Derong Liu
Cesare Alippi
Dongbin Zhao
Amir Hussain (Eds.)

LNAI 7888

Advances in Brain Inspired Cognitive Systems

6th International Conference, BICS 2013
Beijing, China, June 2013
Proceedings

Springer

Lecture Notes in Artificial Intelligence 7888

Subseries of Lecture Notes in Computer Science

Derong Liu Cesare Alippi Dongbin Zhao
Amir Hussain (Eds.)

Advances in Brain Inspired Cognitive Systems

6th International Conference, BICS 2013
Beijing, China, June 9-11, 2013
Proceedings

Springer

Volume Editors

Derong Liu
Dongbin Zhao
Chinese Academy of Sciences, Institute of Automation
The State Key Laboratory of Management and Control for Complex Systems
Beijing 100190, China
E-mail: {derong.liu; dongbin.zhao}@ia.ac.cn

Cesare Alippi
Politecnico di Milano
Dipartimento di Elettronica, Informazione e Bioingegneria
20133 Milano, Italy
E-mail: alippi@elet.polimi.it

Amir Hussain
University of Stirling, Department of Computing Science and Mathematics
Stirling FK9 4LA, UK
E-mail: ahu@cs.stir.ac.uk

ISSN 0302-9743 e-ISSN 1611-3349
ISBN 978-3-642-38785-2 e-ISBN 978-3-642-38786-9
DOI 10.1007/978-3-642-38786-9
Springer Heidelberg Dordrecht London New York

Library of Congress Control Number: Applied for

CR Subject Classification (1998): I.2.11, I.2, H.3-4, F.1, F.2.2, I.4-5

LNCS Sublibrary: SL 7 – Artificial Intelligence

Typesetting: Camera-ready by author, data conversion by Scientific Publishing Services, Chennai, India

Printed on acid-free paper

Springer is part of Springer Science+Business Media (www.springer.com)

Preface

BICS 2013 – The 6th International Conference on Brain Inspired Cognitive Systems—was held in Beijing, China, as a sequel of BICS 2004 (Stirling, Scotland, UK), BICS 2006 (Island of Lesvos, Greece), BICS 2008 (Sao Luis, Brazil), BICS 2010 (Madrid, Spain), and BICS 2012 (Shenyang, China). BICS has now become a well-established conference series on brain-inspired cognitive systems around the world, with growing popularity and increasing quality. Beijing, as the capital of the People's Republic of China, is the nation's political, economic, and cultural center as well as China's most important center for international trade and communications. All participants of BICS 2013 had a technically rewarding experience as well as memorable experiences in this great city.

This book constitutes the proceedings of BICS 2013. BICS 2013 aimed to provide a high-level international forum for scientists, engineers, and educators to present the state of the art of brain-inspired cognitive systems research and applications in diverse fields. The conference featured plenary lectures given by world-renowned scholars, regular sessions with broad coverage, and some special sessions focusing on popular and timely topics.

The conference received 68 submissions from more than 120 authors in 21 countries and regions across four continents. Based on a rigorous review process carried out by the Program Committee members and reviewers, 45 high-quality papers were selected for publication in the conference proceedings. We would like to express our sincere gratitude to all reviewers of BICS 2013 for the time and efforts they generously gave to the conference. We are very grateful to the Institute of Automation of the Chinese Academy of Sciences, the University of Stirling, the Chinese University of Hong Kong, the University of Illinois at Chicago, and the National Natural Science Foundation of China for their financial support. We would also like to thank the publisher, Springer, for their cooperation in publishing the proceedings in the prestigious series of *Lecture Notes in Artificial Intelligence.*

June 2013

Derong Liu
Cesare Alippi
Dongbin Zhao
Amir Hussain

Organization

General Chair

Derong Liu, China

Advisory Committee Chairs

Ruwei Dai, China
Aike Guo, China

Organizing Committee Chairs

Bhaskar DasGupta, USA
Jun Wang, Hong Kong

Program Chairs

Vladimir Bajic, Saudi Arabia
Amir Hussain, UK
Robert Kozma, USA
Liang Zhao, Brazil

Special Sessions Chairs

Erik Cambria, Singapore
Sanqing Hu, China
Dongbin Zhao, China

Finance Chair

Huaguang Zhang, China

Publicity Chairs

Song Ci, USA
El-Sayed El-Alfy, Saudi Arabia

European Liaisons

Mohamed Chetouani, France
Anna Esposito, Italy

Giacomo Indiveri, Switzerland
Mufti Mahmud, Italy
Stefan Wermter, Germany

Publications Chairs

Zeng-Guang Hou, China
Stefano Squartini, Italy

Registration Chair

Qinglai Wei, China

Local Arrangements Chair

Ding Wang, China

Conference Secretariat

Hongliang Li, China

International Program Committee

Peter Andras
Vladimir Bajic
Joao Bertini Jr.
Fabricio Breve
Erik Cambria
Zengqiang Chen
Mohamed Chetouani
Song Ci
Bhaskar DasGupta
El-Sayed El-Alfy
Peter Erdi
Anna Esposito
Marcos Faundez-Zanuy
Takeshi Furuhashi
Michele Giugliano
Stephen Grossberg
Haibo He
Zeng-Guang Hou
Sanqing Hu
Amir Hussain
Giacomo Indiveri
Robert Kozma
Xuelong Li
Hongliang Li
Haihua Liu
Mufti Mahmud
Marcos Quiles
Nicla Rossini
Juergen Schmidhuber
Bjoern Schuller
Stefano Squartini
Jianhua Tao
Isabel Trancoso
Stefano Vassanelli
David Vernon
Ding Wang
Jun Wang
Zhanshan Wang

Qinglai Wei
Luda Werbos
Stefan Wermter
Erfu Yang
Huaguang Zhang
Li Zhang
Dongbin Zhao
Liang Zhao
Qiangfu Zhao

Table of Contents

Silhouette-Based Gait Recognition via Deterministic Learning

Wei Zeng[1,2] and Cong Wang[3]

[1] School of Mechanical & Automotive Engineering, South China University of Technology, Guangzhou 510641, P.R. China
[2] School of Physics and Mechanical & Electrical Engineering, Longyan University, Longyan 364000, P.R. China
zw0597@126.com
[3] School of Automation Science and Engineering, South China University of Technology, Guangzhou 510641, P.R. China
wangcong@scut.edu.cn

Abstract. In this paper, we present a new silhouette-based gait recognition method via deterministic learning theory. We select four silhouette features which represent the dynamics of gait motion and can more effectively reflect the tiny variance between different gait patterns. The gait recognition approach consists of two phases: a training phase and a test phase. In the training phase, the gait dynamics underlying different individuals' gaits are locally-accurately approximated by radial basis function (RBF) networks. The obtained knowledge of approximated gait dynamics is stored in constant RBF networks. In the test phase, a bank of dynamical estimators is constructed for all the training gait patterns. By comparing the set of estimators with a test gait pattern, a set of recognition errors are generated, and the average L_1 norms of the errors are taken as the similarity measure between the dynamics of the training gait patterns and the dynamics of the test gait pattern. The test gait pattern similar to one of the training gait patterns can be recognized according to the smallest error principle. Finally, the recognition performance of the proposed algorithm is comparatively illustrated to take into consideration the published gait recognition approaches on the CASIA gait database (Dataset B).

Keywords: Gait recognition, deterministic learning, silhouette features, gait dynamics, smallest error principle.

1 Introduction

The study of human gait has recently been driven by its potential use as a biometrics for person identification at a distance, which stands in contrast to other biometric techniques involving face, fingerprints, iris, etc. Furthermore, it does not require users' interaction, and is non-invasive and difficult for a subject to conceal and disguise his/her gait characteristics.

The schemes applied in gait recognition can be roughly divided into two categories: model-based [1] and silhouette-based [2] approaches. Current literature

D. Liu et al. (Eds.): BICS 2013, LNAI 7888, pp. 1–10, 2013.

focuses on silhouette-based approaches which directly operate on the gait sequences without assuming any specific model. They usually analyze the spatio-temporal shape and motion characteristics of silhouettes.

Since performance of the gait recognition algorithm increases with the number of appropriate gait features considered, we aim to effectively combine spatio-temporal gait characteristics, statistical and physical parameters of human body. The relative importance of the dynamics of the silhouette feature and the dynamics of physical parameters like joint angles in human gait recognition has been seldom investigated. In [1], the dynamics along the phase portrait of joint angles versus angular velocities was captured as a gait signature to achieve gait recognition. However, there has been very little work on attempting to capture the dynamics in this silhouette feature. The experimental results of this work shed some light on this issue. Compared with [1], our experiments indicate that, for the purpose of gait recognition, the amount of discriminability provided by the dynamics of the silhouette feature is similar to the discriminability provided by the dynamics of physical parameters like joint angles and/or angular velocities. This means that there is very little (if any) loss in using the dynamics of the silhouette feature instead of dynamics of the human body parts.

2 Problem Formulation

Consider a general nonlinear human gait dynamical system in the following form:

$$\dot{x} = F(x; p), \quad x(t_0) = x_0 \tag{1}$$

where $x = [x_1, \ldots, x_n]^T \in R^n$ is the state of the system which represents the gait features, p is a constant vector of system parameters (different p will in general generate different gait patterns). $F(x; p) = [f_1(x; p), \ldots, f_n(x; p)]^T$ is a smooth but unknown nonlinear vector field.

Our objective is to choose suitable human gait features as the states of system (1) and design a dynamic RBF network to identify and approximate the unknown vector $F(x; p)$. The approximation result can be used to represent the human gait dynamics which will be stored and used for gait recognition.

3 Feature Extraction and Gait Signature Derivation

In this section, we investigate four silhouette features which seem suitable for capturing discriminatory gait information from sequences of extracted silhouettes and for representing gait dynamics.

3.1 Silhouette Extraction

Silhouette segmentation is the first step to gait recognition. Firstly, we model the background image and subtract the foreground image from original image. A bounding box is then placed around the part of the motion image that contains the moving person. These boxed binarized silhouettes can be used directly as image features or further processed to derive the width vector and the ratio vector of the silhouette's height and width as in the next item.

3.2 Gait Periodicity

In this paper, we proposed to use the aspect ratio of the boundingbox of moving silhouette (height/width, H-W ratio), which is comparatively stable. By observing, the width of the silhouette was changing periodically with the time-lapse. For each frame in one sequence, the variances of H-W ratio will constitute a gait feature vector, as shown in Fig. 1.

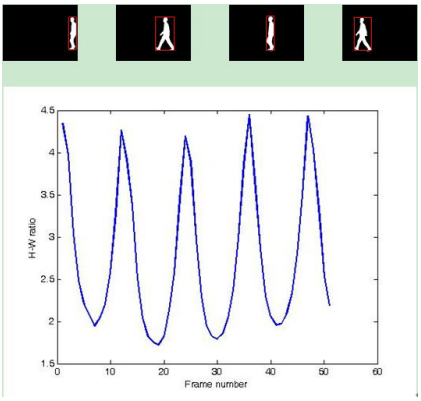

Fig. 1. The H-W ratio curve of a gait sequence

3.3 Width of the Outer Contour of the Binary Silhouette

Distance between left and right extremities of the silhouette gives the width vector. From the binarized silhouette, the left and right boundaries are traced. Width calculation is shown in Fig. 2(a). Here, Y axis denotes the row index and X axis denotes the width associated with the corresponding row. The width along a given row is simply the difference between leftmost and rightmost boundary pixels (1-valued) in that row. For a binary gait image $b(X, Y)$ indexed spatially by pixel location (X, Y), X_Y^1 represents the X-coordinate of the leftmost boundary pixel in the Yth row, and X_Y^2 represents the X-coordinate of the rightmost boundary pixel in the same row. For all rows, the width feature W_d is generated by

$$W_d = max(X_Y^2 - X_Y^1) \tag{2}$$

where d denotes the dth frame binary silhouette. Fig. 2(b) shows the width feature curve of a person for one walking sequence.

3.4 Silhouette Area

Since the total area of the body fluctuates at the same pace as the stride, it reflects the discriminating power of the frame. We then calculate the area A_d of the whole binary silhouette by counting the number of pixels in it, where d denotes the dth frame binary silhouette.

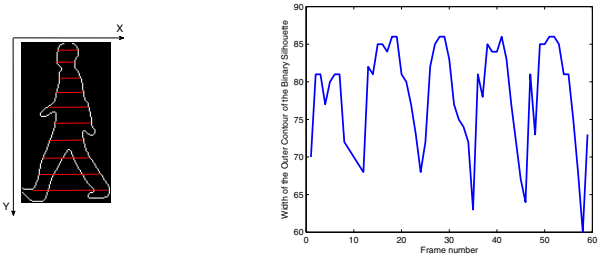

(a) Width feature extraction.

(b) The width of the outer contour of the binary silhouette in a gait sequence.

Fig. 2. Width feature extraction and its representation

3.5 Vertical Coordinate of Centroid of the Outer Contour

The centroid is a fundamental and preliminary feature whose vertical motion is found to be periodic (in time). Apparently, centroid (x_c, y_c) of the binary silhouette (as shown in Fig. 3(a)) can be calculated from the information of the outer contour of the silhouette as follows:

$$x_c = \frac{1}{n_{oc}} \sum_{i=1}^{n_{oc}} X_i \tag{3}$$

$$y_c = \frac{1}{n_{oc}} \sum_{i=1}^{n_{oc}} Y_i \tag{4}$$

where n_{oc} denotes the number of the pixels on the outer contour, (X_i, Y_i) is the coordinate of the pixels (1-valued) on the outer contour. Fig. 3(b) shows the vertical motion curve (variation of y_c) of the centroid of silhouette in a gait sequence.

4 Training and Learning Mechanism Based on Silhouette Features

In this section, we present a scheme for identification of gait system dynamics based on deterministic learning theory.

In order to more accurately describe the human walking, the gait dynamics can be modeled as the following form:

$$\dot{x} = F(x; p) + v(x; p) \tag{5}$$

where $x = [x_1, \ldots, x_n]^T \in R^n$ are the states of system (5) which represent the combined silhouette features of the human body, p is a constant vector of system parameters. $F(x; p) = [f_1(x; p), \ldots, f_n(x; p)]^T$ is a smooth but unknown

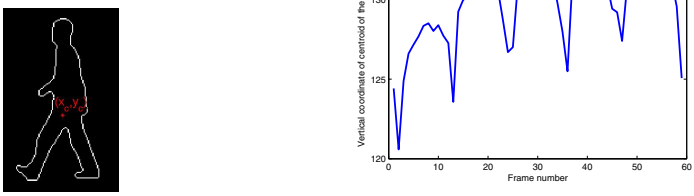

(a) (b)

Fig. 3. (a) Illustration of the centroid of the binary silhouette; (b) variation curve of y_c of the binary silhouette in a gait sequence

nonlinear vector representing the gait system dynamics, $v(x;p)$ is the modeling uncertainty. The system trajectory starting from initial condition x_0, is denoted as $\varphi_\zeta(x_0)$.

Since the modeling uncertainty $v(x;p)$ and the gait system dynamics $F(x;p)$ cannot be decoupled from each other, we consider the two terms together as an undivided term, and define $\phi(x;p) := F(x;p) + v(x;p)$ as the general gait system dynamics. The objective of the training or learning phase is to identify or approximate the general gait system dynamics $\phi(x;p)$ to a desired accuracy via deterministic learning.

Based on deterministic learning theory [3], the following dynamical RBF networks are employed to identify the gait system dynamics $\phi(x;p) = [\phi_1(x;p), \ldots, \phi_n(x;p)]^T$:

$$\dot{\hat{x}} = -A(\hat{x} - x) + \hat{W}^T S(x) \tag{6}$$

where $\hat{x} = [\hat{x}_1, \ldots, \hat{x}_n]$ is the state vector of the dynamical RBF networks, $A = diag[a_1, \ldots, a_n]$ is a diagonal matrix, with $a_i > 0$ being design constants, localized RBF networks $\hat{W}^T S(x) = [\hat{W}_1^T S_1(x), \ldots, \hat{W}_n^T S_n(x)]^T$ are used to approximate the unknown $\phi(x;p)$.

The NN weight updating law is given by:

$$\dot{\hat{W}}_i = \dot{\tilde{W}}_i = -\Gamma_i S(x)\tilde{x}_i - \sigma_i \Gamma_i \hat{W}_i \tag{7}$$

where $\tilde{x}_i = \hat{x}_i - x_i, \tilde{W}_i = \hat{W}_i - W_i^*$, W_i^* is the ideal constant weight vector such that $\phi_i(x;p) = {W_i^*}^T S(x) + \epsilon_i(x)$, $\epsilon_i(x) < \epsilon^*$ is the NN approximation error, $\Gamma_i = \Gamma_i^T > 0$, and $\sigma_i > 0$ is a small value.

With Eqs. (5)-(6), the derivative of the state estimation error $\tilde{x}_i$ satisfies

$$\dot{\tilde{x}}_i = -a_i \tilde{x}_i + \hat{W}_i^T S(x) - \phi_i(x;p) = -a_i \tilde{x}_i + \tilde{W}_i^T S(x) - \epsilon_i \tag{8}$$

By using the local approximation property of RBF networks, the overall system consisting of dynamical model (8) and the NN weight updating law (7) can be summarized into the following form in the region Ω_ζ

$$\begin{bmatrix} \dot{\tilde{x}}_i \\ \dot{\tilde{W}}_{\zeta i} \end{bmatrix} = \begin{bmatrix} -a_i & S_{\zeta i}(x)^T \\ -\Gamma_{\zeta i} S_{\zeta i}(x) & 0 \end{bmatrix} \begin{bmatrix} \tilde{x}_i \\ \tilde{W}_{\zeta i} \end{bmatrix} + \begin{bmatrix} -\epsilon_{\zeta i} \\ -\sigma_i \Gamma_{\zeta i} \hat{W}_{\zeta i} \end{bmatrix} \tag{9}$$

and

$$\dot{\hat{W}}_{\bar{\zeta} i} = \dot{\tilde{W}}_{\bar{\zeta} i} = -\Gamma_{\bar{\zeta} i} S_{\bar{\zeta} i}(x) \tilde{x}_i - \sigma_i \Gamma_{\bar{\zeta} i} \hat{W}_{\bar{\zeta} i} \tag{10}$$

where $\epsilon_{\zeta i} = \epsilon_i - \tilde{W}_{\bar{\zeta} i}^T S_{\bar{\zeta}}(x)$. The subscripts $(\cdot)_\zeta$ and $(\cdot)_{\bar{\zeta}}$ are used to stand for terms related to the regions close to and far away from the trajectory $\varphi_\zeta(x_0)$. The region close to the trajectory is defined as $\Omega_\zeta := Z | dist(Z, \varphi_\zeta) \leq d_\iota$, where $Z = x, d_\iota > 0$ is a constant satisfying $s(d_\iota) > \iota$, $s(\cdot)$ is the RBF used in the network, ι is a small positive constant. The related subvectors are given as: $S_\zeta(x) = [s_{j1}(x), \ldots, s_{j\zeta}(x)]^T \in R^{N_\zeta}$, with the neurons centered in the local region Ω_ζ, and $W_\zeta^* = [w_{j1}^*, \ldots, w_{j\zeta}^*]^T \in R^{N_\zeta}$ is the corresponding weight subvector, with $N_\zeta < N$. For localized RBF networks, $|\tilde{W}_{\bar{\zeta} i}^T S_{\bar{\zeta}}(x)|$ is small, so $\epsilon_{\zeta i} = O(\epsilon_i)$.

According to Theorem 1 in [4], the regression subvector $S_{\zeta i}(x)$ satisfies persistence of excitation (PE) condition almost always. This will lead to exponential stability of $(\tilde{x}_i, \tilde{W}_{\zeta i}) = 0$ of the nominal part of system (9) [5]. Based on the analysis results given in [4], the NN weight estimate error $\tilde{W}_{\zeta i}$ converges to small neighborhoods of zero, with the sizes of the neighborhoods being determined by $\epsilon_{\zeta i}$ and $\|\sigma_i \Gamma_{\zeta i} W_{\zeta i}^*\|$, both of which are small values. This means that the entire RBF network $\hat{W}_i^T S(x)$ can approximate the unknown $\phi_i(x; p)$ along the trajectory φ_ζ, and

$$\phi_i(x; p) = \hat{W}_i^T S(x) + \epsilon_{i1} \tag{11}$$

where $\epsilon_{i1} = O(\epsilon_{\zeta i})$.

By the convergence result, we can obtain a constant vector of neural weights according to

$$\bar{W}_i = mean_{t \in [t_a, t_b]} \hat{W}_i(t) \tag{12}$$

where $t_b > t_a > 0$ represent a time segment after the transient process. Therefore, we conclude that accurate identification of the function $\phi_i(x; p)$ is obtained along the trajectory $\varphi_\zeta(x_0)$ by using $\bar{W}_i^T S_i(x)$, i.e.,

$$\phi_i(x; p) = \bar{W}_i^T S(x) + \epsilon_{i2} \tag{13}$$

where $\epsilon_{i2} = O(\epsilon_{i1})$ and subsequently $\epsilon_{i2} = O(\epsilon^*)$.

Hence, locally-accurate identification of the gait system dynamics $\phi_i(x; p)$ to the error level ϵ^* is achieved along the trajectory $\varphi_\zeta(x_0)$. Time-varying gait dynamical patterns can be effectively represented by the locally-accurate NN approximations of the gait system dynamics, and this representation is time-invariant.

5 Gait Recognition Mechanism

In this section, we present a scheme for rapid recognition of human gait by using the learned gait system dynamics.

Consider a training set containing dynamical human gait patterns $\varphi_\zeta^k,\ k = 1,\ldots,M$, with the kth gait training pattern φ_ζ^k generated from

$$\dot{x} = F^k(x;p^k) + v^k(x;p^k),\quad x(t_0) = x_{\zeta 0} \tag{14}$$

where $F^k(x;p^k)$ denotes the gait system dynamics, $v^k(x;p^k)$ denotes the modeling uncertainty, p^k is the system parameter vector.

As shown in Section 4, the general gait system dynamics $\phi^k(x;p^k) := F^k(x;p^k) + v^k(x;p^k)$ can be accurately identified and stored in constant RBF networks $\bar{W}^{k^T} S(x)$. By utilizing the learned knowledge obtained in the training phase, a bank of M estimators is first constructed for the trained gait systems as follows:

$$\dot{\bar{\chi}}^k = -B(\bar{\chi}^k - x) + \bar{W}^{k^T} S(x) \tag{15}$$

where $k = 1,\ldots,M$ is used to stand for the kth estimator, $\bar{\chi}^k = [\bar{\chi}_1^k,\ldots,\bar{\chi}_n^k]^T$ is the state of the estimator, $B = diag[b_1,\ldots,b_n]$ is a diagonal matrix which is kept the same for all estimators, x is the state of an input test pattern generated from Eq. (5).

In the test phase, by comparing the test gait pattern generated from human gait system (5) with the set of M estimators (15), we obtain the following recognition error systems:

$$\dot{\tilde{\chi}}_i^k = -b_i\tilde{\chi}_i^k + \bar{W}_i^{k^T} S_i(x) - \phi_i(x;p),\quad i = 1,\ldots,n,\quad k = 1,\ldots,M \tag{16}$$

where $\tilde{\chi}_i^k = \bar{\chi}_i^k - x_i$ is the state estimation (or synchronization) error. We compute the average L_1 norm of the error $\tilde{\chi}_i^k(t)$

$$\|\tilde{\chi}_i^k(t)\|_1 = \frac{1}{\mathrm{T}_c}\int_{t-\mathrm{T}_c}^{t} |\tilde{\chi}_i^k(\tau)|d\tau,\quad t \geq \mathrm{T}_c \tag{17}$$

where T_c is the cycle of human gait.

The fundamental idea of human gait recognition is that if one person appearing with the gait pattern similar to the trained human gait pattern s ($s \in \{1,\ldots,k\}$), the constant RBF network $\bar{W}_i^{s^T} S_i(x)$ embedded in the matched estimator s will quickly recall the learned knowledge by providing accurate approximation to the human gait dynamics. Thus, the corresponding error $\|\tilde{\chi}_i^s(t)\|_1$ will become the smallest among all the errors $\|\tilde{\chi}_i^k(t)\|_1$. Based on the smallest error principle, the appearing person can be recognized.

6 Experiments

We evaluate the proposed method on the CASIA gait database (Dataset B). The experiments are implemented using matlab software and tested on an Intel Core i5 3.5GHz computer with 4GB RAM.

The CASIA-B database is a large dataset, including 124 different subjects (93 males and 31 females) with variations in view angle and walking status (normal, in a coat, or with a bag) [6]. Besides, there are 6 sequences from each normal walking subject under one of the 11 viewing angles. Since clothing and carrying condition changes are not in the scope of this paper, only the videos with normal walking status and with a lateral view angle (view angle 90°) are used in this experiment. Fig. 4 shows three sample images in this gait database.

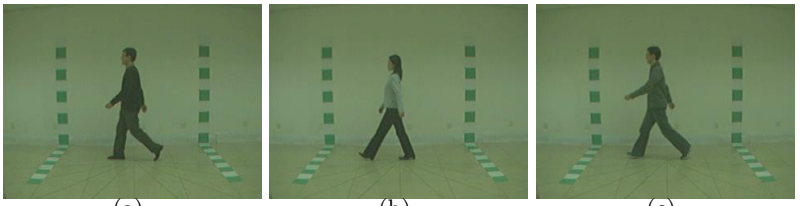

(a) (b) (c)

Fig. 4. Three different sample images in the CASIA-B database with the lateral view and normal walking status

We assign three sequences to training set and the remaining three sequences to testing set for all the 124 subjects. Based on the method described in Section 3, we extract all the 124 persons' silhouette features through the normal walking image sequences, which means the input of the RBF networks $x = [\text{H-W ratio}, W_d, A_d, y_c]^T$. The extracted silhouettes from the databases are normalized, and the size of the silhouettes is 128×88. In order to eliminate the data difference between different silhouette features, all the silhouette feature data is normalized to $[-1, 1]$.

Fig. 5 and Fig. 6 show an example of the training and recognition of person 001 in the 124-person dataset. There are three sequences to training set (labeled '001-nm-01-90' ,'001-nm-02-90' and '001-nm-03-90' in the database) and three sequences to test set (labeled '001-nm-04-90', '001-nm-05-90' and '001-nm-06-90' in the database). In the training phase, the RBF network $\hat{W}_i^T S_i(x)$ is constructed in a regular lattice, with nodes $N = 83521$, the centers μ_i evenly spaced on $[-1, 1] \times [-1, 1] \times [-1, 1] \times [-1, 1]$, and the widths $\eta = 0.15$. The weights of the RBF networks are updated according to Eq. (7). The initial weights $\hat{W}_i(0) = 0$. The design parameters for (6) and (7) are $a_i = 0.5, \Gamma = diag\{1.5, 1.5, 1.5, 1.5\}, \sigma_i = 10, (i = 1, \ldots, 4)$. The convergence of neural weights is shown in Fig. 5, which demonstrates partial parameter convergence, that is, only the weight estimates of some neurons whose centers close to the orbit are activated and updated. These weights converge to their optimal values W_i^*. Based on deterministic learning theory, the gait dynamics $\phi_i^k(x; p^k)$ can be locally-accurately approximated by $\bar{W}_i^{k^T} S_i(x), (k = 1, \ldots, 372)$ along recurrent system trajectory, then these constant weights are stored for each training pattern.

In the test phase, by using the constant networks $\bar{W}_i^{k^T} S_i(x), (k = 1, \ldots, 372)$, 372 RBF network estimators are constructed based on (15). The parameters in (15) and (17) are $b_i = -25$ $(i = 1, \ldots, 4), T_c = 1.2s$. Consider recognition of the test person 001 (represented by the test pattern '001-nm-04-90') by 372 training patterns. The average L_1 norms of the synchronization errors, that is, $\|\tilde{x}_i^k(t)\|_1$ $(k = 1, \ldots, 372)$ are shown in Fig. 6. It is obvious that after certain time, the average L_1 norm generated by the training pattern '001-nm-01-90' becomes smaller than the others.

The recognition performance of the proposed methods is reported in terms of the correct classification rate (CCR). Table 1 compares the performance of the proposed method with that of state-of-the-art silhouette-based methods.

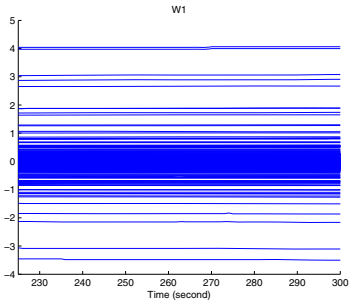

Fig. 5. Partial parameter convergence of $\hat{W}_1$ in one training pattern

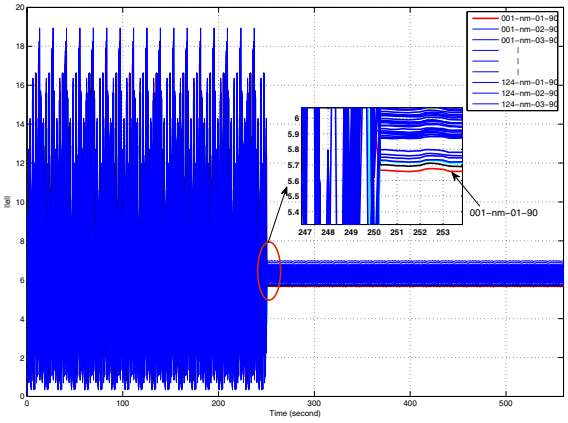

Fig. 6. Recognition result of person 001 by using smallest error principle

Table 1. Comparison of several algorithms on the CASIA-B database (in lateral view and normal walking status)

Algorithms	CCR (%)
Yu 2006 [6]	97.6
Goffredo 2010 [7]	86.5
Zhang 2010 [8]	98.39
Proposed method	98.4

7 Conclusions

A new gait recognition approach based on silhouette features via deterministic learning theory is presented in this paper. Based on the method for feature extraction, the silhouette features representing the gait dynamics can be extracted. The gait system dynamics can be accurately approximated by RBF networks and the obtained knowledge will be stored in constant RBF networks. Then, according to the dynamical estimators and the smallest error principle, the human gait can be recognized.

Acknowledgments. This work was supported by the National Science Fund for Distinguished Young Scholars (Grant No. 61225014), and by the National Natural Science Foundation of China (Grant No. 60934001).

References

1. Zeng, W., Wang, C.: Human Gait Recognition via Deterministic Learning. Neural Networks 35, 92–102 (2012)
2. Ekinci, M., Aykut, M.: Improved Gait Recognition by Multiple-Projections Normalization. Machine Vision and Applications 21(2), 143–161 (2010)
3. Wang, C., Hill, D.J.: Deterministic Learning Theory for Identification, Recognition and Control. CRC Press (2009)
4. Wang, C., Chen, T., Chen, G., Hill, D.J.: Deterministic Learning of Nonlinear Dynamical Systems. International Journal of Bifurcation and Chaos 19(4), 1307–1328 (2009)
5. Farrell, J.: Stability and Approximator Convergence in Nonparametric Nonlinear Adaptive Control. IEEE Transactions on Neural Networks 9(5), 1008–1020 (1998)
6. Yu, S., Tan, D., Tan, T.: A Framework for Evaluating the Effect of View Angle, Clothing and Carrying Condition on Gait Recognition. In: 18th International Conference on Pattern Recognition, pp. 441–444 (2006)
7. Goffredo, M., Bouchrika, I., Carter, J.N., Nixon, M.S.: Self-Calibrating View-Invariant Gait Biometrics. IEEE Transactions on Systems, Man, and Cybernetics-Part B: Cybernetics 40(4), 997–1008 (2010)
8. Zhang, E., Zhao, Y., Xiong, W.: Active Energy Image plus 2DLPP for Gait Recognition. Signal Processing 90(7), 2295–2302 (2010)

An Improved Free Search Approach for Energy Optimization in Wireless Sensor Networks

Zengqiang Chen*, Yuefei Wei, and Qinglin Sun

Department of Automation, Nankai University, Tianjin, 300071, China
{chenzq,sunql}@nankai.edu.cn, weiyuefei@gmail.com

Abstract. In order to maximize the lifetime of a wireless sensor network (WSN), an improved free search (FS) approach, which is called free search with double populations (FSDP), is proposed in this paper. FSDP is a population-based approach which is applied to optimize the energy consumption of a wireless sensor network. A circular network model is adopted and FSDP obtains the optimal solution by finding an optimal transmission path from the nodes of outer girdle bands to the sink node. Simulation results obtained by FSDP show the effectiveness of the proposed optimization approach.

Keywords: Free search algorithm, free search with double populations, wireless sensor networks, energy consumption optimization, network lifetime.

1 Introduction

Wireless Sensor Networks (WSNs) ([1], [2]) are becoming increasingly popular, due to the benefits they bring to many applications as well as the increasing availability and maturity of the underlying technologies. However, since wireless sensor nodes are powered by small batteries, the limited energy supply has constrained the lifetime of a wireless sensor network. This issue has been a long-lasting, fundamental problem faced by wireless sensor networks that are designed for long-term operation.

To overcome this challenge, different methods and techniques (e.g., clustering algorithms [3-4], MAC layer protocols [5-6] and population-based intelligent optimization algorithms [7-9]), which aimed at reducing the energy consumption and extending the network lifetime, were developed in the last few years. In Ref. [3], a hierarchical-based topology called LEACH (Low-Energy Adaptive Clustering Hierarchy) which combines the ideas of energy-efficient cluster-based routing and media access together with application-specific data aggregation was proposed. Researchers also focus on such evolutionary optimization techniques as Ant Colony Optimization (ACO) [8], Particle Swarm Optimization (PSO) [7] and Genetic Algorithm (GA) [9] in attempt to prolong the network lifetime.

Free Search (FS), which was proposed by Kalin Penev and Guy Littlefair in 2003 [10], has proven to be highly efficient and fast in convergence speed comparing to such population-based optimization approaches as GA and PSO. The behavior of each

* Corresponding author.

D. Liu et al. (Eds.): BICS 2013, LNAI 7888, pp. 11–20, 2013.

individual in FS algorithm is not defined and each individual has the freedom to make the decision on how and where to search. In addition, FS is based on the following assumptions: an uncertainty can cope with other uncertainties and the infinity can cope with other infinities [11]. Nevertheless, some drawbacks still exist in FS algorithm like premature convergence. FS is also sensitive to the searching radius: the convergence speed is slower when the searching radius is a little bigger while it is easier to trap into local optima when the searching radius is a little smaller. In this paper, an improved free search approach, called free search with double population (FSDP), is proposed for optimizing data transmission path to the sink node in attempt to achieve the goal of reducing the energy consumption and extending the network lifetime. The simulation results show that an overall good performance can be obtained by FSDP comparing to other algorithms such as FS, PSO and GA.

2 Network Model and Problem Formulation

In order to obtain some related descriptions of nodes of a wireless sensor network, a specific model is necessary. Inspired by the network model mentioned in Ref. [12], a simple circular network model is set up in this study and it is assumed that nodes are uniformly distributed as a set of cycles centered on the sink node and each node in the wireless sensor network has four-stage transmitting power. The sink node is located in the centre of the monitoring area. The distance between two girdle bands is r which is also the range that each node can reach using the lowest transmitting power. The position where the sink node located is referred to as girdle band 0 and the next outside one is girdle band 1, where the first stage nodes distribute and the second stage nodes distribute on the girdle band 2 and so on. In single-hop transmission process, the data transmitted from the $(k+1)^{th}$ stage have to be relayed by the k^{th} stage nodes and then be transmitted to the $(k-1)^{th}$ stage nodes from the k^{th} stage. In order to be convenient for analysis, it is assumed that the distance between the sink node and the nodes distributed in the outmost girdle band is R and number of the nodes in a unit area is 1, with each node only generating one data package in unit time. Besides, it only considers up-load transmission for transmitting the data and does not consider data aggregation. Under these assumptions, the data packages generated by the nodes which are distributed outside the k^{th} girdle band are transmitted by the nodes of the k^{th} girdle band. The total data packages generated by the nodes distributed outside the k^{th} girdle band are $\pi[R^2-(k\cdot r)^2]$. At the same time we can get the number of nodes on the k^{th} girdle band is $\pi[(kr)^2-((k-1)\cdot r)^2]$. Consequently, the data package received by each node on the k^{th} girdle band is shown in formula (1) as follows.

$$D_R(k)=\frac{R^2-(kr)^2}{(kr)^2-((k-1)r)^2} \tag{1}$$

Except for the received data, each node also generates one data package in unit time. Thus, the total data packages to be transmitted by each node on the k^{th} girdle band are as follows.

$$D_T(k)=D_R(k)+1 \tag{2}$$

In multi-hop transmission process, it is assumed that the transmitting distances for each-stage transmitting power of the Nodes are r $2r$, $3r$ and $4r$ respectively. Usually, the communication distance is positively proportion to the n^{th} power of the transmitting power of the transmitter module, where n is the path attenuation coefficient, having a radii between 2 and 6. It is also assumed that the communication channel is idealized when the value of n is equal to 2 and each-stage transmitting power is p_1=1 p_2 = 4, p_3 = 9 and p_4=16, with the receiving power pr = 3. Under the assumptions above, there are four choices to transmit data to the corresponding girdle band for the nodes on the k^{th} girdle band. For this reason, some nodes distributed on the k^{th} girdle band probably cannot receive all the data packages because the data packages generated by some nodes may be transmitted to the other girdle bands without reaching the k^{th} girdle band. The number of the nodes on the k^{th} girdle band is $\pi r^2[k^2-(k-1)^2]$ and the number of the nodes on the $(k+n)^{th}$ girdle band is $\pi r^2[(k+n)^2-(k+n-1)^2]$. Then the ratio between the number of the nodes on the k^{th} girdle band and the number of the nodes on the $(k+n)^{th}$ girdle band, which is $[2k+(2n-1)]/(2k-1)$, can be obtained.

The RTS-CTS handshaking protocol [13] is adopted as the communication protocol of the network, it is assumed that the following equations are satisfied.

$$D_R(k) = R_{RTS}(k) = T_{ACK}(k) = T_{CTS}(k) \tag{3}$$

$$D_T(k) = T_{RTS}(k) = R_{ACK}(k) = R_{CTS}(k) \tag{4}$$

When transmitting one data packet from *Node k* to *Node k-i* (i=1, 2, 3, 4), the transmitted data for *Node k* includes a control frame and a data packet, which is the received data for *Node k-i* (i=1, 2, 3, 4)**.** The received data for *Node k* includes two control frames, which is the transmitted data for *Node k-i* (i=1, 2, 3, 4). Assume that the energy consumption ratio for transmitting a control frame to transmitting a data frame is δ .According to the RTS-CTS handshaking protocol and the ratio of the number of the nodes on the k^{th} girdle band to the number of the nodes on the $(k-i)^{\text{th}}$ girdle band, the energy consumption of the node distributed on the k^{th} girdle band is shown in equations (5) and (6) when transmitting one packet from the k^{th} girdle band to the $(k-i)^{\text{th}}$ girdle band.

$$E_T = P_i[D_T(k)+\delta\cdot T_{RTS}(k)]\cdot\frac{2k-1}{2(k-i)-1}+\mathrm{P_r}\cdot\delta[R_{CTS}(k)+R_{ACK}(k)]\cdot\frac{2(k-i)-1}{2k-1} \tag{5}$$

$$E_R = P_i\cdot\delta[T_{CTS}(k)+T_{ACK}(k)]\cdot\frac{2(k-i)-1}{2k-1}+\mathrm{P_r}[D_R(k)+\delta\cdot R_{RTS}(k)]\cdot\frac{2k-1}{2(k-i)-1} \tag{6}$$

According to Equs.(3) and (4), Equs. (5) and (6) can become a simple form as:

$$E_T = (1+\delta)P_i\cdot D_T(k)\frac{2k-1}{2(k-i)-1}+2\delta\,\mathrm{Pr}\cdot D_R(k)\frac{2(k-i)-1}{2k-1} \tag{7}$$

$$E_R = 2\delta P_i\cdot D_T(k)\frac{2(k-i)-1}{2k-1}+(1+\delta)\mathrm{P_r}\cdot D_R(k)\frac{2k-1}{2(k-i)-1} \tag{8}$$

Assume that the time is t_1 when a data packet is transmitted from the k^{th} girdle band to the $(k-i)^{th}$ girdle band. Then, the energy consumption of nodes distributed on the k^{th} girdle band and the $(k-i)^{th}$ girdle band at t_1 can be obtained respectively.

$$E_{t_1}(k) = E_{t_1-1}(k) + E_T \tag{9}$$

$$E_{t_1}(k-i) = E_{t_1-1}(k-i) + E_R \tag{10}$$

The equations (7)-(10) are the energy consumption model of nodes of wireless sensor network based-on the aforementioned network model and multi-hop routing.

3 Free Search with Double Populations (FSDP)

In this section, the details on the searching process and mechanism of free search (FS) will firstly be given. After that, an improved optimization approach called free search with double populations (FSDP) which is based on free search will be introduced.

3.1 An Overview of Free Search (FS)

Before presentation, it is necessary to have an overview firstly on the notations involved in this paper, showing in Table 1.

Table 1. Notational conventions common to the evolutionary algorithms

Notation	Description
popSize	Population size
Dim	Dimensions of searching space
G	Total number of generations
X0	Initial solutions generated randomly
T	An exploration walk
R_{ji}	Searching radius for each individual
$X_{\min j}$	Lower limit of searching space for the *j-th* individual
$X_{\max j}$	Upper bound of searching space for the *j-th* individual
P_j	Pheromone of the *j-th* individual
S_j	Sensibility of the *j-th* individual

3.1.1 Initialization Process

Before the exploration, some initializations, which include generating the initial solutions in a given searching space and the searching radius of individuals and setting the exploration walk, the population size, the dimensions of searching space, the number of generations and the range of searching space, are necessary.

For the issue of generating the initial swarm, here there are three generation strategies given in the follows. Any one of the three strategies can be used for swarm initialization by FS algorithm, and the first strategy is adopted in this paper. A brief description on the three strategies is given below.

The first method for initialization is to generate random value as the initial solutions and it is expressed in Eq. (11).

$$X_0 = X_{\min} + (X_{\max} - X_{\min}) * random(0,1) \tag{11}$$

The second way is to use fixed values as the initial solutions, that is, the initial solutions are set by us as shown in Eq. (12).

$$x_{0j,i} = a_{ji}, \quad j = 1,2...popSize, \quad i = 1,2...\dim \tag{12}$$

where $\boldsymbol{a_{ji}} \in [\boldsymbol{X_{min}}, \boldsymbol{X_{max}}]$ denotes the value of *i-th* dimension variable of the *j-th* individual and it is a constant. By this way, each individual of the swarm locates in a fixed position within the search-space before exploration.

The third strategy, which is called single value strategy, is shown in Eq. (13). It is similar to the second method with the difference that the corresponding dimensional variable value for all individuals is the same as opposite to that in the second strategy.

$$X_{0j} = C_j \qquad j = 1,2...popSize \tag{13}$$

where $\boldsymbol{C}_j$ is a vector and it is satisfied that:

$$C_j = (c_1, c_2, ...c_{\dim}) \qquad c_i \in [X_{\min}, X_{\max}], i = 1,2...\dim$$

In FS, the searching radius is initialized as follows: R_j=1if $j \in$ [1, *popSize*/4]; R_j=0.5 if $j \in$ [1+ *popSize*/4, 3.*popSize*/4]; R_j=0.01 if $j \in$ [1+3.*popSize*/4, *popSize*].

3.1.2 Exploration Stages

In every generation, each individual will take an exploration walk independently. When finishing an exploration walk, the best fitness value list, the pheromone and the sensibility of each individual will be updated. An exploration walk is limited by a number of steps and the individuals of swarm will move step by step towards the global optima. During the movement within an exploration walk, the position of the individuals will be updated accordingly. The update rule for the individuals' behavior is shown as follows.

$$X_j(t) = X_j(0) - \Delta X_j(t) + 2\Delta X_j(t) random(0,1), \quad t = 1,2...T \tag{14}$$

where *j* denotes the *j-th* individual and the definition of $\Delta X_j(t)$ can be expressed as:

$$\Delta X_j(t) = R_j(X_{\max} - X_{\min}) random(0,1) \tag{15}$$

In the searching process, the behavior of individuals can be evaluated by objective function value. It is assumed that:

$$F_j(t) = F(X_j(t)), F_j = \max(F_j(t)), \quad t = 1 \cdots T$$

where $\boldsymbol{F_j}$ (t) denotes the objective function value of the *j-th* individual at time *t* and $\boldsymbol{F_j}$ denotes a best objective function value found by the *j-th* individual after an exploration walk. After an exploration walk, each individual will achieve an objective function solution by which a pheromone for each individual will be distributed. A pheromone, which is proportional to the objective function value, indicates the quality of the solution found by one individual. The swarm abstracts the information about the locations marked with pheromone which is essential for the search in order to gradually approach the optimal solution. The definition of pheromone is given below :

$$P_j = F_j / \max(F_j) \qquad j = 1 \cdots popSize \tag{16}$$

where $max(\boldsymbol{F}_j)$ denotes the optimal objective function value found by all individuals in an exploration walk. In addition, each individual has a sense which together with pheromone determines the selection of location for the next exploration walk. The definition of sensibility is given in Eq. (17).

$$S_j = S_{\min} + \Delta S_j, \quad \Delta S_j = S_{\min} + (S_{\max} - S_{\min}) rand(0,1),\ j = 1,2..., popSize \quad (17)$$

where S_{min} denotes the minimal sensibility and S_{max} denotes the maximal sensibility respectively. They are satisfied that:

$$S_{\min} = P_{\min}, \qquad S_{\max} = P_{\max}$$

As mentioned above, the pheromone and the sensibility together determine the initial position for the next exploration walk. And it can be updated by Eq. (18).

$$X_j(0) = \begin{cases} X_j(0), P_j < S_j \\ X_j(g), P_j \geq S_j \end{cases}, \quad g = 1,2...G \quad (18)$$

When one of the following criteria is satisfied, it is considered to have found the optimal solution:

- Reaching of the optimisation criteria: $F_{max} \geq F_{opt}$, where F_{max} is maximal achieved solution, F_{opt} is an acceptable value of the objective function.
- Expiration of generation limit: $g > G$, where g is the current value.
- Complex criterion: $F_{max} \geq F_{opt} \parallel g > G$.

3.2 Free Search with Double Populations (FSDP)

In this section, free search with double populations (FSDP) which is based on the free search (FS) algorithm will be presented. Although FSDP is derived from FS, there are three main differences between them. Firstly, FSDP uses two population sets, namely W_1 and W_2 as opposed to the only one W in FS. The function of W_1 in FSDP is the same as that of W in FS. The swarm W_2 is an auxiliary population set whose function in FSDP is to keep the record of the sub-optimal solutions that are discarded by W_1. These potential solutions in W_2 are then used for further exploration. The second difference between the two algorithms is the way they implement the neighbor space R_j. FSDP uses a variable neighbor space R_j for each animal as opposed to FS which uses a set of fixed R_j parameters. Thirdly, FSDP differs from FS in that it adopts a tactics of preserving excellent members.

Initially, two sets W_1 and W_2 are generated by Eq. (11). Two individuals are iteratively sampled from the search region. The best individual is going to W_1 and the suboptimal individual to W_2. The process continues until each set has the same number of individuals as the population size. The FSDP procedure then gradually drives the set W_1 towards the global optimum through the repeated cycles of taking exploration walk, distributing pheromone, generating sensibility, selection and preserving the best individual. For each animal, there are two starting locations: One location is from W_1 and the other is from W_2. During the search process, each animal takes exploration walks respectively from two different starting locations, by Eq. (14) and Eq. (15). The locations from W_1 take exploration walks T_1 and the ones from W_2 take exploration walks T_2. In FSDP, the rule for updating R_j is shown in Eq. (19).

$$R = R_{\max} - g(R_{\max} - R_{\min}) / G \tag{19}$$

Where R_{min} and R_{max} denote the minimal and the maximal search radius respectively, and g denotes the current generation.

After exploration walks, each individual has two tracks. The locations in tracks are evaluated by given evaluation function. Then the best location and suboptimal location can be obtained. The best location is marked. In addition, the suboptimal one replaces the corresponding one in W_2 for next generation. The pheromone in FSDP is calculated by Eq. (20). After that, the sensibility for each individual can be obtained.

$$P_j = F_j / \max(F), \quad j = 1 \cdots popSize \tag{20}$$

where *max(F)* denotes the optimal objective value found so far by the swarm.

As we can observe from the algorithm, there are three major parts like that in FS to be implemented in FSDP algorithm, that is, initialization, exploration and termination. The time complexity of FSDP can be obtained by analyzing the three major parts. we can easily obtain the time complexity of FSDP algorithm which is O (*G.popSize.dim* (T_1+T_2)). Obviously, the performance of FSDP algorithm depends on the parameters of *G*, *dim*, *popSize*, T_1 and T_2. They are described as follows: *popSize* denotes the population size; *dim* denotes the dimensions of a solution; T_1 and T_2 denote an exploration walk of W_1 and W_2 respectively; *G* is the total number of generations.

4 FSDP Based Energy Consumption Optimization in WSN

In this section, the optimization problem based on the above-mentioned network model is proposed and details on FSDP-based optimization process are presented.

4.1 The Objective Function

According to the energy consumption model of nodes, it is obviously known that the total energy consumption for *Node k* consists of two parts which are energy consumption for sending packets and that for receiving. The total energy consumption for *Node k* can be described in Equ. (21).

$$E(k) = E_T(k) + E_R(k) \tag{21}$$

Then the total energy consumption of girdle band *i* can be obtained by Equ. (22).

$$E_i = \sum_{k=1}^{n} E(k), \qquad i = 1, \cdots M \tag{22}$$

where $n = \pi r^2 [i^2 - (i-1)^2]$.

Since the main goal is to minimize the total energy consumption of wireless sensor network and average energy consumption of each girdle band, the objective function for optimization, which is described in Equ. (23), is applied.

$$F(x) = Max(E_i), \quad i = 1,2 \cdots M \tag{23}$$

In Equ. (23), $Max(E_i)$ denotes the maximal energy consumption among each girdle band and M denotes the number of girdle bands which is equal to $\lfloor R / r \rfloor$. The

primary goal for the objective function $F(x)$ is to find out an optimal solution which makes $Max(E_i)$ minimal in the iteration process.

4.2 PSDP for Energy Consumption Optimization

The primarily goal for energy consumption optimization is to achieve the optimal routing path from each girdle band to the sink node through FSDP. The optimal routing path can cause results that energy consumption is much more distributed and lower while data packets are transmitted through the path. The optimization process based on FSDP for energy consumption in WSNs has the following important steps.

Step 1) To generate the initial solutions randomly by (11), and set the network scale which is referred to as the population size.

Step 2) According to the initial solutions, to calculate the energy consumption of each girdle band by Eqs. (7)-(10), then obtain the objective function value by Eq. (23).

Step 3) According to the objective value obtained in Step 2), to update the pheromone by Eq. (20) and the sensibility by Eq. (18).

Step 4) To repeat Step 2) and Step 3) until the expiration criterion is satisfied.

5 Simulation Tests

In this section, the proposed approach is applied to the energy consumption optimization problem. the comparative simulations in this section are based on such algorithms as Free Search (FS), Genetic Algorithm (GA) and Particle Swarm Optimization (PSO). In our simulation experiments, data transmission among nodes deplayed in each girdle band is based on multi-hop routing algorithm, and the experiments will be run 30 independent trials respectively. Further, since it is assumed that *unit* is the unit of data packets generated by nodes in Section. 2, it will also be adopted as the unit of the simulation results shown below.

For the parameter settings, the transmitting power Pt = [1, 4, 9, 16] and the receiving power Pr = 3 can be obtained from Section. 2. Further, Table 2 lists other common parameters related to the network model, and the number of girdle bands M, which is equal to $\lfloor R / r \rfloor$ = 15, can be easily obtained.

Table 2. Common parameter settings of the network model

Parameter	Value	Simple Description
δ	0.15	Energy consumption ratio
R	15	Radius of the circular model
r	1	Distance between each girdle band

For FSDP, the parameter settings are as follows: T_1 = 10; T_2 = 15; G = 50 and the population size of the swarm is 20. For the parameters of FS, it is almost the same as that of FSDP, that is, T = 15; G = 50 and the population size of the swarm is 20. Further, for PSO, the parameter settings are as follows: $c_1 = c_2 = 2.0$; w = 0.7; G = 50

and the population size of the swarm is 20. Lastly, the parameter settings for GA are as follows: $G = 50$; crossover probability $p_c = 0.4$; mutation probability $p_m = 0.05$ and the population size is 20. The simulation results are shown in Fig. 1.

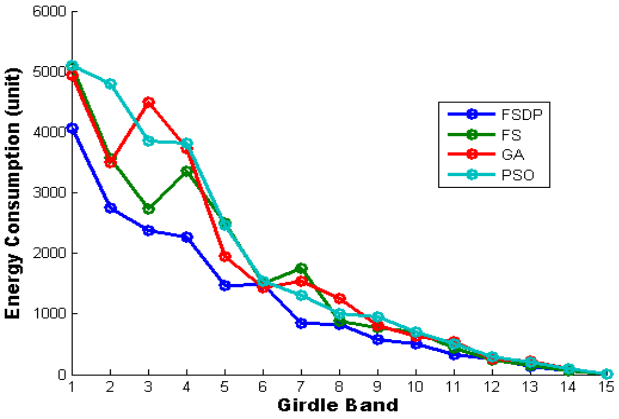

Fig. 1. Energy consumption of girdle bands by FSDP/FS/GA/PSO

Table 3. The total and maximal energy consumption for different approaches

Approach	Total Energy Consumption (*unit*)	Maximal Energy Consumption (*unit*)
FSDP	17967	4059.4
FS	23757	5083.4
GA	25421	4948.8
PSO	26692	5107.4

From Fig. 1, it can be seen that comparing FSDP with FS, PSO and GA, the energy consumption of each girdle band is much lower, and most importantly, the energy consumption among all girdle bands is more uniformly distributed, which is helpful in extending the network lifecycle. Further, as we can observe from Table 3, the maximal energy consumption among each girdle band is 4059.4 units when using the FSDP approach, which reduces by 25.23%, 21.91% and 25.82% respectively comparing with FS, GA and PSO. In addition to the maximal energy consumption, the total energy consumption, which is 17967 units for FSDP, is also smaller than that of all other three methods. The total energy consumptions based on FS, GA, and PSO approach are 23757 units, 25421 units and 26692 units respectively. Thus, FSDP can reduce both the maximal energy consumption of girdle bands and the total energy consumption, which can effectively prolong the lifetime of a wireless sensor network. In conclusion, the FSDP approach can obtain relatively better performance in energy consumption optimization problem of WSN comparing with FS, GA and PSO.

6 Conclusions

In this paper, a novel energy optimization approach (FSDP) is proposed. It is adopts two swarms and elitism strategy based upon FS. Simulations show that it is superior

to FS, GA and PSO in terms of reducing the maximal energy consumption of each girdle band and making a uniform energy distribution among each girdle band, which can effectively prong the lifetime of the WSN networks.

Acknowledgments. This work was supported in part by the National Natural Science Foundation of China (Nos. 61174094, 61273138), the Program for New Century Excellent Talents in University of China (No. NCET-10-0506), the Tianjin Nature Science Foundation under Grant 10JCZDJC15900.

References

1. Lewis, F.L.: Wireless Sensor Networks. Smart Environments: Technologies, Protocols, and Applications. John Wiley, New York (2004)
2. Arampatzis, T., Lygeros, J., Manesis, S.: A Survey of Wireless Sensors and Wireless Sensor Networks. In: Proceedings of IEEE International Symposium on Intelligent Control, pp. 719–724. IEEE Press, Limassol (2006)
3. Heinzelman, W.B., Chandrakasan, A.P., Balakrishnan, H.: An Application-Specific Protocol Architecture for Wireless Micro-sensor Networks. IEEE Trans. on Wireless Communications 1(4), 660–670 (2002)
4. Younis, O., Fahmy, S.: HEED: A Hybrid, Energy-Efficient, Distributed Clustering Approach for Ad-Hoc Sensor Networks. IEEE Trans. on Mobile Computing 3(4), 366–379 (2004)
5. Fariborzi, H., Moghavvemi, M.: EAMTR: Energy Aware Multi-Tree Routing for Wireless Sensor Networks. IET Communications on Wireless Ad-Hop Networks 3(5), 733–739 (2009)
6. Van Dam, T., Langendoen, K.: An Adaptive Energy Efficient MAC Protocol for Wireless Sensor Networks. In: Proceedings of 1st ACM Conference on Embedded Networked Sensor Systems, pp. 171–180. ACM Press, New York (2003)
7. Wang, X., Ma, J.J., Wang, S., Bi, D.W.: Distributed Particle Swarm Optimization And Simulated Annealing For Energy-Efficient Coverage In Wireless Sensor Networks. Sensors 7(5), 628–648 (2007)
8. Lin, C., Wu, G., Xia, F., Li, M., Yao, L., Pei, Z.: Energy Efficient Ant Colony Algorithms For Data Aggregation In Wireless Sensor Networks. Journal of Computer and System Sciences 78(6), 1686–1702 (2012)
9. Jin, S., Zhou, M., Wu, A.S.: Sensor Network Optimization Using A Genetic Algorithm. In: Proceedings of the 7th World Multi-Conference on Systemics, Cybernetics and Informatics, pp. 1–6. Int. Inst. Informatics & Systemics, Orlando (2003)
10. Kalin, P., Guy, L.: Free Search: A Novel Heuristic Method. In: Proceedings of the PREP 2003, pp. 133–134. PREP Press, Southampton (2003)
11. Kalin, P., Guy, L.: Free Search: A Comparative Analysis. Information Sciences 172(1-2), 173–193 (2005)
12. Zhou, Y., Medidi, M.: Sleep-based topology control for wakeup scheduling in wireless sensor networks. In: IEEE 4th Annual Communications Society Conference on Sensor, Mesh and Ad Hoc Communications and Networks, pp. 304–403. IEEE Press, San Diego (2007)
13. Hu, X.M., Zhang, J.: Ant Routing Optimization Algorithm For Extending The Lifetime Of Wireless Sensor Networks. In: IEEE International Conference on Systems, Man and Cybernetics, pp. 738–744. IEEE Press, Istanbul (2010)

How Do Emotional Cues Modulate Readers' Perception of Emotional Arousal during Text Comprehension: An ERP Study

Jinlu Zhang[1,2], Xiaohong Yang[1], and Yufang Yang[1,*]

[1] Key Laboratory of Behavioral Science, Institute of Psychology, Chinese Academy of Sciences, Beijing 100101, China
[2] University of Chinese Academy of Sciences, Beijing 100101, China
{zhangjl,yangxh,yangyf}@psych.ac.cn

Abstract. In an event-related potential experiment, we investigated how the amount and the location of emotional cues in the context influenced readers' perception of emotional arousal during reading comprehension. Participants read short narratives in which the amount of emotional cues and the location of emotional cues varied across conditions: a) the context contained two emotional cues, b) the context contained one emotional cue in the second sentence, c) the context contained one emotional cue in the first sentence, and d) the context contained no emotional cue. Our results showed that compared with contexts including one or no emotional cue, contexts including two emotional cues elicited a higher level of emotional arousal, as reflected by a larger anterior distributed LPP effect. However, the location of the emotional cue was found to have no effect on emotional arousal.

Keywords: emotional perception, emotional cues, emotional arousal, LPP.

1 Introduction

It is intuitively clear that readers can actively process emotional information of a story. There is a body of literature showing that readers can make inferences of the protagonist's emotions [1]–[4]. However, the factors that influence the readers' perception of emotional arousal and the neurocognitive mechanism of the emotional processing during reading comprehension have less been explored. In the current study, we used event-related potentials (ERPs) to investigate whether and how the amount and the location of emotional cues can modulate readers' perception of emotional arousal during text comprehension.

Evidence from earlier behavioral studies of text comprehension has demonstrated that readers can accurately perceive the emotional tone of the events in a story and infer the protagonist's emotions [1]–[4]. In these studies, participants were presented with narratives which described some events that the protagonist encountered. After reading the narrative, participants were presented by a target sentence which was either emotionally consistent or inconsistent with the preceding context. Inconsistent

* Corresponding author.

D. Liu et al. (Eds.): BICS 2013, LNAI 7888, pp. 21–29, 2013.

emotions were found to induce longer reading times than consistent emotions, suggesting that readers can derive inferences about the protagonist's emotions in a story.

Recently, the question of how readers process emotional information in discourse has also been addressed by some ERP studies [5]–[6]. Similar to the earlier behavioral studies, they used short narratives that implicitly described the protagonist's emotions. The main results showed a consistency effect reflected by the ERP index of N400. Namely, a larger N400 was elicited by inconsistent emotions than consistent emotions [5]. In another study, investigators presented affectively positive, negative, or neutral words within non-constraining, neutral contexts. Under the passive reading task, results showed that relative to neutral words, a small, posterior N400 effect to negative and positive words was detected. Later, a widely distributed late positivity was found to be larger to negative than to positive words. This suggested that brain networks of emotional processing appear to exert a continuous influence at several stages on the construction of the emotional meaning of language [6].

The above studies have consistently shown that readers actively keep track of the emotional information during text comprehension. However, little is known about how this process is influenced by other factors. The exception is de Vega et al.'s (1996) study [2], which examined how the amount of emotional cues affected emotional perception during text comprehension. In the cumulative context, they first presented a paragraph which described the protagonist's emotion (for example, positive emotion), then a second paragraph was presented which described the same emotion to the first paragraph. The target sentence described either positive emotion or negative emotion. Results showed that when the target sentence was presented after the first paragraph, reading times of the positive emotional sentences (consistent with the preceding context) were faster than the negative ones. And when the target sentence was presented after the second paragraph, this consistency effect was even more significant, that is, reading times of the positive emotional sentences were even faster than the negative ones. This was interpreted as a strong effect of the amount of emotional cues on the processing of emotional information. However, in this study, the effect of the amount of emotional cues was confounded by the amount of semantic information. Specifically, the addition of the second paragraph not only adds to the amount of emotional cues, but also brought additional semantic information to the text. Thus, in the current study, we aimed to investigate how the amount of emotional cues affects emotion perception during text comprehension while the amount of semantic information was held constant across conditions. We constructed short narratives consisting of three sentences. The first two sentences described events that the protagonist encountered which provided a context of emotion, and the last sentence described the protagonist's emotion with an explicit emotional word (for example, happy) which was emotionally inconsistent with the preceding context . The number of emotional cues varied across conditions: two (both of the first two contextual sentences carried emotional information), one (only one sentence in the context carried emotional information, while another was emotionally neutral), or zero (both of the first two contextual sentences were emotionally neutral).

Furthermore, we were also interested in the location of the emotional cues. Previous studies have shown that the introduction of new information into a text renders old information less available [7]–[8]. The question is whether the introduction of

emotional information in the first or in the second sentence would bring any difference on the perception of emotional arousal. Thus, for the condition which includes one emotional cue, we manipulated the location of the emotional information: the emotional cue was located either in the first sentence or in the second sentence. Thus, all together four conditions were constructed (see Table 1 for an example).

Table 1. Design and sentence examples for the four critical conditions

Condition	Example
(a) Two emotional cues context	(a) 王欣一直都没走出失恋的阴影。她的工作压得她透不过气来。王欣心里真是*欢快*极了。 Wang Xin hasn't come out from the lovelorn shadow. Her work is putting a great strain on her. Wang Xin feels really *happy* in heart.
(b) One emotional cue located in the second sentence	(b) 王欣有一个交往了两年的男朋友。她的工作压得她透不过气来。王欣心里真是*欢快*极了。 Wang Xin has had a boyfriend for two years. Her work is putting a great strain on her. Wang Xin feels really *happy* in heart.
(c) One emotional cue located in the first sentence	(c) 王欣一直都没走出失恋的阴影。她在单位做经理助理的工作。王欣心里真是*欢快*极了。 Wang Xin hasn't come out from the lovelorn shadow. She works as the manager's assistant in the enterprise. Wang Xin feels really *happy* in heart.
(d) Neural context	(d) 王欣有一个交往了两年的男朋友。她在单位做经理助理的工作。王欣心里真是*欢快*极了。 Wang Xin has a boyfriend for two years. She works as the manager's assistant in the enterprise. Wang Xin feels really *happy* in heart.

To address the above two questions, we used event-related potentials (ERP). The ERP components that are of particular relevant are the N400 and the LPP. Usually, N400 effects were found in semantic anomalous conditions or expectation violations (for a review, see [9]). And in the two ERP studies [7]–[8], they also found N400 effect when emotional consistency was manipulated. LPP (late positive potentials) is most related to the emotional arousal [10]–[16], which is just the core question that we were interested in. In the current study, we expected that 1) compared to condition b, c and d, condition a which included more emotional cues would elicit a larger N400 or LPP, meanwhile, condition b and c would elicit a larger N400 or LPP than condition d for the same reason; 2) compared to condition c, condition b in which the emotional cue was located near the target word would elicit a larger N400 or LPP.

2 Methods

2.1 Participants

Twenty healthy university students (mean age 23 years, range 19-26; 10 females) gave informed consent to participate in the experiment. All participants were native speakers

of Mandarin Chinese, right-handed and had normal or corrected-to-normal vision. They were paid a nominal sum for their participation. The data of four participants (2 males and 2 females) were excluded because of poor signal-to-noise ratio or poor performances (two of them fell into sleep when some trials were presenting). Therefore, the final set of participants consisted of sixteen participants (mean age 23 years, range 19-26; 8 females). The experiment was approved by the Academic Committee of the Institute of Psychology, Chinese Academy of Sciences.

2.2 Materials

The critical materials consisted of 160 quadruplets of short texts in Chinese (see Table 1 for examples). Each text consisted of two contextual sentences which respectively described either emotional or neutral events in an implicit way that the protagonist encountered, followed by a final sentence which contained an explicit emotional word (emotionally violated to the preceding context) served as the critical word in the ERP experiment. For the two contextual sentences, we manipulated the number of emotional cues (two in condition a, one in condition b and condition c, zero in condition d) and the location that the emotional cue located when there was only one emotional cue in the context (located in the first sentence in condition b, located in the second sentence in condition c), while the final sentences were the same between the four conditions in one set. To counterbalance the number of positive emotions and negative emotions, we made half of the 160 quadruplets of contexts related to positive emotions while another half related to negative emotions.

These short narratives were assigned to four experimental lists using a Latin square procedure. In each list, 120 filler texts were added. These 120 fillers were all neutral in emotion, and 100 of them were semantically correct while the other 20 ones were semantically anomalous in the final sentences.

In order to ensure that the two emotional events in the materials were in the same level of emotional arousal and the two emotionally neutral events were reliable, we asked another 24 participants (who did not participate in the EEG experiment) to judge the emotional valence and arousal on a 7-point two-direction rating scale (“1”, “2”, “3” indicated positive emotion, with “3” indicating the highest level of positive arousal; “-1”, “-2”, “-3” indicated negative emotion, with “-3” indicating the highest level of negative arousal; “0” indicated neutral). The ANOVA performed on the mean emotional arousal showed that the scores of the positive emotional events were significant higher than the neutral events ($ps < .001$), while the negative emotional events were significant lower than the neutral events ($ps < .001$), but no differences were found between the two emotional events in the contexts for both positive emotional contexts and negative emotional contexts ($ps > .1$), suggesting that the materials fitted well with our design.

2.3 Procedure

Participants were seated in a comfortable chair approximately 80cm from the computer screen in a sound-attenuated room. The stimuli were presented in white color on a black background, with a font size of 18 for all the materials. Each trial started with a central fixation cross presented for 1000 ms. Then the first sentence appeared as a whole

sentence in the center of the screen. Participants were asked to press the space bar when they finished reading the sentence. Then the second sentence appeared and the participants did the same as above. After the two contextual sentences, the final sentence was presented to the participants word by word in the center of the screen. Each word (or sometimes short phrase) was presented for 400 ms, with an additional 100-ms inter-stimulus interval. To ensure that the participants read the materials attentively, there was a comprehension task after about 1/4 trials. Participants were asked to press "F" (false) or "J" (true) button to give a judgment on the questions. Prior to the experimental blocks, participants received a practice block of 14 trials. The experimental session lasted about 1 h.

2.4 Electroencephalogram (EEG) Recording

The EEG was recorded using AC amplifiers. An elastic cap, equipped with 64 Ag/AgCl electrodes according to the International 10-20 system was used. The right mastoid electrode served as the online reference. An electrode placed between Fz and Cz served as the ground. The vertical eye movements and blinks were monitored via a supra- to suborbital bipolar montage. A right to left canthal bipolar montage was used to 13 monitor the horizontal eye movements. All electrode impedances were kept below 5 KΩ during the experiment. EEG data were digitized at a rate of 500Hz, with a band pass filter of 0.05 Hz–100 Hz.

2.5 ERP Data Analysis

ERPs time-locked to the critical words (the emotional words in the last sentences of each texts) were computed for each participant, condition, and electrode site. NeuroScan software 4.3 was used to preprocess the raw EEG data. Ocular artifacts were corrected by NeuroScan software [17]. Data were filtered off-line with a 30 Hz low-pass filter. The data were segmented from 200ms before to 1000ms after the onset of the critical words. A baseline correction was applied from 200 to 0 ms preceding word onset. The artifact rejection criterion was ±70μV. On average, 7.5% of all trials were rejected, with rejections being equally distributed across the four conditions. Then, the EEG data were re-referenced off-line to the average of both mastoids. Finally, trials were averaged in each condition for each participant.

Time window was chosen on the basis of visual inspection and earlier studies: 350–850 ms for LPP effects. All statistical analyses were performed on the mean amplitudes in the selected time window. ERPs were analyzed separately for midline and lateral electrodes. From the 64 electrodes, we first selected six midline electrodes FZ, FCZ, CZ, CPZ, PZ, and POZ. Omnibus ANOVAs for midline electrodes included two within-subject factors: Region (Anterior: FZ and FCZ ; Central: CZ and CPZ; Posterior: PZ and POZ) and Condition (Two emotional cues, one emotional cue in the second sentence, one emotional cue in the first sentence, no emotional cues). In order to cover distributional differences in both the left–right and anterior-to-posterior dimensions, we selected 30 lateral electrodes and formed six lateral regions of interest, with five electrodes each, by crossing Hemisphere (Left/Right) and Region (Anterior/Central/Posterior): left anterior (F1, F3, F5, FC1, and FC5); left central

(C1, C3, C5, CP1, and CP5); left posterior (P1, P3, P5, PO3, and PO5); right anterior (F2, F4, F6, FC2, and FC6); right central (C2, C4, C6, CP2, and CP6); and right posterior (P2, P4, P6, PO4, and PO6). Omnibus ANOVAs for lateral electrodes included three within-subject factors: Hemisphere, Region, and Condition.

Pair-wise comparisons were performed only when the ANOVA revealed a significant effect of Condition. All pair-wise comparisons were adjusted by Bonferroni correction. In addition, the Greenhouse–Geisser correction was applied when evaluating effects with more than one degree of freedom in the numerator. In these cases, the original degrees of freedom and the probability levels were reported.

3 Results

3.1 Behavioral Data

Comprehension rates were high: the accuracy of each participant was over 91%, suggesting that the participants read the texts attentively.

3.2 ERP Data

Fig. 1 shows grand average ERPs elicited by the emotional words for all four critical conditions at nine representative electrodes.

As shown in Fig. 1, compared with the one-emotional-cue context conditions and the neutral context conditions, the two-emotional-cue context conditions elicited a larger positivity with an anterior distribution in the 350–850 ms time window, with no difference among the other three conditions. These observations were statistically verified by ANOVAs performed on the mean amplitudes in the 350–850 ms. The results of the global ANOVAs are shown in Table 2.

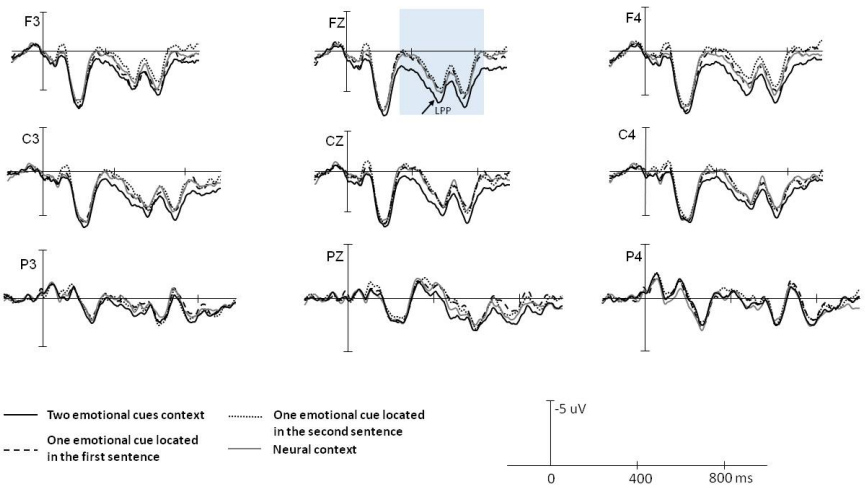

Fig. 1. Grand average ERPs time locked to the emotional words in the target sentences for all four critical conditions at nine representative electrodes

Table 2. Overall analyses of variance in the time window of 350-850 (in milliseconds) over midline and lateral electrodes, for amplitude data from 16 participants

Source	*dfs*	*F*	*p*
Midline electrodes			
Condition	3, 45	2.88	.061
Region	2, 30	32.35	< .001
Condition×Region	6, 90	3.34	.031
Lateral electrodes			
Condition	3, 45	2.07	> .1
Region	2, 30	27.99	< .001
Condition×Region	6, 90	2.98	.04
Condition×Hemisphere	3, 45	1.59	> .1
Condition×Region×Hemisphere	6, 90	1.47	> .1

Midline. The global ANOVA revealed a significant main effect of Region [$F(2, 30) = 32.35$, $p < .001$], a marginally significant main effect of Condition [$F(3, 45) = 2.875$, $p = .061$], and a significant interaction of region×condition [$F(6, 90) = 3.339$, $p = .031$]. Separate analyses for each region revealed a significant effect of condition in the anterior region [$F(3, 45) = 4.70$, $p = .01$], but no reliable effect in the central [$F(3, 45) = 2.75$, $p = .071$] or the posterior region [$F(3, 45) = .855$, $p > .1$]. Further pair-wise comparisons for the anterior region revealed that the two-emotional-cue context conditions elicited larger LPPs than the conditions that the emotional cue located in the second sentence ($p = .001$), the conditions that the emotional cue located in the first sentence ($p = .057$), and the neutral context conditions ($p = .065$). There were no significant differences among the other three conditions ($ps > .1$).

Laterals. The global ANOVA revealed a significant main effect of Region [$F(2, 30) = 27.991$, $p < .001$], but no significant effect of hemisphere [$F(1, 15) = 1.302$, $p > .1$] or condition [$F(3, 45) = 2.072$, $p > .1$]. The results also revealed a significant interaction of region×condition [$F(6, 90) = 2.977$, $p = .04$]. Separate analyses for each region revealed a significant effect of condition in the anterior region [$F(3, 45) = 4.087$, $p = .015$], but no reliable effect in the central [$F(3, 45) = 1.902$, $p > .1$] or the posterior region [$F(3, 45) = .446$, $p > .1$]. Further pair-wise comparisons for the anterior region revealed that the two-emotional-cue context conditions elicited a larger LPP than the conditions that the emotional cue located in the second sentence ($p = .004$), with no significant differences among the other conditions ($ps > .1$).

4 Discussion

Using the event-related potentials (ERPs), the present study investigated how the amount and the location of emotional cues in narratives modulated the perception of emotional arousal during text comprehension. The ERP results showed that the two-emotional-cue conditions elicited larger anterior distributed LPPs than the other three conditions, suggesting that the amount of emotional cues had influence on the emotional arousal. However, the location of the emotional cue did not reveal any effect.

Our results showed that emotional violation in the two-emotional-cue conditions elicited larger LPPs than the two conditions which contained only one emotional cue, suggesting that the more emotional cues in the narratives, the higher level of emotional arousal was elicited. This result coincides with the findings of de Vega et al.'s (1996), which showed shorter reading times for the consistent emotions in the emotional cumulative contexts [2].

Surprisingly, we found that the location of emotional cue had no influence on the perception of emotional arousal such that no significant differences on LPP amplitude of condition b (one emotional cue located in the second sentence) and condition c (one emotional cue located in the first sentence). It appeared that when there was only one emotional cue in the narrative, the emotional arousal of the whole text was the same such that the location of the emotional cue did not affect the perceived emotional arousal. However, in the current study, there were only two sentences in the preceding context. Further study is needed to investigate whether the location of the emotional cue affects emotion perception in narratives where the preceding context contains more sentences.

Interestingly, the emotional sentence following the neutral context showed no difference from the two one-emotional-cue conditions on LPP amplitude. This is quite out of our expectation because in the neutral condition, there was no emotional cue in the preceding sentence so we expected that the emotional word following the neutral context should result the smallest LPP of all conditions. However, comparing the amplitudes of LPP among the conditions, we found that the violation of the emotional word following a neutral context was similar in violation degree to the one-emotional-cue conditions, albeit smaller than the two-emotional-cue condition. As LPP has been consistently found to be sensitive to expectation violation [18]–[20], it is reasonable to infer that emotional words following neutral context also brings expectation violation on the reader.

In addition, different from the studies which found the N400 effects of emotional processing in text comprehension [5]–[6], we found LPP effects. Some investigators suggested that both N400 and LPP reflected expectation violation, the difference was that the increased N400 might reflect difficulties in understanding unanticipated stimuli, while the LPP effect might reflect evaluative incongruence [21]. Our results provided further evidence that LPP is a reliable index of the perception of emotional arousal and the evaluation of emotional incongruence.

Acknowledgments. This research was supported by the National Natural Science Foundation of China (31070989). We thank all the participants for their cooperation.

References

1. Gernsbacher, M.A., Goldsmith, H.H., Robertson, R.R.W.: Do Readers Mentally Represent Characters' Emotional States? Cognition and Emotion 6, 89–111 (1992)
2. de Vega, M., León, I., Díaz, J.M.: The Representation of Changing Emotions in Reading Comprehension. Cognition and Emotion 10, 303–321 (1996)
3. de Vega, M., Díaz, J.M., León, I.: To Know or Not to Know: Belief-Based Emotional Inferences in Comprehension. Discourse Processes 23, 169–192 (1997)

4. Gygax, P., Garnham, A., Oakhill, J.: Inferring Characters' Emotional States: Can Readers Infer Specific Emotions? Language and Cognitive Processes 19, 613–639 (2004)
5. León, I., Díaz, J.M., de Vega, M., Hernández, J.A.: Discourse-Based Emotional Consistency Modulates Early and Middle Components of Event-Related Potentials. Emotion 10(6), 863–873 (2010)
6. Holt, D.J., Lynn, S.K., Kuperberg, G.R.: Neurophysiological Correlates of Comprehending Emotional Meaning in Context. Journal of Cognitive Neuroscience 21(11), 2245–2262 (2008)
7. Binder, K.S., Morris, R.K.: Eye Movements and Lexical Ambiguity Resolution: Effects of Prior Encounter and Discourse Topic. Journal of Experimental Psychology: Learning, Memory, and Cognition 21(5), 1186–1196 (1995)
8. O'Brien, E.J., Duffy, S.A., Myers, J.L.: Anaphoric Inference during Reading. Journal of Experimental Psychology: Learning, Memory, and Cognition 12(3), 346–352 (1986)
9. Kuperberg, G.R.: Neural Mechanisms of Language Comprehension: Challenges to Syntax. Brain Research 1146, 23–49 (2007)
10. Herbert, C., Junghofer, M., Kissler, J.: Event Related Potentials to Emotional Adjectives during Reading. Psychophysiology 45(3), 487–498 (2008)
11. Kissler, J., Herbert, C., Winkler, I., Junghofer, M.: Emotion and Attention in Visual Word Processing—An ERP Study. Biological Psychology 80, 75–83 (2009)
12. Cuthbert, B.N., Schupp, H.T., Bradley, M.M., Birbaumer, N., Lang, P.J.: Brain Potentials in Affective Picture Processing: Covariation with Autonomic Arousal and Affective Report. Biological Psychology 52(2), 95–111 (2000)
13. Schupp, H.T., Cuthbert, B.N., Bradley, M.M., Cacioppo, J.T., Ito, T., Lang, P.J.: Affective Picture Processing: the Late Positive Potential Is Modulated by Motivational Relevance. Psychophysiology 37(2), 257–261 (2000)
14. Schupp, H.T., Cuthbert, B.N., Bradley, M.M., Hillman, C.H., Hamm, A.O., Lang, P.J.: Brain Processes in Emotional Perception: Motivated Attention. Cognition and Emotion 18(5), 593–611 (2004)
15. Schupp, H.T., Junghofer, M., Weike, A.I., Hamm, A.O.: Emotional Facilitation of Sensory Processing in the Visual Cortex. Psychological Science 14(1), 7–13 (2003)
16. Schupp, H.T., Ohman, A., Junghofer, M., Weike, A.I., Stockburger, J., Hamm, A.O.: The Facilitated Processing of Threatening Faces: An ERP Analysis. Emotion 4(2), 189–200 (2004)
17. Semlitsch, H.V., Anderer, P., Schuster, P., Presslich, O.: A Solution for Reliable and Valid Reduction of Ocular Rrtifacts, Applied to the P300 ERP. Psychophysiology 23(6), 695–703 (1986)
18. Cacioppo, J.T., Crites, S.L., Berntson, G.G., Coles, M.G.H.: If Attitudes Affect How Stimuli Are Processed, Should They Not Affect the Event-Related Brain Potential? Psychol. Sci. 4, 108–112 (1993)
19. Cacioppo, J.T., Crites, S.L., Gardner, W.L., Berntson, G.G.: Bioelectrical echoes from evaluative categorizations: I. A Late Positive Brain Potentials that Varies as A Function of Trait Negativity and Extremity. Journal of Personality and Social Psychology 67, 115–125 (1994)
20. De Pascalis, V., Strippoli, E., Riccardi, P.: Personality, Event–Related Potential (ERP) and Heart Rate (HR) in Emotional Word Processing. Pers. Individ. Diff. 36, 873–891 (2004)
21. Baetensa, K., Van der Cruyssena, L., Achtzigerb, A., Vandekerckhovea, M., Van Overwallea, F.: N400 and LPP in Spontaneous Trait Inferences. Brain Research 1418, 83–92 (2011)

The Global-Local Mental Rotation in Divided Attention Paradigm

Yong Niu[1] and Xiang Qiu[2,*]

[1] Students' Psychological Quality Education Center, Beijing Jiaotong University, Beijing, China
niuy2002@yahoo.com.cn
[2] School of Child Development and Education, China Women's University, Beijing, China
xiangqiu@126.com

Abstract. The present study addressed to explore whether precedence of the global rotation over the local rotation existed in a normal/mirror judgment task with divided-attention paradigm. Subjects had to decide whether or not a normal letter appeared at either level of a compound stimulus, Each level of compound stimulus could be rotated 0°, 60°, 120° or 180° separately. The results showed that : The RT and ACC were changed linearly with rotation angle, and the global rotation was faster and more accurately than local rotation. which provided convergent evidence for our previous finding using a focused-attention paradigm. Our findings were discussed in terms of the mechanism of global advantage on mental rotation.

Keywords: mental rotation, global advantage, divided-attention paradigm.

1 Introduction

The perceptual Global Precedence (short for GP) refers to the priority of global processing over local processing in visual perception. It is generally evidenced by using the focused-attention experimental paradigm designed by Navon in 1977. In this paradigm, compound stimuli (global uppercase letters are made up of local uppercase letters) are displayed at short exposure duration. In each trial, the relationship between the identity of the global and local aspects of the compound stimuli are either congruent or incongruent. Subject is required to identify the letter （H or S） at a given level (i.e., global or local) while ignoring the other level. The result showed that reaction times (RTs) to identify global letters are faster than those to identify local letters [1]. Navon proposed that "perceptual processes are temporally organized so that they proceed from global structuring towards more and more fine-grained analysis. In other words, a scene is decomposed rather than built up"[1,2]. From then on, Navon's paradigm was taken as the standard paradigm to examine the GP, and this original study gave rise to many publications[3,4,5]. The consistent

* These authors contributed equally to this work.

D. Liu et al. (Eds.): BICS 2013, LNAI 7888, pp. 30–37, 2013.

findings in the literature are as follows: a main advantage of the global over the local letters and, less often, a global-to-local interference.

Functional equivalence hypotheses, functional similarities between visual mental imagery and perception, had been tested and verified by many studies[6,7]. Mental rotation is one typical transformation of mental images, which had been extensively investigated in cognitive psychology. In the typical experimental design, two stimuli appear in different orientations, and are either identical or are left-right mirror images. The subject's task is to report whether the stimuli are identical or mirror images. With this normal/mirror judgment task, two impressive and consistent finding has been demonstrated in the literature on mental image. the time required to carry out an imaged rotation increases with greater angular disparity between the rotated image and upright [8,9]. Second, by measuring reaction times to variously oriented stimuli presented during the course of mental rotation, it has been established that intermediate states of the internal process have one-to-one correspondence to intermediate orientations of the external object [10-12].

Based on GP in perception and the Functional equivalence hypotheses, Qiu et al combined compound stimuli and rotation task in order to explore whether there was a GP on mental rotation. In their study, Compound stimuli combined with rotation task were used in two experiments. Participants were required to judge whether the large letter or small letter of the compound stimulus was in its regular format or left-right mirror. Experiment 1 was designed to eliminate perceptual global precedence through prolonging the duration of target stimuli. Experiment 2 investigated the global precedence on mental rotation. They found that global rotation was faster than local rotation even when perceptual global precedence was excluded in mental rotation task. This was the first study that differentiated the global advantage on mental rotation from that on perception [13].

A focused-attention experimental paradigm was used in both Navon's study of perception and Qiu's study of mental rotation, in which, subject only need to pay attention to one level of compound stimuli and ignore the other level of compound stimuli. However, Several experiments have shown that attentional manipulation can affect the speed of global and local information processing[2,14,15]. Comparison of dividing attention between the global and the local levels (i.e., conditions in which both levels were relevant) to focusing attention on a single level sometimes showed that when attention was divided between the two levels, global targets had no advantage[16]. Qiu et al(2009)fond the exposure time could mediate the GP in normal/mirror judgment task with divided attention paradigm[17]. In their experiment, stimuli were presented at two exposure durations (unlimited and 80 ms). Subjects had to decide whether or not a normal letter appeared at either level of a compound stimulus. They found when the exposure time was limited as 80 ms, the subjects responded faster to global level of compound stimulus than to local level; when the exposure time was unlimited, the subjects' responses to global level of compound stimulus and to local level were of no difference.

In this study, we investigated whether there was an effect of global advantage on mental rotation with a divided-attention Paradigm. In order to exclude the perceptual global advantage, the exposure time of stimuli was unlimited in our study , as Qiu et al did in her study[17].

2 Methods

2.1 Participants

Eighteen right-handed college students (7 men, mean age 20.0 years old, range 16-21 years old) participated in this study. All of them were right-handed and had normal or corrected-to-normal vision ability.

2.2 Stimuli and Experimental Design

As illustrated in Fig.1, Large letters (normal or mirror-reflected F or R) were composed of small letters (normal or mirror-reflected F or R), which subtended visual angles of 5.71°×3.81°and 0.48°×0.29°, separately. Stimuli were divided into three types: "global-only" when just the global letter was normal, "local-only" when just the local letter was normal and “neither” when neither letter was normal. Each level of compound stimuli could be rotated 0°, 60°, 120°or 180°separately.

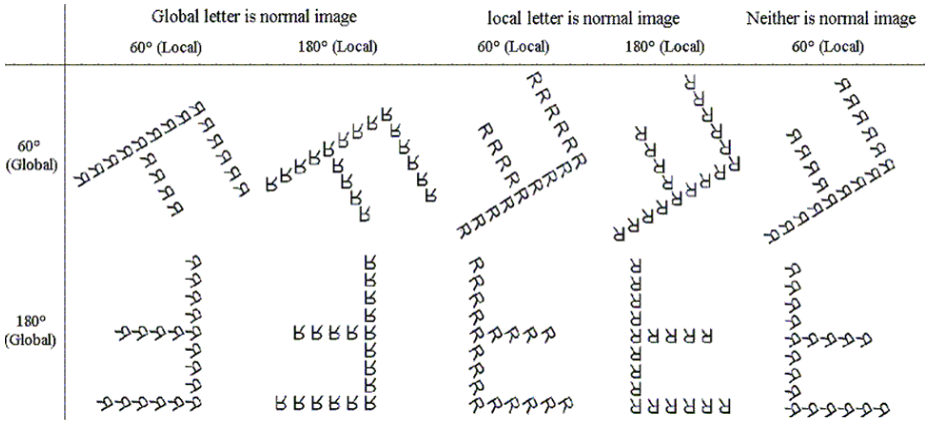

Fig. 1. Samples of stimuli used in present study

Subjects had to divide attention across levels of the compound stimuli and decide whether or not a normal letter appeared at either level of a compound stimulus. Global-only and local-only types of stimuli mapped into positive responses, and neither type of stimuli mapped to negative responses. Only the positive responses were included in analysis. Independent variables were rotation type[1] (global rotation vs local rotation) and orientation (0°, 60°, 120° and 180°). Totally 320 trials were constructed. The overall ratio of positive response to negative response was 1: 1. To

[1] In the present study, rotation type corresponded to the stimulus type. That was to say, when a global-only type of stimulus was displayed, subjects had to rotate the global aspect of the compound stimulus to some angle to determine whether a yes or no response should be made. In the same case, subjects had to rotate the local aspect of the local-only type of compound stimulus to some angle to make a response.

familiarize participants with the task, 12 unrecorded practice trials were added. The stimuli were displayed on a TCL17-in. monitor with a 70-Hz refresh rate at resolution of 1280 × 1024 pixels, connected to a Pentium IV computer. The experiment was programmed with E-Prime software (version 1.1).

2.3 Procedure

Subjects were arranged to sit in front of the computer with the middle and index fingers of her dominant hand placed on two keys of a computer keyboard. Viewing distance was about 60cm. Subjects had to decide whether or not a normal letter appeared at either level of a compound stimulus. Each trial began with the presentation of a fixation point in the center of the computer monitor, 300ms later, a compound stimulus was presented for a maximum of 5000ms or until the participants pressed any button, whichever was the sooner. the stimulus interval was pseudorandom between 1000ms and 1500ms. Participants were asked to make their response as quickly and accurately as possible.

3 Results

RTs that were more than three standard deviations from the mean were discarded from the analysis (approximately 2.26% of the trials). The correlation between RT and correct rate was -0.19, $p > 0.05$, which indicated that there was no speed-accuracy trade-off in our task. RT and accuracy (ACC) were separately subjected to a repeated measure ANOVAs, with rotation type and orientation as factors.

For the RT data, Orientation (4) × Rotation type (2) repeated-measures of analysis of variance (ANOVA) indicated that there were significant main effects of orientation($F(3, 51) = 76.13$, $P<0.001$), and rotation type($F(1, 17) = 4.89$, $P<0.05$), the orientation × rotation type interaction was not significant, $P>0.05$. Participants took longer to respond to global rotation task than to local rotation task, and reaction time was increased with the angular disparity. The post hoc analyses found that the four orientations were significantly different with each other (see Fig. 2).

For the correct rate, Repeated measures of analysis of variance (ANOVA) indicated that there were significant main effects of orientation, $F(3, 51) = 28.97$, $P<0.001$, rotation type($F(1, 17) = 5.30$, $P<0.05$.) and a significant Orientation × rotation type interaction, $F(3, 51) = 7.33$, $P<0.001$. Correct rate decreased with the greater angular disparity. Post hoc analyses found the ACC of 180° condition was significantly lower than those of other three orientation conditions, and the ACC of 0° condition was significantly lower than that of 120° condition, $Ps<0.05$. The accuracy of global rotation task was higher than that of local rotation task. The simple effect test of orientation × rotation type interaction indicated that there was a significant difference between the two rotation types at 120°($F(1, 17)=5.45$, $P<0.05$) and 180° condition, $F(1, 17)=8.41$, $P<0.01$(see Fig. 2).

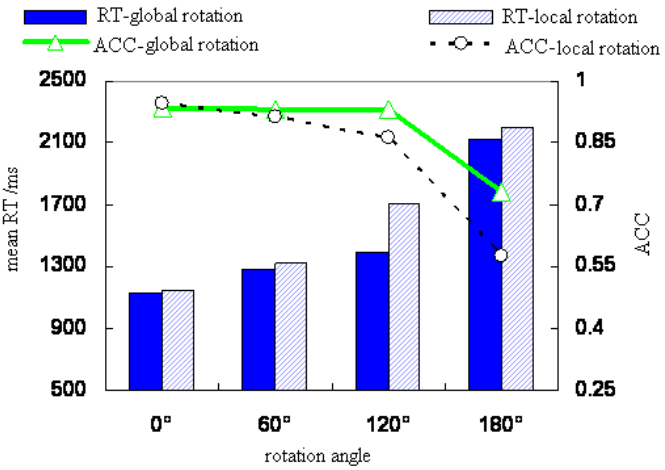

Fig. 2. Mean reaction times (RTs, in milliseconds) and accuracy across conditions

In addition, a further analysis was conducted on rotation rate, which was estimated from the corresponding slopes of the fitted linear functions between RT and orientation [12,13]. A paired-samples T test performed on the intercept of the RT vs. orientation of function revealed no difference between global rotation and local rotation, $t(17)=1.26$, $p>0.05$. A paired-samples T test performed on the slope of mental rotation revealed that the rotation rate of global level of compound stimuli (214.59 degree/sec) was faster than that of local level (162.07degree/sec), $t(17)=2.63$, $p<0.05$.

4 Discussion

The RT and ACC were changed linearly with rotation angle in present study; these results indicated subjects had to take a mental rotation process to complete this normal/mirror judgment task. What's more, there was a global advantage on mental rotation with divieded attention paradigm. The global rotation was faster and more accurately than local rotation. These findings consistent with our another study, in which a global advantage effect on mental rotation was found with a focused-attention design.

According to traditional theories of mental rotation [9,12], functionally independent information processing stages can be differentiated in a mental rotation task. They are at least (1) perceptual encoding, (2) mental rotation itself, (3) judgment of the parity, (4) response selection, and (5) response execution. Empirical evidence suggested either that these processes were organized in a strictly sequential manner [18], or that consecutive processes do overlap but only to a very small extent [11]. It was clear that mental rotation process started after perceptual encoding. Consequently, it was difficult to determine whether the locus of GP locolised in perceptual process or in postperceptual processes. Kimchi thought a factor contribute

to this difficulty was that the manifestation of an effect in a postperceptual process such as mental rotation does not, by itself, rule out the possibility that the effect has its origin in earlier perceptual processing (see also [19]). In order to control the perceptual global advantage in our experiment. We prolong the exposure time of stimulus until to subjective's response. In most researches about global advantage, the exposure duration is less than 200 ms, ranging from 17 ms [4] to 200 ms [20]. Paquet and Merikle [21] found that the interference pattern between the global and the local letters is affected by exposure duration. They presented compound letters for 10, 40, or 100 ms and found unidirectional global-to-local interference only at the shortest exposure duration. At the longer exposure durations, mutual interference effects were observed even though the global aspect was identified faster than the local one. Qiux et al also found when the exposure time was limited as 80 ms, the subjects responded faster to global level of compound stimulus than to local level; when the exposure time was unlimited, the subjects' response to global level of compound stimulus and to local level was of no difference[17]. Just as the Kimchi[16] claimed, Navon's perceptual global-precedence hypothesis is a hypothesis about the development of the percept. It was claimed that global properties had temporal precedence during the microgenesis of the percept. It did not necessarily imply what was salient in the final percept. So, we hypothesized that if the participants had enough time to process both the global and local information, making the global and local information same salient and accessible at the point of final percept, the perceptual global advantage would disappear.

So in our experiment, after displaying stimuli until subjects' response, the perceptual global advantage disappeared, but the result still found a global advantage in this experiment, we interpreted it as the Gp on mental rotation process.

Why there was a precedence of the global rotation over the local rotation? According to our analyse of the intercept and slope of RT vs. orientation linear function, the intercept of global rotation was of no difference from that of local rotation, but the slope of global rotation was significantly larger than that of local rotation. According to the standard model[9,10], the slope of this line estimates rate of rotation, whereas the intercept estimates time for encoding, comparison, decision making and response. That was to say, in this experiment, the RT of global rotation task was faster than that of local rotation lied in that the rate of global rotation was larger than that of local rotation, while the encoding, comparison, decision making and response of the global rotation task were of no difference from that of local rotation task.

Finally, one point should be taken into consideration in the present results. Because of the divided-attention paradigm, the analysis of format congruency for the global rotation and local rotation was impossible.

5 Conclusions

In summary, the present results suggest three conclusions. First, there is a global advantage on mental rotation with a divided-attention paradigm; second, the global

advantage on mental rotation is similar to the perceptual global advantage, but they are not the same thing. Third, the global advantage on mental rotation lies in that the rate of global rotation was larger than that of local rotation, while the encoding, comparison, decision making and response of the global rotation task were of no difference from that of local rotation task.

Acknowledgments. This study was supported in part by Ministry of Education Social Science Fund for young scholars (10YJCXLX038) and General foundation of China women's university (KG1003004).

References

1. Navon, D.: Forest before Trees: the Precedence of Global Features in Visual Perception. Cognitive Psychology 9, 353–383 (1977)
2. Navon, D.: What does a Compound Letter Tell the Psychologist's Mind? Acta Psychologica 114(3), 273–309 (2003)
3. Jiang, Y., Han, S.H.: Neural Mechanisms of Global/local Processing of Bilateral Visual Inputs: an ERP Study. Clinical Neurophysiology 116(6), 1444–1454 (2005)
4. Andres, A.D., Fernandes, M.A.: Effect of Short and Long Exposure Duration and Dual-tasking on a Global-local Task. Acta Psychologica 122(3), 247–266 (2006)
5. Lucie, B., Stéphane, R., Sylviane, V., Sophie, D.: Global Precedence Effect in Audition and Vision: Evidence for Similar Cognitive Styles across Modalities. Acta Psychologica 138(2), 329–335 (2011)
6. Kosslyn, S.M.: Image and Mind. Harvard University Press, Cambridge (1980)
7. Kosslyn, S.M., Thompson, W.L.: When is Early Visual Cortex Activated during Visual Mental Imagery? Psychological Bulletin 129, 723–746 (2003)
8. Zacks, J.M.: Neuroimaging Studies of Mental Rotation: a Meta-analysis and Review. Journal of Cognitive Neuroscience 20, 1–19 (2008)
9. Shepard, R.N., Farrell, J.E.: Representation of the Orientations of Shapes. Acta Psychologica 59, 103–121 (1985)
10. Grégoire, B., Rogier, A.K., William, L.T., Kosslyn, S.M.: Mental Rotation is not easily Cognitively Penetrable. Journal of Cognitive Psychology 23(1), 60–75 (2011)
11. Heil, M.: The Functional Significance of ERP Effects during Mental Rotation. Psychophysiology 39, 535–545 (2002)
12. Cooper, L.A.: Varieties of Visual Representation: How are We to Analyze the Concept of Mental Image. Neuropsychologia 33, 1575–1582 (1995)
13. Qiu, X., Fu, X.L., Sui, D.N., Li, J., Tang, Y.Y.: The Effect of Global Precedence on Mental Rotation of Compound Stimuli. Acta Psychologica Sinica 41, 1–9 (2009)
14. Miller, J.: Global Precedence in Attention and Decision. Journal of Experimental Psychology: Human Perception and Performance 7, 1161–1174 (1981)
15. Blanca, M.J., Lopez-Montiel, D.: Global and Local Dominance with Concentric Hierarchical Stimuli and Orientation Classification Task. Psicothema 19(1), 7–13 (2007)
16. Kimchi, R.: Primacy of Wholistic Processing and Global/local Paradigm: A Critical Review. Psychological Bulletin 112(1), 24–38 (1992)
17. Qiu, X., Fu, X.L., Luo, C.M.: Exposure Time Mediates Perceptual Global Advantage with A Divided-attention Paradigm. In: Proceedings of the 5th International Conference on Natural Computation, vol. 5, pp. 192–194. IEEE Press, Tianjin (2009)

18. Stoffels, E.J.: Inhibition of Concurrent Processes in Letter and Orientation Discrimination. Acta Psychologica Sinica 91, 153–173 (1996)
19. Navon, D.: The Forest Revisited: More on Global Precedence. Psychological Research 43(1), 1–32 (1981)
20. Koivisto, M., Revonsuo, A.: Preconscious Analysis of Global Structure: Evidence from Masked Priming. Visual Cognition 11(1), 105–127 (2004)
21. Paquet, L., Merikle, P.M.: Global Precedence: The Effect of Exposure Duration. Canadian Journal of Psychology 38(1), 45–53 (1984)

An ERP Study of Semantic Anomalies in Second Language Processing

Jia Miao

Language School, Northeasten University At Qinhuangdao,
Qinhuangdao, China
miaojiamail@163.com

Abstract. This study conducts an event-related potential (ERP) study to investigate the temporal neural dynamics of semantic processing in bilinguals. The experiment was done with Korean speakers of English as an L2, divided into two groups depending on their L2 proficiency level. The typical semantic anomaly paradigm was adopted for the material; semantically anomalous sentences end with a word which is not congruent in the sentence context. It was investigated if semantically anomalous stimuli elicit N400. Overall, similar pattern of the N400 effect was observed in the high proficiency group, while no significant effect was found in the low proficiency group. Though the results do not show a complete match in every detail, the study suggests that the bilinguals' semantic processing resembles monolinguals' semantic processing to a significant extent. This study also suggests that proficiency has a close correlation with brain responses in semantic processing in L2.

Keywords: sentence processing, semantic anomaly, semantic congruency, N400, second language.

1 Introduction

How semantic information is retrieved during language comprehension and how the normal brain constructs meaning, especially in real-time, have been major concerns in the study of the sentence processing related to meaning. Event-related potentials (ERPs), an electrophysiological method, have been an alternative to overcome the limitations from behavioral methods and hemodynamic-based brain imaging methods. ERPs is also a high temporal resolution technique that is both a sensitive measure of real-time language processing and a direct manifestation of brain activity. ERPs have been adopted in the researches on processing of meaning since Kutas and Hillyard (1980) first observed a meaning-related ERP component, the N400. The amplitude of the N400 increases when a semantically anomalous word is presented in the sentence as compared with the case of semantically normal(congruent) word.The N400 component is not simply an index of anomaly though. Rather it can be said that it is a part of the brain's normal response to potentially meaningful events (Kutas & Federmeier 2000; Kutas et al. 2000). The amplitude of the N400 varies with semantic congruity, cloze probability of words in a context, word repetition, word frequency,

D. Liu et al. (Eds.): BICS 2013, LNAI 7888, pp. 38–45, 2013.

and semantic category, among others. Its distribution over the scalp has been found to vary depending on the type of eliciting stimulus.

The semantic anomaly sentence paradigm of L1 vs. L2 ERP studies which induces the N400 effect can be distinguished depending on the formation of experiment subject groups. One is between-groups design, which compares an L2 group with an L1 group. The other is within-group design, which focuses on how bilinguals process an L2 as compared to their L1.One of the observations from previous between-group design studies is that bilinguals are slower in their lexical decisions as compared to native speakers of L2 (e.g., Lehtonen & Laine 2003; Portin & Laine 2001). Hahne & Friederici (2001) examined native Japanese speakers who had learned German as an L2 and found with regard to the ERPs to semantic anomalies that the bilinguals showed an N400 effect similar to the one observed in native speakers of German.Proverbio et al. (2002) adopted a within-group design as well as a between-group design. For the processing of semantic errors, they report a reversed pattern of N400 lateralization on scalp distribution for the bilinguals compared with the monolinguals. Semantic incongruence resulted in greater response over the left hemisphere than over the right in bilinguals, while the pattern was reversed in the monolinguals. Moreover, the N400 effect was different in the bilinguals' L1 and L2. Moreno & Kutas (2005) examined the N400 effect using English-Spanish bilinguals and found that the effect varies depending on their proficiency level.

This study investigates the above issues in an experiment with Korean L2 speakers of English. Specifically we will adopt the typical semantic anomaly paradigm to find out their semantic processing pattern.

2 Experiment

2.1 Participants

Two groups of Korean-English bilinguals whose first language is Korean participated in the present experiment. They were all late-learners of English as an L2 and did not have any experience of living in an English native country. All participants were undergraduate college students, right-handed and had normal or corrected to normal vision. None of them had experienced a psychiatric or neurological disease. The group with high English proficiency consisted of 19 advanced L2 speakers of English (12 men; mean age 22.2) who had very high scores on the TOEIC Test (mean 900.5/990, range 855 – 970). The other group of participants consisted of 15 intermediate L2 learners of English (9 men; mean age 23.9) whose English proficiency was significantly lower than that of High group (mean TOEIC score 556/990, range 475–665). Participants gave consent for participation and were paid 20,000 Won for their participation.

2.2 Material

A total of 110 pairs of stimulus sentences consisting of basic English words were devised. Paired sentences shared the sentence frame and all the words except one word at the end.

With the semantic congruity condition, one sentence in each pair was semantically anomalous by virtue of one word and the other was semantically congruous. The critical words always appeared in a sentence-final position. The sentences were 7 to 12 words long with the mean length of 8.5 words. The sentences are illustrated in Table 1. Two lists of 110 sentences were created; each list contained one sentence from each of the 110 sentence pairs. One list was presented to a half of the participants and the other list to the other half. Thus, each subject read 110 sentences consisting of 55 congruous and 55 incongruous sentences. These sentences were presented in a random order.

2.3 Procedure

During the experiment, participants sat in a sound-attenuating, dimly-lit, lectrically shielded recording room. Stimuli were presented on a computer screen approximately 100 cm distant in front of the participants. Sentences were displayed in word by word manner in black Courier New font size 23 on white screen. An initial fixation (XXXX) was presented for 300ms and replaced by first word of the sentence. Each word was presented at the center of the screen for 300ms, followed by a blank screen for 300ms.3 In about one-third of the trials (42 trials) a comprehension question was presented two seconds after the last word of the sentence. The following sentence was initiated with pressing button either to answer the comprehension question or to terminate empty blank. A 10-trial practice session preceded the experimental run. The entire session, including electrode application and removal, lasted about 2 hours.

2.4 EEG Readings

Electroencephalograms (EEGs) were recorded from thirty-two electrodes mounted in an electrode cap (Neuroscan Quikcap). An additional electrode was placed below the right eye to monitor eye blinks. Each electrode was referred to linked mastoids. The EEG recordings were amplified by NeuroScan amplifiers, sampled at 250 Hz, and filtered with a band-pass of 0.1 - 30 Hz. Electrode impedances were kept below 10 kΩ.

2.5 Data Analysis

Three participants were excluded from analysis because of recording error, so a total of 31 participants (16 participants in High group and 15 participants in Low group) were included in the statistical analysis. ERPs were averaged for each individual participant over 1000 ms epoch for the critical words in all conditions, relative to a 200 ms pre-stimulus baseline. Trials with excessive eye-blinks or movements and ones with electrode drift were screened, and contaminated trials were not included in the statistical analysis. Epochs with an elector-oculogram (EOG) response exceeding 100 mv were discarded. Repeated measures analyses of variance (ANOVAs) were performed on the mean amplitude of the ERPs during the two ranges of 300 - 460 ms and 620-800ms, to capture the N400 and P600 component respectively. One ANOVA was conducted for midline sites Fz, Cz, Pz, and Oz only (midline analysis) and one was done comparing electrode sites over left and right hemispheres at different levels of anteriority (scalp topography analysis). The scalp topography analysis also

included the factors of hemisphere (left or right) and anteriority (three levels: anterior, central, and posterior, going from the front to the back of the head), which created six regions: left-frontal (F3, F7, FC3), right-frontal (F4, F8, FC4), left-central (C3, CP3, T7), right-central (C4, CP4, T8), left-posterior (P3, P7) and right-posterior (P4, P8). Three separate ANOVAs were executed to compare electrode sites over left and right hemisphere at each of frontal, cental, and posterior regions.

2.6 Results

The difference ERP waves over selected Fz, Cz, & Pz are shown in Fig 2 and 3. Results from ANOVAs that included factors of High group and Low group are presented in Table 1.

Table 1. Statistics for the N400 & P600 Time Window in High Group and Low Group

	df	High		df	Low	
		F	*P*		*F*	*P*
300-600ms						
Midline analysis						
Main effect	1,15	3.33	.08	1,14	.00	.95
X electrode	3,45	3.50	.02	3,42	1.04	.38
Scalp topography			.			
Main effect	1,15	5.31	.03	1,14	.01	.94
X hemisphere	2,30	4.06	.06	1,14	.13	.72
X Anteriority	2,30	2.12	.13	2,28	.68	.51
X Hemi X Ant		.70	.50	2,28	.36	.69
620-800ms						
Midline analysis						
Mainline effect	1,15	.99	.33	1,14	.31	.58
X electrode	3,45	.59	.62	3,42	1.41	.25
Scalp topography						
Main effect	1,15	.38	.54	1,14	1.06	.32
X Hemisphere	1,15	.52	.48	1,14	.17	.68
X Anteriority	2,30	.53	.59	2,28	.82	.45
X Hemi X Ant	2,30	1.49	.24	2,28	.30	.74

N400(300-460 ms)

High group. The overall effect of semantic congruency was significant in both the midline and topography analyses. At the midline sites, the condition main effects (congruous vs. anomalous) were marginally significant only in Fz [F(1,15)=3.56, p=.079] and Cz [F(1,15)=3.79, p=.071]] in High group. There were also significant interactions with electrode in the midline analysis and marginally significant interactions with hemisphere in the scalp topography analysis. More information on the N400 component in High group is shown in Table 2.

Low group. No significant effects were found in both the midline and scalp topography analysis in Low group.

Table 2. N400 component in High Group

		onset(ms)	amp(μV)	Peak(ms)	amp(μV)
CZ	anomalous	342	-1.26	404	-2.60
	congruent	360	0.46	412	-0.32
FZ	aomalous	360	-1.91	408	-2.9
	congruent	360	0.44	412	0.32
PZ	anomalous	348	0.82	408	-0.57
	congruent	352	1.55	424	0.35

P600 or LPC(620-800ms)

High group. The LPC time-window did not show an overall effect of semantic congruency in the midline and scalp topography analyses. Also, no interactions were found for the effects of semantic congruency in either the midline or scalp topography analyses. However, there was a significant effect in Pz ($F(1, 15)=4.45$, $p=.05$).

Low group. No significant effects were found in both the midline and scalp topography analyses including interaction effects.

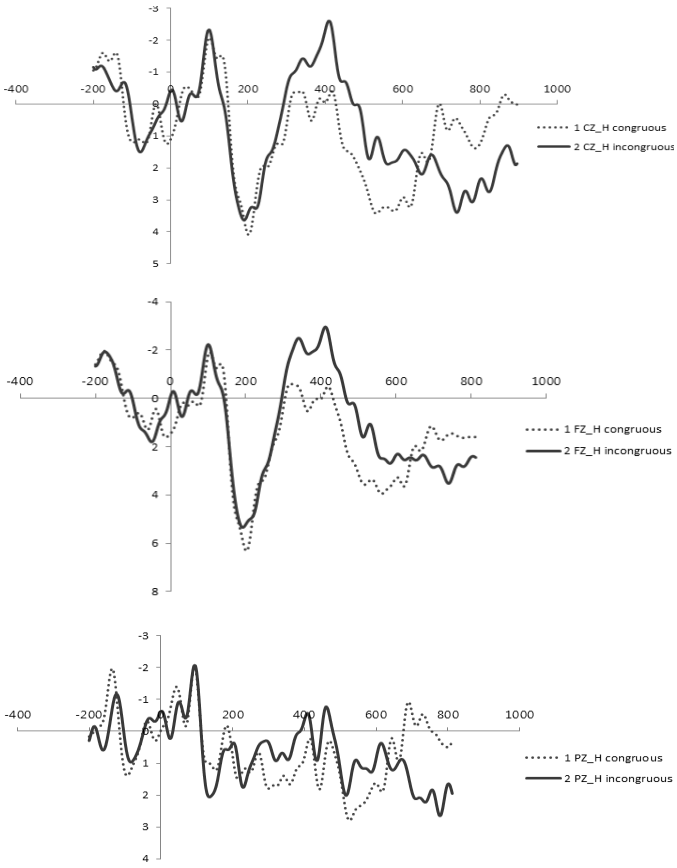

Fig. 1. Grant-average ERP Waveforms for Semantically Congruous and Incongruous Words at Cz. Fz and Pz in High Group

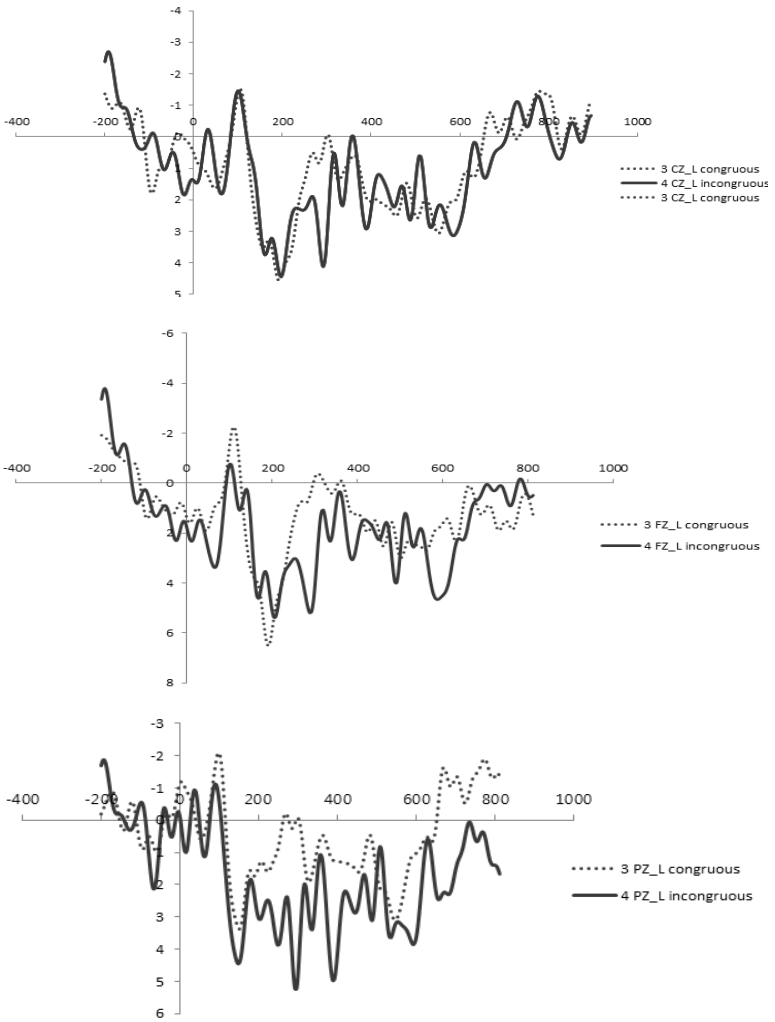

Fig. 2. Grant-average ERP Waveforms for Semantically Congruous and Incongruous Words at Fz and Cz in Low Group

3 Discussion

The results of the experiment show that the semantic congruency effect is found in Korean bilinguals' ERP responses. That is, the N400 effect was observed with ERPs having more negativity around 400 ms after semantically anomalous stimuli. This result, however, was limited to the high proficiency group and not observed in the low proficiency group.

As for the amplitude of the N400 component observed in High group, it was not significantly different from the numbers observed in other N400-related researches

(e.g., Moreno & Kutas 2005, Zhou et al. 2010). It was often found in L2 ERP researches, the peak latency of the N400 component shows a delay. But no significant delay in the peak latency was observed in the N400 of High group in this study.

The current study also suggests that proficiency plays an important role in L2 processing. The semantic congruency effect was found in the N400 component in high proficiency group only; the N400 effect was not found in low proficiency group. And the effect was consistently observed in all the participants in High group. Given this, bilinguals with high L2 proficiency seem to have the capacity to comprehend the words in the given sentence appropriately and notice the semantic anomaly involving excessive load of processing. On the other hand, the low proficiency group does not show any significant congruency effect and their ERP responses to semantic anomaly do not show the pattern observed in L1 English speakers. All the participants of the current experiment were late-learners of English as an L2 and have never been put in an emersion setting of English. However, the high proficiency group showed a pattern consistent with L1 speakers of English. This confirms that proficiency is a significant factor affecting semantic processing in L2.

4 Conclusion

In this paper, we presented an experimental study examining event-related potentials in bilinguals. The study suggests that the bilinguals' semantic processing resembles monolinguals' semantic processing to a significant extent. The study also strongly suggests that proficiency has a close correlation with brain responses in semantic processing. Although there still remain issues to be resolved further, especially what exactly prevents the elicitation of N400 in Low group, whether semantic aspects other than congruency can also elicit N400 in Korean bilinguals' L2 as in monolinguals' L1, and what exactly is involved in observed differences in distribution of the effect (e.g., no significant effect at Pz in High group), this study illuminates the neural dynamics of semantic processing in Korea-English bilinguals and shows how ERPs can be implemented to answer the theoretical questions brought up in the field of L2 research.

Acknowledgements. This research was supported by Qin Huang-dao City Soft-Science Research Plan Project grant (2012025A022).

References

1. Hahne, A., Friederici, A.D.: Processing a second language: Late learners' comprehension mechanisms as revealed by event-related brain potentials. Bilingualism: Language and Cognition 4(2), 123–141 (2001)
2. Kutas, M., Federmeier, K.D.: Electrophysiology reveals semantic memory use in language comprehension. Trends in Cognitive Sciences 4(12), 463–470 (2000)

3. Kutas, M., Federmeier, K.D., Coulson, S., King, J.W., Munte, T.F.: Language. In: Cacioppo, J.T., Tassinary, L.G., Berntson, G.G. (eds.) Handbook of Psychophysiology, 2nd edn., pp. 576–601. Cambridge University Press, Cambridge (2000)
4. Kutas, M., Hillyard, S.A.: Reading senseless sentences: brain potentials reflect semantic incongruity. Science 207, 203–205 (1984); Kutas, M., Hillyard, S.A.: Brain potentials during reading reflect word expectancy and semantic association. Nature 307, 161–163 (1980)
5. Lehtonen, M., Laine, M.: How word frequency affects morphological processing in mono- and bilinguals. Bilingualism: Language and Cognition 6, 213–225 (2003)
6. Moreno, E.M., Kutas, M.: Processing semantic anomalies in two languages: An electrophysiological exploration in both languages of Spanish–English bilinguals. Cognitive Brain Research 22(2), 205–220 (2005)
7. Portin, M., Laine, M.: Processing cost associated with inflectional morphology in bilingual speakers. Bilingualism: Language and Cognition 4, 55–62 (2001)
8. Proverbio, A.M., Cok, B., Zani, A.: Electrophysiological measures of language processing in bilinguals. Journal of Cognitive Neuroscience 14(7), 994–1017 (2006); Slabakova, R.: Is there a critical period for semantics? Second Language Research 22, 302–338 (2002)
9. Van Petten, C., Luka, B.J.: Neural bases of semantic context effects in electromagnetic and hemodynamic studies. Brain and Language 97, 279–293 (2006)
10. Zhou, X., Jiang, X., Ye, Z., Zhang, Y., Lou, K., Zhan, W.: Semantic integration processes at different levels of syntactic hierarchy during sentence comprehension: an ERP study. Neuropsychologia 48 (2010)

Hybrid Real-coded Genetic Algorithm and MIMO CMAC NN Classifier for Solving Medical Data Classification Problems

Jui-Yu Wu*

Department of Business Administration,
Lunghwa University of Science and Technology, Taiwan
jywu@mail.lhu.edu.tw

Abstract. Medical diagnosis is widely viewed as binary classification problems. To reduce classification error and parametrization of an efficient classifier, this work develops a hybrid real-coded genetic algorithm (RGA) and MIMO cerebellar model articulation controller neural network (CMAC NN) classifier. The parameter settings of the MIMO CMAC NN classifier are optimized using the RGA approach. Classification problems are then solved using the MIMO CMAC NN classifier. The performance of the proposed RGA-MIMO CMAC NN classifier is evaluated using two real-world datasets, i.e. diabetes and cancer datasets. The classification errors obtained using the RGA-MIMO CMAC NN classifier are compared with those obtained using individual MIMO CMAC NN classifier and published classifiers (e.g., genetic programming-based, NN-based and GA-based classifiers) for diabetes and cancer datasets. Experimental results indicate that the classification errors obtained using the proposed RGA-MIMO CMAC NN classifier are smaller than those of some individual and hybrid published classifiers. Moreover, the proposed approach can reduce parametrization of the MIMO CMAC NN classifier. Hence, the proposed RGA-MIMO CMAC NN classifier is highly promising for use as alternative classifier for solving medical data classification problems.

Keywords: classification, genetic algorithm, cerebellar model articulation controller, neural network classifier.

1 Introduction

Classification is a critical issue in many research domains, such as machine learning (ML) and data mining (DM)[1]. Medical diagnosis can be viewed as binary classification problems. In classification problems, an instance (patient's case) is assigned to a predefined class (disease or non-disease) based on various features (e.g., symptoms, signals and clinical history) [2]. Many ML and DM classifiers have been used to solve classification problems. For instance, Mazurowski et al. [3] presented neural network

* Corresponding author.

D. Liu et al. (Eds.): BICS 2013, LNAI 7888, pp. 46–56, 2013.

(NN) classifiers for computer-aided medical diagnosis problems. Gadaras and Mikhailov [4] developed a novel fuzzy classification framework for medical diagnosis problems. Barakat et al., [5] used a support vector machine (SVM) classifier for the diagnosis of diabetes. Quteishat et al., [6] developed a modified fuzzy min-max NN classifier and a genetic algorithm (GA)-based rule extractor for the medical diagnosis task. Wang et al. [7] analyzed and compared the performance of various SVM classifiers based on three various kernel functions for 20 real-world datasets. Wu [8] developed a MIMO cerebellar model articulation controller (CMAC) NN classifier to solve medical data classification problems and chemical analysis of glass splinters. The NN and SVM classifiers have the certain limitation that uses trial and error to find the optimal user-defined parameters. To overcome this limitation, many hybrid classifiers have been developed [9, 10]. Hybrid algorithms outperform individual algorithms in solving certain problems, and they can solve general problems more efficiently [11]. To develop an efficient classifier and reduce its parametrization, this work presents a hybrid classifier based on MIMO CMAC NN classifier [8] and real-coded GA (RGA) method. The proposed RGA-MIMO CMAC NN classifier consists of an external RGA approach and the internal MIMO CMAC NN classifier. The external RGA method is used to optimize the optimal parameter settings of the internal MIMO CMAC NN classifier, and the internal MIMO CMAC NN classifier is applied to solve benchmark medical classification problems. The performance of the RGA-MIMO CMAC NN classifier is compared with that of individual MIMO CMAC NN classifier and many published classifiers from the literature [12-15].

2 Related Works

2.1 Real-coded Genetic Algorithm

RGA methods have been successfully used to solve optimization problems [16]. RGA approaches use three genetic operations, i.e. selection, crossover and mutation, to explore and exploit the solution space. This work describes these operations [17, 18].

1. Selection Operation

A selection operation selects strong individuals from a current population based on their fitness function values and then reproduces these individuals into a crossover pool. The several selection operations developed include the roulette wheel, ranking and tournament methods. This work uses the normalized geometric ranking method, as follows:

$$p_j = q'(1-q)^{rank-1}, \quad j = 1, 2, \ldots, ps_{\text{RGA}} \tag{1}$$

where p_j = probability of selecting individual j; q = probability of choosing the best individual (here q = 0.35); $q' = \dfrac{q}{1-(1-q)^{ps_{\text{RGA}}}}$; $rank$ = individual ranking based on fitness value, where 1 represents the best ($rank = 1, 2, \ldots, ps_{\text{RGA}}$); ps_{RGA} = population size of the RGA method.

2. Crossover Operation

While exploring the solution space by creating new offspring, the crossover operation randomly selects two parents from the crossover pool, and then uses these two parents

to generate two new offspring. This operation is repeated until the $ps_{\mathrm{RGA}}/2$ is satisfied. The whole arithmetic crossover is easily implemented, as follows:

$$\mathbf{v}_1^{'} = \alpha \times \mathbf{v}_1 + (1-\alpha) \times \mathbf{v}_2 \tag{2}$$

$$\mathbf{v}_2^{'} = (1-\alpha)\mathbf{v}_1 + \alpha \times \mathbf{v}_2 \tag{3}$$

where $\mathbf{v}_1$ and $\mathbf{v}_2$ = parents; $\mathbf{v}_1^{'}$ and $\mathbf{v}_2^{'}$ = offspring; α = uniform random number in the interval [0, 1.5].

3. Mutation Operation

Mutation operation can increase the diversity of individuals (candidate solutions). Multi-non-uniform mutation is described as follows:

$$x_{\mathrm{trial},n} = \begin{cases} x_{\mathrm{current},n} + (x_n^u - x_{\mathrm{current},n})\, pert(g_{\mathrm{RGA}}) & \text{if } U_1(0,1) < 0.5 \\ x_{\mathrm{current},n} - (x_{\mathrm{current},n} - x_n^l)\, pert(g_{\mathrm{RGA}}) & \text{if } U_1(0,1) \geq 0.5 \end{cases} \tag{4}$$

where $pert(g_{\mathrm{RGA}}) = \left[U_2(0,1)\left(1 - \frac{g_{\mathrm{RGA}}}{g_{\max,\mathrm{RGA}}}\right)\right]^2$, perturbed factor; $U_1(0,1)$ and $U_2(0,1)$ = uniform random variable in the interval [0, 1]; $g_{\max,\mathrm{RGA}}$ = maximum generation of the RGA method; g_{RGA} = current generation of the RGA approach; $x_{\mathrm{current},n}$ = current decision variable x_n; $x_{\mathrm{trial},n}$ = trial candidate solution x_n.

2.2 MIMO CMAC NN Classifier

The network topology of the MIMO CMAC NN classifier comprises five cells, which are an input space ($\mathbf{X}_{\mathrm{in}}$), a sensory cell ($\mathbf{S}$), an association cell ($\mathbf{A}$), a physical memory cell ($\mathbf{P}$) and an output cell ($\mathbf{Y}$). The MIMO CMAC NN classifier transforms input values into output values using a series of mapping operations and then updates the weights using a least mean squared (LMS) algorithm. The implementation of the MIMO CMAC NN classifier is described as follows [8].

Step 0: Initialize paremeter settings

Many parameters must be set, such as size of weight table (k), learning rate (β), quantization size (Q_i) and generalization size (g).

Step 1: Quantize the input vector

Each input pattern undergoes a quantization operation to transform continuous or label (such as 1, 2, 3) attributes into discrete indexes, as follows.

$$s_{ij} = \left\lfloor \left(\frac{Q_i}{x_{\mathrm{in},i}^{\max} - x_{\mathrm{in},i}^{\min}} \right) \times \left(x_{ij} - x_{\mathrm{in},i}^{\min} \right) \right\rfloor - 1, \tag{5}$$

$$i = 1, 2, \ldots, i_{\max} \quad j = 1, 2, \ldots, n_{\mathrm{total}}$$

$$s_{ij} = 0, \text{ if } s_{ij} < 0 \tag{6}$$

where s_{ij} = quantization index of component $x_{\text{in},i}$ of input pattern j; $x_{\text{in},ij}$ = component $x_{\text{in},i}$ of input pattern j; $x_{\text{in},i}^{\min}$ = minimum value of input vector $\mathbf{x}_{\text{in},i}$; $x_{\text{in},i}^{\max}$ = maximum value of input vector $\mathbf{x}_{\text{in},i}$; $i_{\max}$ = dimension of input space; n_{total} = total number of input patterns; $\lceil \cdot \rceil$ = rounded number.

Step 2: Create random tables and weight tables

A sensory cell comprises random tables. The size of each random table can be computed using

$$C_i = Q_i + g - 1, \quad i = 1, 2, \ldots, i_{\max} \tag{7}$$

where C_i = size of the random table of input vector $\mathbf{x}_{\text{in},i}$.

Each random table i consists of uniform random numbers generated from the interval [0, k/2].

Step 3: Generate an address table

Many-into-few mapping operations are performed using a bitwise XOR operator-based hash coding. An address table is then created.

Step 4: Calculate the actual output

The actual output values can be calculated using Eq. (8), as follows.

$$y_{o,pj} = \mathbf{a}^T \mathbf{w}_p, \; p = 1, 2 \quad j = 1, 2, \ldots, n_{\text{train}} \tag{8}$$

where $y_{o,pj}$ = actual output from neuron p of input pattern j; n_{train} = number of input patterns for training;

$\mathbf{a} = \begin{bmatrix} a_1 \\ a_2 \\ \vdots \\ a_k \end{bmatrix}$, association vector in cell $\mathbf{A}$; $\mathbf{w}_p = \begin{bmatrix} w_{p1} \\ w_{p2} \\ \vdots \\ w_{pk} \end{bmatrix}$, weight table p in cell $\mathbf{P}$.

Step 5: Implement the LMS algorithm

The MIMO CMAC NN classifier modifies the weights by applying a supervised learning algorithm based on the LMS algorithm. The $\mathbf{w}_p$ ($p = 1, 2, ..., p_{\max}$) is independently updated, as follows.

$$\begin{aligned} & w_{pl}(epoch+1) = w_{pl}(epoch) + \frac{\beta(y_{d,pj} - y_{o,pj})}{g} \\ & l = 1, 2, \ldots, k \quad j = 1, 2, ..., n_{\text{train}} \quad p = 1, 2, ..., p_{\max} \quad epoch = 1, 2, \ldots, epoch_{\max} \end{aligned} \tag{9}$$

where $y_{d,pj}$ = desired output from desired vector p of input pattern j; $w_{pl}(epoch)$ = value of weight l from weight table p in *epoch*; $w_{pl}(epoch+1)$ = value of weight l from weight table p in *epoch*+1; $epoch_{\max}$ = maximum epoch number

Step 6: Evaluate the training classification error

A neuron output is classified as 1 when its original value is greater than or equal to 0.5, or as 0 when its value is less than 0.5. A training classification error ($CE_{\text{train}}\%$) is used as a performance index, as follows.

$$CE_{\text{train}} = \left(\frac{n_{\text{train}} - n_{\text{accuracy}}}{n_{\text{train}}} \right) \times 100 \tag{10}$$

where n_{accuracy} = number of instances for determining accuracy.

Step 7: Measure the test classification error

The input pattern j ($j = n_{\text{train}}+1, n_{\text{train}}+2,..., n_{\text{total}}$) is used as the test dataset. The actual outputs of recall of the MIMO CMAC NN classifier can be calculated from the weight table $\mathbf{w}_p$ ($p = 1, 2, ..., p_{\max}$) that was obtained in the training stage (Steps 1–6). The generalization accuracy of the MIMO CMAC NN classifier is then evaluated using a test $CE_{\text{test}}\%$ that obtained using Eq. (10) though the test dataset.

3 Method

Figure 1 shows the pseudo-code of the proposed RGA-MIMO CMAC NN classifier. The best parameter settings of the internal MIMO CMAC NN classifier are optimized using the external RGA approach, and two medical data classification problems are solved using the internal MIMO CMAC NN classifier.

External RGA:

Step 1: Initialize the parameter settings

Parameter settings are given such as ps_{RGA}, crossover probability $p_{\text{c,RGA}}$ and mutation probability $p_{\text{m,RGA}}$. The candidate solutions (individuals) of the external RGA method represent the optimized parameters (β, Q_i, g) of the internal MIMO CMAC NN classifier. Therefore, an available population is randomly generated using ps_{RGA} from [x_n^l, x_n^u], such as the lower and upper boundaries of Q_i [Q_i^l, Q_i^u], the lower and upper boundaries of g [g^l, g^u] and the lower and upper boundaries of β [β^l, β^u].

Step 2: Compute the fitness function value

Internal MIMO CMAC NN classifier:

The external RGA method offers parameter settings Q_i, g and β for the internal MIMO CMAC NN classifier. Subsequently, Steps 0–7 of the internal MIMO CMAC NN classifier are implemented. The internal MIMO CMAC NN classifier returns the best $CE_{\text{test}}\%$ to external RGA approach.

end

The fitness function value $fittness_j$ of the external RGA approach is the best $CE_{\text{test}}\%$ obtained using the internal MIMO CMAC NN classifier, as follows:

$$fitness_j = CE_{\text{test}}\%,\ j = 1, 2, \ldots, ps_{\text{RGA}} \tag{11}$$

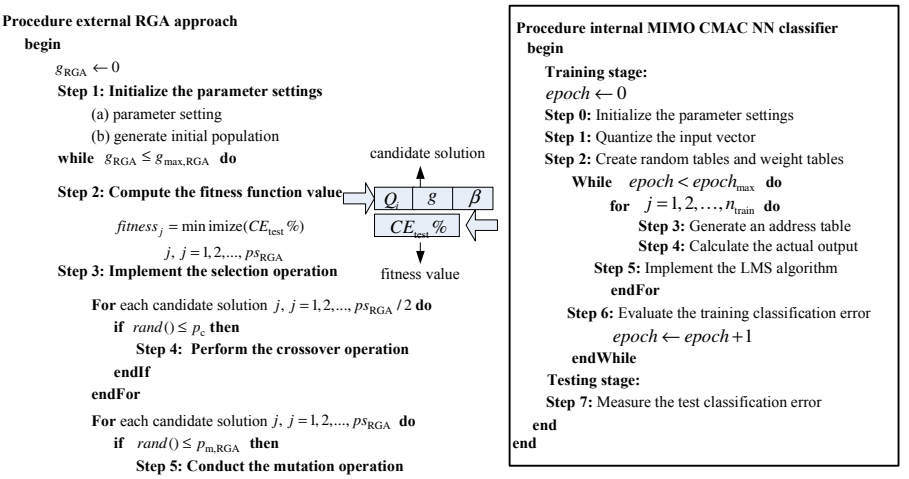

Fig. 1. The pseudo-code of the RGA-MIMO CMAC NN classifier

Step 3: Implement the selection operation

The parents in a crossover pool are selected using Eq. (1).

Step 4: Perform the crossover operation

Candidate solutions are created using Eqs. (2) and (3). The operation $[\cdot]$ (rounded number) is used to the generate candidate solutions since the parameters Q_i and g have integer values.

Step 5: Conduct the mutation operation

A solution space is exploited using Eq. (12).

$$x_{\text{trial},n} = \begin{cases} \left[x_{\text{current},n} + (x_n^u - x_{\text{current},n})\, pert(g_{\text{RGA}}) \right], \text{if } U_6(0,1) < 0.5 \\ \left[x_{\text{current},n} - (x_{\text{current},n} - x_n^l)\, pert(g_{\text{RGA}}) \right], \text{if } U_6(0,1) \ge 0.5 \end{cases}, n = 1,2$$

$$x_{\text{trial},n} = \begin{cases} x_{\text{current},n} + (x_n^u - x_{\text{current},n})\, pert(g_{\text{RGA}}), \text{if } U_7(0,1) < 0.5 \\ x_{\text{current},n} - (x_{\text{current},n} - x_n^l)\, pert(g_{\text{RGA}}), \text{if } U_7(0,1) \ge 0.5 \end{cases}, n = 3 \quad (12)$$

where $[\cdot]$ = rounded number.

Step 6: Implement an elitist strategy

This work updates the population using an elitist strategy. A situation in which the $fittness_j$ of candidate solution j in the new population is larger than that in the

current population suggests that the weak candidate solution j is replaced. Additionally, a situation in which the $fittness_j$ of candidate solution j in the new population is equal to or worse than that in the current population implies that the candidate solution j in the current population survives. In addition to maintaining the strong candidate solutions, this strategy eliminates weak candidate solutions.

External steps 2 to 6 are repeated until the $g_{\max,\mathrm{RGA}}$ value of the external RGA approach is met.

Table 1 lists the parameter settings of the proposed RGA-MIMO CMAC NN classifier. The RGA-MIMO CMAC NN classifier was run independently 30 times and summarizes mean CE_{train} %, mean CE_{test} %, mean computational CPU time (MCCT), mean Q_i, mean g and mean β.

4 Results

The proposed RGA-MIMO CMAC NN classifier was coded in MATLAB programming language, and executed on a Pentium D 3.0 (GHz) personal computer. To fairly compare the experimental results obtained using the proposed classifier with that of obtained using individual and hybrid classifiers, the PROBEN1 datasets [14] are used. In PROBEN1 datasets, three permutations of the patterns are available for the diabetes and cancer datasets. This work uses the first 50% of a dataset for training and the last 25% of the dataset in test. The proposed classifier was executed 30 times for each test dataset.

Table 1. Parameter settings of the RGA-MIMO CMAC NN classifier

Methods	Parameter settings	Search space
the external RGA approach	$p_{\mathrm{c,RGA}} = 1$, $ps_{\mathrm{RGA}} = \{2, 4\}$ $p_{\mathrm{m,RGA}} = 0.5$ $g_{\max,\mathrm{RGA}} = 3$	$[Q_i^l, Q_i^u]$ = [30, 50] $[g^l, g^u]$ = [50, 120] β $[\beta^l, \beta^u]$ = [0.05, 0.1]
the internal MIMO CMAC NN classifier	$epoch_{\max}$= 30 k =10000	

4.1 Experimental Results of the RGA-MIMO CMAC NN Classifier for Diabetes Dataset

Table 2 lists experimental results obtained by using the proposed RGA-MIMO CMAC NN classifier to the diabetes1, 2 and 3. According to this table, increasing the parameter ps_{RGA} increases the MCCT. Moreover, the t test is performed for the mean CE_{test}% s obtained using the parameter ps_{RGA} ={2, 4}, indicating that the differences of the mean CE_{test}% s obtained using the parameter ps_{RGA} ={2, 4} are statistically different for diabetes1 and 3, since the P values (0.007 and 0.015) of the t

test are smaller than the significance level of 0.05. This work prefers the results obtained using ps_{RGA} =4, since the MCCTs are acceptable and CE_{test} % s are small. Therefore, the best parameter settings of the internal MIMO CMAC NN classifier are (β, Q_i, g) = (42, 93, 0.08) for diabetes1, (β, Q_i, g) = (37, 93, 0.08) for diabetes2 and (β, Q_i, g) = (36, 96, 0.07) for diabetes3.

Table 2. Experimental results of the RGA-MIMO CMAC NN classifier for diabetes1, 2 and 3

	$p_{\mathrm{c,RGA}}$ = 1, $p_{\mathrm{m,RGA}}$ = 0.5												*P* value
	ps_{RGA} = 2						ps_{RGA} = 4						
	mean CE_{train} %	mean CE_{test} %	MCCT (sec.)	mean Q_i	mean g	mean β	mean CE_{train} %	mean CE_{test} %	MCCT (sec.)	mean Q_i	mean g	mean β	
diabetes1	10.81	25.24	99.68	41	91	0.07	10.43	24.69	168.59	42	93	0.08	0.007*
diabetes2	10.48	27.03	101.02	40	96	0.08	10.48	26.55	166.36	37	93	0.08	0.056
diabetes3	10.85	23.47	101.97	38	98	0.07	11.02	22.90	168.46	36	96	0.07	0.015*

(The "*" represents the difference of CE_{test} % obtained using ps_{RGA} ={2, 4} are statistically different.)

Table 3 compares the experimental results obtained using the RGA-MIMO CMAC NN classifier with those obtained using individual MIMO CMAC NN classifier [8], genetic programming (GP)-based classifiers [13, 15], NN classifier [14] and modular GA-based classifier [12]. In Table 3, the individual MIMO CMAC NN classifier used trail and error to manipulate parameters (e.g., Q_i, g and β) and obtained the best CE_{test} %. This table indicates that the CE_{test} % s obtained using the RGA-MIMO CMAC NN classifier are statistically smaller than those obtain using the individual MIMO CMAC NN classifier for diabetes1 and 2, since the *P* values of the *t* test are smaller than the significance level of 0.05. Moreover, the CE_{test} % s of the RGA-MIMO CMAC NN classifier are significantly lower than those of GP-based classifier [15] for diabetes2 and 3. Furthermore, the CE_{test} % s obtained using the RGA-MIMO CMAC classifier and the NN classifier [14] are identical to each other for diabetes1, 2 and 3. Additionally, the CE_{test} % of the RGA-MIMO CMAC classifier is smaller that of the GP-based classifier [13] for diabetes2. Moreover, the CE_{test} % s obtained using the RGA-MIMO CMAC classifier are lower than the modular GA-based classifier [12] for diabetes1 and 3.

Table 3. Comparison of experimental results of the proposed RGA-MIMO CMAC NN classifier with those of obtained using publised classifiers for diabetes1, 2 and 3

	GP-based classifier [15]	NN classifier [14]	linear GP-based classifier [13]	modular GA-based classifier [12]	MIMO CMAC NN classifier [8]	RGA-MIMO CMAC NN classifier	MIMO CMAC NN classifier [8] vs. RGA-MIMO CMAC NN classifier
datasets	mean CE_{test} %	mean CE_{test} %	mean CE_{test} %	mean CE_{test} %	mean CE_{test} %	mean CE_{test} %	*P* value
diabetes1	24.84	24.10	23.96	25.86	25.57	24.69	0.000
diabetes2	30.36	26.42	27.85	26.89	27.53	26.55	0.000
diabetes3	26.09	22.59	23.09	24.69	23.33	22.90	0.068

4.2 Experimental Results of the RGA-MIMO CMAC NN Classifier for Cancer Dataset

Table 4 lists experimental results obtained using the proposed RGA-MIMO CMAC NN classifier to the cancer1, 2 and 3. According to this table, increasing the parameter ps_{RGA} increases the MCCT. Additionally, the difference of the mean CE_{test}% obtained using the parameter ps_{RGA} ={2, 4} are statistically different for cancer2, since the *P* value (0.005) of the *t* test is smaller than the significance level of 0.05. This work prefers the results obtained using ps_{RGA} = 4, because the MCCTs are acceptable and CE_{test}% s are small. Hence, the best parameter settings of the internal MIMO CMAC NN classifier are (β , Q_i , g) = (40, 96, 0.07) for cancer1, (β , Q_i , g) = (41, 88, 0.08) for cancer2 and (β , Q_i , g) = (37, 92, 0.07) for cancer3.

Table 4. Experimental results of the RGA-MIMO CMAC NN classifier for diabetes1, 2 and 3

	$p_{\text{c,RGA}}$ = 1, $p_{\text{m,RGA}}$ = 0.5												*P* value
	ps_{RGA} = 2						ps_{RGA} = 4						
	mean CE_{train} %	mean CE_{test} %	MCCT (sec.)	mean Q_i	mean g	mean β	mean CE_{train} %	mean CE_{test} %	MCCT (sec.)	mean Q_i	mean g	mean β	
cancer1	1.45	3.87	97.29	40	93	0.08	1.55	3.83	167.17	40	96	0.07	0.573
cancer2	1.42	3.77	98.04	40	94	0.08	1.17	3.56	160.56	41	88	0.08	0.005*
cancer3	1.24	3.26	98.30	37	94	0.07	1.16	3.16	161.62	37	92	0.07	0.258

(The "*" represents the difference of CE_{test} % obtained using ps_{RGA} ={2, 4} are statistically different.)

Table 5 compares the experimental results obtained using the RGA-MIMO CMAC NN classifier with those obtained using individual MIMO CMAC NN classifier [8], GP-based classifiers [13, 15], NN classifier [14] and modular GA-based classifier [12]. According to this table, the CE_{test}% s obtained using the RGA-MIMO CMAC NN classifier are statistically smaller than those obtain using the individual MIMO CMAC NN classifier for cancer2 and 3, since the since the *P* values of the *t* test are smaller than the significance level of 0.05. Moreover, the CE_{test}% s obtained using the RGA-MIMO CMAC NN classifier are smaller that those obtained using GP-based classifiers [13, 15] and NN classifier for cancer2 and 3.

Table 5. Comparison of experimental results of the proposed RGA-MIMO CMAC NN classifier with those of obtained using publised classifiers for Cancer1, 2 and 3

	GP-based classifier [15]	NN classifier [14]	linear GP-based classifier [13]	modular GA-based classifier [12]	MIMO CMAC NN classifier [8]	RGA-MIMO CMAC NN classifier	MIMO CMAC NN classifier [8] vs. RGA-MIMO CMAC NN classifier
datasets	mean CE_{test} %	mean CE_{test} %	mean CE_{test} %	mean CE_{test} %	mean CE_{test} %	mean CE_{test} %	*P* value
cancer1	2.46	1.38	2.18	–	3.94	3.83	0.083
cancer2	6.08	4.77	5.72	–	3.77	3.56	0.009
cancer3	4.47	3.70	4.93	–	3.59	3.16	0.000

(A dashed line '–' in a cell indicates an element that was not reported in a particular test.)

The proposed RGA-MIMO CMAC NN classifier has the following advantages:

1. Parameter manipulation of the internal MIMO CMAC NN classifier is based on the solved classification problems. Owing to their ability to solve classification problems efficiently, the external RGA method replaces the trial and error to manipulate the parameters (i.e. β, Q_i and g).
2. In additionally to obtaining the optimum parameter settings of the internal MIMO CMAC NN classifier, the RGA-MIMO CMAC NN classifier can reduce CE_{test} % against individual MIMO CMAC NN classifier for the diabetes and cancer datasets.
3. Moreover, by outperforming some published classifier, the proposed method reduces the parametrization for the internal MIMO CMAC NN classifier.

5 Conclusions

This work develops a hybrid classifier that integrates a RGA method with the MIMO CMAC NN classifier. The proposed RGA-MIMO CMAC NN classifier is applied to two benchmark medical datasets: diabetes and cancer datasets. Experimental results indicate that the RGA-MIMO CMAC NN classifier outperforms some individual and hybrid classifiers for the test datasets. Therefore, the RGA-MIMO CMAC NN classifier can be regarded as efficient classifier to solve medical data classification problems.

References

1. Mastrogiannis, N., Boutsinas, B., Giannikos, I.: A Method for Improving the Accuracy of Data Mining Classification Algorithms. Computers & Operations Research 36(10), 2829–2839 (2009)
2. Bojarczuk, C.C., Lopes, H.S., Freitas, A.A., Michalkiewicz, E.L.: A Constrained-Syntax Genetic Programming System for Discovering Classification Rules: Application to Medical Data Sets. Artificial Intelligence in Medicine 30(1), 27–48 (2004)
3. Mazurowski, M.A., Habas, P.A., Zurada, J.M., Lo, J.Y., Baker, J.A., Tourassi, G.D.: Training Neural Network Classifiers for Medical Decision Making: The Effects of Imbalanced Datasets on Classification Performance. Neural Networks 21(2-3), 427–436 (2008)
4. Gadaras, I., Mikhailov, L.: An Interpretable Fuzzy Rule-Based Classification Methodology for Medical Diagnosis. Artificial Intelligence in Medicine 47(1), 25–41 (2009)
5. Barakat, N., Bradley, A.P., Barakat, M.N.H.: Intelligible Support Vector Machines for Diagnosis of Diabetes Mellitus. IEEE Transactions on Information Technology in Biomedicine 14(4), 1114–1120 (2010)
6. Quteishat, A., Lim, C.P., Tan, K.S.: A Modified Fuzzy Min-Max Neural Network with a Genetic-Algorithm-based Rule Extractor for Pattern Classification. IEEE Transactions on Systems, Man and Cybernetics, Part A: Systems and Humans 40(3), 641–650 (2010)

7. Wang, S.J., Mathew, A., Chen, Y., Xi, L.F., Ma, L., Lee, J.: Empirical Analysis of Support Vector Machine Ensemble Classifiers. Expert Systems with Applications 36(3), part 2, 6466–6476 (2009)
8. Wu, J.Y.: MIMO CMAC Neural Network Classifier for Solving Classification Problems. Applied Soft Computing 11(2), 2326–2333 (2011)
9. Wu, C.H., Ken, Y., Huang, T.: Patent Classification System Using a New Hybrid Genetic Algorithm Support Vector Machine. Applied Soft Computing 10(4), 1164–1177 (2012)
10. Sartakhti, J.S., Zangooei, M.H., Mozafari, K.: Hepatitis Disease Diagnosis Using a Novel Hybrid Method based on Support Vector Machine and Simulated Annealing (SVM-SA). Computer Methods and Programs in Biomedicine 108(2), 570–579 (2011)
11. Poorzahedy, H., Rouhani, O.M.: Hybrid Meta-Heuristic Algorithms for Solving Network Design Problem. European Journal of Operational Research 182(2), 578–596 (2007)
12. Zhu, F., Guan, S.: Feature Selection for Modular GA-based Classification. Applied Soft Computing 4(4), 381–393 (2004)
13. Brameier, M., Banzhaf, W.: A Comparison of Linear Genetic Programming and Neural Networks in Medical Data Mining. IEEE Transactions on Evolutionary Computation 5(1), 17–26 (2001)
14. Prechelt, L.: Proben1－A Set of Neural Network Benchmark Problems and Benchmarking Rules, Universität Karlsruhe (1994)
15. de Falco, I., Cioppa, A.D., Tarantino, E.: Discovering Interesting Classification Rules with Genetic Programming. Applied Soft Computing 1(4), 257–269 (2002)
16. Tang, P.-H., Tseng, M.-H.: Adaptive Directed Mutation for Real-Coded Genetic Algorithms. Applied Soft Computing 13(1), 600–614 (2013)
17. Houck, C.R., Joines, J.A., Kay, M.G.: A Genetic Algorithm for Function Optimization: A Matlab Implementation. North Carolina State Univ., Raleigh (1995)
18. Wu, J.Y.: Solving Constrained Global Optimization Problems by Using Hybrid Evolutionary Computing and Artificial Life Approaches. Mathematical Problems in Engineering 2012, Article ID 841410, 1–23 (2012)

Research on Electromagnetic Coupling Artificial Neural Network with Spatial Topology*

Ziyin Wang, Mandan Liu**, Xiang Ren, and Yicheng Cheng

Key Laboratory of Advanced Control and Optimization for Chemical Processes
(East China University of Science and Technology),
Ministry of Education, Shanghai 200237
liumandan@ecust.edu.cn

Abstract. In this paper, an emerging artificial neural network (ECANN) is proposed. Abstracting from a latest research in neuroscience, electromagnetic coupling among neuron activities is introduced into the model. Besides, the overall network can be viewed as a system with physical significance of circuitry, and each neuron is presented as differential equation. At the mean time, the spatial grid topology is employed in order to develop its parallelism. This artificial neural network is designed for fitting and predicting dynamic data, and has successfully worked in simulation part of this paper.

Keywords: Artificial neural network, Electromagnetic coupling, Spatial topology, Process identification.

1 Introduction

Artificial neural network(ANN) is the abstraction of biological neural network[1]. Until now, neuroscience has not been constructed completely but, large numbers of neuroscientists are working on it. New developments continuously nourish the field, while the old theory is being modified. Therefore, it's necessary to study new ANN models with new achievements in neuroscience.

Neuroscientists have found spontaneous fluctuations in brain activity with the help of functional magnetic resonance imaging(fMRI)[4-5]. The study shows those fluctuations can't be simply regarded as noise, but meaningful in neural coding and brain function[2-3]. A recent study has shown that high-frequency component (>300Hz) of local field potential(LFP) by each neuron bioelectricity activity will affect other neuron's membrane potential through the rapidly alternating electric field induced by LFP[6].

In neurobiology, it is shown that the neuron action can be modeled with differential equations[7-9]. However, when it comes to the neuron models of ANN used for data fitting, e.g. BP neural network, they are generally presented by nonlinear algebraic equations, which is somewhat lack in the ability of dynamic data handling.

* Supported by the project of produce, study and research of Guangdong, China, granted number: 2010B090400477 and by "the Fundamental Research Funds for the Central Universities".

** Corresponding author.

D. Liu et al. (Eds.): BICS 2013, LNAI 7888, pp. 57–65, 2013.

The action potential arises and attenuates swiftly, whose time span is approximately 1 ms[7], and accordingly makes the actuating current on the nerve fiber alternate rapidly. This induced electromotive force will have an impact on the interaction among synapses, at the same time, rapidly alternating electric field will affect the neuron membrane potential directly. Based on the analysis of those phenomenon mentioned above, we combined the neural network with electromagnetic coupling in the form of differential equations through electromagnetic mechanism. Even as it does not exist physical connections between two neurons, they still may interact indirectly with the method of electromagnetic induction. Moreover, the ANN model in this paper has never been put forward, which gives a new sight of circuitry and electromagnetic field and the spatial grid topology.

2 Development of Electromagnetic Coupling Neuron Model

Consider a neural network with n neurons, a typical neuron j is connected with $m\ (m \le n)$ neurons, which forms m nerve fibers. As shown in figure 1.

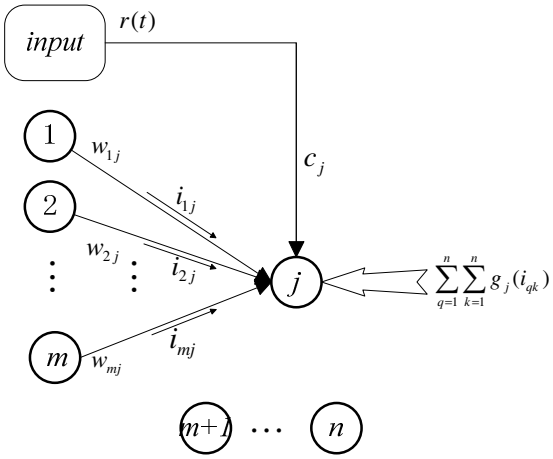

Fig. 1. Electromagnetic coupling neuron model

If neuron i $(i = 1,...,m)$ is connected with neuron j, neuron j will be stimulated by neuron i and produce the actuating current i_{ij} on the specific nerve fiber. We adopt the convention that the direction of i_{ij} is from i pointing to j. If the actual direction of i_{ij} is not the same as the positive direction we have defined, then i_{ij} can be described as the opposite. Mathematically, $i_{ij} = -i_{ji}$. Meanwhile, neuron j is also stimulated by external input $c_j r(t)$, where $r(t)$ is the external input signal and c_j is the weight on the connection between external input to neuron j. Besides, other actuating currents affect the excitation intensity of neuron j with the method of

electromagnetic induction, which can be stated as $\sum_{q=1}^{n}\sum_{k=1}^{n} g_j(i_{qk})$, where $g_j(i_{qk})$ refers to a quantified value that actuating current of neuron q pointing to neuron k affect the excitation intensity of neuron j. Likewise, $\sum_{q=1}^{n}\sum_{k=1}^{n} g_j(i_{qk})$ refers to the combined effect of all the associated actuating currents on neuron j.

Moreover, neural coding and neural computation are based on the membrane potential of neurons in the field of neuroscience. Consequently, the excitation intensity of a single neuron corresponds to the value of its potential. In this model, we consider actuating current is caused by the potential difference between two associated neurons.

The single neuron model can be built as the following:

$$u_j = f[\sum_{i=1}^{n} w_{ij} i_{ij} + c_j r(t)] + \sum_{q=1}^{n}\sum_{k=1}^{n} g_j(i_{qk}) \tag{1}$$

$$i_{ij} = \frac{1}{R_{ij}}(u_i - u_j) \tag{2}$$

Where u_j is a real number that denotes the excitation intensity of neuron j; R_{ij} is the equivalent resistance of the nerve fiber between neuron i to neuron j; w_{ij} refers to the weight on the connection between neuron i to neuron j; $f(\bullet)$ is a continuous sigmoidal function ranging from -1 to +1, that is, $f(x) = \frac{2}{1-e^{-x}} - 1$. $\sum_{q=1}^{n}\sum_{k=1}^{n} g_j(i_{qk})$ is named as electromagnetic coupling term. For further discussion, see the next part.

According to electromagnetic induction law and Biot-Savat-Laplace law, induction current can be calculated as follows:

$$i^{*}_{j-qk}(t) = A_{j-qk} \cdot \frac{di_{qk}(t)}{dt} \tag{3}$$

where A_{j-qk} can be seen as a constant with physical significance.

With respect to neuron j, the stimulation part caused by electromagnetic induction is the sum of all the associated actuating currents. Meanwhile, to guarantee the dimension of the electromagnetic coupling term agrees with that of potential, resistance term R_j is added:

$$\sum_{q=1}^{n}\sum_{k=1}^{n} g_j(i_{qk}) = R_j \cdot \sum_{q=1}^{n}\sum_{k=1}^{n} A_{j-qk} \frac{di_{qk-j}(t)}{dt} \tag{4}$$

For simplicity , assume that the mechanism of electromagnetic induction is taken into account only when the actuating current is close to the neurons specified, and consequently, electromagnetic coupling term can be rewritten as:

$$\sum_{q=1}^{n}\sum_{k=1}^{n} g_j(i_{qk}) = \sum_{i=1}^{n} v_{ij}\frac{d(u_i - u_j)}{dt} \tag{5}$$

Coalesce the coefficients in equation 4, the single neuron model can be represented as:

$$u_j = f\{\sum_{i=1}^{n} w_{ij}(u_i - u_j) + c_j r(t)\} + \sum_{i=1}^{n} v_{ij}\frac{d(u_i - u_j)}{dt} \tag{6}$$

where $v_{qk,j} = R_j \cdot A_{j-qk}$.

Equation 6 is the final model of single neuron. For convenience, define the following 3 matrices:

$$\mathbf{W} = \begin{pmatrix} w_{1,1} & w_{1,2} & \cdots & w_{1,n} \\ w_{2,1} & \ddots & & w_{2,n} \\ \vdots & & \ddots & \vdots \\ w_{n,1} & w_{n,1} & \cdots & w_{n,n} \end{pmatrix}, \quad \mathbf{V} = \begin{pmatrix} v_{11} & v_{12} & \cdots & v_{1n} \\ v_{21} & \ddots & & v_{2n} \\ \vdots & & \ddots & \vdots \\ v_{n1} & v_{n1} & \cdots & v_{nn} \end{pmatrix}, \quad \mathbf{C} = \begin{pmatrix} c_1 \\ c_2 \\ \vdots \\ c_n \end{pmatrix}$$

Where $\mathbf{W}, \mathbf{V}, \mathbf{C}$ refer to the weight matrix of actuating current term, electromagnetic coupling term and external input term, respectively.

3 Development of ECANN Model

3.1 Network Architecture

Different connectivities yield different network behaviors[1]. In this paper, a regular spatial grid topology is employed, which is more beneficial to improve the ability of parallelism as well as reduce the dimension of parameter. This spatial structure derived from a research written by Hafting et al.(2005) . Figure 2 shows a schematic of a cube grid with 27 neurons, and the adjacent neurons have the same distance. Also, we assume that $w_{ij} = w_{ji} = 0$ if the physical connective exists between neuron i and neuron j, and $w_{ij} \neq 0$, $w_{ji} \neq 0$ otherwise.

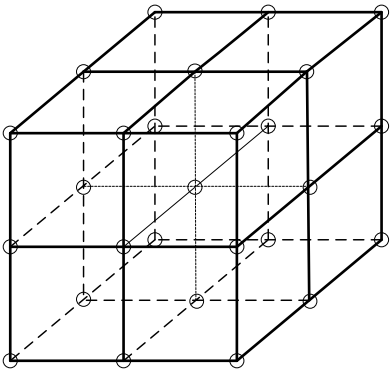

Fig. 2. ECANN architecture: spatial grid topology

3.2 ECANN Model

Let $W_j^* = \sum_{i=1}^{n} w_{ij}, V_j^* = \sum_{i=1}^{n} v_{ij}$, and the overall system with n neurons can be described by equation 6 in vector notation as:

$$\begin{pmatrix} u_1 \\ u_2 \\ \vdots \\ u_n \end{pmatrix} = f\left\{ \mathbf{W}^T \begin{pmatrix} u_1 \\ u_2 \\ \vdots \\ u_n \end{pmatrix} - \begin{pmatrix} W_1^* & & & \\ & W_2^* & & \\ & & \ddots & \\ & & & W_n^* \end{pmatrix} \begin{pmatrix} u_1 \\ u_2 \\ \vdots \\ u_n \end{pmatrix} - r(t) \begin{pmatrix} c_1 \\ c_2 \\ \vdots \\ c_n \end{pmatrix} \right\} - \mathbf{V}^T \begin{pmatrix} \dot{u}_1 \\ \dot{u}_2 \\ \vdots \\ \dot{u}_n \end{pmatrix} + \begin{pmatrix} V_1^* & & & \\ & V_2^* & & \\ & & \ddots & \\ & & & V_n^* \end{pmatrix} \begin{pmatrix} \dot{u}_1 \\ \dot{u}_2 \\ \vdots \\ \dot{u}_n \end{pmatrix} \tag{7}$$

Define $\mathbf{U} = (u_1, u_2, ..., u_n)^T, \hat{\mathbf{W}}^* = diag(W_1^*, W_2^*, ..., W_n^*), \hat{\mathbf{V}}^* = diag(V_1^*, V_2^*, ..., V_n^*)$.
Assuming that $(\mathbf{V^T} - \hat{\mathbf{V}}^*)$ is invertible, equation 7 can be written as the form of state space expression:

$$\dot{\mathbf{U}} = (\mathbf{V^T} - \hat{\mathbf{V}}^*)^{-1} \left\{ f[(\mathbf{W^T} - \hat{\mathbf{W}}^*)\mathbf{U} + \mathbf{C}r(t)] - \mathbf{U} \right\} \tag{8}$$

Equation 8 is the state space equation of ECANN. It is complicated to solve the problem with numerical solution, which will have great influence on the quality of real-time operation. We introduce difference solution to the model here. Meanwhile, assuming that $\left(\frac{\mathbf{V^T} - \hat{\mathbf{V}}^*}{\Delta t} + \mathbf{I}_{n \times n} \right)$ is invertible, we have that:

$$\mathbf{U}(k+1) = \left(\frac{\mathbf{V^T} - \hat{\mathbf{V}}^*}{\Delta t} + \mathbf{I}_{n \times n} \right)^{-1} \left\{ f\left[(\mathbf{W^T} - \hat{\mathbf{W}}^*)\mathbf{U}(k) + \mathbf{C}r(k+1) \right] + \frac{\mathbf{V^T} - \hat{\mathbf{V}}^*}{\Delta t} \mathbf{U}(k) \right\} \tag{9}$$

Where $\mathbf{I}_{n \times n}$ is a n dimensional unit matrix.

Equation 9 presents the iterative formula of ECANN. The operation network calculates as the given formula other than solving differential equations, which is helpful to reduce the time complexity of operation system.

4 ECANN Applied in Process Identification

The model of ECANN is essentially a high-order nonlinear system with differential equations. Figure 3 and figure 4 show the schematics of Input-output of the network and the real-time system with ECANN for dynamic data fitting, respectively.

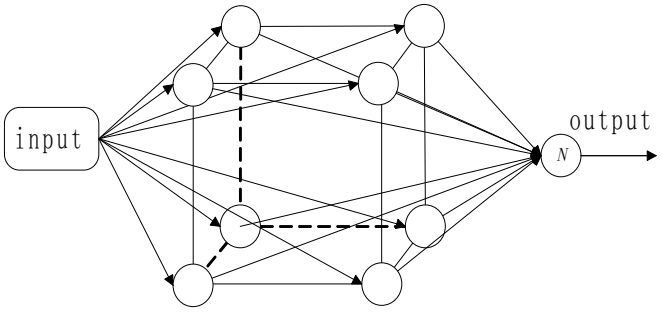

Fig. 3. Input-output of ECANN

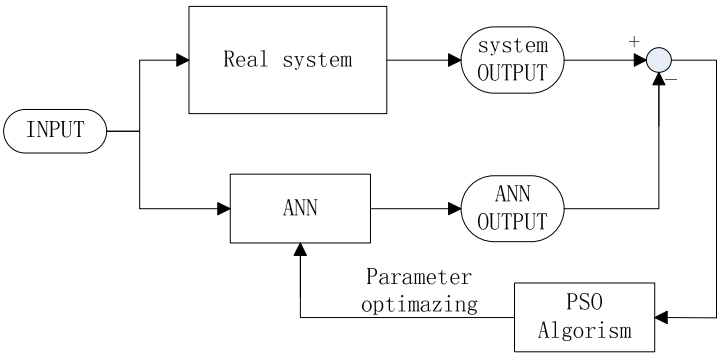

Fig. 4. The real-time system with ECANN for dynamic data fitting

Figure 3 gives a sight of the basic procedure of the network that operates. Firstly, each neuron's input is weighed input of the external real-time input, then give neuron N the weighed outputs of every neuron. Neuron N is a traditional neuron whose threshold is zero. The excitation intensity of neuron N satisfies the algebraic equation:

$$u_N = f(\sum_{j=1}^{n} h_j u_j - 0) \tag{10}$$

Where h_j denotes the connection weight of neuron j in output layer.

Figure 4 presents an offline optimization system. To begin with, give an external input to the real-time system and we can get a set of input/output data from time t_0 to t. Meanwhile, give the same input signal to the network mentioned above. Similarly, a set of output data caused by the network is obtained. Our goal is to minimize the quadratic cost function with the difference between output caused by the network and the real-time system, and apply the particle swarm optimization(PSO) algorithm to optimize the weights in the network. As the learning proceeds, the algorithm can find the optimal weights, and the network is capable of approximating the real-time system.

For PSO algorithm, the initial value of inertial weight is set as 0.9, as the learning proceeds, it decays to 0.4; defining the global acceleration coefficient and the past acceleration coefficient (learning rate) to be 0.3, respectively; the maximum number of iteration is 800.

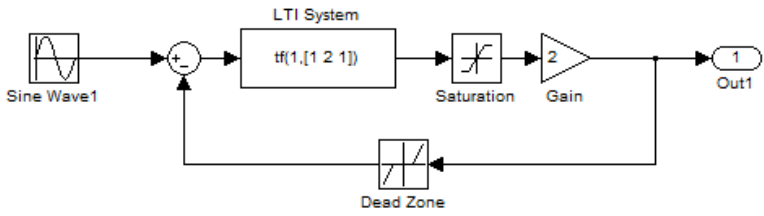

Fig. 5. Block diagram

The structure diagram is depicted in figure 5. Where LTI System block is the linear part of the system whose transfer function is $F(s)=\frac{1}{s^2+2s+1}$. saturation element ranges from -0.8 to 0.8. Dead zone ranges from -0.5 to 0.5.

In order to test the generalization ability of ECANN model. Here, three input signals are given. As shown in figure 6.

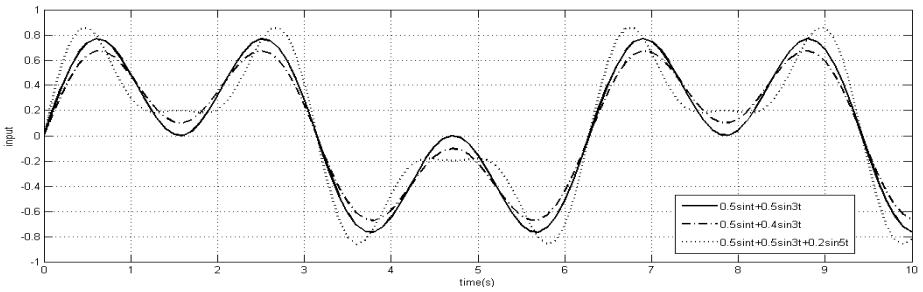

Fig. 6. Input signal

The solid line corresponds to signal 1 $r(t)=0.5\sin(t)+0.5\sin(3t)$, the chain line corresponds to signal 2 $r'(t)=0.5\sin(t)+0.4\sin(3t)$ and the dashed line corresponds to signal 3 $r''(t)=0.5\sin(t)+0.5\sin(3t)+0.2\sin(5t)$.

Let the simulation time be 10 time units, train the network with input signal 1 and the corresponding output of the system as figure 4 shows. Afterwards, to forecast the output of the system when the input signal is slightly altered, give signal 2 and signal 3 as input signal to the model that has been trained, then, we can get the simulation results, which shows in figure 7.

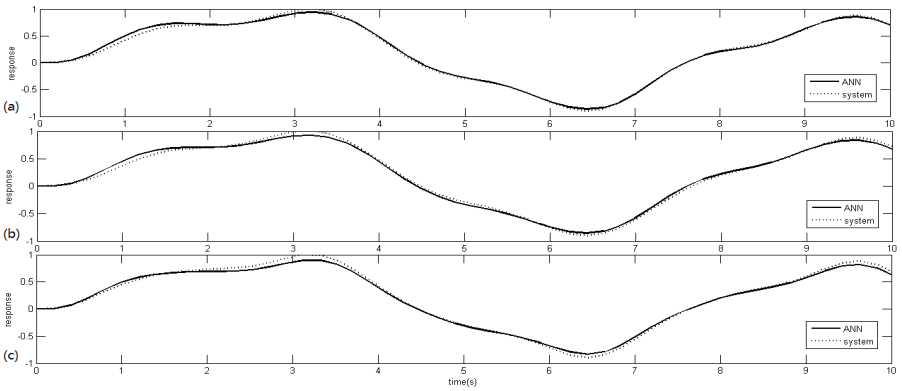

Fig. 7. Identification performance of outputs, the solid line corresponds to the ECANN model and the dashed line corresponds to the system: (a)signal 1; (b)signal 2; (c)signal 3

And before that, the data has been normalized with the following equation:

$$\hat{y} = 2\frac{y - y_{min}}{y_{max} - y_{min}} - 1 \tag{11}$$

Define the mean square root error(MSE) as follows:

$$e = \sqrt{\frac{1}{N_{sample}} \sum_{i=1}^{N_{sample}} (y_i^* - y_i)^2} \times 100\% \tag{12}$$

MSE of three input signals between the actual output and that estimated from the model is 2.7735%, 4.198% and 5.041%, respectively. It is shown that the ECANN model performs a good job in dynamic data fitting with great generalization ability.

5 Conclusion

Abstracting from a latest research in Neuroscience, we researched on a dynamic artificial neural network based on the electromagnetic coupling. To conclude, this neural network reveals several advantages compared with the traditional ANN used for data fitting:

- The single neuron model is described as the form of differential equation, which is more likely as biological neuron in mechanism[7-9], and consequently, ECANN is capable of dynamic data fitting.
- The overall network can be viewed as a circuitry, the actuating current is related to the difference of the excitation intensity of neurons. Meanwhile, suppose that the excitation intensity of artificial neuron corresponds to the membrane potential of biological neuron, the product of the potential difference and the conductance is exactly the current.
- Numeric solution to solve differential equation was abandoned in solving the nonlinear differential equation, which can obtain an applicable computational speed compared with traditional neural networks used for data fitting.

It has been tested that the ECANN has the ability in dynamic data fitting and approximating the overall dynamic system, which has profound consequence in the field of dynamic modeling, and it also proved that the model in this paper has great potential.

References

1. Jain, A.K., Mao, J., Mohiudin, K.M.: Artificial neural networks: A tutorial. Computer 29(5), 31–34 (1996)
2. Fox, M.D., Raichle, M.E.: Spontaneous fluctuations in brain activity observed with functional magnetic resonance imaging. Nature Rev. Neurosci. 8, 700–711 (2007)
3. Biswal, B., Yetkin, F., Haughton, V., Hyde, J.: Functional connectivity in the motor cortex of resting human brain using echo-planar MRI. Magn. Res. Med. 34, 537–541 (1995)

4. Foster, D.J., Wilson, M.A.: Reverse replay of behavioral sequences in hippocampal place cells during the awake state. Nature 440, 680–683 (2006)
5. Kenet, T., Bibitchkov, D., Tsodyks, M., Grinvald, A., Arieli, A.: Spontaneously emerging cortical representations of visual attributes. Nature 425, 954–956 (2003)
6. Anastassiou, C.A., Perin, R., Markram, H., Koch, C.: Ephaptic coupling of cortical neurons. Nature Neuroscience 12(2), 217–223 (2011)
7. Hodgkin, A.L., Huxley, A.F.: A quantitative description of,emnrane current and its application to conduct and excitation in nerve. Physiol. 117, 500 (1952)
8. Fitzhugh, R.: Impulses and physiological states in models of nerve membrane. Biophys. 1, 445 (1961)
9. Hindmarsh, J.L., Rose, R.M.: A model of neuronal bursting using three coupled first order differential equations. Proc. R. Soc. London 221(B), 87 (1984)
10. Hafting, T., Fyhn, M., Molden, S., Moser, M., Moser, E.I.: Microstructure of a spatial map in the entorhinal cortex. Nature 436(7052), 801–806 (2005)

General Change Detection Explains the Early Emotion Effect in Implicit Speech Perception

Aishi Jiang[1,2], Jianfeng Yang[1], and Yufang Yang[1,*]

[1] Key Laboratory of Behavioral Science, Institute of Psychology, Chinese Academy of Sciences, Beijing 100101, China
[2] Graduate University of Chinese Academy of Sciences, Beijing 100049, China
{jiangas,yangjf,yangyf}@psych.ac.cn

Abstract. Emotional prosody differentiates neutral sound at emotional category and acoustic features. To investigate the neural mechanism of early emotion perception in speech, one approach is using spectrally rotated sound of emotional sound as a neutral stimulus to match acoustic features. However, rotating sound involves the change of intelligence of the sound. Here the current event-related potential (ERP) study tested whether the mismatch negativity (MMN) invoked by the emotion stimuli reflects the emotion perception or change salience in oddball paradigm. Results revealed both emotion and rotation of the sound invoked MMNs, and larger negativity was found for rotated than emotional sounds. It suggested the perceived salience of change may determine the mismatch effects in implicit speech perception, and revealed that MMN effect in the early stage of emotion prosody perception can be explained in the domain-general change detection.

Keywords: Emotional Prosody, Event Related Potential (ERP), Mismatch Negativity (MMN).

1 Introduction

Vocal communication is an important way to convey emotional signals. Human express his or her emotion, not only by the verbal content, but also by suprasegmental properties such as pitch, intensity and duration. The variation of acoustic parameters, termed as emotional prosody, has been reported also in nonhuman primates [1] and is evident throughout human ontogeny and evolution of speech [2]. The interesting is increasing on the rapid differentiation of vocal emotion signals which remain unclear.

Previous implicit oddball studies have shown that human brain detects vocal emotion around 200ms after stimulus onset. Under sounds unrelated task, the brain responses were compared between frequent neutral standard stimuli and occasionally interrupted emotional deviants [2, 3]. Then the fronto-central MMN evoked by subtracting the brain responses to standards from that to deviants were considered as the indicator of sensitivity to emotional categories differences implicitly.

* Corresponding author.

D. Liu et al. (Eds.): BICS 2013, LNAI 7888, pp. 66–74, 2013.

Correspondingly, enhanced responses in human middle superior temporal sulcus have been demonstrated for angry relative to neutral prosody [4].

The quick differentiation of emotional sounds from neutral sounds may require detection of emotion significance as well as the accompanying low-level acoustic properties. As we know, each emotional category vocalization has its unique physiological ‘‘imprint’’ and is expressed with distinct pattern of acoustic properties [5]. For instance, compared with neutral utterance, anger is characterized by fast speech rate, high mean fundamental frequency (F0), F0 variability and sound intensity. Therefore, in previous oddball studies of emotional prosody, acoustic properties systematically differed between neutral standards and emotional deviants. Thus the question emerges whether these mismatch responses actually reflect the detection of emotional significance change, or low-level perceptual acoustic features change, or both change.

Our current study aims to text this question with MMN as an index of early stimulus encoding, by employing two type deviant stimuli: emotional deviant sounds and theirs matched acoustically counterparts which lacked emotional information. Acoustically matched neutral counterparts were obtained by spectrally rotated technique, which preserves amplitude envelope and duration information, pitch and pitch variation while distorting spectral information. Previous studies of emotional prosody sometimes used spectrally rotated counterparts as acoustically matched neutral counterparts [6, 7]. Here we manipulated emotional information and its acoustic properties using the original emotional sounds and their spectrally rotated counterparts as deviant stimuli compared to neutral standard sounds. From neutral standards to emotional sounds deviants, two types information changed: emotional significance and its acoustic properties (e.g. increasing pitch and intensity). From neutral standards to spectrally rotated deviants which were also neutral, only acoustic properties changed. Supposing emotional information are perceived and invoke MMN, emotional deviants will elicit larger MMN than theirs spectrally rotated counterparts. Furthermore, the MMN evoked by rotated stimuli of neutral original sounds was tested to investigate whether the early brain response for emotional sounds reflect the emotion perception or domain general change detection in implicit speech perception.

2 Methods

2.1 Participants

Twenty-nine university students (17 females; mean age = 22.79 years, range = 19 – 27 years) participated in the experiment. All participants were healthy, right-handed native speakers of Mandarin Chinese with no history of hearing deficits. They provided written informed consents and were paid an hourly stipend. Data of two female were excluded from the final analysis because of excessive artifacts.

2.2 Materials and Design

Sixteen Chinese pseudo-syllables produced by a trained actress in happy and neutral prosody were used in current study. Then 16 neutral and 16 happy sounds were spectrally rotated as the acoustically matched neutral stimuli which share low-level acoustic features but without affective properties [6, 7]. In addition, the sound intensity of neutral sounds was enhanced to the intensity level of happy sounds as baseline sounds with Praat [8].

In all, five type sounds were contained: neutral sounds (N) and happy sounds (H), spectrally rotated versions of neutral and happy original sounds (rH and rN), as well as the neutral sounds with enhanced intensity (Ni), with 16 stimuli each type. The acoustic parameters (duration, intensity, pitch) measured using Praat were analyzed statistically, and one-way ANOVA was performed. The main effects were significant for intensity, F (4, 75) = 116.52, $p < .001$; and for pitch, F (4, 75) = 88.68, $p < .001$; but not for duration, F (4, 75) = 1.95, $p = .11$. Multiple comparisons (Bonferroni corrected) revealed that happy original and rotated sounds have higher intensity and higher pitch than neutral original and rotated sounds ($ps < .05$); While no significances were found on duration, intensity and pitch between original sounds and theirs spectrally rotated counterparts ($ps > 0.1$).

A. Stimuli presentation

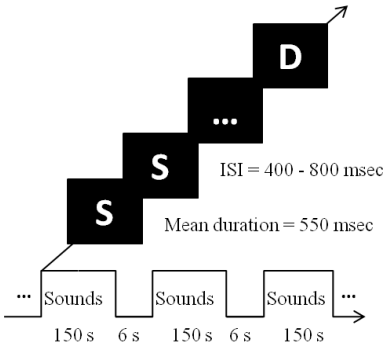

B. Stimuli example

	Standards	Deviants
H	N_1 N_2 … N_{16}	$H_{1\sim16}$
rH	N_1 N_2 … N_{16}	$rH_{1\sim16}$
rN	N_1 N_2 … N_{16}	$rN_{1\sim16}$
Ni	N_1 N_2 … N_{16}	$Ni_{1\sim16}$
C	$H_{1\sim16}$, $rH_{1\sim16}$, $rN_{1\sim16}$, $Ni_{1\sim16}$	

Fig. 1. (A) Experiment procedure and stimuli presentation. (B) Materials examples in one block: N (neutral sounds), H (happy sounds), rH (spectrally rotated versions of happy sounds), rN (spectrally rotated versions of neutral sounds), and Ni (neutral sounds with enhanced intensity).

The oddball paradigm was conducted and 16 neutral sounds were randomly presented as standard stimuli (see Fig.1). The presentation of multiple standard stimuli varied the template acoustically and phonetically, thus just the memory trace of neutral standard category was provided [2]. Other four type sounds were assigned to different conditions (H, rH, rN and Ni conditions) as deviant stimuli separately. In detail, in each block of H condition, 16 happy sounds were presented as deviants; then from neutral standards to happy deviants, two types information changed: emotion and its accompanying acoustic properties. In each block of rH condition, 16 spectrally rotated

stimuli of happy sounds were presented as deviants, therefore only acoustic properties changed from neutral standards to deviants. In each block of rN condition, 16 spectrally rotated sounds of neutral sounds were presented as deviant stimuli, and then both emotion and acoustic parameters remained unchanged. In each block of Ni condition, 16 neutral sounds with enhanced intensity were presented as deviants, and then only the simple acoustic parameter of intensity changed. In addition, an equiprobable control condition (C condition) was created by picking up deviant sounds from H, rH, rN and Ni conditions, providing control stimuli with the same physical characteristics and probability of occurrence as deviants in other four conditions.

2.3 Procedure

Participants were seated comfortably in a sound-attenuating chamber at a distance about 120 cm away from the computer monitor to minimize eye movements. They were asked to watch a silent movie (with subtitles on) while auditory stimuli were presented. The volume of sounds was adjusted for each participant to ensure that all sounds presented via headphones were heard clearly.

A block design was used and each block contained 112 standard stimuli and 16 deviants (12.5% probability for deviants) from one condition (see Fig.1). Each stimuli was presented at a rate of per 1.1 s (the average duration of sounds was 550ms), with the jittered inter-stimulus interval (ISI) from 400 to 800ms. Each block lasted about 150 s, followed by a 6 s silence. Four blocks were contained in each condition, and then 20 blocks in all were mixed randomly in five runs. The participant toke a 2-3 minutes rest after each run and the total experimental time was about an hour.

2.4 EEG Data Acquisition and Preprocessing

The EEG was recorded with 66 Ag-AgCl electrodes mounted in an elastic cap (NeuroScan system). Scalp electrodes were referenced to the tip of the nose. Vertical electrooculogram (EOG) were recorded supra- and infra-orbitally at the left eye. Horizontal EOG was recorded from the bilateral orbital rim. EEG and EOG were digitized at 500 Hz with an amplifier bandpass of 0.01–100 Hz. Impedances were kept below 5 kΩ. ERP averages were computed with a 100-msec baseline and a 600-msec ERP time window. Trials with artifacts exceeding the amplitude of ±75μV were excluded and about 57 trails per condition remained for averaging.

Brain responses to each type deviants were averaged as deviant ERP waveforms, and brain responses to standards preceding each deviant stimulus were averaged as standard ERP waveforms. Furthermore, brain responses to four type control stimuli in C condition were averaged as control waveforms, separately. Two type difference waves were calculated: Traditional deviant-minus-standard difference waves, which were obtained by subtracting the responses to standards from that to deviants in the same condition; Deviant-minus-control difference waves, obtained by subtracting the responses to control stimuli from deviants, with the same physical characteristics and probability of occurrence for more genuine mismatch responses [9].

The grand average ERPs for each condition were illustrated in Fig. 2 and 3. The repeated measure ANOVAs were conducted by 4 (Deviant type: H, rH, rN and Ni) × 3

(Region: frontal, central and parietal) × 3 (Hemisphere: left, middle and right) in consecutive mean amplitude latency bins of 10ms from 0 to 300ms post-stimulus onset, and nine electrodes (F3, FZ, F4, C3, CZ, C4, P3, PZ, P4) were chosen for analysis. According to visual inspection and consecutive short time analysis, the following time range was chosen as interest time window for further analysis: 190 – 240ms. Greenhouse–Geisser-corrected p-values were used, and only significant main effect and interactions including critical factor will be reported in the following.

3 Results

3.1 The Deviant-Minus-Standard Difference Waves

The repeated ANOVA on deviant-minus-standard difference waves (see Fig. 2) revealed significant main effects for Deviant type, F (3, 78) = 4.99, $p < .01$; and for Region, F (2, 52) = 6.25, $p < .01$. The typical fronto-central distributed pattern of MMN was observed [10] that brain responses were more negative over frontal and central than parietal ($ps < .05$), while no difference between frontal and central was found ($p > .05$). The Deviant type interacted with Region, F (6, 156) = 3.28, $p < .05$. The simple main effects of Deviant type were significant over frontal and central regions ($ps < .05$). Further simple analysis revealed that similar difference waves were evoked in rH and rN conditions ($p > .05$); while they were more negative than that in H condition ($ps < .05$); and in turn more negative than Ni condition ($ps < .05$).

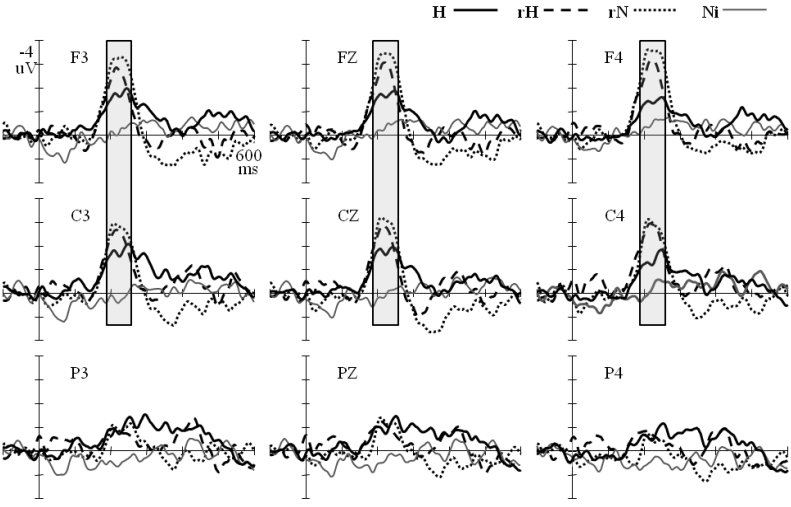

Fig. 2. ERP waveforms for deviant-minus-standard difference waves. Grand average difference waves with nine electrodes (F3, FZ, F4, C3, CZ, C4, P3, PZ and P4) are illustrated. At 190 – 240ms, larger fronto-central MMNs were elicited by deviants in rH and rN conditions comparing to H condition, while no mismatch response was elicited in Ni condition.

3.2 The Deviant-Minus-Control Difference Waves

The repeated ANOVA on deviant-minus-control difference waves (see Fig. 3) revealed marginal significant main effects for Deviant type, F (3, 78) = 2.25, p = .09; and for Region, F (2, 52) = 4.69, p < .05. The typical fronto-central distributed pattern of MMN was also observed [10]. Deviant type interacted with Region, F (6, 156) = 2.62, p < .05. Simple main effects of Deviant type were also significant over frontal and central regions (*ps* < .05). Further simple analysis revealed that in frontal region, no significance of difference waves was found between rH and rN conditions (*ps* > .05); while they were more negative than MMN in H condition marginal significantly (p = .07); and in turn more negative than that in Ni condition (*ps* < .05). Meanwhile in central region no significance of difference waves was found between rH and rN conditions (*ps* > .05); and the difference waves in rH condition were more negative than H condition (p < .05); and in turn more negative than in Ni condition (*ps* < .05).

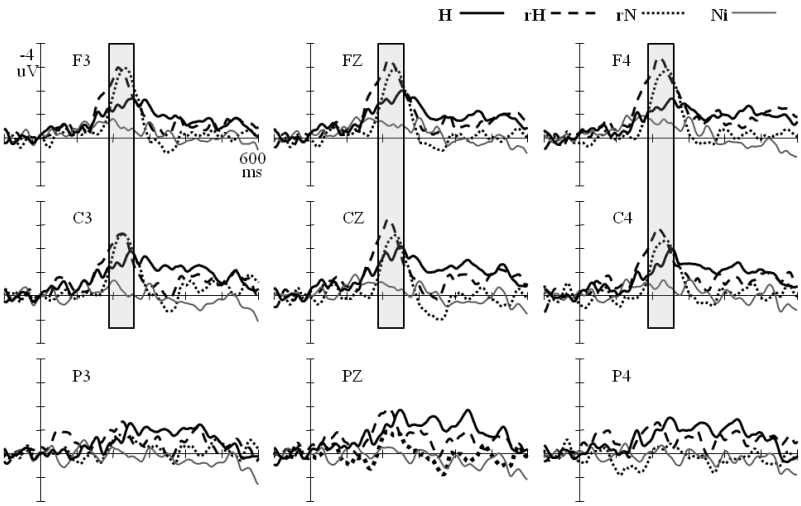

Fig. 3. ERP waveforms for deviant-minus-control difference waves. Similar results pattern was demonstrated as deviant-minus-standard waves. At 190 – 240ms, larger fronto-central mismatch responses were elicited by deviants in rH and rN conditions than H condition, while no mismatch response was elicited in Ni condition.

4 Discussion

Our experiment focused on whether vocal emotional information was encoded at an early cognitive level. Results demonstrated that although emotional deviant sounds invoked MMN, enhanced MMN was invoked by spectrally rotated sounds. The detection of emotional information can't explain this result. Since from neutral standards to emotional deviants, both emotion and acoustic properties changed; while

from neutral standards to spectrally rotated sounds which share low-level acoustic features with emotional sounds.

It is more possible that the perceived salience of change determine the mismatch effects during the early perception of emotional prosody. Based on the characteristics of MMN, larger of perceptive salience of deviants will invoke larger amplitude and earlier latency of MMN [11]. For emotional stimuli, due to the social and evolutionary importance, emotional information change is considered very prominent and can invoke MMN. This is also supported by a number studies demonstrating that emotional information can be detected and distinguished from neutral sounds implicitly [2]. While for spectrally rotated stimuli, even larger MMNs were invoked, indicating that more prominent information was perceived from neutral standards to spectrally rotated sounds. As previous studies demonstrated that from human unrotated voices to spectrally rotated sounds, amplitude envelope and duration information, pitch and pitch variation were preserved; while spectral information was distorted [7]. Actually syllable information and human vocal quality disappeared at the same time, and the rotated stimuli sound very weird. Therefore, the change from neutral unrotated standards to rotated deviant sounds would be perceived prominent and invoked even more larger MMN than emotional deviant sounds. Furthermore, two type spectrally rotated stimuli originating from neutral and emotional sounds invoked similar MMNs. This result strongly excluded the possibility that physical properties changes invoked the mismatch effects. If the MMN effects observed were due to the acoustic parameters differentiation, the brain responses of two type spectrally rotated stimuli should be different. Then it could be inferred that the larger MMN evoked by spectrally rotated stimuli might reflect a differential brain response to rotated versus unrotated sounds that is entirely unrelated to their emotional significance.

The perceived salience of change may determine the mismatch effects during early emotional prosody perception, and the domain-general change detection is considered at the early stage. This conclusion was supported by previous studies showing that early ERP components were modulated by physical properties such as pitch [3] and so on, in a bottom-up manner. More importantly, gradual and systematic amplitude increases of early P2 component were found to have relation with gradual increases of emotional intensity of voices [12] and faces [13], indicating the emotional intensity affected the early emotional prosody perception.

Spectrally rotated stimuli, due to its properties of matched acoustic features while lacking the affective perceptual quality, have been served as the unintelligible baseline condition in language comprehension studies [14]; and as acoustically matched neutral sounds in emotional prosody studies [6,7]. For instance, Warren et al. (2006) compared the perception of nonverbal emotional vocalizations to the spectrally rotated baselines, to test the brain regions responsible for arousal and valence of prosodic emotion. However, our current experiment found that the change from unrotated versus rotated sounds invoked large mismatch effects in implicit oddball paradigm, then it is inferred that the spectrally rotated properties would be perceived very prominent and invoked its corresponding brain responses. New confusing factor may be introduced by using rotated sounds. Caution should be exercised when

employing spectrally rotated stimuli as acoustically matched unintelligible baseline stimuli or neutral control sounds. Better acoustically matched stimuli should be considered in future.

In addition, neutral deviant sounds with enhanced intensity invoked no mismatch effect. Sound intensity contours do not bring any significant information when used alone [15]. Then the brain responses to minor change of intensity would be eliminated or delayed when more salient variations (changes of emotion and spectrally rotated properties) were contained in experimental context [16].

In summary, by comparing brain responses to emotional sounds and its spectrally rotated counterparts in implicit oddball paradigm, the roles of emotional information and its accompanying physical properties were separated and tested, and our study yields novel insights on early perception mechanism of emotional prosody. We demonstrate that perceived salience of change may determine the mismatch effects, and the domain-general change detection is considered at the early stage of emotional prosody perception.

Acknowledgements. This research was supported by the Natural Science Foundation of China (31070989), Open Research Fund of the State Key Laboratory of Cognitive Neuroscience and Learning (CNKOPYB0909). The authors would like to thank Lu Gao for technical support.

References

1. Ghazanfar, A.A., Santos, L.R.: Primate Brains in the Wild: the Sensory Bases for Social Interactions. Nat. Rev. Neurosci. 5(8), 603–616 (2004)
2. Thönnessen, H., Boers, F., Dammers, J., Chen, Y.-H., Norra, C., Mathiak, K.: Early Sensory Encoding of Affective Prosody: Neuromagnetic Tomography of Emotional Category Changes. Neuroimage 50, 250–259 (2010)
3. Goydke, K.N., Altenmüller, E., Möller, J., Münte, T.F.: Changes in Emotional Tone and Instrumental Timbre are Reflected by the Mismatch Negativity. Cognitive. Brain. Res. 21(3), 351–359 (2004)
4. Grandjean, D., Sander, D., Pourtois, G., Schwartz, S., Seghier, M.L., Scherer, K.R., et al.: The Voices of Wrath: Brain Responses to Angry Prosody in Meaningless Speech. Nat. Neurosci. 8(2), 145–146 (2005)
5. Juslin, P.N., Laukka, P.: Communication of Emotions in Vocal Expression and Music Performance: Different Channels, Same Code? Psychol. Bull. 129(5), 770–814 (2003)
6. Sauter, D.A., Eimer, M.: Rapid detection of emotion from human vocalizations. J. Cognitive. Neurosci. 22(3), 474–481 (2010)
7. Warren, J.E., Sauter, D.A., Eisner, F., Wiland, J., Dresner, M.A., Wise, R.J.S., et al.: Positive Emotions Preferentially Engage an Auditory–motor "mirror" System. J. Neurosci. 26(50), 13067–13075 (2006)
8. Boersma, P., Weenink, D.: Praat: Doing Phonetics by Computer (Version 5.1. 30) (Computer program) (retrieved March 24, 2010)
9. Jacquemot, C., Pallier, C., LeBihan, D., Dehaene, S., Dupoux, E.: Phonological Grammar Shapes the Auditory Cortex: A Functional Magnetic Resonance Imaging Study. J. Neurosci. 23(29), 9541–9546 (2003)

10. Näätänen, R., Kujala, T., Winkler, I.N.: Auditory Processing that Leads to Conscious Perception: A Unique Window to Central Auditory Processing Opened by the Mismatch Negativity and Related Responses. Psychophysiology 48, 4–22 (2010)
11. Näätänen, R., Paavilainena, P., Rinne, T., Alho, K.: The Mismatch Negativity (MMN) in Basic Research of Central Auditory Processing: A Review. Clin. Neurophysiol. 118, 2544–2590 (2007)
12. Chen, X., Yang, Y.: When Brain Differentiates Happy from Neutral in Prosody? In: 6th International Conference on Speech Prosody, Shanghai (2012)
13. Utama, N.P., Takemoto, A., Koike, Y., Nakamura, K.: Phased Processing of Facial Emotion: An ERP Study. Neurosci. Res. 64, 30–40 (2009)
14. Friederici, A.D., Kotz, S.A., Scott, S.K., Obleser, J.: Disentangling Syntax and Intelligibility in Auditory Language Comprehension. Hum. Brain. Mapp. 31, 448–457 (2010)
15. Audibert, N., Aubergé, V., Rilliard, A.: The Prosodic Dimensions of Emotion in Speech: the Relative Weights of Parameters. In: Interspeech 2005, Lisbon, pp. 525–528 (2005)
16. Zevin, J.D., Yang, J., Skipper, J.I., McCandliss, B.D.: Domain General Change Detection Accounts for "Dishabituation" Effects in Temporal-parietal Regions in Functional Magnetic Resonance Imaging Studies of Speech Perception. J. Neurosci. 30, 1110–1117 (2010)

Time-Dependent Multivariate Multiscale Entropy Based Analysis on Brain Consciousness Diagnosis

Li Ni[1], Jianting Cao[2,3], and Rubin Wang[1]

[1] East China University of Science and Technology
Meilong Road 130, Shanghai 200237, China
[2] Saitama Institute of Technology
1690 Fusaiji, Fukaya-shi, Saitama 369-0293, Japan
[3] Brain Science Institute, RIKEN
2-1 Hirosawa, Wako-shi, Saitama 351-0198, Japan
8nl@163.com, cao@sit.ac.jp

Abstract. The recently introduced multivariate multiscale sample entropy (MMSE) well evaluates the long correlations in multiple channels, so that it can reveal the complexity of multivariate biological signals. The existing MMSE algorithm deals with short time series statically whereas long time series are common for real-time computation in practical use. As a solution, we novelly proposed our time-dependent MMSE as an extension of MMSE. This helps us gain greater insight into the complexity of each section of time series, respectively, producing multifaceted and more robust estimates than the standard MMSE. The simulation results illustrated the effectiveness and well performance in the brain death diagnosis.

Keywords: EEG signals, Approximate entropy, Sample entropy, Brain death diagnosis.

1 Introduction

Brain death is defined as the complete, irreversible and permanent loss of all brain and brainstem functions. Under the definition, however, it's hard to conduct brain death judgement precisely for some clinical reasons. Traditional clinical tests are expensive, time consuming, and even dangerous in some cases (e. g., apnea test etc.). To avoid above disadvantages, we have proposed a EEG preliminary examination procedure before the test of spontaneous respiration, which makes the test easier, more effective and brings less risks[1]. To determine quasi brain death (QBD, where quasi- means that it's a preliminary decision), EEG which is known to us an important clinical tool for the observing brain signals, has been widely available in many countries to evaluate the absence of cerebral cortex function[1–3]. Our research aim is to provide several signal processing tools to determine brain death based on EEG analysis, and help clinicians conduct the diagnosis in the practical operation.

D. Liu et al. (Eds.): BICS 2013, LNAI 7888, pp. 75–82, 2013.

The complexity of nonlinear physiologic signals has been wildly used in evaluating the differences between health and disease states. The information of complexity contained by a physiologic time series directly reflect the state of such physiologic system[4]. The concept of entropy has been extensively available for complexity measures. Approximate entropy (ApEn) and sample entropy (SampEn) are effective approaches used in the complexity analysis, and help us have a better understanding of biological system[5, 6].

Costa has calculated a SampEn for each coarse-gained time series plotted as a function of the scale factor. This procedure to figure out an entropy for each scale is called multiscale entropy (MSE)[7], where features of multiple scale are taken into account. The coarse-grained procedure essentially represents a linear smoothing and decimation of the original time series. As a consequence, only coarse-scale or low-frequency components are captured; the high-frequency components at fine scales are lost[8, 9].

This paper presents the time-dependent extensions, since the static methods can only deal with a limited length of time series whereas the analysis of the data of long recording length is common in a biological system. The analysis on a small segment of the original data may probably cause a larger error and even a fault (for example, the segment is seriously contaminated by noise), causing misleadingness. So that the time-dependent method enables us to gain a more comprehensive and global view into a complex system. On the other hand, such dynamic method can decrease the amount of calculation in a simulation process and improve the efficiency for an analysis on a full data.

2 Methods of EEG Data Analysis

2.1 Approximate Entropy (ApEn)

In ApEn, the limited time series of N points, $U = [u_1, u_2, ..., u_N]$ represented by the form of m-dimension vectors as $X_i = [u_i, u_{i+1}, ..., u_{i+m-1}]$ and $X_j = [u_j, u_{j+1}, ..., u_{j+m-1}]$, where $i, j \leq N - m + 1$. The max distance between X_i and X_j can be calculated by

$$d[X_i, X_j] = max_{k=1,2,...,m}[|u_{i+k-1} - u_{j+k-1}|], \tag{1}$$

where d is the maximum norm in the reconstructed phase space of the system under study.

Given a threshold r and each $i \leq N-m+1$, let B_i^m be the number of vectors X_j within r of X_i, and we define

$$C_i^m(r) = \frac{B_i^m}{N-m+1}, \ where \ i \leq N-m+1, \tag{2}$$

and $\phi^m(r)$ as mean of $C_i^m(r)$

$$\phi^m(r) = \frac{1}{N-m+1} \sum_{i=1}^{N-m+1} \ln C_i^m(r). \tag{3}$$

Equation (2) is mainly defined to calculate the possibility that for each Xi and Xj, the two vectors are similar within the threshold r, while Equation (3) is used to calculate the mean of entropy known as the regularity of a time series in dimension m.

By finding $\phi^{m+1}(r)$, $ApEn(r, m, N)$ takes the form as

$$ApEn(m, r, N) = \phi^m(r) - \phi^{m+1}(r). \tag{4}$$

This is how ApEn is defined to measure the self-similarity of the time series[5].

2.2 Sample Entropy (SampEn)

SampEn deals with same m-dimension vectors X_i and X_j as defined in ApEn. The distance between two vectors is calculated by Eq. (1). In SampEn, let A_i^m denotes the number of vectors X_j within r of X_i times $(N-m)^{-1}$, for j ranges from 1 to $N-m+1$ and $j \neq i$, excluding self-matches. We then define A^m as mean of A_i^m, for all $1 \leq i \leq N-m+1$, and takes the form as

$$A^m = \sum_{i=1}^{N-m+1} \frac{A_i^m}{N-m+1}. \tag{5}$$

By increasing the space dimension to $m+1$, and also repeat the steps in Eqs. (1), (5), we can obtain A^{m+1}. Then SampEn can be obtained by

$$SampEn(m, r, N) = -\ln\left(\frac{A^{m+1}(r)}{A^m(r)}\right). \tag{6}$$

This is how SampEn is defined to measure the self-similarity of the time series[5, 6].

2.3 Multiscale Entropy Analysis

Given an one-dimensional discrete time series of length N, $U = [u_1, u_2, ..., u_N]$, by averaging the data points within non-overlapping window of the increasing scale factor ϵ, then we can have a coarse-grained time series as

$$x_j^\epsilon = \frac{1}{\epsilon} \sum_{i=(j-1)\epsilon+1}^{j\epsilon} u_i, \ where \ 1 \leq j \leq N/\epsilon. \tag{7}$$

For each new reconstructed time series of scale ϵ, find its corresponding SampEn and plot it as a function of the scale factor. The length of such time series is ϵ times shorter than the original ones, however, when $\epsilon = 1$, they are in the same length.

Similarly, for the algorithm of MMSE, the number of channels should be taken into account. Given the multivariate time series $\{u_{k,i}\}_{i=1}^N$, $k = 1, 2, ..., p$ where p

denotes the number of variables and N the number of samples in each variable, then the coarse-grained time series take the form as

$$x_{k,j}^{\epsilon} = \frac{1}{\epsilon} \sum_{i=(j-1)\epsilon+1}^{j\epsilon} u_{k,i}, \ where\ 1 \leq j \leq N/\epsilon\ and\ k = 1, 2, ..., p. \tag{8}$$

Also for each new reconstructed time series of scale ϵ, find its corresponding MSampEn (it is defined in Eq. (10)) and plot it as a function of the scale factor.

2.4 Multivariate Embedding

To calculate multivariate sample entropy, we first need to generate multivariate embedded vectors according to Takens embedding theorem for multivariate case which is first generalized by Cao et al.[10]. Given that there are p time series $\{u_{k,i}\}_{i=1}^{N}$, for $k = 1, 2, ..., p$ generated through p measurement functions $h_k(y_i)$ from the same system, the multivariate embedded reconstruction takes the form as

$$\begin{aligned} X_m(i) = [u_{1,i}, ..., u_{1,i+(m_1-1)\tau_1}, u_{2,i}, ..., u_{2,i+(m_2-1)\tau_2}, ..., \\ u_{p,i}, ..., u_{p,i+(m_p-1)\tau_p}], \end{aligned} \tag{9}$$

where embedding vector $M = [m_1, m_2, ..., m_p]$, time lag $\tau = [\tau_1, \tau_2, ..., \tau_p]$ and total dimension $m = \sum_{k=1}^{p} m_k$, $k = 1, 2, ..., p$.

2.5 Multivariate Sample Entropy

Form multivariate embedded vectors $X_m(i)$ and $X_m(j)$. Similar with the algorithm of SampEn, find $A^m(r)$ as first step, then for each channel, keep other variables unchanged and let $m_k = m_k + 1$, and find $A^{m+1}(r)$ (Both $A^m(r)$ and $A^{m+1}(r)$ are the average over all k and all i). Then multivariate sample entropy (MSampEn) can be defined as

$$MSampEn(M, \tau, r, N) = -\ln\left(\frac{A^{m+1}(r)}{A^m(r)}\right), \tag{10}$$

where r is the tolerance level, N is the time series length, M and τ are defined above.

For MMSE calculation, we've known that MSampEn is plotted as a function of scale factor. In order to describe such MSampEn-MSE-combined computing process, here we denote $MSampEn(M, \tau, r, N)_{\epsilon}$ as the mathematical expression, where the subscript ϵ represents the scale upon which MSampEn is calculated.

2.6 Time-Dependent Extensions of MMSE

Over all the channels, the original time series is divided into, for example, n_0 segments, with a certain time resolution $t^{'}$ for dynamic analysis. That is to say, for the time series $\{u_{i,k}(t)\}_{i=1}^{N}$ of the moving non-overlapping time windows from

time t_0 to T, where $t = t_0 + n \times t^{'}$, $T \geq t$ and $n = 0, 1, 2, ..., n_0$, MSampEn is then calculated over all scales. So that the expressions of time-dependent MMSE can be obtained as

$$MSampEn(M, \tau, r, N)_{t,\epsilon} = -\ln\left(\frac{A_{t,\epsilon}^{m+1}(r)}{A_{t,\epsilon}^{m}(r)}\right), \tag{11}$$

where $A_{t,\epsilon}^{m}(r)$ and $A_{t,\epsilon}^{m+1}(r)$ are both calculated in a certain time window t with the scale factor ϵ.

3 Experimental Results

In our present study, the EEG experimental protocols were executed in the ICUs of Huashan hospital, Shanghai. The EEG data were directly recorded at the bedside of patients's where high environmental noise from medical machines seriously corrupted recording procedure. The EEG recording instrument was a portable NEUROSCAN ESI-32 amplifier associated with a note computer. During EEG recording, a total of nine electrodes were placed on the forehead of the patients. Six channels were placed at corresponding electrodes (Fp1, Fp2, F3, F4, F7, F8), two electrodes (A1, A2) were placed on the ears as reference and an additional channel, GND, served as the ground, whose sampling rates were all set as $1000Hz$ and resistances of electrodes were set under $8k\Omega$. Experimental data were obtained from 35 patients (19 male, 16 female) of ages ranging from 17 to 85 years old; 19 of them were diagnosed to be comatose and the left were brain deaths.

3.1 Results for MSE and MMSE

For MSE calculation, we simulated SampEn in each time scale. Because of the shortened data length in large scales, we looked into a much longer data length of $N = 20000$ points as a compensation. Here, we gave an statistic of the total 35 patients with $m = 2$ and $r = 0.15 \times SD$ (*standard deviation*) as shown in **Fig. 1**.

For shorter scales, coma patients (red circle) showed lower complexity than QBD patients (blue asterisk), while for larger scales (larger than 58 in this case), coma patients showed higher complexity. Except the obvious difference in the value of MSE in scales, we found that for the coma patient, the value of entropy monotonically increase. On the contrary, for the QBD patient, the value of entropy almost monotonically decrease over multiple time scales. This indicates that EEG waveform of the coma patients may have much stronger self-similarity than the QBD patients in shorter scales and may become weaker in larger scales. Because the averaged data points destruct the correlation of the rhythm, but smooth the recorded environmental noise, which is an evident that brain activity exist in the comatose patients. So we propose that the monotonic property of the curves could be another criterion of brain death judgement, where monotonic property of these two states remarkably differs.

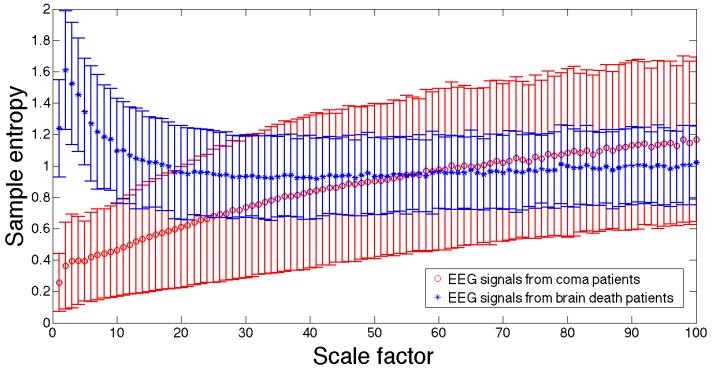

Fig. 1. Result of MSE for each 20 s ($N = 20000$) EEG data sampled from of 35 patients via a single channel with the threshold $r = 0.15 \times SD$ and scale factor ϵ ranges from 1 to 100

According to the recently introduced MMSE methods[9, 11], we could apply it to analyze EEG data here for a more comprehensive and systematic view. Our experimental data was recorded in six channels simultaneously, so the values of the parameters used to calculate MSampEn are $N = 20000$, $m = 2$, $\tau = 1$ and $r = 0.15$ for each channel. The data of different channels is normalized before analysis to make it comparable. As shown in **Fig. 2**, over the shorter time scales, MSampEn values differ for both states, which are larger for the QBD state in comparison with the coma state. Around the scale factor 33, then the magnitude happens to reverse and then keep steady over larger scales.

The obtained result for MMSE is similar with MSE, since they have maintained the common features over all the scales. This result is consistent with the fact that, unlike coma patients, brain activities of QBD patients contains complex structure across multiple time scales.

3.2 Results for Time-Dependent MMSE

For the real-time application such as monitoring a state of the patient, it is necessary to introduce time-dependent MMSE to explore the brain wave activity changes of the patients over time. As shown in **Fig. 3**, results obtained in the 3D graphics contain more comprehensive information (a) (b), which indicates that our obtained criteria of an arbitrary selected short segment of time series are also available in a time-dependent situation.

The novelly introduced time-dependent MMSE is methodologically better than standard MMSE, which calculates multivariate sample entropy in a moving time window, respectively. Compared to the static measures, our extensions allow us to gain more accurate and robust estimates. The proposed time-dependent extensions of the existent methods can deal with data in a full length, but the standard methods can only deal with data in a limited length. It is worthy mentioning that the analysis on one short segment of the original data may probably lead to a larger error and even a fault (for example, the short segment is often seriously

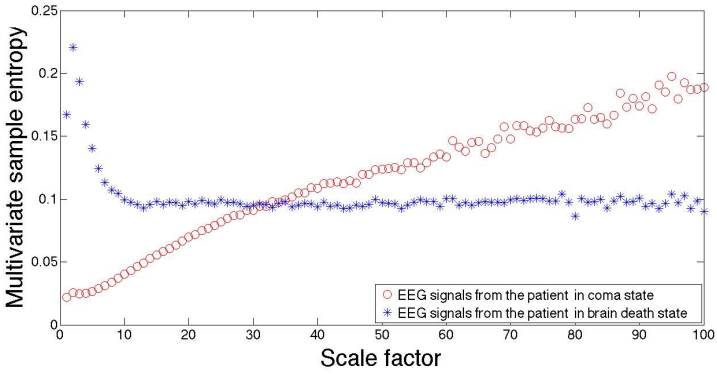

Fig. 2. Result of MMSE for each 20 s ($N = 20000$) EEG data sampled from of the certain patient via six channels with the threshold $r = 0.15$ and scale factor ϵ ranges from 1 to 100

contaminated by noise), causing misleadingness. To that case, the proposed time-dependent MMSE can be available for sifting large errors out from the reasonable results, decreasing the effect of noise in the data post-process. Moreover, the static methods on a very long time series may bring a heavy amount of calculation during the simulation process, however, if we compute in each short segments, respectively, by the proposed time-dependent MMSE, then the simulation process becomes more efficient and practical. As a consequence, the results of each segments are obtained and results of whole time series are also statistically estimated. Eventually, relying on the real-time technique, the trend of the signal over time can be well estimated, so that the dynamic method we proposed could contribute to our future-planned work, such as designing a prediction system or an automatic alarm system for the brain death diagnosis and other fields.

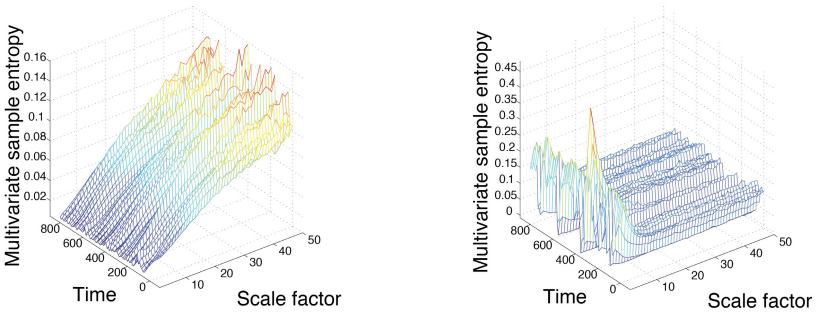

(a) (b)

Fig. 3. Results of time-dependent MMSE for the coma patient (a) and brain death patient (b), both analyzing a 800 s time of the data with a time resolution of 10 s

4 Conclusion

This paper has proposed the recently introduced complexity analysis based on calculating entropy of a time series in physiologic systems. Especially for MSE and MMSE measures, we firstly found two criteria on the judgement of quasi-brain-death. One is the value of entropy over shorter scales and another is its asymptotic and monotonic property over larger scales. Based on these criteria, we gain insight into a set of unknown raw data and obtain the result which is identical to the clinical brain death determination completely. For time-dependent extension, simulation results show great potential of its methodology and application in EEG signal processing.

Acknowledgments. This work was supported by KAKENHI (21360179, 22560425) (JAPAN), also supported by the Key Project of National Science Foundation of China (11232005) (CHINA).

References

1. Cao, J., Chen, Z.: Advanced EEG signal processing in brain death diagnosis. In: Signal Processing Techniques for Knowledge Extraction and Information Fusion, pp. 275–297. Springer (2008)
2. Guatama, T., Mandic, D.P., Van Hulle, M.M.: The delay vector variance method for detecting determinism and nonlinearity in time series. Physica D: Nonlinear Phenomena 190(3-4), 167–176 (2004)
3. Eelco, F., Wijdicks, M.: Brain death worldwide. Neurology 58, 20–25 (2002)
4. Taylor, R.M.: Reexaming the definition and criteria of death. Seminars in Neurology 17, 265–270 (1997)
5. Pincus, S.M.: Approximate entropy as a measure of system complexity. Proceedings of the National Academy of Sciences of the United State of America 88(6), 2297–2301 (1991)
6. Richman, J.S., Moorman, J.R.: Physiological time-series analysis using approximate entropy and sample entropy. AJP-Heart and Circulatory Physiology 278(6), 2039–2049 (2000)
7. Costa, M., Goldberger, A.L., Peng, C.-K.: Multiscale entropy analysis of complex physiologic time series. Physical Review Letters 89(6), 68–102 (2002)
8. Hu, M., Liang, H.: Adaptive multiscale entropy analysis of multivariate neural data. IEEE Transactions on Biomedical Engineering 59(1), 12–15 (2011)
9. Ahmed, M.U., Li, L., Cao, J., Mandic, D.P.: Multivariate multiscale entropy for brain consciousness analysis. In: Annual International Conference of the IEEE Engineering in Medicine and Biology Society, EMBC 2011, pp. 810–813 (2011)
10. Cao, L., Mees, A., Judd, K.: Dynamic from multivariate time series. Physica D: Nonlinear Phenomena 121(1-2), 75–88 (1998)
11. Li, L., Saito, Y., Looney, D., Cao, J., Tanaka, T., Mandic, D.P.: Data fusion via fission for the analysis of brain death. In: Evolving Intelligent Systems: Methodology and Applications, pp. 279–320. Springer (2010)

Cognitive Styles as Motivating Factors of Language Learners' Metaphorical Competence: A Case Study Based on Riding's CSA

Peng Wang and Chunlei Hao

Liren College, Yanshan Universitiy, 438 Heibei Street, 066004, Qinhuangdao, Hebei, China

Abstract. The paper aims to reveal the relationship between learners' cognitive styles and their metaphorical competence in English. The paper reviewed the influence of cognitive styles on SLA and the cognitive origin of metaphorical competence. The paper made a case study to look into the correlations; the case study investigated the participants' metaphorical competence in English by the designed tests, and examined their cognitive styles by Riding's CSA. The data analysis showed cognitive styles are motivating factors of metaphorical competence: the styles of verbal-imagery dimension have impact on metaphorical awareness, and holistic-analytic dimension have influence on metaphorical comprehension. Participants in the case study showed an obvious tendency of verbal style; participants tending toward holistic style were more sensitive to conceptual metaphor, and participants tending to be analytic performed better in metaphorical comprehension. Achievements in the field of cognitive styles provide new angles to researches into metaphorical competence.

Keywords: cognitive styles, metaphorical competence, Riding's CSA.

1 Introduction

Teachers and students now do more practice in listening, speaking, cultural awareness and even communication strategies while learning English, however, students who can pronounce a native like English cannot achieve the conceptual fluency in the communication, for they use English words and structures as carriers of Chinese concepts. Based on researches into conceptual metaphor and cognitive psychology, the absence of metaphorical competence in language teaching and learning is the main cause. Metaphorical Competence includes the capacity to figure out conceptual metaphors and mental imageries in the target language, and the capacity to use conceptual schema in communication [1]. Since the metal process shapes the language, and the cognitive linguistics interests in how language reveals the process, linguists look into the issue with the reference of cognitive science.

Cognitive styles "describe the manner in which people perceive, conceptualize, organize and recall information" [2]. They have great influence on language learning, and studies on the applications to language teaching have a long history, therefore,

D. Liu et al. (Eds.): BICS 2013, LNAI 7888, pp. 83–91, 2013.

cognitive styles are important factors when looking into issues in SLA. Metaphorical competence originates from cognitive sciences; it develops with the basis of improvements of cognitive linguistics, cognitive psychology and other relevant cognitive sciences.

2 Cognitive Styles and the Issues of Language Learning

The cognitive theories see language comprehension from a descriptive view: comprehension of spoken and written discourses is an active, constructive process, and it implements from attentional and encoding processes by utilization of the meaning interpreted. Language production involves selection and organizational processes in order to express meaning. Cognitive styles uncover an individual's characteristics and consistent approach to perceiving, organizing, and processing information. Many studies on cognitive styles showed that it influences a student's general approach to learning, and language learning in particular [3]. Researchers' focus on learners' cognitive styles and the application of their studies make the language teaching learner-centered, effective and efficient.

2.1 Cognitive Styles' Influence on SLA

When learners became the focus of researches into learning, there is a linkage between cognitive styles and learning. Cognitive styles refer to "preferred or habitual pattern of mental functioning; patterns of attitudes interests that affect what an individual will pay most attention to in a learning situation; a tendency to seek situations compatible with one's one learning patterns; and a tendency to use certain leaning strategies and avoid others"[4], when applied to learning. Cognitive-style researches in the 1920s and 1930s addressed such phenomena as perceptual speed and flexibility. The field independence–field dependence (FI–FD) construct in the late 1940s started with Witkin's efforts to distinguish variations in proprioception and perception of the vertical [5]. The style or dimension of Field dependence/independence (FD/FI) has received the greatest attention in the field of language acquisition. O'Malley and Chamot [6] concluded that students with the style of FI have better performance in imitation and listening comprehension than the performance of FD students, and FI students are good at communication, while FD students tend to be more proficient in language.

Cognitive styles influence language learning strategies choice among learners in the studies done by Cohen [7], Macintyre and Gardner [8], Ehrman and Oxford [9]: most FD learners preferred memory-related and compensation strategies while most FI learners preferred social, affective and memory-related strategies.

2.2 Cognitive Origin of Metaphorical Competence

The issues of conceptual metaphor and metaphorical competence actually belong to cognitive science, since their physiological foundation comes from cognition

development. Deane found the area in brain called "inferior parietal lobe", which is at the back of Broca's area and above Wernicke's area, is the key processing unit of space and language information, and its hurts lead to aphasia [10]. Deane's findings provided the solid evidence of Lakoff's "specialization of form hypothesis" proposed in 1987. The hypothesis assumed the existence of that area in brain, and pointed out special and language thoughts are carried out by the same structure in brain. Regier found certain structures in brain and even worked out "image-schemas" by the imitative model [11], which was first assumed by cognitive linguists. Many researchers realized that "metaphor cannot be seriously considered without reference to the extensive areas of cognitive science" [12]. Findings in cognitive science such as cognitive psychology, neural theory of language are the basis of developments of researches into metaphorical competence.

Since cognitive styles and metaphorical competence have the same psychological origin of cognitive science, cognitive styles have influence on learners' metaphorical competence theoretically.

2.3 Assessment of Cognitive Styles

The cognitive style of Field dependent/field independent is the early types, and it is usually measured by the Group Embedded Figures Test (GEFT), in which the participant must locate simple figures within more complex ones. It lacks an adequate and symmetrical means of measurement, and cannot truly reflect the subjects' individualized cognitive styles.

Riding and Cheema have collected more than 30 names of cognitive styles. They classified them into two basic dimensions of styles, one is holistic-analytic dimension, which represents that individuals prefer to processing information holistically or partially, and the other is verbal-imagery dimension, which represents that individuals tend to comprehend by words or by images [13]. The software system of Cognitive Styles Analysis (CSA) is the instrument; it is cognition-entered, activity-oriented, focusing on organization and processing in the cognition process, which ground on specific situation of education. The system of CSA can be applied to concrete learning tasks. The two dimensions in CSA are independent and related, thus, participants' cognitive styles can be described as holistic-verbal, holistic-imagery, analytic-imagery, and analytic-verbal. Riding also made up four fabricated persons when elaborated on cognitive styles, the person of analytic-verbal dimension is good at memorizing and presenting in words, he prefers to finish tasks by himself, and keeps distance when communicating with strangers; the person of analytic-imagery dimension is good at expressing by figures and pictures, and writes or talks in a brief way, she likes to have one companion but does not like more people working together; the person of holistic-verbal dimension lacks planning and feels difficult to tell positions, but he is good at communicating and expressing in words; the person of holistic-imagery dimension prefers learning from figures and pictures, her speaking sounds unnatural and with hesitation, and she is friendly and eager to making friends[14].Since CSA can tell the precise position in the four dimensions of styles, and personalizes the subjects' cognitive styles, thus the description of styles is more accurate than the description showed by GEFT.

3 A Case Study

A case study was carried out to look into the relationship between cognitive styles and learners' metaphorical competence in English.

3.1 Instrument for Cognitive Styles Measurement

The case study use Riding's CSA as the instrument for cognitive styles measurement, it is a computer-based, objective and bipolar measurement of the holistic/analytic cognitive style continuum and the verbal/imagery cognitive style continuum. In the verbal-imagery part of CSA, participants attempt to judge the statements whether they are right or not. There are 48 statements in all, in which 24 belong to concept sort items; the other 24 belong to imagery sort. For each sort of the statements, half are right. Participants read sentence appeared on the screen and judge whether it is right or not according to categorization in general sense. The computer records the reaction time of each item. As Table 1 shows, *V* represents the reaction time of verbal questions, and *I* represents the reaction time of imagery questions. If the value of V/I is less than or equal to 1.01, it shows the participant prefers verbal style ;and if the value more than or equals to 1.15, the participant shows a preference of imagery style, if the value stands in the range, the participant is called a dual-channel style.

Table 1. Scales for V/I dimension

	Verbal	dual-channel	Imagery
V/I	≤1.01	1.02~1.14	≥1.15

In the analytic part, the participants have to find a simple shape embedded in a more complex one. A simple figure and a complex figure are displayed side by side on the computer screen. The participants have to answer the question appeared on the screen "Is shape A contained within shape B" by pressing the button "correct" or "incorrect". The computer repeats 3 times for exercises, and 20 times with different shapes for the real test. In the part designed to measure holistic processing, the participants judge whether pairs of complex geometric figures are same or different. There are two images presented on the screen, this time participants have to press buttons for the question "is the shape A identical to shape B". This part also involves 3 exercises and 20 real questions, including 10 pairs with identical shapes. In both parts of the test the computer records the reaction times of the participants, W represents the total reaction time of holistic test, and A represents the total reaction time of analytic test. If the value W/A is less than or equals to 0.90, it means the participant prefers a holistic style; if the value is more than or equals to 1.17, the participant manifest an analytic style; if the value lies in range of 0.91 and 1.16, the participant shows a preference of intermediate style.

Table 2. Scales for W/A dimension

	Holistic	Intermediate	Analytic
W/A	≤0.90	0.91~1.16	≥1.17

3.2 Design of Tests on Metaphorical Competence

A paper test is designed for metaphorical competence including three sections, test on metaphorical awareness, test on comprehension and test on creativity. The test is designed with reference to Littlemore's test [15] and Jiang's test [16] on metaphorical competence. All the sentences contain conceptual metaphor in the tests are examples from Ungerer and Schmid' An Introduction to Cognitive Linguistics [17].

Section A is a test on metaphorical awareness. The test comprises 16 sentences of 8 pairs, for each pair there is one sentence contains conceptual metaphor, the other one is the ordinary sentence. The counterpart of each metaphorical sentence is paraphrased by three native-speaker professors of linguistics in United States. The test asked participants to sense conceptual metaphor in each pair, namely, to find out and sign the sentence with conceptual metaphor within limited time, for example, in the pairs of "He is without direction in life. He doesn't know what to do for his life." The former one contains the metaphor +LIFE IS JOURNEY+, the latter one is ordinary sentence, and the participants choose the former one to gain a score. These sentences represent different kinds of metaphors, 3 are structural metaphors, 3 are ontological metaphors, and 2 are orientational metaphors.

Section B is test on metaphorical comprehension. The test asks participants to classify the metaphorical sentences according to different source domains. The test shows participants a target domain ARGUMENT, meanwhile provides several source domains including BUILDING, JOURNEY, BATTLE, and CONTAINER. The test takes the first sentence as example "1.We have set out to prove that bats are birds." the participants write down "1" after the column +AN ARGUMENT IS A BUILDING+ , and each correct classification equals a score.

Section C is test on metaphorical creativity, it asks participants to produce more source domains for the target domain FRIEND by creating sentence like "a friend is a light, which drives away our fear and depression, brings us hope and confidence, and leads us to the right way to success". The topic of "friend" is familiar to students in college, and it is easy for them to express. They have to create as more sentences as they can within 15 minutes; the three native-speaker professors with linguistics background scored the sentences, sentences without grammar mistakes or conceptual mistake equals a score.

3.3 Participants and Testing Procedure

The participants are 61 non-English major students from a university in Qinhuangdao. 14 of them neither complete all parts of the tests, nor are their answers up to standard. There are 47 left with different levels of English, including 5 freshmen, 17 sophomores, and 25 juniors, and 31 of them have already passed CET-4, 22 of them have passed CET-6. 27 of them are male while 20 female.

30 students have taken part in the pilot study. After the pilot study, the researcher has made some refinements to the instructions and materials, to guarantee that the participants thoroughly understand the instructions and there is no new word for them. Proper timing is also found in the pilot study.

The main study was carried out as an examination. Participants were told to attend an interesting exam for English learning, and they were asked to take their laptops. A teacher showed them how to answer the questions up to standard, and 4 assistants installed the software of CSA for them. Participants were asked to take the test on MC first, 35 minutes later the papers were collected; then, participants worked on the test on cognitive styles CSA by following the directions on the screen. During the tests, teachers helped the participants to meet the requirements.

Reliability and validity of the tests are also ensured by scoring. Tests on metaphorical awareness and comprehension are designed as objective questions, and the answers to the questions are fixed, teachers scored according to the fixed answers. Test on awareness has a full mark of 8 scores, and the comprehension part has a full mark of 9 scores. For the test on creativity in English, only the sentences without grammar mistakes or conceptual mistakes are scored, then the native-speaker professors with linguistic background made a review for the results, and each metaphor gained a score. The scores the participants gain in each section show their metaphorical competence: the more scores the participants get in section A, the more sensitive they are to conceptual metaphors; high scores in section B shows the participants have a better understanding of conceptual metaphor; and high scores in section C means the participants have a good common of metaphorical creativity.

3.4 Data Analysis and Discussion

After the scoring, all the data collected were analyzed by SPSS 11.5, including the data coming from CSA.

The data analysis of test on metaphorical competences showed: the participants have the awareness of conceptual metaphor and the ability of metaphorical comprehension; they are aware of orientational metaphors, but not sensitive to ontological metaphors. They performed better in understanding primary metaphors than understanding complex metaphors: they performed worse in test on metaphorical creativity and they cannot create proper metaphors since the created metaphors are translations of the same Chinese conceptual metaphors. Since the current study focus on the relationship between cognitive styles and metaphorical competence, the paper looks into participants' cognitive styles and the correlative analysis with metaphorical competence.

In the current study, the average records of CSA showed that participants had a tendency of verbal type in the verbal-imagery dimension (SD=0.13) and an intermediate type in the holistic-analytic dimension. (SD=0.16), as table 3 below illustrated. Although this conclusion of participants' cognitive styles comes from the average person or the ideal person, the facts are that most participants belong to verbal type, and half of them belong to the holistic style and half of them belong to the analytic style, or most of them belong to the intermediate type. The results,

however, showed a tendency of participants' cognitive styles, and the results provided evidence for looking into the interrelations.

Table 4 shows the Pearson correlation between verbal-imagery dimension and metaphorical awareness is 0.420 when the significance is at the 0.01 level, the Pearson correlation between holistic-analytic dimension and metaphorical comprehension is 0.369 when the significance is at the 0.05 level. It means that styles of verbal-imagery dimension have impact on participants' metaphorical awareness to conceptual metaphor, and holistic-analytic dimension has influence on participants' metaphorical comprehension.

Table 3. Participants' average cognitive styles

	Mean	Std. Deviation	N
verbal-imagery	.9936	.12742	47
Holistic-analytic	1.0030	.16256	47

Table 4. Correlations between cognitive style and MC

		Metaphorical awareness	Metaphorical Comprehension	Metaphorical Creativity
verbal-imagery	Pearson Correlation	.420(**)	-.077	-.045
	Sig. (2-tailed)	.003	.608	.766
	N	47	47	47
Holistic-analytic	Pearson Correlation	-.031	.369(*)	-.038
	Sig. (2-tailed)	.838	.011	.799
	N	47	47	47

** Correlation is significant at the 0.01 level (2-tailed).

* Correlation is significant at the 0.05 level (2-tailed).

People with holistic style prefer to process information holistically, the verbal styles prefer to express messages by words and the imagery styles prefer to use psychological images. In the current study, 31 of participants have already passed CET-4, and 22 of them have passed CET-6, which means 65.96% of the participants have a good command of English. It coincides with the results of CSA that participants had a tendency of verbal type.

There is no linear correlation between the two dimensions and the aspects of metaphorical competence from scatter grams, but the scatter distribution showed participants of holistic style tend to be more sensitive to conceptual metaphors than those of analytic style. Littlemore found that speed in finding meaning in metaphor was significantly related to the holistic cognitive styles [15], which is accord with the results above. Participants' metaphorical awareness is tested by distinguish sentences

with conceptual metaphors from ordinary sentences in the limited time, namely the test showed whether they are sensitive to analogy in the sentence, and the holistic styles are much more sensitive. The scatter distributions showed the analytic styles tend to perform better in metaphorical comprehension than the holistic styles. The test on metaphorical comprehension asked participants to group sentences with metaphors according to different source domains in limited time. People of analytic style prefer to plan and organize by certain structure or system, participants of the style feel natural and orderly to group conceptual metaphors.

4 Conclusion

Language is an important evidence of conceptual system; different languages have different conceptual systems. Language acquisition is somewhat the acquisition of conceptual system. Therefore, conceptual fluency becomes the final goal of language learning, and learners' metaphorical competence receives more and more attentions. The case study showed that cognitive styles have influence on learners' metaphorical competence; the holistic style have a better awareness of conceptual metaphors, and the analytic styles are better in metaphorical comprehension. Since cognitive styles are motivating factors of learners' metaphorical competence, researches into the cultivation of learners' metaphorical competence cannot ignore the influence of cognitive styles. Exercises for improvement of metaphorical competence in textbooks or in class also need to involve the factors of learners' cognitive styles. The current study is a trail to researches into motivating factors of metaphorical competence, and researches into metaphorical competence connected with the traditional issues in second language acquisition, such as cognitive styles, provides a multi-perspective for the cultivation of learners' metaphorical competence.

References

1. Danesi, M.: Semiotics in Language Education. Mouton de Gruyter, Berlin (2000)
2. Ellis, R.: Instructed Second Language Acquisition: Learning in the Classroom. Blackwell, Oxford (1990)
3. Riding, R.J.: On the assessment of cognitive style: A commentary on Peterson, Deary and Austin. Personality and Individual Differences 34(5), 893–897 (2003)
4. Reid, J.M.: The Learning Style Preferences of ESL Students. TESOL Quarterly 21(1), 87–111 (1987)
5. Witkin, H.A., Goodenough, D.R.: Cognitive Styles, Essence and Origins: Field Dependence and Field Independence. International Universities, New York (1981)
6. O'Malley, J.M., Chamot, A.U.: Learning Strategies in Second Language Acquisition. Cambridge University Press, Cambridge (1990)
7. Cohen, A.D.: Language learning: Insight for Learners, Teachers, Researchers. Heinle & Heinle, Boston (1990)
8. MacIntyre, P.D., Gardner, R.C.: Anxiety and second language learning: toward a theoretical clarification. Language Learning 39(2), 251–275 (1989)

9. Ehrman, M., Oxford, R.: Effects of sex differences, Career Choice, and Psychological Type on Adults' Language Learning Strategies. The Modern Language Journal 72(3), 253–265 (1988)
10. Deane, P.: Syntax in Mind and Brain. John Benjamins, Amsterdam (1992)
11. Regier, T.: The Human Semantic Potential: Spatial Language and constrained connectionism. MIT Press, Cambridge (1996)
12. Holme, R.: Mind, Metaphor and Language Teaching. Palgrave Macmillan, New York (2004)
13. Riding, R.J., Cheema, I.: Cognitive styles—an overview and integration. Educational Psychology 11(3 &4), 193–215 (1991)
14. Riding, R.J., Wright, M.: Cognitive style, personal characteristics and harmony in student flats. Educational Psychology 15(3), 337–346 (1995)
15. Littlemore, J.: Metaphoric competence: a possible language learning strength of students with a holistic cognitive style? TESOL Quarterly 35(3), 456–491 (2001)
16. Jiang, M.: An Empirical Study of the Development of Metaphorical Competence of Chinese English Major Learners. Foreign Language Teaching Abroad 4, 27–34 (2006) (in Chinese)
17. Ungerer, F., Schmid, H.J.: An introduction to cognitive linguistics. Foreign Language Teaching and Research Press, Beijing (2008)

EEG Signal Classification Using the Event-Related Coherence and Genetic Algorithm

Chunying Fang [1,2], Haifeng Li[1], and Lin Ma[1]

[1] Harbin Institute of Technology, School of Computer Science and Technology, Harbin, China
{Lihaifeng,malin_li}@hit.edu.cn
[2] Heilongjiang Institute of Science and Technology, School of Computer and Information Engineering, Harbin, China
fcy3333@163.com

Abstract. The reliable operation of brain-computer interfaces (BCIs) based on spontaneous electroencephalogram (EEG) signals requires an accurate classification and recognition of multichannel EEG. The design of EEG representations and classifiers for BCI are open research questions whose difficulty stems from the need to extract complex spatial and temporal patterns from noisy multidimensional time series obtained from EEG measurements. This paper proposes a Genetic algorithm (GA) and Support Vector Machine (SVM) hybrid approach to accomplish this EEG classification task for potential BCI applications. An Oddball stimulus program and evoked event-related coherence program were designed to evaluate our method. The present study systematically evaluates the performance of the one channel pair event-related coherence feature set for EEG signal classification of auditory task. A GA approach for feature selection is presented which used to reduce the dimension of event-related coherence feature parameters. With the base classifiers of SVM, classification experiments are carried out upon real EEG recordings. Experimental results suggest the feasibilities of the new feature set, and we also derive some valuable conclusions on the performance of the EEG signal classification methods. The high recognition rates and the method's procedural and computational simplicity make it a particularly promising method for achieving real-time BCI system based on evoked potential event-related coherence in the future.

Keywords: EEG signal classification, Event-related coherence, Genetic algorithm, BCI.

1 Introduction

The electroencephalography(EEG) classification is one important part of the brain computer interface (BCI)[1], EEG is relatively more convenient, harmless and inexpensive than other methods[2] which provides a direct measure of cortical activity with millisecond temporal resolution[3]. By training the computer to recognize and classify EEG signals, users could manipulate the machine by merely thinking about what they want it to do within a limited set of choices[4]. Particularly relevant to the present study is a growing number of EEG classification studies which depends on

D. Liu et al. (Eds.): BICS 2013, LNAI 7888, pp. 92–100, 2013.

both the features and the classification algorithm employed. A great variety of features have been attempted to design BCI such as amplitude values of EEG signals [5], Band Powers (BP) [6], Power Spectral Density (PSD) values [7] [8], Auto Regressive (AR) and Adaptive Auto Regressive (AAR) parameters [9] [10], Time-frequency features [11] and inverse model-based features [12] [13] [14]. The used classification algorithms divided into five different categories: linear classifiers, neural networks, nonlinear Bayesian classifiers, nearest neighbor classifiers and combinations of classifiers in BCI systems [15]. However, as we know it may be difficult to build a good single classifier if feature parameters are high dimensionality and the training set is comparatively small.

Finding a suitable representation of EEG signals is the key to learning a reliable discrimination [16, 17].Oscillatory states are the most remarkable features of EEG activity, according to this view, the rhythmic synchronization during oscillatory states can serve to enhance perception, learning, and the transmission of neuronal signals between different regions of the brain[18].The EEG coherence analysis gives important information on EEG changes in long distance connections in brain areas upon application of perception/cognitive stimulations[19]. Until now, there is no study in the literature related to the analysis of event-related coherence as the feature parameters in the EEG signals classification. In a number of experiments, we found that the event-related coherence (ERCoh) from two bipolar channels (F4-M2) over the frontal and temporal areas during auditory change could be significant differentiated at different times ($p=0.035$), primarily within low alpha (8-10Hz) frequency band. Based on experience with the auditory change study, we sought to replicate the design using an ERCoh-based BCI. Furthermore, we discriminate the standard and deviant auditory stimulus. This article combined feature selection technique with the aim of reducing the number of required trials. The classifier used is a Support Vector Machine [20]. The results show that, the classification accuracy of the proposed method reaches 93% as compared to the current reported best accuracy of 84%. To this end, firstly, we designed the Oddball stimulus program and evoked potential event-related coherence experimental program, the collected EEG signals is pre-processed and pattern recognition which contained evoked potential signal, the evoked potential event-related coherence BCI system is established based on signal acquisition and processing model. The high recognition rates and the method's procedural and computational simplicity make it a particularly promising method for achieving real-time BCI system based on evoked potential event-related coherence in the future.

2 Method and Experiments

This research attempts to find a new feature parameter set and optimum algorithm to deal with the EEG signal to achieve the increase in the accuracy. The proposed model in five phases (see Fig.1), preprocessing, feature extraction, feature selection, classification, with EEG signal finally is classified into standard auditory stimuli or deviant auditory stimuli.

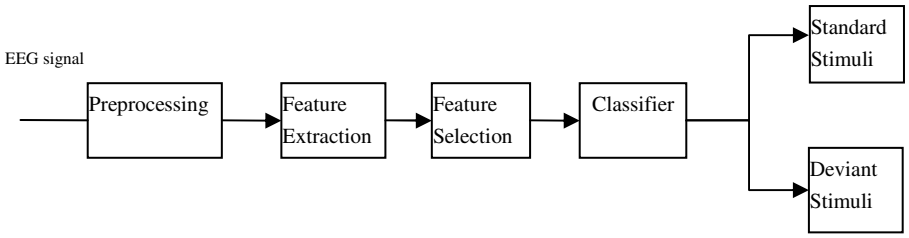

Fig. 1. Event-related coherence BCI system model

2.1 Preprocessing

The continuous electroencephalogram (EEG) was collected with Neuroscan NuAmps Amplifier, using Quick Cap with 64-channel Ag/AgCl electrodes according to the extended international 10-20 system. The reference electrode was placed on the nose tip. The vertical EOG was recorded from the right eye by supra- and infra-orbital electrodes, and horizontal EOG were recorded from electrodes on the outer canthi of both eyes. EEG and EOG signals were amplified from DC to 100 Hz at a sampling rate of 500 Hz. The electrode impedance was less than 5 kΩ throughout the experiment. After EOG artifact correction, the EEG was transformed offline to the epoch from 50ms pre-stimulus to 550ms post-stimulus. The trials contaminated with artifacts greater than ±100μV were rejected before averaging. The EEG segments were averaged separately for 150 ms with 50ms duration conditions, and the averaged ERPs were smoothed through a low-pass digital filter at 20 Hz (24 dB/octave).

2.2 Feature Extraction

We found that the event-related coherence (ERCoh) from two bipolar channels (F4-M2) over the frontal and temporal areas during auditory change could be significant differentiated at different times (p=0.035), primarily within low alpha (8-10Hz) frequency band. So we extracted the event-related coherence of F4-M2 during auditory change in the low alpha frequency band. Event-related coherence is a frequency dependent measure of the degree of linear relatedness between two channels. This symmetric measurement is computed from a collection of EEG epochs sampled from either ongoing or event-related activity. High coherence implies that amplitudes at a given frequency are correlated across EEG samples, moreover, that tends to be a constant phase angle (or time lag) between the two signals [21].

$$R_{xy} = \frac{\sum_i (x_i - \overline{x})(y_i - \overline{y})^*}{\sqrt{\sum_i (x_i - \overline{x})(x_i - \overline{x})^* \sum_i (y_i - \overline{y})(y_i - \overline{y})^*}} \quad (1)$$

Where x_i and y_i is a pair of real numbers sampled on occasion *i*. Each time series can be translated to the frequency domain as a frequency spectrum of complex numbers $x_i(f)$ and $y_i(f)$. The result is a complex correlation spectrum; finally, the coherence spectrum consists of set of real numbers ranging between 0 and 1, with 0 in the case of independence and 1 in the case of a perfect linear relationship. For each frequency, this number measures the proportion of variance in the data that can be accounted for a best-fit linear relationship between the two variables. ERCoh is computed from epoch EEG data using the coherence formulas already given. However, the frequency of interest is preselected, and the results are a function of time with respect to the event at time zero. The real and imaginary parts come from sweep-by-sweep complex demodulation rather than from sweep-by -sweep FFT.

2.3 Feature Selection

Reducing the number of features will help the classifier learn a more robust solution and achieve a better generalization performance. Feature selection algorithms fall into two categories based on whether or not they perform feature selection independently of the learning algorithm that constructs the classifier. If the technique performs feature selection independently of the learning algorithm, it follows a filter approach. Otherwise, it follows a wrapper approach [22]. Genetic algorithms can find the most efficient features of the whole space, it has been demonstrated the most efficient feature selection method for learning areas and hence has less chance to get local optimal solution than other algorithms [23] [24] [25].

Genetic algorithm belongs to the wrapper approach; therefore, classifier is very important, and we use support vector machine (SVM) classifier in this paper. The algorithm flow is shown in Figure 2.

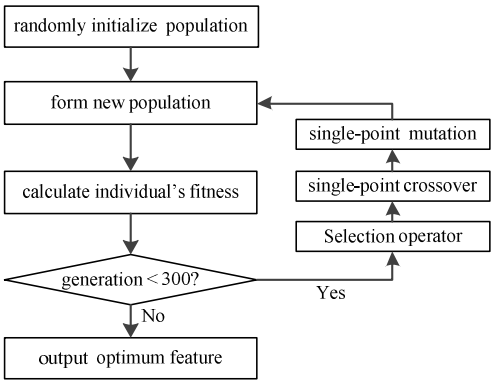

Fig. 2. The genetic algorithm flow

Encode Problem. Firstly, we must encode the problem. Here, we use a binary coded chromosome GA to select optimum feature descriptor subset for event-related coherence. Each code, namely a chromosome, corresponds to a solution of the problem.

Each gene on chromosome represents an input of the independent feature and its value can only be "0" or "1". If a gene's value is "1", it indicates that the corresponding feature is involved in the selected feature descriptor subset. On the contrary, the "0" indicates that the corresponding feature is not involved in the selected feature descriptor subset.

Initial Population. Let m as the number of feature descriptors, N the size of population. Commonly, population size N is $20 < N < 100$ and we use 60 in this paper. Chromosome of m genes is used to represent whether the corresponding feature is involved in the selected feature descriptor subset. In initial population $P = \{p_1, p_2, \cdots, p_N\}$, the genes of all individuals are randomly generated. Namely, each gene in a chromosome has value "0" or "1" randomly.

Fitness Function. Classification accuracy of SVM classifier is used to evaluate the fitness of individuals. In detail, we use the reciprocal of sum of the test set's squared errors as the fitness function, it is quite straightforward to see that.

$$f(p_k) = 1 \Big/ \sum_{i=1}^{n} (\hat{t}_i - t_i)^2 \tag{2}$$

Where $\hat{T} = \{\hat{t}_1, \hat{t}_2, \cdots, \hat{t}_n\}$ represent the predictive value of the test set classified by SVM using feature descriptor subset which p_k represents, $T = \{t_1, t_1, \cdots, t_n\}$ represent the true value of the test set, and n is the test data size.

Selection Operator. The selection operator determines an individual's genetic probability to the next generation population based on the individual's fitness. The processing is as follows:

Firstly, sum the fitness of all individual in the population:

$$F = \sum_{k=1}^{N} f(p_k) \tag{3}$$

Secondly, calculate the relative fitness of individual p_k in the population, which indicates the probability of the individual selected and inherited to the next generation:

$$\Pr(p_k) = f(p_k)/F \tag{4}$$

Finally, the simulated roulette to generate a random number between (0, 1), to determine the number of each individual selected. Obviously, larger individual's selection probability will lead to more repeatedly selected. Crossover operator uses single-point mode. The mutation operator in this paper uses the single-point mutation. We proceed with the next generation until the process reaches the maximum iteration 300 generation. When the process ends, the fittest individual is output as the optimum feature selection result.

2.4 Experiments

To this end, we designed an experiment which Fourteen healthy right-handed volunteers (4 males, 10 females; age=24.1±5.7 years) participated in this study. To eliminate circadian rhythm effects, the present experiment was carried out between 10:00 a.m. and 3:00 p.m. The task was an adaptation of the novelty "oddball" paradigm with an auditory modality, in which two types of stimuli, 1000 Hz frequent (75%) tones as non-target standard stimuli, infrequent (15%) 2000 Hz tones as targets, and rare (15%), All stimuli were presented binaurally at a sound level of 90 dB, with an exposure time of 100 ms and an inter-stimulus interval (ISI) of 600ms. The experimental session consisted of four blocks of 100 trials each, with a short time break between blocks. The EEG signal was recorded while participants were watching a self-selected, subtitled and silent film. Participants were instructed to ignore the acoustic stimuli. The continuous electroencephalogram (EEG) was collected with Neuroscan NuAmps Amplifier, using Quick Cap with 64-channel Ag/AgCl electrodes according to the extended international 10-20 system.

The event-related coherence was analyzed for low alpha (8-10 Hz) frequencies ranges, the 10 trials are were divided into one epoch in the time range of 50ms before and 550ms after the onset of auditory stimuli. The event-related coherence values for F4-M2 electrode pair were averaged across the single trials if the number of accepted trails is greater than three. The event-related coherence 302 dimension feature set is selected to form the new feature subset by genetic algorithm. The feature subset is examined with the classifier SVM, finally, the number of feature subset is 13 dimensions.

2.5 Results

SVM follows a procedure to find the separating hyperplane with the largest margin between two classes. It is based on statistical learning theory. The open source LibSVM is used to realize the SVM classifier. Firstly, to the single subject, we train the models using the two kinds(standard, deviant) of samples epoch which every epoch is consisted with 10 single trails and test is the same, the number of accept trails is greater than three to compute the event-related coherence, the accuracy rate is as shown in Table 1. Secondly, we choose ten subjects to analysis by the same method, the train set is 600 standard auditory stimuli and 100 deviant stimuli, and the test is 213 standard stimulus and 34 deviant stimulus group. The classified method is different. One is GMM(Gaussian mixture model) classifier, one is SVM(Support Vector Machine), the other is that the event-related coherence feature is selected and classified by GA and SVM, Results are as shown in table 2. Finally, the number of feature select subset is 13 dimensions, the selected feature is concentrated period of time from 100ms to 150ms and from 250ms to 300ms.

Table 1. Results of classification of single subject

	Subject 1	*Subject 2*	*Subject 3*	*Subject 4*	*Subject 5*
Accuracy	93.2%	87.2%	93.1%	93.8%	86.1%

Table 2. Results of classification of ten subjects (difference methods)

	GMM	*SVM*	*GA+SVM*
Ten subjects	53.8%	82.8%	86.6%

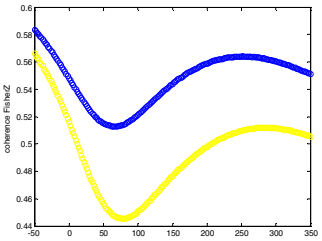

Fig. 3. The event-related coherence (Fisher-Z)(the blue is standard, the yellow is deviation)

3 Conclusions

In this paper we have presented an approach to auditory recognition based on the processing of EEG signals because the event-related coherence of auditory standard and deviation are significant differentiated (see Fig 3). Usually, the EEG signals are recorded from an electrode hat with many electrodes, such as 64, 128, and 256. Even if some electrodes unrelated to the desired task are removed, the number of remaining electrodes may still be large. In order to develop a reliable and efficient EEG signal classification system with less number of electrodes, we designed this experiment, among all fourteen subjects, we choose the relatively stable ten subject data sample and preprocess a total of 947 EEG epochs from two kinds of auditory stimuli. The number of data points in each epoch F4-M2 electrode pair is 302 depends on the event-related coherence. The classification ability of event-related coherence feature set can be measured through classification accuracy. From table 1, the best classification results in these sessions were 93.8% for subject S4, the time taken for the least three trails is lesser than 2s (1800ms). We made significant improvements in the accuracy and speed by employing powerful machine learning algorithms for classification and developing a new dynamic feature in this method. Two-class experiments show that utilization of the event-related coherence parameters as features and genetic algorithm as feature selection improve correct classification at the cost of decreased complexity and computations.

Two bipolar EEG channels prior to the reported multichannel experiment even though in the multichannel experiment no feedback was given. it can be expected that in the latter case the classification accuracy is lower [26] . However, There are shortcomings in my paper, firstly, one difficulty encountered in such a study concerns the lack of published objective comparisons between classifiers [15] [27]. Secondly, one of the major limitations on this research is the lack of the number of the subjects. In the future, find the best parameter configuration and adaptive method for each subject should be investigated. Apart from the current considered base classifiers, the

performance of some other classifiers such as k-nearest-neighbor [29] can be further investigated as well. Although our studies were done on healthy subjects, there is a chance that BCI systems such as the one presented in this paper may someday provide potentially the only communication channel for severely disabled people who are otherwise unable to articulate their thoughts and needs[28].

Acknowledgements. Our thanks to supports from the National Natural Science Foundation of China (61171186, 61271345), Key Laboratory Opening Funding of MOE-Microsoft Key Laboratory of Natural Language Processing and Speech (HIT.KLOF.20110xx), and the Fundamental Research Funds for the Central Universities (HIT.NSRIF.2012047). The authors are grateful for the anonymous reviewers who made constructive comments.

References

1. Šťastný, J., Sovka, P., Stančák, A.: EEG Signal Classification: Introduction to the Problem. Radioengineering 12, 51–55 (2003)
2. Curran, E.A., Stokes, M.J.: Learning to control brain activity: a review of the production and control of EEG components for driving brain–computer interface (BCI) systems. Brain Cogn. 51, 326–336 (2003)
3. Jahankhani, P., Kodogiannis, V., Revett, K.: EEG signal classification using wavelet feature extraction and neural networks. In: International Symposium on Modern Computing, pp. 52–57 (2006)
4. Garrett, D., Peterson, D.A., Anderson, C.W., Thaut, M.H.: Comparison of Linear and Nonlinear Methods for EEG Signal Classification. IEEE Transactions on Neural Systems and Rehabilitation Engineering 11, 141–144 (2003)
5. Kaper, M., Meinicke, P., Grossekathoefer, U., Lingner, T., Ritter, H.: Bci competition data set iib: support vector machines for the p300 speller paradigm. IEEE Transactions on Biomedical Engeneering 51(6), 1073–1076 (2004)
6. Pfurtscheller, G., Neuper, C., Flotzinger, D., Pregenzer, M.: Eeg-based discrimination between imagination of right and left hand movement. Electroencephalography and Clinical Neurophysiology 103, 642–651 (1997)
7. Chiappa, S., Bengio, S.: Hmm and iohmm modeling of eeg rhythms for asynchronous bci systems. In: European Symposium on Artificial Neural Networks, ESANN (2004)
8. Millan, J.R., Mourino, J.: Asynchronous BCI and local neural classifiers: An overview of the Adaptive Brain Interface project. IEEE Transactions on Neural Systems and Rehabilitation Engineering, Special Issue on Brain-Computer Interface Technology (2003)
9. Penny, W.D., Roberts, S.J., Curran, E.A., Stokes, M.J.: Eeg-based communication: a pattern recognition approach. IEEE Transactions on Rehabilitation Engeneering 8(2), 214–215 (2000)
10. Pfurtscheller, G., Neuper, C., Schlogl, A., Lugger, K.: Separability of eeg signals recorded during right and left motor imagery using adaptive autoregressive parameters. IEEE Transactions on Rehabilitation Engineering 6(3) (1998)
11. Wang, T., Deng, J., He, B.: Classifying eeg-based motor imagery tasks by means of time-frequency synthesized spatial patterns. Clinical Neurophysiology 115(12), 2744–2753 (2004)

12. Qin, L., Ding, L., He, B.: Motor imagery classification by means of source analysis for brain computer interface applications. Journal of Neural Engineering, 135–141 (2004)
13. Kamousi, B., Liu, Z., He, B.: Classification of motor imagery tasks for brain-computer interface applications by means of two equivalent dipoles analysis. IEEE Transactions on Neural Systems and Rehabilitation Engineering 13, 166–171 (2005)
14. Congedo, M., Lotte, F., Lecuyer, A.: Classification of movement intention by spatially filtered electromagnetic inverse solutions. Physics in Medicine and Biology 51(8), 1971–1989 (2006)
15. Lotte, F., Congedo, M., Lécuyer, A., Lamarche, F., Arnaldi, B.: A Review of Classification Algorithms for EEG-based Brain-Computer Interfaces. Journal of Neural Engineering 4 (2007)
16. Sun, S., Zha, C.: An optimal kernel feature extractor and its application to EEG signal classification. Neurocomputing 69, 1743–1748 (2006)
17. Inouye, T., Shinosaki, K., Iyama, A., Matsumoto, Y.: Localization of activated areas and directional EEG patterns during mental arithmetic. Electroencephalography and Clinical Neurophysiology 86(4), 224–230 (1993)
18. Anderson, C.W., Devulapalli, S.V., Stolz, E.A.: Determining mental state from EEG signals using neural networks. Scientific Programming 4(3), 171–183 (1995)
19. Anderson, C.W., Devulapalli, S.V., Stolz, E.A.: EEG signal classification with different signal representations. In: Girosi, F., Makhoul, J., Manolakos, E., Wilson, E. (eds.) Neural Networks for Signal Processing V, pp. 475–483. IEEE Service Center, Piscataway (1995)
20. Suykens, J.A.K., Van Gestel, T., De Brabanter, J., De Moor, B., Vandewalle, J.: Least Squares Support Vector Machines. World Scientific, Singapore (2002)
21. Neuroscan Edit4.5.American
22. Yang, J., Honavar, V.: Feature subset selection using a genetic algorithm. Intelligent Systems and their Applications, 44–49 (1998); Iowa State Univ.
23. Ren, J., Qiu, Z., Fan, W., Cheng, H., Yu, P.S.: Forward Semi-Supervised Feature Selection. In: Washio, T., Suzuki, E., Ting, K.M., Inokuchi, A. (eds.) PAKDD 2008. LNCS (LNAI), vol. 5012, pp. 970–976. Springer, Heidelberg (2008)
24. Bu, H., Zheng, S., Xia, J.: Genetic algorithm based Semi-feature selection method. In: 2009 International Joint Conference on Bioinformatics, Systems Biology and Intelligent Computing, pp. 521–524 (2009)
25. Oh, I.S., Lee, J.S., Moon, B.R.: Hybrid genetic algorithms for feature selection. IEEE Transactions on Pattern Analysis and Machine Intelligence 26(11), 1424–1437 (2004)
26. Pfurtscheller, G., Neuper, C., Flotzinger, D., Pregenzer, M.: EEG based discrimination between imagination of right and left hand movement. Electroenc. Clin. Neurophys 103(5), 1–10 (1997)
27. Schalk, G., McFarland, D.J., Hinterberger, T., Birbaumer, N., Wolpaw, J.R.: Bci2000: a generalpurpose brain-computer interface (bci) system. IEEE Transactions on Biomedical Engeneering 51(6), 1034–1043 (2004)
28. Thulasidas, M., Guan, C., Wu, J.: Robust Classification of EEG Signal for Brain–Computer Interface. IEEE Transactions on Neural Systems and Rehabilitation Engineering 14(1) (2006)
29. Sun, S., Zhang, C., Zhang, D.: An experimental evaluation of ensemble methods for EEG signal classification. Pattern Recognition Letters 28, 2157–2163 (2007)

Research on Formation Control for Hybrid Multi-robot Based on Leader-Follower

Cuicui Zhang and Yong Zhang

School of Electrical Engineering, University of Jinan, Jinan 250022, China
zhangc1124@163.com, cse_zhangy@ujn.edu.cn

Abstract. For the problem of formation control of multiple robot system, a kind of formation control for hybrid Multi-robot based on Leader-Follower is proposed in this paper. The main leader searches an optimal path fast by using GPSO-PF algorithm, which is starting point to the target point, at the same time, using KLSPI algorithm avoids obstacle independently; The movement of the second leader in accordance with the key points, which are planned by the main leader, and combined with their own sensor information and formation width adjust formation shape, which make the followers and its matched the second leader keep expected distance and angle relation, then control formation shape. Simulation results are given to demonstrate the effectiveness of the proposed formation control method.

Keywords: multi-robot system, formation control, leader-follower, obstacle avoidance.

1 Introduction

There is generally some animal's group formation behavior such as fish, birds in nature, which is a reflection of the cooperation. They have the characteristics of keeping a certain set shape or fixed relative position in movement process so that resist outside intruders or stalk its prey. Inspired by this, some researchers introduce this formation behavior of animals into formation control problem of multiple mobile robot system, which makes multi-robot system outbalance single robot in some ways.

(1) The accuracy and validity of acquiring environmental information;
(2) The benefit to coordination and cooperation between individuals;
(3) The improvement of work efficiency;
(4) Against outside invasion ability and system robustness enhancement.

Formation control problem has already been applied in many fields. for example, the specific formation of multi-robot system can be used to handle large objects in industry; Multiple independent cars are used to complete the tasks of investigation, patrol after formation in the military; Police field, multiple mobile robots compose arc to surround or capture the invaders through the formed formation; Completing the tasks of harvest crops, seeding[1] in Civil; Aerospace field, they are used to explore in the unknown area, not only reduce the high cost, but also make the ability of individual

D. Liu et al. (Eds.): BICS 2013, LNAI 7888, pp. 101–109, 2013.

robot of the system to full play; In addition, they also can be used to search and rescue work in some special occasions (flood or earthquake). Therefore, the research of formation control problem will have important theoretical and realistic significance.

AS robot cooperation system [2] typical and representative one of the key technologies, robot formation control includes formation formed and formation control [3]. At present, according to solve different ways of thinking of the formation control, basically have three algorithms: leader-follower, based on behavior [4-5] and virtual structure [6-9]. Among them, leader-follower [10-12] was put forward by the German economist Heinrich Freiherr for the first time in 1934, which is a kind of method of using the earliest, widely popular of Multi-robots formation control method. For the formation group of multi-robots, the basic idea is that one or several robots are designated as the leader, the rest of the robots are followers, followers only holding the relationship of position or direction between the matched leaders. This method not only simplifies the complex formation control problem, and but also its structure is easy to expand; the overall performance of the formation shape won't be big affected because of increasing or decreasing the number of robot. Due to the lack of system formation feedback mechanism, when motion state of the pilot or the follower goes wrong, this may lead to the failure of formation. Therefore, in view of the shortcomings of above traditional leader-follower method, formation control method for hybrid multi-robot based on the leader-follower is proposed by this paper.

This paper is organized as follows. In Sect. II, a description of GPSO-PF algorithm is presented and the mobile robot autonomous obstacles avoidance based on KLSPI algorithm is explained. In Sect.III, formation control for hybrid multi-robot based on Leader-Follower is described in detail. To show the effectiveness of the proposed algorithm, simulation results are given in Sect.IV. Conclusions are given in the last section.

2 Description of the Algorithm

2.1 GPSO-PF Algorithm

In order to solve the problem of traditional particle filtering method, which are lack of particle and to realize the system state estimation by increasing the number of particles (initial state unknown), usually integrate in thought of PSO based on the particle filter algorithm, its purpose is to optimize particle filter sampling process, and finally make particle motion to the large area of posterior probability value. Using PSO algorithm can make all particles of particle set to large area movement of posterior probability value, but particle velocity of the algorithm can't be controlled without special mechanism, so it's difficult to determine the parameters value such as the maximum speed and position. Hence, GPSO-PF algorithm is adopted by this paper. Specific implementation steps of particle filter based on GPSO algorithm are as follows.

Step1. The acquisition of measurement value

$$Z_k \sim f = \exp\left[-\frac{1}{2R_k}(Z_k - \hat{Z}^{i}_{k|k-1})^2 \right] \tag{1}$$

Among formula, z_k means the latest measurement value; $\hat{z}_{k|k-1}$ means prediction measuring value.

Step2. Initialization

In the moment of k=0, sampling N particles from the importance density function, and with $\left\{x_{0:k}^i, 1/N\right\}_{i=1}^N$ presentation, importance density function adopts transfer prior probability.

$$x_k^i \sim q(x_k^i \mid x_{k-1}^i, z_k) = p(x_k^i \mid x_{k-1}^i) \tag{2}$$

Step3. Calculation of importance weights

$$w_k^i = w_{k-1}^i p(z_k \mid x_k^i) = w_{k-1}^i \exp\left[-\frac{1}{2R_k}(z_k - \hat{z}_{k|k-1}^i)^2\right] \tag{3}$$

Combined with the optimal value, calculate each particle update speed and position with the following formula, which make particle approach the real state.

$$v_{k-1}^i = |randn|\,(p_{pbest} - x_{k-1}^i) + |Randn|\,(p_{gbest} - x_{k-1}^i) \tag{4}$$

$$x_k^i = x_{k-1}^i + v_{k-1}^i \tag{5}$$

Among formula, $|randn|$ and $|Randn|$ are positive random number which $abs[N(0,1)]$ emerges.

Step4. Resampling process

If $N_{eff} = 1/\sum_{i=1}^{N}(w_k^i)^2 \le N_{th}$, then go resampling, the original weighted sample will be mapped the same weighted sample.

Step5. Output

State estimation, variance estimation:

$$\hat{x}_k = \sum_{i=1}^{N_1} w_k^i x_k^i \tag{6}$$

$$p_k = \sum_{i=1}^{N_1} w_k^i (x_k^i - \hat{x}_k) \bullet (x_k^i - \hat{x}_k)^T \tag{7}$$

Step6. Determine whether the end or not, if end then it exits the algorithm, otherwise, returns Step2.

Using the above GPSO-PF algorithm for robot path trajectory is superior to PSO-PF algorithm. It is used to control the update of velocities of the particles by the Gaussian distribution. This method has good convergence.

2.2 The Mobile Robot Autonomous Obstacles Avoidance Based on KLSPI Algorithm

Kernel-based least squares policy iteration (KLSPI) is a kind of approximate policy iteration algorithm by introducing the Gaussian kernel function in LSPI algorithm. Kernel function and the corresponding reproducing kernel Hilbert space are introduced into policy iteration process thought, which can be equated to the nucleation algorithm existing linear space policy iteration algorithm. The specific steps of the algorithm are as follows.

(1) Set

①Definite kernel function $k(\bullet,\bullet)$ and its parameters;

②Algorithm stop condition and sparse change threshold u ;

③Initial strategy of random generation π_0 ;

④In the initial conditions, the observed data.

(2) Initialization of algorithm: Set iterations $t = 0$

(3) Loop

①Using $KLSTD-Q$ algorithm of integrated the approximate linear correlation analysis estimates behavior function of the current data set;

②In the current of function estimation, using the formula $\pi[t+1] = \arg\max_a Q^{\pi[t]}(s,a)$ calculates policy of optimization and improvement, and gets a new greedy policy π_{t+1} ;

③The new policy π_{t+1} produce new data sample set;

④ $t = t+1$, return①. Until the algorithm meet the requirements then stop.

Viewing $[x_t, y_t, \theta_t]$ as the position of robot in the global coordinate system; $[x_t, y_t]$ means abscissa and ordinate of the robot; θ_t is an angle between forward direction of the robot and X-axis. Figure 1(a) is a diagram of robot motion. $(s_0 \sim s_5)$ are equipped with six ultrasonic sensors in front of the robot. Assumed that d is detection range of each sensor; angle is 30. As shown in Figure 1(b). Markov decision process was showed with tetrad $\{S, A, R, P\}$, S means state space; A means action space; P means the state transition probability, meet no aftereffect; R means return function. Supposing six sensors detected environmental information means the model state. Optional action is showed by the discretization combination $(1)[0.5,0.5],(2)[0.5,0],(3)[0,0.5]$ of double angular velocity.

$$r_t = \begin{cases} -1000, & \text{(I)} \\ -k(D-d_l)-k(D-d_r), & \text{(II)} \\ -k(D-d_l), & \text{(III)} \\ -k(D-d_r), & \text{(IV)} \\ 0, & \text{(V)} \end{cases} \tag{8}$$

Remark1: K is proportional constant greater than zero; D is safe obstacle avoidance distance; d_l is average reading of left sensor; d_r is the average reading of the right sensor.

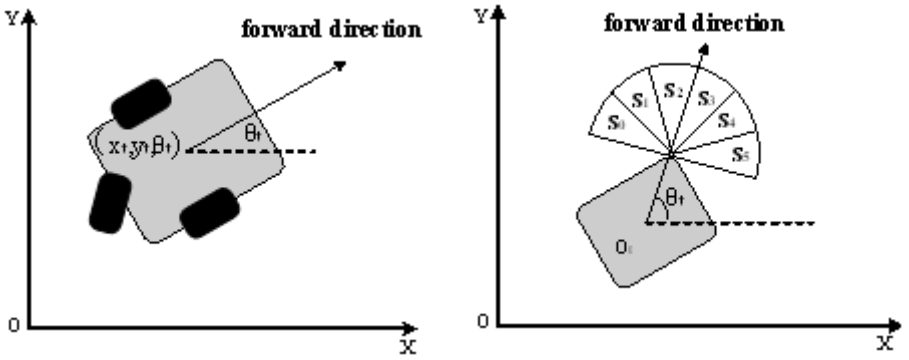

(a) Robot model (b) Robot sensor configurations

Fig. 1. Schematic diagram of mobile robot system

3 Formation Control for Hybrid Multi-robot Based on Leader-Follower

The robots of hybrid multi-robot formation control based on the leader-follower are divided into three roles: main leader, the second leaders and followers. Figure 2 is formation control chart for hybrid multi-robot. As shown in Figure 2, we observed that the formation control block consists three layers from top to bottom. The tasks of each layer are described as follows.

Top layer: With your own motion information and environmental information of observation, the main leader searches a safety path from the current position to the target point using GPSO-PF algorithm, and at the same time, plans a series of key points for the second leader of the middle layer according to its trajectory, sensor data and the width of the formation.

The middle layer: The movement of the second leader in accordance with the key point of the main leader planning and formation shape is adjusted by its own sensor information and formation width. The follower's desired movement is controlled by the closed-loop $l-\varphi$ controller.

Bottom layer: Solid control layer, which task is to keep expected distance and angle relation between the follower and its matched the second leader and completes autonomous obstacle-avoiding movement.

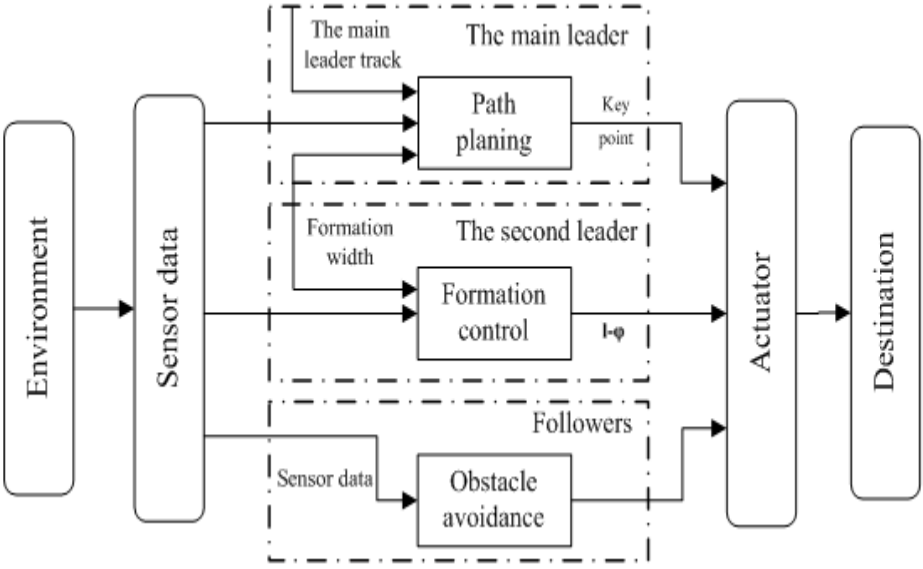

Fig. 2. Formation control structure diagram of hybrid multi-robot

In the hybrid formation control method, it is important to the key point main leaders planed to the second leader's trajectory, because the key position of the formation process is not constant. Combined with the situation of their own position information and the sensor data of observation, the second leader can make changes to the original point for adapting the environment preferable, and keep the shape of formation. Specific implementation principle is described as follows.

(1)Assume that the key points allow width of the formation to pass.

①when all the both sides machine of the whole formation can pass the current key point, at present, the second leaders need to keep main leader's position.

②when the left or right edge of the robot of whole formation can't pass the current key point and the right or left edge of the robot can pass. At this time, the whole formation can pass completely by adjusting the position of the second leader make it have certain offset toward the right or left .

(2)If the current point don't allow the existing width of the formation pass, then keep the position of original point unchanged. When the second leader move to the key point, just inform the pairing followers to take formation transformation strategy and formation's width narrow to pass the narrow area. Then the original shape of formation restores and continues to move to goal. Figure 3 shows a formation transformation example. When a set of robot of the vertical formation encounter narrow channel, longitudinal formation will be changed into triangle formation with formation

transformation strategy and then triangle formation will be changed into line formation. Then formation reverse and maintain the original formation go forward when pass the narrow area.

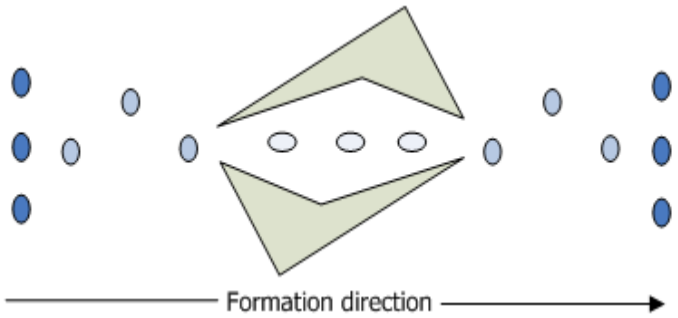

Fig. 3. Formation transformation example

4 Simulation Result

With the help of robot simulation platform Player/Stage, a simulation environment field is established. Player/Stage is an open source system [13], which provides internal interface and simulation environment for robot system. As a multithreaded robot drive server, the design of Player has independent language and supports any number of the client. Stage is a kind of simulation tool, which is used to simulate robot, sensor and obstacles of two-dimensional bitmap environment. The virtual equipment can be controlled by Player. This paper use four Amigobot robots, which are equipped with laser, sonar, position sensor as the research object, the initial position of robot are set randomly. Supposing robot 1 is the main leader; the robot 2 is the second leader; the robot 3, 4 are followers; static obstacles position are unknown. The purpose is to control the robot 2, 3, 4 to the target point (8, 6) position with triangular formation without collision.

Simulation results are shown in Figure 4. A simulation condition that four robots adopt the traditional leader-follower formation method is shown in Figure 4(a). The front of the robot (red dot) stands for a leader; the rest three robots are followers. It is not difficult to find that the last robot (blue dot) broke away from formation for meet obstacles resulting in failure of formation when formation travels to point (3, 4) position. Figure 4(b) shows that simulation result of four robot using hybrid formation method. Among them, in front of the robot (yellow dot) represents the main leader; red curve means the second leader's trajectory; blue and green curve corresponding to the path of two followers. As can be seen from the graph, when the whole formation can pass the obstacles channel, the second leader just along the main leaders' track or to the right (left) has certain offset in order that the whole formation pass completely. When the width of the formation can't pass the narrow obstacles area, at this case, the second

leader inform followers to enable formation transformation strategy so that the whole formation get through, then continue to move to target point with triangle formation. In a word, using hybrid formation method not only avoids the failure of formation as shown in Figure 4(a), but also can adjust the formation timely in the light of information of obstacles of the environment and have well the effectiveness of formation keeping.

(a) Leader-follower (b) Hybrid formation method

Fig. 4. Simulation results graph of formation control

5 Conclusion

Based on closed-loop $l-\varphi$ control and KLSPI obstacle avoidance algorithm, a kind of formation control method for hybrid multi-robot has been presented. The trajectory of the main leaders is optimized and the affects of mutations of the leader's state acts on follower are reduced by the GPSO-PF algorithm. Consequently, the stability of the formation has been improved. Simulation results show that this method can maintain desired formation shape and complete formation task. But this paper studies formation control problem based on the environment there only static obstacles. Future work is focused on the formation control problem of environment existing dynamic obstacles.

Acknowledgments. This work was supported in part by the Shandong Provincial Natural Science Foundation of China under Grant 2009CIA01001.

References

1. Su, Z., Lu, J.: Research approach to formation control of multiple mobile robots. Robot 25(1), 88–91
2. Tan, M., Fan, Y., Xu, G.: Research on control and cooperation for swarm robot systems. Robot 23(2), 178–182 (2001)

3. Ren, D., Lu, G.: Thinking in formation control. Control and Decision 20(6), 601P–606P (2005)
4. Lawton, J.R.T., Beard, R.W., Young, B.J.: A decentralized approach to formation maneuvers. IEEE Transactions on Robotics and Automation 19(6), 933–941 (2003)
5. Lawton, J.R.T., Beard, R.W., Young, B.J.: A Decentralized Approach to Elementary Formation Maneuvers. In: International Conference on Robotics and Automation, pp. 2728–2733 (2000)
6. Ghommam, J., Saad, M., Mnif, F.: Formation path following control of unicycle-type mobile robots. In: Proceedings of IEEE International Conference on Robotics and Automation, pp. 1966–1972 (2008)
7. Ren, W., Beard, R.W.: Formation feedback control for multiple spacecraft via virtual structures. IEE Proc. - Control Theory & Applications 151(3), 357–368 (2004)
8. Balakrishnan, S.N., Xin, M., Pernicka, H.J.: Multiple spacecraft formation control with O-D Method. In: Control Theory & Applications, pp. 485–493 (2007)
9. Egerstedt, M., Hu, X.: Formation Constrained Multi-Agent Control. IEEE Transaction on Robotics and Automation 17(6), 947–951 (2001)
10. Fujii, M., Yamamoto, T., Fujinami, T.: Stable formation driving of mobile robots with hybrid strategy. In: Dynamic Systems Approach for Embodiment and Soeiality, pp. 142–238 (2003)
11. Cheng, L., Wang, Y., Zhu, Q.: Communication-based multiple mobile robots formation control system. In: IEEE International Conference on Machine Learning and Cyberneties, pp. 127–132 (2004)
12. Das, A.K.: A vision-based formation control framework. IEEE Transaction on Robotics and Automation 18(5), 813–825 (2002)
13. Vaughan, R.T., Howard, A., Gerkey, B.P.: Stage User Manual 1.3. Player/Stage Project (2002), `http://playerstage.sourceforge.net`

A New Bio-inspired Unsupervised Learning Method

Kaijian Weng[1], Guoyuang Liang[1], and Xinyu Wu[1,2]

[1] Guangdong Provincial Key Laboratory of Robotics and Intelligent System,
Shenzhen Institutes of Advanced Technology, Chinese Academy of Sciences, China
[2] Department of Mechanical and Automation Engineering,
The Chinese University of Hong Kong, Hong Kong SAR, China

Abstract. Unsupervised learning has been widely used in many areas such as pattern recognition. However, it is usually difficult to acquire accurate representation of pattern within a limited period of time. Unsupervised learning, in general, is likely to be more common in brain than supervised learning. In this paper, we propose a new neural network based unsupervised learning method and evaluate its applications on 1-D and 2-D pattern learning. Our approach is inspired by recent researches on the physiological process of neural connection and brain activity. A bipolar weight scheme based on biological neural connection mechanism is presented. Moreover, we have also noticed the synaptic plasticity of brain plays an important role in learning. A new brain-inspired short-term and long-term scheme is applied in our method to adjust weights during the learning process. Experimental results of learning over 1-D and 2-D patterns demonstrate the proposed method is effective and high-efficiency.

Keywords: Unsupervised learning, Neural network, Neural plasticity, Sparse representation.

1 Introduction

Unsupervised learning is widely used in pattern recognition and artificial intelligence. For unsupervised learning or feature selection, accuracy of pattern representation and efficiency of learning are considered to be significant. Although lots of methods have been proposed in pervious works [1], [2], [3], there are still some problems, such like how to extract accurate representation of pattern, how to learn efficiently.

Self-organizing maps (SOM) [3] is one of the most famous bio-inspired models for unsupervised learning, which is an artificial neural network. It has become a very powerful and effective tool for various fields ranging from modeling the computational maps in brain to pattern recognition. One of the most important properties of SOM is that it can approach input patterns by adjusting weights so that it can acquire representations of patterns, which is critical to unsupervised learning. It can preserve the topological property of input space which is considered to be another important property. However, there are some limitations with SOM. It approaches input by competition and dynamically adjusting weights of winners and the neurons near the winner. Thus, the ability to extract good representation greatly depends on the initial

D. Liu et al. (Eds.): BICS 2013, LNAI 7888, pp. 110–117, 2013.

conditions of the system, such as values of weights, and parameters changed with time. It is usually hard for this kind of system to have accurate representation of pattern for its limited capability of adaption to representation similarity and selectivity. For example, when current input is similar enough to a previous one, there may not be any new representation generated. In an opposite case, more than one neuron may have very similar representation, which will eventually leads to redundancy. Weight adjustment in SOM usually follows Hebb's rule [4] which is simply controlled by input and output. It is unstable and vulnerable to noises.

Biological brain, such as human brain, non-human mammal's brain and even bird's brain, which has been evolving for over millions of years, is a powerful and robust system that can acquire useful information and filter noises from complex nature world [5], [6], [7]. Though the distinct mechanisms of information processing in brain are still uncertain, some evidences from brain research have revealed some underlying principles on how brains acquire and process information [8], [9], [10].

According to these researches, a new method of unsupervised learning is presented which is a neural network that aims to filter information robustly and statistically from input, acquire good representations of patterns and high efficiency of learning. In order to adjust weights for the accurate and efficient representations to inputs, we use short-term mechanism combined with long-term mechanism on the basis of synaptic plasticity which is always ignored in traditional neural network. In addition, in order to control the similarity and selectivity more easily, we propose a bipolar weight scheme in which one neuron connects to other neurons by not only excitatory connections but also inhibitory connections. This scheme is inspired by biological neural connection mechanism which widely exists in biological brain. Results of 1-D and 2-D pattern learning demonstrate our method is anti-noise and effective in representing pattern.

2 Method

The method of unsupervised learning we presented in this paper is essentially based on neural network model, where relations between inputs and outputs depend on weights adjusted during learning. Competition exists among neurons and the winner of competition has the right to adjust its weights and parameters.

2.1 Bipolar Weight

In traditional neural network model, such as SOM, weight is unipolar. That means there is only positive weight in neural network. In biological brain, however, excitatory and inhibitory connections are observed to collaborate together enabling biology to complete various tasks. For example, in visual cortex, this mechanism is considered to be the basis of visual pattern perception. Following the same mechanism, we define a bipolar weight in our system. Basically, there are two kinds of weight, namely positive weight and negative weight, which contribute to excitation and inhibition of each neuron respectively. The output of each neuron is decided by excitation and

inhibition. The positive weights of each neuron represent the pattern learned, the more input is similar to the pattern, the higher response will be. In other words, by positive weights, neuron connects strongly to the inputs that fire frequently when this neuron is winner and connects weakly to the other inputs, while the form of negative weights is totally contrary. So the distinction is enhanced and is expected to produce better learning results than traditional neural network. For example, when a new pattern occurs and one of the previous learned patterns is a part of this new pattern, without inhibition, the neuron representing the previous pattern will reach the strongest response as the previous pattern occurs. In this case, the new pattern will not be learned. That is definitely unexpected. The inhibitory strength is controlled by initial parameters and is self-adaptive in learning period, so that the selectivity or distinction of representation in neural network can be easily tuned. The details of the scheme are formulated as follows:

$$Y_j^{\pm} = \text{sigmoid}^{\pm}\left(\frac{\sum \sigma \cdot \min\left(X_i^{\pm}, WL_{ij}^{\pm}\right) + (1-\sigma) \cdot \min\left(X_i^{\pm}, WS_{ij}^{\pm}\right)}{\sum W_{ij}^{\pm}}\right), \tag{1}$$

$$X_i^{+} = X_i\,, X_i^{-} = 1 - X_i, \tag{2}$$

$$Y_j = Y_j^{+} - Y_j^{-}, \tag{3}$$

$$\text{sigmoid}^{\pm}(x) = \frac{1}{1+e^{-a^{\pm}(x-b^{\pm})}}, \tag{4}$$

$$b_{j+}^{T+1} = Y_{j+}^{T} - s,\ b_{j-}^{T+1} = Y_{j-}^{T} + s, \tag{5}$$

where $Y_j^{\pm}$, the excitatory response and inhibitory response of the j_{th} neuron, affect the final out of the j_{th} neuron Y_j. X_i is the i_{th} original input. $WL_{ij}^{\pm}$ refer to positive and negative long-term weight of the i_{th} input and the j_{th} neuron. $WS_{ij}^{\pm}$ refer to positive and negative short-term weight of the i_{th} input and the j_{th} neuron. σ is used to adjust the proportion of short-term and long-term weight. $a^{\pm}$ and s are initially preset constants used to control similarity and selectivity, while $b_{j\pm}$ are self-adaptive variables changed with time in the j_{th} neuron. (5) indicates that the system can adjust by itself according to response of output.

2.2 Weight Adjustment

For weight adjustment impacts on what to learn, it is significant to learning in a neural network. Thus a statistical and anti-noise learning mechanism or method is expected. In traditional neural network model weight usually is adjusted directly by input and output. However, in biological brain, plasticity of synapse is controlled by not only presynaptic response and postsynaptic response, but also transmitters in neural cell and gene inside nucleus [8]. The former lasts for a short period and the latter creates new synapses is long-term and even permanent. In this method a new mechanism of adjusting weights is proposed on the basis of [8]. As mentioned above, there are positive and negative weights in this model. Each positive and negative weight is

subdivided to short-term and long-term weight. For a neuron, short-term weights are changed quickly by input and output, and long-term weights are controlled by hidden variables. The details of discrete form are shown below:

$$\Delta WL_{\pm} = \rho_{\pm} \cdot [\text{sigmoid}(PI_{\pm}) \cdot Sw(X_{\pm} - WL_{\pm}) - \text{sigmoid}(-PD_{\pm}) \cdot Sw(X_{\pm} - WL_{\pm})], \tag{6}$$

$$\Delta PI_{\pm} = (X_{\pm} - WL_{\pm}) - \delta \cdot PI_{\pm} \cdot [1 - Sw(X_{\pm} - WL_{\pm})], \tag{7}$$

$$\Delta PD_{\pm} = (WL_{\pm} - X_{\pm}) - \delta \cdot PD_{\pm} \cdot [1 - Sw(WL_{\pm} - X_{\pm})], \tag{8}$$

$$PI_{\pm}^{T+1} = \Delta PI_{\pm} + PI_{\pm}^{T},\ PD_{\pm}^{T+1} = \Delta PD_{\pm} + PD_{\pm}^{T}, \tag{9}$$

$$\Delta WS_{\pm} = \rho_{\pm} \cdot [X_{\pm} - WS_{\pm}], \tag{10}$$

$$WL_{\pm}^{T+1} = \Delta WL + WL_{\pm}^{T},\ WS_{\pm}^{T+1} = \Delta WS_{\pm} + WS_{\pm}^{T}, \tag{11}$$

$$Sw(x) = \begin{cases} 1, & x \geq 0 \\ 0, & x < 0 \end{cases}, \tag{12}$$

where $WL_{\pm}$ and $WS_{\pm}$ represent long-term weight and short-term weight respectively. $PI_{\pm}$ and $PD_{\pm}$ are hidden variables modeling the chemical transmitters and genetic effect in neural cells. $\rho_{\pm}$ is learning step size. Constant δ is used to adjust the force of the second part in (7) and (8). (6) indicates that long-term weight is directly affected by not only input but also the hidden variables. (7) and (8) show that $PI_{\pm}$ and $PD_{\pm}$ are determined by external and internal factors. External factor is affected by $X_{\pm}$ and $WL_{\pm}$, and internal factor enables $PI_{\pm}$ and $PD_{\pm}$ to decrease spontaneously under certain condition. These two variables enable long-term weight to change smoothly and filter noise. Since the response of winner is set to 1, the output do not directly impact both $WL_{\pm}$ and $WS_{\pm}$. The reason of using two kinds of weights $WL_{\pm}$ and $WS_{\pm}$, includes two aspects. On one hand, $WL_{\pm}$ is changed smoothly, so it is anti-noise and stable. On the other hand, $WS_{\pm}$ changes quickly which enable neuron to approach pattern quickly though the presence of noisy so that the neuron becomes the winner in next round if the same pattern is input again. That will greatly raise the learning efficiency.

3 Results

We have designed three experiments with dataset ranges from the simplest 1-D patterns to complex 2-D patterns to evaluate performance of the presented method.

3.1 1-D Pattern Learning

First of all, we build a minimal system with one input and one neuron. In this experiment we aim to show how neuron learns from input statistically and filters noise. So there is only long-term positive weight. ρ_{+} is set to 0.5. δ is set to 0.3.

We use three inputs added with different kinds of noises illustrated in the left column of Fig.1. The results of long-term weight corresponding to the inputs are shown in the right column of Fig.1. The time span of input is 300 seconds, and the sampling rate is 1 time per second. In Fig.1 (a), the input is set to 1 in the first half of time span added with Gaussian noise and decrease to 0 added with stronger Gaussian noise every 10 sampling points in the last half. The long-term weight of the neuron, shown in Fig.1 (b), increases gradually within a short period at the beginning, then it reaches a stable state under which the value of weight undulates slightly. Though Impulse noise interfere with the input in (c) every 10 sampling points in the first half of time span, the result in (d) is similar with (b). In Fig.1 (f), input is added with strong impulse noise every 5 sampling points. However, long-term weight does not change sharply. Note that, the response value of weight is scaled by 10^{-3}. These results show that the long-term weight based on the scheme of weight adjustment can filters noise and learns from input statistically.

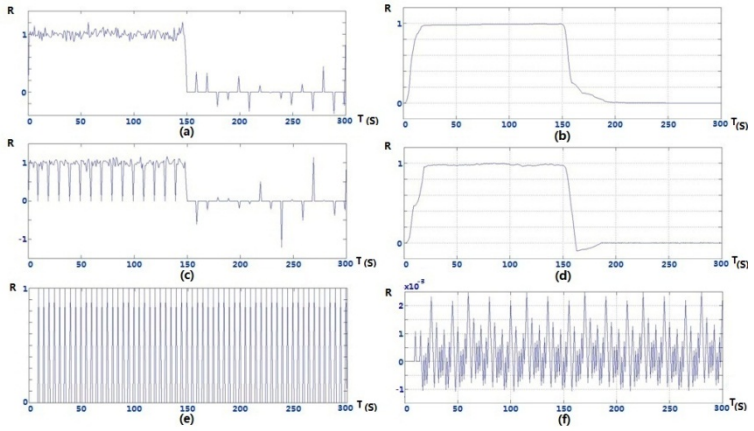

Fig. 1. The left three graphs show the inputs. The training results of long-term weight are shown on the right column. R and T denote response value and time respectively in each graph. Note that response value of weight is scaled by 10^{-3} in the last graph (f).

Then we build a complete system which has 100 inputs and one neuron in order to demonstrate the method is effective in learning 1-D pattern. The weights are initialized with random numbers. a^+ and a^- are set to 50 and 20. The s and σ are set to 0.1. $\rho_\pm$ and δ are the same in the first experiment. Five 1-D patterns with Gaussian noise and impulse noise are used as the input. We train the system for 100 epochs in each round. Each epoch contains the five patterns. The experiment is repeated for 10 rounds, since the noises added to input are random. Correlation shown in (13) is used to evaluate the difference between the representation and the patterns.

$$C = \frac{\sum WX}{\sqrt{\sum X^2}\sqrt{\sum W^2}}, \tag{13}$$

where W is the long-term weight after training and X refers to the pattern.

The first pattern and corresponding training results are illustrated in the second row in Fig.2. As we can see, the noise acutely interferes with the original pattern. However, weights do not fluctuate widely. Here, we define CPR as the correlation between prototype of pattern and representation to evaluate the accuracy of representation. ACPR refers to the average CPR of 10 rounds. We define ATC as the average training number of epochs when CPR reaches 99% of ACPR to evaluate the efficiency of learning. The results are shown in Table 1. After 10 rounds training, ACPR of each pattern is larger than 0.98 indicating that the representations of patterns are accurate. Results of ATE indicate that it needs a few iterations (ATE < 30) to acquire accurate representations.

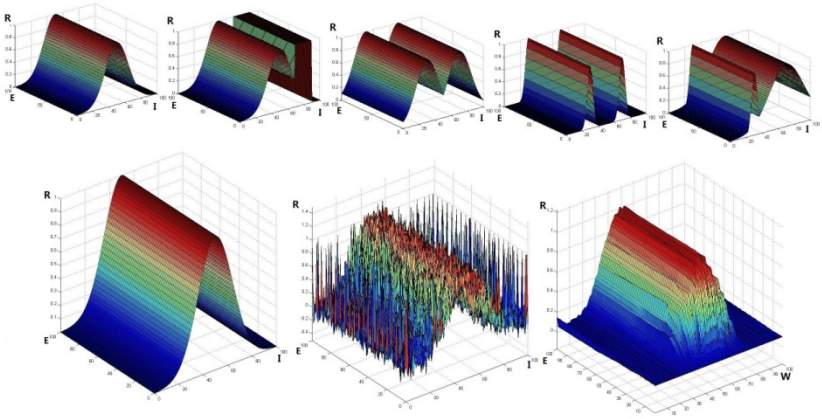

Fig. 2. The first row shows the five different patterns as input. In all graphs, E and R represent epoch and response respectively. I and W denote input and WL(long-term weights).The first pattern, the first pattern added with noise and the corresponding training result are shown on the second row.

Table 1. The five different patterns are in the left column. CPR is correlation between prototype of pattern and representation of result after 100 epochs training, and ACPR is average CPR of 10 rounds. ATE refers to average training epoch of 10 rounds when CPR reaches 99% of ACPR.

Input pattern	ACPR	ATE of CPR>0.99*ACPR
Pattern 1	0.9978	11.8
Pattern 2	0.9989	9.1
Pattern 3	0.9995	5
Pattern 4	0.9865	26.2
Pattern 5	0.9976	13

3.2 2-D Pattern Learning

We extend the system to a more complex one that contains 20 neurons to have demonstration on more challenging 2-D pattern learning. The positive weights of each neuron are set to a Gaussian-like shape randomly, and the negative weights are initialized to zero. The receptive field of each neuron has the size of 64 by 64 as same as

the size of input image. All the parameters are as the same in the second experiment. The dataset contains 10 different 2-D patterns shown in Fig.3. The experiment is repeated for 10 rounds. In each round the system are trained for 100 epochs. We define ACPN as the average correlation between prototype pattern without noise and pattern with noise to measure the strength of noise inference. We use sparseness to evaluate the redundancy of representation which is formulated as follows:

$$S_i = \frac{\sum_j N_{ij}}{N_{max}}, \quad N_{ij} = \begin{cases} 1, & C_{ij} \geq 0.9 \text{ and } C_{ij} = \max_i C_{ij} \\ 0, & otherwise \end{cases}, \tag{14}$$

where S_i is the sparseness of representation of the i_{th} pattern, N_{max} is the total number of neurons in the system, C_{ij} refers to the correlation between representation of the j_{th} neuron and the i_{th} pattern.

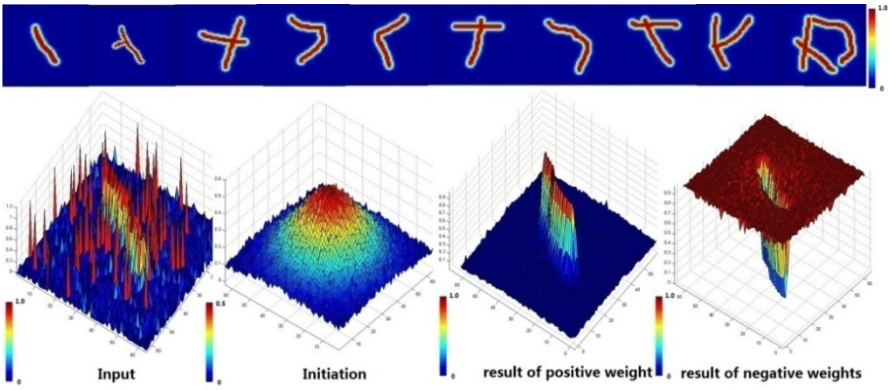

Fig. 3. The first row shows the 10 2-D patterns. The second row, from left to right, presents the first input pattern with noise, initiation of positive long-term weights, positive long-term weights of the neuron that represents the first pattern after training, and negative long-term weights of the neuron after training. Color bars illustrate range of value.

Table 2. ACPN refers to the average correlation between prototype pattern without noise and pattern with noise. ACPR and ATE are defined as the same in Table 1. AS refers to the average sparseness of representation of 10 rounds training.

Input pattern	ACPN	ACPR	ATE	AS
Pattern 1	0.7834	0.9859	54.1	0.05
Pattern 2	0.8380	0.9940	50.2	0.05
Pattern 3	0.8879	0.9963	38.3	0.05
Pattern 4	0.8835	0.9966	46.4	0.05
Pattern 5	0.8733	0.9963	46.5	0.05
Pattern 6	0.8837	0.9962	39.6	0.05
Pattern 7	0.8647	0.9954	44.7	0.05
Pattern 8	0.9066	0.9971	40.8	0.05
Pattern 9	0.8965	0.9966	39.9	0.05
Pattern 10	0.9214	0.9966	27.8	0.05

The evaluation results are listed in Table 2. Though small ACPN (as low as 0.7834) is in presence which means the noise interference is strong, ACPR, however, still reaches as high as 0.98 (mostly above 0.99), indicating the system is able to give accurate pattern representations. In addition, ATE is less than 60 for all input patterns, which verifies the proposed method is quick and efficient as well. Another important feature is sparse representation. Only one neuron out of 20 neurons (AS = 0.05) is needed to build representation for each of all 10 input patterns, as shown in Table 2.

4 Conclusion

In this paper, two kinds of bio-inspired schemes are proposed in our new unsupervised learning method. The experimental results demonstrate that the learning method can acquire accurate and low redundant representation and good efficiency of learning. Our next step is to compare with other methods by more experiments and apply this method on some pattern recognition models, such as the hierarchical model of visual cortex.

Acknowledgments. This work is partially supported by Guangdong Innovative Research Team Program (201001D0104648280), Shenzhen Nanshan Research and Design Special Fund 'Research for the Key technology of Intravenous Infusion Dispensing Robot' with Project No. KC2012JSYB0050A and Shenzhen Key Lab for Computer Vision and Pattern Recognition (CXB201104220032A).

References

1. MacQueen, J.B.: Some Methods for classification and Analysis of Multivariate Observations. In: Proceedings of 5th Berkeley Symposium on Mathematical Statistics and Probability, pp. 281–297. University of California Press (1967)
2. Bremner, D., Demaine, E., Erickson, J., Iacono, J., Langerman, S., Morin, P., Toussaint, G.: Output-sensitive algorithms for computing nearest-neighbor decision boundaries. Discrete and Computational Geometry 33, 593–604 (2005)
3. Kohonen, T.: Self-Organized Formation of Topologically Correct Feature Maps. Biological Cybernetics 43, 59–69 (1982)
4. Hebb, D.O.: The organization of behavior. Wiley & Sons, New York (1949)
5. Olshausen, B.A., Field, D.J.: Emergence of simple-cell receptive field properties by learning a sparse code for natural images. Nature 381, 607–609 (1996)
6. Carlson, E.T., Rasquinha, R.J., Zhang, K., Connor, C.E.: A Sparse Object Coding Scheme in Area V4. Current Biology 21, 228–293 (2011)
7. Li, N., Dicarlo, J.J.: Unspuervised Natural Experience Rapidly Alters Invariant Object Representation in Visual Cortex. Science 321, 1502–1507 (2008)
8. Kandel, E.R.: The Molecular Biology of Memory Storage: A Dialogue Between Genes and Synapses. Science 294, 1030–1038 (2001)
9. Anzai, A., Peng, X., Van Essen, D.C.: Neurons in monkey visual area V2 encode combinations of orientations. Nat. Neurosci. 10, 1313–1321 (2007)
10. Hegde, J., Van Essen, D.C.: Temporal Dynamics of Shape Analysis in Macaque Visual Area V2. J. Neurophysiol. 92, 3030–3042 (2004)

Research on Resource Scheduling of Cloud Based on Improved Particle Swarm Optimization Algorithm

Yan Wang, Jinkuan Wang, Cuirong Wang, and Xin Song

College of Information Science and Engineering
Northeastern University, Shenyang, 110004, China
holdwangyan@gmail.com

Abstract. Resource of cloud computing has the characteristics of dynamic, distribution, complexity. How to have the effective scheduling according to the users' QoS (Quality of Service) demand and in order to maximize the benefits is the challenge encountered in cloud computing resource allocation. In this paper, according to the characteristics of the resources of cloud computing, considering the constraints of time and budget needs of users, we designed the scheduling model of resource based on particle swarm optimization algorithm, and used the IPSO (Improved Particle Swarm Optimization algorithm) for global search to obtain the multi-objective optimization solutions that satisfies the requirements. Experimental results show that: when the IPSO applied to the resource of cloud computing compares with other algorithms, it has faster response time and could take efficient use of resource to meet the users' QoS requirements in solving multi-objective problems.

Keywords: cloud computing, QoS requirements, resource scheduling Particle, Swarm Optimization.

1 Introduction

How to provide the quality assurance for a variety of users is one of the key issues in cloud computing. Researchers considering the SLA (Service-Level Agreement)[1], propose the consistency of policy-based optimal time task scheduling resource management that users share higher bid to get more shared maintenance to ensure the user to configure the service level [2]. At the same time, the method of research of economic is introduced and game theory is used to analyze resource allocation in cloud computing [3-5]. Considering the interests of the providers of resource of cloud computing, improvement of the effectiveness of pricing is also a hot problem [6,7]. For the providers of resource, they can achieve a more efficient allocation of resources and usage through load balancing [8,9] and automatically expand, but it also brings the danger of the service failure and the service quality degradation. Therefore, how to insure the QoS, help providers efficiently organize or allocate resource, and establish a reasonable compromise between the two levels is very meaningful. This also puts forward higher requirements on the load balancing mechanism. Scheduling algorithms and models about the cloud resource load

D. Liu et al. (Eds.): BICS 2013, LNAI 7888, pp. 118–125, 2013.

balancing are proposed in [10,11], and solution of load balancing about cloud resource in business application are included in [12], although, these methods don't fully consider the needs of the users' QoS.

The basic of cloud computing is the mode of service according to the needs. Resource scheduling in cloud computing is actually the scheduling of service. And the value of cloud computing is the advantages of it in business and the users' satisfaction. Among them, the users' satisfaction is based on the service quality which is offered by the cloud computing. And the running time and cost is the main factors.

In this background, this paper tries to combine new-style optimization method suitable for the allocation of resource in cloud computing. According to the time and cost of resource scheduling problem, the characteristics of cloud computing and scheduling algorithm, we establish the corresponding scheduling model and propose the resource scheduling strategy based on IPSO. The experiments verify the feasibility of the design of IPSO. Meanwhile, comparing with the classical particle swarm algorithm, the proposed algorithm in running time and cost of total performance has a certain advantage.

2 Optimization Scheduling Model of Cloud Resource

2.1 Description of the Problem

Many different lengths of kinds of tasks can be assigned and there are different kinds of resource, give the following agreement:

a. Use the batch mode. That makes enough reasonable tasks mapping strategy.
b. The task in the scheduling process is independent.
c. The resource at the same time can only be offered to one task.
d. One task only has one kind of resource.
e. Once the task runs, the resource offered to the task can't be offered to other task until this task finishes its work.

2.2 Model

The model of resource scheduling is as follows:

a. The set of resources is $S = \{s_1, s_2, ..., s_j, ..., s_m\}$, the set of tasks is $X = \{x_1, x_2, ..., x_i, ..., x_n\}$.

b. For the allocation of resource s_j to the task x_i, the cost is c_{ij}, the expected running time is t_{ij}, the longest running time and the biggest spending that designated by the user are $T_{\max}$ and $C_{\max}$.

c. The mapping relation between tasks and resource is:

$$P = \begin{vmatrix} p_{11} & p_{12} & \cdots & p_{1j} \\ p_{21} & p_{22} & \cdots & p_{2j} \\ \cdots & \cdots & \cdots & \cdots \\ p_{i1} & p_{i2} & \cdots & p_{mn} \end{vmatrix} \tag{1}$$

Here, $p_{ij} = \begin{cases} 1, s_j \text{ is used by } x_i \\ 0, x_i \text{ doesn't use } s_j \end{cases}$

The users' Qos demand is $q = \{q_i^1, q_i^2, ..., q_i^n\}$, each dimensional is denoted by a utility function to represent what the users gained when they select resource. This paper considers efficiency of cost, efficiency of running time and the total utility as follows:

$$U_i'(q_i') = \theta_i'(C_{\max} - \sum_{i=1}^{n}\sum_{j=1}^{m} c_{ij}) \tag{2}$$

$$U_i''(q_i'') = \theta_i''(T_{\max} - \sum_{i=1}^{n}\sum_{j=1}^{m} t_{ij}) \tag{3}$$

$$U_i(q_i) = \lambda_1 U_i'(q_i') + \lambda_2 U_i''(q_i'') \tag{4}$$

$$E = \max[\sum_i U_i(q_i)] \tag{5}$$

Here, θ_i'、θ_i'' is the weight and $\lambda_1 + \lambda_2 = 1$.

3 IPSO

3.1 Design of Code

In the basic particle swarm algorithm, speed and displacement model is in the continuous numerical solution, but in this paper, resource scheduling problem is a discrete problem, so the model of speed and displacement is improved.

a. In the calculation of the speed v, take discrete coding according to one binary.

b. In the calculation of the displacement y, if the particles fly out of the boundary, it is equal to the boundary value, to ensure that the particles fly in the target space.

3.2 Design of Constraints

Dynamically adjusted based on the constraints to meet the inertia weight value ω, in order to ensure that the particles have larger inertia when the difference between the

actual value and the constraints is large. Doing this, it can have a wide range of exploring. With search, the actual values and the constraints are getting closer and closer, then ω decreases, prompting the particles in the small-scale mining global best position. ω is defined as follows:

$$\omega = \begin{cases} \dfrac{\sum |U_i(q_i) - D_i|}{\sum |T_{\max} + C_{\max} - D_i|} + 0.8, \\ \dfrac{\sum |U_i(q_i) - D_i|}{\sum |T_{\max} + C_{\max} - D_i|} \le 0.6 \\ 1.4, else \end{cases} \tag{6}$$

Here, D_i as an expense of the cost and the running time.

Definition of ω can ensure its value in [0.8,1.4], making it in balance of "explore" and "mining", also, better convergence speed and fitness value.

3.3 Multi-objective Optimization with Pareto

This paper introduces the Pareto multi-objective evolutionary method to overcome the diversity of the poor population and lack of prior knowledge. By solving the front-end, while depending on the constraints, it obtains the optimal solution.

Definition 1: given a multi-objective optimization problem $f(x)$, the set of feasible solution for the optimization objectives is S, if there is a feasible solution $x' = \{x_1', x_2', ..., x_n'\}, (x' \in S)$, for each solution $x' \in S$, $f(x') = \overset{opt}{x' \in S} f(x)$ is always true, x' is called the global optimum or global extreme point.

Definition 2: assumptions p and q are different individuals in evolutionary groups pop, if there are the relationship that p dominates q, must meet the following two conditions:

a. For all the sub-goals, p is better than q, that is $f_k(p) \le f_k(q), (k = 1, 2, ..., r)$.

b. There are at least a sub-goal that p is better than q, that is $\exists l \in \{1, 2, ..., r\}, f_l(p) \le f_l(q)$.

Here r is the number of sub-goals.

In this case, p is the non-dominated and q is dominated.

The steps of the solution are as follows:

Step 1: Initialization

a. Generate a population randomly, and the population is formed by many maps. We make first map for initial particles, set the initial velocity, test each particle whether meet the constraint condition, if not satisfied, have a initialization again.

b. Calculate the multi-objective adaptive value of each individual particle in the population, check the Pareto dominant, and store the non-inferior solution particle in the storage area f of Pareto solution set. f at least needs two particles, if not, then have a random generation.

Step 2: Adaptive Value Evaluation

Calculate the adaptive value of each particle, and use vector form for storage.

Step 3: Update of Particle

a. Update the velocity and position of individual particle, and select a value from the current Pareto solution randomly as the optimal solution in the whole population.

b. If updated particles do not satisfy the constraint conditions, then delete the particle and have a new generate randomly.

Step 4: Update f

a. According to definition 1 and 2, check the Pareto dominant situation of each particle, if a dominant particle is not a bad solution with comparison of particles in f, then put the particle in f as a Pareto solution.

b. If a particle in f is controlled by the new deposit particle, then delete the particle in f.

Step 5: Cycle

If algorithm meets the biggest iterations condition, stop the algorithm, if not, then return to step 2 continue to search. Otherwise output the mapping scheme met the constraint, then assign to a scheduling model.

4 Experimental and Results Analysis

The purpose of solution of constraint is transformation of multi-objective optimization into single objective optimization.

Parameters are as follows: the cost is selected in (1,10) randomly, and the expected implement time is selected in the interval (0.01, 1.00) randomly. The number of particle is 20, learning factor is $C_1 = C_2 = 0.9$, crossover probability is 0.8, then with equal probability for resources cross and mutation rate is 0.5.

Figure 1 and Figure 2 are the comparison of the cost using the PSO algorithm and IPSO algorithm. As shown in Figure 1 and Figure 2, in fixed number of cases (number of tasks for 100, the number of resource for 10), the experimental results show that from the beginning to the 40^{th} generation, the curve with PSO algorithm has some jitter, not very smooth, and that with the IPSO algorithm is more smooth. At about the 35^{th} generation, the algorithm with IPSO is beginning to has the convergence, but as that of the PSO, the beginning of the convergence is at about the 45^{th} generation. The reason is that we modify the weight value ω as shown in

formula (6), as it is fixed in some value range, while, this promotes the algorithm has the fast convergence. And from which it also can be seen that the value ω is an important parameter, especially for the system performance.

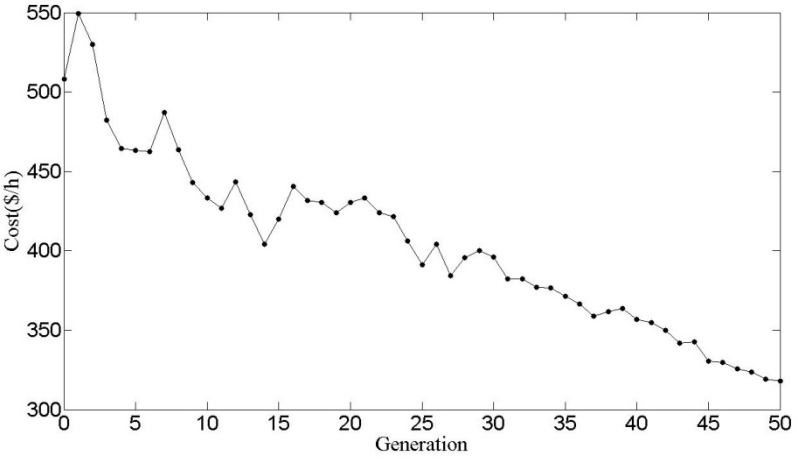

Fig. 1. Cost of PSO

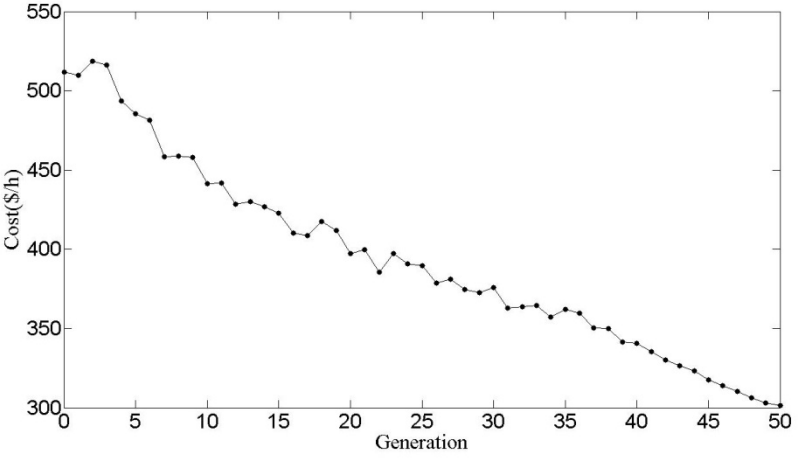

Fig. 2. Cost of IPSO

The running time of the two algorithms is shown in Figure 3 and Figure 4, as follows. Results show that the running time of the comparison is almost the same with these two algorithms, except at some generation that the time using the IPSO is short. But the whole curve of the IPSO algorithm is smooth, comparing to the PSO algorithm, before the 35th generation, the running time of which is low or high, not

very stable. The source is that the IPSO uses the method Pareto and the multi-objective optimization solutions are obtained, so which reflecting on the Figure is the decline curve without fluctuation.

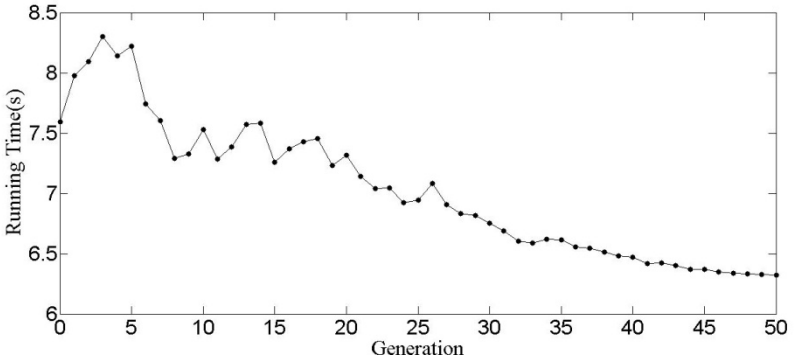

Fig. 3. Running Time of PSO

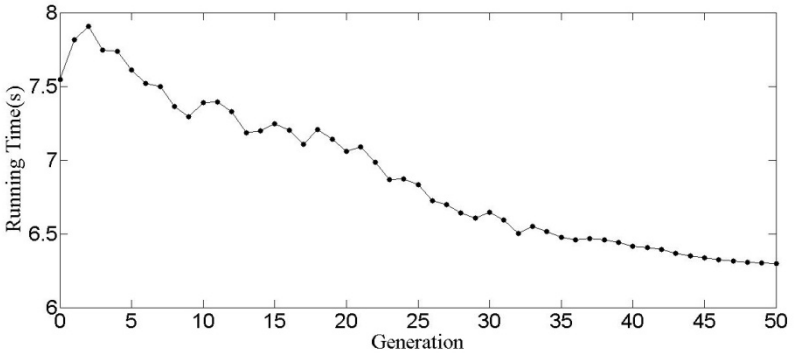

Fig. 4. Running Time of IPSO

5 Conclusion

In this paper, considering the influence of multi-objective optimization, we solve the scheduling problem of Cloud resource. We have described a resource scheduling model with IPSO algorithm for QoS constrained cloud resource, considered the cross and mutation of the genetic algorithm, and the Pareto method for Optimization. Experimental results show that the model can enhance the effective, and have a better search speed, showing certain superiority.

Acknowledgment. THE research work was supported by the Research and Development of Qinhuangdao Science and Technology Plan Self-financing Project under Grant No. 2012021A102.

References

1. Maurer, M., Emeakaroha, V.C., Brandic, I., Altmann, J.: Cost-Benefit Analysis of an SLA Mapping Approach for Defining Standardized Cloud Computing Goods. J. Future Generation Computer Systems. 28(1), 39–47 (2012)
2. Younge, A.J., von Laszewski, G., Wang, L.Z., Lopez-Alarcon, S., Carithers, W.: Efficient Resource Management for Cloud Computing Environments. In: Green Computing Conference, pp. 357–364. IEEE Press, New York (2010)
3. Wei, G., Vasilakos, A.V., Zheng, Y.: A Game-Theoretic Method of Fair Resource Allocation for Cloud Computing Services. J. Supercomputing 54(2), 252–269 (2010)
4. An, B., Vasilakos, A.V.: Evolutionary Stable Resource Pricing Strategies. In: Proceedings of ACM SIGCOMM 2009, pp. 17–21. ACM Press, New York (2009)
5. An, B., Lesser, V., Irwin, D.: Automated Negotiation with Decommitment for Dynamic Resource Allocation in Cloud Computing. In: 9th International Conference on Autonomous Agents and Multi-Agent Systems, pp. 981–988. ACM Press, New York (2010)
6. Mihailescu, M., Teo, Y.: Strategy-Proof Dynamic Resource Pricing of Multiple Resource Types on Federated Clouds. In: Frasson, C., McCalla, G.I., Gauthier, G. (eds.) ITS 1992. LNCS, vol. 608, pp. 337–350. Springer, Heidelberg (1992)
7. Gao, H.Q., Xing, Y.: Research on Cloud Resource Management Model Based on Economics. J. Computer Engineering and Design 31(19), 4139–4142 (2010)
8. Chen, Q., Deng, Q.N.: Cloud Computing and Key Techniques. J. Journal of Computer Application 29(9), 2562–2567 (2009)
9. Zhao, C., Wang, S.: Load Balancing Based on Cloud Model. J. Microelectronics & Computer 29(3), 167–169 (2012)
10. Chang, H., Tang, X.: A Load-Balance Based Resource Scheduling Algorithm under Cloud Computing Environment. In: Luo, X., Cao, Y., Yang, B., Liu, J., Ye, F. (eds.) ICWL 2010 Workshops. LNCS, vol. 6537, pp. 85–90. Springer, Heidelberg (2011)
11. Fang, Y., Wang, F., Ge, J.: A Task Scheduling Algorithm Based on Load Balancing in Cloud Computing. In: Wang, F.L., Gong, Z., Luo, X., Lei, J. (eds.) Web Information Systems and Mining. LNCS, vol. 6318, pp. 271–277. Springer, Heidelberg (2010)
12. Tejaswi, R.: Windows azure platform. Apress, New York (2009)

An Associative Memory Based on the Immune Networks: Perspectives on Internal Image with Antibody Dynamics

Chung-Ming Ou[1] and Chung-Jen Ou[2]

[1] Department of Information Management, Kainan University, Luchu 338, Taiwan
cou077@mail.knu.edu.tw
[2] Department of Electrical Engineering, Hsiuping University of Science and Technology, Taichung 412, Taiwan
crou@mail.hust.edu.tw

Abstract. Immune memory can be regarded as an equilibrium state of immune network system with nonlinear dynamical behavior. The rapid response of immune systems to the second-time antigen is owing to the stable structure of memory state forming by a closed idiotypic immune network. Internal image of an antigen is defined while memory state is formed via such network. A dynamical system of cell population based on antibody chains and tree structure is proposed which explains how the memory state is formed in the immune network. We also propose a network dynamics model of idiotypic immune network based on cross-reactive correlation matrix to fill the gap of weaker assumption for artificial immune memory. Mathematical theory of associative memory is also explored, particularly, combining network structure and dynamical systems are some breakthrough in this paper. We realize that cyclic idiotypic immune network and dynamical systems can be a cooperative description for immune memory.

Keywords: idiotypic immune network, immune memory, antibody chain, internal image.

1 Introduction

It is well-known that the injection of a given amount of some antigen into a mammal's body will stimulate the production of antibodies directed against that antigen, if the antibody is with a high affinity for that antigen. The immune system of the animal has thus learned to produce high quantities of the antibody directed against that very antigen, which is called vaccinated. Therefore, the biological immune system can learn itself and memorize the characteristics of invading antigens.

Memory in a physical system refers to the ability of the system to preserve information of its environment at some previous time. Memory mechanism of biological immune systems is still a mystery. From computational biology viewpoints, memory mechanism in immune systems can be regarded some physical

D. Liu et al. (Eds.): BICS 2013, LNAI 7888, pp. 126–135, 2013.

systems. There are basically two theories to explain the immune memory [1]. The first one is the theory of memory cells, which are generated after the B-cell proliferations. These cells will remain for an immune memory in the human body until the death of the individual. On the other hand, Immune memory mechanism can be explained through Jerne's immune network theory by investigation them as complex adaptive systems [2]. Immune memory belongs to a class of sparse and distributed associative memory [3] The concept of artificial immune memory is the following. Complex adaptive systems (CASs) have to deal with constant change of environment. Based on memory mechanism, CASs can **respond** immediately to the same or similar environment. Here we are adopting immune memory mechanisms in CASs. According to [4], it is an ongoing research topics to exploit relationship between immune memory and internal image. The internal image can be regarded as a portion of immune memory of antigen [5].

Immune memory mechanism can also be modeled from immune network theory [2] [6]. Jerne also proposed that once the foreign antigen is removed, the immune system will restore some information of such antigen by some memory mechanism. The debate of whether memory cell theory or associative property is true have been discussed. The immune memory can be explained by the following network view point. Assuming that antibody Ab_1 is produced by modeling the stimulating antigen, the production of Ab_1 is increased in the presence of another type of antibody Ab_2. The population of T-helper cell TH_1 specified by Ab_1 is also increased. In this way, Ab_2 can be considered as some "internal image" of this antigen. This image will be remained after the antigen is removed. The interactions can be a long chain with length greater than 2.

Many idiotypic network models focus on the interactions between antibodies and antigens. The network interactions provides a dynamical memory, by keeping the concentrations of antibodies, in particular those internal images [7]. However, how immune systems recalls similar antigen is still unknown. From computations view points, it is worthwhile considering state transitions which represents the network dynamics of such unfamilar pathegon. If this antigenic state converges, then immune systems gain some control and activate some (associative) recall process.

The major goal of this paper is to study the associative memory based on statistical immunodynamics inspired by [8]. This network structure will proved to be major contributions to the immune memory mechanism. The related research can be referred to Abbattista et al. [9]. The arrangement of this paper is as follows. In section 2, some preliminary knowledge of immune memory is introduced. In section 3, dynamical behavior of idiotypic immune network is described. Simulation analysis of immune network memory is also given.

2 Background Knowledge

2.1 Immune Responses

While a specific antigen invades human body, the immune system will respond by producing some antibodies which can eliminate this invaded antigen. It has

three phases, namely, first immune response, second immune response and cross-reactive response. For the first invaded antigen, the immune systems will massively produce the antibody which binds to Ag. Therefore the amount of antigen will be reduced tremendously after the peaking and tended to some constant value. We can say that immune systems are turned to the memory state. For the second phase, the same antigen invades and the antibody Ab will take much less time than that of first immune response to reach the population peak. Therefore this antigen cannot proliferate tremendously. This is the reason why we don't get sick at this stage. On the other hand, if a similar antigen Ag' invades, then the same antibody Ab will also proliferate soon and eliminate Ag' population. We will analyze the network transitions between each phases. Once the first immune response has activated, we are particularly interested in the third stage, namely the associate memory mechanism for the immune response to similar antigens.

2.2 Idiotypic Immune Network

Idiotypic network theory implies that immune systems will mimic the presence of the antigen even after it is destroyed [3]. In this way, antibody and receptor of the lymphocytes can recognize each other. The epitope of antibody molecule is called an "idiotope". An epitope of antigen A_g is recognized by the antibody molecule Ab_1 and by the receptor molecule on the lymphocyte of LU_1. The antibody Ab_1 and the receptor of LU_1 have the idiotope which is recognized by antibody Ab_2 and the receptor on the lymphocyte of LU_2. Continuously, we reach an antibody Ab_N, while the antibody Ab_1 and the receptor on the lymphocyte of LU_1 also recognize idiotopes on antibody Ab_N. Ab_N constitutes an internal image of the antigen A_g. Network forming by interactions between lymphocyte interactions. This Ab_n constitutes an internal image of the antigen Ag, see Figure 1. The idiotypic network theory has been proposed as a central aspect of the associative properties of immune memory [3] [10]. However, computational aspect of this paradigm needs to be further explored.

For simplicity, it is reasonable that we consider antibodies rather than LUs of IINs from both network dynamics and population dynamics perspectives. Some immune network models can be contributed to this antibody dynamics such as [11]. Such antigen-antibody interactions can be a long sequence structure, namely, an antibody chain, which is formerly defined as follows.

Definition 1. *For an idiotypic immune network* $\langle \{LU_i\}_{i=1}^{N}, M \rangle$*, an antibody chain* $AC = \{Ab_1, Ab_2, \cdots Ab_N\}$ *is defined as follows.*

- $Ab_i \in LU_i$*, for all* $i = 1, 2, \cdots N$*.*
- Ab_i *can recognize* Ab_{i+1}*, namely,* $Ab_i \rightarrow Ab_{i+1}$*, for all* $i = 1, 2, \cdots N-1$
- $Ab_N \rightarrow Ab_1$*.*

The final element of the antibody chain Ab_N interests us. It can stimulus the antibody Ab_1 even the Ag is destroyed. In this way, population of Ab_1 will be stable in small amount. In particular, its role in immune memory can be analyzed by network dynamics.

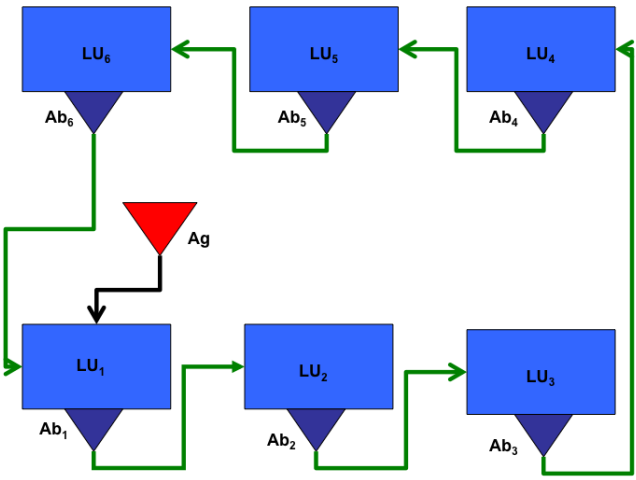

Fig. 1. Schematic diagram of the idiotypic immune network

2.3 Immune Memory

Immune system will react rapidly to the same or similar antigens which had invaded the same human body before. This phenomenon implies that immune system can "memorize" associatively the formations of previously invaded antigens. One major evidence for immune memory is that it is strongly affected by the populations of soluble antibodies in the blood. Therefore some variable quantified the immune memory can be correlated to the amount of antibodies. In fact, this is a major inspiration for this research, but different angle from computational biology.

Immune memory mechanism is not fully understood so far; according to Smith et al. [3], at the end of an immune response, when the antigen is cleared, the B cell population decreases, leaving a persistent sub-population of memory cells. The newer view of memory cells is that they are not intrinsically longer-lived than virgin cells, but that memory depends instead on the persistence of antigen [12]. However, some researches, especially those related to immune network theory, imply that mechanisms of immune memory is formed by rather cyclic idiotypic networks than specific memory cells [11]. Immunologists have discovered the vaccination mechanism for human immune systems for a long time. This takes advantages of so-called the associative memory of immune systems. The associative memory mechanism can be explain as follows [13]. If the secondary antigen is "similar" to the primary one, the set of antibodies activated by this antigen will overlap with the one activated by the primary antigen. The similarity between antigens can be defined by affinity of molecules. This memory is able to store and recall patterns when immune systems need. Associative recall is a general phenomenon of immune memory [3].

3 Main Results

3.1 Tree Structure of Idiotypic Immune Network

Perelson [14] suggested a tree structure with varied levels for idiotypic immune networks. A_g is the root note. Level 1 is the collection of all antibodies which are complementarily matching with A_g. Level 2 is the collection of all antibodies which are complementarily with those at level 1. In this way, we may construct a tree structure for antibody chain (Figure 2).We also define the directed edge $\rightarrow$ from antibody at higher level to the one at lower level. Based on this structure $T = \{A_g, AC, \rightarrow\}$, all possible internal images for a given antigen can be searched within some antibody populations. We also observe the existence of internal image can be guaranteed if and only if second level is inward and outward according to some affinity relation $\rightarrow$.

Proposition 1. *The tree structure of idiotypic immune network* $T = \{A_g, AC, \rightarrow_\epsilon\}$ *satisfies the following properties: (1) Each antibody in* AC *can be located at most one level; (2) The edge can only exist between adjacent level; (3) If* AC *is closed, then its length is even; (4) If* AC *is closed, then number of level of* T *is equal to* $\frac{N}{2} + 1$*. (5) Internal image must locate at the level 2. (6) The internal image exists if and only if* $Level(AC) = \frac{N}{2} + 1$*.*

This is obvious by definition of tree structure. If $Ab_i \in AC$ is located to Level i of T and $Ab_1 \rightarrow Ab_i$. Then Ab_i has to be located to Level 2. If $Ab_i \rightarrow Ab_j$, then Ab_j must be located at level $i + 1$. If the length of the left AC is equal to m, then the number of level is also m by the closeness of AC. The right AC is $N - m$, which is also even. However, m and $N - m$ must have difference equal to 2 by the closeness of AC and the fact that Ab_N must be located at level 2. Therefore the length of AC is equal to m+(m-2)=2m-2, which must be even. According to (3), N must be even. Ab_N and Ab_2 are at the level 2; Ab_{N-1} and Ab_3 are at the level 3; continuing in this way, $Ab_{N/2+1}$ is the unique antibody located the level $\frac{N}{2} + 1$. If $Level(AC) < \frac{N}{2} + 1$, then $length(AC_j) < \frac{N}{2} + 1$. Therefore, $length(AC) \leq \frac{N}{2} + \frac{N}{2} - 1 = N - 1$, which is a contradiction. Therefore $Level(AC) = \frac{N}{2} + 1$.

If an internal image is highly complementary match with Ab_1, then it can be regarded as an reasonable stimulus for Ab_1 even Ag is eliminated. Ab_1 plays a pivotal role for internal image. If the ϵ of the ϵ-complementary match between Ab_1 and Ag is higher, then the internal image and Ag are more similar. From mathematical viewpoint, it is still a question that Ag and its internal image may be of low similarity.

The network-layered structure for CIINs provide some evidences that the population dynamics cannot provide, such as recall process of immune memory. Every closed antibody chain $T(AC)$ can be represented as a k-level tree structure, where $k = \frac{N}{2} + 1$. Furthermore, internal image Ab_N must locate at level 2.

Theorem 1. *For idiotypic immune network* $\rightarrow$ *as the relation of "being recognized", the internal image of an antigen exists if and only if*

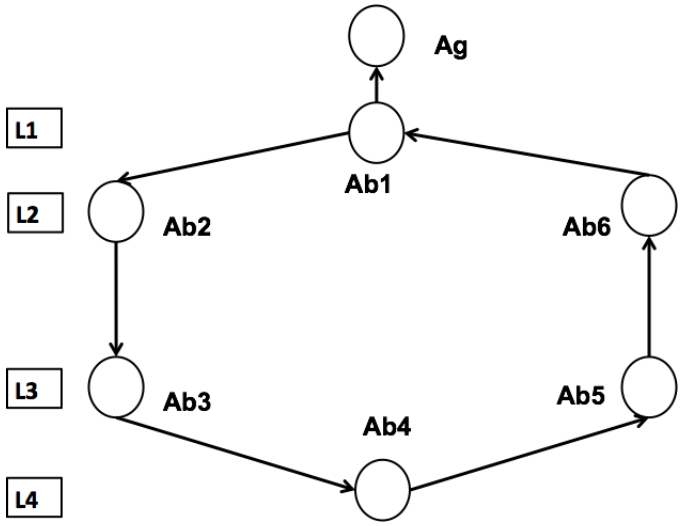

Fig. 2. Antibody Chain for Cyclic idiotypic Immune Network

- *The tree structure of AC one antibody path* P_1 *with length* $\frac{N}{2}+1$ *and the other one* $\frac{N}{2}-1$*, for some even integer* N*.*
- $P_1(end) \rightarrow P_2(1)$*.*
- $P_2(end)$ *is an internal image.*

3.2 Network Dynamics Based on Autocorrelation Matrix

From immunology viewpoints, a better antibody chain has the following two aspects: the first is that it will respond fast to the second-time antigenic invasion; the second one is that it will act adaptively to the similar antigenic invasion. The question is how to build some mathematical model to connect the concepts of tree structure with the dynamics of immune responses such as immune memory and recall ? Most importantly, response to a similar antigen rather than second. This is related to associative memory mechanism [15] [16].

The attractor networks proposed by [17] defined by tree structures can generate a dynamics. It is a transition of states represented by nodes of antigens. A network dynamics F can be defined on states of network S as follows. An antigen will induce an antibody chain, which will generate a network dynamics for interpreting immune memory formation and recall process. Moreover, this attractor network dynamics can interpret the associative property of immune memory while population dynamics cannot. Let F be a function defined on state space **S**. For a given state $S(t)$ at time t, the network dynamics can be defined as a transition of state S from time t to time $t+1$, namely, S(t+1)=F(S(t)). According to the basic concept of dynamical systems, we may define an attractor μ of the network dynamics F, if there exists a state S such that $F^n \rightarrow u$, as $n \rightarrow \infty$, where t is a temporal variable and S is the state variable. Now we define the

associative memory based on stability analysis of equilibrium points (states) of such network dynamics.

Definition 2 (Associative Memory). *For an immune network* $\{AC, F\}$*, if there exists a set of* p *antigenic patterns,* $\{\mu^1, \mu^2, \cdots, \mu^p\}$ *which are attractors of the network dynamics* F*, then we say the immune network can memorize* p *patterns of antigens associatively.*

The stable states of immune networks can guarantee that if an antigenic format fallen into the basin of attraction of μ_k, then by memory recalling process, this antigen can invoke the same antibody proliferation immediately. The following question arises: what is the mathematical model of network dynamics F, if an antigen-antibody chain (Ag, AC) is given. We will first concentrate on some binary-valued function F to illustrate the dynamics of immune memory, rather than on discussing some complex and high-dimensional dynamical systems.

This mechanism is named autocorrelation matrix memory (ACMM) inspired by [17]. For an antigen Ag, there exists an antibody chain AC such that it is a CIIN. This AC will induce a autocorrelation matrix W as

$$W = \frac{1}{n} \sum_{i=1}^{N-1} Ab_i^T * Ab_{i+1} \tag{1}$$

Given a pattern S such as an antigen as an initial state $X(0)$, the network dynamics of W is given by $X(t+1) = sgn(W \cdot X(t))$, where $sgn(x_i(t)) = 1$, if $x_i(t) > 0$; $sgn(x_i(t)) = -1$, if $x_i(t) < 0$. If $X(t) \to S$, as $t \to \infty$, then we call S a memory format (MF). Therefore, an antigen activates an antibody chain whose network dynamics can generate antigenic memory format.

3.3 Associative Memory Formed by the Immune Systems

How immune memory pertains associativity is still a mystery for scientists even for the advances and success of vaccinations for more than 300 years. However, we propose a network dynamics model to describe this mechanism from computational immunology viewpoints. An immune network $\langle \{LU_i\}_{i=1}^N, M \rangle$ is equipped with with associative memory, if for any $\epsilon > 0$, there exists $\alpha > 0$, such that whenever a new antigen Ag' with $d(Ag, Ag') < \alpha$ implies that $Ag' \to_\epsilon Ab_1$.

If a new antigen Ag', which is very similar to the previous invaded antigen Ag, invades human body, then the antibody Ab_1 which binds Ag can also bind Ag' and invokes another immune response. For an antigen Ag activating the antibody chain AC, the network dynamics defined on pattern space for memory formation and recall with $s(t+1) = W \cdot s(t)$ must induce attractors, where W is some state transition matrix. This means, starting from an initial configuration s which is sufficiently closed to (or overlapped with) one Ab_i, the system will flow to a fixed point of the dynamics, which is either the pattern itself or the configuration with high overlap with that pattern.

Memory Recall Process Based on Network Dynamics. Once the same or "similar" antigen to Ag invades immune systems again, the memory recall process of the immune systems will be activated by comparing the memory format generated and stored in the previous antigenic invasion of Ag. From system dynamics, we can define such similar antigens by basin of attraction. Suppose the same antigen Ag invades the immune systems again, then network dynamics F, namely, $F^n(Ag)$ will immediately converges to memory format of Ag, say $M(Ag)$. On the other hand, if some similar antigen Ag' invades, the network dynamics $F^k(Ag')$ converges to the same $M(Ag)$ if $Ag' \in BA(Ag)$. Therefore, basin of attraction of Ag is the major criterion that Ag' will activate the Ab_1 and the same antibody chain.

The third question we are interested here is the following. For a similar antigen Ag', whether the original antibody chain AC activated by Ag can also produce immune response effectively to this mutated Ag' ? In this way, the immune network reflects a decent associative memory. If the internal image Ab_N is similar to Ag, then it is also similar to Ag'. If for initial condition $X(0)$, we have the following network dynamics of recall process inspired by [16] and [18].

$$X(i) = sgn(\frac{1}{n}\sum_{i=1}^{N-1}(Ab_i X(i-1))Ab_{i+1}^T) \tag{2}$$

Therefore, if $X(0) = Ag$ and $\{Ab_k\}_k$ is a set of antibodies with sufficiently high dimension , then Ab_1 is recall at $t = 1$, as $X(1) = Ab_1$. In the same way, $X(2) = Ab_2$, $X(3) = Ab_3$, or the stored antibody sequence of Ag is recalled. Once the same antigen Ag invades, $Ab_1, Ab_2, \cdots, Ab_N$ are activated successively. On the other hand, If a similar antigen Ag' invades, then the recall process can be computed as follows.

$$\begin{aligned} X(1) &= sgn(\frac{1}{n}\sum_{k=0}^{N-1}(Ab_k Ag')Ab_{k+1}^T) \approx (Ag \cdot Ag')Ab_1 \\ &= \alpha_1 \cdot Ab_1 \end{aligned} \tag{3}$$

where $\alpha < 1$ is a small positive number. In the similar fashion, $X(k) = \alpha_k \cdot Ab_k$. Therefore this similar antigen Ag' will activate antibodies $\alpha_1 Ab_1, \cdots, \alpha_N Ab_N$.

Based on (3), there exists $\lambda > 0$ such that $d(Ag, Ag') < \lambda$ implies that $d(F^k(Ag'), Ab_k) < \lambda_k$. If $\lambda_K \approx \frac{1}{k}$, then this network dynamics can guarantee that $F^k(Ag')$ is approximately equal to internal image Ab_N. Therefore, CI-INs, from computation viewpoints, is stable for memory recall. However, we are interested in the critical value for λ such that network dynamics will deviate the antibody chain. Figure 3 is a simulation that a particular network dynamics activated by a specific antibody chain recall completely some mutated antigen.

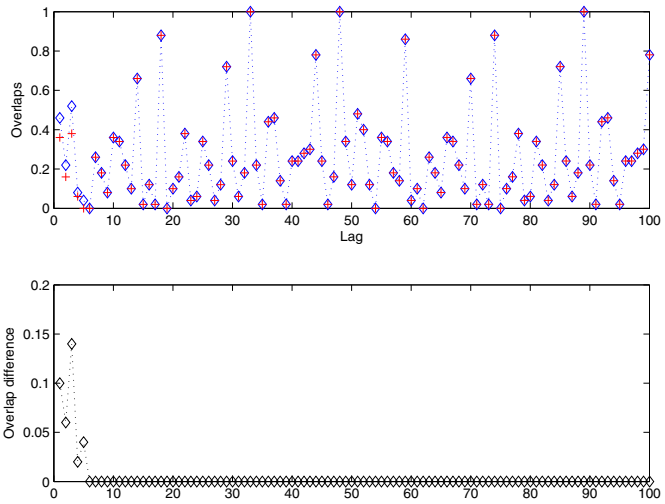

Fig. 3. Stable Network Dynamics for Immune Memory Recall

4 Conclusions

We propose immune memory mechanism based on the closed idiotypic immune network. The latter is analyzed by some tree structure. The formation of immune memory can be deduced by close loop of the cell's interactions, in particular, by antibody dynamics such as internal image recognition. Network dynamics which describes the immune memory formation and recall process is modeled based on autocorrelation matrix of antibody chains. This mechanism is associative by analyzing the state transitions of mutated antigens.

Acknowledgement. The author would like to thank support from National Science Council of Taiwan under the grant number NSC-101-2221-E-424-006.

References

1. de Castro, A.: A network model for clonal differentiation and immune memory. Physica A 355, 408–426 (2005)
2. Jerne, N.: Towards a network theory of the immune system. Ann. Immunol (Inst. Pasteur) 125C, 373 (1974)
3. Smith, D., Forrest, S., Perelson, A.: Immunological memory is associative. In: Artificial Immune Systems and Their Applications, The International Conference on the Multi-Agent Systems Workshop Notes, Kyoto, pp. 62–70 (1996, 1999)
4. Fernandez, J., Acostra, G., Mayosky, M.: From network-to-antibody robustness in a bio-inspured immune system. BioSystems 104, 109–117 (2011)
5. Bona, C.: Internal image concept revisited. In: Proceeding of the Society for Experimental Biology and Medicine 213, 32–42 (1996)

6. Parisi, G.: A simple model for the immune network. Proceedings of the National Academy of Sciences 87, 429–433 (1990)
7. Barra, A., Agliari, E.: Stochastic dynamics
8. Amari, S.I., Maginu, K.: Statistical neurodynamics of associative memory. Neural Networks 1, 63–73 (1988)
9. Abbattista, F., Gioia, G.D., Santo, G.D., Fanelli, A.: An asspciative memory based on the immune networks. In: Proceedings of the IEEE Internatinal Conference on Neural Networks, pp. 519–523 (1996)
10. Farmer, J., Packard, N., Perelson, A.: The immune system, adaptation, and machine learning. Physica 22D, 187–204 (1986)
11. Sonoda, T.: Formation and stability of a memory state in the immune network. J. Physical Society of Japan 81(4), 1408–1424 (1992)
12. Matzinger, P.: Memories are made of this? Nature 369, 605–606 (1994)
13. Borowik, B., Borowik, B., Kucwaj, J., Laird, S.: Associative memory of artificial immune systems. Annales UMCS Informatica AI X 2, 111–122 (2010)
14. Perelson, A.S.: Immune network theory. Immunological Reviews 10, 5–36 (1989)
15. Gutfreund, H.: The Physics of Neural Network: Spin Glasses and Biology. In: Steinl, D. (ed.) World Scientific Publishing (1992)
16. Morita, M.: Associative memory with nonmonotone dynamics. Neural Networks 6, 115–126 (1993)
17. Kohonen, T.: Self-Organization and Associative Memory. Springer (1983)
18. Oda, M., Miyajima, H.: Autocorrelation associative memory using refractory period of neurons. Electronics and Communications in Japan, Part 2 87(8), 41–52 (2004)

Effects of Emotional Content on Working Memory: Behavioral and Electrophysiological Evidence*

Yi-Xiang Jin[1,2], Xue-Bing Li[1,**], and Yue-Jia Luo[3,**]

[1] Key Laboratory of Mental Health, Institute of Psychology, Chinese Academy of Sciences, 100101 Beijing, China
{jinyx,lixb}@psych.ac.cn
[2] University of Chinese Academy of Sciences, 100049 Beijing, China
[3] State Key Laboratory of Cognitive Neuroscience and Learning, Beijing Normal University, 100875 Beijing, China
luoyj@bnu.edu.cn

Abstract. Effects of emotional content on working memory performance and the underlying neural mechanism were explored in this study, with a time-locked delayed matching-to-sample task (DMST) and a high-temporal resolution event-related potential (ERP) technique. Faster RTs and higher accuracy were observed in positive stimuli, while slower RTs and lower accuracy in negative stimuli. At encoding, an enhanced anterior P2 component was elicited by negative compared to neutral stimuli; at retention, the sustained slow wave (SW) showed a more positive deflection for both positive and negative stimuli compared to neutral stimuli during early and middle periods; at retrieval, a significant N400 old-new effect was observed and this effect for positive stimuli tended to be largest. The findings suggest that positive stimuli enhance working memory performance by facilitating retention and retrieval processing, while negative stimuli impede working memory performance as the negative emotion may be avoided during retrieval in spite of privileged processing during previous encoding and retention.

Keywords: positive emotion, negative emotion, working memory, event-related potentials.

1 Introduction

Numerous studies have demonstrated that emotional events tend to be remembered better than events without emotional relevance [1-3]. Emotions influence memory at various stages of information processing with the amygdala playing an important role in encoding, consolidation, and long-term retrieval [4].

* This research was partially supported by National Nature Science Foundation of China (NSFC 30930031, 30900441), National Basic Research Program of China (973 Program, 2011CB711001), National Key Technologies R&D Program (2009BAI77B01), Global Research Initiative Program (GRIP, NIH 1R01TW007897) and Key Laboratory of Mental Health of Institute of Psychology of Chinese Academy of Sciences.

** Co-corresponding authors.

D. Liu et al. (Eds.): BICS 2013, LNAI 7888, pp. 136–144, 2013.

However, most previous studies of emotion and memory were concentrated on long-term memory [5, 6, 7, 8], only a few on working memory, and the findings of relationship between emotion and working memory mainly focused on the behavioral level [9, 10]. Therefore, the effect of emotional content on working memory processes and underlying neural mechanism remains unclear.

In the present study, we aimed to investigate the influence of emotion on working memory that refers to a system used for the temporary storage and manipulation of information necessary for a range of more complex cognitive activities [11]. A delayed matching-to-sample task (DMST) was adopted that comprised three phases: target, delay, and probe. Distinct brain processing procedures can be separated by the three phases with this paradigm: information encoding in the target phase, information retention in the delay phase, and information retrieval in the probe phase [12].

Two critical issues were concerned. One is whether participants' working memory performance would be affected by the emotional content of memorized stimuli. The other is how the emotional content has the effect on encoding, retention and retrieval phases of working memory. The participants' performance of DMST with emotional and neutral stimuli was examined, and the event-related potential (ERP) technique was employed to measure the precise time course of the cortical activation.

2 Methods

2.1 Participants

Forty-six Chinese undergraduate and graduate students (22 males, 24 females; mean age = 21.3 ± 1.9 years) participated in the study. All were right-handed with normal or corrected-to-normal vision and had no previous neurological/psychiatric history. The participants received monetary compensation for their time and gave their informed consent in accordance with the IRB at the Institute of Psychology at the Chinese Academy of Sciences.

2.2 Stimuli

One hundred and twenty Chinese words (40 positive, 40 negative, and 40 neutral ones) were selected from Chinese Affective Words System (CAWS) [11]. Three categories of words were matched for word frequency [$F(2,117) = 0.034$, $p = 0.967$]. In accordance with the CAWS scoring, the average valence and arousal scores were 6.99 ± 0.21 and 5.67 ± 0.52 for positive words, 2.83 ± 0.23 and 5.75 ± 0.83 for negative words, and 5.04 ± 0.31 and 4.42 ± 0.68 for neutral words. Positive and negative words differed from each other in terms of emotional valence, but not in terms of emotional arousal, whereas both positive and negative words differed from neutral words in terms of both arousal and valence. An ANOVA on the valence scores of positive, neutral, and negative words yielded a significant main effect of valence [$F(2,117) = 2671.28$, $p < 0.001$], and post hoc tests showed significant differences between the valence scores of all three categories (all ps < 0.001). Also, an ANOVA

on the arousal scores of positive, negative, and neutral words yielded a significant main effect of arousal [$F(2,117) = 46.84$, $p < 0.001$], and post hoc tests showed significant differences between the arousal scores of both positive and negative words and those of neutral words ($ps < 0.001$), but no significant difference between positive and negative words ($p = 0.581$).

The stimuli were presented in central vision on the computer monitor (white words on a black background). Each item subtended a maximum vertical visual angle of approximately 10° and a maximum horizontal angle of approximately 5°.

2.3 Procedure

The participants were seated in an electrically isolated, sound- and light-attenuated room and viewed a computer monitor from a distance of 80 cm.

All of the trials began with a cross fixation (500-800 ms), then two target words were presented side by side in the center of the screen for 300 ms. After a short delay (2700-3000 ms), a word was presented as a probe stimulus for 300 ms, followed by a 1000 ms blank. The participants were asked to decide whether the probe word was "old" or "new" (i.e., whether the probe word was congruent or incongruent with one of the preceding two target words), and were instructed to try to respond as correctly and quickly as possible. Half of the participants were told to press the "F" key with their left index finger for "old" stimuli and the "J" key with their right index finger for "new" stimuli. Old and new stimuli were presented in equal proportions. For the other half of participants, the assignment of the response hand was reversed.

The emotional valence of the target and probe words in one trial was consistent, and 40 trials were included in each emotional condition. It meant that each word was presented twice as target word and once as probe word. The order of the trials was fully randomized by the E-prime program.

2.4 ERP Recordings and Analysis

The electroencephalogram (EEG) was recorded from 64 scalp sites using Ag/AgCl electrodes mounted in an elastic cap (NeuroScan Inc.), with the reference on the right mastoid. Horizontal eye movements were monitored with bipolar electrodes placed symmetrically on the outer canthus of each eye, and vertical movements were monitored with bipolar electrodes situated above and below the left eye. All electrode impedances were kept below 5 kΩ. The EEG and EOG were bandpass filtered between DC and 100 Hz and were sampled at a digitization rate of 500 Hz. To allow off-line analysis, they were digitally filtered with a 16 Hz lowpass filter. Trials with various artifacts were rejected with a criterion of ± 100 μV. The ERPs were averaged for trials with correct responses.

The ERP waveforms were time locked to the onset of the target and probe stimuli, respectively. The averaged epoch for the target stimulus-locked ERP was 3500 ms, ranging from 500 ms before the onset of the target stimuli to 3000 ms after the target

stimuli. The averaged epoch for the probe stimulus-locked ERP was 1200 ms, which included a 200 ms pre-probe baseline.

The following 18 sites were chosen for statistical analysis for both the target stimulus-locked ERP and probe stimulus-locked ERP components: frontal (F3, FZ, F4), frontocentral (FC3, FCZ, FC4), central (C3, CZ, C4), centroparietal (CP3, CPZ, CP4), parietal (P3, PZ, P4), and parietooccipital (PO5, POZ, PO6).

A repeated-measures analysis of variance (ANOVA) of each probe stimulus-locked ERP component was conducted with four factors: emotion (positive/negative/neutral), probe type (old/new), laterality (left/midline/right), and anterior-posterior scalp location (F/FC/C/CP/P/PO). And for each target stimulus-locked ERP component, there were three factors: emotion, laterality and anterior-posterior scalp location. The Greenhouse-Geisser correction was used to compensate for sphericity violations.

3 Results

3.1 Behavioral Results

ANOVAs were conducted on response times (RT) and accuracy scores (percent correct) with the following factors: emotion (positive/negative/neutral) and probe type (old/new).

An ANOVA of the RTs revealed a significant main effect of emotion [$F(2,90) = 5.612$, $p = 0.005$, $\eta^2 = 0.111$], and an emotion × probe type interaction [$F(2,90) = 5.789$, $p = 0.004$, $\eta^2 = 0.114$]. Fisher's LSD test revealed that RTs were faster for positive rather negative words ($p = 0.007$). Simple effects analyses showed an emotional effect only on old words [$F(2,90) = 13.149$, $p < 0.001$], not on new words. RTs of old words were fastest for positive items, and slowest for negative items (positive < neutral, $p = 0.019$; neutral < negative, $p = 0.003$; positive < negative, $p < 0.001$).

Analyses of accuracy yielded a significant main effect of probe type [$F(1,45) = 6.735$, $p = 0.013$, $\eta^2 = 0.130$] and an emotion × probe type interaction [$F(2,90) = 4.138$, $p = 0.019$, $\eta^2 = 0.084$]. The main effect showed that the accuracy of new words was higher than that of old words. Similar to results of RTs, simple effects analyses of accuracy showed an emotional effect only on old words [$F(2,90) = 4.081$, $p = 0.020$], not on new words. Furthermore, for old words, positive items were recognized more accurately than negative items ($p = 0.015$), and neutral items tended to be recognized more accurately than negative items ($p = 0.075$) (see Fig. 1).

3.2 ERP Results

ERPs were quantified by measuring the mean amplitudes of P2 component at encoding and slow wave (SW) at retention during target stimulus-locked epoch, as well as N400 at retrieval phase during probe stimulus-locked epoch. Averaged data were analyzed using repeated-measures ANOVAs and post hoc Bonferroni tests.

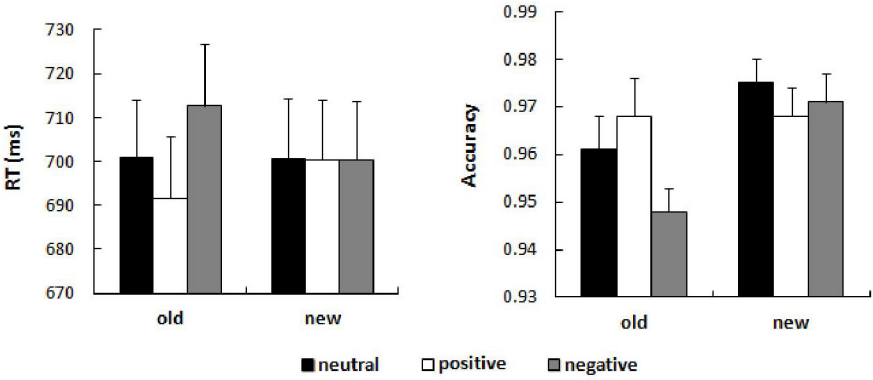

Fig. 1. Response time (RT) and Accuracy (Error bars represent standard errors) of neutral, positive and negative items in old and new words

Target Stimulus-locked ERPs

P2. A fronto-central positive-going voltage deflection observed 150–210 ms following target onset was identified as the P2 component. An ANOVA of the mean amplitudes of P2 measured at 9 anterior electrodes (F3, FZ, F4, FC3, FCZ, FC4, C3, CZ, C4) revealed a significant main effect of emotion [$F(2,90) = 3.478$, $p = 0.035$, $\eta^2 = 0.072$], and post hoc tests showed a significant difference between negative and neutral words ($p = 0.048$), but neither between positive and neutral words ($p = 0.124$), nor between positive and negative words ($p = 1.000$), reflecting an enhancement of the P2 amplitude for negative words rather than for neutral words.

SW. Sustained negative slow wave shifts showed condition-related differences over the whole scalp region. The mean amplitudes of the SW were measured at three consecutive epochs (400-800 ms, 800-2000 ms, 2000-3000 ms) at the 18 electrodes. The ANOVAs yielded a significant main effect of emotion during an early epoch [400-800 ms; $F(2,90) = 11.199$, $p < 0.001$, $\eta^2 = 0.199$] and a middle epoch [800-2000 ms; $F(2,90) = 4.736$, $p = 0.011$, $\eta^2 = 0.095$], but not during a late epoch [2000-3000 ms; $F(2,90) = 1.576$, $p = 0.212$, $\eta^2 = 0.034$]. At 400-800 ms, post hoc tests showed a significant difference between positive words and neutral words (positive > neutral, $p = 0.006$) and between negative and neutral words (negative > neutral, $p < 0.001$), but not between positive and negative words ($p = 1.000$). Analyses yielded analogous results at 800-2000 ms (positive > neutral, $p = 0.075$; negative > neutral, $p = 0.019$; positive versus negative, $p = 1.000$). These results indicated that the SW showed a more positive deflection for emotional words than neutral words during both early and middle epochs, but not during a late epoch (see Fig. 2).

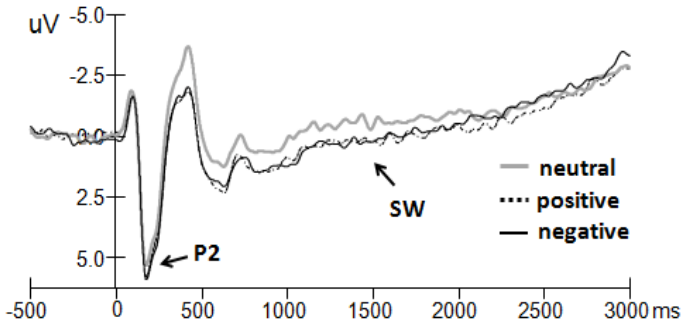

Fig. 2. Grand average target stimuli-locked ERPs for positive, negative and neutral stimuli at the FCZ electrode site

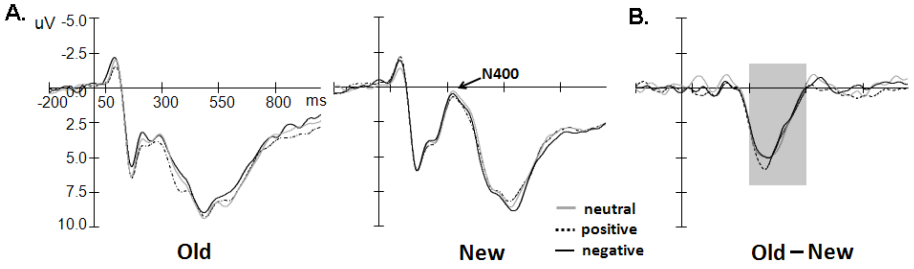

Fig. 3. Grand average probe stimuli-locked ERPs for positive, negative and neutral stimuli at the CZ electrode site, separately for (A) old and new items, and (B) the difference waves (old minus new)

Probe Stimulus-locked ERPs

N400. An ANOVA of the mean amplitudes of N400 (300-550 ms) measured at the 18 electrodes revealed a significant main effect of probe type [so-called old-new effect; $F(1,45) = 156.942$, $p < 0.001$, $\eta^2 = 0.777$], and a main effect of emotion [$F(2,90) = 2.922$, $p = 0.059$, $\eta^2 = 0.061$], but no significant emotion × probe type interaction. Post hoc tests found that the old words elicited a more positive deflection than new words ($p < 0.001$). ERPs for positive words were more positive than those for neutral items ($p = 0.051$), but no significant difference was found between negative and neutral words, nor between positive and negative words. Although a follow-up analysis of difference waves (old stimuli ERPs minus new stimuli ERPs) did not show a significant emotion effect, there was a tendency for a larger old-new effect for positive words than that for negative or neutral items (see Fig. 3).

4 Discussion

The aims of this study were to assess the effects of positive and negative emotion on working memory and find out the possible underlying neural mechanism. The current behavioral and ERP results confirmed our predictions of significant effects of emotional content on working memory task performance and ERP correlates with encoding, retention and retrieval processes.

First, the behavioral data showed that RTs were faster for positive than neutral words, and slower for negative than neutral words. Accordingly, accuracy was higher for positive words and lower for negative words. These emotional effects were observed only in old items, not in new items. The evidence suggested that positive emotion enhances performance of the working memory task while negative emotion impedes it, which was consistent with previous studies on relationship between emotion and long-term memory. Such as, Inaba, Nomura and Ohira found that the recognition speed of correct responses to positive words was faster than those to negative and neutral words, and ERP old-new effect (this will be explained below) were greater for emotional targets than for neutral targets [14]. Hence, the behavioral results implied that the memory bias to positive information also exists in the working memory system.

Second, the target stimuli-locked ERP data showed an enhanced anterior P2 component for negative words as compared with neutral words. This result was in line with other studies showing that cues signaling threat of shock, compared to safety, prompted enhanced P2 component [15]. It is well known that aversive information has the ability to draw attention automatically [16]. The P2 is regarded as an important attention–related component, and the similar emotional effect on P2 was observed in Carretie and colleagues' study with an implicit emotional task. They found that P2 showed higher amplitudes in response to negative stimuli than in response to positive stimuli [17]. During the encoding process of working memory, attention acts a very important role, so it is not surprised that P2 amplitude was enhanced for negative words, as compared with neutral and positive ones. At retention, the sustained SW showed a more positive deflection for both positive and negative words compared with neutral words during early and middle periods. Several studies have elucidated that the long-duration slow wave was specifically indexed sustained mnemonic operations during the retention phase [18], and the SW was sensitive to task difficulty, as reducing in amplitude with increasing memory load [19]. The current changes of SW for both positive and negative stimuli indicated that emotional content has abilities to facilitate the maintenance function of working memory, and then decreases task difficulty.

Finally, the probe stimuli-locked ERP data showed a robust N400 old-new effect at retrieval. It has long been known that, relative to new words, the N400 amplitudes elicited by correctly classified old words in tests of recognition memory are more positive-going [20, 21]. The so-called N400 old-new effect is thought to reflect familiarity-driven recognition [5], a form of recognition memory held by some authors to be independent of recollection, and to underlie recognition judgments associated with "Know" rather than "Remember" responses [22]. Further, for both old

and new items, average amplitudes elicited by positive words were more positive-going than those elicited by neutral words, accompanied with a tendency of a larger old-new difference for positive words than that for negative or neutral items. This result suggested that there was a positive bias during memory retrieval, in other words, positive emotion enhanced the retrieval processing of working memory.

Based on the present behavioral and electrophysiological results, we found that positive emotion improved the working memory performance by facilitating the retention and retrieval processing of working memory. Negative emotional content exhibited the enhancement effect during encoding and retention periods of working memory. However, this enhancement effect failed to keep to the retrieval phase, which might be due to the negative avoidance motivational system [23], thus negative emotion didn't improve, instead, impaired the performance of working memory task. As is explained, the mere presence of a negatively valenced object results immediately in the activation of a negative avoidance motivational system, that is to say, in such a system, negative objects have "avoidance motives" attached to them [24].

5 Conclusion

In summary, this study combined a time-locked DMST paradigm and a high-temporal resolution ERP technique to investigate the emotional effects on working memory. The findings suggest that positive stimuli enhance working memory performance by facilitating the retention and retrieval processing. However, negative stimuli impede working memory performance possibly due to the avoided response during retrieval phase.

References

1. Doerksen, S., Shimamura, A.P.: Source memory enhancement for emotional words. Emotion 1, 5 (2001)
2. Dolcos, F., Cabeza, R.: Event-related potentials of emotional memory: encoding pleasant, unpleasant, and neutral pictures. Cogn. Affect. Behav. Neurosci. 2, 252–263 (2002)
3. Bradley, M.M., Greenwald, M.K., Petry, M.C., Lang, P.J.: Remembering pictures: pleasure and arousal in memory. J. Exp. Psychol. Learn. Mem. Cogn. 18, 379 (1992)
4. LaBar, K.S., Cabeza, R.: Cognitive neuroscience of emotional memory. Nat. Rev. Neurosci. 7, 54–64 (2006)
5. Maratos, E.J., Allan, K., Rugg, M.D.: Recognition memory for emotionally negative and neutral words: An ERP study. Neuropsychologia 38, 1452–1465 (2000)
6. Johansson, M., Mecklinger, A., Treese, A.C.: Recognition memory for emotional and neutral faces: An event-related potential study. J. Cognitive Neurosci. 16, 1840–1853 (2004)
7. Kensinger, E.A., Corkin, S.: Two routes to emotional memory: Distinct neural processes for valence and arousal. PNAS 101, 3310 (2004)
8. Weymar, M., Löw, A., Hamm, A.O.: Emotional memories are resilient to time: Evidence from the parietal ERP old/new effect. Hum. Brain Mapp. 32, 632–640 (2011)

9. Kensinger, E.A., Corkin, S.: Effect of negative emotional content on working memory and long-term memory. Emotion 3, 378 (2003)
10. Luethi, M., Meier, B., Sandi, C.: Stress effects on working memory, explicit memory, and implicit memory for neutral and emotional stimuli in healthy men. Front. Behav. Neurosci. 2 (2008)
11. Baddeley, A.: Working memory. Science 255, 556–559 (1992)
12. D'Esposito, M., Postle, B.R., Rypma, B.: Prefrontal cortical contributions to working memory: evidence from event-related fMRI studies. Exp. Brain Res. 133, 3–11 (2000)
13. Wang, Y.N., Zhou, L.M., Luo, Y.J.: The pilot establishment and evaluation of Chinese Affective Words System. Chin. Ment. Health J. 22 (2008)
14. Inaba, M., Nomura, M., Ohira, H.: Neural evidence of effects of emotional valence on word recognition. Int. J. Psychophysiol. 57, 165–173 (2005)
15. Weymar, M., Bradley, M.M., Hamm, A.O., Lang, P.J.: When fear forms memories: Threat of shock and brain potentials during encoding and recognition. Cortex (in press)
16. Huang, Y.X., Luo, Y.J.: Temporal course of emotional negativity bias: An ERP study. Neurosci. Lett. 398, 91–96 (2006)
17. Carretié, L., Mercado, F., Tapia, M., Hinojosa, J.: Emotion, attention, and the 'negativity bias', studied through event-related potentials. Int. J. Psychophysiol. 41, 75 (2001)
18. Drew, T.W., McCollough, A.W., Vogel, E.K.: Event-related potential measures of visual working memory. Clin. EEG Neurosci. 37, 286–291 (2006)
19. Mecklinger, A., Pfeifer, E.: Event-related potentials reveal topographical and temporal distinct neuronal activation patterns for spatial and object working memory. Cogn. Brain Res. 4, 211 (1996)
20. Finnigan, S., Humphreys, M.S., Dennis, S., Geffen, G.: ERP 'old/new' effects: memory strength and decisional factor (s). Neuropsychologia 40, 2288–2304 (2002)
21. Friedman, D., Johnson, R.: Event-related potential (ERP) studies of memory encoding and retrieval: A selective review. Microsc. Res. Techniq. 51, 6–28 (2000)
22. Gardiner, J.M., Java, R.I., Richardson-Klavehn, A.: How level of processing really influences awareness in recognition memory. Can. J. Exp. Psychol. 50, 114 (1996)
23. Chen, M., Bargh, J.A.: Consequences of automatic evaluation: Immediate behavioral predispositions to approach or avoid the stimulus. Pers. Soc. Psychol. Bull. 25, 215–224 (1999)
24. Lang, P.J., Bradley, M.M., Cuthbert, B.N.: Emotion, attention, and the startle reflex. Psychol. Rev. 97, 377 (1990)

A Computationally and Cognitively Plausible Model of Supervised and Unsupervised Learning*

David M.W. Powers[1,2]

[1] CSEM Centre for Knowledge & Interaction Technology, Flinders University, Adelaide, South Australia
[2] Beijing Municipal Lab for Multimedia & Intelligent Software, BJUT Beijing, China
powers@acm.org

Abstract. Both empirical and mathematical demonstrations of the importance of chance-corrected measures are discussed, and a new model of learning is proposed based on empirical psychological results on association learning. Two forms of this model are developed, the Informatron as a chance-corrected Perceptron, and AdaBook as a chance-corrected AdaBoost procedure. Computational results presented show chance correction facilitates learning.

Keywords: Chance-corrected evaluation, Kappa, Perceptron, AdaBoost.

1 Introduction

The issue of chance correction has been discussed for many decades in the context of statistics, psychology and machine learning, with multiple measures being shown to have desirable properties, including various definitions of Kappa or Correlation, and the psychologically validated ΔP measures. In this paper, we discuss the relationships between these measures, showing that they form part of a single family of measures, and that using an appropriate measure can positively impact learning.

1.1 What's in a "Word"?

In the Informatron model we present, we will be aiming to model results in human association and language processing. The typical task is a word association model, but other tasks may focus on syllables or rimes or orthography. The "word" is not a well-defined unit psychologically or linguistically, and is arguably now a backformed concept from modern orthology. Thus we use "word" for want of a better word, and the scare quotes should be imagined to be there at all times, although they are frequently omitted for readability! (Consider "into" vs "out of", "bring around" vs "umbringen".)

* An extended abstract based on an earlier version has been submitted for presentation to the Cognitive Science Society (in accordance with their policy of being of "limited circulation").

D. Liu et al. (Eds.): BICS 2013, LNAI 7888, pp. 145–156, 2013.

1.2 What's in a "Measure"?

A primary focus of this paper is the inadequacy of currently used measures such as Accuracy, True Positive Rate, Precision, F-score, etc. Alternate chance-corrected measures have been advocated in multiple areas of cognitive, computational and physical science, and in particular in Psychology in the specific context of (unsupervised) association learning [1-3], where ΔP is considered "the normative measure of contingency".

In parallel, discontent with misleading measures of accuracy was building in Statistics [4,5], Computational Linguistics [6] and Machine Learning [7] and extended to the broader Cognitive Science community [8]. Reversions to older methods such as Kappa and Correlation (and ROC AUC, AUK, etc.) were proposed and in this paper we explore learning models that directly optimize such measures.

2 Informedness, Correlation and DeltaP

The concept of chance-corrected accuracy measures has been reinvented several times in several contexts, with some of the most important being Kappa variants [4,5]. This is an *ad hoc* approach that subtracts from accuracy (Ac) an estimate of the chance-level accuracy (EAc) and renormalizes to the form of a probability K=(Ac–EAc)/(1–EAc). But different forms of chance estimate, different forms of normalization, and different generalizations to multiple classes or raters/predictors, lead to a whole family of Kappa measures of which ΔP turns out to be one, and ΔP' another [9]. The geometric mean of these two unidirectional measures is correlation, which is thus a measure of mean association over both directions of an A↔B relation between events. Perruchet and Pereman [3] focus on an A, B word sequence and define ΔP as a chance-corrected version of TP = P(B|A), corresponding to Precision (proportion of events A that predict B correctly), whilst ΔP' corrects TP' = P(A|B) which is better known as TPR, Sensitivity or Recall, meaning the proportion of events B that are predicted by A – on the assumption that forward prediction A→B is normative. They argue for comparing TP with a baseline of how often event B occurs when not preceded by A so that ΔP = P(B|A) – P(B|¬A) and ΔP' = P(A|B) – P(A|¬B).

Empirically ΔP' is stronger than ΔP in these experiments, and TP and TP' are much weaker, with TP failing to achieve a significant result for either Children or Adults in their experiments. Why should the reverse direction be stronger? One reason may be that an occurrence in the past is more definite for the speaker and has been more deeply processed for the hearer. Furthermore, often a following segment may help disambiguate a preceding one. Thus in computational work at both word level and phoneme/grapheme level, the preceding two units and the succeeding three units, seem to be optimal in association-based syntax and morphology learning models [10,11], and two-side context has also proven important in semantic models [12]. However, Flach [7] and Powers [8] independently derived ΔP'-equivalent measures, not ΔP, as a skew/chance independent measure for A→B predictions as the information value relates to (and should be conditioned on) the prevalence of B not A.

In view of these Machine Learning proofs we turn there to introduce and motivate definitions in a statistical notation that conflicts with that quoted above from the

Psychology literature. We use systematic acronyms [7,8] in upper case for counts, lower case for rates or probabilities. In dichotomous Machine Learning [7] we assume that we have for each instance a Real class label which is either Positive or Negative (counts, RP or RN, rates rp=RP/N and rn=RN/N where we have N instances labelled). We assume that our classifier, or in Association Learning the predictor, specifies one Predicted class label as being the most likely for each instance (counts, PP or PN, probs pp and pn). We further define True and False Positives and Negatives based on whether the prediction P or N was accurate or not (counts, TP, TN, FP, FN; probs tp, tn, fp, fn; rates tpr=tp/rp, tnr=tn/rn, fpr=fp/rn).

Table 1. Prob notation for dichotomous contingency matrix

	+R	−R	
+P	tp	fp	pp
−P	fn	tn	pn
	rp	rn	1

Whilst the above systematic notation is convenient for derivations and proofs, these probabilities (probs) are known by a number of different names and we will use some of these terms (and shortened forms) for clarity of equations and discussions.

The probs rp and rn are also known as Prevalence (Prev) and Inverse Prevalence (IPrev), whilst pp and bn are Bias and Inverse Bias (IBias) resp. Also Recall and Sensitivity are synonyms for true positive rate (tpr), whilst Inverse Recall and Specificity correspond to true negative rate (tnr). The term rate is used when we are talking about the rate of finding or recalling the real item or label, that is the proportion of the real items with the label that are recalled. When we are talking about the accuracy of a prediction in the sense of how many of our predictions are accurate we use the term accuracy, with Precision (Prec) or true positive accuracy being tpa=tp/pp, and Inverse Precision or true negative accuracy being tna=tn/pn, and our (perverse) prediction accuracy for false positives being fpa=fp/pp. We also use fpa and fna correspondingly for the perverse accuracies predicting the wrong (false) class. Names for other probs [13] won't be needed.

The chance-corrected measure ΔP' turns out to be the dichotomous case of Informedness, the probability that a prediction is informed with respect to the real variable (rather than chance). This was proven based on considerations of odds-setting in horse-racing, and is well known as a mechanism for debiasing multiple choice exams [8,13]. It has also been derived as skew-insensitive Weighted Relative Accuracy (siWRAcc) based on consideration of ROC curves [7]. As previously shown in another notation, it is given by:

$$\Delta P' = tpr - fpr = tpr + tnr - 1 = Sensitivity + Specificity - 1 \quad (1)$$

The inverse concept is Markedness, the probability that the predicting variable is actually marked by the real variable (rather than occuring independently or randomly). This reduces to ΔP in the dichotomous case:

$$\Delta P = tpa - fpa = tpa + tna - 1 = Prec + IPrec - 1 \quad (2)$$

As noted earlier, the geometric mean of ΔP and ΔP' is Matthews Correlation (Perruchet & Pereman, 2004), and kappas and correlations all correspond to different normalizations of the determinant of the contingency matrix [13]. It is noted that ΔP' is recall-like, based on the rate we recall or predict each class, whilst ΔP is precision-like, based on the accuracy of our predictions of each label.

The Kappa interpretation of ΔP and ΔP' in terms of correction for Prevalence and Bias [9,13] is apparent from the following equations (noting that Prev<1 is assumed, and Bias<1 is thus a requirement of informed prediction, and E(Acc)<1 for any standard Kappa model):

$$\text{Kappa} = (\text{Accuracy}–E(\text{Acc})) / (1–E(\text{Acc}))$$
$$\Delta P' = (\text{Recall} – \text{Bias}) / (1 – \text{Prevalence}) \quad (3)$$
$$\Delta P = (\text{Precision}–\text{Prevalence})/(1 – \text{Bias}) \quad (4)$$

If we think only in terms of the positive class, and have an example with high natural prevalence, such as water being a noun say 90% of the time, then it is possible to do better by guessing noun all the time than by using a part of speech determining algorithm that is only say 75% accurate [6]. Then if we are guessing our Precision will follow Prevalence (90% of our noun predictions will be nouns) and Recall will follow Bias (100% of our noun occurences will be recalled correctly, 0% of the others).

We can see that these chance levels are subtracted off in (3) and (4), but unlike the usual kappas, a *different* chance level estimate is used in the denominator for normalization to a probability – and unlike the other kappas, we actually have a well defined probability as the probability of an informed prediction or of a marked predictor resp. The insight into the alternate denominator comes from consideration of the amount of room for improvement. The gain due to Bias in (3) is relative to the chance level set by Prevalence, as ΔP' can increase only so much by dealing with only one class – how much is missed by this blind 'positive' focus of tpr or Recall on the positive class is captured by the Inverse Prevalence, (1 – Prevalence).

Informedness and Markedness in the general multiclass case, with K classes and the corresponding one-vs-rest dichotomus statistics indexed by k, are simply

$$\text{Informedness} = \Sigma_k \text{Bias}_k \Delta P'_k \quad (5)$$
$$\text{Markedness} = \Sigma_k \text{Prev}_k \Delta P_k \quad (6)$$

Informedness can also be characterized as an average cost over the contingency table cells c_{pr} where the cost of a particular prediction p versus the real class r is given by the Bookmaker odds: what you win or lose is inversely determined by the prevalence of the horse you predict (bet on) winning (p=r) or losing (p≠r) – using a programming convention for Boolean expressions here, (true,false)=(1,0), define Gain G_{pr} to have

$$G_{pr} = 1/(\text{Prev}_p–D_{pr}) \quad \text{where } D_{pr} = (p≠r) \quad (7)$$
$$\text{Informedness} = \Sigma_p \text{Bias}_p [\Sigma_r c_{pr} G_{pr}] \quad (8)$$

Here the nested sum is equivalent to $\Delta P'_p$ and represents how well you do on a particular horse p (a probability or pay off factor between 0 and 1). The outer sum is (5) and shows what proportion of the time you are betting on each horse.

The formulae can also be recognized in the equiprevalence case as the method of scoring multiple choice questions. With 4-horse races or 4-choice questions, all

equally likely, and us just guessing, Bias = Prev = ¼, and we have three chances of losing ¼ and one of gaining ¾. We likely select the correct answer one time in four, and our expected gain is 0: ¼ / ¼ – ¾ / ¾. The odds are ¾ : ¼ but we normally multiply that out to integers so we have 3 : 1.

If we were four poker players all putting in a quarter before looking at our cards, we would have a dollar in the pool and whatever I gain someone else has lost, but my expected loss or gain is 0: 3 * ¼ + 1 * ¾. There is $1 or an Informedness of 1, at stake for every bet we make here.

3 Association Learning and Neural Networks

We have seen that chance-corrected ΔP measures are better models both from a statistical point of view (giving rise to probabilities of an informed prediction or marked predictor) and also from an empirical psychology perspective (reflecting human association strength more accurately). They also have the advantage over correlation of being usable separately to provide directionality or together to provide the same information as correlation. This raises the question of whether our statistical and neural learning models reflect appropriate statistics. The statistical models traditionally directly maximize accuracy or minimize error, without chance correction, and many neural network and convext boosting models can shown to be equivalent to such statistical models, as we show in this section and the next. Our question is whether these can be generalized with a bioplausble chance-correcting model.

3.1 The Generalized Perceptron

Perceptrons (or Φ-machines) as the heart of the leading supervised neural networks, and (Linear or Kernel) Support Vector Machines as the common classifier of choice in Machine Learning, are actually equivalent models, seeking a (linear) separating boundary (hyperplane) between the positive and negative examples. If the examples are indeed linearly separable (or we can find an appropriate non-linear kernel to separate them), then SVM focuses on just one more example than there are dimensions in the separating hyperplane (the support vectors) in order to maximize the no-man's land between. In this case, both Perceptron and SVM will be perfect on the training data, and the early stopping margin Perceptron [14] or the SVM will actually do better on unseen data for not having tried to minimize the sum of squared error (SSE) as is effectively done when non-separable.

Multilayer Perceptrons or MLP (usually trained with some form of backpropagation) and Simple Recurrent Networks or SRN [15] are both networks of Perceptrons and inherit the SSE statistics as well as the backpropagation training method, which is acknowledged not to be particularly bioplausible [16] although attempts have been made to bridge the gap [17]. Other ways of training supervised and unsupervised networks are possible, and have been used in language learning experiments, including more complex recurrent networks [16,18]. But all these networks tend to use some variant of the Hebbian learning rule (10) – the main difference being whether update always takes place (unsupervised or association

models) or takes place only under specific conditions (supervised models based on updates as correction only).

We now consider how these neural network and learning models fail to match the desired chance-corrected probability estimates and empirical association experiments, and develop an alternate model that does. We follow the same conventions that Boolean yes/no events are represented by (1,0) for (true,false), but note that many neural models use (1,-1) including MLP/BP with the tanh transfer function as f() which is argued to better balance the effort expended on positive and negative examples. However, biologically plausible networks conventionally separate out excitatory (+ve) and inhibitory (-ve) roles. On the other hand, there are issues modeling inhibition with subtraction given we assume neural activity (unlike kappas) can't go negative. We will discuss a multiplicative variant of the Perceptron shortly (Winnow), and we propose a model of synapse that is not strictly excitatory or inhibitory, but rather divisive (or facilitative) – noting that, due to the possibilities of scaling activity on both sides, the +ve/-ve distinction is moot.

3.2 A Family of Neural Update Rules

The Hebb [19] update rule can be characterized as "the neurons that fire together wire together" [17], with the basic neuron accumulation and update equations being shown in (9) & (10), where X is a collection of instances represented as a sequence of attribute vectors (and corresponds to a set of input neurons per attribute), and Y is a corresponding sequence of real class labels (desired output for each output neuron), while Z is the sequence of predicted class labels (actual output for each output neuron), which we show in summation form as well as in matrix form (with its omitted subscripts and implied sum over the inner subscripts):

$$Z = \theta(XW) ; \quad Z_{ik} = f(\Sigma_j\, g(X_{ij})\, W_{jk}) \tag{9}$$

$$W = XY; \qquad W_{jk} = \Sigma_{ij}\, X_{ij}\, Y_{jk}; \qquad \Delta W_{jk} = \lambda X_{ij}\, Y_{jk} \tag{10}$$

In (9) we see two alternative formulations involving a threshold function as in the original Perceptron and a transfer function as in the Multilayer Perceptron, which can be the identity function, but is usually a smoothed 'sigmoid' variant of the threshold function to allow for a finite amplification factor for backpropagation rather than an infinitely fast change as we move infinitesimally through a threshold. We also show a function g(X) which may reflect recursively deeper layers of a MLP, or a radial basis or other transformation as used by SVMs. Voting, bagging, boosting and stacking ensembles may also be construed to obey (9) for appropriate choices of f() and g().

In (10) we see the original Hebb update rule in three forms. The first two forms are the 'batch update' versions in matrix and summation notations, whilst the third is the 'incremental' version, and also includes a learning rate $\lambda \leq 1$. This is repeated for each example, often more than one each and sometimes in random order, adding ΔW to W each time. For sparse (word to word) association learning, W_{jk} simply corresponds to unnormalized c_{jk} contingency table entries of (8), being normalized counts $c_{jk} = C_{jk}/N = W_{jk}/N$.

The standard Perceptron rule, by contrast, only updates if the wrong answer is given – in matrix or summation form the Boolean is again interpreted numerically and defines a matrix of binary values, whilst in incremental form either the binary or "if Boolean" interpretation can be used (no change if false):

$$W_{jk} = \Sigma_{ij}\ X_{ij}\ Y_{jk}\ (Y_{jk} \neq Z_{jk}); \qquad \Delta W_{jk} = \lambda X_{ij}\ Y_{jk}\ (Y_{jk} \neq Z_{jk}) \tag{11}$$

The Margin Perceptron is a venerable variant of the Perceptron that has more recently been shown to have desirable margin optimization properties similar to an SVM [14]. The update rule becomes

$$W_{jk} = \Sigma_{ij}\ X_{ij}\ Y_{jk}\ (\gamma > |Y_{jk} Z_{jk}|);\ \Delta W_{jk} = \lambda X_{ij}\ Y_{jk}\ (\gamma > |Y_{jk} Z_{jk}|) \tag{12}$$

Here the parameter γ represents the margin width, but can be set to 1 [14] if X and W are not explicitly normalized (as here). A soft modification of this variant, that takes less account of possibly noisy margin violations is

$$W_{jk} = \Sigma_{ij}\ X_{ij}\ Y_{jk}\ (1 - |Y_{jk} Z_{jk}|);\ \Delta W_{jk} = \lambda X_{ij}\ Y_{jk}\ (1 - |Y_{jk} Z_{jk}|) \tag{13}$$

Winnow [20] is a variant on the Perceptron that uses multiplication rather than addition to update the weights, in order to eliminate the contribution of irrelevant attributes, characterized by quotient rather than difference:

$$W_{jk} = \Pi_j\ (Y_{jk} \geq Z_{jk}) * \alpha; \qquad QW_{jk} = (Y_{jk} \geq Z_{jk}) * \alpha \tag{14}$$

Note that where an error occurs for negative (Y=0) class member the corresponding weight is zeroed. Winnow2 is less severe and uses the reversible

$$QW_{jk} = (Y_{jk} \geq Z_{jk}) * \alpha + (Y_{jk} < Z_{jk}) / \alpha = (Y_{jk} \geq Z_{jk})\ ?\ \alpha : \alpha^{-1} \tag{15}$$

Note too that Winnow's weight is exponential in the number of up corrected examples (14), and Winnow2 is exponential in differential counts of up vs down corrections (15). Taking the logarithm gives us a Perceptron-like algorithm that reflects Information rather than Prevalence, but Information is inverse to log(Prob) giving weight to surprise value or novelty rather than weight of numbers or ubiquity.

Often authors of neuroplausible models have the rider that cells may correspond to a cluster of neurons rather than one. We actually show cells that are explicitly clusters of neurons in Fig. 1(a), revealing exemplar shadow and mirror cells in inset (b).

3.3 The Informatron

To model chance-correction, we require a matrix that reflects Informedness gains (in "dollars") rather than counts (10) or errors (11-13). Considering each predictor separately, this profit matrix corresponds to the inner sum of (8) and thus

$$W_{jk} = \Sigma_j\ X_{ij}\ Y_{jk}\ \ G_{jk} \tag{16}$$

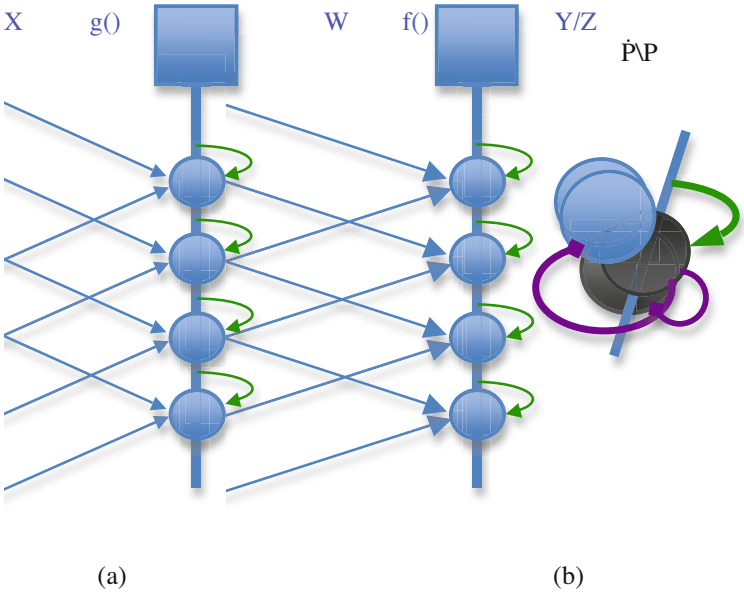

Fig. 1. The Informatron

It will be noted that no update (delta) rule is shown, although one could be if the prevalences, and hence the Gain matrix, were assumed known. We however assume that $Prev_r$ is *not* known but accumulated within the model, as shown in Fig. 1 as P.

Figure 1 shows representative synapses of a feature association or learning network to the left, corresponding to g() in (9). This is assumed to be recursively definable using the same model, which is also able to be self-organizing since it models associations between natural inputs or features, and corresponds to the perceptual and linguistic processing necessary to recognize a word from its phonological or orthological input representation. The model is thus agnostic as to whether it is unsupervised, or implicitly or explicitly supervised by feedback with or without recurrence [10,15], or may follow a similar model to the ones presented here, which is a single association stage. We make a connection to boosting and ensemble techniques here, and thus can also call it a weak learner or an individual classifier. These concepts will be picked up in the next section.

In Fig. 1(a) columns of round cells represent the before and after terms in a temporal association sequence [3]. We see here excitatory neurons obeying the standard Hebbian learning rule (10), the synapses between the columns reflecting the joint probability of the events (independent of time sequence or causality), but the simplified graphic should not be taken as precluding connections within a column – indeed the columns are shown separate only for didactic purposes and all units are activated by "words".

The square event sync cells (X_{ek}) synapse on all the shadow cells (Y_{sk}) below them with the same Hebbian learning (10), the vertical axon with curved dendritic synapses reflecting the simple (marginal) probability of the "word" events. Because they are always 1, the marginal probabilities are learned, rather than the contingencies between

two concept neurons. (The square cells may be regarded in electronic engineering terms as underlying system clocks enabling a bank of cells; in cognitive neuroscience terms they may be reflected in Event Related Potentials such as the P300 and BP.)

Arrow heads represent excitatory synapses with Hebbian learning. Diamond heads represent facilitatory synapses with divisive rather than subtractive or thresholded effect, and so facilitation of the foreground neuron accumulating joint probability by the background shadow neuron accumulating marginal probability, as shown in the glide out detail of Fib. 1(b). We now show an equation corresponding to (7-8) clarifying the role of the shadow neurons:

$$Z_{ik} = f(\Sigma_j\, g(X_{ij})\, W_{jk} / S_{ik}) \text{ with } S_{ik} = Y_{ek} - D_{ik} \quad (17)$$

Note that the inhibitory effect of the shadow neuron represents the normalization by prevalence of (7) & (8), but the Hebbian synaptic modification of associating foreground is independent of this gain factor. The D_{ik} (which might correspond to a mismatch negativity effect and might be involved in disabling Hebbian learning and achieving Perceptron-like learning) is not illustrated for space reasons (but is a standard neural circuit involving a comparator neuron and the illustrated memory or mirror neuron, with information assumed to shift through layers at the data rate, which may also be clocked by "P300" event synchronization).

Whilst (17) is simple and reflects (8), the neural model is thus far very speculative and challenges biological plausibility with some new proposals and assumptions. Furthermore it doesn't explicitly give multiclass Informedness but that is a straightforward higher level embedding, and it doesn't model features or kernels, which is an obvious lower level recursion. We now clarify how we see the shadow and mirror neurons implementing S_{ik} and give an idea of the complexity of the model suggested in Fig. 1(b).

We assume that signals shift through of the order of four layers of memory neurons, as suggested by Cohen's Magical Number Four, providing short term memory essential for associations to form and comparisons to be made, although we show only one such neuron in Fig. 1(b) as that is all that is needed for our purposes to retain the prediction. Note that all logic functions including XOR and EQV can be achieved by two layers of Perceptron-like neurons acting as NAND or NOR gates [21]. These XOR and EQV circuits correspond to our ($p \neq r$) resp. ($p=r$), allowing comparison of prediction and reality in our model. We have explained how Prevalence P_k is directly accumulated using standard Hebbian learning conditioned by the event clock e, as Y_{ek} – and the Inverse Prevalence $\dot{P}_k = 1-P_k = \Sigma_{l \neq k}\, P_l$ can be calculated from e using the divisive operator as shown in Fig. 1(b) or accumulated by lateral synapsing of all other Prevalences similar to many famous models that actually sidestepped the question of complexity of their learning unit [18].

Given the complexity is reasonable, and is indeed reduced from O(N) to O(1) by our divisive operator, the remaining question is how parsimonious the model is. The accumulation of both contingency and prevalence information is standard Hebbian, the assumption of comparison of predictor and predicted is implicit in all the Hebbian and Perceptron rules we have considered – update depends on what happens on both sides of the synapse in all the rules (10-16). The divisive alternative to subtractive inhibition is equivalent to a single transistor and a more straightforward modulation of the signal (similar to Perceptron vs Winnow).

4 Fusion and Boosting

We also noted earlier that both MLPs and Boosting can also be modelled by (9), and in particular AdaBoost [22] assumes a weak learner g() and uses that to learn a strong learner in a very similar way to the Perceptron algorithms we have been considering. If the first layer of AdaBoost is a Decision Stump or Perceptron or Linear SVM, then AdaBoost corresponds to a two stage training mechanism for a two layer Perceptron. The first layer, the weak learners are trained using a standard algorithm selected to be fast rather than strong, and merely has to satisfy a weak learner criterion, namely that it can be expected with high probability to learn a classifier that will do better than chance. However, the standard algorithms define that as Error <0.5, or Accuracy >0.5, where Error is the sum of fp and fn, and Accuracy is the sum of tp and tn (Table 1), and Accuracy + Error = 1, which we abbreviate as Acc = 1 – Err.

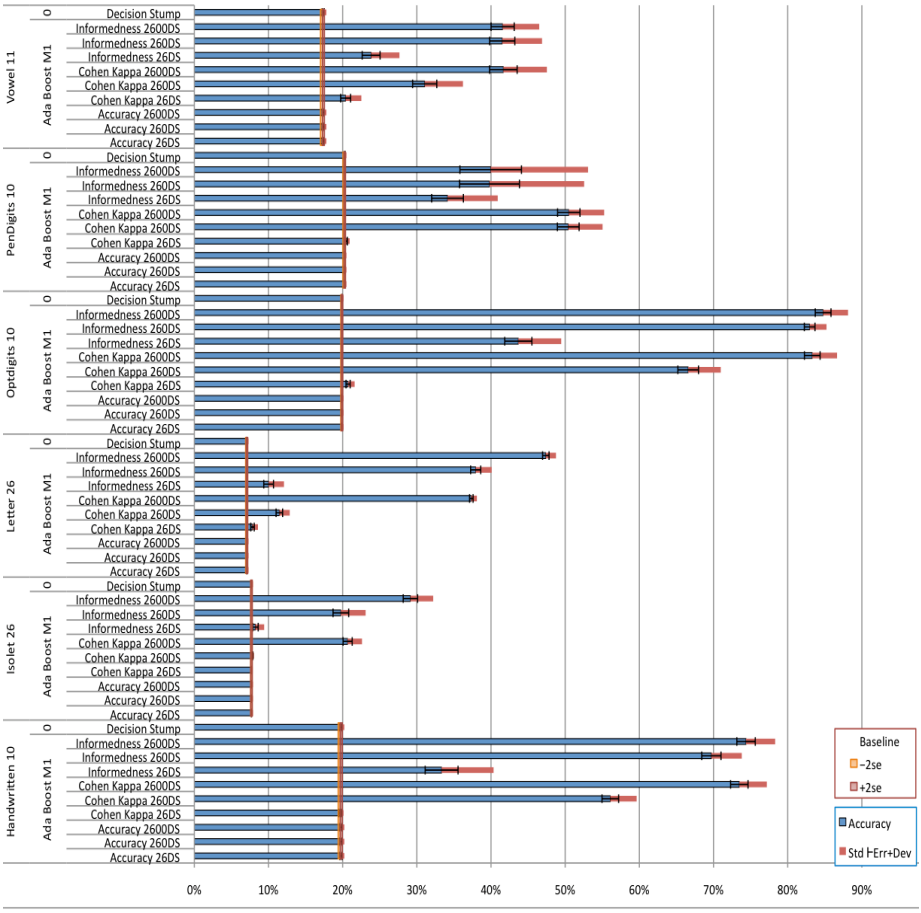

Fig. 2. Accuracy of AdaBoost variants with Decision Stump weak learner

AdaBoost sets the weight associated with each trained classifier g() to the log of the odds ratio Acc / Err, iterating while there is room for improvement (Acc < 1) and it is doing better than 'chance' (Acc > 0.5 in the standard model). Note that as Kappa = (Acc-E(Acc)) / (1-E(Acc)) goes from -1 to +1, Acc goes from 0 to 1, and the same applies for any other Kappa or Correlation measure including ΔP and ΔP' (and ROC AUC). A technique to fix this is simply to calculate $Gini_K = (K+1)/2$, where Gini (being originally designed for ROC AUC) can be applied to any chance-corrected measure K where 0 marks the chance level, mapping this chance level to ½. We can run any boosting algorithm with chance-corrected measure K by replacing Acc by $Gini_K$.

To complete the discussion of AdaBoost, it suffices to note that the different trained classifiers result from training the same weak learner on different weightings (or resamplings) of the available training set, with weights given by the odds Acc / Err.

We have now introduced a neural model that directly implements ΔP or ΔP' (which is purely a matter of direction and both directions are modelled in Fig. 1). We have also shown how a chance-corrected measure can be used for boosting, whether ΔP or ΔP' or Informedness, Markedness or Correlation, The question that follows is whether they are actually useful as learning criteria. For simplicity, we do not consider the bioplausible implementation of the neural net from this perspective, but a direct implementation of Informedness and Markedness in the context of AdaBoost.

5 Results and Conclusions

The most commonly used training algorithm today is SVM, closely followed by AdaBoost, which is actually usually better than SVM when SVM is boosted rather than the default Decision Stump (which is basically the best Perceptron possible based on a single input variable). To test our boosting algorithm, which we call AdaBook because of its Bookmaker corrected accuracy), we used standard UCI Machine Learning datasets relating to English letters (recognizing visually, acoustically or by pen motion). These were selected consistent with our language focus.

AdaBoost in its standard form fails to achieve any boosting on any of these datasets! AdaBook with either Cohen's Kappa [4] or Powers' Informedness [8] doubles, triples or quadruples the accuracy (Fig. 2). Thus we have shown that the use of chance-corrected measures, ΔP rather than TP or TPR, etc. is not only found empirically in Psychological Association experiments, but leads to improved learning in Machine Learning experiments. This applies equally to supervised learning and unsupervised "association" learning or "clustering", and can be applied simultaneously in both directions for "coclustering" or "biclustering" [10,11,18,23].

N.B. Informedness and Information are related through Prevalence P and Euler's constant γ: $\ln P + \gamma \approx \Sigma_{p=1}^{P} 1/p$. This allows an Informatron to accumulate Information.

Acknowledgements. This work was supported by CNSF Grant 61070117, BNSF Grant 4122004, ARC TS0689874, DP0988686 & DP110101473, and the Importation and Development of High-Caliber Talents Project of the Beijing Municipal Institutions.

References

1. Ward, W.C., Jenkins, H.M.: The display of information and the judgement of contingency. Canadian Journal of Psychology 19, 231–241 (1965)
2. Shanks, D.R.: The psychology of association learning. CUP, Cambridge (1995)
3. Perruchet, P., Peereman, R.: The exploitation of distributional information in syllable processing. J. Neurolinguistics 17, 97–119 (2004)
4. Cohen, J.: A coefficient of agreement for nominal scales. Educational and Psychological Measurement, 37–46 (1960)
5. Fleiss, J.L.: Statistical methods for rates and proportions, 2nd edn. Wiley, Chichester (1981)
6. Entwisle, J., Powers, D.M.W.: The Present Use of Statistics in the Evaluation of NLP Parsers. In: NeMLaP3/CoNLL98 Joint Conference, pp. 215–224. ACL (1998)
7. Flach, P.A.: The Geometry of ROC Space: Understanding Machine Learning Metrics through ROC Isometrics. In: Proceedings of the Twentieth International Conference on Machine Learning (ICML 2003), pp. 226–233 (2003)
8. Powers, D.M.W.: Recall and Precision versus the Bookmaker. In: International Conference on Cognitive Science, pp. 529–534 (2003)
9. Powers, D.M.W.: The Problem of Kappa. In: 13th Conference of the European Chapter of the Association for Computational Linguistics, pp. 345–355 (2012)
10. Powers, D.M.W.: Neurolinguistics and Psycho-linguistics as a Basis for Computer Acquisition of Natural Language. SIGART 84, 29–34 (1983)
11. Powers, D.M.W.: Goals, Issues and Directions in Machine Learning of Natural Language and Ontology. SIGART Bulletin 2(1), 101–114 (1991)
12. Finch, S.P.: Finding Structure in Language. Ph.D. thesis, University of Edinburgh (1993)
13. Powers, D.M.W.: Evaluation: From Precision, Recall and F-Measure to ROC, Informedness, Markedness & Correlation. Journal of Machine Learning Technologies 2(1), 37–63 (2011)
14. Collobert, R., Bengio, S.: Links between Perceptrons, MLPs and SVMs. IDIAP Research Report, Dalle Molle Institute for Perceptual Artificial Intelligence (2004)
15. Elman, J.L.: Finding structure in time. Cognitive Science 14, 179–211 (1990)
16. Elman, J.L., Bates, E.A., Johnson, M.H., Karmiloff-Smith, A., Parisi, D., Plukett, K.: Rethinking innateness: A connectionist perspective on development. MIT Press, Cambridge (1996)
17. Munakata, Y., Pfaffly, J.: Hebbian learning and development. Developmental Science 7(2), 141–148 (2004)
18. Powers, D.M.W., Turk, C.C.R.: Machine Learning of Natural Language. Springer, Berlin (1989)
19. Hebb, D.O.: The organization of behaviour. Wiley, New York (1949)
20. Littlestone, N.: Learning Quickly When Irrelevant Attributes Abound: A New Linear-threshold Algorithm. Machine Learning, 285–318 (1988)
21. McCulloch, W.S., Pitts, W.H.: A logical calculus of the ideas immanent in nervous activity. Bulletin of Mathematical Biophysics 5, 115–133 (1943)
22. Shapire, R.E., Freund, Y.: Boosting. MIT Press, Cambridge (2012)
23. Leibbrandt, R.E., Powers, D.M.W.: Frequent frames as cues to part-of-speech in Dutch: why filler frequency matters. In: 32nd Annual Meeting of the Cognitive Science Society (CogSci 2010), pp. 2680–2685 (2010)

Is ERP Old/New Effect Related to Familiarity Memory Modulated by Emotion?

Pengyun Wang[1,2], Yue Wu[3], Jie Gao[4], Wenqi Yang[3], Baoxi Wang[1,2], and Juan Li[1,*]

[1] Center on Aging Psychology, Key Laboratory of Mental Health, Institute of Psychology, Chinese Academy of Sciences, Lincui Road 16, Chaoyang District, Beijing 100101, China
[2] Graduate School, Chinese Academy of Sciences, Beijing, China
[3] School of Psychology, Beijing Normal University, Beijing, China
[4] Department of Psychology, Langfang Normal College, Langfang, China
{Pengyun.Wang,Yue.Wu,Jie.Gao,Wenqi.Yang,
Baoxi.Wang,Juan.Li,LNCS}@Springer.com

Abstract. This study used a modified Remember/Know paradigm to examine whether the old/new effects related to familiarity modulated by emotion. A series of positive, neutral and negative pictures were presented to young adults, and they were asked to watch the pictures carefully like watching TV. After 24 hours, the electroencephalogram was recorded when the participants were performing a recognition memory test with "Remember", "low-confidence Know", "medium-confidence Know", "high-confidence Know", or "New" judgments to each picture. The results showed that the early frontal old/new effect (FN400) in aggregative Know responses of high and medium confidence was found in emotional pictures, but not in neutral ones. The results suggested that the electrophysiological index of familiarity could be affected by emotion.

Keywords: Familiarity, emotion, ERP, FN400, remember, know.

1 Introduction

Emotional stimuli tend to be more easily remembered than neutral ones, a phenomenon termed "emotional memory advantage" [1]. Emotional stimuli attract more attention and are processed more fully, which in turn enhances memory by increasing the distinctiveness with which they are encoded [2]. This effect has been observed for pictures, words, autobiographical experiences, and sounds [3].

Previous studies revealed that emotion had different effect for two distinct memory processing: familiarity and recollection. Familiarity is the feeling that an event has occurred before, but details of this memory are missing; recollection refers to a controlled retrieval of a past event that is accompanied by detailed and associated information of the event, such as time and location [4]. A well-established neural index of familiarity and recollection memory function relying on scalp event-related potentials (ERP) were a 300–500 ms mid-frontal old/new effect (FN400) and a late

* Corresponding author.

D. Liu et al. (Eds.): BICS 2013, LNAI 7888, pp. 157–164, 2013.

positive complex (LPC) with parietal maxima occurring in a 500–700 or 500–800 window, separately [5]. Mostly studies suggest recollection benefits more from emotional materials, but familiarity, as a faster and more automatic process, is less affected by emotional content [2, 4, 6]. However, some studies used the electrophysiological measures or neuroimage method found familiarity memory was modulated by emotion [7, 8].

The Remember/Know paradigm is often used to test the recollection and familiarity. Consistent with the emotional memory advantage phenomenon, a common finding with the Remember/Know task is that the frequency of Remember judgments is increased when test items have an emotional content, whereas Know items tend to remain largely unaffected by emotion (Dewhurst and Parry, 2000; Ochsner, 2000; Kensinger and Corkin, 2003). However, the Know responses inevitably include "lucky guess" to some extent. "Guesses" is not a veritable memory processing. In this line, "guesses" in the Know responses may dilutes the emotional effect in familiarity represented by Know responses. According to the study of Voss, Lucas, and Paller in 2010 [9], Know responses were subdivided into high-, medium-, and low-confidence categories. Only the categories which are above the random chance level are used as a representation for familiarity. Using this modified Remember/Know task, in the present study, we want to investigate whether the ERP old/new effect on familiarity is modulated by emotion.

2 Method

2.1 Participants

Sixteen healthy right-handed under graduate students without history of neurological or psychiatric disorders (9 females, mean age of 20.9, SD=3.8) took part in this study. They completed two experimental sessions with a 24 hours interval, and were paid (120 RMB) for their participation. This study was approved by the ethics committee of the Institute of Psychology, Chinese Academy of Sciences. Written informed consent was obtained from each participant.

2.2 Stimuli

750 pictures (250 for each valence) used in the normal procedure of the current study were obtained from the International Affective Pictures System (IAPS) [10]. 60 alongside similar additional pictures obtained from the Internet using Google Image™. Before being used in the experiment, pictures were re-sized and converted into a 435×327 pixel format, with a resolution of 72 pixels/inch. The pictures were scored for valence and arousal after the retrieval stage. Mean valence and arousal scores were in line with expectations. There were no significant difference between positive and negative pictures in arousal, but they were both higher than neutral ones, $F(2, 747) = 268.62$, $p < .001$. The entire set of pictures was separated into 2 equal sets (A and B) that were alternatively "old" (previously studied) or "new" (unstudied) during the test stage, counterbalanced across participants.

2.3 Procedure

The study was separated into an encoding stage and a retrieval stage, separated by about 24 hours' interval. This interval was consistent with evidence that the effects of emotion on the Remember/Know task are optimal after a long period of consolidation [11]. At the encoding stage, participants viewed the pictures of one of the sets (A or B, counterbalanced across subjects) displayed on a 17" screen, using E-prime™. Emotional and neutral pictures were intermixed, and the order of presentation was fully randomized. In each trial, a fixation (white cross on black background) was displayed for a randomly varying duration (from 1500 to 2000 ms) following a picture displayed for 3000 ms. Participants were asked to look at it carefully like watching a TV. After that, they were asked to finish the Positive Affect Negative Affect Schedule (PANAS) [12].

In the retrieval stage, participants undertook a surprise memory test in which they viewed all the pictures (sets A and B) in a random order, with "old" and "new" items intermixed. In each trial, a fixation (white cross on black background) was displayed for a randomly varying duration (from 1500 to 2000 ms) and followed by a test picture displayed for 5000 ms at most. Next, a screen prompted participants to use five buttons to categorize each stimulus as old or new using response categories on the basis of a modified "remember/know" paradigm [9, 13].

Subjects had previously been given the following instructions as used in Schaefer et al.'s study [14]: "You may recognize the picture very vividly and remember specific details about its previous occurrence. In other words, a remember response implies that you recall something specific that happened when you first encountered this picture, during the first session of this experiment. This may include recalling what you thought when you first encountered this picture, or anything else that happened when you first saw this picture. However, you may just have a feeling of knowing the picture, when you cannot recall specific details about its first occurrence, but simply know that you have seen it before. And the new responses indicated that the word was not presented earlier." Know responses were subdivided into high-, medium-, and low-confidence categories." Scalp electroencephalographic activity (EEG) was recorded during the retrieval session.

There was a practice session using the pictures for practice before the formal retrieval session. During that, each relevant condition was explained using examples and practiced until the participant understood. The experimenter emphasized that the difference between Remember and know was not because of confidence or memory strength. Both Remember and Know may have high memory strength. The main difference was whether there was detailed information was recalled.

After the retrieval session, participants were administrated to finish ratings by a 5-point version of the Self-Assessment Manikin (SAM), a scale evaluating the valence (positive, neutral, or negative) and the level of perceived arousal (calm/aroused) [15]. Participants used the SAM scales to rate their emotional response with a key press.

2.4 Electrophysiological Recordings

Scalp electroencephalographic activity (EEG) was recorded from a 64-channels cap (NeuroScan) at a rate of 500 kHz and an impedance ≤10 kΩ. EEG data was high-pass filtered offline (0.01 Hz), digitally converted to an average mastoids reference, corrected for eye movements [16] and segmented into epochs between 200 ms before and 1500 ms after picture onset. For each channel, epochs with a difference between the maximum and minimum voltage amplitude > 100 μV were rejected (after eye movement artifact correction).

Averaged data was smoothed (30 Hz, 12 dB) and baseline corrected, and participants with less than 16 artifact-free trials in at least one relevant condition were excluded from the analysis. ERP waveforms were created through averaging EEG data for "Remember" trials (correctly recognized items followed by a "Remember" judgment), "high" trials (correctly recognized items followed by a high confidence of "Know" judgment), "medium" trials (correctly recognized items followed by a medium confidence of "Know" judgment), "low" trials (correctly recognized items followed by a low confidence of "Know" judgment), and "New" (N) trials (correctly rejected unstudied items) separately for positive, negative and neutral items.

Mean ERP amplitudes were extracted in two time windows (300–500, 500–800,) corresponding to the two old–new effects targeted by this study: the FN400 and the LPC, respectively. These time windows were selected following both a careful examination of our waveforms and a review of previous findings [5, 17]. We created 6 scalp regions spanning over anterior and posterior regions and left, midline and right laterality: Left Anterior (F5, F3, FC3), Midline Anterior (F1, Fz, F2), Right Anterior (F6, F4, FC4), Left Posterior (P5, P3, PO5), Midline Posterior (P1, Pz, P2) and Right Posterior (P4, P6, PO6).

2.5 Data Analysis

For In order to obtain a memory discrimination score, a Pr score [P (hits) −P (false alarms)] [18] was calculated separately for Remember, and Know judgments in each confidence level. In addition, all Know scores were corrected by dividing it by the probability of an item to not receive an Remember judgment (1−R). This correction was necessary to obtain independent estimates of R and K [19].

On the basis of behavior data results, Remember, medium- and high-confidence Know responses indexed veridical memory rather than hits on the basis of pure chance responding. Low-confidence Know responses, however, were likely based on uninformed guessing. Therefore, we aggregated the medium- and high- confidence Know as to Know+, which represented Familiarity in contrast to recollection represented by Remember responses.

According to the aim of the present study, only the two old–new ERP effects, the FN400 and the LPC, needed to calculate to represent familiarity and recollection. In line with the present studies [5], we only analyzed the ERP for Know+ responses in time window 300-500 in anterior regain (FN400), and the ERP for Remember responses in time window 500-800 in posterior regain (LPC). Thus, for FN400 ERP

effect, a repeated-measures ANOVA was computed including the following factors: (1) Response (Know+ vs. New); (2) Emotion (Positive vs. Neutral vs. Negative); (3) Laterality (Right vs. Midline vs. Left). Similarly, for LPC ERP effect, a repeated-measures ANOVA was computed including the following factors: (1) Response (Remember vs. New); (2) Emotion (Positive vs. Neutral vs. Negative); (3) Laterality (Right vs. Midline vs. Left).

All statistical analyses were carried out with the Statistical Package for Social Sciences version 20.0 (SPSS Inc., Chicago, IL). The Bonferroni correction for multiple comparisons was applied when necessary. The degrees of freedom for the within-subjects comparisons were corrected for deviance from sphericity (Greenhouse-Geisser).

3 Result

3.1 Behavior Performance

As showed in Figure 1, there were no significant main effects of Emotion, $F(2, 14) = 1.47$, $p = .263$, $\eta^2 = .17$, or Response, $F(1, 15) = 0.21$, $p = .657$, $\eta^2 = .01$. The Emotion × Response interaction was significant, $F(2, 14) = 4.92$, $p = .024$, $\eta^2 = .41$. Simple effect test and Post Hoc test revealed that the negative pictures were remembered better than neutral ones in remember responses, $F(2, 30) = 4.63$, $p = .018$, however, there was no difference between emotional and neutral pictures in know+ responses, $F(2, 20) = 1.37$, $p = .270$. The results suggested the emotional enhancement effect (especially for negative valence) could be found in recollection, while familiarity was not affected by emotion.

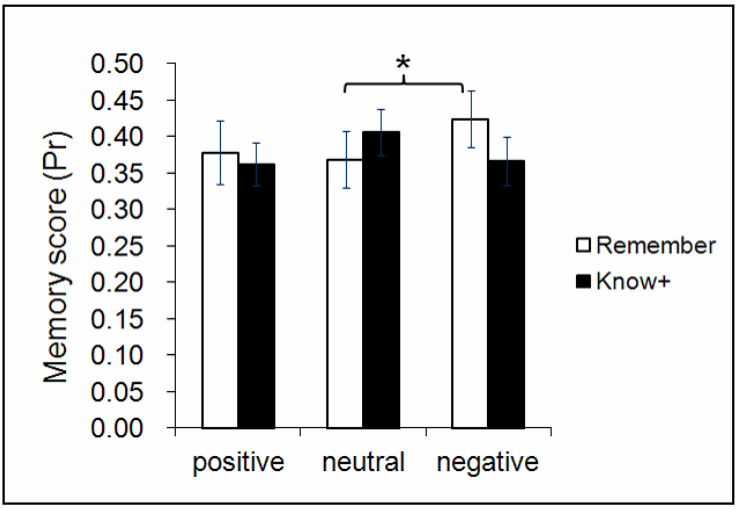

Fig. 1. The behavioral performance of Remember and Know+ responses for emotional and neutral pictures. *Note*. * $p < .05$.

3.2 FN400 Old/New Effect

Starting at about 300 ms, a large frontal old-new effect for "know +" responses was observed mainly for positive and negative pictures. Statistical analysis revealed a significant main effect of response, $F(1, 15) = 23.12$, $p < .001$, $\eta^2 = .61$, and an emotion × response interaction, $F(4, 12) = 4.74$, $p = .016$, $\eta^2 = .51$. Simply effect test revealed there were significant FN400 old/new effects for both positive pictures, $F(1, 15) = 8.58$, $p = .010$, and negative pictures, $F(1, 15) = 12.87$, $p = .003$, however, there was no FN400 old/new effect for neutral pictures, $F(1, 15) = 0.03$, $p = .872$. There were no other significant main or interaction effect (all ps > .05).

3.3 LPC Old/New Effect

Large LPC old-new effect for "remember" responses was observed in 500-800 window for all pictures. The effect was not difference between emotional and neutral pictures. Statistical analysis revealed a significant main effect of Response, $F(1, 15) = 28.25$, $p < .001$, $\eta^2 = .65$, a main effect of Laterality, $F(2, 14) = 11.29$, $p = .001$, $\eta^2 = .62$, and an Response × Laterality interaction, $F(2, 14) = 16.23$, $p < .001$, $\eta^2 = .70$. Simply effect test and Post Hoc test suggested the interaction reflected the significant LPC old/new effect was larger in midline sites, $F(1, 15) = 40.14$, $p < .001$, than in left sites, $F(1, 15) = 18.81$, $p = .001$, and in right sites, $F(1, 15) = 21.92$, $p < .001$. There were no other significant main or interaction effect (all ps > .05).

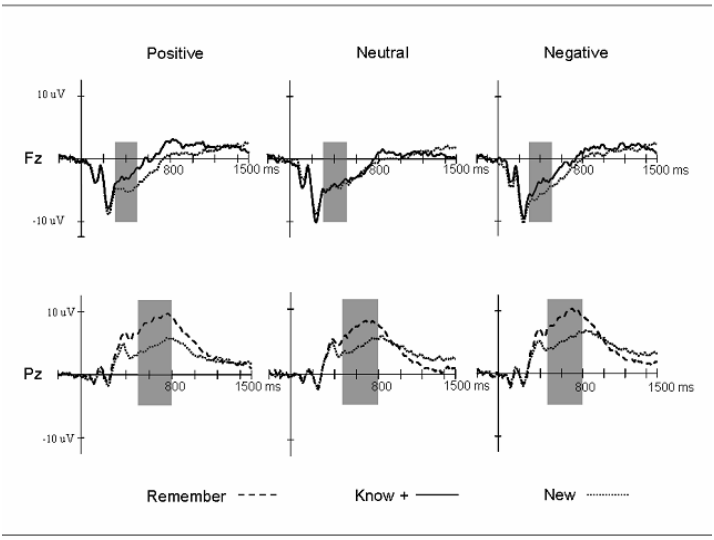

Fig. 2. FN400 and LPC for emotional and neutral pictures

4 Discussion

In the present study, we investigated the emotional memory effect on familiarity induced by purified Know responses (Know+). The result indicated that although there was no emotional effect in behavioral performance on familiarity, the FN400 old/new effect for Know+ responses was found only for emotional (both positive and negative) pictures. It was suggested at least the Electrophysiological index of familiarity could be modulated by emotion. There were obvious LPC old/new effects in both emotional and neutral pictures. Although the statistical analysis did not show a significant difference, form observation of the waveform, the old/new effect seemed larger in positive and negative valence than in neutral valence. Moreover, the behavioral data indicated the negative pictures were remembered better than neutral ones. It was in line with the previous study [20].

The most important finding in present study was that the FN400 old/new effect for the pictures accompanied by a Know+ judgment was modulated by emotion. In contrast to this result, Schaefer, Pottage, & Rickart (2011) also found this emotional modulation for FN400 old/new effect occurs mainly for old items accompanied by a Remember judgment but not for Know judgment [14]. They interpreted this as Remember/Know task primarily as a measure of phenomenal quality of memories, and emotion can exert a significant influence on variations of item memory strength. In our opinion, however, the results were not inconsistent in these two studies. Because participants may rely on both familiarity and recollection when doing a Remember response. Thus, the FN400 old/new effect found in the Remember responses was also an evidence for familiarity. Therefore, the results of both the present study and study of Schaefer et al. in 2011 suggested that the old/new ERP effect on familiarity could be modulated by emotion.

Acknowledgments. This work was supported by the National Natural Science Foundation of China (31271108, 30911120494 and 31070916), the National Science & Technology Pillar Program of China (2009BAI77B03), the Knowledge Innovation Project of the Chinese Academy of Sciences (KSCX2-EW-J-8), and CAS/SAFEA International Partnership Program for Creative Research Team (Y2CX131003).

References

1. Murphy, N.A., Isaacowitz, D.M.: Preferences for Emotional Information in Older and Younger Adults: a Meta-analysis of Memory and Attention Tasks. Psychol. Aging. 23, 263–286 (2008)
2. Ochsner, K.N.: Are Affective Events Richly Recollected or Simply Familiar? The Experience and Process of Recognizing Feelings Past. J. Exp. Psychol. Gen. 129, 242–261 (2000)
3. Spaniol, J., Voss, A., Grady, C.L.: Aging and Emotional Memory: Cognitive Mechanisms Underlying the Positivity Effect. Psychol. Aging. 23, 859–872 (2008)

4. Dolcos, F., LaBar, K.S., Cabeza, R.: Remembering One Year Later: Role of the Amygdala and the Medial Temporal Lobe Memory System in Retrieving Emotional Memories. PNAS Proceedings of the National Academy of Sciences of the United States of America 102, 2626–2631 (2005)
5. Rugg, M.D., Curran, T.: Event-related Potentials and Recognition Memory. Trends. Cogn. Sci. 11, 251–257 (2007)
6. Johansson, M., Mecklinger, A., Treese, A.C.: Recognition Memory for Emotional and Neutral Faces: an Event-related Potential Study. J. Cogn. Neurosci. 16, 1840–1853 (2004)
7. Langeslag, S.J.E., Van Strien, J.W.: Age Differences in the Emotional Modulation of ERP Old/new Effects. Int. J. Psychophysiol. 70, 105–114 (2008)
8. Fenker, D.B., Schott, B.H., Richardson-Klavehn, A., Heinze, H.J., Duzel, E.: Recapitulating Emotional Context: Activity of Amygdala, Hippocampus and Fusiform Cortex During Recollection and Familiarity. Eur. J. Neurosci. 21, 1993–1999 (2005)
9. Voss, J.L., Lucas, H.D., Paller, K.A.: Conceptual Priming and Familiarity: Different Expressions of Memory During Recognition Testing With Distinct Neurophysiological Correlates. J. Cognitive. Neurosci. 22, 2638–2651 (2010)
10. Lang, P.J., Bradley, M.M., Cuthbert, B.N.: International Affective Picture System (IAPS): Affective Ratings of Pictures and Instruction Manual. Technical. Report. A–8. University of Florida, Gainesville, FL (2008)
11. Sharot, T., Yonelinas, A.P.: Differential Time-dependent Effects of Emotion on Recollective Experience and Memory for Contextual Information. Cognition 106, 538–547 (2008)
12. Watson, D., Clark, L.A., Tellegen, A.: Development and Validation of Brief Measures of Positive and Negative Affect: the PANAS Scales. J. Pers. Soc. Psychol. 54, 1063 (1988)
13. Tulving, E.: Memory and Consciousness. Canadian Psychology/Psychologie Canadienne 26, 1–12 (1985)
14. Schaefer, A., Pottage, C.L., Rickart, A.J.: Electrophysiological Correlates of Remembering Emotional Pictures. Neuroimage 54, 714–724 (2011)
15. Bradley, M.M., Lang, P.J.: Measuring Emotion: the Self-Assessment Manikin and the Semantic Differential. J. Behav. Ther. Exp. Psychiatry. 25, 49–59 (1994)
16. Berg, P., Scherg, M.: A Multiple Source Approach to the Correction of Eye Artifacts. Electroencephalogr. Clin. Neurophysiol. 90, 229–241 (1994)
17. Voss, J.L., Paller, K.A.: Remembering and Knowing: Electrophysiological Distinctions at Encoding but not Retrieval. Neuroimage 46, 280–289 (2009)
18. Snodgrass, J.G., Corwin, J.: Pragmatics of Measuring Recognition Memory: Applications to Dementia and Amnesia. J. Exp. Psychol. Gen. 117, 34 (1988)
19. Yonelinas, A.P., Jacoby, L.L.: The Relation Between Remembering and Knowing as Bases for Recognition: Effects of Size Congruency. J. Mem. Lang. 34, 622–643 (1995)
20. Johansson, M., Mecklinger, A., Treese, A.: Recognition Memory for Emotional and Neutral Faces: An Event-Related Potential Study. J. Cognitive. Neurosci. 16, 1840–1853 (2004)

Characteristics of Verbal Serial List Learning in Amnestic Mild Cognitive Impairment: A Profile Analysis of Learning Curve, Retention, Interference, and Serial Position Effect

Pengyun Wang[1,2] and Juan Li[1,*]

[1] Center on Aging Psychology, Key Laboratory of Mental Health, Institute of Psychology, Chinese Academy of Sciences, Lincui Road 16, Chaoyang District, Beijing 100101, China
[2] Graduate School, Chinese Academy of Sciences, Beijing, China
{Pengyun.Wang,Juan.Li,LNCS}@Springer.com

Abstract. Amnestic Mild cognitive impairment (aMCI) is generally considered as a transitional stage between normal aging and a clinical diagnosis of dementia. In the present study, we aimed to investigate the memory impairment features in verbal serial list learning measured by Auditory Verbal Learning Test WHO/UCLA version in aMCI in depth. The results indicated that aMCI patients had a shallower learning curve than normal older adults. However, aMCI patients showed normal retentions, normal proactive and retroactive interference, as well as normal serial position effect. Those results contribute to deeper understanding of memory impairment features in aMCI and indicate areas that can be targeted for intervention.

Keywords: Mild cognitive impairment, aMCI, Memory, AVLT.

1 Introduction

Mild cognitive impairment (MCI) is generally considered as a transitional stage between normal aging and a diagnosis of probable clinical dementia [1]. Amnestic MCI (aMCI) is a subtype in which patients show early memory impairment but do not fulfill the criteria for dementia [2]. Approximately 80% of individuals with aMCI progress to Alzheimer's dementia (AD) at a clinical follow-up after 6 years [1]. It is thus important to investigate the nature of memory deficit in people with aMCI and to identify them at a very early stage.

Previous research has demonstrated that AD patients showed a gentler learning curve and deficits in intertrial acquisition and consolidation than normal older adults on verbal item learning tests [3]. In the present study, we used a verbal item learning test (Auditory Verbal Learning Test WHO/UCLA version, AVLT) [4] to investigate the learning curve in people with aMCI. Besides, we also wanted to investigate the retention, proactive and retroactive interference, and serial positions effect, in order to give a profile description of memory pattern in aMCI patients.

* Corresponding author.

D. Liu et al. (Eds.): BICS 2013, LNAI 7888, pp. 165–171, 2013.

2 Method

2.1 Participants

Thirty-eight older adults diagnosed with aMCI (15 men, 23 women) and 38 healthy older adults (normal control, NC; 15 men, 23 women) were evaluated by experienced psychiatrists from memory disorder clinics and were diagnosed through a consensus procedure. All participants completed a battery of neuropsychological tests, a clinical assessment, and neuroimaging examinations when applicable.

The clinical assessment included a survey of participants' medical history, a basic physical exam, as well as the Neuropsychiatric Inventory, the Activities of Daily Life, the Global Deterioration Scale, the Clinical Dementia Rating, the Hachinski Ischemic Score, and the Structured Clinical Interview for DSM Disorders (depression and anxiety parts only). Research assistants with a background in psychology administered the neuropsychological battery, and psychiatrists were responsible for the clinical assessment. All the research assistants and clinicians had been intensively trained. High inter-rater reliability (above 90%) was obtained at a consensus diagnosis meeting in which the neuropsychological and clinical data were reviewed. The screening process was standardized with a comprehensive Case Report Form recorded for each participant. Experienced psychiatrists performed all clinical diagnoses.

Diagnosis of aMCI was satisfied Petersen's aMCI criteria [1]: (a) Self-report or knowledgeable informant report of subjective memory impairment for at least 6 months, as assessed by direct questioning during initial screening interview. (b) Objective evidence of impairment in memory with scores of Paired Associative Learning Test (subtest of Clinical Memory Test) [5] falling at least 1.5 standard deviations below age and education-matched norms. (c) Preserved general cognitive functions as confirmed by a normal range of the Mini-Mental State Examination (MMSE, for the Chinese version of the MMSE, the most commonly-used criterion for normal general cognition is an MMSE score ≥ 24 for those who had received more than 7 years of education and MMSE score ≥ 20 for those who had received less than 7 years of education) [6]. (d) No significant impact of cognitive deficits on the participant's daily activities, as confirmed by a ADL score of no greater than 20. (e) Nonfulfillment of the Diagnostic and Statistical Manual of Mental Disorders (DSM–IV) criteria for dementia, confirmed by reviewing screening data, neuropsychological testing data, and any available medical records.

Inclusion criteria for the NC group were as follows: (a) normal general cognitive function, (b) normal objective memory performance, and (c) normal activities of daily living. Exclusion criteria for both groups were as follows: (a) significant visual and/or auditory impairment; (b) current diagnosis of, or history of significant medical, neurological, or psychiatric illness, and (c) history of alcohol or substance abuse.

This study was approved by the ethics committee of the Institute of Psychology, Chinese Academy of Sciences. Written informed consent was obtained from each participant. All participants were given a report documenting their performance on the neuropsychological tests, as well as little tokens of appreciation for their participation.

Parts of demographic and neuropsychological characteristics of the aMCI and NC groups are presented in Table 1. All aMCI participants were closely matched with healthy older adult participants in terms of age, gender distribution, and education. Individuals with aMCI scored significantly lower on the Mini-Mental State Examination (MMSE) although all of their scores were in the normal range. The aMCI group showed significant deficits in working memory (Digit Span Forward and Backward Subtest, Chinese version of the Wechsler Memory Scale-Revised) [7], visual spatial ability (Chinese version of Block Design Subtest of the Wechsler Intelligence Scale Revised) [8], and language ability through a verbal fluency test [9], compared to the NC group. There were no significant group differences on semantic memory, which was determined through a category fluency test [9].

Table 1. Demographic data and neuropsychological test data by group

Variable or test	NC (n = 38)		aMCI (n = 38)		*t*
	Mean	SD	Mean	SD	
Age (in years)	69.16	6.35	69.47	7.17	0.20
Education (in years)	8.21	2.33	7.76	2.76	1.32
MMSE	27.95	1.90	24.95	2.90	5.33***
Digit span (forward)	10.00	1.83	8.37	2.78	3.02**
Digit span (backward)	5.87	2.11	3.95	1.49	4.59***
Verbal fluency (fa)	7.18	3.38	5.16	3.02	2.76**
Category fluency (vegetables)	15.92	4.47	14.66	4.06	1.29
Block design	27.76	8.18	20.71	7.63	3.39***

Notes. ** $p < .01$, *** $p < .001$.

2.2 Measures and Procedure

The administration of the AVLT (WHO-UCLA version) involves study and test trials of 2 lists of 15 concrete nouns (1 critical list and 1 distracter list). Stimulus words were read aloud at a rate of approximately 1 word per second. Participants were instructed to remember as many words as possible and to recall them in any order. Words on the critical list were presented in the same order for the 5 study-test trials. After the fifth test trial of the critical list, participants performed 20 min of non-memory-related activities, after which they were again asked to recall the words from the critical list (trial 6). Subsequently, the distracter list was presented for 1 study-test trial (trial 7). Immediately following this study-test trial of the distracter list, participants were asked to recall all the words from the critical list (trial 8). The timing of the presentation of the distracter list was adjusted from the position after the fifth study-test trial in the initial WHO/UCLA version [4] in order to get a delayed recall performance unaffected by the distracters. Only the first 5 study-test trials were analyzed according to the purpose of the present study.

2.3 Data Analysis

Statistical analyses were carried out with the Statistical Package for Social Sciences (SPSS) version 20.0. T test were performed to examine the group differences in demographic variables and other neurocognitive function measures. Mixed-design analysis of variance (ANOVA) was conducted to analyze the learning curve, retention, proactive and retroactive interference, as well as serial position effect. Bonferroni correction for multiple comparisons was applied when necessary.

3 Result

3.1 Learning Curve

The analysis on trials 1 through 5 revealed that the aMCI patients performed worse than NC, $F(1, 74) = 48.73$, $p < .001$, $\eta^2 p = 0.40$. A main effect of trial was significant, $F(4, 71) = 65.61$, $p < .001$, $\eta^2 p = 0.79$. Pairwise comparison indicated that trial-by-trial performance increased significantly, all ps $< .001$, expected trial 4 vs. 5 ($p > .05$). Moreover, there was a significant interaction between group and trial, $F(4, 71) = 3.84$, $p = .007$, $\eta^2 p = 0.18$. Subsequently simple effect and pairwise analysis revealed that, for both groups, scores increased significantly over the four trial, all ps $< .01$, expected trial 4 vs. 5 (ps $> .05$). As evident from inspection of Figure 1, this interaction is due to less of an increase in performance across trials for aMCI patients as compared to NC.

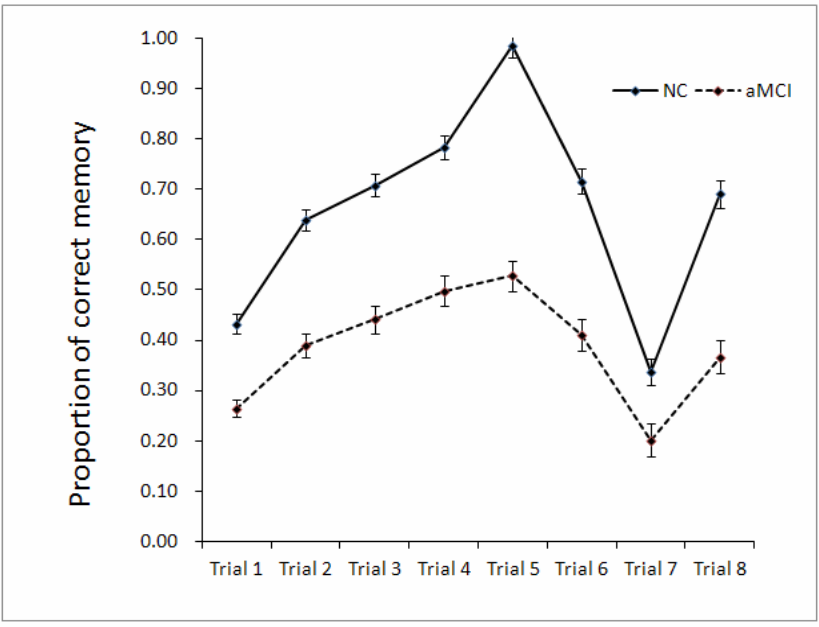

Fig. 1. The learning curve of AVLT for aMCI and NC groups

3.2 Retention

The trial 5 versus trial 6 comparison examines the retention of list words after 20 min relative to the most likely 'best' performance after five consecutive learning trials. The main effect for Group was significant, $F(1, 73) = 18.55$, $p < .001$, $\eta^2 p = 0.20$. And the main effect for Trial was significant, $F(1, 73) = 4.94$, $p = .029$, $\eta^2 p = 0.06$. The Group x Trial interaction was not significant, $F(1,73) = 0.75$, $p = .390$, $\eta^2 p = 0.01$. The result indicated that the retention of memory was not impairment in aMCI patients, although their memory ability was declined obviously.

3.3 Proactive and Retroactive Interference

The extent to which prior learning interferes with the recall of a new word list can be evaluated by comparing the number of words recalled after the first presentation of the first word list to the number of words recalled from the distractor list (trial 1 vs. trial 7). The main effect for Group was significant, $F(1,72) = 38.64$, $p < .001$, $\eta^2 p = 0.35$. The main effect for Trial was also significant, $F(1,72) = 18.21$, $p < .001$, $\eta^2 p = 0.20$. However, the Group × Trial interaction was not significant, $F(1,72) = 0.87$, $p = .353$, $\eta^2 p = 0.01$. It suggested that, like NC, the aMCI patients had normal proactive interference, although their memory ability was impaired.

The extent to which learning a new list interferes with recall of a previously learned list may be examined by comparing recall at trial 6 (prior to presentation of the distractor list) to recall at trial 8 (following presentation of the distractor list). The main effect for Group was significant, $F(1,71) = 33.26$, $p < .001$, $\eta^2 p = 0.32$. The main effect for Trial was also significant, $F(1,71) = 8.10$, $p = .006$, $\eta^2 p = 0.10$. However, the Group × Trial interaction was not significant, $F(1,71) = 0.62$, $p = .435$, $\eta^2 p = 0.01$. It suggested that, like NC, the aMCI patients had normal retroactive interference, although their memory ability was impaired.

3.4 Serial Positions Effect

To provide a more complete characterization of multi-trial performance, we examined performance on the AVLT across various serial positions of the presentation of items. As described previously [3], performance across the serial positions was collapsed into three segments: 'Primacy' is performance collapsed across serial positions 1-3, 'asymptote' is performance collapsed across positions 5-11, and 'recency' is performance collapsed across serial positions 13-15. Means across individual subject's values for each of the three segments and for the five critical study-test trials was showed in figure 2.

The main effect for Group was significant, $F(1,72) = 53.21$, $p < .001$, $\eta^2 p = 0.43$. The main effect for Trial was also significant, $F(2,71) = 14.41$, $p < .001$, $\eta^2 p = 0.29$. However, the Group × Trial interaction was not significant, $F(2,71) = 0.21$, $p = .809$, $\eta^2 p = 0.01$. It suggested that, like NC, the aMCI patients had normal serial positive effect, although their memory ability was impaired.

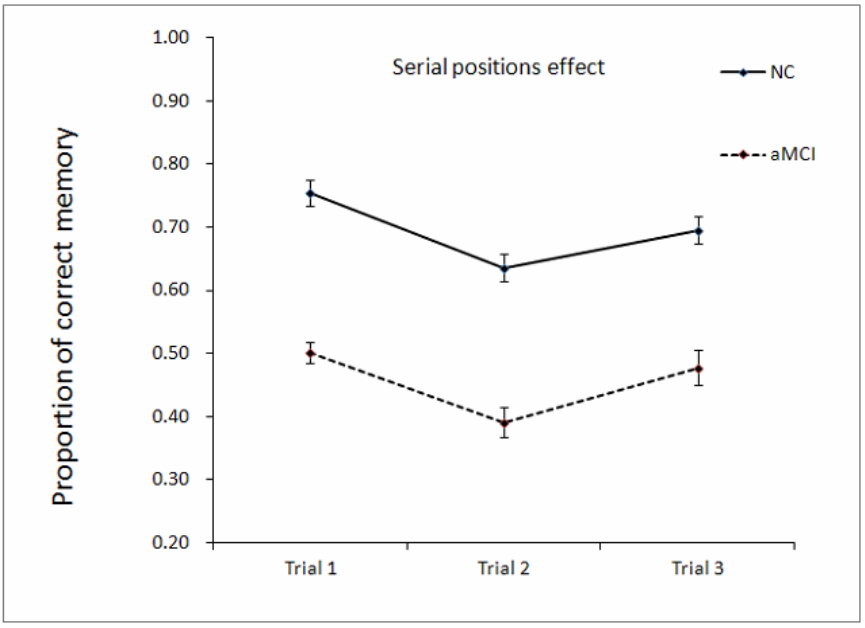

Fig. 2. Serial positions effect in aMCI and NC

4 Discussion

The result indicated that the retention of memory was not impairment in aMCI patients, although their memory ability was declined obviously. It suggested the memory impairment in aMCI patients may be mainly because of their deficit in encoding new information, but not of retention. However, we cannot rule out the possibility that the interaction came from scale effects [10, 11], since there were clear differences in score in Trial 1.

The present found obvious proactive interference in aMCI patient as in NCs, which was consistent with prior studies [12, 13], but not [14]. In analysis of retroactive interference, Libon et al. (2011) found that, as compared to NC groups, aMCI patients appeared to be very susceptible to the deleterious effect of the interference test condition along with greater penetration of list B words into subsequent list A recall [14]. However, in the present study, we did not found that the aMCI patients were susceptible for distracters. As mentioned above, however, we cannot rule out the possibility that the interaction came from scale effects, since there were clear differences in score in each calculated trial.

A normal serial positions effect was found in both NC and aMCI groups. The rationale of serial positions effect may come from the effect of proactive and retroactive interference, or may be because of the different effect of short term memory and long term memory. The present study suggested that although the performance of aMCI patients was impaired, the memory pattern in serial positions was the same as the NCs.

The current study gave a profile analysis of learning curve, retention, proactive and retroactive interference, as well as serial positions effect in aMCI patients. Our results, together with those of previous studies, contribute to deeper understanding of memory function impairment in aMCI and indicate areas that can be targeted for intervention.

Acknowledgments. This work was supported by the National Natural Science Foundation of China (31271108, 30911120494 and 31070916), the National Science & Technology Pillar Program of China (2009BAI77B03), the Knowledge Innovation Project of the Chinese Academy of Sciences (KSCX2-EW-J-8), and CAS/SAFEA International Partnership Program for Creative Research Team (Y2CX131003).

References

1. Petersen, R.C.: Mild Cognitive Impairment as a Diagnostic Entity. J. Intern. Med. 256, 183–194 (2004)
2. Petersen, R.C., Doody, R., Kurz, A., Mohs, R.C., Morris, J.C., Rabins, P.V., et al.: Current Concepts in Mild Cognitive Impairment. Arch. Neurol-Chicago 58, 1985–1992 (2001)
3. Woodard, J.L., Dunlosky, J., Salthouse, T.A.: Task Decomposition Analysis of Intertrial Free Recall Performance on the Rey Auditory Verbal Learning Test in normal Aging and Alzheimer's Disease. J. Clin. Exp. Neuropsyc. 21, 666–676 (1999)
4. Maj, M., Satz, P., Janssen, R., Zaudig, M., Starace, F., Delia, L., et al.: WHO Neuropsychiatric AIDS Study, Cross-sectional Phase-II - Neuropsychological and Neurological Findings. Arch. Gen. Psychiat. 51, 51–61 (1994)
5. Cooperative, CMS.: The Manual of Clinical Memory Test (rev. ed.). Institute of Psychology, Chinese Academy of Sciences, Beijing (1996)
6. Zhang, M.Y.: Handbook of Rating Scales in Psychiatry. Hunan Science and Technology Press, Changsha (1998)
7. Gong, Y.X., Jiang, D.W., Deng, J.L., Dai, Z.S., Zhou, Q.Z., Xie, G.Y., Li, Y., Hua, X.X.: Manual of Wechsler Memory Scale—Chinese Version. Hunan Medical College Press, Changsha (1989)
8. Gong, Y.X.: Manual of Wechsler Adult Intelligence Scale-Chinese version. Chinese Map Press, Changsha (1992)
9. Spreen, O., Strauss, E.: A Compendium of Neuropsychological Tests: Administration, Norms, and Commentary. Oxford University Press, USA (1998)
10. Wagenmakers, E.J., Krypotos, A.M., Criss, A.H., Iverson, G.: On the Interpretation of Removable Interactions: A Survey of the Field 33 Years after Loftus. Mem. Cognit., 1–16 (2012)
11. Loftus, G.R.: On Interpretation of Interactions. Mem. Cognit. 6, 312–319 (1978)
12. Loewenstein, D.A., Acevedo, A., Luis, C., Crum, T., Barker, W.W., Duara, R.: Semantic Interference Deficits and the Detection of Mild Alzheimer's Disease and Mild Cognitive Impairment Without Dementia. J. Int. Neuropsych. Soc. 10, 91–100 (2004)
13. Loewenstein, D.A., Acevedo, A., Agron, J., Duara, R.: Vulnerability to Proactive Semantic Interference and Progression to Dementia among Older Adults with Mild Cognitive Impairment. Dement. Geriatr. Cogn. 24, 363–368 (2007)
14. Libon, D.J., Bondi, M.W., Price, C.C., Lamar, M., Eppig, J., Wambach, D.M., et al.: Verbal Serial List Learning in Mild Cognitive Impairment: A Profile Analysis of Interference, Forgetting, and Errors. J. Int. Neuropsych. Soc. 17, 905–914 (2011)

Ontology-Based Collaborative Filtering Recommendation Algorithm

Zijian Zhang, Lin Gong, and Jian Xie

School of Mechanical Engineering,
Beijing Institute of Technology, Beijing, 100081, China
bitie_zzj@foxmail.com

Abstract. E-learning system for knowledge points recommended primarily uses traditional collaborative filtering algorithm. Similarity calculation of knowledge points is often based on user rating above the intersection of knowledge points. The different semantic relations between knowledge points are not well considered, which results in the low recommended accuracy. This paper proposed an Ontology-based collaborative filtering recommendation algorithm, which could help users find the nearest neighbors even if the scores of knowledge points are little or zero. Through experiment, this algorithm was compared to traditional collaborative filtering recommendation algorithms. The new method achieved a better recommendation.

Keywords: collaborative filtering, similarity calculation of knowledge points, semantic relations, ontology.

1 Introduction

With the development of the World Wide Web, a lot of people are turning to e-learning via web[1]. But the users are facing mass information of learning resources, it is very difficult to find needed resources. More and more scholars dedicate to the study of the recommendation algorithm [2].

In order to guarantee that the recommendation system has a relatively precise recommendation under the condition of real-time, researchers have proposed a variety of different recommendation algorithm, which is widely used in collaborative filtering recommendation system. Typestry is the earliest proposed collaborative filtering recommendation system, but target users are required explicitly to point out the similarity to other users with their own behavior[3]. GroupLens is based on user ratings automated collaborative filtering recommendation system for recommending videos and News [4]. Ringo recommendation system and Video recommendation system by electronic mail way recommend music and videos [5, 6]. Breese and others have a deep analysis on a variety of collaborative filtering algorithm and their improvement. The traditional collaborative filtering recommendation is through users' nearest neighbors to get recommendation results. Item-based collaborative filtering recommendation firstly calculates the correlation between the items, and then predicts ungraded items' ratings through users' ratings on related items.

D. Liu et al. (Eds.): BICS 2013, LNAI 7888, pp. 172–181, 2013.

Nearest neighbors collaborative filtering recommendation is one of the most successful recommended techniques[7], which is based on such an assumption: if different users scored the same items with similar ratings, their other items' ratings will also be similar. The basic idea of the algorithm is that the scores of ungraded items are approximated by the items' ratings which are scored by the target users' nearest neighbors.

In order to identify the target users' nearest neighbors, it is necessary to measure the similarity between users. However, with the expansion of the scale of the E-learning system, the number of users and knowledge points data increases dramatically. User rating data is extreme sparsity[8], which makes traditional similarity measurement methods to get the set of latest knowledge not accurate enough, resulting in the algorithm recommendation's lowering quality.

In order to solve the problem that user rating data is extremely sparse, the singular value decomposition which is referred to as SVD is proposed to reduce the items space dimension [9]. But dimensionality reduction may lead to the information loss and search quality's degradation, which makes this method hard to guarantee recommendation's effect when dealing with arbitrary high dimensional problems[10].Because of this, a collaborative filtering recommendation technology based on Item Rating is proposed. Through the estimation of user rating to supply users-items matrix, it can reduce the data sparsity, and negative impact on the calculation results. Because this algorithm to calculate similar items still adhere to the traditional similarity calculation methods, and did not consider classified information of the items, the recommendation's quality is declined. Based on the former work, a collaborative filtering recommendation algorithm based on items classified information is put forward [11]. The modified conditional probabilities are used to compute similarity between items, and to estimate items' scores. Through filling the users-items matrix, users' similarity can be calculated according to the filled users - items matrix, and we can achieve good results with this method . However, the algorithm still scores all items as a single vector to calculate user's similarity and conduct the selection of the nearest neighbors. The accuracy of the algorithm is affected to some extent .

In this paper, Ontology-based collaborative filtering algorithm overcame the deficiencies of traditional vector-based similarity comparison method, which strictly matches the properties of the object. and improved the accuracy of the recommendation.

2 The Traditional Similarity Measure for Collaborative Filtering

The methods of similarity measure between users include the following: cosine similarity, correlation similarity and adjusted cosine similarity[12]:

2.1 Cosine Similarity

The user ratings are regarded as the n-dimensional item space vectors. The similarity between users is measured by the cosine of the angle between vectors.

User i and user j in the space of n-dimensional item ratings are expressed as vectors $\vec{i}$, $\vec{j}$, the similarity between user i and user j is

$$sim(i, j) = \cos(\vec{i}, \vec{j}) = \frac{\vec{i} \cdot \vec{j}}{\left|\vec{i}\right| \cdot \left|\vec{j}\right|}. \tag{1}$$

2.2 Adjusted Cosine Similarity

Cosine similarity measure method does not consider the different users' rating scale problem. The adjusted cosine similarity measure improves the above defects through subtracting the item's average score. The items' collection which is scored by user i and user j is represented by I_{ij} , I_i denotes the items' collection, which is scored by user i ; I_j denotes the items' collection, which is scored by user j , the similarity between user i and user j is :

$$sim(i, j) = \frac{\sum_{c \in I_{ij}} (R_{i,c} - \overline{R}_i)(R_{j,c} - \overline{R}_j)}{\sqrt{\sum_{c \in I_i} (R_{i,c} - \overline{R}_i)^2} \sqrt{\sum_{c \in I_j} (R_{j,c} - \overline{R}_j)^2}}. \tag{2}$$

$R_{i,c}$ denotes the score of item c from user i. $\overline{R}_i$ and $\overline{R}_j$ respectively denote the average score of items scored by user i , user j .

2.3 Correlation Similarity

The items' collection which is scored by user i and user j is represented by I_{ij} , the similarity between user i and user j is measured by the Pearson Correlation Coefficient:

$$sim(i, j) = \frac{\sum_{c \in I_{ij}} (R_{i,c} - \overline{R}_i)(R_{j,c} - \overline{R}_j)}{\sqrt{\sum_{c \in I_{ij}} (R_{i,c} - \overline{R}_i)^2} \sqrt{\sum_{c \in I_{ij}} (R_{j,c} - \overline{R}_j)^2}}. \tag{3}$$

$R_{i,c}$ denotes the score of item c from user i , $\overline{R}_i$ and $\overline{R}_j$ respectively denote the average score of items scored by user i , user j .

Generally speaking, the three ways are vector-based similarity calculations and strictly match between the object properties.

Cosine similarity measures the user rating as a vector, using the cosine of the angle of the vector to measure the similarity between users. It does not contain the statistical characteristics of user ratings. Adjusted cosine similarity method is based on cosine similarity subtracts the items' average ratings which are scored by users. However, the method is embodied correlation rather than similarity between users, correlation and similarity are clearly two different concepts. Similarity reflects the polymerization characteristics, while the correlation reflects the combination of features; Correlation similarity method is based on the joint scored items to evaluate users' similarity. If all scored items between users are common scored items, correlation similarity is so equivalent with adjusted cosine similarity. Although the users ratings on the common items do perfectly reflect the similarity degree between users, but correlation similarity evaluation method is not actually feasible, because of the common items rated by users which are extremely rare. Due to the extreme sparsity of user rating data, filling the users - items matrix is proposed as an improved method.

3 Ontology-Based Collaborative Filtering Recommendation Algorithm

3.1 The Construction of Ontology

In order to improve the accuracy of similarity calculation based on the traditional "intersection" vector in the E-learning system, this paper proposed the following method: predicting user ratings for knowledge points was essentially to find out the relationship between the scored knowledge points and the not scored knowledge points. This contact is the similarity between the two knowledge points, if the rated knowledge points have higher similarity with the not scored knowledge points, the two knowledge points are scored more similarly.

Ontology is used to build the semantic modeling about users' interested knowledge points. If users search the knowledge point A, E-learning system can be considered that user is interested in knowledge point A. Interested knowledge points can be semantic descripted by the lessons group characteristics knowledge ontology. Knowledge point A can be located as a feature node in lessons group characteristics concept ontology, the similarity between knowledge point A with other knowledge points in the ontology can be calculated offline.

Construct a lessons group characteristics of knowledge ontology. In the lessons group characteristics knowledge ontology, the first layer is lessons group, the second layer is a branch of the lessons group courses, the third layer is relevant sections of the courses, and the fourth layer is each chapters' specific knowledge points. Each specific knowledge point corresponds to a knowledge instance. As shown in the figure below, it can be used to describe the hierarchy of knowledge points.

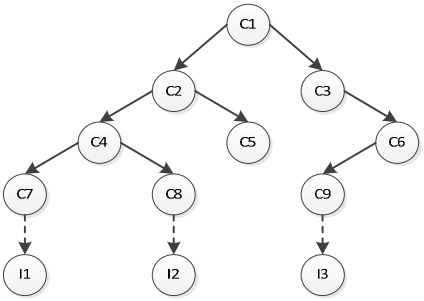

Fig. 1. Lessons group characteristics knowledge ontology

Through the above description for lessons group characteristics knowledge ontology, for example, the course of applied statistics has the characteristics of knowledge points : estimation method and skewness. The statistics lessons group characteristics knowledge ontology can be constructed.

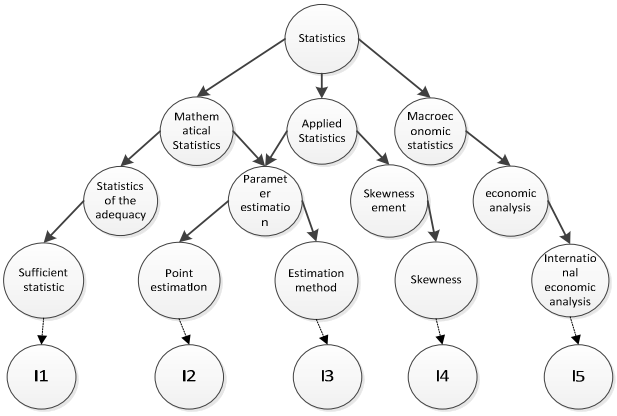

Fig. 2. Statistics lessons group characteristics knowledge ontology

This lessons group characteristics knowledge ontology can describe the users interested in knowledge points of curriculum level.

3.2 Knowledge Similarity Algorithm

3.2.1 Similarity Calculation

Get the collection of all knowledge points $C = \{C_1 C_2 C_3 \ldots\ldots C_n\}$,n denotes the number of knowledge points, $\mathrm{sim}(C_i, C_j)$ denotes the similarity between C_i and C_j , the calculation is as follows:

$$\mathrm{sim}(C_i, C_j) = \begin{cases} \dfrac{\mathrm{a} \times \left(\mathrm{d}(C_i) + \mathrm{d}(C_j)\right)}{\left(\mathrm{CE}(C_i, C_j) + \mathrm{a}\right) \times 2 \times \mathrm{Dep} \times \max\left(\left|\mathrm{d}(C_i) - \mathrm{d}(C_j)\right|, 1\right)} & C_i \neq C_j \\ 1 & C_i = C_j \end{cases}. \tag{4}$$

$\mathrm{d}(C_i)$ and $\mathrm{d}(C_j)$ respectively denote the level of knowledge point C_i and C_j in the ontology, $\mathrm{CE}(C_i, C_j)$ denotes the shortest way from C_i to C_j, Dep denotes the maximum depth in the ontology, a is a given parameter, usually $a \geq 0$.

Obviously, the level of knowledge points in the statistics lessons group characteristics knowledge ontology is 4,the maximum depth is 4. The above formula can be simplified as follows:

$$\mathrm{sim}(C_i, C_j) = \begin{cases} \dfrac{\mathrm{a}}{\left(\mathrm{CE}(C_i, C_j) + \mathrm{a}\right)} & C_i \neq C_j \\ 1 & C_i = C_j \end{cases}. \tag{5}$$

The similarity between knowledge points can be calculated according to the above formula.

3.2.2 The Algorithm Test

As figure 2 shown, the shortest path between "point estimation" and "estimation method" is 2, and their similarity is $\dfrac{\mathrm{a}}{(2+\mathrm{a})}$. The shortest path between "skewness" and "estimation method" is 4, their similarity is $\dfrac{\mathrm{a}}{(4+\mathrm{a})}$.The shortest path between "international economic analysis" and "estimation method" is 6,their similarity is $\dfrac{\mathrm{a}}{(6+\mathrm{a})}$,obviously $\dfrac{\mathrm{a}}{(2+\mathrm{a})} > \dfrac{\mathrm{a}}{(4+\mathrm{a})} > \dfrac{\mathrm{a}}{(6+\mathrm{a})}$ .If the path between the two knowledge points is too long, the similarity between the two knowledge points is very low, which is consistent with common sense.

3.2.3 The Implementation of Collaborative Filtering Recommendation Algorithm Based on Ontology

In this paper, according to the proposed recommendation algorithm, recommended results are produced. The algorithm described as follows:

Input: users–scored knowledge points matrix is $R\ (m,n)$,the similarity between knowledge points is $\mathrm{sim}(C_i, C_j)$.

Output: the target user U_i recommendation rating on knowledge point i.

Step 1: retrieve the users' interested knowledge points. Filling the current users – scored knowledge points matrix $R\ (m,n)$.

Table 1. The current users–scored knowledge points matrix

	C_1	C_2	$\cdots$	C_j	$\cdots$	C_n
U_1	R_{11}	R_{12}	$\cdots$	R_{1j}	$\cdots$	R_{1n}
U_2	R_{21}	R_{22}	$\cdots$	R_{2j}	$\cdots$	R_{2n}
$\vdots$	$\vdots$	$\vdots$	$\ddots$	$\vdots$		$\vdots$
U_i	R_{i1}	R_{i2}	$\cdots$	R_{ij}	$\cdots$	R_{in}
$\vdots$	$\vdots$	$\vdots$		$\vdots$	$\ddots$	$\vdots$
U_m	R_{m1}	R_{m2}	$\cdots$	R_{mj}	$\cdots$	R_{mn}

U_i denotes user i, C_j denotes knowledge point j, R_{ij} denotes the rating of knowledge point j which user i scores.

Step 2: Calculating the similarity between knowledge points. Based on the previously proposed algorithm, $\mathrm{sim}(C_i, C_j)$ is calculated. For knowledge point C, searching the top k of nearest neighbors $neighbors = \{C_1, C_2, \ldots, C_k\}$, $C \notin neighbors$,in condition of $\forall a \in [1,k], \forall b \in [k+1,n], sim(\mathrm{C}, C_a) > sim(\mathrm{C}, C_b)$ is established.

Step 3: Generate recommendation results. Find the nearest neighbors of the knowledge points, produce the appropriate recommendation.

p_{u_i,c_t} is the prediction score of C_t which is not scored by U_i,which can be got from the scored neighbors of C_t, Computation formula is as follows:

$$p_{u_i,\mathrm{c}_t} = \overline{R}_{c_t} + \frac{\sum_{c_i \in neighbors_{\mathrm{c_t}}, u_j \in U} (R_{\mathrm{u_j},c_i} - \overline{R}_{c_i}) \times sim(C_{\mathrm{t}}, C_{\mathrm{i}})}{\sum_{c_i \in neighbors_{\mathrm{c_t}}} sim(C_{\mathrm{t}}, C_{\mathrm{i}})}. \tag{6}$$

$sim(C_t, C_i)$ denotes the similarity between C_t and C_i ,The users' collection is represented by $U = \{U_1, U_{2,\ldots,} U_m\}$. R_{u_j, c_i} denotes the rating of knowledge point C_i which U_i scores. $\overline{R}_{c_t}$ and $\overline{R}_{c_i}$ respectively denote the average score of knowledge point C_t and C_i . Through the above method, predict all ungraded knowledge points' score and then the top g of highest prediction score of knowledge points' knowledge instances are recommended as results feding back to the current users.

4 Experiment and Analysis

In this paper, data from the MovieLens site is used to compare the proposed algorithm with traditional collaborative filtering algorithm. Movielens is the state university of Minnesota, Grouplens computer science research team gathering for the collaborative filtering algorithm of data set, which includes 943 users ,1682 movies,100000 score (rating value: 1-5) records. Each user has at least evaluated 20 films, and it includes the users' simple demographic information and classified information of the movies. This paper will use these data to verify the effectiveness of collaborative filtering recommendation algorithm based on ontology.

Recommended quality evaluation criteria are mainly two categories: statistical accuracy metrics and decision-support accuracy metrics. The mean absolute error(MAE) in the statistical accuracy metrics is a commonly used measurement method.

In this paper, the mean absolute error is taken as a metrics. The MEA can evaluate the accuracy of the forecasts, by calculating deviation between the prediction score of knowledge points and the actual score of knowledge point. If the MAE is smaller, the recommended quality is higher. Predicted user ratings collection $\{p_1, p_2, \ldots, p_n\}$, the actual user rating collection $\{q_1, q_2, \ldots, q_n\}$, the mean absolute error formula is as below:

$$\mathrm{MAE} = \frac{\sum_{i=1}^{N} |p_i - q_i|}{N}. \tag{7}$$

In order to test the proposed algorithm improvements in accurately predicting score, the traditional project-based collaborative filtering recommendation method (using the cosine similarity, adjusted cosine similarity and collection similarity) and the proposed recommendation algorithm are used to recommend knowledge points, the number of collection knowledge points nearest neighbors is set to 5, 10, 15, 20, 25. Respectively, the above five sets of data are used to predict score, as shown below:

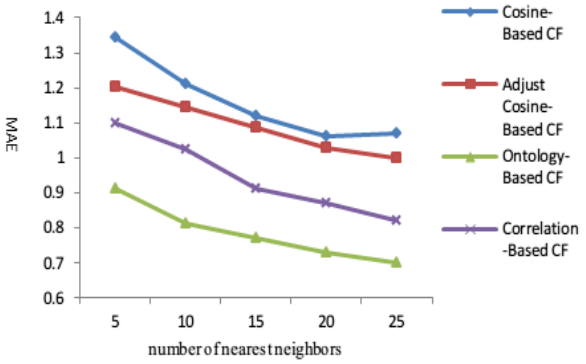

Fig. 3. The result of the experiment

The result of experiment shows that the proposed collaborative filtering algorithm's MAE is always the smallest when the number of nearest neighbors is set to5, 10, 15, 20, 25. That proves our approach to predict score of knowledge points is more accurate than traditional collaborative filtering algorithm. After analysis, The reason is as follow: the similarity between not scored knowledge point and scored knowledge point is 0, when using traditional collaborative filtering algorithm to calculate. The way to calculate similarity is not accurate. According to the semantic relationship between the two knowledge points, the similarity can be calculated more accurate with the proposed collaborative filtering algorithm. Because of that, we can have higher recommendation quality with the proposed approach.

5 Conclusions

This paper has a deep analysis of traditional collaborative filtering recommendation algorithm's problem, in the situation of a few user ratings knowledge points and the data extreme sparse when the E-learning system startup. In order to solve the problem, collaborative filtering recommendation algorithm based on ontology is put forward to calculate the similarity of user rating knowledge points. Experimental results show that using this algorithm can not only solve the problems of few user ratings and data extreme sparse in case of the system "cold start" phenomenon, but also improve the quality and accuracy of the recommendation system. The focus of future research is how to apply the proposed algorithm to the actual knowledge recommendation system.

References

1. Sangodiah, A., Heng, L.E.: Integration of data quality component in an ontology-based knowledge management approach for e-learning system. In: 2012 International Conference on Computer and Information Science, ICCIS 2012 - A Conference of World Engineering, Science and Technology Congress, ESTCON 2012, June 12-14, vol. 1, pp. 105–108. IEEE Computer Society, Kuala Lumpur (2012)

2. Perugini, S., Gon, C.C., Alves, M.A., Fox, E.A.: Recommender systems research: A connection-centric survey. J. Intell. Inf. Syst. 23, 107–143 (2004)
3. Goldberg, D., Nichols, D., Oki, B.M., Terry, D.: Using collaborative filtering to weave an information tapestry. Commun. ACM 35, 61–70 (1992)
4. Resnick, P., Iacovou, N., Suchak, M., Bergstrom, P., Riedl, J.: GroupLens: an open architecture for collaborative filtering of netnews, pp. 175–186 (1994)
5. Shardanand, U., Maes, P.: Social information filtering: algorithms for automating "word of mouth", pp. 210–217 (1995)
6. Hill, W., Stead, L., Rosenstein, M., Furnas, G.: Recommending and evaluating choices in a virtual community of use, pp. 194–201 (1995)
7. Sang, H.C., Young-Seon, J., Jeong, M.K.: A Hybrid Recommendation Method with Reduced Data for Large-Scale Application. IEEE Transactions on Systems, Man, and Cybernetics, Part C: Applications and Reviews 40, 557–566 (2010)
8. Ying, Y.: The personalized recommendation algorithm based on item semantic similarity. In: Ma, M. (ed.) Communication Systems and Information Technology. LNEE, vol. 100, pp. 999–1004. Springer, Heidelberg (2011)
9. Zhao, L., Hu, N.J., Zhang, S.Z.: Algorithm design for personalization recommendation systems. Journal of Computer Research and Development 39, 986–991 (2002)
10. Varshney, K.R., Willsky, A.S.: Linear Dimensionality Reduction for Margin-Based Classification: High-Dimensional Data and Sensor Networks. IEEE Transactions on Signal Processing 59, 2496–2512 (2011)
11. Feng, Z.J., Xian, T., Feng, G.U.O.J.: An Optimized Collaborative Filtering Recommendation Algorithm. Journal of Computer Research and Development 10, 34 (2004)
12. Sarwar, B., Karypis, G., Konstan, J., Riedl, J.: Item-based collaborative filtering recommendation algorithms. In: Proceedings of the 10th International Conference on World Wide Web, pp. 285–295. ACM, Hong Kong (2001)

A Memory Stimulating Brain-Computer Interface

Kelgere Ramesh Abhinandan

Telecommunication Department, PESIT, 100-ft-Ring Road, Banashankari 3rd stage, Bangalore-85, India
abhinandanramesh@gmail.com

Abstract. In the current existing technology, literally everything is digital and machines are built and tuned to understand and respond to human gestures. In this paper, the human computer interaction platform is used for the treatment of the disorders, *SHORT TERM MEMORY LOSS* and *ANTEROGRADE AMNESIA*. Victims of these disorders tend to forget stuffs after a short interval of time, but they have the ability to recover the lost memory and remember things, when a picture or a story or a scene relating to the lost memory incident is portrayed to them. This paper presents an idea of building a brain-computer interface to help the victims recover their lost memory by the visualization of the previously happened incident in a virtual frame. According to the theory proposed, the signals are extracted using Electroencephalography and conditioned for use in real world. These signals are stored in a processor and fed back to the brain to create a virtual vision so that the lost memory can be induced.

Keywords: Brain-Computer Interface, Virtual Vision, Memory Stimulator, Artificial Brain for the Short Term Memory Loss patients.

1 Introduction

Deja vu, a French word representing a dilemma of having seen someone or something somewhere but unable to correlate it to the memory. How about just closing the eyes and picturizing that particular forgotten event in a virtual frame of vision? This is possible when Electronics and the Computer Science takes control of the brain. But the real challenge is to merge the different platforms offered by the Neuroscience, Electronics and Computer Science domains. This paper provides an excellent forum to fold all these domains into a single dimension and create a new *Brain Inspired System.* How about using this idea in the medical research field for the stimulation of memory in the *Short Term Memory Loss* and *Anterograde amnesia* patients.

The *Anterograde amnesia* patients lose the ability to transfer new information to long-term memory after a brain injury, while long-term memories from before the injury remain intact. Oftentimes, the brain being a powerful and miraculous organ, will "remap" itself or remapping can be achieved through brainstorming by showing the previously happened incidents in the form of a virtual vision or images or video clips resulting in the patient regaining the ability to store memories. But the virtual vision seems so close to real as if it is happening right in front of their eyes as

D. Liu et al. (Eds.): BICS 2013, LNAI 7888, pp. 182–191, 2013.

compared to the normal real world pictures. So, this method provides an efficient way of brainstorming thereby helping the brain to remap. This paper proposes a system to induce the virtual vision in the patient.

Short term memory loss is a recent new disorder observed with certain people. People affected with the *Short term memory loss* have the tendency to forget everything happened around them after a short interval of time, let's say a day for example. After a day, they won't even have the faintest idea of what happened around them, be it the recent memory or the long term memory. It is like a fresh start for them everyday, unable to remember anything. But the bright part is that they can remember those lost memory incidents, if something similar to the lost memory incident occurs again in front of them. In brain, we are interested in the memory regions and the visual cortex region. As we all know, brain is a dense network of neurons, the vision signals in the visual cortex region of the brain passes through a dense neural network in the form of electrochemical signals and reach the memory region of the brain. In the memory region, there are three sub regions- short term memory region, long term memory region and the remote memory area. For the short term memory loss patients, short term memory region is perfectly fine and works normal but the long term memory region will be impaired, so they won't be able to remember anything after certain period of time. But all the incidents will be deeply embedded in their long term memory area or the remote memory area but unable to access them. So, when a similar stimulus in the form of a virtual vision is induced, this stimulus acts like a driving force and helps them to remember the incident by correlating it to the hidden memory from the long term or remote memory region. The patients even forget their own family members and close personal friends for that matter of fact, but if they are showed with the snaps of them being together, they tend to remember what happened. Let's say, suppose a short term memory loss victim went to a movie with his mother and doesn't remember one bit about it a week later. How about with the help of this system, the victims can visualize the exact picture of being with his mom in a theatre in his head and thereby helping to remember their previous meeting. This paper is divided into three sections as shown in Fig. 1.

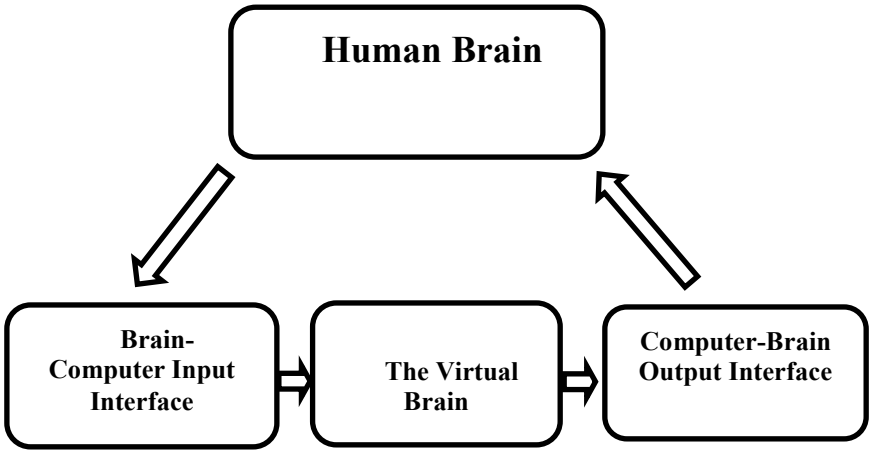

Fig. 1. Block diagram of the system

1.1 Brain-Computer Input Interface

This section houses components that records the electrical activity of the brain and conditions those signals. A number of techniques and devices exist to track the signals produced in the brain like *EEG (Electroencephalography) and EMOTIV (Epoc).* The signals generated by the brain are recorded by measuring the junction potential across the neurons using the electrodes placed on the scalp using some conducting gels. This is the method used in EEG. The signals obtained are processed for usefulness in the real world.

1.2 The Virtual Brain

This section refers to an embedded system consisting of a Digital Signal Processor, a processor which takes care of all the signal processing and signal handling mathematical operations to be carried out. This acts like a Central Processing Unit (CPU) of the entire system.

1.3 Computer-Brain Output Interface

This section consists of the interfacing of certain components required to feedback the signals back into the brain. We use the Faraday's laws of Electro-Magnetic Induction to induce the signals back into the brain.

2 Brain-Computer Input Interface

Communication inside the brain happens just like normal communication systems through electrochemical signals between the neurons which are very similar to electrical signals. But we cannot hack into the neurons directly and extract the signals. So the technique of EEG (Electroencephalography) gives us a platform to read the brain signals. Using this, we can study the behavior of brain waves in the neural network when an event takes place.

Let's take a simple example, say the perception of color blue through the eyes. When color blue is seen for the first time, signals will be generated in the visual cortex region of the brain. Now whenever we perceive the same color blue through our eyes again, signals generated in the brain have a similar pattern (certain similar characteristics in their frequency and spectral power density) to those obtained during the previous perception of the same color. This concept is proved with the help of Functional Magnetic Resonance Imaging (FMRI). This is a type of specialized brain and body scan used to map neural activity in the brain or spinal cord of humans or animals by imaging the change in blood flow related to energy use by the brain cells. The resulting brain activation can be presented graphically by color-coding the strength of activation across the brain or the specific region studied. And with similar color coding, the image obtained by the perception of the color blue by a single person at two different occasions are similar. In the same way, when the same person

(face to be specific) is seen at different occasions, the signals generated in the brain follow a specific similar pattern.

Since the brain signals are very weak, they should be fed to a high precision amplifier tuned to a gain *G* (let's say G = 1000) to amplify the signal strength making it compatible for useful processing in the real world. These amplified signals will be fed to a band pass filter with bandwidth tuned to the frequency range of the brain signals as cited in table 1 to eliminate the out of the frequency band noise signals. Since the frequency range is very less, we need accurate filter and amplifier to eliminate the noise and other undesired signal effects.

Table 1. Brain Wave Specifications

Parameters		Values
Brain wave Frequencies	EEG- beta waves	0.5 to 4 Hz
	EEG-delta waves	8 to 13 Hz
	EEG-theta waves	4 to 7 Hz
	EEG-alpha waves	13 to 30 Hz
Resting potential		-70mV
Magnetic flux around a Neuron		9 to 48 gauss ($9*10^{-4}$ to $48*10^{-4}$ tesla)

3 The Virtual Brain

This section deals with the idea for processing and encoding of the signals coming from the previous section. To achieve this, a simple embedded system consisting of a digital signal processor (DSP) and a microcontroller circuitry is proposed. An amplifier is introduced at a later stage.

The signals from the previous stage should be fed to the analog to digital converter pins in the controller board and the digitized signals will be fed to a DSP. Now, the fourier transform of these signals are obtained. The fourier transform maps the signals onto frequency space. The distribution of amplitudes and the phase of the signals at discrete frequencies over the frequency range of the signals are noted. This data will be stored in a file in a memory. Now the signal enters into feature extraction phase, where the necessary features representing the face are extracted removing all the unwanted information. This feature extracted data will have an identifier to the corresponding fourier transform spectral information data of the same signal. Feature extraction is required because the same person might be seen in two different backgrounds, with varying lightness. So, in order to avoid discrepancies in face classification due to lightness or other factors, feature extraction is carried out. These

features are now encoded using eigen vectors approach as in [1] and later used to classify the new incoming signal from the ones present in the database.

3.1 Building the Database

We know that each and every brain is unique. The way every brain responds to a given excitation is different. So we need to build a database for a particular brain to store all the signals that are sensed and encode them in a way, the classification becomes easy. We use the concept of eigen vectors for face recognition as given in [1]. Let's say five people are sensed. The corresponding signals generated in the brain are extracted and brought into the feature extraction phase after going through all the stages mentioned above. Now let the signals be A_1,A_2,A_3,A_4,A_5. The average signal of the set is given by

$$avg = 1/5 \sum_{n=1}^{n=5} A_n \, . \tag{1}$$

Each signal differs from the average by

$$\Delta = A_i - avg \, . \tag{2}$$

A set of m orthonormal vectors U_n which best describes the data is seeked through Principal Component Analysis. The j_{th} vector is chosen such that

$$V_j = 1/5 \sum_{n=1}^{n=5} \left[\left(U_n^T \right) (avg)_n \right]^2 . \tag{3}$$

is a maximum subject to

$$\left(U_g^T \right) (U_l) = P_{gl} = \begin{bmatrix} 1 & if & g = l \\ & & \\ 0 & & otherwise \end{bmatrix} . \tag{4}$$

The vectors U_j and V_j are the eigen vectors and eigen values respectively. Thus the necessary features are extracted from the signals are encoded and stored in the database.

3.2 Classification of the Face Signals

Now suppose a new signal S comes from the brain. It is transformed into its eigen face components using a simple operation

$$B_k = \left(U_g^T \right) (S - avg) \quad \text{for k = 1,2 .. 5} \, . \tag{5}$$

A weight vector is formed, $W_k=[B_1,B_2,B_3,B_4,B_5]$ that represents the contribution of each eigen face in representing the input face image, treating the eigen faces as basis set for face images. The signal q that maximizes the distance

$$[E_k]^2 = \left\| W - W_q \right\|^2 \tag{6}$$

is found where W_q is a vector describing the q_{th} signal. The input signal is a face signal stored in the database if the Euclidian distance E_k is below a threshold value t_E. Now let the mean input adjusted image be

$$mean = S - avg \tag{7}$$

Its projection onto face space is

$$mean_f = \sum_{i=1}^{i=5} (B_i)(U_i) \tag{8}$$

The distance between image and face space is

$$E^2 = \left\| mean - mean_f \right\|^2 \tag{9}$$

Now if $E_k < t_E$ and $mean_j < t_E$, classify the signal as associated with the vector W_q. If $E_k > t_E$ and $mean_j < t_E$, it means that it is a new face signal and added to the database, else if $E_k > t_E$ and $mean_j > t_E$, the signal is discarded. If there is a match for the new input signal among the signals stored in the database, the fourier transform data corresponding to the stored signal is taken from the memory and a digital signal is regenerated from that spectral information.

Now these signals should be fed to the digital to analog converter pins of the controller to obtain the analog signals. These analog signals will be fed to a similar amplifier used in the input interface section to amplify the weak brain signals but with gain factor set to inverse value of G. The gain of the amplifier in the first stage was noted as *G*. This amplifier is now tuned to a gain 1/*G* (1/1000=0.001) to nullify the initial amplification and fed to a pass band amplifier tuned to the brain signals frequency range as cited in table 1. The signals from the amplifier will be as similar to the brain signals initially tracked with the help of EEG. Since the signals are regenerated in the DSP from the amplitude and phase spectrum with the amplitude reduced by 1/G and filtered by a pass band filter, the signals are perfectly bound to the frequency range and the amplitude rest assured to be less than that of the rest potential (as given in table 1) because when the regeneration of the signal happens, the spectral power density remains constant. Hence these will be very similar to the brain signals obtained initially. Thus the safety of the brain is taken care since the signals are similar to the brain signals.

4 Computer-Brain Output Interface

This section proposes an idea designed to feedback the signals back to the brain using the Faraday's laws of Electromagnetic Induction but with a feasible simple approach

instead of a huge mesh of wires as mentioned in [2], because it is very difficult to monitor the flow of currents and the magnetic flux in that huge collection of wires. When the signals are passed through a conductor which is kept across a neural network, it induces electrical signals E= dΦ/dt (in the form of potential) in the neural network due to *Electromagnetic Induction*. This phenomenon of inducing signals is referred to as *TRANSCRANIAL MAGNETIC STIMULATION* in medical terms. Here, brain itself is the neural network. The conductor used here is a straight conducting wire bent into a series of coils as shown in Fig. 2.

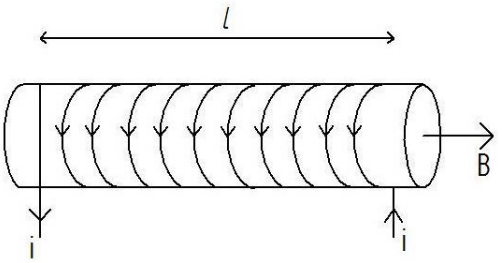

Fig. 2. The wire Assembly

When the current in the wire changes, magnetic field is induced which is concentrated in the centre parallel to the axis of the coils. According to amphere's law, the magnetic field produced is given by,

$$B = \mu Ni / l \tag{10}$$

Let the number of turns be 20 and length be 6 cms. Considering the maximum value of flux from table 1, we get

$$I_{\max} = \left(48*10^{-4}*6*10^{-2}\right)/\left(4\pi*10^{-7}*20\right) = 11.46A \tag{11}$$

So even in the extreme cases, the current will be around 11A. When these signals are passed through a conductor, as the amplitude of these signals varies with time since the brain signals are the varying pulses, the current changes corresponding to the change in the amplitude of the signal. This is proved with the help of amphere-maxwell's law which states that,

$$\oint_s B.ds = \mu i + \left((1/\mu\varepsilon)\left(\partial\left(\int E.dA\right)/\partial t\right)\right) \tag{12}$$

Now consider an imaginary loop located inside the wire arrangement. By amphere's law, we know that line integral of B around this loop is zero. Since it encloses no electrical currents (it can be also assumed that the circuital electric field passing through the loop is constant under such conditions: a constant or constantly changing current through the solenoid). Now with B=9*10^{-4} Tesla,

$$\int ds = 2\pi r(r+h) \tag{13}$$

$$\int dA = 2\pi rh \tag{14}$$

$$E = V / I \tag{15}$$

Solving and removing all constant terms we get,

$$i\alpha\left(\partial V / \partial t\right) \tag{16}$$

When the signals from the previous section are passed through a conductor, since they vary with time, the current in the conductor also varies corresponding to the change in the amplitude of the voltage as given by (**16**). This changing current creates a magnetic flux which induces electrical signals in the brain in the form of potential. Since the brain signals are of feeble amplitude, the current also will be very less. So, a core of ferromagnetic material such as an iron or a better electromagnet which satisfies the equation (16) should be placed inside the hollow space created by the wire arrangement to create stronger magnetic fields to induce the electrical signals, though the field strength has to be confined within the limits as cited in table 1. But the wire arrangement has to be properly insulated in order to avoid any direct contact with the brain and placed on the visual cortex region of the brain to induce the signals specific to the vision region of the brain. The placement of the wire arrangement on the head and the volume of the brain in which the signal is induced are as shown using geometry and integral equations in Fig. 3 and Fig. 4 respectively.

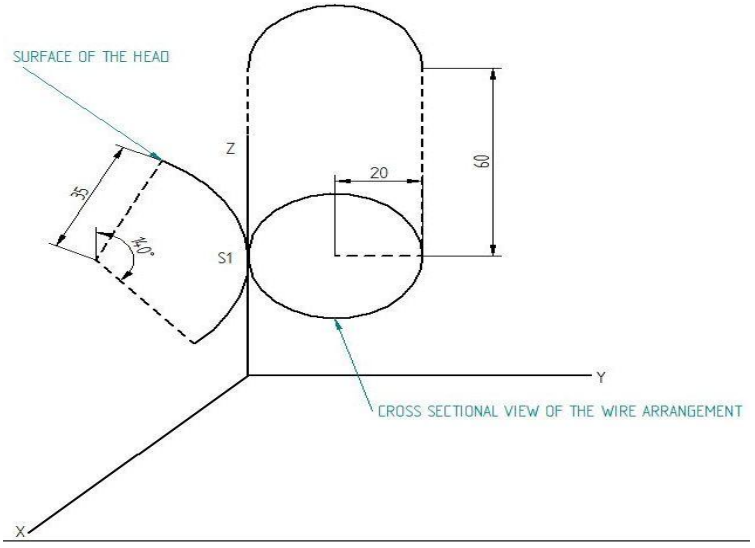

Fig. 3. Cross sectional view of the placement of the wire assembly on the head (Measurements specified are in millimeters)

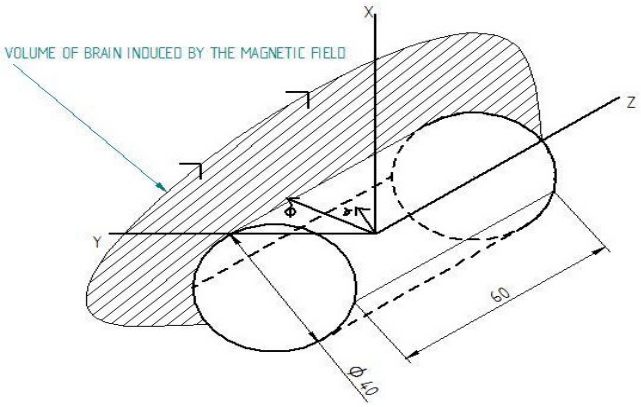

Fig. 4. Shaded portion gives the region of the brain induced by magnetic field (Measurements specified are in millimeters)

4.1 Calculations Corresponding to Fig. 3.

Portion of the head in contact with the wire assembly,

$$S_1 = \left(3.5*10^{-2}*140*\pi\right)/(180) = 8.54*10^{-2}\,m \tag{17}$$

4.2 Calculations Corresponding to Fig. 4.

Solving using cylindrical co-ordinates, Φ, z and r vary as given in (**18**). Therefore, the volume of the brain that the signals will be induced is

$$V = \int_{z=0}^{0.067\pi/9} \int_{\phi=0}^{0.035} \int_{r=0} r \; dr \; d\phi \; dz = 0.875*10^{-4}\,m^3 \tag{18}$$

5 Conclusion

This paper aims at developing a treatment for the *Short term memory loss* and *Anterograde amnesia* victims. A system is proposed to help them recover their lost memory which is very near to reality. With advancement in the fabrication technologies, all the amplifier, filter, processor, controller, brain sensor IC's and the wire arrangement can be integrated into a very small board and included in a system like head phones so that it can always be used by the patients without any overhead. Hope this adds a new dimension to the existing medical technology. With even more improvements in sensors used to read the signals, more accuracy can be obtained.

Acknowledgments. I'm extremely thankful to my Asst. Professor AKSHAY G ECE Dept. PESIT, NAVEEN M N EEE Dept. PESIT, JAIDEV M S R medical college for their help and support.

References

1. Turk, M., Pentland, A.: "Eigen Faces for Recognition", vision and modeling group. The Media Laboratory, MIT
2. Naveen, M.N.: A Complete Interface Device. In: ICCRD 2011, China (2011)
3. Choudhury Roy, D.: Linear Integrated Circuits, 4th edn.
4. Halliday, D., Resnick, R., Walker, J.: Fundamentals of Physics, 6th edn.
5. Duda, R.O., Hart, P.E., Stork, D.G.: Pattern Classification, 2nd edn.
6. Mitra, S.K.: Digital Signal Processing – Computer Based Approach
7. Palaniappan: Brain Computer Interface Design Using Band Powers Extracted During Mental Tasks. In: 2nd International IEEE EMBS Conference Neural Engineering (2005)
8. Palaniappan: A new brain-computer interface design using fuzzy ARTMAP. In: Neural Systems and Rehabilitation Engineering

Differences in Allocations of Attention to Faces during Affective Learning of Chinese People

Junchen Shang and Xiaolan Fu*

State Key Laboratory of Brain and Cognitive Science, Institute of Psychology, Chinese Academy of Sciences, Beijing, China
fuxl@psych.ac.cn

Abstract. If one neutral object predicts a rewarding or threatening outcome, this object will acquire affective value, and this process is known as affective learning. Western participants showed robust affective learning in previous research. Moreover, affective learning influenced face perception. However, the mechanism of this phenomenon remains unclear. In the present study, we used eye-tracking to investigate whether Chinese participants paid more attention to faces paired with sentences describing negative behaviors in the learning phase. Consistent with Western participants, Chinese participants learned affective information of faces. In addition, the gaze patterns showed that Chinese participants looked more at faces presented with negative and neutral sentences than those presented with positive faces. The present research indicates that affective learning is not impacted by culture. Moreover, participants pay more attention at faces paired with negative and neutral sentences during learning, which may lead to different affective learning effects.

Keywords: affective learning, culture, eye-tracking, face processing.

1 Introduction

Affective learning is a process in which one neutral object (the conditioned stimulus, or CS) acquires affective value after paired with another emotional stimulus (the unconditioned stimulus, or US) [1]. Over past years, affective learning has been extensively studied by researchers from social psychology, learning psychology and consumer science (for a review see [2]). For example, one previous study paired neutral words with electric shocks, and found that participants rated the words which paired with the onset of shock more negatively than the words which paired with the offset of shock [3]. Past research usually used biological significant US (e.g., electric shocks) to form affective learning [4-7]. However, recent evidence showed that affective learning can also be formed under minimal conditions [1, 8, 9]. For instance, when a neutral face was paired with a sentence describing positive or negative behavior, participants learned the affective value of the neutral face [1]. That is, participants judged the neutral faces which had been paired with positive sentences as

* Corresponding author. 16 Lincui Road, Chaoyang District, Beijing 100101, China.

D. Liu et al. (Eds.): BICS 2013, LNAI 7888, pp. 192–200, 2013.

more positive, trustworthy and likeable than faces which had been paired with negative sentences [1, 10]. Affective learning phenomenon is so robust that a patient with hippocampal lesions exhibited similar learning effects as normal people [10].

Although there is ample evidence that people can learn affective value of faces under minimal conditions, previous studies were mainly reported from Western cultures. There is little evidence whether East Asians would show similar affective learning effects, since culture backgrounds influences emotional processes [11]. Nonetheless, since affective learning is robust in Western culture, Eastern Asians may show the similar learning effects. In this study, we directly tested affective learning effects in mainland Chinese. We predicted that Chinese participants would evaluate neutral faces paired with negative sentences as more negative, while evaluate neutral faces paired with positive sentences as more positive [1].

Affective learning not only impacted judgments of the learned faces, but also influenced visual processing of these faces. For instance, faces which were paired with negative sentences dominated longer in visual consciousness than faces paired with neutral and positive sentences, in a binocular rivalry paradigm [8]. In a related study, Todorov et al. [12] showed that faces paired with negative sentences evoked stronger activity in left STS than faces paired with positive sentences when participants were asked to complete one-back recognition task after learning, using fMRI method. However, why sentences describing negative behavior resulted in stronger visual processing and neural activity remains unclear. Anderson et al. [8] suggested that participants might learn the negative information better than the neutral and positive information. It is also possible that negative behaviors have higher information and affective value than positive behaviors [13], which would cause more neutral activity to analyze social intentions [12]. However, to our knowledge, no research directly tested these interpretations. Understanding why affective learning influenced face perception is critical. The present study aimed to fill in this gap.

Furthermore, previous research only examined the stages after learning, while ignored the learning phase, except Davis et al. [14]. Davis et al. [14] reported that the activity in the medial ventral amygdala and dorsal amygdala/substantia innominata to both negative and positive faces was stronger than neutral faces. In addition, the lateral ventral amygdala showed stronger activity to negative than positive faces, also, stronger activity to positive than neutral faces. Thus, faces paired with negative sentences evoked more neural response in amygdala. It is possible that the faces associated with negative sentences attract more attention in the learning phase, which leaded to stronger visual processing and neural activity in the stages after learning.

Based on previous research, we attempted to explore whether faces paired with different valenced behavior associated with different attentional resources during learning. Since eye-tracking is widely used to study attention (e.g., for a review, see [15]), we decided to use eye-tracking to explore attention to faces. The experiment was modeled upon Bliss-Moreau et al. [1], which showed that Western participants learned affective value of faces under minimal conditions. We extended previous research to Chinese participants, using Asian faces as stimuli. In the first phase of the experiment, participants were presented with 24 unfamiliar faces paired with verbal descriptions of negative, neutral and positive behaviors. The face-sentence pairs were counterbalanced between participants. Simultaneously, we monitored participants'

eye movements. In the second phase, participants were presented with the 24 learned faces plus 8 novel faces. And participants were asked to indicate whether their gut reactions to the faces were positive, neutral or negative.

In sum, the goal of the present study was two folds. First, we explored whether affective learning effect in Chinese people is similar with Westerns. Second, we tested the attention allocation of Chinese participants during the learning phase. We hypothesized that Chinese participants would show similar affective learning effects as Western people. Moreover, we hypothesized that participants fixed more on the faces presented with sentences describing negative behavior, than those paired with neutral and positive sentences. We are the first to test these hypotheses in an Asian sample.

2 Methods

2.1 Participants

Twenty-eight Chinese students (4 men, 24 women, M_{age} = 23.14, SD_{age} = 2.70) participated in this study. They were recruited through internet. All participants had normal or corrected-to-normal vision. Participants were paid for participation. Each subject signed an informed consent form for the experiment.

2.2 Materials

32 Chinese faces were obtained from a face database [16] and a face set developed by our lab. All faces were neutral, containing 16 males and 16 females. These faces were divided into four groups, and participants learned to pair three groups with sentences describing positive, neutral, and negative behavior, leaving one group as novel faces. The sentences paired with each face group were counterbalanced across participants. The images were 360×400 pixels, subtending 10° of visual angle horizontally and 11° of visual angle vertically. The images were cropped around the face to exclude hair and ears using Adobe Photoshop CS and adjusted to the same luminance. Images incorporated with sentences were presented on a 1280×1024 pixel white background and displayed on a 19-in LCD monitor at a distance of 60 cm from the participant. Moreover, we selected 24 descriptions of behavior (8 positive, 8 neutral, 8 negative sentences) from previous studies [1, 17]. The sentences were translated to Chinese. The stimuli were presented by SMI experiment center software (SensoMotoric Instruments, Germany).

2.3 Eye-tracking

Eye movements were recorded at a sampling rate of 500 Hz with an infrared camera on an iView X Hi-Speed 1250 system (SensoMotoric Instruments, Germany). Head movements were reduced by chin and forehead rests. Only the left eye of each participant was tracked.

2.4 Procedure

Participants sat in a room with dim light. Prior to the experiment, calibration of eye fixations was conducted using a nine-point fixation procedure to make sure that the eye tracker was accurately tracking the left eye of each participant when they looked at different areas on the screen.

The main experiment consisted two phases: learning phase and test phase. We modified the paradigm of previous studies [1, 12]. During the learning phase, the participants were presented with 24 face-sentence pairs, and were instructed to remember the pairs by imaging each person performing the behavior described in the corresponding sentence (e.g., was arrested on suspicion of child beating). In the beginning of each trial, a fixation cross was presented in the center of the screen for 1 s. After that, one face-sentence pair was shown for 5 s and then disappeared. The intertribal interval was 1 s, after which the next trial started. Each face-sentence pair was presented four times in random order.

In the test phase, the faces presented in learning phase and 8 novel faces were displayed and participants were told to categorize each face as positive, neutral or negative. Each trial started with a 1-s fixation cross. After that, a face was shown on the left or right side of the screen for 3 s. After that, participants were asked to indicate whether the face was positive, neutral, or negative. They were required to report their gut reactions. The next trial started after the participants responded.

3 Results

Analyses were performed on the behavioral data collected during the test phase and on eye movement data in the learning phase. One participant whose eye movements were not successfully tracked was excluded from the analyses. Another two participants were excluded because the program crashed, thus leaving 25 participants for data analysis.

3.1 Behavioral Data

As expected, Chinese participants showed the similar affective learning pattern as Westerners [1]. We calculated the mean percentage of each participant's categorizations based on valence of behavioral act with which face was paired. We performed a two-tailed 1-sample t test to compare means to chance level responding (.33 or 33%). Means, standard errors, and statistical tests were presented in Figure 1. After paired with a valenced sentence for four times, neutral faces acquired positive or negative value. Faces paired with positive sentences were significantly more likely than chance to be judged as positive, $t(24) = 3.43$, $p < .01$, significantly less likely to be judged as negative, $t(24) = -7.50$, $p < .001$, and were judged as neutral at chance levels, $t(24) = .97$, $p > .05$. Similarly, faces paired with negative sentences were significantly more likely than chance to be judged as negative, $t(24) = 6.10$, $p < .001$, significantly less likely to be judged as positive or neutral, ts < -2.88, ps $< .01$. Faces paired with neutral sentences, as well as novel faces, were more likely than chance to be judged as neutral, ts > 4.80, ps $< .001$, significantly less likely to be judged as

negative, *t*s < -2.90, *p*s < .01. And faces paired with neutral sentences were significantly less likely than chance to be judged as positive, $t(24) = -3.90$, $p < .001$. Moreover, novel faces were judged as positive at chance levels, $t(24) = -1.70$, $p > .10$.

To test whether valence of sentences influenced affective learning about faces, we performed a one-way ANOVA, with learning effect as dependent variable (i.e. mean percentage of trials on which participants judged valence of the faces just as the valence of sentences they were paired with), and the valance of sentences (positive, neutral, negative) as the independent variable. The main effect of valence was significant, $F(2,48) = 5.79$, $p < .01$, $\eta^2 = .194$. Post-hoc test (LSD corrected) revealed that negative affective learning effect ($M = .63$) was significantly greater than positive ($M = .49$) and neutral ($M = .54$) conditions, *p*s < .05.

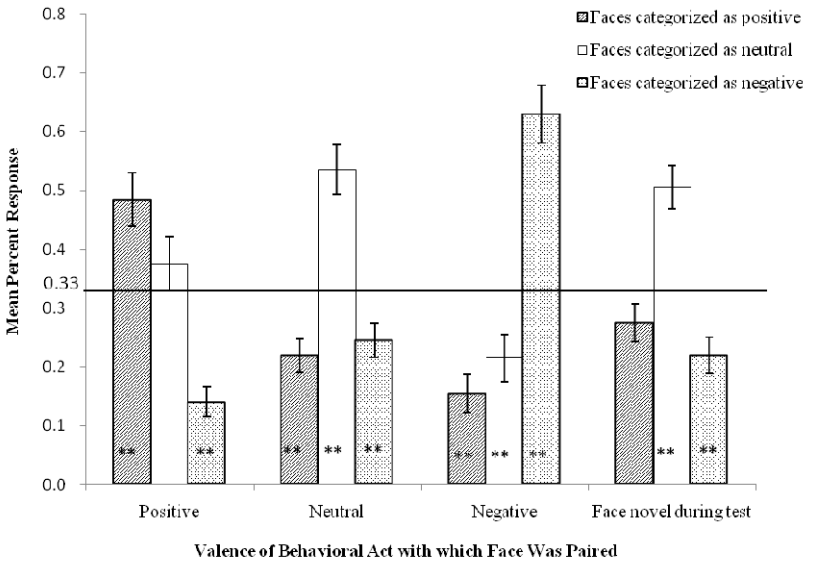

Fig. 1. Mean percentage of categorizations based on valence of behavioral act with which face was paired. Columns with asterisks are different from chance. * $p < .05$, ** $p < .01$.

3.2 Gaze Patterns

The eye-tracking data was analyzed with BeGaze software (SensoMotoric Instruments, Germany). Five face areas of interest (AOI) were manually defined for each stimulus: the whole face area, the eyes, the nose, the mouth, according to previous research [18-20]. Research about eye-tracking suggested that the number and duration of fixations revealed the time during which people process visual information in an AOI [21], reflecting orienting of visual attention [19]. Thus, we measured the number and duration of fixations to each face. We also measured the number of fixations to the eyes, nose and mouth. The trials of unreliable recording (i.e., trials with no fixations on faces) were excluded.

Two one-way ANOVAs with valences of sentence paired with faces (positive, neutral, negative) as independent variable, and number and duration of fixations as

dependent variables were performed. There was significant difference in number of fixations to faces paired with different valenced sentences, $F(2,48) = 3.92$, $p = .026$, $\eta^2 = .140$. Post-hoc test (LSD corrected) showed that participants made more fixations to the faces paired with negative and neutral sentences than those paired with positive sentences, $p = .024$, $p = .05$ (Figure 2). However, there was no difference in number of fixations between faces paired negative and neutral sentences, $p = .446$.

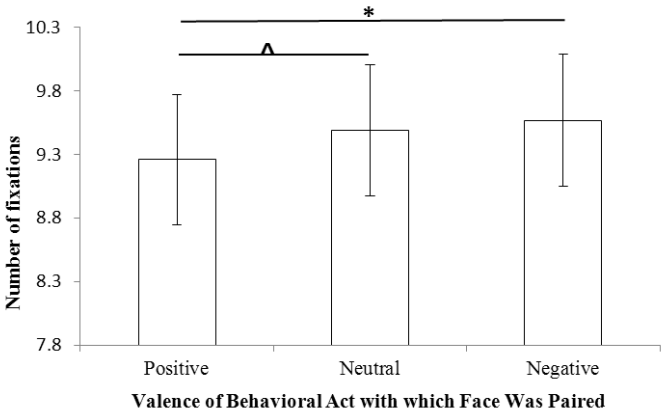

Fig. 2. Number of fixations to faces based on valence of behavioral act with which face was paired during the learning phase. * $p < .05$, ^ $p = .05$.

There was also significant difference in duration of fixations to faces paired with different valenced sentences, $F(2,48) = 3.93$, $p = .026$, $\eta^2 = .141$. Post-hoc test (LSD corrected) showed that participants looked more at faces paired with negative and neutral sentences than those paired with positive sentences, $p = .008$, $p = .047$ (Figure 3). Again, there was no differences between faces paired with negative and neutral sentences, $p = .54$.

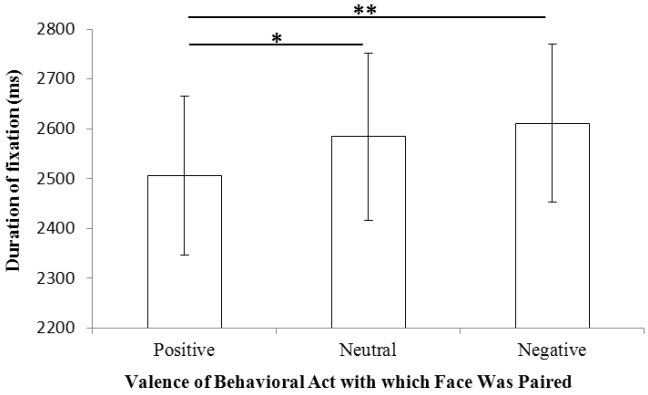

Fig. 3. Duration of fixation to faces based on valence of behavioral act with which face was paired during the learning phase. * $p < .05$, ** $p < .01$.

Moreover, a 3 (AOI: eyes, nose, mouth) × 3 (valence of sentences: positive, neutral, negative) repeated-measures ANOVA on number of fixations to each AOI was performed to test whether there was difference in orienting of visual attention to different face regions. A significant effect was found for AOI, $F(2,48) = 26.38$, $p < .001$, $\eta^2 = .52$. Post-hoc test (LSD corrected) revealed that participants made more fixations to the eyes than the nose and mouth, and more fixations to the nose than the mouth, ps < .01 (Figure 4). However, there was no significant effect for valence of sentences, or interaction between AOI and valence of sentences, Fs < 1.

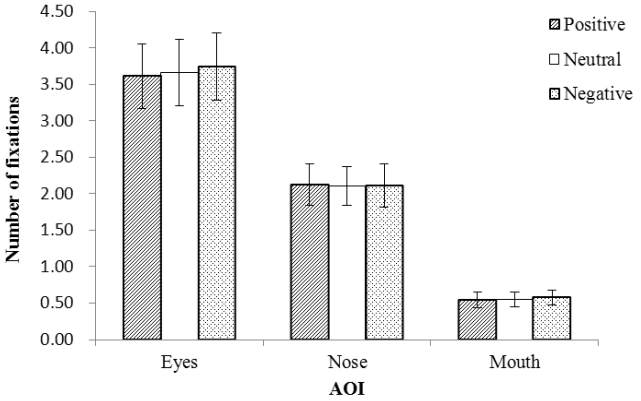

Fig. 4. Number of fixations to AOIs for faces paired with sentences describing different valenced behavior during learning

4 Discussion

This study confirmed that Chinese participants learned affective value of neutral faces under minimal conditions, which is consistent with previous research on Western participants [1, 9]. Chinese people were likely to judge neutral faces as positive after the faces were paired sentences of positive behavior for four times, and were likely to judge neutral faces as negative after the faces were paired with sentences of negative behavior for four times. This finding suggested that affective learning is a robust phenomenon which was not influenced by culture. In addition, participants were better able to learn negative value of neutral faces, compared with neutral and positive condition.

The eye-tracking data partly supported the behavioral results. The durations and number of fixations to faces paired with negative and neutral sentences were greater than those paired with positive sentences. This may reflect increased attention to faces associated with negative sentences than positive sentences, suggesting greater degree of affective learning during the test phase. These findings were generally consistent with results by Anderson et al. [8], which suggested longer dominant durations in visual consciousness of neutral faces paired with negative sentences, in binocular rivalry. Moreover, these results were consistent with [12], which found faces paired

with negative sentences evoked stronger neural response than those paired with positive sentences. In addition, our findings also consistent with previous studies which showed that negative stimuli attracted attention [22, 23].

Furthermore, the eye-tracking data revealed that people oriented more attention to the eyes rather than nose or mouth, suggesting that the eyes were the most important for extracting information during learning of face-sentence pairs. This finding was also consistent with previous research about eye-movements of face perception [19, 24].

However, there was no significant difference in the number and duration of fixations to faces paired with neutral sentences compared with those paired with negative sentences. It was hard to explain. Maybe neutral sentence did not provide salient affective information. Thus it was hard to remember the neutral faces, resulting in greater number and duration of fixations. Future research needs to further investigate this possibility.

In sum, this study not only replicates the affective learning phenomenon of Westerns in a Chinese sample, but also extends to investigate allocation of attention during learning phase. Our results are the first to show different allocations of attention to faces during affective learning using eye-tracking, which suggest different affective learning effects. The present study provides evidence to explain difference in face perception after learning. Also, this may enhance our understanding of the mechanism of minimal affective learning.

Acknowledgments. This research was supported in part by grants from 973 Program (2011CB302201) and the National Natural Science Foundation of China (61075042).

References

1. Bliss-Moreau, E., Barrett, L.F., Wright, C.I.: Individual differences in learning the affective value of others under minimal conditions. Emotion 8(4), 479–493 (2008)
2. De Houwer, J., Thomas, S., Baeyens, F.: Association learning of likes and dislikes: A review of 25 years of research on human evaluative conditioning. Psychological Bulletin 127(6), 853–869 (2001)
3. Zanna, M.P., Kiesler, C.A., Pilkonis, P.A.: Positive and negative attitudinal affect established by classical conditioning. Journal of Personality and Social Psychology 14(4), 321–328 (1970)
4. Damaraju, E., Huang, Y.M., Barrett, L.F., Pessoa, L.: Affective learning enhances activity and functional connectivity in early visual cortex. Neuropsychologia 47(12), 2480–2487 (2009)
5. Lim, S.L., Padmala, S., Pessoa, L.: Affective learning modulates spatial competition during low-load attentional conditions. Neuropsychologia 46(5), 1267–1278 (2008)
6. Lim, S.L., Pessoa, L.: Affective learning increases sensitivity to graded emotional faces. Emotion 8(1), 96–103 (2008)
7. Padmala, S., Pessoa, L.: Affective learning enhances visual detection and responses in primary visual cortex. The Journal of Neuroscience 28(24), 6202–6210 (2008)
8. Anderson, E., Siegel, E.H., Bliss-Moreau, E., Barrett, L.F.: The Visual Impact of Gossip. Science 332(6036), 1446–1448 (2011)

9. Verosky, S.C., Todorov, A.: Generalization of affective learning about faces to perceptually similar faces. Psychological Science 21(6), 779–785 (2010)
10. Todorov, A., Olson, I.R.: Robust learning of affective trait associations with faces when the hippocampus is damaged, but not when the amygdala and temporal pole are damaged. Social Cognitive and Affective Neuroscience 3(3), 195–203 (2008)
11. Han, S., Northoff, G.: Culture-sensitive neural substrates of human cognition: A transcultural neuroimaging approach. Nature Reviews Neuroscience 9(8), 646–654 (2008)
12. Todorov, A., Ida Gobbini, M., Evans, K.K., Haxby, J.V.: Spontaneous retrieval of affective person knowledge in face perception. Neuropsychologia 45, 163–173 (2007)
13. Skowronski, J.J., Carlston, D.E.: Negativity and extremity biases in impression formation. Psychological Bulletin 105, 131–142 (1989)
14. Davis, F.C., Johnstone, T., Mazzulla, E.C., Oler, J.A., Whalen, P.J.: Regional response differences across the human amygdaloid complex during social conditioning. Cerebral Cortex 20(3), 612–621 (2009)
15. Rayner, K.: Eye movements in reading and information processing: 20 years of research. Psychological Bulletin 124(3), 372–422 (1998)
16. Wang, Y., Luo, Y.: Standardization and assessment of college students' facial expression of emotion. Chinese Journal of Clinical Psychology 13(4), 396–398 (2005)
17. Fuhrman, R.W., Bodenhausen, G.V., Lichtenstein, M.: On the trait implications of social behaviors: Kindness, intelligence, goodness, and normality ratings for 400 behavior statements. Behavior Research Methods, Instruments, & Computers 21, 587–597 (1989)
18. Blais, C., Jack, R.E., Scheepers, C., Fiset, D., Caldara, R.: Culture shapes how we look at faces. PLoS One 3(8), e3022 (2008)
19. Vassallo, S., Cooper, S.L., Douglas, J.M.: Visual scanning in the recognition of facial affect: is there an observer sex difference? Journal of Vision 9(3), 1–10 (2009)
20. Wu, E.X.W., Laeng, B., Magnussen, S.: Through the eyes of the own-race bias: eye-tracking and pupillometry during face recogniton. Social Neuroscience, iFirst, 1–15 (2011)
21. Noton, D., Stark, L.: Eye movements and visual perception. Scientific America 224, 35–43 (1971)
22. Fox, E., Lester, V., Russo, R., Bowles, R., Pichler, A., Dutton, K.: Facial expressions of emotion: Are angry faces detected more efficiently? Cognition & Emotion 14(1), 61–92 (2000)
23. Öhman, A., Flykt, A., Esteves, F.: Emotion drives attention: detecting the snake in the grass. Journal of Experimental Psychology: General 130(3), 466–478 (2001)
24. Jansari, A., Rodway, P., Goncalves, S.: Identifying facial emotions: valence specific effects and an exploration of the effects of viewer gender. Brain and Cognition 76, 415–423 (2011)

Magnetically Tunable Photonic Crystal Fibers Bragg Grating

Yong Zhao[1,2], Yuyan Zhang[1,3], and Yan Zhao[3]

[1] College of Information Science and Engineering,
Northeastern University, Shenyang 110004, China
[2] State Key Laboratory of Synthetical Automation for Process Industries
Northeastern University, Shenyang 110819, China
[3] Shenyang Institute of Engineering, Shenyang 110136, China
zhaoyong@ise.neu.edu.cn, {zhangyy,zhaoyan}@sie.edu.cn

Abstract. The multi-resonant peaks of magnetic fluid (MF) filled photonic crystal fiber Bragg grating (PCFBG) with different core diameters were researched under external magnetic field (H). The magnetically induced tuning properties of the MF-filled PCFBG with 3μm core diameter were investigated theoretically. The results show that the different modes have different magnetic sensitivity. The relationships between core diameter and the resonant peak of the MF-filled PCFBG were analyzed and simulated under H=200Oe. The results show that the number of resonant peak increases with D_{core} increasing, and a blue shift of resonant peak is observed with D_{core} increasing.

Keywords: photonic crystal fiber, magnetic fluid, reflection spectrum, Bragg grating.

1 Introduction

Photonic crystal fiber gratings (PCFBGs) have developed for 12 years, and some unprecedented superiority were shown [1]. Up to now, practical applications of PCFBGs are very few, and they have a great development potential. The PCFBGs based material-filled show a greater development opportunities and development space.

The magnetic fluid (MF) is a novel functional material in optical field, which has the magnetic and the fluidity. The refractive index of MF is sensitive to external magnetic field [2]. So the air holes of the PCFBGs were filled with the MF, the equivalent refractive index of the PCFBGs cladding will be changed with the magnetic field, which lead to the reflection spectrums of the MF-filled PCFBG changing with magnetic field.

In this paper, we analyze theoretically the characteristics changes of photonic crystal fiber grating filled MF. Basis on these theoretical, we figure out and simulate the spectral characteristics and mode coupling behaviors of the MF-filled PCFBG, and research the magnetically-induced tuning properties of the MF-filled PCFBG, which establish a firm theoretical foundation for their further expansion studies.

D. Liu et al. (Eds.): BICS 2013, LNAI 7888, pp. 201–207, 2013.

2 Theoretical Basis

The effects that the effective refractive index of the MF-filled PCFBG vs. external magnetic field were analyzed using the finite element method (FEM). The reflection spectral was obtained using the coupled mode theory. The resonant wavelength and coupling coefficient of the MF-filled PCFBG were calculated based on Bragg grating coupled mode theory. The formulation of the FEM here considered is based on the Maxwell equation. It reads

$$\nabla\left[\frac{1}{\varepsilon_r}\nabla\times h(r)\right]=k_0^2\mu_r h(r) \tag{1}$$

Where ε_r, μ_r respectively are the dielectric constant and the magnetic permeability of medium, $h(r)=He^{-\gamma z}$ is magnetic field, $k_0=2\pi/\lambda$ is the wave number in the vacuum, λ is the wavelength. H is the field distribution on the transverse plane and $\gamma=\alpha+jk_0n_{\text{eff}}$ is the complex propagation constant with the attenuation constant α and the effective index n_{eff}. we analyze the propagation of light in a PCF by applying the FEM.

For the fiber Bragg gratings (FBGs), the resonant wavelengths for the fundamental mode couplings are determined by phase-matching condition [3]

$$\lambda_B=2n_{co}P_{FBG} \tag{2}$$

The ith resonant wavelengths for the cladding mode couplings are determined by

$$\lambda_{FBG,i}=(n_{co}+n_{clad,i})P_{FBG} \tag{3}$$

Where Λ is grating period, n_{eff} and $n_{\text{clad,i}}$ are the effective indices of the fundamental mode and the effective indices of the cladding mode respectively. Based on the coupled-mode theory, we obtain the transfer matrix expression

$$\begin{bmatrix}R_i\\T_i\end{bmatrix}=F_i\begin{bmatrix}R_{i-1}\\T_{i-1}\end{bmatrix} \tag{4}$$

$$F_i=\begin{bmatrix}\cosh(\gamma_B\Delta z)-i\frac{\sigma}{\gamma_B}\sinh(\gamma_B\Delta z) & -i\frac{k}{\gamma_B}\sinh(\gamma_B\Delta z)\\ i\frac{k}{\gamma_B}\sinh(\gamma_B\Delta z) & \cosh(\gamma_B\Delta z)+i\frac{\sigma}{\gamma_B}\sinh(\gamma_B\Delta z)\end{bmatrix} \tag{5}$$

Where R_i, T_i, R_{i-1} and T_{i-1} are the amplitudes of forward and reverse light field before and after through the i section grating, respectively. F_i is the transfer matrix of the i section grating. $\gamma_B=\sqrt{\kappa^2-\sigma^2}$ with "dc" coupling coefficient κ and "AC" coupling coefficient σ .According to $R_0(-L/2)=1$ and $T_0(-L/2)=0$ and

$$\begin{bmatrix}R_m\\T_m\end{bmatrix}=F_mF_{m-1}F_{m-2}\cdots F_1\begin{bmatrix}R_0\\T_0\end{bmatrix}=F\begin{bmatrix}1\\0\end{bmatrix} \tag{6}$$

The grating reflection coefficient $\rho = T_m / R_m$. Based on the above theoretical model, the reflection spectrum of the MF-filled PCFBG can be simulated.

3 Simulations and Analysis

3.1 The Models of PCFs and Calculation Parameters

Fig.1 shows the structures of PCF. The cross-sectional of PCF contains a pure silica core surrounded with four hexagons of air holes characterized by a diameter d and the hole to hole spacing Λ of 9μm and 10μm respectively. The refractive index of substrate n_{si} =1.4466, the diameter of fiber D=125μm, the refractive index of core n_{core}=1.4566, the diameter of core Dcore= 3μm, the diameter of inner cladding d_{clad}=4Λ-d=31μm. The water-based Fe_3O_4 with concentration of 1.2 g/ml was selected as filling material, and the filling length was 2cm. When H increased from 0Oe to300 Oe, the corresponding n_{MF} decreased from 1.44714 to 1.43318 [4].

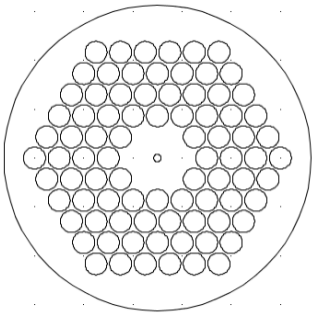

Fig. 1. The cross section of the PCF

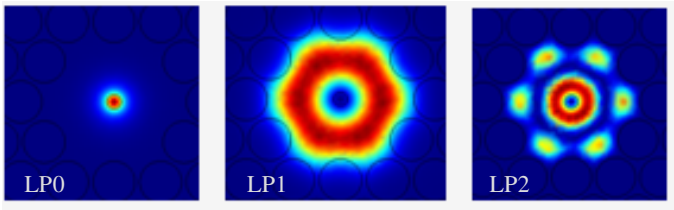

Fig. 2. Field distribute on of each mode of PCF

3.2 The Calculation of Each Mode

The mode field distributions of PCF were calculated and the results were shown in Fig.2. It can be seen that the PCF have three kind transmission modes. One is the coupling between the forward and reverse propagation of the fundamental mode LP0,

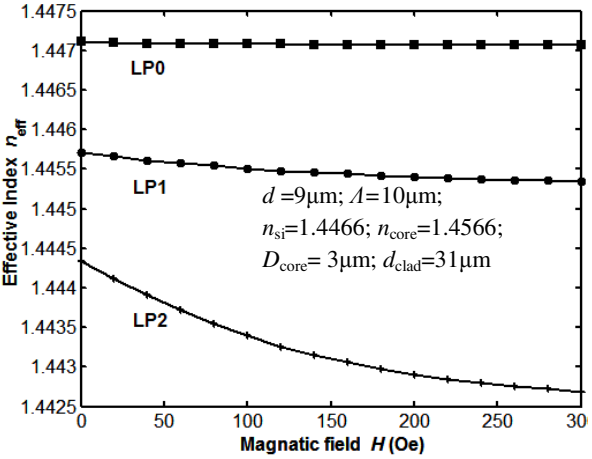

Fig. 3. Mode effective refractive indexes Re(n_{eff}) vs.magnetic fields under λ=1550nm

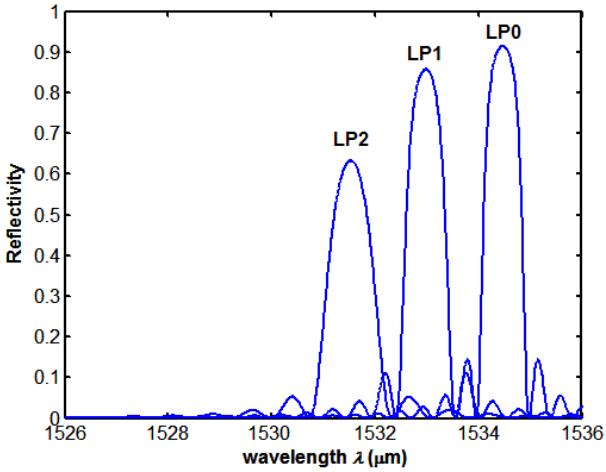

Fig. 4. Reflection spectrum of MF-filled PCFBG under the wavelength λ =1550nm

and others are the coupling between the fundamental mode and the cladding mode (LP1and LP2). The reason is that the V values (n_{co}, n_{cl} are the indices of core and the effective indices of the first eigenmode.) of PCF are greater than , which do not meet the conditions of single-mode transmission [5]. Under λ=1550nm and the magnetic field H is between 0Oe and 300Oe, we analyze the effects the H on the mode effective refractive index Re(n_{eff}) of the MF-filled PCFs. The results were shown in Fig.3. It can be seen, firstly, the Re(n_{eff}) of the PCF reduces with the H increasing. The reason is that the nMF is decreasing with the H enhancing, and then t Re(n_{eff}) is decreasing. Secondly, the Re(n_{eff}) of the PCF reduces with mode increasing, and the higher the mode is, the faster is the changing of Re(n_{eff}) with H. The Re(n_{eff}) of LP0 is independent of magnetic field due to mode field confined to the core and almost no

leakage loss. But the Re(n_{eff}) of LP1 and LP2 are dependent on magnetic field due to mode field penetrated into the cladding holes region and generating leakage loss. The higher the mode is, and the greater is the leakage loss.

3.3 The Reflection Characteristics of the MF-filled PCFBG

The Bragg gratings were inscribed in the above structure PCFs. The grating length L=2cm. The grating period .The refractive index modulation depth. The grating is divided into 100 sections. Under λ=1550nm and the H is 100Oe, 200Oe and 300Oe respectively, We simulate the effects the H on the reflection spectrum of MF-filled PCFBG by applying transfer matrix theory, as shown in Fig.4. Three resonant peaks correspond to the resonant mode in Fig.2. The LP0 resonant peak λ_{0B} is generated by coupling between positive core mode and negative core, and other resonant peaks (λ_{1B} and λ_{2B}) were generated by coupling between core mode and cladding mode. It was found that λ_{0B} is about 1534.35nm, λ_{1B} is about 1532.95nm and λ_{2B} is about 1531.48nm. The reason is that the electric field of cladding modes in the core grating region is weak, and overlap integral of this electric field and the core mode electric field is smaller.

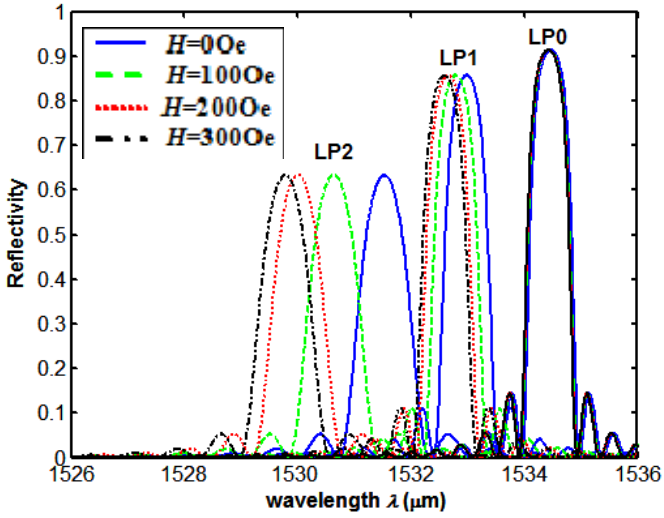

Fig. 5. Reflection spectrum of MF-filled PCFBG under different magnetic field

Fig.5 shows the reflection spectrum of MF-filled PCFBG under different H (H=0Oe, H=100Oe, H=200Oe and H=300Oe,). It can be seen, firstly, the λ_{0B} does not change almost. Secondly, the λ_{1B} change very small and λ_{1B} is changed from1532.55nm to1533.01nm corresponding to H from 300Oe to 0Oe. Finally, λ_{2B} change faster from 1529.78nm to1531.50nm corresponding to H from 300Oe to 0Oe. It can be conclude that the higher the mode is, the faster is the changing of resonant peaks with H. The cladding modes and the fundamental mode have different magnetic sensitivity, which can be use to achieve multi-parameter measurement.

3.4 The Relationships between Core Diameter and the Resonant Peak of the MF-filled PCFBG

The D_{core} is 2nm, 3nm, 4nm respectively, the reflection spectrum of the MF-filled PCFBG with under H=200Oe were analyzed, as shown in Fig.6.

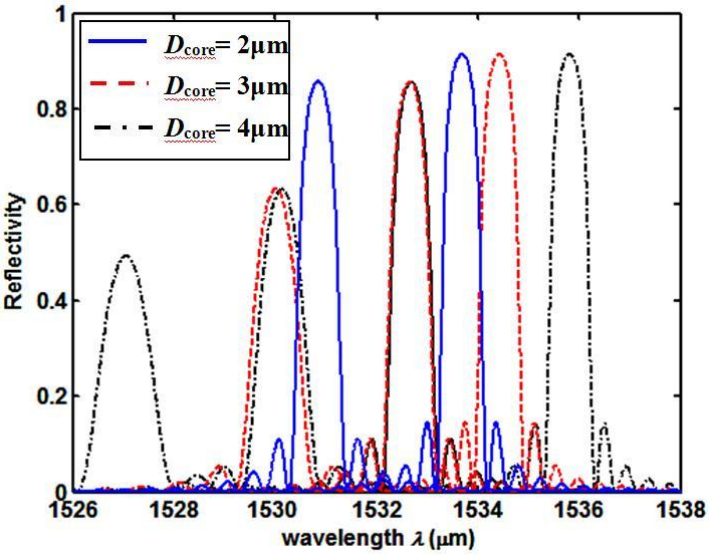

Fig. 6. Reflection spectrum of MF-filled PCFBG under different D_{core}

It was found, firstly, there are double resonance peaks when D_{core}=2μm, and the corresponding resonant wavelength is about 1530.95nm and1533.67. There are three resonance peaks when D_{core}=3μm, and the corresponding resonant wavelength is about 1530.09nm, 1532.67nm and 1534.35nm. There are four resonance peaks when D_{core}= 4μm, and the corresponding resonant wavelength is about 1527.05nm, 1530.25nm, 1532.68nm and 1535.75nm. The largest resonance peaks are generated by the fundamental mode, and the rest of the resonant peaks are generated by the cladding modes. Secondly, the number of resonant peak increases with D_{core} increasing. The reason is that the phase matching conditions of the cladding modes were excited with D_{core} increasing. Finally, a blue shift of resonant peak is observed with D_{core} increasing. The reason is that the Re(n_{eff}) of the transmission mode decreases with D_{core} increasing, and the resonant wavelength shift to long wavelength.

4 Conclusion

In this article, we analyze theoretically the characteristics changes of photonic crystal fiber grating filled MF by applying the FEM, the coupled mode theory and transfer matrix method. Basis on these theoretical, we established the MF-filled PCFBG simulation model. The spectral characteristics and mode coupling behaviors of the

MF-filled PCFBG were figured out and simulated, and the magnetically-induced tuning properties of the MF-filled PCFBG were researched. The relationships between the resonant wavelength and H for different coupling modes were investigated. It can be concluded that the cladding modes and the fundamental mode have different magnetic sensitivity, which can be use to achieve multi-parameter measurement at the same time. In addition, we analyzed and simulated the relationships between core diameter and the resonant peak of the MF-filled PCFBG. The results show that the number of resonant peak increases with D_{core} increasing, and a blue shift of resonant peak is observed with D_{core} increasing. As a result, when PCFG will be used for multi-parameter sensing, you can get to meet the design requirements of multi-resonant peak through the designing rationally core diameter size.

Acknowledgments. This work was supported in part by Specialized Research Fund for the Doctoral Program of Higher Education under Grant 20100042110029, Program for New Century Excellent Talents in University under Grant NCET-08-0102, the Fundamental Research Funds for the Central Universities under Grant 110204002 and 110604009, Natural Science Foundation of China under Grant 60972164, the Science and Technology Program of Shenyang under Grant No. F11-264-1-70, F10-205-1-80 and Science & Technology Research of LiaoNing Provincial under Grant No. L2011235.

References

1. Andrea, C., Domenico, P., Agostino, I.: Microstructured Fiber Bragg Gratings. Journal of Lightwave Technology 11, 1663–1697 (2009)
2. Zhao, Y., Zhang, Y.Y., Lv, R.Q., Wang, Q.: Novel optical devices based on the tunable refractive index of magnetic fluid and their characteristics. Journal of Magnetism and Magnetic Materials 323, 2987–2996 (2011)
3. Liu, R., Qu, R.H., Cai, H.W., Fang, Z.J.: Analysis of the transmission spectral characteristics of fiber Bragg grating in photonic crystal fibers. Acta Optica Sinica 26, 1007–1012 (2006) (in Chinese)
4. Liu, T., Chen, X.F., Di, Z.Y., Zhang, J.F.: Tunable magneto-optical wavelength filter of long-period fiber grating with magnetic fluids. Applied Physics Letters 91, 121116 (2007)
5. Mortensen, N.A., Nielsen, M.D., Folkenberg, J.R.: Modal cutoff and the V parameter in photonic crystal fibers. Optics Letters 28, 1879–1881 (2003)

Optimal Tracking Control for a Class of Nonlinear Time-Delay Systems with Actuator Saturation

Ruizhuo Song[1], Wendong Xiao[1], and Qinglai Wei[2]

[1] School of Automation and Electrical Engineering,
University of Science and Technology Beijing,
Beijing, 100083, P.R. China
ruizhuosong@163.com
[2] Key Laboratory of Complex Systems and Intelligence Science,
Institute of Automation, Chinese Academy of Sciences,
Beijing, 100190, P.R. China

Abstract. In this paper, a new iterative ADP algorithm is proposed to deal with the optimal tracking control problem for a class of time-delay systems with actuator saturation. By the problem transformation, the optimal regulation problem is obtained. For overcoming the difficulty from actuator saturation, the nonquadratic performance functional is presented for the optimal regulation problem. A novel ADP algorithm is established to get the optimal solution of the HJB equation of the nonlinear time-delay systems. A simulation example is given to illustrate the performance of the proposed method.

Keywords: Adaptive dynamic programming, optimal tracking control, time-delay, nonquadratic performance functional.

1 Introduction

Delay phenomena are very common in practical systems, such as, economic, biological and physiological systems [1]. In the past few decades, the Stabilization and control of time-delay systems has always been the key focus in the control filed [2], [3], [4], [5]. The discrete and continuous linear time-delay systems have been studied in [6], [7], [8], [9] and [10]. For nonlinear time-delay system, due to the complexity of systems, the optimal controller is very difficult to obtain.

It is well known that dynamic programming is very useful in solving the optimal control problems [11]. But it is often computationally untenable to run dynamic programming. In the early 1970's, Werbos set up the basic strategy for ADP [12] to overcome the "curse of dimensionality" of dynamic programming. In recent years, ADP algorithms have made great progress [13], [14], [15], [16]. In [17], an optimal infinite-horizon control scheme for a class of nonlinear systems with time delays was proposed based on ADP algorithm. By introducing a delay matrix function, the explicit expression of the optimal control function was obtained. The optimal control was iteratively obtained using the iteration ADP

D. Liu et al. (Eds.): BICS 2013, LNAI 7888, pp. 208–215, 2013.

algorithm. In [18], an optimal tracking controller was proposed for a class of nonlinear discrete-time systems with time delays based on a novel HDP algorithm. The novel algorithm contained state updating, control policy iteration and performance index iteration. But most of the results of the study are about the infinite-horizon optimal control. Few results relate to the finite-horizon optimal control based on ADP algorithm. In [19], a new ADP algorithm was proposed to solve the nearly finite-horizon optimal control problem for discrete time-delay systems through the framework of Hamilton-Jacobi-Bellman (HJB) equation.

In spite of significant progress on ADP algorithm in the optimal control field, within the radius of our knowledge, it is still an open problem about how to solve the optimal tracking control problem for nonlinear time-delay systems with actuator saturation based on ADP algorithm. In this paper, this open problem will be explicitly figured out. First, the optimal tracking problem is transformed to the optimal regulation problem. Then, the nonquadratic performance functional is presented, and a new iterative ADP algorithm is established to achieve the optimal tracking control solution with convergence analysis. At last, a simulation example is given to illustrate the performance of the proposed method.

This paper is organized as follows. In Section 2, we present the problem formulation. In Section 3, the optimal tracking control scheme is developed based on iterative HDP algorithm and the convergence proof is given. In Section 4, one example is given to demonstrate the effectiveness of the proposed control scheme. In Section 5, the conclusion is given.

2 Problem Formulation

In this paper, we consider the following unknown nonlinear systems

$$x(k+1) = F(x(k), x(k-h), u(k)), \tag{1}$$

where the control $u(k) \in \Re^m$ and the state $x(k), x(k-h) \in \Re^n$. $x(k) = 0, k \leq 0$. $F(x(k), x(k-h), u(k)) = f(x(k), x(k-h)) + g(x(k), x(k-h))u(k)$ is unknown continuous function. It is assumed the state is completely controllable and bounded in $\Omega \subset \Re^n$ and $F(0,0,0) = 0$. We denote $u(k) = [u_1(k) \quad u_2(k) \quad ... \, u_m(k)]^{\mathrm{T}} \in \Re^m$, $u_i^{min} \leq u_i(k) \leq u_i^{max}, i = 1, ..., m$, where u_i^{min} and u_i^{max} are the saturating bounds for the ith actuator. In this paper, we assume that the unknown system (1) is controllable in Ω, i.e., there exists analytic control policy which makes the system track the specified signal.

Define the state error as follows

$$e(k) = x(k) - \eta(k), \tag{2}$$

where the reference orbit $\eta(k)$ is generated by the n-dimensional autonomous system as follows

$$\begin{aligned} \eta(k+1) &= S(\eta(k)), \\ \eta(0) &= \varepsilon_2(k), -h \leq k \leq 0 \end{aligned} \tag{3}$$

in which $\eta(k) \in \Re^n$, $S(\eta(k)) \in \Re^n$ and ε_2 is the initial state, $\varepsilon_2(-h) = \cdots = \varepsilon_2(-1) = 0$.

Then we have

$$e(k+1) = F(x(k), x(k-h), u(k)) - S(\eta(k)). \tag{4}$$

So the optimal tracking control problem is transformed to the optimal regulation problem. The performance index function is defined as

$$J(e(k), v(k)) = \sum\nolimits_{i=k}^{\infty} \{Q(e(i)) + W(v(i))\}, \tag{5}$$

where $Q(e(i)), W(v(i))$ are positive definite, and $U(e(i), v(i)) = Q(e(i)) + W(v(i))$ is the utility function. $v(k) = u(k) - u_e(k)$, where $u_e(k)$ denotes the steady control input corresponding to the desired trajectory $\eta(k)$.

Inspired by [20], we let

$$Q(e(i)) = X^{\mathrm{T}}(i-h)QX(i-h), \tag{6}$$

and

$$W(v(i)) = 2\int_0^{v(i)} \phi^{-\mathrm{T}}(s)Rds, \tag{7}$$

where $X(i-h) = [e(i-1); e(i-2); ...; e(i-h)]$, Q, R are positive define, and we assume that R is diagonal for simplicity of analysis, $s \in \Re^m$, $\phi \in \Re^m$, $\phi^{-1}(v(i)) = [\psi^{-1}(v_1(i))\ \psi^{-1}(v_2(i))\ \cdots\ \psi^{-1}(v_m(i))]^{\mathrm{T}}$, $\psi(\cdot)$ is a bounded single mapping function and belonging to C^p $(p \geq 1)$ and L_2. Moreover, it is a monotonic increasing function with its first derivative bounded by a constant M.

Let $J^*(e(k)) = \min\limits_{v(k)} J(e(k), v(k))$ denote the optimal performance index function, and let $v^*(k)$ denote the corresponding optimal control law. According to Bellman's principle of optimality, the optimal performance index function $J^*(e(k))$ should satisfy the following HJB equation

$$J^*(e(k)) = \min_{v(k)} \{Q(e(k)) + W(v(k)) + J^*(e(k+1))\}, \tag{8}$$

and the optimal controller $u^*(k)$ should satisfy

$$v^*(k) = arg\min_{v(k)} \{Q(e(k)) + W(v(k)) + J^*(e(k+1))\}. \tag{9}$$

3 Optimal Tracking Control Scheme for Nonlinear Time-Delay Systems

For obtaining the optimal tracking controller, we design a new iterative algorithm as follows.

First, we start with initial iteration performance index function $J^{[0]}(.) = 0$ which is not necessarily the optimal performance index function. Then we find the control vector $v^{[0]}(k)$ as follow

$$v^{[0]}(k) = \arg\min_{v(k)} \{Q(e(k)) + W(v(k))\}, \tag{10}$$

and the performance index function is updated as

$$J^{[1]}(e(k)) = \min_{v(k)} \{Q(e(k)) + W(v(k))\}, \tag{11}$$

and the state is updated as follow

$$e(k+1) = F(x(k), x(k-h), u^{[0]}(k)) - S(\eta(k)), \tag{12}$$

where $u^{[0]}(k) = v^{[0]}(k) + u_e(k)$.

Moreover, for $i = 1, 2, ...$ the iterative ADP algorithm iterates between

$$v^{[i]}(k) = \arg\min_{v(k)} \left\{Q(e(k)) + W(v(k)) + J^{[i]}(e(k+1))\right\}, \tag{13}$$

and

$$J^{[i+1]}(e(k)) = \min_{v(k)} \left\{Q(e(k)) + W(v(k)) + J^{[i]}(e(k+1))\right\}, \tag{14}$$

and, the state of time-delay system updates as follow

$$e(k+1) = F(x(k), x(k-h), u^{[i]}(k)) - S(\eta(k)), \tag{15}$$

where $u^{[i]}(k) = v^{[i]}(k) + u_e(k)$.

For the proposed algorithm, the convergence analysis will be given in the next part.

Lemma 1. *Let* $\left\{\mu^{[i]}(k)\right\}$ *be any arbitrary sequence of control policies, and* $\left\{u^{[i]}(k)\right\}$ *is the policies expressed as in (13). Let* $J^{[i]}$ *be as in (14) and* $\Lambda^{[i]}$ *as*

$$\Lambda^{[i+1]}(e(k)) = Q(e(k)) + W(\mu^{[i]}(k)) + \Lambda^{[i]}(e(k+1)), \tag{16}$$

where $e(k+1)$ *is under the action of* $\mu^{[i]}(k)$*. For the same initial States, if* $J^{[0]}(\cdot) = \Lambda^{[0]}(\cdot) = 0$*, then* $J^{[i+1]}(e(k)) \leq \Lambda^{[i+1]}(e(k)), \forall i$.

Lemma 2. *Let the sequence* $J^{[i+1]}(e(k))$ *be defined by (14). If the system is controllable, then there is an upper bound* Y *such that* $0 \leq J^{[i+1]}(e(k)) \leq Y$*,* $\forall i$.

Theorem 1. *Define the cost function sequence* $\left\{J^{[i]}\right\}$ *as in (14) with* $J^{[0]}(\cdot) = 0$*, the control law sequence* $\left\{v^{[i]}(k)\right\}$ *as in (13). Then we can conclude that* $\left\{J^{[i]}\right\}$ *is nondecreasing sequence satisfying* $J^{[i+1]}(e(k)) \geq J^{[i]}(e(k))$*,* $\forall i$.

Proof: We define a new sequence $\left\{\Phi^{[i]}(e(k))\right\}$ as follows

$$\Phi^{[i]}(e(k)) = Q(e(k)) + W(v^{[i]}(k)) + \Phi^{i-1}(e(k+1)), \tag{17}$$

with $\Phi^{[0]}(.) = J^{[0]}(.) = 0$. And $J^{[i+1]}(e(k))$ is updated by (14).

In the following part, we prove $\Phi^{[i]}(e(k)) \leq J^{[i+1]}(e(k))$ by mathematical induction.

First,we prove it holds for $i = 0$. Notice that

$$J^{[1]}(e(k)) - \Phi^{[0]}(e(k)) = Q(e(k)) + W(v^{[0]}(k)) \geq 0. \tag{18}$$

Thus for $i = 0$, we get

$$J^{[1]}(e(k)) \geq \Phi^{[0]}(e(k)). \tag{19}$$

Second, we suppose that $J^{[i]}(e(k)) \geq \Phi^{[i-1]}(e(k))$, for $i-1$, $\forall e(k)$. Then for i, since

$$J^{[i+1]}(e(k)) = Q(e(k)) + W(v^{[i]}(k)) + J^{[i]}(e(k+1)), \tag{20}$$

and

$$\Phi^{[i]}(e(k)) = Q(e(k)) + W(v^{[i]}(k)) + \Phi^{i-1}(e(k+1)), \tag{21}$$

so we can get

$$J^{[i+1]}(e(k)) - \Phi^{[i]}(e(k)) = J^{[i]}(e(k+1)) - \Phi^{i-1}(e(k+1)) \geq 0. \tag{22}$$

Therefore, by the mathematical induction, we have

$$J^{[i+1]}(e(k)) \geq \Phi^{[i]}(e(k)), \forall i. \tag{23}$$

In addition, from Lemma 1 we know that $J^{[i]}(e(k)) \leq \Phi^{[i]}(e(k))$. Therefore we have

$$J^{[i]}(e(k)) \leq \Phi^{[i]}(e(k)) \leq J^{[i+1]}(e(k)), \tag{24}$$

which proves that $\left\{J^{[i]}(e(k))\right\}$ is a bounded nondecreasing sequence. Hence we conclude that $\left\{J^{[i]}(e(k))\right\}$ is a convergent sequence as $i \to \infty$.

4 Simulation

In this paper, we consider the following nonlinear time-delay system [21].

$$\begin{aligned} x(k+1) =& f(x(k), x(k-2)) + g(x(k), x(k-2))u(k) \\ x(k) =& \varepsilon_1(k), -2 \leq k \leq 0 \end{aligned} \tag{25}$$

where

$$f(x(k), x(k-2)) = \begin{bmatrix} 0.2x_1(k)\exp\left(x_2(k)\right)^2 x_2(k-2) \\ 0.3\left(x_2(k)\right)^2 x_1(k-2) \end{bmatrix},$$

and

$$g(x(k), x(k-1), x(k-2)) = \begin{bmatrix} x_2(k-2) & 0.2 \\ 0.1 & 1 \end{bmatrix}.$$

The desired orbit $\eta(k)$ is defined as follows

$$\eta(k+1) = A\eta(k), \tag{26}$$

with

$$A = \begin{bmatrix} \cos wT & \sin wT \\ -\sin wT & \cos wT \end{bmatrix}, \eta(0) = \begin{bmatrix} 0 \\ 1 \end{bmatrix},$$

where $T = 0.1s$, $w = 0.8\pi$.

In this paper, it is assumed that the control constraint is set to $|u_i(k)| \leq 0.3$. Firstly, we give the initial states as $\varepsilon_1(-2) = \varepsilon_1(-1) = \varepsilon_1(0) = \begin{bmatrix} 0.05 & -0.05 \end{bmatrix}^T$. The implementation of the algorithm is at the time instant $k = 3$. The maximal iteration step i_{max} is 200. We choose three-layer BP neural networks as the critic network and the action network with the structure $2-8-1$ and $6-8-2$, respectively. The iteration time of the weights updating for two neural networks is 50. The initial weights are chosen randomly from $[-0.15, 0.15]$, and the learning rate is $\alpha_a = \alpha_c = 0.01$. Then we get the simulation results. The convergence curve of the performance index function is shown in Fig. 1. The state trajectories are shown in Fig. 2 and Fig. 3. The corresponding state error curves are given as Fig. 4. It is clear from the simulations that the new iterative algorithm in this paper is very effective.

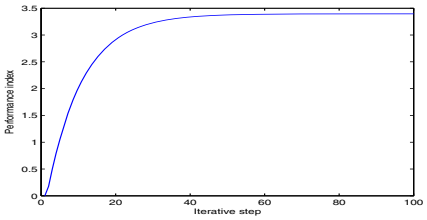

Fig. 1. The performance index function

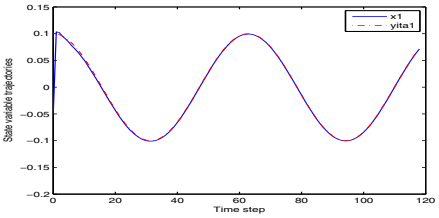

Fig. 2. The state variable trajectory x_1 and desired trajectory η_1

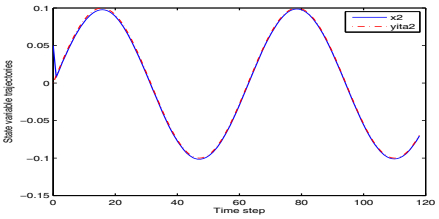

Fig. 3. The state variable trajectory x_2 and desired trajectory η_2

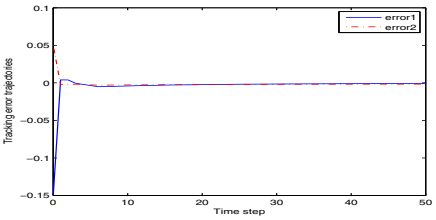

Fig. 4. The state error trajectories e_1 and e_2

5 Conclusion

This paper proposed a new iterative ADP algorithm to solve the optimal tracking control problem for a class of time-delay systems with actuator saturation. The optimal tracking problem was transformed to the optimal regulation problem. The nonquadratic performance functional was presented for overcoming the actuator saturation. A new ADP algorithm was proposed to deal with the optimal control for time-delay systems. At last, a simulation example was given to illustrate the performance of the proposed method.

Acknowledgment. This work was supported in part by the Open Research Project under Grant 20120106 from SKLMCCS, and the Fundamental Research Funds for the Central Universities FRF-TP-13-018A.

References

1. Manu, M.Z., Mohammad, J.: Time-delay systems analysis, optimization and applications. North-Holland, New York (1987)
2. Wang, M., Ge, S.S., Hong, K.S.: Approximation-Based Adaptive Tracking Control of Pure-Feedback Nonlinear Systems With Multiple Unknown Time-Varying Delays. IEEE Transactions on Neural Networks 21(11), 1804–1816 (2010)
3. Phat, V.N., Trinh, H.: Exponential Stabilization of Neural Networks With Various Activation Functions and Mixed Time-Varying Delays. IEEE Transactions on Neural Networks 21(7), 1180–1184 (2010)
4. Shao, H.Y., Han, Q.L.: New Delay-Dependent Stability Criteria for Neural Networks With Two Additive Time-Varying Delay Components. IEEE Transactions on Neural Networks 22(5), 812–818 (2011)
5. Tong, S.C., Li, Y.M., Zhang, H.G.: Adaptive Neural Network Decentralized Backstepping Output-Feedback Control for Nonlinear Large-Scale Systems With Time Delays. IEEE Transactions on Neural Networks 22(7), 1073–1086 (2011)
6. Chyung, D.H.: Discrete optimal systems with time delay. IEEE Transactions on Automatic Control 13(1), 117 (1968)
7. Chyung, D.H., Lee, E.B.: Linear optimal systems with time delays. SIAM J. Control 4(3) (November 1966)
8. Chyung, D.H.: On the controllability of linear systems with delay in control. IEEE Transactions on Automatic Control 15(2), 255–257 (1970)

9. Chyung, D.H.: Controllability of Linear Systems with Multiple Delays in Control. IEEE Transactions on Automatic Control 15(6), 694–695 (1970)
10. Phat, V.N.: Controllability of discrete-time systems with multiple delays on controls and states. International Journal of Control 49(5), 1645–1654 (1989)
11. Bellman, R.E.: Dynamic Programming. Princeton Univ. Press, Princeton (1957)
12. Werbos, P.J.: Advanced forecasting methods for global crisis warning and models of intelligence. General Systems Yearbook 22, 25–38 (1977)
13. Wang, F.Y., Zhang, H.G., Liu, D.R.: Adaptive dynamic programming: an introduction. IEEE Computational Intelligence Magazine 4(2), 39–47 (2009)
14. Zhang, H.G., Wei, Q.L., Liu, D.R.: An iterative adaptive dynamic programming method for solving a class of nonlinear zero-sum differential games. Automatica 47(1), 207–214 (2011)
15. Zhang, H.G., Wei, Q.L., Luo, Y.H.: A novel infinite-time optimal tracking control scheme for a class of discrete-time nonlinear systems via the greedy HDP iteration algorithm. IEEE Transactions on Systems, Man, and Cybernetics, Part B: Cybernetics 38(4), 937–942 (2008)
16. Zheng, C., Jagannathan, S.: Generalized Hamilton-Jacobi-Bellman formulation-based neural network control of affine nonlinear discrete-time systems. IEEE Transactions on Neural Networks 19(1), 90–106 (2008)
17. Wei, Q.L., Zhang, H.G., Liu, D.R., Zhao, Y.: An optimal control scheme for a class of discrete-time nonlinear systems with time delays using adaptive dynamic programming. ACTA Automatica Sinica 36(1), 121–129 (2010)
18. Zhang, H.G., Song, R.Z., Wei, Q.L., Zhang, T.Y.: Optimal Tracking Control for a Class of Nonlinear Discrete-time Systems with Time Delays Based on Heuristic Dynamic Programming. IEEE Transactions on Neural Networks 22(12), 1851–1862 (2011)
19. Wang, F.Y., Jin, N., Liu, D.R., Wei, Q.L.: Adaptive dynamic programming for finite-horizon optimal control of discrete-time nonlinear systems with ϵ-error bound. IEEE Transactions on Neural Networks 22, 24–36 (2011)
20. Zhang, H.G., Luo, Y.H., Liu, D.R.: Neural-network-based near-optimal control for a class of discrete-time affine nonlinear systems with control constraints. IEEE Transactions on Neural Networks 20, 1490–1503 (2009)
21. Zhang, H., Song, R., Wei, Q., Zhang, T.: Optimal Tracking Control for a Class of Nonlinear Discrete-Time Systems With Time Delays Based on Heuristic Dynamic Programming. IEEE Transactions on Neural Networks 22(12), 1851–1862 (2011)

Improved Efficiency of Road Sign Detection and Recognition by Employing Kalman Filter

Usman Zakir[1], Amir Hussain[1], Liaqat Ali[1], and Bin Luo[2]

[1] COSPIRA Laboratory, Division of Computing Science,
School of Natural Sciences University of Stirling, Stirling FK9 4LA
[2] Intelligent Computing and Signal Processing, Anhui University, Hefei, Anhui, China
usmanzakir@gmail.com, {a.hussain,lal}@cs.stir.ac.uk,
luobin@ahu.edu.cn

Abstract. This paper describes an efficient approach towards road sign detection, and recognition. The proposed system is divided into three sections namely: *Road Sign Detection* where *Colour Segmentation* of the road traffic signs is carried out using HSV colour space considering varying lighting conditions and *Shape Classification* is achieved by using Contourlet Transform, considering possible occlusion and rotation of the candidate signs. *Road Sign Tracking* is introduced by using Kalman Filter where object of interest is tracked until it appears in the scene. Finally, *Road Sign Recognition* is carried out on successfully detected and tracked road sign by using features of a Local Energy based Shape Histogram (LESH). Experiments are carried out on 15 distinctive classes of road signs to justify that the algorithm described in this paper is robust enough to detect, track and recognize road signs under varying weather, occlusion, rotation and scaling conditions using video stream.

Keywords: Road Signs, HSV, Contourlet Transform, LESH, Colour Segmentation, Autonomous Vehicles, Kalman Filter and SVM.

1 Introduction

RSDR (*Road Sign Detection and Recognition*) has drawn considerable research attention in recent years, due to its challenging nature as a computer vision problem. Road signs have a direct impact on ones daily life as possible life threats can easily be formed due to lack of concentration or ignorance. In recent years, a number of Driver *Assistance Systems* have been proposed and implemented including vision-based algorithms, claiming to be efficient towards the RSDR. In addition, due to increased amount of possible threats on the roadside, the impact of the road signs on the road users has considerably increased during the last decades. Many new road signs have been introduced according to the necessity and due to increase usage of the roads. Vehicle driver specially needs to learn to identify all road signs for road safety. For example a driver requires the knowledge of cyclist signs, pedestrian signs, obligatory signs and advisory signs etc. and ignorance of any sign can cause possible accident hazards. In conjunction to other ADAS *(*Advanced Driver Assistance Systems) such as lane departure warning systems, in-car navigation systems, adaptive cruise control system, automatic parking etc., the RSDR systems help in detecting and translating

D. Liu et al. (Eds.): BICS 2013, LNAI 7888, pp. 216–224, 2013.

the road signs for the attention and understanding of drivers. Specifically, drivers with visual impairments can benefit from this important computer based visual aid. In more sophisticated systems, the RSDR systems can utilise other features of ADAS such as adaptive cruise control system to automatically drive the vehicle according to varying road speeds. Highway agencies and road maintenance engineers have the responsibilities to maintain the roads and the state of signposting, which are vital for the safety of the road users. The RSDR can be used for road sign inventory and inspection purposes. Damaged, occluded, tilted, rotated, colour faded road signs can be recognised and replaced to reduce possible risks. With the RSDR, the inventory and inspection process can be made semi automatic where video footage of the road with signage information is recorded, prior to locating and investigating a particular damage. Generally, road signs consist of three properties; firstly *colour* such as Red, Green, Blue or Brown etc. represents them. Secondly, they consist of a particular *shape* such as Circular, Triangular, Octagonal, or Square etc. The *inner contents* of the road signs represent the third property, which may vary depending on the application of the road sign. In this paper we have provided improvement to the algorithm [7] considering the importance of using above mentioned properties separately by focusing different problems including various lighting conditions, scaling, angular rotation and occlusion. For clarity of presentation this paper has been organized as follows: In addition to this section in which the research problem was introduced and its practical relevance was highlighted, Section-2 provides exiting State of the Art, Section-3 presents the System Overview providing details about each operational stage. Section-4 provides the experimental results obtained and an analysis of the results leading to the conclusions that are provided in Section-5.

2 State of the Art

This section introduces existing literature in the application domain of the RSDR. The study of these approaches will conceptually compare the performance of the state-of-the-art to the performance of the proposed algorithm in the following section. This allows fair comparison, particularly when no standard dataset is available for researchers to carry out performance analysis. Fig 1 illustrates the general framework used in the majority of the RSDR approaches proposed in the literature. These approaches largely differ due to the differences in the algorithms used within each of the three functional blocks of Fig 1.

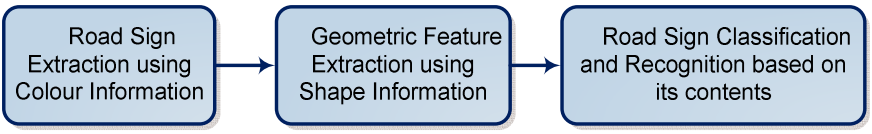

Fig. 1. General framework of Road Sign Detection and Recognition

Road sign detection from an image or image sequence is the first key step of the RSDR. An extensive investigation of existing literature [1] , [2] has been made which reflects that using the properties of colour and shape or joint information carries out

the detection step. Secondly road sign recognition is performed on the contents of the candidate road signs and is mostly dependent on an extensive shape analysis and classification. In addition, road sign tracking is adopted by some researchers to enhance the accuracy of the detection and recognition stages and to reduce the computational cost of having not to repeat the above processes on each video frames. A detailed taxonomy is provided in [2] shows the varying ranges and combinations of the algorithms utilised by the RSDR systems in the literature within the three key stages (see Fig 1). Colour based segmentation is achieved by using different colour models, Shape is also considered as an important feature of the road sign representation and Contents are recognised by utilizing various feature extraction techniques and classifiers. The next section aims to overcome previous research gaps in designing a robust RSDR system that is capable of performing on video streams under wide variations of illumination and environmental conditions.

3 System Overview

The proposed RSDR system comprises of three key stages, which are detailed in this section. For better understanding of proposed RSDR, Fig 2 is given to describe a complete RSDR framework whereas Fig 4 is provided to further explain the framework with example input and output of the RSDR system.

3.1 Road Sign Detection

Road Sign Detection of the system represents a key stage of detecting an outdoor object that could possibly be a road sign. To aid this detection process; colour and shape properties of the road sign are utilised which are detailed in following subsections.

(a) Colour Segmentation

The taxonomy presented in [2] highlights the fact that the colour segmentation is majorly initiated by employing a computer based colour space. Video footage/images captured by a digital camera are not always appropriate to perform the desired image processing tasks. Different video systems such as NTSC (National Television System Committee), PAL (Phase Alternating Line) and SECAM (Séquentiel Couleur à Mémoire) that are used to capture the Videos/images, significantly affect the original (i.e. raw) pixel intensity values by Gamma Encoding [3]. The Gamma is represented with the Greek letter γ, has encoding and decoding standard values according to the above-mentioned video systems. The videos/images captured for experimental purposes have adopted the NTSC video system, which encodes gamma at the rate $\gamma = 1/2.2$. Therefore, this non-linearity in the videos/images is required to be decoded in order to achieve pre processing task prior to Pixels of Interest (POI) selection by using HSV (Hue, Saturation, and Value) colour space [1], [4]. In the segmentation process; pixels belonging to Red, Blue and Green colours, are represented by 1 and rest of the pixels are treated as background or 0. The corresponding bounding boxes of the segmented object(s) are analysed according to its centre and corner points as illustrated in [1].

(b) Shape Classification

Apart from colour of the road sign, shape is the second most distinctive attribute that can be used to further identify the type of a road sign. The input images to the shape classification module are the binary images resulting by applying the colour based segmentation algorithms.

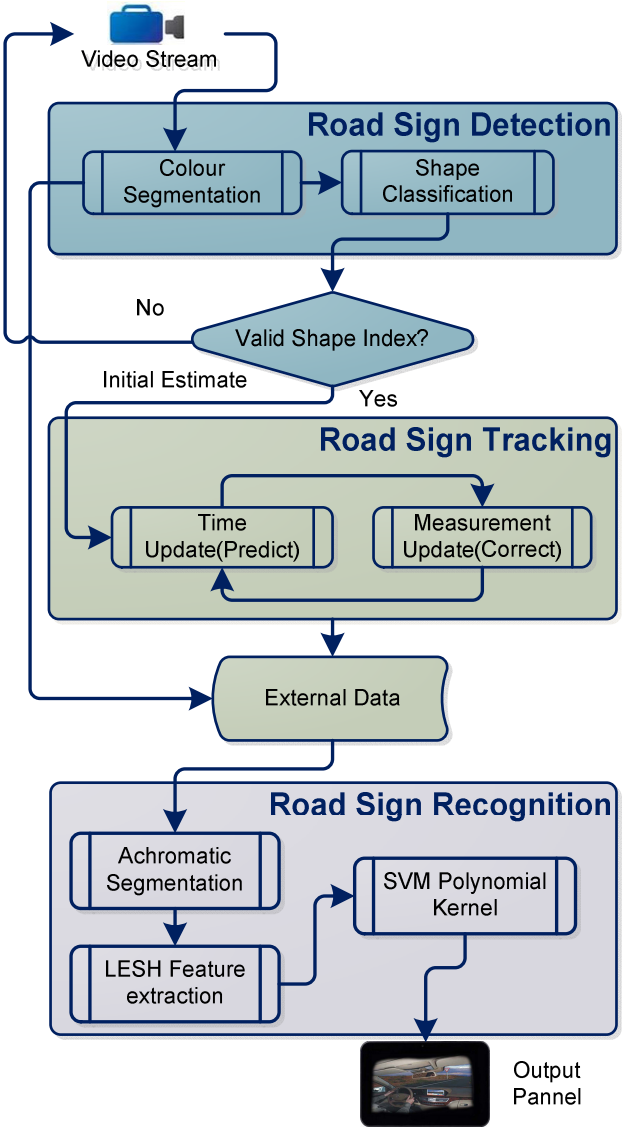

Fig. 2. RSDR framework

The binary input images are pre processed in such a way that only outer candidate shapes are considered in later processing stages of shape classification. The shape features are extracted by using Contourlet Transform [5] and SVM polynomial kernel [6] is employed to classify the extracted features. The robustness of the proposed shape identification and classification is particularly tested on road signs with abnormal appearances, i.e. ones that are partially occluded, may be of different sizes (scale) and orientations. The shape-based analysis of road signs is helpful in two ways in the RSDR. Firstly, it removes the false positives extracted as candidate road signs during colour-based segmentation. Secondly, subsequent tracking and detailed content recognition in road signs will only be performed on road signs belonging to a particular shape group i.e., circular, rectangular or triangular.

3.2 Road Sign Tracking

Road Sign Tracking is well introduced as a process between road sign detection and road sign recognition. The procedure is carried out by using Kalman Filter [8] where identified blob of interest representing geometric shape is tracked and considered as same object for the life of its appearance in the scene. Tracking system is aided with some vital information extracted from the road sign detection process; that is colour, shape, location and size of the object, kept stored as object signatures. Colour and shape information provides the relevance to previously tracked object of same colour and shape information respectively. Location information helps in predicting the position of the object in next iteration and narrows down the search region at the same time. Size information ensures that the detected blob gets bigger in dimensions in the next iteration. Object is tracked at three stages; firstly, initial estimate is gathered about the position of the object in the video frame. Object signature helps to obtain the initial position of an object and a square search region is constructed to narrow down the search area. Secondly, Prediction of the object position is made with in the square search region which periodically changes according to the new position of the tracked object. Correction of measurements in terms of actual and predicted positions of an object is the final stage in the tracking process. At the end of each successful tracking, signatures of the object are updated and road sign is cropped from the original image for later stage of its contents recognition.

3.3 Road Sign Recognition

Once the candidate sign gets qualified through road sign detection and tracking stages of RSDR, it initiates the process of recognition and classification of the road sign contents. The recognition process comprises of the LESH [1] features extraction of the road sign contents and training/testing of these features by employing SVM polynomial kernel [6]. The candidate road signs, which are validated in first two stages i.e. *Road Sign Detection* and *Road Sign Tracking*, are further processed to obtain the valid road sign contents for feature extraction. The internal contents of road signs are normally represented as black and white colours. These white and black areas can be extracted by simple black and white region extraction using adaptive threshold. After obtaining the binary images, the connected components from the binary image are extracted which removes the noisy objects (non sign objects) at the same time. The image(s) are normalised to a square dimensional image of size

128×128 and at the same time converted to grey level image. It should be reminded that the image normalisation to a fixed dimensional size and its grey level conversion, are the valid input requirements for LESH feature extraction. The next stage is to extract the LESH features of the normalized images, which are obtained through the pre processing stage. LESH features are obtained by computing the local energy along each filter orientation of image sub-region. The overall histogram represents the concatenated histograms, which are computed along each sub-region of the image. These extracted LESH features from different classes of road signs are trained and classified with the help of multiclass SVM polynomial kernel. The next section provides details of the experimental setup and acquired results by utilising aforementioned algorithm.

4 Experimental Setup and Results

This section provides details of the experiments carried out on the video samples, which were recorded during varying outdoor lighting conditions. The resolution 640×480 pixels is used to capture testing video samples where as 2592×1944 pixels resolution is used to capture images for training purposes. The hardware comprises of *Canon IXUS80IS* digital camera for image and video acquisition, Pentium 4 Dual Core 3.2 Ghz, and 4 GB of RAM. The RSDR application is developed and tested by using Visual Studio .Net and signal and image processing toolboxes of MATLAB.

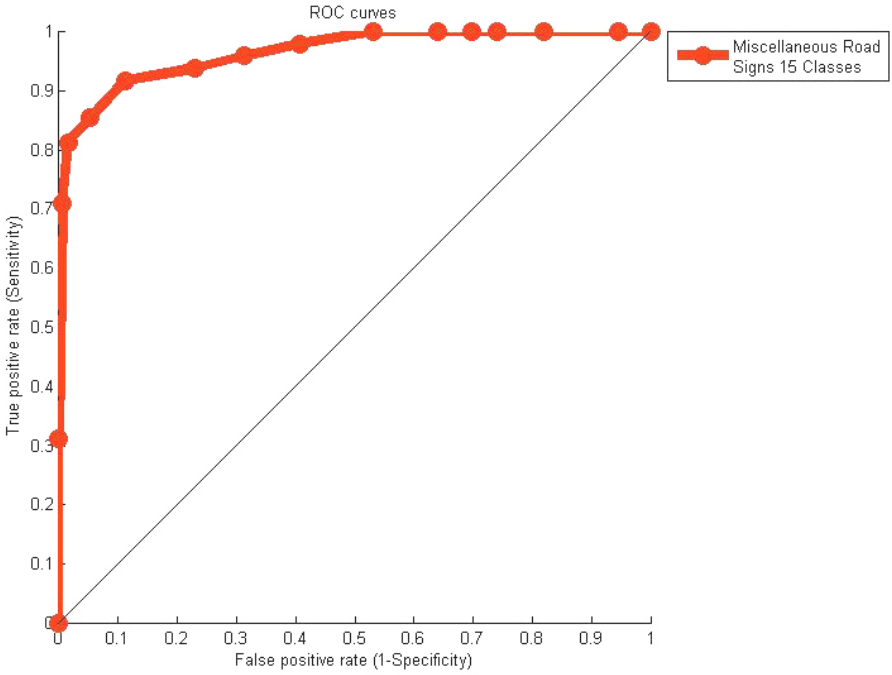

Fig. 3. ROC curve of Set-1, Set-2 and Set-3 road signs

The experiments are carried out on same dataset used in [7] where 15 different classes are used in detection and recognition stages. Speed limit signs i.e. '15','30','40','50' and,'70' are given class labels as T1, T2, T3, T4 and T5 respectively and collectively they are named as *Set-1* signs. *Set-2* represents different triangular signs, i.e., 'GIVEWAY', 'Round About', 'Bend to Left Ahead', 'T-Junction' and 'Slippery Road' which are given class labels as T6, T7, T8, T9 and T10 respectively. *Set-3* is a further group of miscellaneous road signs (e.g. Advisory and Obligatory etc.) i.e. '*Priority*', '*Stop*', '*Turn Left*', '*No Entry*' and '*Round About*', and they are given class labels for this experiment as *T11, T12, T13, T14 and T15* respectively. The training of road signs is performed on 40 image samples per class and it is carried out offline. The testing is performed on the video samples which represents road signs, captured during varying lighting and environmental conditions, with changes in scale and includes partial occlusion. Table 1 is provided to show the comparison of RSDR accuracies along with number of frames and total number of signs used in *Set-1*, *Set-2* and *Set-3* respectively. ROC (Receiver Operating Characteristic) curve for tested *Set-1, Set-2 and Set-3* road signs is presented in Fig 3 where true positives are plotted against false positives.

Table 1. Comparison of RSDR accuracies

Label Index	Type of Sign[7]	Number of Frames	Total Signs	Accuracy %[7]	Accuracy % Proposed System
T1-T5	Set-1	1670	186	94.0 - 98.0	98.0-99.0
T6-T10	Set-2	1535	276	93.1 - 97.0	97.0-99.0
T11-T15	Set-3	830	103	76.0 - 91.2	95.0-97.5

5 Conclusion

In this paper we have presented a novel approach towards road sign detection and recognition. *Road Sign Detection* stage comprises of *Colour Segmentation* and *Shape Classification*; where *Colour Segmentation* of the road traffic sign is carried out using HSV colour space considering varying outdoor lighting conditions and *Shape Classification* is achieved by using Contourlet Transform; considering possible occlusion and rotation of the candidate sign. *Road Sign Tracking* is achieved by using Kalman Filter where object of interest is tracked until it appears in the scene. *Road Sign Recognition* stage introduces the SVM classifier with Local Energy based Shape Histogram (LESH) features. The experiments are carried out on 15 different classes of road signs considering varying levels of illumination and environmental conditions proves the effectiveness of proposed approach. Overall accuracy figures of 97.5-99.0% have been reported which shows vital improvement that are compared in Table 1. In future, current work will be utilised towards the development of real time application of RSDR to further aid currently available ADAS systems.

(a) Input Image/ Frame

(b) Red Colour Segmentation

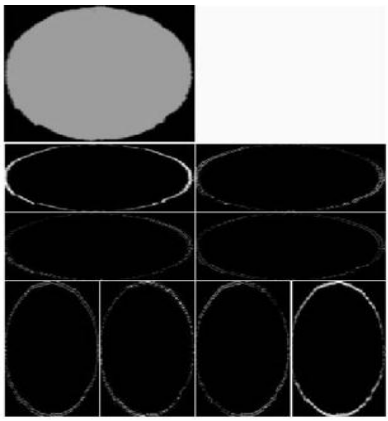

(c) Contourlet Representation of Colour Segmented Object

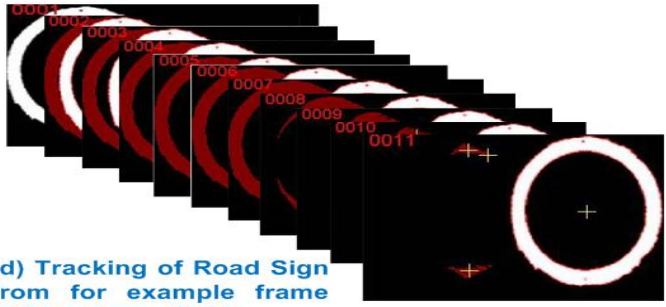

(d) Tracking of Road Sign from for example frame 0001 to frame 0011

(e) Complete Coloured Sign

(f) Achromatic Segmentation

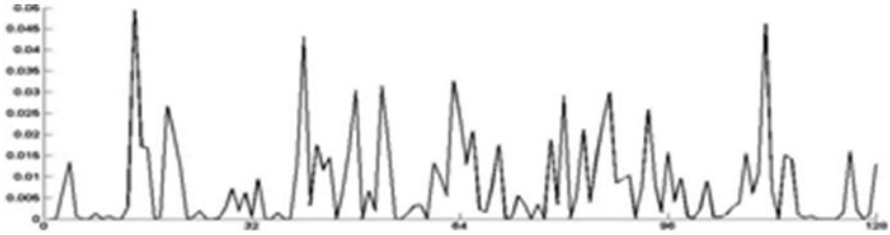

(g) LESH feature Vector for 15 speed limit road sign

Fig. 4. An explained framework of RSDR with example input and output

Acknowledgments. The Royal Society of Edinburgh (RSE) and the National Natural Science Foundation of China (NNSFC) support Professors Amir Hussain and Bin Luo under the RSE-NNSFC joint project (2012-2014). Professors Hussain and Luo are also supported by a grant from the British Council in China for their collaborative research project (2013-15).

References

1. Zakir, U., Zafar, I., Edirisinghe, A.E.: Road Sign Detection and Recognition by using Local Energy Based Shape Histogram (LESH). International Journal of Image Processing 4(6), 566–582 (2011) ISSN: 1985-2304
2. Automatic Road Sign Detection and Recognition, PhD Thesis, Computer Science Loughborough University (2011), http://lboro.academia.edu/usmanzakir/Papers/1587192/Automatic_Road_Sign_Detection_And_Recognition
3. Gamma Correction, http://en.wikipedia.org/wiki/Gamma_correction
4. Zakir, U., Leonce, J.N.A., Edirisinghe, A.E.: Road sign segmentation based on colour spaces: A Comparative Study. In: Proceedings of the 11th Iasted International Conference on Computer Graphics and Imgaing, Innsbruck, Austria (2010)
5. Do, N.M., Vetterli, M.: The Contourlet Transform: An Efficient Directional Multi resolution Image Representation. IEEE Transactions on Image Processing 14(12) (2005)
6. Duin, W.P.R., Juszczak, P., Paclik, P., Pekalska, E., de Ridder, D., Tax, J.M.D., Verzakov, S.: PRTools4.1, A Matlab Toolbox for Pattern Recognition, Delft University of Technology (2007)
7. Zakir, U., Edirishinghe, E.A., Hussain, A.: Road Sign Detection and Recognitionfrom Video Stream using HSV, Contourlet Transform and Local Energy basedShape Histogram. In: Zhang, H., Hussain, A., Liu, D., Wang, Z. (eds.) BICS 2012. LNCS, vol. 7366, pp. 411–419. Springer, Heidelberg (2012)
8. Kalman, E.R.: A new approach to linear filtering and prediction problems. IEEE Trans. of the ASME, Journal of Basic Engineering 82 (1960)

Prospective Emotion Regulation in Smokers as Reflected in Self-reports, Facial Electromyographic and Electroencephalogram Activity

Lingdan Wu, Markus H. Winkler, Marta Andreatta, and Paul Pauli

Department of Psychology, University of Würzburg, 97070 Würzburg, Germany
{Lingdan.Wu,Markus.H.Winkler,Marta.Andreatta,
Paul.Pauli,lingdan43}@gmail.com

Abstract. Nicotine addiction is the most prevalent type of drug addiction that has been described as a cycle of spiraling dysregulation of the brain reward systems. It was assumed that addicts may perform less well than healthy nonsmokers in cognitive emotion regulation tasks. The current study applied the appraisal frame paradigm to investigate how smokers differ from nonsmokers on cognitive emotion regulation. Sixty participants (22 nonsmokers, 19 nondeprived smokers and 19 12-h deprived smokers) completed emotion regulation tasks while emotional responses were concurrently recorded as reflected by self-ratings and psychophysiological measures. The results indicated that nondeprived smokers and deprived smokers performed as well as nonsmokers on the emotion regulation task. The lack of group differences in multiple emotional responses (i.e., self-reports, facial EMG activity and brain EEG activity) suggests that nicotine addicts have no deficit in cognitive emotion regulation of natural rewards via appraisal frames.

Keywords: Nicotine addiction, Emotion regulation, EMG, EEG.

1 Introduction

Previous studies found that appraisal frames preceding negative pictures could manipulate emotional responses as indexed by self-reports, facial electromyographic (EMG), and the late positive potential (LPP), an event-related potential (ERP) component involved in emotional processing (Wu et al., 2012; Foti & Hajcak, 2008).

The present study builds on the previous work by examining the prospective emotion regulation via appraisal frames in smokers. Clinical and functional imaging studies have noted that smokers are characterized by a decreased use of cognitive appraisal strategies and by malfunction in PFC regions as compared to nonsmokers (Goldstein & Volkow, 2011; Sutherland et al., 2012). Smoking deprivation further affected performances on a variety of cognitive tasks related to attention, memory and emotion. In particular, abstinence from smoking (e.g., overnight deprivation) has been found to induce more negative experience, less attention and smaller emotional reactions to nonsmoking stimuli (Cinciripini et al., 2006; Dar et al., 2010;

D. Liu et al. (Eds.): BICS 2013, LNAI 7888, pp. 225–234, 2013.

Lam et al., 2012). Therefore, it might be assumed that smokers would show deficit in cognitive emotion regulation, and that overnight deprivation from smoking would worsen this deficit. However, no study to date has specifically investigated emotion regulation via appraisal frames in nicotine addicts, not to mention the effect of smoking deprivation on cognitive emotion regulation. Therefore, this study aimed to investigate whether and how smokers or deprived smokers may differ from nonsmokers on cognitive emotion regulation via appraisal frames.

To address the above issue, the present study recruited smokers who regularly smoke more than 10 cigarettes per day during at least the last 12 months, and compared their emotion regulation ability with a group of nonsmokers who had smoked 2 or fewer cigarettes in their lifetime. Half of the smokers were allowed to smoke as usual and the other half were required to refrain from smoking 12 hours before they came to the experiment, thus forming a deprived smoking group and a nondeprived smoking group. The reports of emotional experience, cravings to smoke and psychophysiological responses during emotion regulation were examined using measures of self-rating scales, facial electromyography (EMG) activity, and electroencephalogram (EEG) activity.

I predicted that smokers have deficits in cognitive emotion regulation: smokers would respond to appraisal frames with smaller changes in subjective emotional experience, EMG and EEG activities as compared to nonsmokers, and this impairment would be more pronounced in deprived smokers as compared to nondeprived smokers.

2 Method

2.1 Participants

In total, 35 nonsmokers (18 females) and 70 smokers (35 females) were recruited through online advertisements and posters. Participants were screened over phone or email to determine that they were either smokers or nonsmokers. Participant's mean age was 24.74 years old (range 18-40). They had a high school diploma or equivalent, were not taking any prescription drugs and were fluent German speakers. Smokers were defined as persons who smoked an average of at least 10 cigarettes per day during at least the last 12 months, while nonsmokers (NS) were persons who had smoked fewer than 2 cigarettes in their lifetime. Smokers were randomly assigned to one of two groups: nondeprived smoking group and deprived smoking group. Individuals in the nondeprived smoking group (NDS) were asked to smoke as normal and to consume one cigarette immediately before they came to the laboratory. Individuals in the deprived smoking group (DS) were required to abstain from smoking over-night for about 12 hours prior to their appointments.

Further exclusion criteria included: 1) having personal history of drug addiction excluding nicotine dependence; 2) having current psychiatric or neurological disorders; 3) currently taking any smoking cessation medications and/or attending smoking cessation programs. According to these criteria, a total of 33 nonsmokers (16 females), 27 nondeprived smokers (15 females) and 28 deprived smokers

(15 females) were confirmed to participate in the experiment. Most participants were students from the University of Würzburg and received either money (6 euro/h) or course credit. Deprived smokers were compensated with an extra 10 euro for their efforts to abstain from smoking.

2.2 Materials

In total, 25 neutral scenes, 50 positive scenes and 50 negative scenes were selected from the International Affective Picture System (IAPS; Lang et al., 2005). Auditory narratives were recorded in advance including 125 neutral narratives, 50 negative narratives for the negative pictures and 50 positive narratives for the positive pictures. The auditory narratives were presented binaurally via speakers with a sound intensity of 68dB. Self-Assessment Manikins (SAM; Bradley and Lang, 1994) were used to measure stimulus evoked valence and arousal. A portable Smokerlyzer® carbon monoxide (CO) monitor (Bedfont Scientific Ltd, Kent, U.K.) was used to verify participants' smoking status.

2.3 Procedure and Apparatus

After reading the instructions for the experiment and signing the informed consent, participants completed a simple CO test and filled out the questionnaire. The questionnaire set included a general demographics questionnaire, the Fagerström Test for Nicotine Dependence (FTND; Heatherton, Kozlowski, Frecker & Fagerstrom, 1991), the German version of the State Trait Anxiety Inventory questionnaire (STAI; Laux, Glanzmann, Schaffner, and Spielberger, 1981), and the German version of the Beck Depression Inventory questionnaire (BDI; Hautzinger et al., 1995). Participants were then seated in a comfortable chair in a sound attenuated and dimly lit room. Electroencephalograph (EEG) sensors and facial electromyography (EMG) sensors were attached. To decrease demand characteristics, participants were informed that their skin conductance was to be measured as they viewed some pictures.

Each trial began with a white fixation cross presented on a black screen for a period ranging randomly from 4 to 5 sec. The fixation cross turned to blue one second before the onset of the auditory narratives which could last from 2 to 4 sec. Half of the positive pictures were preceded by positive narratives (positive-positive condition) and half of the negative pictures were preceded by negative narratives (negative-negative condition). The other halves of the emotional pictures were preceded by neutral narratives (neutral-positive condition and neutral-negative condition). All of the neutral pictures were preceded by neutral narratives (neutral-neutral condition). Following each narrative, there was a 1 sec delay and then the corresponding picture was presented for 4 sec. At the offset of each picture, the SAM scales appeared on the screen and participants rated how they felt during picture presentation. At the end of

the test, participants completed the German version of the Emotion Regulation questionnaire (ERQ, Gross & John, 2003). And then, they were debriefed and thanked.

2.4 Psychophysiological Data Recording and Data Reduction

The continuous EMG and EEG were recorded at 1000 Hz through a V-Amp 16 amplifier (Brain Products Inc., Gilching, Germany). The pairs of two 7-mm Ag/AgCl electrodes were placed over the left eye (corrugator) and left cheek (zygomaticus) according to guidelines provided by Fridlund and Cacioppo (1986). The EMG data was re-referenced to obtain bipolar recordings. The raw signal was filtered with a band-pass filter from 30 Hz to 500 Hz and a 50 Hz notch filter. Subsequently, the data were rectified and smoothed using a 125 ms moving average filter. Trials with an EMG activity above 8 μV or below -8 μV during the baseline (mean EMG activity over 1000 ms preceding picture onset) and above 30 μV or below -30 μV during picture presentation were excluded. Before statistical analysis, EMG activity was measured as the difference between the mean activity during the 4 sec picture period and the 1 sec baseline. The corrugator activity and zygomaticus activity were scored as the average activity in the time window 300–4000 ms over the corrugator supercilii and zygomaticus major muscle respectively.

Based on previous research indicating that the LPP is typically maximal at posterior and parietal sites, the EEG was recorded using an EasyCap (EasyCap, Hersching, Germany) from 10 positions including FCz, Cz, CPz, Pz, C1, C2, CP1, CP2 (Foti & Hajcak, 2008), and the left and right mastoids. EEG data was band-pass filtered between 0.01 and 20 Hz and then segmented (−100 to 4000 ms with respect to stimulus onset). Subsequently, the data was corrected for ocular artifacts using the method developed by Gratton et al. (1983). An automated procedure was used to reject remaining artifacts according to the following criteria: a voltage step of more than 50.00 μV between sample points, a voltage difference of more than 300.00 μV within a trial, and a maximum voltage difference of less than 0.50 μV within 100 ms intervals. EEG recordings were then re-referenced to the numeric mean of mastoids, and baseline corrected (-100 ms).

Self-reports, EMG and ERPs were constructed by averaging trials per each condition per participant. Based on previous research indicating that the LPP is typically maximal at posterior and parietal sites (Foti & Hajcak, 2008), the LPP was scored as the average activity in the time window 300–4000 ms at CPz, CP1, and CP2.

2.5 Statistical Analyses

First of all, multivariate analyses (MVA) were conducted to test for differences among nonsmokers, nondeprived smokers and deprived smokers in the questionnaire scores. I examined the effects of appraisal frames on subjective experience and psychophysiological responses among smokers and nonsmokers. Difference scores were calculated by subtracting data scores of the baseline condition (i.e., neutral narratives preceding neutral pictures) from each condition. The difference scores of

the EMG and the EEG activity were then submitted to a repeated analyses of variance (ANOVA) with picture valence (positive, negative) and appraisal frame (neutral, emotion consistent) as within-subject factors, and group (NS, NDS, DS) as a between-subjects factor. Dependent variables included self-reported valence, self-reported arousal, self-reported craving, corrugator activity, zygomaticus activity, and LPP. Paired t-tests were conducted to further examine main effects. For all analyses the alpha-level was set at .05. The Greenhouse-Geisser correction was applied when the assumption of sphericity was violated. The uncorrected degrees of freedom and effect sizes (partial eta-squared, η^2_p) are reported.

3 Results

3.1 The Demographic Characteristics of Participants

Multivariate analyses (MVA) indicated that comparing to nondeprived smokers, deprived smokers had lower CO level (F (1, 36) = 17.38, $p < .01$, $\eta^2_p = .33$), and nonsmokers had lower BDI scores (F (1, 39) = 4.47, $p < .05$, $\eta^2_p = .68$). No other comparisons among the three groups reached statistical significance (ps > .11).

3.2 Effect of Appraisal Frame on Self-reported Valence and Arousal

Mean changes in self-reports depending on emotion conditions are depicted in Fig.1.

Self-Reported Valence. The ANOVA revealed main effects of picture valence (F (1, 57) = 351.77, $p < .01$, $\eta^2_p = .86$) and appraisal frame (F (1, 57) = 21.87, $p < .01$, $\eta^2_p = .28$). However, the main effect of group did not reach statistical significance (F (2, 57) < 0.001). There was a significant interaction effect of picture valence by appraisal frame (F (1, 57) = 200.38, $p < .01$, $\eta^2_p = .78$). Thus, the negative-negative condition was rated as more negative than the neutral-negative condition (t (59) = 15.14, $p < .01$). And the positive-positive condition was rated as more positive than the neutral-positive condition (t (59) = -9.39, $p < .01$). None of the other interaction effects reached statistical significance (ps > .53).

Self-Reported Arousal. The ANOVA revealed main effects of picture valence (F (1, 57) = 89.89, $p < .01$, $\eta^2_p = .61$) and appraisal frame (F (1, 57) = 20.01, $p < .01$, $\eta^2_p = .26$). The main effect of group was not significant (F (2, 57) = 0.04, $p = .96$, $\eta^2_p = .00$). There was a significant interaction effect of picture valence by appraisal frame (F (1, 57) = 33.55, $p < .01$, $\eta^2_p = .37$). Follow-up t-tests revealed that the negative-negative condition was rated as more arousing than the neutral-negative condition (t (59) = 7.89, $p < .01$).). However, there was no reliable difference between positive-positive and neutral-positive conditions (t (59) = 1.23, $p = .22$). None of the other interaction effects reached statistical significance (ps > .24).

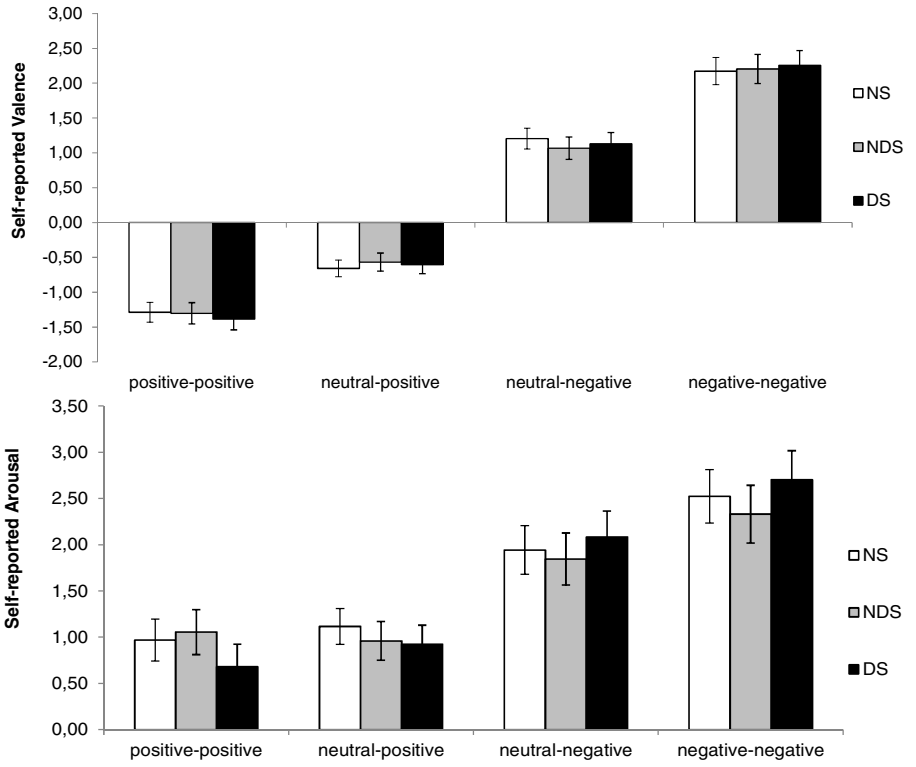

Fig. 1. Effect of appraisal frames on ratings of valence and arousal across nonsmokers (NS), nondeprived smokers (NDS) and deprived smokers (DS). Depicted are changes in self-reported valence (top) and self-reported arousal (bottom) as a function of appraisal frame among the three groups. Each bar represents the difference score between neutral condition and one of the four conditions (positive-positive, neutral-positive, neutral-negative, and negative-negative). Error bars represent standard error of the mean (SEM).

3.3 Effect of Appraisal Frame on Psychophysiological Responses

Mean changes in EMG activity and LPP activity are depicted in Fig. 2.

Corrugator Activity. The a priori *t*-tests showed that corrugator activity was higher in the negative-negative condition compared to the neutral-negative condition (t (59) = 2.39, $p < .05$). The exploratory comparison of the corrugator activity between the positive-positive and neutral-positive conditions also reached statistical significance (t (59) = -2.01, $p = .05$), indicating decreased corrugator activity in the positive-positive condition compared to the neutral-positive condition.

The ANOVA revealed a significant main effect of picture valence (F (1, 57) = 20.64, $p < .01$, $\eta^2_p = .27$). Neither the main effect of appraisal frame (F (1, 57) = 0.32, $p = .57$, $\eta^2_p = .01$) nor the main effect of group (F (1, 57) = 0.05, $p = .95$, $\eta^2_p < .001$) reached statistical significance. The interaction effect of picture valence by appraisal frame was significant (F (1, 57) = 8.76, $p < .01$, $\eta^2_p = .13$). None of the other interaction effects reached statistical significant (ps > .52).

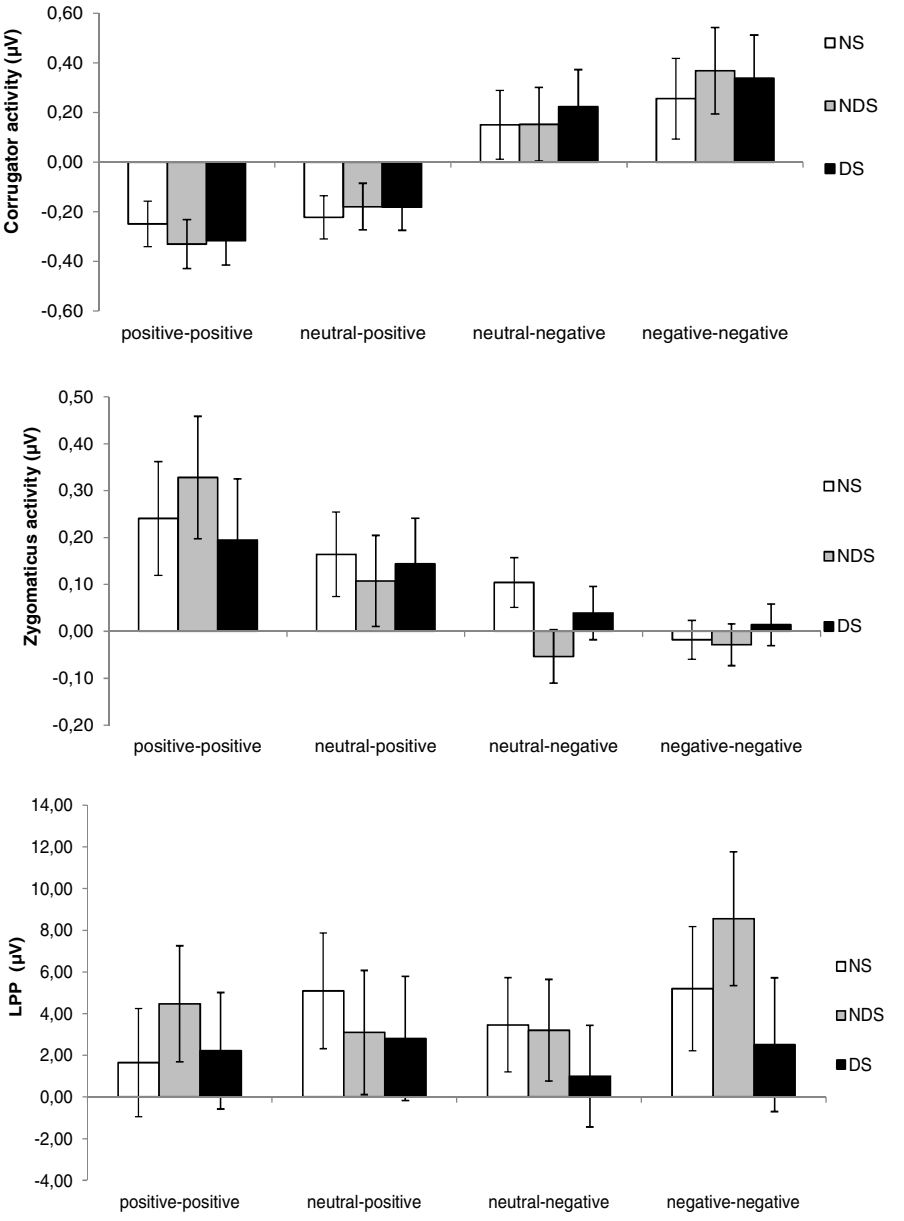

Fig. 2. Effect of appraisal frames on facial EMG activity and on LPP activity across nonsmokers (NS), nondeprived smokers (NDS) and deprived smokers (DS). Depicted are changes in corrugator activity (top), zygomaticus activity (middle) and LPP activity (bottom) as a function of appraisal frame of the three groups. Each bar represents the difference score between one of the four conditions (positive-positive, neutral-positive, neutral-negative, and negative-negative) and the neutral condition. Error bars represent standard error of the mean (SEM).

Zygomaticus Activity. The a priori *t*-tests showed that zygomaticus activity was higher in the positive-positive than the neutral-positive condition (t (59) = 2.03, $p < .05$). The exploratory comparison of the zygomaticus activity between the negative-negative conditions compared to the neutral-negative conditions failed to reach statistical significance (t (59) = -1.27, $p = .11$).

The ANOVA revealed a significant main effect of picture valence (F (1, 57) = 10.88, $p < .01$, $\eta^2_p = .16$), but neither the main effect of appraisal frame (F (1, 57) = 1.23, $p = .27$, $\eta^2_p = .02$) nor the main effect of group (F (1, 57) = 0.09, $p = .91$, $\eta^2_p = .00$) reached statistical significance. None of the interaction effects was significant (*ps* > .20) except for the interaction effect of picture valence by appraisal frame (F (1, 57) = 5.78, $p < .05$, $\eta^2_p = .09$).

LPP Activity. The a priori paired *t*-tests revealed that LPP activity was greater in the negative-negative than the neutral-negative condition (t (59) = 2.07, $p < .05$). The exploratory *t*-test comparing the positive-positive condition to the neutral-positive condition was not significant (t (59) = 0.58, $p = .28$). The ANOVA revealed that none of the main effects and interaction effects reached statistical significance (*p*s > .13).

4 Discussion

This study examined whether the three groups of participants differ in their cognitive ability to regulate emotion via appraisal frames and whether smokers' performance on emotion regulation task is predicted by smoking dependence as measured by questionnaires. To address these issues, the present study investigated participants' responses under emotion-congruent conditions (i.e., neutral-neutral, negative-negative and positive-positive) that is when there was no emotional confliction between appraisal frames and emotional pictures, and two distinct emotion-incongruent conditions (i.e., neutral-negative and neutral-positive) during which participants were primed by neutral appraisal frames to down regulate the emotions elicited by the picture.

The present study did not find group difference in cognitive emotion regulation. Namely, smokers and nonsmokers showed equal emotional regulation on the explicit level (subjective ratings) and the implicit level (the psychophysiological responses). Specifically, under emotion-incongruent conditions (i.e., neutral-positive, and neutral-negative), all participants responded to emotional pictures with less arousing and more neutral ratings together with reduced amplitude of EMG and EEG activity, as compared to corresponding emotion-congruent conditions (i.e., positive-positive, and negative-negative). These results suggested that both smokers and nonsmokers can take advantage of appraisal frames to regulate their emotions. Importantly, the abstinence from smoking did not influence participants' efficiency of this regulation strategy. Therefore, it is concluded that smokers are not impaired in ability to regulate emotion via appraisal frames.

These results did not support the hypothesis that nicotine addicts have a deficit in cognitive emotion regulation. Previous imaging studies have demonstrated that heavy smokers have abnormal brain activities in the PFC regions that are assumed to be

responsible for cognitive emotion regulation (Goldstein & Volkow, 2011; Sutherland et al., 2012; Damasio, 1996). A possible explanation could be that the task used in this study was too easy to detect deficits in smokers. There was a floor effect which could indicate that cognitive efforts based on PFC regions were not necessarily involved. Thus, with the help of preceding appraisal frames, all participants could alter their interpretations of emotional stimuli and thus regulate emotions without much cognitive effort. Therefore, to draw more convincing conclusions, future studies should apply more difficult challenges of emotion regulation.

In conclusion, this study suggests that smokers do not differ from nonsmokers in their emotional responses and their ability to cognitively regulate emotions. With the help of preceding appraisal frames, all participants could simultaneously alter emotional experience and corresponding psychophysiological responses. This study revealed the efficacy of appraisal frames in modulating multiple systems of positive as well as negative emotional responses. In addition, it was determined that smoking dependence and abstinence from smoking influence neither emotional response to nonsmoking stimuli, nor emotion regulation via appraisal frames.

Acknowledgments. This work was supported by the German Research Foundation (GRK 1253/1 scholarship to LW, FOR 605-PA 566/9-1, and SFB-TRR 58 project B01].

References

1. Cinciripini, P.M., Robinson, J.D., Carter, B.L., Lam, C., Wu, X., de Moor, C.A., Wetter, D.W.: The effects of smoking deprivation and nicotine administration on emotional reactivity. Nicotine Tob. Res. 8(3), 379–392 (2006)
2. Dar, R., Frenk, H.: Can one puff really make an adolescent addicted to nicotine? A critical review of the literature. Harm Reduct. J. 7, 28 (2010)
3. Kober, H., Kross, E.F., Mischel, W., Hart, C.L., Ochsner, K.N.: Regulation of craving by cognitive strategies in cigarette smokers. Drug Alcohol Depend 106(1), 52–55 (2010)
4. Born, J.M., Lemmens, S.G.T., Martens, M.J.I., Formisano, E., Goebel, R., Westerterp-Plantenga, M.S.: Differences between liking and wanting signals in the human brain and relations with cognitive dietary restraint and body mass index. American Journal of Clinical Nutrition 94(2), 392–403 (2011)
5. Lang, P.J., Bradley, M.M., Cuthbert, B.N.: Technical Report A-6, International affective picture system (IAPS): digitized photographs, instruction manual and affective ratings (University of Florida, Gainesville, FL.) (2005)
6. Bradley, M.M., Lang, P.J.: Measuring emotion: the Self-Assessment Manikin and the Semantic Differential. J. Behav. Ther. Exp. Psychiatry 25(1), 49–59 (1994)
7. Mayr, F.B., Spiel, A., Leitner, J., Marsik, C., Germann, P., Ullrich, R., Jilma, B.: Effects of carbon monoxide inhalation during experimental endotoxemia in humans. American Journal of Respiratory and Critical Care Medicine 171(4), 354–360 (2005)
8. Mucha, R.F., Geier, A., Pauli, P.: Modulation of craving by cues having differential overlap with pharmacological effect: evidence for cue approach in smokers and social drinkers. Psychopharmacology 147(3), 306–313 (1999)

9. Stippekohl, B., Winkler, M., Mucha, R.F., Pauli, P., Walter, B., Vaitl, D., Stark, R.: Neural responses to BEGIN- and END-stimuli of the smoking ritual in nonsmokers, nondeprived smokers, and deprived smokers. Neuropsychopharmacology 35(5), 1209–1225 (2010), doi:10.1038/npp.2009.227
10. Fridlund, A.J., Cacioppo, J.T.: Guidelines for human electromyographic research. Psychophysiology 23(5), 567–589 (1986)
11. Gratton, G., Coles, M.G., Donchin, E.: A new method for off-line removal of ocular artifact. Electroencephalogr Clin. Neurophysiol. 55(4), 468–484 (1983)
12. Sutherland, M.T., McHugh, M.J., Pariyadath, V., Stein, E.A.: Resting state functional connectivity in addiction: Lessons learned and a road ahead. Neuroimage 62(4), 2281–2295 (2012)
13. Damasio, A.R.: The somatic marker hypothesis and the possible functions of the prefrontal cortex. Philosophical Transactions of the Royal Society B-Biological Sciences 351(1346), 1413–1420 (1996)
14. Goldstein, R.Z., Volkow, N.D.: Drug addiction and its underlying neurobiological basis: neuroimaging evidence for the involvement of the frontal cortex. Am. J. Psychiatry 159(10), 1642–1652 (2002)
15. Koob, G.E., Le Moal, M.: Addiction and the brain antireward system. Annual Review of Psychology 59, 29–53 (2008)
16. Berridge, K.C.: Pleasures of the brain. Brain and Cognition 52(1), 106–128 (2003)
17. Lam, C.Y., Robinson, J.D., Versace, F., Minnix, J.A., Cui, Y., Carter, B.L., Cinciripini, P.M.: Affective Reactivity During Smoking Cessation of Never-Quitters as Compared With That of Abstainers, Relapsers, and Continuing Smokers. Experimental and Clinical Psychopharmacology 20(2), 139–150 (2012)
18. Wu, L.D., Winkler, M.H., Andreatta, M., Hajcak, G., Pauli, P.: Appraisal frames of pleasant and unpleasant pictures alter emotional responses as reflected in self-report and facial electromyographic activity. International Journal of Psychophysiology 85(2), 224–229 (2012)
19. Foti, D., Hajcak, G.: Deconstructing reappraisal: Descriptions preceding arousing pictures modulate the subsequent neural response. Journal of Cognitive Neuroscience 20, 977–988 (2008)
20. Goldstein, R.Z., Volkow, N.D.: Dysfunction of the prefrontal cortex in addiction: neuroimaging findings and clinical implications. Nature Reviews Neuroscience 12(11), 652–669 (2011)
21. Sutherland, M.T., McHugh, M.J., Pariyadath, V., Stein, E.A.: Resting state functional connectivity in addiction: Lessons learned and a road ahead. Neuroimage 62(4), 2281–2295 (2012)

Conceptual Clustering of Documents for Automatic Ontology Generation

Reshmy Krishnan[1], Amir Hussain[2], and Sherimon P.C.[3]

[1] Department of Computing, Muscat College, Muscat, Sultanate of Oman
reshmy_krishnan@yahoo.co.in
[2] Department of Computing Science and Mathematics, University of Stirling, Scotland, UK
hussain.doctor@googlemail.com
[3] Faculty of Computer Studies, Arab Open University, Muscat, Sultanate of Oman
sherimon@aou.edu.com

Abstract. In Information retrieval, Keyword based retrieval is unsatisfactory for user needs since it can't always retrieve relevant words according to the concept. Since different words can represent the same concept (polysemy) and one word can represent different concepts (homonymy), mapping problem will lead to word sense Disambiguation. Through the implementation of domain dependent ontology, concept based information retrieval (IR) can be achieved. Since Semantic concept extraction from keywords is the initial phase for automatic construction of ontology process, this paper propose an effective method for it. Reuters21578 is used as the input of this process, followed by indexing, training and clustering using self-Organizing Map. Based on the feature vector, the clustering of documents are formed using automatic concept selections, in order to make the hierarchy. Clusters are represented hierarchically based on the topics assigned .Ontology will be generated automatically for each cluster, based on the topic assigned.

Keywords: homonymy, polysemy, Information retrieval, indexing, feature vector, Self-Organizing Map, Clustering.

1 Introduction

Internet is the vast source of information, so people are struggling to get relevant information and eliminate irrelevant information according to the query. The information needs of people are in concept space. Keyword based retrieval is unsatisfactory for users' needs since it can't always retrieve relevant words according to the concept. Even though words represent concepts in human language, mapping from words to concepts is many to many. Mapping problem will lead to word sense disambiguation as different words can represent the same concept and one word can represent different concepts, [2]. The semantic relationship between the related words makes the capturing more tedious. In an internet searching even though user specified words are not there in many documents, semantic information will be present in them. If such documents are not retrieved, effective information retrieval will not happen in searching. Concept based retrieval can solve this problem in a successful way. A model using ontologies will be a valuable method for retrieving documents based on

D. Liu et al. (Eds.): BICS 2013, LNAI 7888, pp. 235–244, 2013.

the concepts [21][5]. Even though ontological model consists of two tasks such as extraction of semantic concepts from keywords and actual construction of ontology [5], we focus on the 'semantic extraction' which is the initial phase in this paper. Identifying the proper concepts from the input documents is the challenge in this task. For achieving this task we are doing a series of process such as clustering and hierarchical representation of documents.

Initially clustering will be done from the documents after indexing and training using self-organizing map. In data clustering, related documents can be grouped together. Using a vector space model, preprocessing of the clustering can be done [34]. In the preprocessing phase, parsing and indexing are the two important processes have to be done. In parsing, filtering of words is done using the basic 'stop list' of common English words to remove the words with little information to contribute to discriminate the documents through the stemming process. Since each document is represented in vector space model, feature vector has to be identified. To generate best words which will be taken as feature vector, frequency of each word in document is recorded using TFIDF value. Less frequent terms will be getting more weightage than the more frequent terms because of the TFIDF equation. Using a continuous training of these featured vectors, self-organizing map can make clusters of related words. Self-Organizing map, which is the most commonly used Artificial Neural Network, is used in different applications such as data visualization, data clustering, pattern recognition etc. We can think SOM as a "nonlinear projection" of probability density function p(x) of the high-dimensional input data vector x onto the two dimensional display. This makes SOM optimally suitable for application to the problem of the visualization and cluster of complex data [20].

Our goal is to construct the ontology automatically, so hierarchical representation of concepts must be done after clustering. Clustered concepts in the documents can be represented in a hierarchical way using the hierarchical clustering. A top-down approach is deployed for the hierarchical assignment. We are assigning the topics according to the concepts in the clusters. Super class will be represented in the top and subclasses will be represented in the leaf nodes.

The rest of the paper is organized as follows. Section 2 reviews the state of the art in conceptual clustering and hierarchical assignment of clusters. Section 3 explains our methodology for the clustering using SOM and Section 4 presents Implementation and results. Finally concluding remarks are given in Section 5.

2 State of Art

There is a strong requirement in the information retrieval research area in recent years due to the enormous growth in the number of text databases available on-line and need for better techniques to access this databases[1],[15]. Since the future web – semantic web-consists of pages containing texts and semantic mark up, the current IR techniques are unable to exploit the semantic knowledge within the documents and hence cannot give precise answers to precise queries [5]. Information retrieval models can be distinguished such as Keyword based Information Retrieval Model and content based IR model [2]. In the first one, Information retrieval model is based on keyword

indexing systems; frequency of occurrence of a keyword is taken into account [4]. Using the first one we can do data retrieval and latter gives us Information retrieval. As the name implies, the main task in information retrieval is to find information rather than data. Keyword based access can do the data retrieval which aims to provide data sets which fit the keywords of a query.

To gain maximum precision and recall in the information retrieval system, ontology is employed as the best method [5], [6]. Even though work has been done in the two directions of ontology employment such as Query expansion through the use of semantically related terms and the use of conceptual distance measures, they are not suitable for automatic ontology construction because of manual construction [7],[8],[9],[10]. Since Initial phase of automatic construction of ontology involves the clustering of documents, document clustering is an important area to be focused. Various methods had been proposed for clustering the documents. Vector Space Model is used in the preprocessing phase of clustering methods [15]. In order to cluster the documents self-organizing map is used as a better method [16], [17], [18].

Different methods were proposed to construct hierarchy after text categorization. To display a set of web pages on a site, a method is proposed in which hierarchy is constructed using self-organizing map [11]. Hierarchy based on the statistical method was proposed as referenced in [12]. Hotho et al. [13] propose various clustering techniques to view text documents with the help of ontology.

3 Methodology for Semantic Extraction and Hierarchical Representation

3.1 Extraction of Text from SGM

The most widely used text categorization corpus reuters 21578 is used for extracting documents. The text collection consists of 21578 documents which are in SGM extension [21]. These text files with SGM extension is known as SGML files. SGML stands for Standard Generalized Markup Language, which is used to share information digitally. It consists of custom tags that describe structure and content of information included in the document [9].

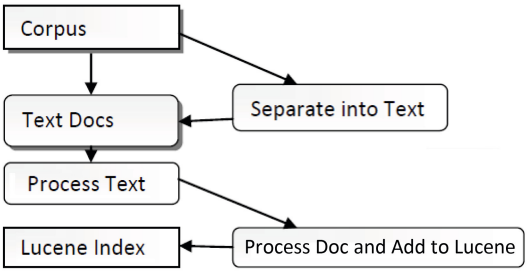

Fig. 1. Extraction of texts and indexing

Text documents are extracted from SGM formatted text corpus and can be viewed using 'view documents'. This extracted text documents being sent to Lucene index. Before sending the documents to the Lucene, we are processing it and removing all the stop words and do the stemming. During this process, words shorter than 3 letters are discarded and performing stop word extraction. Stop word are the words which can be removed during the processing of text [22]. Any group of words can be chosen as the stop words for a given purpose [22]. Derived words ending with 'ing', 'ly' etc. are shrinked to their base or root [23].

3.2 Indexing the Documents with Lucene

The extracted textual information from the documents is sent to Lucene for indexing. A common full text library Lucene is used for indexing. Parsers used are different for different documents in Lucene for indexing [24]. Here SGML parser is used which does preprocessing such as filtering the SGML tags and output the text content. Writing the tokens and related information into index file will be done after retrieving them from text contents by Lucene Analyzer. Indexing the documents with Lucene consists of two steps, preparing the text files and creating index.

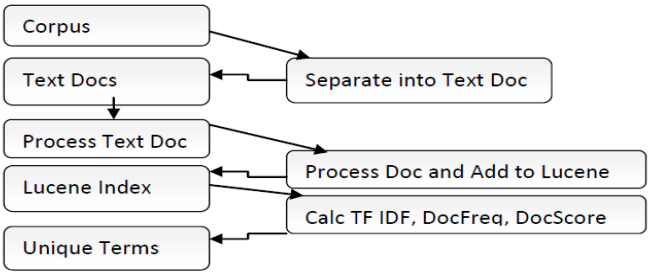

Fig. 2. Lucene Indexing

3.3 Construction of Feature Vector

A key process in our method is finding feature vector as feature vector is the input for the self-organizing map. Selecting independent and appropriate feature is the key to any pattern recognition algorithm in text categorization. Features are usually numeric [25]. An n dimensional vector of numerical features that represent some objects is the feature vector [26]. Numerical representation of objects is used as feature vector in machine learning algorithms as numerical representation of objects promotes processing. In this method unique terms are taken as the feature vector. For identifying unique terms, score values, TF values, and TFIDF values for all the terms in the documents are calculated.

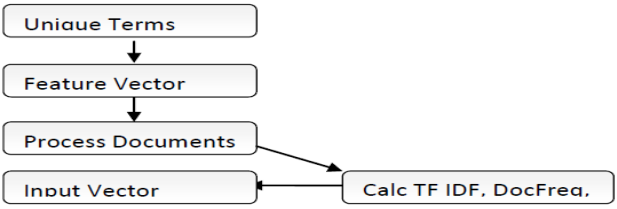

Fig. 3. Input vector

TF (term frequency) is a numerical statistic to calculate the frequency of a word in a document. Inverse document frequency factor (IDF) is associated with TF to reduce the weight of very frequently occurring terms in corpus and increases the weight of terms that occur rarely. TFIDF is often used as a weighting factor in text mining and information retrieval. The relative frequency of words in a specific document compared to the frequency of that word over the entire document corpus is determined by TFIDF value [27]. Using this calculation terms which are common in specific group have high TFIDF value than the common words like articles and prepositions.

3.4 Semantic Clustering

In concept based retrieval, clustering should be done according to the meaning or semantic content of terms. In semantic clustering, closer related words are grouped together and more distantly related ones are keeping apart. Two effective methods for deploying semantic clustering are using ontology and using vector space model [28]. Here we are focusing vector space model to correlate words and textual contents from the text corpus and then going for a hierarchical representation. Self-Organizing map is an efficient neural alternative for clustering with an additional topological property.

Self-Organizing Map Ideas is first introduced by C. von der Malsburg (1973), developed and refined by T. Kohonen (Finland) (1982). Neural network algorithm is using unsupervised competitive learning.

In SOM we do the method of making a two dimensional array, or map, and randomize it. Then presenting the training data to the map and let the cells on the map compete to win in some way (Euclidean distance is usually used). Stimulate the winner and some friends in the “neighborhood” (Update weight matrix). We do this a bunch of times. The result is a two dimensional “weight” map.

There are two main steps in SOM such as Training and Testing. At the end of iterative training best node will be found out. Followed by Training we do the testing by using the weights from training.

3.5 SOM Training

To find the best node, training process is used in SOM. During training high dimensional input data is mapped to two dimensional output topology spaces. Feature

vector x represents the input data and reference vector 'w' represents each node in output map. Random values are assigned to reference vector initially and comparing with randomly selected input data during the process. Cosine functions are used to measure the distance between these two. The lowest distance of input data and reference vector is the best matching node c.

$$\Delta Wi = \eta(t) \times \Delta (i, c) \times (x\text{-}wi) \quad (1)$$

i is the neighboring node, t is discrete time coordinate, and η (t) is learning and learning rate function. Topologically closed best matching nodes and neighboring nodes are updated. When the process continues, nearby regions of output map gains similarity for clusters of similar data vectors.

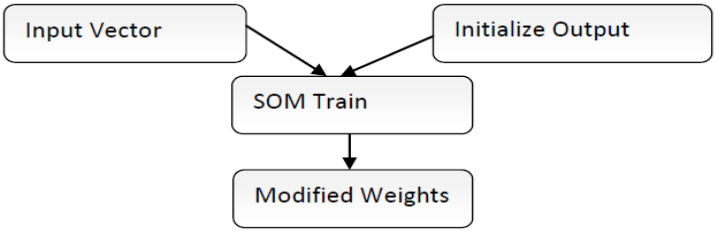

Fig. 4. SOM Training

3.6 SOM Testing

After training we are testing with different values of input vector, but with the same values of weight vector which is obtained from the above step. As the SOM knows which input vector is most related (i.e. less differed) output units by comparing the output weights, the clusters are formed that is an input vector represent a document and an output weight or output unit represents a cluster.

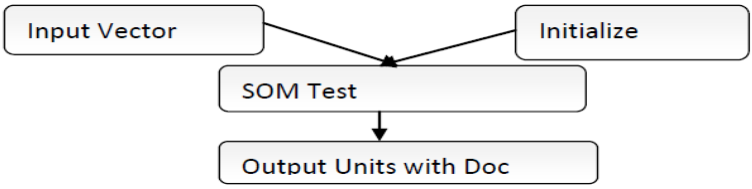

Fig. 5. SOM Testing

4 Implementation and Result

The most widely used text categorization corpus Reuters 21578 is used for extracting documents. Text documents are extracted form SGM formatted text corpus and can be viewed using 'view documents'. First we are using to get top unique terms which can be used as the feature vector i.e. input to the SOM. For e.g. if there are 500

documents, there will be 500 separate arrays (the size of array is based on the feature vector which are simply the unique terms) of values, and these values are got by calculating document score for each and every word in the feature vector with the corresponding document.

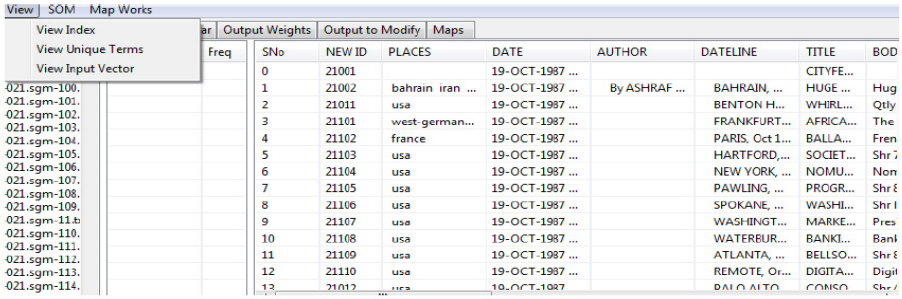

Fig. 6. Extracting text from SGM and Indexing

The extracted textual information from the documents is sent to Lucene for indexing. Before sending the documents to the Lucene we are processing it and removing all the stop words and do the stemming. Since feature vector is the input for the self-organizing map, finding feature vector is a key process in our method. In this method unique terms are taken as the feature vector. For identifying unique terms, Score values, TF values, TFIDF values for all the keywords in the documents are calculated. Since we don't know which values should be used in the Feature Vector we are using the Unique Terms obtained from the Document itself (Fig.7)

Before sending the input vector to the SOM we are normalizing it. Each SOM input data is represented by a vector of features x. Each node in the output map has a reference vector w.

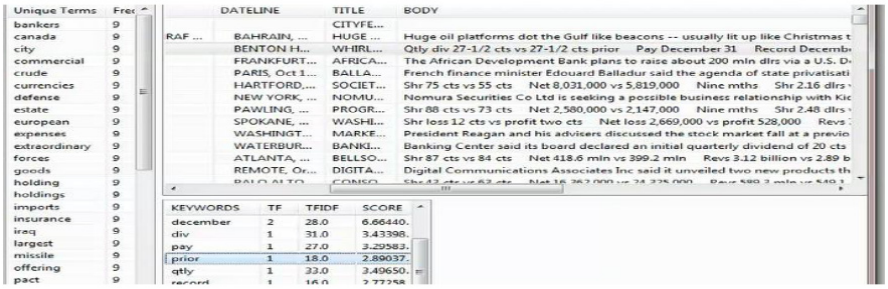

Fig. 7. Finding unique words

The reference vector has the same dimension as the feature vector of input data. Initially the reference vector is assigned to random values. Initially randomly selected input data vector from input data set is compared with all reference vectors w. During

learning process the above step is repeated until the learning rate is decreased to a lowest value. As a result we will get modified weight vectors.

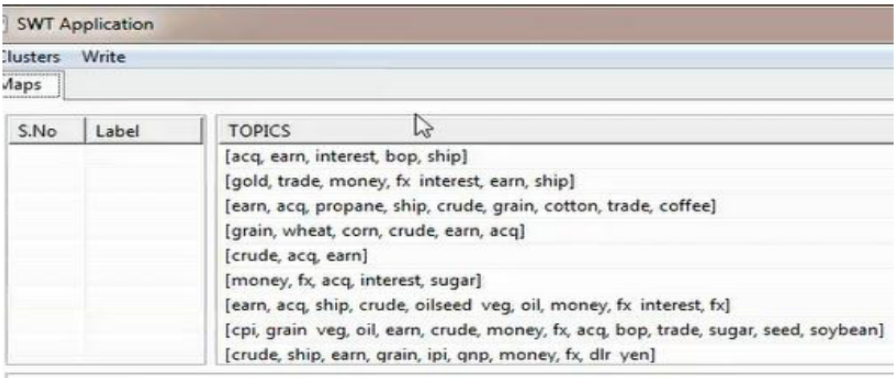

Fig. 8. Topics formation

After training we are testing with different values of input vector, but with the same values of weight vector which is obtained from the above step. As the SOM knows which input vector is most related (i.e. less differed) output units by comparing the output weights, the clusters are formed from output weight. Once the clusters are formed, we have to assign topic the document cluster. So the Cluster should contain some topics representing the Documents from which the hierarchical representation will be formed.

Clustered concepts (topics) in the documents can be represented in a hierarchical way using the hierarchical clustering. A top-down approach is deployed for the hierarchical assignment [7], [33]. We are assigning the topics according to the concepts in the clusters. Super class will be represented in the top and subclasses will be represented in the leaf nodes.

5 Conclusions and Future Work

In information retrieval, keyword based retrieval is unsatisfactory for users' needs since it can't always retrieve relevant words according to the concept. In an internet searching even though user specified words are not there in many documents, semantic information will be present in them. Initially clustering will be done from the documents after indexing and training using self-organizing Map. Indexing was done using Lucene and best words were taken as the unique words which are used as feature vector. Based on the feature vector values for each document, SOM is performed to make clusters. Cluster label will be the superclass and topics will be the subclasses in the ontology. A top-down approach is deployed for the hierarchical assignment. We are assigning the topics according to the concepts in the clusters. Super class will be represented in the top and subclasses will be represented in the

leaf nodes. OWL files will be generated automatically from this hierarchy and labels assigned in the hierarchy and can be viewed in the Editor Protégé. Automatic ontology construction can be extended with the generation of properties of the classes automatically.

References

1. Bedini, I., Nguyen, B.: Automatic Ontology Generation: State of the Art. Journal of Molecular Evolution 44(2), 226–233, 02 (1997, 2005)
2. Reshmy, K., Hussain, A., Sherimon P.C.: Retrieval of Semantic Concepts Based on Analysis of Texts for Automatic Construction of Ontology. In: Huang, T., Zeng, Z., Li, C., Leung, C.S. (eds.) ICONIP 2012, Part I. LNCS, vol. 7663, pp. 524–532. Springer, Heidelberg (2012)
3. Lin., C.-Y.I., Ho, C.-S.: An Ontology-Based Approach to Acquiring Domain Knowledge for Requirement Analysis. In: Proc. Natl. Sci, Counc. ROC (A), vol. 24(1), pp. 44–60 (2000)
4. Bohring, H., Auer, S.: Mapping XML to OWL Ontologies. In: 3rd International Conference on Advanced Computer Theory and Engineering (ICACTE), vol. 6, pp. V6-517 – V6-519 (2010)
5. Reshmy, K., Hussain, A., Sherimon P.C.: Automatic ontology construction of unstructured documents using semantic clustering: Applied Ontology (communicated, 2013)
6. Thomas, M., Hussain, A.: Novel logistic regression models to aid the diagnosis of dementia. (Elsevier) Expert Systems with Applications 39(3), 3356–3361 (2012)
7. Bedini, I., Nguyen, B., Gardarin, G.: B2B Automatic Taxonomy Construction. In: International Conference on Enterprise Information systems, ICEIS 2008, pp. 325–330 (2008)
8. Guarino, N., Masolo, C., Vetere, G.: OntoSeek: Content-based Access to the Web. IEEE Intelligent Systems 14(3), 70–80 (1999)
9. Khan, L.: Ontology-based Information Selection, Ph.D. Thesis, University of South California (2000)
10. Smeaton, F., Rijsbergen, V.: The Retrieval Effects of Query Expansion on a Feedback Document Retrieval System. The Computer Journal 26(3), 239–246 (1993)
11. Woods, W.: Conceptual Indexing: A Better Way to Organize Knowledge. Technical Report of Sun Microsystems (1999)
12. Khan, L., McLeod, D.: Audio Structuring and Personalized Retrieval Using Ontology. In: Proc. of IEEE Advances in Digital Libraries, Library of Congress, Bethesda, MD, pp. 116–126 (May 2000)
13. Khan, L., McLeod, D.: Disambiguation of Annotated Text of Audio Using Ontology. In: Proc. of ACM SIGKDD Workshop on Text Mining, Boston, MA (August 2000)
14. Elliman, D., Pulido, J.R.G.: Automatic Derivation of On-line Document Ontology. In: 15th European Conference on Object Oriented Programming, MERIT 2001, Budapest, Hungary (June 2001)
15. Hotho, A., Mädche, A., Staab, S.: Ontology-based Text Clustering. In: Workshop Text Learning: Beyond Supervision (2001)
16. Myat, N.N., Hla, K.H.S.: A combined approach of formal concept analysis and text mining for concept based document clustering. In: Proceedings of the 2005 IEEE/WIC/ACM International Conference on Web Intelligence, September 19-22, pp. 330–333 (2005)

17. Salton, G.: Automatic text processing: the transformation, analysis, and retrieval of information by Computer, Reading, and Mass. Addison-Wesley, Wokingham (1988)
18. Kaski, S., et al.: Creating an order in Digital Libraries with self-organizing Map. In: Proc. WCNN 1996 World Congress on Neural Networks, pp. 814–817. Lawrence Erlbann and INNS Press, Mahwah (1996)
19. Freeman, R., Yin, H., Allinson, N.M.: Self-Organizing Maps for Tree View Based Hierarchical Document Clustering. In: Proceedings of the IEEE IJCNN 2002, Honolulu, Hawaii, May 12-18, vol. 2, pp. 1906–1911 (2002)
20. Mehotra, et al.: Self-Organizing Maps, Elements of Artificial Neural Networks, p. 189. MIT Press (1997)
21. Khan, L., Luo, F.: Ontology Construction for Information Selection. In: 14th IEEE International Conference on Tools with Artificial Intelligence (ICTAI 2002), p. 122 (2002)
22. http://www.daviddlewis.com/resources/testcollections/reuters21578/readme.txt
23. http://www.ehow.com/facts_5676704_file-extension-sgm_.html
24. http://en.wikipedia.org/wiki/Stop_words
25. http://en.wikipedia.org/wiki/Stemming
26. http://www.ibm.com/developerworks/library/wa-lucene/
27. http://en.wikipedia.org/wiki/Features_pattern_recognition
28. http://en.wikipedia.org/wiki/Feature_vector
29. http://en.wikipedia.org/wiki/Tf%E2%80%93idf
30. http://en.wikipedia.org/wiki/Semantic_similarity
31. Mehotra, et al.: Self-Organizing Maps, Elemets of Artificial Neural Networks, p. 189. MIT Press (1997)
32. Biébow, B., Szulman, S.: TERMINAE: A linguistics-based tool for the building of a domain ontology. In: Fensel, D., Studer, R. (eds.) EKAW 1999. LNCS (LNAI), vol. 1621, pp. 49–66. Springer, Heidelberg (1999)
33. Lonsdale, D., Ding, Y., Embley, D., Melby, A.: Peppering knowledge sources with SALT: Boosting conceptual content for ontology generation (2002)
34. Dahaba, M.Y., Hassanb, H.A., Rafea, A.: TextOntoEx: Automatic ontology construction from natural English text Expert systems with applications, pp. 1474–1480 (February 2008)

A Basal Ganglia Inspired Soft Switching Approach to the Motion Control of a Car-Like Autonomous Vehicle

Erfu Yang[1], Amir Hussain[1], and Kevin Gurney[2]

[1] Division of Computing Science and Mathematics,
University of Stirling, Stirling FK9 4LA, UK
{eya,ahu}@cs.stir.ac.uk
[2] Department of Psychology,
University of Sheffield, Sheffield S10 2TP, UK
k.gurney@shef.ac.uk
http://www.cs.stir.ac.uk/cogcobras/

Abstract. This paper presents a new brain-inspired, switching control approach for a car-like autonomous vehicle using a basal ganglia (BG) model as an action selection mechanism. The problem domain has challenging nonholonomic and state constraints which imply no single stabilizing controller solution is possible by time-invariant smooth state feedback. To allow the BG make the correct controller selection from a family of candidate motion controllers, a fuzzy logic-based salience model using reference and tracking error only is developed, and applied in a soft switching control mechanism. To demonstrate the effectiveness of our approach for motion tracking control, we show effective control for a circular trajectory tracking application. The performance and advantages of the proposed fuzzy salience model and the BG-based soft switching control scheme against a traditional single control method are compared.

Keywords: Brain-inspired computing, basal ganglia, cognitive computation, autonomous vehicles, motion control, soft switching, multiple controller systems, action selection,fuzzy logic.

1 Introduction

Autonomous vehicle systems (AVS) have the ability to perform dangerous, repetitive and automated tasks in remote or hazardous environments. The potential for AVS to accomplish challenging tasks in many important applications such as intelligent transportation, security and environment monitoring etc. has drawn together interdisciplinary researchers [1, 2]. Future surveillance systems for indoor and outdoor (including security) applications will require mission platforms that are autonomous, asynchronous, adaptive and highly sensitive in complex, time-varying and possibly hostile environments [3]. Autonomous surveillance systems developed with autonomous vehicles (ASAVs) can be used for missions that are generally difficult to be accomplished by a static platform in the existence of

D. Liu et al. (Eds.): BICS 2013, LNAI 7888, pp. 245–254, 2013.

incomplete or inaccessible information, non-deterministic, unknown and hostile environments. One important application area of the ASAVs is the life-detection. It is of great significance in earthquake relief, medical attention, disaster rescue, and anti-terrorism, etc.

Much of the recent research work on biologically-inspired and intelligent control systems for autonomous vehicles, including for Mars' rovers and DARPA Challenges, has been carried out in the USA. For example, a Biologically Inspired System for Map-based Autonomous Rover Control has been developed in NASA's Jet Propulsion Laboratory for long duration missions [1, 2, 4]. The development of autonomous vehicle systems for applications such as visual surveillance has raised many new research issues related to both information processing and adaptive control of autonomous vehicles under complex and dynamic environments [3].

One research problem in autonomous vehicle systems is how to accurately track and exactly follow the specified path by avoiding obstacles and potential risks in extreme outdoor/indoor environments. Another research problem in autonomous vehicle systems is how to choose a right behavior by taking a right motion controller from a family of possible candidates. This research challenge is concerned with designing adaptive autonomous vehicle controllers and adaptive switching of autonomous vehicle controllers to improve the vehicle's surveillance and motion control capabilities. In recent years some researchers have conducted both theoretical and application studies on switching control [1, 2, 5, 6].

An understanding of how automatic processing is learnt in the brain will have profound consequences in neuroscience,psychology,adaptive control theory and artificial intelligence,etc [1, 2, 6]. The objective of this paper is to develop a new brain-inspired, adaptively switching control strategy for a car-like autonomous vehicle with challenging state and nonholonomic constraints [7] by exploiting similarities between system architectures in control engineering and the basal ganglia in animal brains. The motion control in this paper is based on the vehicle's kinematics model. In a three-stage modular architecture for autonomous vehicle control, it receives the desired trajectory generated from the first stage 'trajectory planning' module. The outputs from the motion control stage will be providing the reference inputs to the dynamics-based inner control module. This paper will only fucus on the motion control module due to page limit.

The outcomes from this study can be utilized to the research for the next generation of neurobiologically inspired autonomous visual surveillance systems in which innovative radar image processing methods are being explored to extract the required image information for multiple object detection, micro-motion detection and tracking. For intelligent transportation systems, brain-inspired cognitive control would have potential impact on developing next-generation smart cars that can safely self-drive in complex driving environments.

2 Statement of the Switching Control Problem

The configuration of a car-like autonomous vehicle under consideration in this paper is denoted by $\boldsymbol{q} := (x, y, \theta, \psi)^T \in \mathbb{R}^4$ with (x, y) being the Cartesian

location of the center of the rear wheels, θ being the heading angle between the body axis and the horizontal axis, and ψ representing the steering angle with respect to the vehicle body. L is the distance between the location (x, y) and the middle point of the driving wheels. This system has 2 degrees of nonholonomy since the constraints on the system arise by allowing the wheels to roll and spin, but not slip [8]. The Pfaffian constraints applied on the autonomous vehicle are of the following form:

$$\sin(\theta+\psi)\,\dot{x} - \cos(\theta+\psi)\,\dot{y} - L\cos\psi\,\dot{\theta} = 0, \quad \sin\theta\,\dot{x} - \cos\theta\,\dot{y} = 0 \tag{1}$$

The nonlinear control model of the autonomous vehicle is represented by [9]

$$\dot{x} = \cos\theta\, u_1, \quad \dot{y} = \sin\theta\, u_1, \quad \dot{\theta} = \tfrac{1}{L}\tan\psi\, u_1, \quad \dot{\psi} = u_2 \tag{2}$$

where, v is the driving speed, $u_1 = v\cos\psi$ and $u_2 = \dot{\psi}$ corresponds to the translational velocity of the rear wheels, and the velocity of the angle of the steering wheels, respectively. In addition, the steering angle ψ is further constrained by $|\ \psi\ | \leq M,\ \ (0 < M < \pi/2)$. In [8], it was proven that the autonomous vehicle could be driven from one position and orientation to another position and orientation in finite time under an appropriate motion controller.

Suppose a family of appropriate motion controllers $\boldsymbol{\{C_i\}}$ $(i = 1, N)$ have been developed for controlling this car-like autonomous vehicle, the research problem in this paper is thus stated as:

Problem 1 (Switching Control Problem). *For the autonomous vehicle system (2), under the aforementioned constraint condition, over the time period* $[0, T]$ *how can we choose the right motion controller from a set of candidates* $\boldsymbol{\{C_i\}}$ *(*$i = 1, N$*) and let the vehicle track a feasible trajectory* $\boldsymbol{q_d}$ *which connects the initial state* $\boldsymbol{q(0)}$ *and the final state* $\boldsymbol{q(T)}$*?*

If at one time only the best controller is selected, it is called as 'hard' switching. If all the controllers are gated to form a synthesized one for achieving the desired control specification, it is defined as 'soft' switching. Due to its smoother nature over the selection process, the soft switching with the BG-based selection mechanism is studied in this paper.

3 Motion Tracking Controllers via Input-Output Feedback Linearization

3.1 Input-Output Feedback Linearization

To explicitly deal with the state constraint, the change $\psi = M\tanh w$ is first made, where w is an auxiliary variable. A dynamic compensator $\dot{u}_1 = p_1, \dot{p}_1 = \mu_1$ in which μ_1 is a new control input is then introduced. The new control system model is described by [8]:

$$\dot{x} = \cos\theta\, u_1,\ \dot{y} = \sin\theta\, u_1,\ \dot{\theta} = \tan(M\ \tanh w)\, u_1/L := \eta_1(w)\, u_1$$
$$\dot{w} = \mu_2,\ \dot{u}_1 = p_1,\ \dot{p}_1 = \mu_1 \tag{3}$$

Denoting $\boldsymbol{x}= (x, y, \theta, w, u_1, p_1)^T$, $y_1 = x$, $y_2 = y$, and $\boldsymbol{u}= (\mu_1, \mu_2)^T$, the coordinates transformation $\boldsymbol{z = \Phi(x)}$ is made as [8]

$$z_1 = y_1 = x, z_2 = \dot{y}_1 = \dot{x} = \cos\theta\, u_1, z_3 = \ddot{y}_1 = \ddot{x} = -\sin\theta\, \eta_1(w)\, u_1^2 + \cos\theta\, p_1$$
$$z_4 = y_2 = y, z_5 = \dot{y}_2 = \dot{y} = \sin\theta\, u_1, z_6 = \ddot{y}_2 = \ddot{y} = \cos\theta\, \eta_1(w)\, u_1^2 + \sin\theta\, p_1 \tag{4}$$

In the new coordinates the nonlinear control system (3) can be completely decoupled into the following two linear SISO subsystems, i.e.,

$$\dot{z}_1 = z_2, \dot{z}_2 = z_3, \dot{z}_3 = v_x,\ \dot{z}_4 = z_5, \dot{z}_5 = z_6, \dot{z}_6 = v_y \tag{5}$$

where $v_x = y_1^{(3)} = x^{(3)}, v_y = y_1^{(3)} = y^{(3)}$. Moreover, we have:

$$\boldsymbol{\alpha(x) + \rho(x)\, u = v} \tag{6}$$

where

$$\boldsymbol{\alpha(x)} = \begin{pmatrix} -\cos\theta\, \eta_1^2(w)\, u_1^3 - 3\, \sin\theta\, \eta_1(w)\, u_1\, p_1 \\ -\sin\theta\, \eta_1^2(w)\, u_1^3 + 3\, \cos\theta\, \eta_1(w)\, u_1\, p_1 \end{pmatrix} \tag{7}$$

$$\boldsymbol{\rho(x)} = \begin{pmatrix} \cos\theta & -\frac{\partial \eta_1}{\partial w} \sin\theta\, u_1^2 \\ \sin\theta & \frac{\partial \eta_1}{\partial w} \cos\theta\, u_1^2 \end{pmatrix} \tag{8}$$

in which $\frac{\partial \eta_1}{\partial w} = M\ \sec^2(M\ \tanh w)\, \mathrm{sech}(w)/L$.

3.2 Motion Tracking Controllers

The motion controller design for trajectory tracking is now based on the obtained feedback linearization forms. Assume that the desired, feasible trajectory $(x_d(t), y_d(t))^T$ is given by the position coordinates in the form of time functions. The output tracking error is denoted by $(e_x, e_y)^T = (x - x_d, y - y_d)^T$. The purpose of motion controller is that the car-like autonomous vehicle can be driven to asymptotically track the desired trajectory from some initial tracking error $(e_x(0), e_y(0))^T$, and both e_x and e_y converge to zero as $t \to +\infty$.

If we have the following two *Hurwitz* polynomials [8]

$$H_1(s) = s^3 + \lambda_2\, s^2 + \lambda_1\, s + \lambda_0,\ H_2(s) = s^3 + \gamma_2\, s^2 + \gamma_1\, s + \gamma_0 \tag{9}$$

So the motion controller is first designed in the new coordinates as follows

$$v_x = x_d^{(3)} - \lambda_2\, (z_3 - \ddot{x}_d) - \lambda_1\, (z_2 - \dot{x}_d) - \lambda_0\, (z_1 - x_d)$$
$$v_y = y_d^{(3)} - \gamma_2\, (z_6 - \ddot{y}_d) - \gamma_1\, (z_5 - \dot{y}_d) - \gamma_0\, (z_4 - y_d) \tag{10}$$

If the constant real coefficients $\{\lambda_2, \lambda_1, \lambda_0\}$ and $\{\gamma_2, \gamma_1, \gamma_0\}$ can be chosen appropriately such that:1)The change of coordinates (4) is invertible; 2) The decoupling matrix $\boldsymbol{\rho(x)}$ is nonsingular. Then,the following motion controller

$$\boldsymbol{u = \rho^{-1}(x)\,(v - \alpha(x))} \tag{11}$$

will make the vehicle to asymptotically track the desired trajectory from some initial tracking error $(e_x(0), e_y(0))^T$, and both e_x and e_y converge to zero as $t \to +\infty$ [8]. To form a bank of motion controllers $\boldsymbol{\{C_i^x\}}$ and $\boldsymbol{\{C_i^y\}}$ $(i = 1, N)$ under different control requirements, we just need to pick up the different real coefficients of $H_1(s)$ and $H_2(s)$, i.e., $\{\lambda_2, \lambda_1, \lambda_0\}$ and $\{\gamma_2, \gamma_1, \gamma_0\}$, respectively.

4 Basal Ganglia-Inspired Soft Switching Approach

The key role of the BG which acts as a central selector or 'switch' in the brain, mediating conflicting action requests, and allowing the most urgent or salient requests to be selected for behavioural expression [6, 10, 11]. Therefore, in this paper we will aim to propose a BG-based soft switching approach by employing the BG 'action-selection' model developed in [10, 11] that is both biologically plausible and computationally efficient. All the controllers (actions or channels in the BG model) in the candidate bank are developed to work using the same adaptive procedure and a selection among the various controller options is made in terms of action request signals, i.e., salience.

In Fig.1, the proposed BG-based soft switching control architecture is given. Since the original MIMO (multi-inputs multi-outputs) nonlinear vehicle control system can now be decoupled by taking advantage of input-output feedback linearization technique into two SISO (single input single output) subsystems, two BG selection models are used in the proposed approach to deal with each SISO subsystem separately. Moreover, this decoupling property can also greatly facilitate and simplify the design of fuzzy salience model which provides salience signals for each BG to make the selection from the motion controller bank of each subsystem, i.e., $\boldsymbol{\{C_i^x\}}$ and $\boldsymbol{\{C_i^y\}}$ $(i = 1, N)$. In this paper, we only take $N = 3$ to illustrate how our proposed BG-based soft switching approach works.

Both the reference signal (x_d, y_d) and tracking error (e^x, e^y) are used to form the salience signals for controller(action) requests. The action request vector $\boldsymbol{s^x} = (s_1^x, s_2^x, s_3^x)$ and $\boldsymbol{s^y} = (s_1^y, s_2^y, s_3^y)$ are then supplied to the BG selection mechanism for each SISO subsystem. The BG's outputs are the set of signals $\boldsymbol{\sigma^x} = (\sigma_1^x, \sigma_2^x, \sigma_3^x)$ and $\boldsymbol{\sigma^y} = (\sigma_1^y, \sigma_2^y, \sigma_3^y)$, respectively. The gating signals $\boldsymbol{g^x}$ $= (g_1^x, g_2^x, g_3^x)$ and $\boldsymbol{g^y} = (g_1^y, g_2^y, g_3^y)$ which mimic inhibition on their targets (the controllers themselves) [1], and defined by:

$$g_i^x = \begin{cases} 1 - \sigma_i^x/\sigma_0^x & \text{if } 1 - \sigma_i^x/\sigma_0^x > 0 \\ 0 & \text{otherwise} \end{cases} \tag{12}$$

$$g_i^y = \begin{cases} 1 - \sigma_i^y/\sigma_0^y & \text{if } 1 - \sigma_i^y/\sigma_0^y > 0 \\ 0 & \text{otherwise} \end{cases} \tag{13}$$

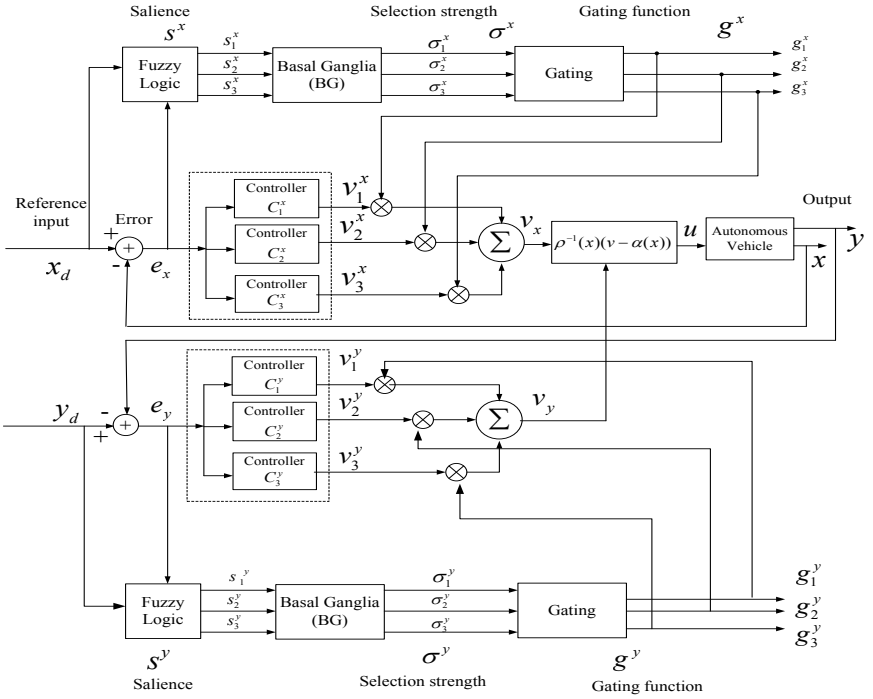

Fig. 1. Architecture for the BG-based soft switching control

To make a soft selection, the three component controllers in each SISO subsystem are mixed together to form v_x and v_y, respectively, i.e.,

$$v_x = \frac{1}{g_x}\sum_i g_i^x v_i^x, \quad v_y = \frac{1}{g_y}\sum_i g_i^y v_i^y \tag{14}$$

in which $g_x = \sum_i g_i^x$ and $g_y = \sum_i g_i^y$. Furthermore, we define $\boldsymbol{v} = (v_x, v_y)$.

The dynamics in the BG model [10, 11] can make that the mixing of motion controllers is smoothly done (less 'bumping' at switch over). Moreover, the mix of controllers in (14) is made in a natural, bio-inspired way [1].

5 Fuzzy Logic Salience Model and Its Action Surface

One challenging issue in applying the BG-based selection mechanism to any control engineering systems is how to form/generate salience signals from sensory inputs, system states and performance metrics or their combinations. Therefore, a salience model needs to be built first. It is designed as input to the selection mechanism for covert selective attention. Mathematically speaking, the salience model is a nonlinear mapping, i.e., $\boldsymbol{S} = \boldsymbol{f}(\boldsymbol{X})$ in which $\boldsymbol{X}, \boldsymbol{S}$ are the input and

output vectors with appropriate dimensions, representing input variables and salience signals which can then be used by the BG for action selection.

In recent years there has been increasing interest in applying fuzzy logic to autonomous vehicles and robotic control field [2, 5]. It is becoming a promising method for dealing with complex modeling issues and system uncertainties/noises. Therefore, it is a natural option for us to build a fuzzy logic-based model to generate the salience signals needed by the BG selection mechanism in the proposed soft switching scheme.

In developing the fuzzy salience models, two inputs (reference and error) and three salience outputs for action requests are used. The other information of different combinations between the reference and error signals can be implicitly included in fuzzy rules and inference procedure. For every SISO subsystem, each input and output fuzzy variable has 3 fuzzy triangular memberships. The Mamdani fuzzy inference system (FIS) are developed with the following 11 rules:

1. **IF** (*reference* is *low*) **OR** (*error* is *small*) **THEN** (*Salience 1* is *weak*) (*Salience 2* is *strong*) (*Salience 3* is *weak*);
2. **IF** (*reference* is *medium*) **OR** (*error* is *medium*) **THEN** (*Salience 1* is *average*) (*Salience 2* is *weak*) (*Salience 3* is *average*);
3. **IF** (*reference* is *high*) **OR** (*error* is *large*) **THEN** (*Salience 1* is *strong*) (*Salience 2* is *average*) (*Salience 3* is *average*);
4. **IF** (*reference* is *low*) **AND** (*error* is *small*) **THEN** (*Salience 1* is *weak*) (*Salience 2* is *weak*) (*Salience 3* is *weak*);
5. **IF** (*reference* is *medium*) **AND** (*error* is *medium*) **THEN** (*Salience 1* is *average*) (*Salience 2* is *average*) (*Salience 3* is *average*);
6. **IF** (*reference* is *high*) **AND** (*error* is *large*) **THEN** (*Salience 1* is *strong*) (*Salience 2* is *strong*) (*Salience 3* is *strong*);
7. **IF** (*reference* is *low*) **AND** (*error* is *medium*) **THEN** (*Salience 1* is *weak*) (*Salience 2* is *average*) (*Salience 3* is *strong*);
8. **IF** (*reference* is *medium*) **AND** (*error* is *small*) **THEN** (*Salience 1* is *weak*) (*Salience 2* is *average*) (*Salience 3* is *average*);
9. **IF** (*reference* is *medium*) **AND** (*error* is *large*) **THEN** (*Salience 1* is *strong*) (*Salience 2* is *average*) (*Salience 3* is *strong*);
10. **IF** (*reference* is *high*) **AND** (*error* is *medium*) **THEN** (*Salience 1* is *average*) (*Salience 2* is *weak*) (*Salience 3* is *strong*);
11. **IF** (*reference* is *high*) **AND** (*error* is *small*) **THEN** (*Salience 1* is *strong*) (*Salience 2* is *average*) (*Salience 3* is *weak*);

The action surface for the whole fuzzy salience model is shown in Fig.2.

6 Simulation Results

In this section, simulation results are provided to illustrate the effectiveness of the proposed BG-based soft switching approach for the motion control of the car-like autonomous vehicle with the constrained steering angle by applying it to the circular trajectory tracking control like [8]. However, the aim of the simulation in this paper is to have a performance comparison under noisy environment.

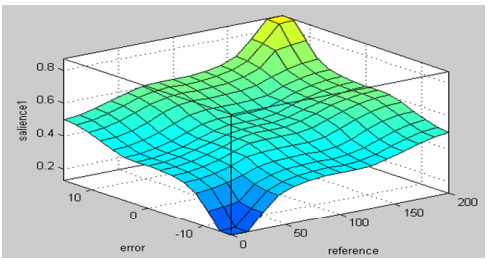

(a) Action surface for salience 1

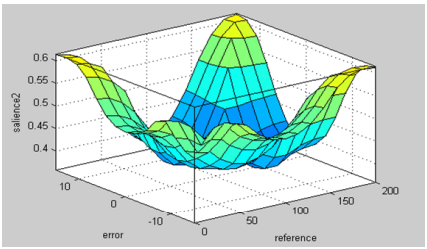

(b) Action surface for salience 2

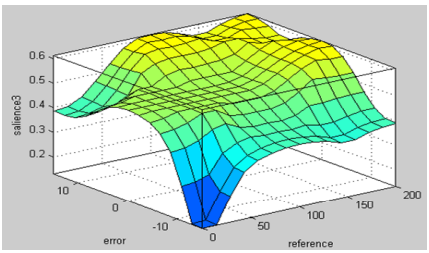

(c) Action surface for salience 3

Fig. 2. Action surfaces of the fuzzy salience model

Therefore, some white noises are added to the control system model to mimic measurement uncertainties.

The desired trajectory is given by $x_d(t) = R\cos(\omega t),\ y_d(t) = R\sin(\omega t)$. Where R and ω are appropriate positive constants. The circular trajectory tracking for the vehicle without the BG in the loop was simulated with the following controller parameters and initial conditions

$$\begin{aligned}&\lambda_2 = \gamma_2 = 0.3, \lambda_1 = \gamma_1 = 0.03, \lambda_0 = \gamma_0 = 0.001, R = 15, L = 1, \omega = 0.01\pi \\ &x(0) = 5, y(0) = 3, \theta(0) = 0, \psi(0) = 0, u_1(0) = 0.5, p_1(0) = 0, M = \pi/3\end{aligned} \tag{15}$$

For the BG-based soft switching control, the three candidate controllers were constructed as follows

1. For Controller 1: $\lambda_2 = \gamma_2 = 0.3, \lambda_1 = \gamma_1 = 0.03, \lambda_0 = \gamma_0 = 0.001$;
2. For Controller 2: $\lambda_2 = \gamma_2 = 0.6, \lambda_1 = \gamma_1 = 0.11, \lambda_0 = \gamma_0 = 0.006$;
3. For Controller 3: $\lambda_2 = \gamma_2 = 1.5, \lambda_1 = \gamma_1 = 0.75, \lambda_0 = \gamma_0 = 0.125$;

The time histories of state variables during the trajectory tracking control are plotted in Fig. 3. Fig. 4 also shows the $x - y$ trajectory comparison of the BG-based soft switching control and a pure single motion controller for the circular tracking under system noises. From these figures, it has been shown that in this noisy environment the performance of a single, pure feedback linearization-based motion controller can be very poor. However, BG-based soft switching control scheme could significantly improve the performance for motion tracking control.

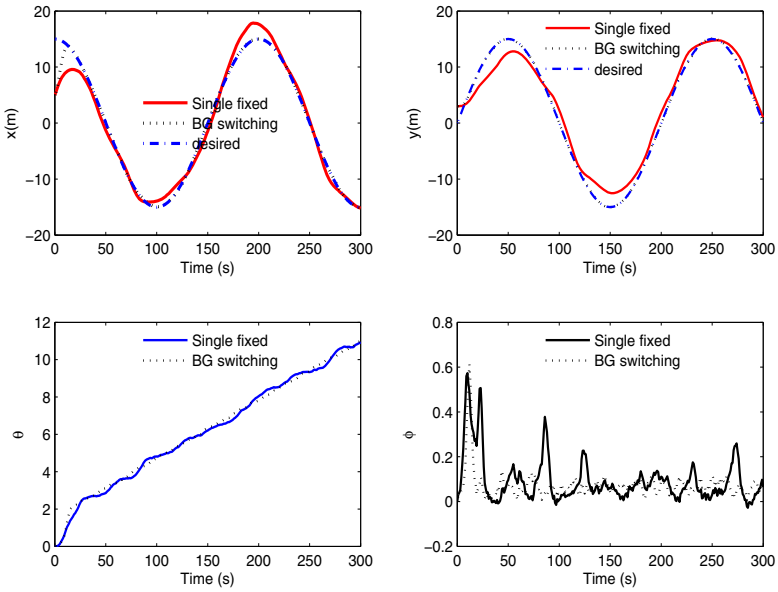

Fig. 3. States in the circular tracking with BG-based switching and a single feedback linearization motion controller under noises

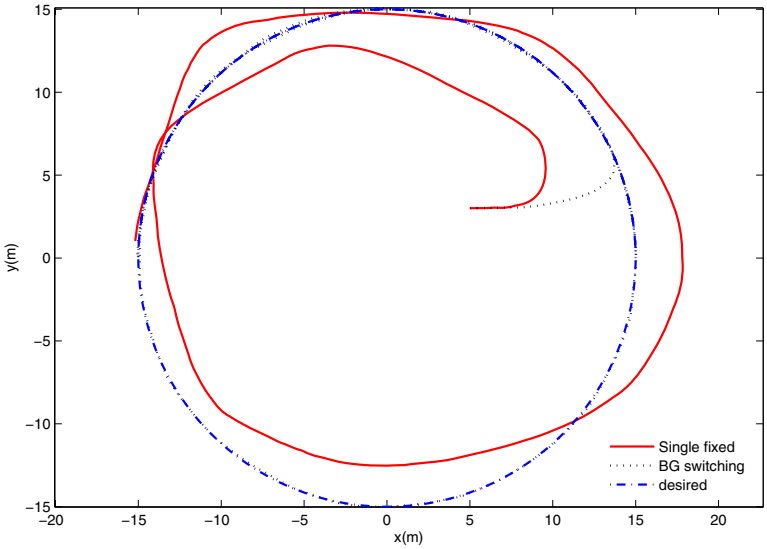

Fig. 4. $x - y$ trajectory comparison for BG-based switching and a single feedback linearization motion controller under noises

7 Conclusions

A new brain-inspired switching control approach has been presented in this paper for more efficiently and adaptively control the motion of a car-like autonomous

vehicle with challenging state and nonholonomic constraint. In the proposed approach, a functional BG model was implemented to make a soft selection from a family of candidate controllers. Furthermore, a fuzzy logic-based salience model using reference and tracking error only has been developed and applied in the BG-based soft switching control approach for the challenging motion control of a car-like autonomous vehicle. The performance and advantages of using the proposed fuzzy salience model and the BG-based soft switching control against the traditional single control method have been demonstrated.

Acknowledgments. This work is supported by the UK Engineering and Physical Sciences Research Council (EPSRC) [grant number EP/I009310/1]. Both Erfu Yang and Amir Hussain are also supported by The Royal Society of Edinburgh (RSE) and The National Natural Science Foundation of China (NNSFC) under the RSE-NNSFC joint projects (2012-2014) with Prof Jun Wang, Beihang University, and Prof Bin Luo, Anhui University, China. The support from our industrial partners SciSys UK Ltd., and Industrial Systems Control (ISC) Ltd. is greatly appreciated.

References

1. Yang, E., Hussain, A., Gurney, K.: Neurobiologically-inspired soft switching control of autonomous vehicles. In: Zhang, H., Hussain, A., Liu, D., Wang, Z. (eds.) BICS 2012. LNCS, vol. 7366, pp. 82–91. Springer, Heidelberg (2012)
2. Hussain, A., Abdullah, R., Yang, E., Gurney, K.: An intelligent multiple-controller framework for the integrated control of autonomous vehicles. In: Zhang, H., Hussain, A., Liu, D., Wang, Z. (eds.) BICS 2012. LNCS, vol. 7366, pp. 92–101. Springer, Heidelberg (2012)
3. Giulio, R., James, U., Graham, B., Durrant-Whyte, H.: Radar-based perception for autonomous outdoor vehicles. Journal of Field Robotics 28(6), 894–913 (2011)
4. Huntsberger, T.: Biologically inspired autonomous rover control. Autonomous Robots 11, 341–346 (2001)
5. Abdullah, R., Hussain, A., Warwick, K., Zayed, A.: Autonomous intelligent cruise control using a novel multiple-controller framework incorporating fuzzy-logic-based switching and tuning. Neurocomputing 71, 2727–2741 (2008)
6. Gurney, K., Hussain, A., Chambers, J., Abdullah, R.: Controlled and automatic processing in animals and machines with application to autonomous vehicle control. In: Alippi, C., Polycarpou, M., Panayiotou, C., Ellinas, G. (eds.) ICANN 2009, Part I. LNCS, vol. 5768, pp. 198–207. Springer, Heidelberg (2009)
7. Kolmanovsky, I., McClamroch, N.H.: Developments in nonholonomic control problems. IEEE Control Systems Magazine 15(6), 20–36 (1995)
8. Yang, E., Gu, D., Mita, T., Huo, H.: Nonlinear tracking control of a car-like mobile robot via dynamic feedback linearization. In: Proc. Control 2004, Bath, UK (2004)
9. Sastry, S.: Nonlinear Systems-Analysis, Stability, and Control. Springer-Verlag New York, Inc. (1999)
10. Gurney, K., Prescott, T., Redgrave, P.: A computational model of action selection in the basal ganglia. I. a new functional anatomy. Bio. Cybern. 84, 401–410 (2001)
11. Gurney, K., Prescott, T., Redgrave, P.: A computational model of action selection in the basal ganglia. II. analysis and simulation of behaviour. Bio. Cybern. 84, 411–423 (2001)

Hierarchically Arranged Mutualism of Neural Circuit Ecosystems

Derek Harter

Department of Computer Science
Texas A&M University - Commerce, Commerce, TX 75429
Derek.Harter@tamuc.edu

Abstract. Neural reuse theories of the development of the functional structure of the brain [1] state that it is normal and common that neural circuits evolved for one purpose can and will be exapted (exploited, recycled and redeployed) by newer and later developed functions. This organizational hypothesis of the nature of neural evolution supports many observations on how and why the embodied nature of cognition works. In this paper we introduce the neural reuse paradigm, and relate it to theories of hierarchically arranged mutualisms in the development of natural ecosystems. In such nested structures of functional mutualism, the ecosystems evolve to support more diverse types of species (or functions) [2]. This diversity has many advantages for natural ecosystems. We will argue that these same concepts can be applied to understanding the functional ecosystem of the evolved neural circuits of the brain. We will discuss how these ideas relate to the robustness and flexibility of embodied cognitive functioning and discuss ways that this concept could be tested in natural neural networks and artificial cognitive systems.

Keywords: embodied cognition, cooperative network dynamics, hierarchical networks.

1 Neural Reuse and Hierarchical Organization

Anderson's neural reuse hypothesis, also known as massive redeployment hypothesis (MRH) [3,1], takes the reuse of neural circuitry for various cognitive purposes to be a central organizational principle. This basic hypothesis suggests that anytime a new cognitive function is evolving (and the structural neural circuits are being selected to support the newly evolving cognitive functionality), existing neural circuits and functions are likely to be invoked and reused to support the new functionality. This makes sense for many reasons. We know that this is fundamentally the way that natural selection works, new functionality cannot be anticipated by natural selection thus when environmental conditions change, existing structure and function will be favored and shaped to cope with such pressures. Further, neural circuits represent use of a limited resource, both in space and energy costs. It is expensive to build new structures, and to provide the energy needed to operate the structures. Thus wherever possible, reuse

D. Liu et al. (Eds.): BICS 2013, LNAI 7888, pp. 255–260, 2013.

of circuits for 2, 3 or many functions makes sense given the profound resource constraints placed on the living organism.

Given that neural reuse is common, we should expect that the general architecture of the function and structure of neural circuits will have several properties. The MRH expects and makes several predictions about the nature of these structural and functional relations. We would hypothesize that phylogenetically older brain areas should be redeployed and reused more frequently than newer evolved structures, simply because they have had more time to be available to be selected and exapted by other functions for reuse. We would also expect older areas to show more localization, because when they were developed there were fewer circuits they themselves could redeploy. Newer areas should show opposite patterns, relying both on a greater number of other circuits to carry out their functions, and using more widely deployed circuits (activity over many more brain areas) since there were more circuits in more locations that might possibly be exapted when they developed.

The MRH of functional and structural development of neural circuits gives a hypothesis of the structure of relations and modular architecture we would expect to observe of naturally evolved neural systems. Likewise, given the nested, hierarchical nature of the functional relations we would expect, we can make predictions about how cognitive functions may be supported, and the expected properties of those cognitive functions. For example, MRH is well supported by observations about the embodied nature of cognition, as well as observed patterns of neural activity during cognitive tasks. There is evidence that watching actions, imagining actions, and doing actions all activate similar networks of brain regions [4]. We see that when we perceive objects or object names, this activates brain regions associated with grasping [5]. This last effect has been associated with so called mirror neuron systems, where motor areas known to be active in performing particular functions (grasping, walking, etc.) will also be active when observing others performing those actions, or when reasoning about the intentions of others by observing their actions [6].

In fact, these types of cognitive reuse are associated with and used to explain embodied viewpoints of cognition. In embodied theories of cognition, higher-level or more abstract cognitive functions are thought to be grounded in lower-level functions (e.g. understanding time concepts by mapping them onto left-right or up-down spatial dimensions) [7]. There are several flavors of embodied, grounded or metaphor-theory views of cognition. MRH is compatible with most of these views, but by making specific predictions about the underlying evolutionary and structural properties of the neural circuits, may be useful in contrasting and sharpening the differences between the various views of embodiment [8].

2 Nested Mutualism and Robust Ecosystems

The main contribution of this article, then, is to connect up ideas about neural reuse in the development of functional cognitive circuits to work on cooperative network dynamics that lead to the nested or hierarchical arrangement of mutual

cooperation/competition functional networks in things such as biological ecosystems and social based market systems. One observation driving this connection is to note that in some ways the hierarchical and nested modular architecture of brain circuits suggested by MRH seem to imply a fragile system of functional network dynamics. Given that some neural areas of cognitive functions are massively reused by many other areas, one might imagine a brittle system where small injuries or failures lead to total systems failure. It is true that damage to these important hub centers will lead to a total system break down. But the overall impression of the biological brain is one of robustness, both to isolated failures or injuries, as well as robustness in achieving overall intentional goals when faced with novel difficulties.

Competition and cooperation (mutualism) has been studied in the context of several types of functional networks, including biological ecosystems [9,2], financial networks [10], and other social networks. A common theme in the evolution (or assembly rules) of such systems is the idea of growing the network along paths of least resistance, with simple constraints that minimize competition. For example, in ecological networks, plants and animals compete for resources among both competing species as well as among members within their own species. Competition among members within a species is always a constraint within such networks. Another factor, the mutual cooperation or benefits between species, also evolve in such systems (for example pollinators helping plants procreate in exchange for food resources). It has been shown that in purely competitive ecological networks [11], the biodiversity (or number of species) that the system can support has an absolute limit. However, when cooperative mutualism is allowed, this constraint is lessened or removed all together, allowing much greater levels of biodiversity to evolve in the system. It appears that the structure of the mutualistic networks is essential to supporting this greater biodiversity, and depends on a type of nested (hierarchical) mutualism network.

In the types of networks studied under this idea of nested mutualism (ecological networks, financial networks, etc.), the assembly rules usually look similar in nature to one another. For example, in ecological networks species join the network in order of increasing specialization, usually in ways that minimize competitive resistance. This means that natural ecosystems first evolve generalist species, usually simpler and hardy. Biodiversity increases when new species join the ecosystem. However, when a new species evolves in an ecosystem, it must evolve in the context of the already (successfully) filled niches of the existing species. Thus new species will form and develop to exploit niches that are not already filled (which minimizes their direct competition with other already established species). In addition, some of the most valuable unexploited niches in any given time and place of an existing ecosystem will revolve around opportunities provided by existing species, opportunities that often include developing a mutual cooperative benefit between the newly evolving specialist species and the existing established species in the ecosystem.

These fundamental dynamics lead to a natural nestedness of functional relations among the organisms of an evolving ecosystem, where ever more specialized

species evolve to form mutual cooperative associations with existing successful species. Bastolla et. al. [9] among others have shown that the greatest support for the greatest biodiversity of such ecosystems is obtained when the architecture of the functional relation among the species have certain properties of nestedness. This type of development, where established generalists give rise to niches that can be filled by newly developed specialists give rise to network disassortativity, in which nodes with few connections (specialists) tend to be connected to nodes with many connections (generalists). Further, in the studies on ecological networks and other types of nested functional organizations, it has been suggested that the structure is fundamental to supporting an ever expanding and increasing level of complexity. This nesting of more and more specialized function may not be unlimited, but given the right type of nested mutual cooperative relations it can support a very diverse and robust set of species (functions) in the network. This robustness has many advantages for a biological ecosystem in withstanding changing or adverse shocks from the environment, and once established is self-sustaining.

3 Robust Functional Performance of Neural Circuits

The preceding section should make it clear that brain circuit information processing networks share many of the same architectural and developmental features being explored in network analysis and models applied to other types of functional networks. The MRH hypothesis of neural reuse makes the claim that the same type of generalist to specialist assembly is expected and seen in the evolution of brain function. In the ecosystem of the brain, generalist functions evolve first to fill the low-hanging fruit of the environmental niche (basic functions of perception and action, maintenance of bodily functions, etc.). But the information processing ecosystem of organisms that continue to complexify their behavioral repertoire must create a nested hierarchy of mutual competitive/cooperative relations that support (rather than limit) the continuing development of specialist functions. Further, each specialist function that develops can be seen as filling a new niche, and will work best by reusing (and cooperating with) existing functional circuits already present in the environment when the new function is developing.

In other words, here is the important point of the preceding thoughts about the MRH relation to cooperative network dynamics of biological ecosystems. The question is: Why might hierarchical or nested mutual organization be beneficial? The answer from biological ecosystems and other types of hierarchical self-organizing functional networks appears to be that nested mutualism allows for, not unlimited, but vastly more levels of nested hierarchical specialization than networks that don't have the right types of nesting or that don't evolve specializations that reuse existing generalist functions. This robustness of the information processing ecosystem of neural circuits has several implications. First of all, as already mentioned, we would expect that certain types of failures or injuries will have disastrous consequences, while others can and will be easily

absorbed by the diverse ecosystem of a nested mutualistic network. So the death of a hub species can results in the collapse of a biological ecosystem, and likewise in collapse in an information processing network. However, the robustness of the mutualistic network will allow such systems to withstand many other types of serious injuries or threats relatively unharmed. But this robustness is not simply a factor in the injury or damage to the physical components of the network. Again by analogy, in a biological ecosystem, the continued increasing specialization supported by the ecosystem gives rise to many unique functions. As this diversity of function increases, the biodiversity of the ecosystem increases and in a self-catalytic type of way supports even more varied niches for even more varied specialization opportunities. We believe that the impressive ability of the human information processing network importantly and crucially relies on the self-catalytic nature of increasing specialization of functions supported by the nested mutualistic nature of the massively redeployed neural circuits.

However, the preceding discussion should not lead you to believe that the authors are only proposing an analogy between biological ecosystems (and other types of hierarchical functional networks) and biological information processing networks. The important insights are into the relation and structure of the functional network that naturally develop in such systems. Though it has not been confirmed, there is certainly strong evidence that the biological brain is structurally organized as a small-world, scale-free network [12,13]. Further work is needed to understand the exact nature of the hierarchical nesting of functional relations, and to what degree and how these may mirror functional relations in other types hierarchically organized networks.

4 Conclusions

In this article we have introduced the reader to two different areas of research, the massive redeployment hypotheses of neural reuse of brain information circuits (and its relationship to embodied theories of cognition), and the network dynamic analysis of functional networks, such as biological ecosystems. We have shown that exciting findings in network science analysis of functional networks have illustrated some interesting properties of how nested hierarchical mutualism supports increasing specialization of function in such networks. We have made the explicit link that this same type of nested mutualism observed in biological ecosystem networks may also explain some of the properties of MRH theory. Further, these observations help us understand the impressive robust functioning of biological information processing networks. Further work is needed in order to analyze the functional relation of brain function networks to confirm the nested disassortativity structure of these circuits. Such an understanding would be useful in being able to understand embodied cognitive performance of human behavior, and to being able to replicate the robustness of the nature of cognitive performance in artificial systems.

Acknowledgments. The ideas and work described in this paper were supported by DOE grant #DE-SC0001132 and NSF grant #0916749, as well as by a Texas A&M University faculty development grant. Numerical work performed on the Lion compute cluster at Texas A&M University - Commerce.

References

1. Anderson, M.L.: Neural reuse: A fundamental organizational principle of the brain. Behavioral and Brain Sciences 33, 245–313 (2010)
2. Sugihara, G., Ye, H.: Cooperative network dynamics. Nature 458, 979–980 (2009)
3. Anderson, M.L.: Massive redeployment, exaptation, and the functional integration of cognitive operation. Synthese 159(3), 329–345 (2007)
4. Decety, J., Grèzes, J.: Neural mechansims subserving the perception of human actions. Trends in Cognitive Science 3, 172–178 (1999)
5. Chao, L.L., Martin, A.: Representation of manipulable man-made objects in the dorsal stream. Neuroimage 12, 478–484 (2000)
6. Rizzolatti, G., Craighero, L.: The mirror-neuron system. Annual Review of Neuroscience 27, 169–192 (2004)
7. Gallese, V., Lakoff, G.: The brain's concepts: The role of the sensory-motor system in conceptual knowledge. Cognitive Neuropsychology 22(3-4), 455–479 (2005)
8. Anderson, M.L.: On the grounds of (x)-grounded cognition. In: Calvo, P., Gomila, T. (eds.) Handbook of Cognitive Science, ch. 21, pp. 423–435. Elsiver (2010)
9. Bastolla, U., Fortuna, M.A., Pascual-Garcia, A., Ferrera, A., Luque, B., Bascompte, J.: The architecture of mutualistic networks minimizes competition and increases biodiversity. Nature 458, 1018–1021 (2009)
10. May, R.M., Levin, S.A., Sugihara, G.: Ecology for bankers. Nature 451, 893–895 (2008)
11. Bastolla, U., Lassig, M., Manrubia, S.C., Valleriani, A.: Biodiversity in model ecosystems, i: coexistence conditions for competing species. Journal of Theoretical Biology 235, 521–530 (2005)
12. Bassett, D.S., Bullmore, E.: Small-World brain networks. The Neuroscientist 12(6), 512–523 (2006)
13. Boccaletti, S., Latora, V., Moreno, Y., Chavez, M., Hwang, D.-U.: Complex networks: structure and dynamics. Physics Reports 424, 175–308 (2006)

What You Talk About Is What You Look At?

Shulan Lu and Lonnie Wakefield

Department of Psychology, Texas A & M University–Commerce, TX, 75429-3011
lu.shulan@gmail.com

Abstract. Studies in event perception have shown that people sort ongoing experiences into neat and tidy event packages instead of unedited recordings of the world. For events unfolding along multiple tracks, there is evidence that humans impose boundaries onto them and perceive them to be one psychological entity (i.e., temporal chunking). Language users have been shown to use the differences in the beginning states of activities to describe the event sequence of simultaneous events. The current study investigated whether language users have a perceptual bias toward the beginning states while describing event sequences. Participants viewed films of simultaneous events, and described the temporal relationship of events. Throughout the experiments, their eye movements were recorded. The results did not show a compelling bias in visual attention toward the beginning boundaries. We present the findings of our eye tracking study and discuss the results in the context of the interplay between nonlinguistic and linguistic representations of events.

Keywords: event structure, temporal chunking, end state, temporal language.

1 Introduction

Many everyday events occur in parallel, whereas when we talk about events we are forced to structure and relate them in a linear fashion. How do people parse a myriad array of perceptual information into meaningful events and transform it into linguistic representations that are sufficiently simple for communication? Studies have demonstrated the close correspondence between event perception and language [1][2]. This coordination first requires language users to spontaneously segment a constant flux of information into meaningful events. Language users must then map the perceptual event representations onto some mental representations in order to be able to communicate their understanding of the events [3].

1.1 Event Perception

Studies in cognitive science have consistently demonstrated that humans impose structures upon the available information to understand and navigate their perceptions and guide their actions in the ongoing world. For example, Gestalt psychologists have demonstrated quite a few grouping principles that humans use in organizing visual information [4]. The principle of closure illustrates how humans tend to impose completion upon the incomplete, but connecting contours. The principle of proximity

D. Liu et al. (Eds.): BICS 2013, LNAI 7888, pp. 261–270, 2013.

illustrates how humans impose grouping on objects that are near each other. Each of these principles illustrates how the human minds organize the information in the environment into neat, tidy packages instead of unedited raw recordings of the world. Another example is how humans use schema to perceive and later remember the activities they experience [5].

In recent years, studies in event perception have demonstrated how humans segment the flux of perceptual information streams into a series of discrete events [6] [7]. The ongoing world is thus packaged into perceptual parts and tagged as meaningful events. This temporal chunking of perceptual experience is crucial to the understanding of consciousness, where our phenomenological experiences are segmented and distinctions are made in terms of what is now versus what was before [8] [9]. There have been many experiments demonstrating how event boundaries guide the comprehension, memory, and re-representation of conscious experiences (e.g., [10]).

Using the classic Newtson task [11], Zacks and his colleagues investigated how perceivers segment events that unfold along a single track (i.e., one agent in service of one goal at a time) [7]. While watching video clips of everyday activities, participants indicated when an event ends and another begins by pressing the spacebar on a computer keyboard. The results showed that perceivers segment sequential everyday activity at multiple time scales simultaneously. For example, indicated boundaries for fine and coarse grained event segmentation will not have a random relationship. Instead, the boundary of fine grained event segments (e.g. clean a fish tank) will be temporally and hierarchically aligned with the boundary of the coarse grained event (e.g. pouring water). Event segmentation is more than identifying the right boundariess of events. Perceivers have to monitor the unfolding of fine-grained events and see how they group together forming a larger meaningful units.

In one experiment of the Zacks et al. study [7], participants were asked to describe events while they segment the events. The results showed that describing events during segmentation reinforced participants to build a hierarchical partonomic structure, where fine grained events are not only part of the coarse grained event units but also align to the corresponding event boundaries temporally. The coarse unit descriptions tend to be actions on a new object, whereas the fine unit descriptions tend to be actions on different parts of the same object. In a nut shell, talking about the ongoing events guided perceivers to focus on the goal completion states of events rather than merely observing the events.

Lu, Harter, and Graesser [12] investigated how people perceive simultaneous events. The temporal parameters of the stimulus events were varied based on Allen's 7 temporal relations [13] [14]. Upon viewing the stimulus events, participants made judgments on temporal relations by performing a 7-alternative forced choice task. The results showed that perceivers group the simultaneous perceptual stream as one event by imposing a unit boundary upon them instead of imposing separate event markers on each steam. In this manner, we sort ongoing experiences into event packages following one another linearly.

Imagine the following scenario. John begins to read a newspaper while continuing to drink coffee. By the time he is done with the newspaper, he is still drinking his coffee. This is an example of DURING activity in Allen's representation, where one activity (i.e., reading newspaper) occurs entirely during the time frame of the other (i.e., drinking coffee). For perceivers, there appears to be three spans occurring one after another: (a) John drinking the coffee alone first (initial span); (b) John drinking the

coffee and reading a newspaper (coterminous span); and (c) John finishing the coffee. People may describe these two activities as the following: John drank the coffee while reading the newspaper. When they are asked about the sequence of the events, people frequently say the following: John drank the coffee before he read the newspaper. If they are asked about the more detailed parameters of temporal relations, people frequently say the following: John began to drink coffee first, then read the newspaper while sipping his coffee. He finished reading the newspaper before he was done with the coffee. This last description includes the three sub-events and marked the event boundaries. It is reasonable to raise the question as to the relationship between the perceptual and linguistic representations of events. Does talking about the sequence of simultaneous events map onto the event structure being perceived? Alternatively, does language have its own quirks and linguistic structure does not directly correspond to event structure?

1.2 Linguistic Representations of Simultaneous Events

Lu and Wakefield investigated how people talk about simultaneous events [15]. Participants viewed films of simultaneous events, and performed linguistic acceptability judgments. The results showed that event boundaries played a significant role in how people talk about the sequence of simultaneous events. More specifically, people talk about the order of simultaneous events primarily using *before* instead of *after,* and calibrate their uses of *before* depending on the differences between beginning states. In the above example activities of John drinking the coffee and reading a newspaper, participants judged the following sentence A based on the differences in beginning states to be linguistically acceptable: he drank the coffee before he read the newspaper (i.e., the beginning of *drinking the coffee* precedes the beginning of the sub-event *reading the newspaper*). However, participants did not perceive the following sentence B to be acceptable based on the differences in the end states: he read the newspaper before he drank the coffee (i.e., the ending of *reading the newspaper* precedes the ending of *drinking the coffee*).

In the experiment reported by Lu and Wakefield [15], the events in the before sentences were described following the iconicity principle [16], whereas the events in the after sentences were opposite to the order in which events unfolded. To what extent might the results be affected by the sentence order? That is, if the sentence A was syntactically transformed into the following, would language users still perceive it to be acceptable? Before he read the newspaper, he drank the coffee. It is possible that before may not apply to most of the simultaneous events once it is moved to the beginning of a sentence because the event order in the sentence violates the iconicity principle. Furthermore, after may apply to most of the simultaneous events once it is at the beginning of a sentence. This possibility was investigated in a separate study. The exact same materials and procedure in the Lu and Wakefield study were used other than changes in sentences [15]. Consistent with the previous results [15], participants tended to compute the differences of the beginning states of events to calibrate their uses of before regardless of event order in a sentence.

This bias toward using the beginning state to calibrate the sequence of simultaneous events is not consistent with the prevalent literature that describes the importance of end goal states of events. This raises the question as to whether the

beginning state bias, emerging out of the linguistic acceptability judgments of event sequence, reflects the perceptual encoding bias. Language is known to favor some features over other features [17] [18]. Furthermore, naming a certain feature leads people to think about the various relational associations that a particular feature has. This raises the possibility that the bias toward the beginning state is the byproduct of talking about event sequence. Studies have proposed that linguistic systems have a tendency to resolve ambiguity earlier on [19] [20]. The earlier resolution of which event precedes also meets the demands of pragmatics and cognitive load. It seems difficult to communicate using the end states, particularly in the case of event Y ends prior to event X but begins later than event X. It violates the iconicity principle if people need to think about the end states first and the beginning states second.

2 An Eye Tracking Study of Perceiving and Describing Event Sequence

To address these alternative possibilities, we performed an eye tracking study. Participants were asked to describe the temporal relations of fish swimming events while their eye movements were recorded. We used fish swimming events as opposed to human enacting actions, because the fish swimming events are simpler for the purpose of eye tracking. Considering the cognitive load of describing events may add to that of perceiving simultaneous events, participants were allowed to describe events when they were ready to speak.

To what extent do people fixate on the beginnings versus ends? Do people fixate as much at the end states as the beginning states during event perception? Or does describing event temporal relations bias the perceptual system to attend more to the beginnings as opposed to the ends? Our previous study showed that people tended to use before to describe the temporal order of simultaneous events. Would people use more before than after words in their spontaneous descriptions of event temporal relations?

3 Method

Participants
Nineteen introductory psychology students at University of Memphis participated in exchange for course credit. One of the data sets was corrupted, and it was not included in the analysis.

Materials
The fish swimming animations used in Lu et al. [12] were used. As described in Lu et al., all stimuli were constructed based on Allen's 7 temporal relations [13] [14]. For each event temporal relation, there were 6 different animations. A total of 42 animations were used. There were seven randomized orders of presentations for the experiment.

One question that remained in the Lu and Wakefield study [15] was how frequently people might use *before* and *after* in describing simultaneous events. A list of verbs, adverbs, prepositions and conjunctions that encode the temporal relations were selected

from Lu [21]. The following are some example words: (a) anticipate, precede, follow after, succeed, go with, overlap, (b) before, earlier, previously, in advance, after, later, next, subsequently, at the same time, simultaneously, for now, and (c) prior to, soon after, until, when, while, during, in the course of. The complete word list was presented on a computer screen during the exposure and training phase only.

Apparatus

An Applied Science Laboratory Model 501 eye tracker was used in the study. Eye movements were recorded 60 times per second (once every 17 ms). Accuracy of the gaze position record varied within 0.5 degrees visual angle. Participants were seated about 700mm in front of the stimulus monitor.

Video and audio of the experimental session were recorded through a VCR. The VCR recorded a TV screen that displayed the ongoing events in each animation and a superimposed image of what the left eye was fixating on. The superimposed image was generated by the eye tracking equipment. Each participant wore a small microphone, which was connected to the VCR, so their verbal descriptions were recorded.

Procedure

Participants were told they will be viewing animations of fish swimming events. Participants received the following instructions, "While you view the animation, try to describe the time relations between the fish swimming events using one or two succinct sentences. For example, the light fish swims before the dark fish, but stopped after the dark fish. Or another example, the light fish and the dark fish swim simultaneously. The words or phrases underlined in these examples tell us the time relations between the two fish swimming events. Of course, these are just ***arbitrary*** examples. Describe the events and time relations in a way, which is most natural to you and which is understandable to others who do not see the animations. Before you speak, please hit S on the keyboard". The two example descriptions were frequently used in the pilot study.

Participants were presented with the word list described earlier on the computer screen. Participants were told that these words are example words that describe the time relations between events. The experimenter read each word to participants and pointed to the word on the screen. Upon completion, the word list screen was removed. Then participants received trial animations and practiced performing the task by following the instructions. Participants also positioned their finger next to the S key on the keyboard.

When participants felt ready for the experiment task, they went through a 9-point eye tracker calibration procedure. Upon completing the calibration, participants viewed one animation at a time and described event temporal dynamics when they were ready. Calibration was checked periodically throughout the experiment session.

Results and Discussion

We used the points of times where the fish swimming motion launches and stops as the physical event boundaries. Only those eye fixations overlay on top of the motion onset and offset were accounted as the fixations on the event boundaries. Those fixations cast right after the onset and offset of the motion were not included as the fixations on the

event boundaries. We believe a strict definition would reduce the subjectivity in categorizing the fixations.

An analysis of variance was performed on the proportions of eye fixations, using an event temporal relation (6) x event boundary (beginning versus end) design. We did not include the EQUAL events in the analysis, because EQUAL denotes two events that begin and end at exactly the same time. There were significant interactions of event temporal relations with event boundaries, F (5, 85) = 3.54, MSE = .02, $p < .006$, partial $\eta^2 = .17$. There were significant main effects of event temporal relations, F (5, 85) = 4.35, MSE = .02, $p < .001$, partial $\eta^2 = .20$. There were not significant main effects of event boundaries, F (1, 85) = .58, MSE = .02, $p = .46$, partial $\eta^2 = .03$.

For BEFORE (two activities being completely apart for some time), OVERLAP (two activities overlapping in time partially), and DURING (one activity occurring within the temporal span of the other activity), the comparison analysis did not show more fixations at the beginning boundaries than the end boundaries. The equal amount of fixations at the beginning versus end boundaries demonstrated the ongoing segmentations of events. MEET (two activities abutting each other in time), START (two activities beginning at the same time), and FINISH (two activities ending at the same time) events had motion changes that were very close in time. For example, START activities both began at the same time. Naturally, participants tended to miss overlaying their eye fixations on the change points in events when monitoring the two separate streams of motion. The interaction effects of event temporal relations with event boundaries were thus largely due to the differences in following event streams that were simultaneous versus somewhat linear. It is notable that there were many fixations that were cast right after the onsets and offsets of the motion in the latter three types of activities.

Participants launched their descriptions at different points of the experiment phase. Five participants were during mode speakers who always launched their descriptions while events were unfolding, whereas seven participants were after mode speakers who always launched their descriptions upon event completion. Six participants did not have a preferred mode of description. For example, the MEET animations were described after the completion of both events 51% of the time, whereas 49% of the time descriptions were launched during events. These results suggested that these participants were not engaged in a consistent pattern of event perception and description planning. Thus, these data were not included in the further analysis of eye fixations.

Table 1 showed the proportions of eye fixations at the beginnings versus the ends for the after and the during mode participants. Overall, the after mode participants had more fixations at the event boundaries than the during mode participants. Even though describing events while events unfolding consumed visual attention, there were still significant amounts of eye fixations being cast squarely on the event boundaries. This indicates that attending to event boundaries is an integral part of describing the sequence of simultaneous events. To complete the task, participants only needed to keep track of the order in which events unfolded. Participants did not need to actively predict and follow the event boundaries using eye movements.

Table 1. Mean Beginning and End Fixation Proportions by Description Mode

Mode	Breakpoint	Event Temporal Relations					
		BEFORE	MEET	OVERLAP	START	DURING	FINISH
During	Beginning	.34(.17)	.33(.20)	.27(.13)	.22(.09)	.22(.19)	.37(.19)
	End	.28(.08)	.27(.28)	.26(.17)	.30(.18)	.12(.14)	.12(.14)
After	Beginning	.51(.14)	.38(.14)	.49(.22)	.35(.20)	.32(.21)	.46(.22)
	End	.50(.19)	.49(.21)	.41(.27)	.43(.27)	.38(.23)	.28(.13)
Total	Beginning	.45(.18)	.36(.16)	.40(.21)	.29(.17)	.28(.20)	.42(.20)
	End	.41(.18)	.40(.26)	.35(.24)	.38(.24)	.27(.23)	.21(.15)

The eye fixations of the after mode participants should reveal the bias that is brought about by planning descriptions. However, there were not statistically significant differences in fixations at the beginnings versus the ends for any event temporal relation except FINISH. This again demonstrated attending to event boundaries as they occur is an integral part of describing events. The differences in the beginning states were crucial to describe the FINISH activity, whereas the differences in the end states were the only differences of the two activities in the START relation. This asymmetry between the fixation patterns of FINISH versus START provided some indication that attending to the beginning states may play a slightly greater role in talking about event sequence.

Besides START and FINISH, DURING is another representative simultaneous events, whereas BEFORE, MEET and OVERLAP has more linearity in their event component. The DURING mode speakers tended to cast more fixations on the beginnings of events, which might be another indication of a greater weight on beginning boundaries when talking about event sequences. One may argue that beginning boundaries are less recent in memory and thus speakers might be more likely to fixate on the beginnings. However, this does not weaken the beginning state hypothesis, in that speakers forecast the needs of using the beginning boundaries in describing events and keep track of them.

A question arises as to how people used the before versus after in their event descriptions. Lu and Pierce [23] looked at the linguistic characterization of the event descriptions, however, this research did not constrain the tense, aspect, and sentence structures of the spontaneous descriptions. We could not make a direct comparison with the Lu and Wakefield study in terms of the properties of before versus after used.

In addition, people frequently used verbs such as start and stop in their descriptions. There were not significant differences between the uses of these two verbs across all three modes of descriptions [23]. Can this lack of differences speak to the representations of beginning and end states in talking about the sequence of simultaneous events? The following two considerations preclude it as evidence for

comparing perceptual versus linguistic representations in describing the sequence of simultaneous events. First, words such as start and stop do not impose any interpretation of the event sequence per se. Second, due to the nature of the experiments, we could not control the timing of uttering "start / stop" and that of launching the fixations toward event boundaries. It is not clear if the uses of such linguistic markers were the alignment between the perceptual and linguistic representations or merely the byproduct of participants aiming to give thorough descriptions of what they saw.

4 General Discussion

Understanding how people talk about events is important for understanding nonlinguistic representations of events. Lu and Wakefield demonstrated that language users tend to use the order in which beginning states of two events unfold in describing the sequence of simultaneous events [15]. The current study provided eye movements data demonstrating the explicit visual marking of event boundaries. The current study showed that attending to both beginning and end boundaries of events are an integral part of describing event temporal relations. There is some indication that attending to the beginning boundaries might be more important in describing event temporal relations. Nevertheless, there is no consistent pattern that a greater amount of eye fixations occur on the beginning boundaries than on the end boundaries.

Language has been shown to guide event perception when language is recruited to perform the task [22]. When describing spatial motion events, English speakers typically focus on the manner of the motion by using verbs such as slide and walk, whereas Greek speakers typically focus on the path such as approach and ascend. This indicates the possibility that people get trained to perceive events via language. The eye movement data showed that participants tend to zoom onto the event components encoded in their native languages. However, such effects of language are modulated by the event processing tasks. When participants were asked to freely inspect the events instead of verbally describing the events, their visual attention allocation was not affected by which language they speak.

The after mode speakers in the current study are somewhat similar to the participants who were assigned to freely inspect the events in the Paragragou et al. study [22], whereas the during mode speakers are somewhat similar to the participants who were assigned to speak in their native languages. However, talking about the sequence of simultaneous events in either of the modes did not demonstrate proportionally greater bias toward the beginning boundaries. This raises the question as to how the asymmetry between event perception and talking about event sequences emerged. This asymmetry may be primarily due to the constraints of pragmatics. If people primarily use end states to calibrate the event sequence, then it would not be clear to other language users which event gets initiated earlier at all. One of the functions of language is to highlight the relational properties in the world. Linguistic devices serve to support and guide the perception of contingency relations between events [24]. Furthermore, using the beginning states gives the word *before* greater coverage in usage. For example, people can talk about the sequence of uninstantiated events when using *before*. In the sentence *John drank lots of red bull*

before he beat his tennis opponent, the event of beating the tennis opponent may not happen.

In closing, the current study revealed a method in which we could examine the interplay of perceptual representations and linguistic representations. In future studies, it would be worthwhile to assign participants to describe events while events unfold versus describing events after events unfold. It would also be worthwhile to manipulate the pragmatics aspects of the task. An exciting question for future work based on these results would be to ask: How do our goals in communication impact the temporal chunking of conscious experiences?

Acknowledgments. This work is supported by a grant from Texas Advanced Research Program, a grant from US National Science Foundation (#0916749), and a grant from Texas A & M University – Commerce Faculty Research Enhancement. We thank Derek Harter for his comments on an earlier draft, and Gang Wu for formatting this article.

References

1. Miller, G.A., Johnson-Laird, P.N.: Language and perception. Harvard University Press, Cambridge (1976)
2. Talmy, L.: Semantics and syntax of motion. In: Kimball, J.P. (ed.) Syntax and Semantics, vol. 4, pp. 181–238. Academic Press, New York (1975)
3. Talmy, L.: Toward a cognitive semantics. MIT Press, Cambridge (2000)
4. Wertheimer, M.: Laws of organization in perceptual forms. First published as Untersuchungen zur Lehre von der Gestalt II, in Psycologische Forschung, 4, 301-350; Translation published in W. A. Ellis (eds.). A source book of Gestalt psychology, pp. 71-88. Routledge&KeganPaul, London (1923/1938)
5. Bartlett, F.C.: Remembering: A study in experimental and social psychology. Cambridge University Press, Cambridge (1932)
6. Zacks, J.M., Tversky, B.: Event structure in perception and conception. Psychological Bulletin 127, 3–21 (2001)
7. Zacks, J.M., Tversky, B., Iyer, G.: Perceiving, remembering, and communicating structure in events. Journal of Experimental Psychology: General 130, 29–58 (2001)
8. James, W.: The principles of psychology, vol. 1. Henry Holt, New York (1890)
9. Zacks, J.M.: How we organize our experience into events. Psychological Science Agenda 24 (2010)
10. Zacks, J., Speer, N., Reynolds, J.R.: Segmentation in reading and film comprehension. Journal of Experimental Psychology: General 138, 307–327 (2009)
11. Newtson, D.: Attribution and the unit of perception of ongoing behavior. Journal of Personality and Social Psychology 28, 28–38 (1973)
12. Lu, S., Harter, D., Graesser, A.C.: An empirical and computational investigation of event temporal relations. Cognitive Science 33, 344–373 (2009)
13. Allen, J.F.: Towards a general theory of action and time. Artificial Intelligence 23, 123–154 (1984)

14. Allen, J.F.: Time and time again: The many ways to represent time. International Journal of Intelligent Systems 6, 341–355 (1991)
15. Lu, S., Wakefield, L.: The role of event boundaries in language: Perceiving and describing the sequence of simultaneous events. In: Zhang, H., Hussain, A., Liu, D., Wang, Z. (eds.) BICS 2012. LNCS, vol. 7366, pp. 198–207. Springer, Heidelberg (2012)
16. Zwaan, R.A., Radvansky, G.A.: Situation model in language comprehension and memory. Psychological Bulletin 123, 162–185 (1998)
17. Lu, S., Franceschetti, D.R.: Perceiving and describing motion events. Behavioral and Brain Sciences 26, 295–296 (2003)
18. Tversky, B.: Tools for thought. In: Benedetti, B., Cooks, V. (eds.) Language and Bilingual Cognition, pp. 131–139. Psychology Press, New York (2011)
19. Clark, H.H.: Bridging. In: Schank, R.C., Nash-Webber, B.L. (eds.) Theoretical Issues in Natural Language Processing, pp. 169–174. Association for Computing Machinery, New York (1975)
20. Gennari, S.P.: Temporal references and temporal relations in sentence comprehension. Journal of Experimental Psychology: Learning, Memory, and Cognition 30, 877–890 (2004)
21. Lu, S.: Perceiving, remembering, and describing event temporal relations. Dissertation Abstract International 65(06), 3191 (2004)
22. Papafragou, A., Hulbert, J., Trueswell, J.: Does language guide event perception? Evidence from eye movements. Cognition 108, 155–184 (2008)
23. Lu, S., Pierce, D.: Perceiving and describing event temporal dynamics. In: Bara, B.G., Barsalou, L., Bucciarelli, M. (eds.) Proceedings of the 27th Annual Meeting of the Cognitive Science Society, pp. 1349–1354. Erlbaum, Mahwah (2005)
24. Moens, M., Steedman, M.: Temporal ontology and temporal reference. Computational Linguistics 14, 15–28 (1988)

Cryptanalysis of Truong et al.'s Fingerprint Biometric Remote Authentication Scheme Using Mobile Device

Muhammad Khurram Khan[1], Saru Kumari[2], Mridul K. Gupta[3], and Fahad T. Bin Muhaya[4]

[1] Center of Excellence in Information Assurance, King Saud University, Riyadh, Kingdom of Saudi Arabia
mkhurram@ksu.edu.sa
[2] Department of Mathematics, Agra College, Agra, Uttar Pradesh, India
saryusiirohi@gmail.com
[3] Department of Mathematics, Chaudhary Charan Singh University, Meerut, Uttar Pradesh, India
mkgupta2002@hotmail.com
[4] Prince Muqrin Chair for IT Security, King Saud University, Saudi Arabia
fmuhaya@ksu.edu.sa

Abstract. In 2010, Chen et al. focused at the vulnerability of smart card based authentication systems owing to leakage of secret information from smart card. They proposed a scheme with a view to boost the security of such authentication systems. However, in 2012, Truong et al. found Chen et al.'s scheme weak at resisting replay attack and spoofing attacks; thereby they proposed an improved scheme to counterfeit these weaknesses. Undoubtedly, the improved scheme by Truong et al. is free from defects pointed out on Chen et al.'s scheme, but here we show that problems like impersonation attacks, password guessing, etc are adhered with its design. We show that Truong et al.'s scheme violates Chen et al.'s aim to get rid of information-leak hazard from the smart card or mobile device based authentication schemes.

1 Introduction

Last decades have witnessed a significant advancement in communication networks. Authentication mechanisms are playing key role in imparting network services to a large number of remote users. This scenario automatically brings with it a concern about the security of existing authentication protocols. There are many user authentication schemes [1-9] using smart card and key agreement schemes [10-12]. According to Kocher and Messerges [13,14], the information stored inside a smart card can be revealed. With this thought, Rhee et al. proposed a remote user authentication scheme [15] without using smart cards. In 2010, Chen et al. [16] also pondered that information leakage is a crucial cause for vulnerability of various schemes [17-22]. In addition, they targeted Khan et al.'s mobile device based scheme [23] for the same drawback. To remove this drawback, Chen et al. [16] extended the approach used by Khan et al. [23] and proposed a new scheme. Recently, Truong et al. [24] showed that Chen et al.'s scheme is unable to protect user's anonymity,

D. Liu et al. (Eds.): BICS 2013, LNAI 7888, pp. 271–277, 2013.

suffers from identity-theft and its consequences, etc. In addition, Truong et al. proposed an improved protocol [24] over Chen et al.'s scheme.

In this paper, we display that Truong et al.'s scheme [24] incorporates impersonation attacks and password guessing attack via information-leak from mobile device. Thus, we make obvious that the flaw of information-leak from smart card or mobile device, on which Chen et al. pondered and worked, evolves again in Truong et al.'s scheme. In addition, we demonstrate that impersonation attacks are also possible using only an intercepted login request, which makes the scheme more vulnerable. Rest of the paper is ordered as follows: In Section 2, we review Truong et al.'s scheme. Section 3 is about security issues of Truong et al.'s scheme. And the conclusion is given by Section 4.

2 Review of Truong et al.'s Scheme

The scheme consists of four phases: the registration phase, the login phase, the mutual authentication and session key agreement phase, and the password change phase. Each of the phases is described as follows:

2.1 Registration Phase

This phase is used to register the user with server S. It is conducted over a secure channel indicated by '⇒'. The steps involved are described as follows:

1) U_i chooses its identity ID_i, password PW, and a random nonce N.
2) Computes $h(PW \oplus N)$ and gives the imprint of his fingerprint on the sensor.
3) $U_i \Rightarrow S$: Registration request = $\{ID_i, h(PW \oplus N), F_i)\}$, here F_i is the fingerprint template of U_i.

On receiving the registration request of U_i, the server performs the following steps using his secret key x, cryptographic hash function $h(.)$ and cryptographic keyed-hash function $h_k(.)$ with a secret key k:

4) Generates a random value e. Computes:
   $hpw = h(PW \oplus N) \oplus F_i$, $E_i = hpw \oplus h(x \| e)$,
   $R_i = h(ID_i \oplus h(x \| e)) \oplus hpw$ and $V_i = h_{h(IDi \oplus h(x \| e))}(F_i)$.
5) $S \Rightarrow U_i$: Secret Information = $\{R_i, V_i, E_i, e, h(.), h_k(.)\}$.

On receiving the secret information from server, U_i stores it along with N into his mobile device. U_i's mobile device now contains $\{R_i, V_i, E_i, e, h(.), h_k(.), N\}$

2.2 Login Phase

This phase facilitates user to login to the server S. For this, U_i inserts his identity ID_i, password PW and imprints his fingerprint F_i on the sensor. Then the mobile device of U_i performs the following steps:

1) Computes $hpw = h(PW \oplus N) \oplus F_i$, $A_i = R_i \oplus hpw$.
2) Verifies if $h_{Ai}(F_i) = V_i$. If so, then the mobile device proceeds to next step; otherwise, it lapse the session.
3) Generates a random nonce N_U and calculates $C_1 = N_U \oplus E_i \oplus hpw$, $C_2 = h_{Ai}(N_U)$ and $CID = ID_i \oplus N_U$.
4) $U_i \rightarrow S$: Login request = $\{CID, e, C_1, C_2\}$, where '→' denotes a public channel.

2.3 Mutual Authentication and Session Key Agreement Phase

In this phase, both, the server and the user, verify the authenticity of each other. Description of the steps performed by user and server is as follows:

On receiving the login request of U_i , first S performs the following steps:
1) Retrieves B_i (=N_U) = $h(x \| e) \oplus C_1$, $ID_i = CID \oplus N_U$ and checks the validity of ID_i format.
2) Check if $C_2 = h_{h(IDi \oplus h(x \| e))}(N_U)$. If not so, rejects the login request; otherwise, accepts login request and temporarily stores ID_i till the end of the session.
3) Generates a random nonce N_S and computes:
$S_1 = h(h(ID_i \oplus h(x \| e)) \| N_S \| B_i)$.
4) $S \rightarrow U_i$: $\{N_S, S_1\}$.

On receiving $\{N_S, S_1\}$, from S, the user performs the following steps to authenticate the server:
5) Verifies if $S_1 = h(A_i \| N_S \| N_U)$. If so, then the legitimacy of server gets confirmed; otherwise lapse the session.
6) $U_i \rightarrow S$: $\{S_2\}$. Computes $S_2 = h((E_i \oplus hpw) \| N_S)$.

On receiving $\{S_2\}$ from U_i, the server S performs the following:
7) Verifies whether $S_2 = h(h(x \| e) \| N_S)$. If so, authenticity of U_i is confirmed; otherwise this session is lapsed.

At the end of session both U_i and S independently compute the session key. S computes session key as $SK = h(h(ID_i \oplus h(x \| e)) \| h(x \| e) \| N_S \| B_i)$ and U as $SK = h(A_i \| (E_i \oplus hpw) \| N_S \| N_U)$.

2.4 Password Change Phase

The password change phase facilitates the user to change his password PW to a new one, say PW^*. Following are the steps performed by the user and its mobile device:

1) U_i inserts his identity ID_i , password PW and imprints his fingerprint F_i into its mobile device.
2) The mobile device computes $hpw = h(PW \oplus N) \oplus F_i$, and checks if $h_{(Ri \oplus hpw)}(F_i) = V_i$. If not so, then the mobile device stops further action. Otherwise, allows the user to insert a new password PW^*.
3) The mobile device computes $hpw^* = h(PW^* \oplus N) \oplus F_i$, $R_i^* = R_i \oplus hpw \oplus hpw^*$, $E_i^* = E_i \oplus hpw \oplus hpw^*$ and replace R_i and E_i with R_i^* and E_i^* respectively.

3 Cryptanalysis of Truong et al.'s Scheme

3.1 User and Server Impersonation Attack Using Only an Intercepted Login Request via ID Guessing

Suppose U_A intercepts a login request $\{CID, e, C_1, C_2\}$ of U_i. Now, U_A performs the following steps:

1) Computes $CID \oplus C_1$, which needs to be $ID_i \oplus h(x \| e)$.
2) Computes the hash of $ID_i \oplus h(x \| e)$ and thus obtains $A_i = h(ID_i \oplus h(x \| e))$, which is a secret shared between U_i and S. The value A_i acts as key for keyed hash function $h_k(.)$.
3) Guesses ID_i^* as identity of U_i , computes $h^*(x \| e) = ID_i^* \oplus [ID_i \oplus h(x \| e)]$ and obtains $N^* = C_1 \oplus h^*(x \| e)$.
4) Computes $C_2^* = h_{Ai}(N^*)$ and checks if $C_2 = C_2^*$. If so, it implies that he has correctly guessed the identity of U_i and has correctly obtained the value $h(x \| e)$.

Now, U_A possess $A_i = h(ID_i \oplus h(x \| e))$ and $h(x \| e)$. Thus, he can easily mount user and server impersonation attack on the scheme in the following manner:

1) U_A generates a random nonce N_A and computes $C_{A1} = N_A \oplus h(x \| e)$, $C_{A2} = h_{Ai}(N_A)$ and $CID_A = ID_i \oplus N_A$.
2) $U_A \rightarrow S$: Login request $\{CID_A, e, C_{A1}, C_{A2}\}$.

On receiving $\{CID_A, e, C_{A1}, C_{A2}\}$, the server S performs the following steps:

3) Obtains $N_A = C_{A1} \oplus h(x \| e)$, $ID_i = CID_A \oplus N_A$, and checks ID_i, which is obviously valid.
4) Checks if $h_{h(IDi \oplus h(x \| e))}(N_A) = C_{A2}$, which obviously holds. S generates a random nonce N_{AS}, and computes $S_{A1} = h(h(ID_i \oplus h(x \| e)) \| N_{AS} \| N_A)$ and sends $\{ N_{AS}, S_{A1}\}$.

On receiving $\{ N_{AS}, S_{A1}\}$, the attacker U_A performs as follows:

5) Computes $S_{A2} = h(h(x \| e)) \| N_{AS})$ and sends it to S.

On receiving S_{A2}, the server S, performs the following

6) Computes $h(h(x \| e)) \| N_{AS})$ and checks if it is equal to the received S_{A2}, which obviously holds. At last, U_A computes $SK = h(A_i \| h(x \| e) \| N_{AS} \| N_A)$, which is exactly the same session key that the server calculates.

In this way, U_A can successfully impersonate U_i and S without knowing password of U_i, without having mobile device of U_i, and without the imprint of fingerprint F_i of U_i.

3.2 User and Server Impersonation Attack Using Information Extracted from Mobile Device of U_i and an Intercepted Login Request

In Truong et al.'s scheme, it is very easy to relate a mobile device with its corresponding login request $\{CID, e, C_1, C_2\}$ because the random value e is common in both. Consider the situation when an attacker U_A somehow [13-14, 25-26]

successfully extracts the information $\{R_i, V_i, E_i, e, h(.), h_k(.), N\}$ from mobile device of U_i. Now, using the values extracted from mobile device and one of its corresponding intercepted login requests, U_A can obtain secret values shared between U_i and S in the following manner:

1) Obtains $I = h(ID_i \oplus h(x \| e)) \oplus h(x \| e) = E_i \oplus R_i$, using values from mobile device.
2) Obtains $L = ID_i \oplus h(x \| e) = C_1 \oplus CID$, using values from login request.
3) Computes $A_i = h(I) = h(ID_i \oplus h(x \| e))$, which is a secret shared between U_i and S. The value A_i acts as key for keyed hash function $h_k(.)$.
4) Computes $h(x \| e) = I \oplus A_i = [h(ID_i \oplus h(x \| e)) \oplus h(x \| e)] \oplus A_i$, which is another secret value embedded in the mobile device of U_i. The value $h(x \| e)$ has key role in the entire login-authentication phase and legally only S can compute it.

Now, U_A possess $A_i = h(ID_i \oplus h(x \| e))$ and $h(x \| e)$. Thus, he can easily mount user and server impersonation attack on the scheme in similar way as demonstrated in previous subsection:

3.3 Password Guessing Attack

We further extend the previous scenario to password guessing attack. U_A having the values $\{R_i, V_i, e, h(.), h_k(.), N\}$ extracted from the mobile device and possessing $A_i = h(ID_i \oplus h(x \| e))$ and $h(x \| e)$ can easily guess the password of U_i as explained below:

1) Computes $h(x \| e) \oplus E_i$ which needs to be $hpw = h(PW \oplus N) \oplus F_i$.
2) Guesses a password PW^*, computes $h(PW^* \oplus N)$ using N and obtains $F_i^* = hpw \oplus h(PW^* \oplus N)$.
3) Checks if $h_{h(IDi \oplus h(x \| e))}(F_i^*) = V_i$. If so, then U_A now possesses PW as well as the imprint of fingerprint F_i of U_i.

U_A may use these values of U_i to access other servers on behalf of U_i as it is convenient for a user to keep same password for different servers.

4 Conclusion

We have shown that Truong et al.'s improved scheme is insecure for both, server and user. An adversary can cheat both entities of the protocol. An adversary cannot only impersonate as legal communicating parties, he can guess the user's password as well. We have demonstrated that this comes true for the adversary due to information-leak from user's mobile device. As a result, the displacement of Chen et al.'s journey, which was aimed at removing the information-leak (from smart card or mobile device) vulnerability, turns to zero. We have also enlightened the fact that a login request alone is enough to breach the security of the scheme. In our view, such crucial aspects must not be overlooked while improving an existing scheme.

Acknowledgements. This paper is supported by NPST Program by King Saud University Project Number 09-INF883-02.

References

1. Hwang, M.S., Li, L.H.: A New Remote User Authentication Scheme using Smart Cards. IEEE Transactions on Consumer Electronics 46(1), 28–30 (2000)
2. Sun, H.M.: An Efficient Remote User Authentication Scheme using Smart Cards. IEEE Transactions on Consumer Electronics 46(4), 958–961 (2000)
3. Chein, H.Y., Jan, J.K., Tseng, Y.M.: An Efficient and Practical Solution to Remote Authentication: Smart Card. Computers and Security 21(4), 372–375 (2002)
4. Liao, I.E., Lee, C.C., Hwang, M.S.: A Password Authentication Scheme over Insecure Networks. Journal of Computer and System Sciences 72(4), 727–740 (2006)
5. Lee, J.K., Ryu, S.R., Yoo, K.Y.: Fingerprint based Remote User Authentication Scheme using Smart Cards. Electronics Letters 38(2), 554–555 (2002)
6. Lin, C.H., Lai, Y.Y.: A Flexible Biometrics Remote User Authentication Scheme. Computer Standards & Interfaces 27(1), 19–23 (2004)
7. Khan, M.K., Zhang, J.: Improving the Security of 'a Flexible Biometrics Remote User Authentication Scheme'. Comput. Stand. Interfaces 29, 82–85 (2007)
8. Yuan, J., Jiang, C., Jiang, Z.: A Biometric-Based User Authentication for Wireless Sensor Networks. Wuhan University Journal of Natural Sciences 15, 272–276 (2010), http://dx.doi.org/10.1007/s11859-010-0318-2
9. Kumari, S., Gupta, M.K., Kumar, M.: Cryptanalysis And Security Enhancement of Chen et al. 's Remote User Authentication Scheme Using Smart Card. Central European Journal of Computer Science 2(1), C60–75C (2012)
10. He, D., Chen, J., Hu, J.: A Pairing-free Certificateless Authenticated Key Agreement Protocol. International Journal of Communication Systems 25(2), 221–230 (2012)
11. Guo, H., Xu, C., Mu, Y., Li, Z.: A Provably Secure Authenticated Key Agreement Protocol for Wireless Communications. Computers and Electrical Engineering 38, 563–572 (2012)
12. Wang, R.C., Juang, W.S., Lei, C.L.: Provably Secure And Efficient Identification and Key Agreement Protocol with User Anonymity. Journal of Computer and System Sciences 77, 790–798 (2011)
13. Kocher, P.C., Jaffe, J., Jun, B.: Differential power analysis. In: Wiener, M. (ed.) CRYPTO 1999. LNCS, vol. 1666, pp. 388–397. Springer, Heidelberg (1999)
14. Messerges, T.S., Dabbish, E.A., Sloan, R.H.: Examining Smart-card Security under the Threat of Power Analysis Attacks. IEEE Transactions on Computers 51(5), 541–552 (2002)
15. Rhee, H.S., Kwon, J.O., Lee, D.H.: A Remote User Authentication Scheme Without using Smart Cards. Computer Standards and Interfaces 31(1), 6–13 (2009)
16. Chen, C.L., Lee, C.C., Hsu, C.Y.: Mobile Device Integration of a Fingerprint Biometric Remote Authentication Scheme. International Journal of Communication Systems (2011), http://dx.doi.org/10.1002/dac.1277
17. Sun, D.Z., Huai, J.P., Sun, J.Z., Li, J.X.: Cryptanalysis of a Mutual Authentication Scheme Based on Nonce and Smart Cards. Computer Communications 32(6), 1015–1017 (2009)
18. Hsu, C.L.: Security of Chein et al.'s Remote User Authentication Scheme using Smart Cards. Computer Standards and Interfaces 26(3), 167–169 (2004)
19. Ku, W.C., Chen, S.M.: Weaknesses and Improvements of an Efficient Password based Remote User Authentication Scheme using Smart Cards. IEEE Transactions on Consumer Electronics 50(1), 204–207 (2004)
20. Xiang, T., Wong, K.W., Liao, X.: Cryptanalysis of a Password Authentication Scheme over Insecure Networks. Journal of Computer and System Sciences 74(5), 657–661 (2008)

21. Wang, X.M., Zhang, W.F., Zhang, J.S., Khan, M.K.: Cryptanalysis and Improvement on two Efficient Remote User Authentication Scheme using Smart Cards. Computer Standards and Interfaces 29(5), 507–512 (2007)
22. Khan, M.K., Kim, S.K., Alghathbar, K.: Cryptanalysis and Security Enhancement of a 'More Efficient & Secure Dynamic ID-based Remote User Authentication Scheme'. Computer Communications 34(3), 305–309 (2010)
23. Khan, M.K., Zhang, J., Wang, X.: Chaotic Hash based Fingerprint Biometric Remote User Authentication Scheme on Mobile Devices. Chaos, Solitons & Fractals 35(3), 519–524 (2008)
24. Truong, T.T., Tran, M.T., Duong, A.D.: Robust Mobile Device Integration of a Fingerprint Biometric Remote Authentication Scheme. In: Proceedings of 26th IEEE International Conference on Advanced Information Networking and Applications, pp. 678–685 (2012)
25. Bellcore Press Release. New Threat Model Breaks Crypto Codes, Bellcore Press Release (September 1996)
26. Yen, S.M., Joye, M.: Checking Before Output Not Be Enough Against Fault-based Cryptanalysis. IEEE Transactions on Computers 49(9), 967–970 (2002)

Study on the Statistical Test for String Pseudorandom Number Generators

Lequan Min*, Longjie Hao, and Lijiao Zhang

School of Mathematics and Physics
University of Science and Technology Beijing, Beijing 100083, China
minlequan@gmail.com

Abstract. Many fields need random and pseudorandom numbers, especially in cryptographic applications. d-bit segment binary pseudorandom numbers can be more easily used for block encryption. This paper studies on the statistical test for binary d string pseudorandom number generator (PRNG). Three postulates on the randomness for ideal pseudorandom d-bit segment sequences have been proposed. Based on the FIPS140-2 tests, a statistical test suite for d-bit segment sequences generated by PRNG has been proposed. Using the test suite tests the 100 key streams generated by RC4 PRNG and Matlab PRNG, respectively. The test results show that in the two 100 key streams generated via the two PRNGs with different seeds, about 97% 8-bit strings have passed the test suite, respectively. Using the key streams generated via the two PRNGs encrypts an RGB image. The results have shown that the encrypted RGB images have significant stream encryption avalanche effect.

Keywords: Information Theory, Pseudorandom Number String, Randomness Postulate, FIPS 140-2 Test, New Test Standard.

1 Introduction

Pseudorandom numbers are widely used in many fields such as simulations of physical systems[1], cryptography[2], entertainment[3], and computer simulation[4]. John von Neumann was the first contributor in computer based random number generators. Today algorithmic PRNGs have replaced almost all random number tables and hardware random number generators in practical uses.

The well-known public-domain statistical testing packages for RNGs/PRNGs are DIEHARD Test Suite (Marsaglia 1996, [5]), the FIPS140-2 Test Suite, and the SP800-22 Test Suite implemented by the National Institute of Standards and Technology (NIST) of the USA ([6], [7]). DIEHARD Test Suite contains several statistical tests but has drawbacks and limitations. The sequence of tests as well as the parameters of these tests (sample size, etc.) are fixed in the package. The sample sizes are not very large: the entire test suite runs in a few seconds of CPU time on a standard desktop computer[8].

* Corresponding author.

D. Liu et al. (Eds.): BICS 2013, LNAI 7888, pp. 278–287, 2013.

FIPS140-2 test suite consists of four tests: Monobit test, Pork test, Run test and Long Run test. Each test needs a single stream of 20,000 one and zero bits from keystreams generation. Any failure in the required intervals of the tests means the sequence of stream must be rejected. Ref. [9] has analyzed the required intervals of the FIPS140-2 tests.

The NIST 800-22 Test Suite consists of 16 statistical tests that were developed to test the randomness of (arbitrarily long) binary sequences produced by either hardware or software based cryptographic random or pseudorandom number generators [7]. Each statistical test is formulated to test a specific ***null hypothesis*** (H_0): the sequence being tested is random. A significance level (α) can be chosen for the tests. If $P - value \geq \alpha$, then the null hypothesis is accepted; i.e., the sequence appears to be random. Typically, α, is chosen in the range $[0.001, 0.01]$. NIST 800-22 test suite is more strict than the FIPS140-2 test suite. A binary sequence which has passed all tests of FIPS140-2 test suite may not pass all tests in the NIST 800-22 Test Suite.

d-bit segment binary pseudorandom numbers can be more easily used for block encryption. Recently, a novel stream encryption scheme with avalanche effect is introduced. Using this scheme and an ideal pseudorandom number generator to generate d-bit segment binary key streams, one can encrypt a plaintext such that by using any key stream generated from a different seed to decrypt the ciphertext, the decrypted plaintext will become an avalanche-like text which has $(2^d - 1)/2^d$ consecutive one's with a high probability[10].

The aim of this paper is to study the statistical tests for d-bit segment PRNGs. Similar to the Golomb's three postulates on the randomness that pseudorandom sequences should satisfy[11], the postulates on the randomness that d-bit segment pseudorandom sequences have been proposed. Based on the FIPS140-2 tests, a statistical test suite for d-bit segment sequences generated by pseudorandom number generator (PRNG) has been introduced. Using the test suite tests the key streams generated by RC4 PRNG and Matlab PRNG. The results show that they have passed the tests of the test suite.

The rest of this paper is organized as follows. Section 2 introduces the Randomness Postulates on d-bit PRNG. Section 3 discusses the statistical test standards for string pseudorandom number generators. Section 4 gives the examples for RC4 PRNG and Matlab PRNG. Finally, some concluding remarks are given in Section 5.

2 Randomness Postulates on d-Bit Segment PRNGs

A binary random sequence generation is like the flying game. If one tosses a fair coin, there will be two possible outcomes: the face-up side is head or tail after the coin has landed on the ground. There is a 1/2 probability that one guesses correctly which side of the coin will be the face-up side.

If one tosses a fair polyhedron with 2^d faces, there will be 2^d possible outcomes: the face-up side is one of the 2^d faces after the polyhedron has landed on the ground. There is only a $1/2^d$ probability that one guesses correctly which face of the polyhedron will be the face-up side.

Similarly to the fair polyhedron flying game and based on the Golomb's three postulates on the randomness that pseudorandom sequences should satisfy [11], we can propose the following postulates on the randomness that pseudorandom d-bit segment sequences should satisfy.

Postulates. An ideal PRNG which generates binary d-bit key streams has the following properties:

(1) **Balance Property.** In one period of a pseudorandom key streams generated by the PRNG, if the period $p = n \times 2^d$, then the number of each different d-bit segment is equal to n. If the period p is not an integer multiple of 2^d, then the difference between the numbers of different d-bit segments is at most one.

(2) **Run Distribution Property.** In a pseudorandom sequence with the length of $n2^d$, the frequency of runs of length k[1] is $1/2^{kd}$. The numbers of the same length $\{0, 1, \cdots, 2^d - 1\}$ runs are the same.

(3) **Ideal Autocorrelation Property.** Change the d-bit binary sequence ϵ with length n into its corresponding decimal number sequence. Denote by

$$\epsilon = \epsilon_1 \epsilon_2 \cdots \epsilon_n.$$

The autocorrelation function $AC(k)$ has two values for a period. Explicitly:

$$\begin{aligned} AC(k) &= \frac{1}{p} \sum_{i=1}^{p} (1 - |sign(\epsilon_i - \epsilon_{i+k})|) \\ &= \begin{cases} 1 & for\ k = np \\ \dfrac{1}{2^d} & otherwise \end{cases} \end{aligned}$$

3 Statistical Test Suite

Similar to the Monobit test, Pork test, Run test and Longest Run test for binary $\{0, 1\}$ sequence, here we propose the Monobit test, Pork test, Run test and Longest Run test for d-bit segment binary sequence as follows.

(1) Change the d-bit binary sequence ϵ with length n into its corresponding decimal number sequence $\{0, 1, \cdots, 2^d - 1\}^n$. Denote by

$$\epsilon = \epsilon_1 \epsilon_2 \cdots \epsilon_n. \tag{1}$$

(2) For any $\epsilon_i \in \epsilon$, denote $2^d - 1 - \epsilon_i$ by $\sim \epsilon_i$.

[1] k consecutive same d-bit strings is called a run with length k.

(3) For each fixed i, taking ϵ_i and $\sim \epsilon_i$ consecutively from ϵ. Then we obtain $2^d/2$ new sequences and denote them by

$$E_i = E_{n_1} E_{n_2} \cdots E_{n_i}, i = 1, 2, \cdots, 2^d/2. \tag{2}$$

Monobit Test. For any fixed i and E_i, replace $\epsilon_i \in E_i$ by 1, and $\sim \epsilon_i$ by zero. Denote the new sequence by

$$\tilde{\epsilon}_i = \tilde{\epsilon}_{n_1} \tilde{\epsilon}_{n_2} \cdots \tilde{\epsilon}_{n_i}.$$

Denote $X_k = 2\tilde{\epsilon}_{n_k} - 1$, then $S_{n_i} = X_1 + X_2 + \cdots X_{n_i} = 2(\tilde{\epsilon}_{n_1} + \tilde{\epsilon}_{n_2} + \cdots + \tilde{\epsilon}_{n_i}) - n_i$. *Assume* $\tilde{\epsilon}_i$ is a sequence of independent identically distributed Bernoulli random variables, then[7]

$$\frac{S_{n_i}}{\sqrt{n_i}} \sim N(0, 1)$$

where $N(0, 1)$ is a standard normal distribution.

The confident interval of $S'_{n_i} = \tilde{\epsilon}_{n_1} + \tilde{\epsilon}_{n_2} + \cdots + \tilde{\epsilon}_{n_i}$ with significant level α is given by

$$\frac{n_i}{2} - \frac{\sqrt{n_i}}{2} Z_{\frac{\alpha}{2}} \leq S'_{n_i} \leq \frac{n_i}{2} + \frac{\sqrt{n_i}}{2} Z_{\frac{\alpha}{2}}$$

where $Z_{\frac{\alpha}{2}}$ (Matlab command $norminv(1 - \alpha/2)$) is the inverse of the normal cumulative distribution function. In the case $n = 10000 \times 2^d$, $n_i = 20000$. Let $\alpha = 0.0001$, the calculated result is given in the second column in Table 1 which is the same as the required interval given by the FIPS 140-2 test.

Run Test. Let

$$E_i = E_{n_1} E_{n_2} \cdots E_{n_i}, i = 1, 2, \cdots, 2^d/2$$

be defined by (2).

(a) Lengths of Runs are less than 6

Pick up the runs of length k from an ϵ_i and $\sim \epsilon_i$ bit streams and construct a new bit stream. Replace each ϵ_i run of length k by 1, and $\sim \epsilon_i$ run of length k by 0. Then we obtain an one and zero bit sequence $\epsilon' = \epsilon'_1 \epsilon'_2 \cdots \epsilon'_{n'_i}$ where n'_i is the length of the new bit string. Assume ϵ' is a sequence of independent identically distributed Bernoulli random variables, then similar to the analysis in the case of the Monobit test, we obtain

$$\frac{S_{n'_i}}{\sqrt{n'_i}} \sim N(0, 1).$$

The confident interval of $S'_{n'_i} = \epsilon'_1 + \epsilon'_2 + \cdots \epsilon'_{n'_i}$ with significant level α is given by

$$\frac{n'_i}{2} - \frac{\sqrt{n'_i}}{2} Z_{\frac{\alpha}{2}} \leq S'_{n'_i} \leq \frac{n'_i}{2} + \frac{\sqrt{n'_i}}{2} Z_{\frac{\alpha}{2}}.$$

For an ideal ϵ_i and $\tilde{\epsilon}_i$ d-bit pseudorandom stream, the length n_i' of a bit sequence ϵ' generated via the runs of length k should be equal to $n/2^{d+k}$. In the case $n = 10000 \times 2^d$, $n_i' = 10000/2^k$. Let $\alpha = 0.0001$, the calculated confident intervals are listed in the second column in Table 1.

(b) All Runs are larger than 5

Picking up all the runs whose length $k's$ are larger than 5 forms a sequence. Using the following rules to change it into a new sequence consisting of $\{0, 1\}$.

If the member E_{n_k} of a run is less than $2^d/2 - 1$, then replace the run by 0. Otherwise replace the run by 1.

Denote the new sequence by $\epsilon' = \epsilon_1'\epsilon_2' \cdots \epsilon_{n'}'$, where n' is the length of the new bit string. Assume ϵ' is a sequence of independent identically distributed Bernoulli random variables, then similar to the analysis in the case of the Monobit test, we obtain

$$\frac{S_{n'}}{\sqrt{n'}} \sim N(0, 1).$$

The confident interval of $S_{n'}' = \epsilon_1' + \epsilon_2' + \cdots \epsilon_{n'}'$ with significant level α is given by

$$\frac{n'}{2} - \frac{\sqrt{n'}}{2} Z_{\frac{\alpha}{2}} \leq S_{n'}' \leq \frac{n'}{2} + \frac{\sqrt{n'}}{2} Z_{\frac{\alpha}{2}}.$$

In the case $n = 10000 \times 2^d$, the length n' of the sequence ϵ' length k should be equal to $10000/2^6$. Let $\alpha = 0.0001$, the calculated confident intervals are listed in the second column in Table 1.

Poker Test. For each fixed

$$E_i = E_{n_1} E_{n_2} \cdots E_{n_i}, i = 1, 2, \cdots, 2^d/2.$$

replace $\epsilon_i \in E_i$ by 1, and $\sim \epsilon_i$ by zero. Denote the new sequence by

$$\tilde{\epsilon}_i = \tilde{\epsilon}_{n_1} \tilde{\epsilon}_{n_2} \cdots \tilde{\epsilon}_{n_i}.$$

Divide a sequence of $\tilde{\epsilon}_i$ into fix$(n_i/4)$ consecutive 4-bit segments. Denote $f(i)$ to be the number of each 4-bit value $i - 1$, where $1 \leq i \leq 16$ and $m = fix(n_i/4)$. Then calculate the following:

$$N = \frac{16}{m} \sum_{i=1}^{16} f(i)^2 - m. \tag{3}$$

Assume the the 4-bit segments are distributed independently and identically. Then the statistic quality

$$\begin{aligned} N &= \frac{16}{m} \sum_{i=1}^{16} f(i)^2 - m \\ &= \sum_{i=1}^{16} \frac{m}{1/16} (\frac{f(i)}{m} - \frac{1}{16})^2 \end{aligned}$$

obeys χ^2 distribution. Hence the confident interval of the statistic quality of N with significant level α is given by

$$\chi^2_{1-\frac{\alpha}{2}}(15) \leq N \leq \chi^2_{\frac{\alpha}{2}}(15),$$

where $\chi^2_\alpha(15)$ (Matlab command chi2inv(α,15)) is the inverse of the χ^2 cumulative distribution function with free degree 15. In the case $n = 10000 \times 2^d$, $m = 5000$. Let $\alpha = 0.0001$, the calculated confirmation interval is given in Table 1.

Table 1. The required intervals of the Monobit Test, Pork Tests, Run Test. Here MT, PT, and LT represent the Monobit Test, Pork Test and Long Run Test, respectively. The significant level $\alpha = 0.0001$. The k represents the length of the run of a tested sequence.

Test Item	Test Standard Required Intervals	Randomness Postulates
MT	9,725∼10,275	10000
PT	2.16∼46.17	χ^2distribution
LT	< 26	—
k	Run Test	Run Test
1	2,362∼2,638	2,500
2	1,153∼1,347	1,250
3	556∼694	625
4	264∼361	313
5	122∼191	156
6+	122∼191	156

4 Statistical Tests

4.1 Statistical Tests for RC4 Algorithm

RC4 was designed by Ron Rivest of RSA Security in 1987, and widely used in popular protocols such as Secure Sockets and computer systems.

The RC4 algorithm generates 8-bit pseudorandom streams. Using the Matlab command, this algorithm can be described as follows.

```
L=8; K=randint(1,2^L, [0 2^L-1]);
S=[0:2^L-1]; j=0;
for i=1:2^L
j=mod(j+S(i)+K(i),2^L);
Sk=S(j+1); S(j+1)=S(i); S(i)=Sk;
end
l=1; C=zeros(1,20000/8+10); j=0;i=0; k=1;
for l=1:10000×2^d
i=mod(i+1,2^L); j=mod(j+S(i+1),2^L);
Sk=S(j+1); S(j+1)=S(i+1); S(i+1)=Sk;
C(k)=S(mod(S(j+1)+S(i+1),2^L)+1);
k=k+1;
end
```

Table 2. The tested Mean ± SD of all $E_i's$ defined by (2) for the 100 8-bit key streams with length 10000×2^8 generated by the RC4 PRNG the Matlab PRNG, respectively. Here MT, PT, and LT represent the Monobit Test, Pork Test and Long Run Test, respectively; k represents the length of the run of a tested sequence.

Test item	bits $\{\varepsilon_i, \sim \varepsilon_i\}$	Random Postulates	RC4 Mean ± SD	MATLAB Mean ± SD
MT	ε_i	10000	10000± 99.583	10001±99.80
	$\sim \varepsilon_i$	10000	9999.9±100.18	9998.5± 99.169
PT	–	χ^2distribution	14.99±5.4847	14.965± 5.444
LT	ε_i	−−	13.62±1.8923	13.62± 1.8623
	$\sim \varepsilon_i$	−−	13.617±1.8576	13.62±1.8437
k			Run Test	
1	ε_i	2500	2500.3±49.517	2500.2±50.038
	$\sim \varepsilon_i$	2500	2500.1± 49.969	2496.6±50.081
2	ε_i	1250	1250.2 ± 32.799	1249.7± 32.492
	$\sim \varepsilon_i$	1250	1249.9± 33.146	1249.8±32.615
3	ε_i	625	624.97± 23.333	625.24± 23.448
	$\sim \varepsilon_i$	625	625.42± 23.338	624.86±23.088
4	ε_i	313	312.26 ±16.799	312.17 ±16.81
	$\sim \varepsilon_i$	313	312.28±16.616	312.59 ±16.79
5	ε_i	156	155.95 ±12.181	156.09 ± 12.087
	$\sim \varepsilon_i$	156	156.17 ±11.914	156.34 ±12.057
6^+	ε_i	156	156.39 ± 11.903	156.15 ± 11.801
	$\sim \varepsilon_i$	156	156.13 ±11.819	156.38± 11.982

Now use the statistical tests to test the 100 keystreams randomly generated by the command K=randint(1,2^L, [0 2^L-1]) in RC4 algorithm. There are about 3% $E_i's$ cannot pass the all tests.

Calculate the means and the standard deviations (SD) of the test items in all $E_i's$ defined by (2). The results are shown in 4th column in Table 2. Observe that the keystreams have sound 8-bit segment randomness.

4.2 Statistical Tests for Matlab Algorithm

Use the Matlab command randint(2^8*10000,1,[0,2^8-1]) one 100 times to generate 100 8-bit segment keystreams. Use the statistical tests to test the 100 keystreams. There are about 3% $E_i's$ cannot pass the all tests. Calculate the means and the standard deviation (SD) of the test items in all $E_i's$ defined by (2). The tested results are shown in 5th column in Table 2. Observe that the keystreams have sound 8-bit segment randomness.

4.3 Encryption Tests

Definition([10]) Let $\mathcal{P} = \{p_1, p_2, \cdots, p_n\}$ be a binary key stream with d-bit segments generated by a PRNG, $\mathcal{M} = \{m_1, m_2, \cdots, m_n\}$ a binary plaintext

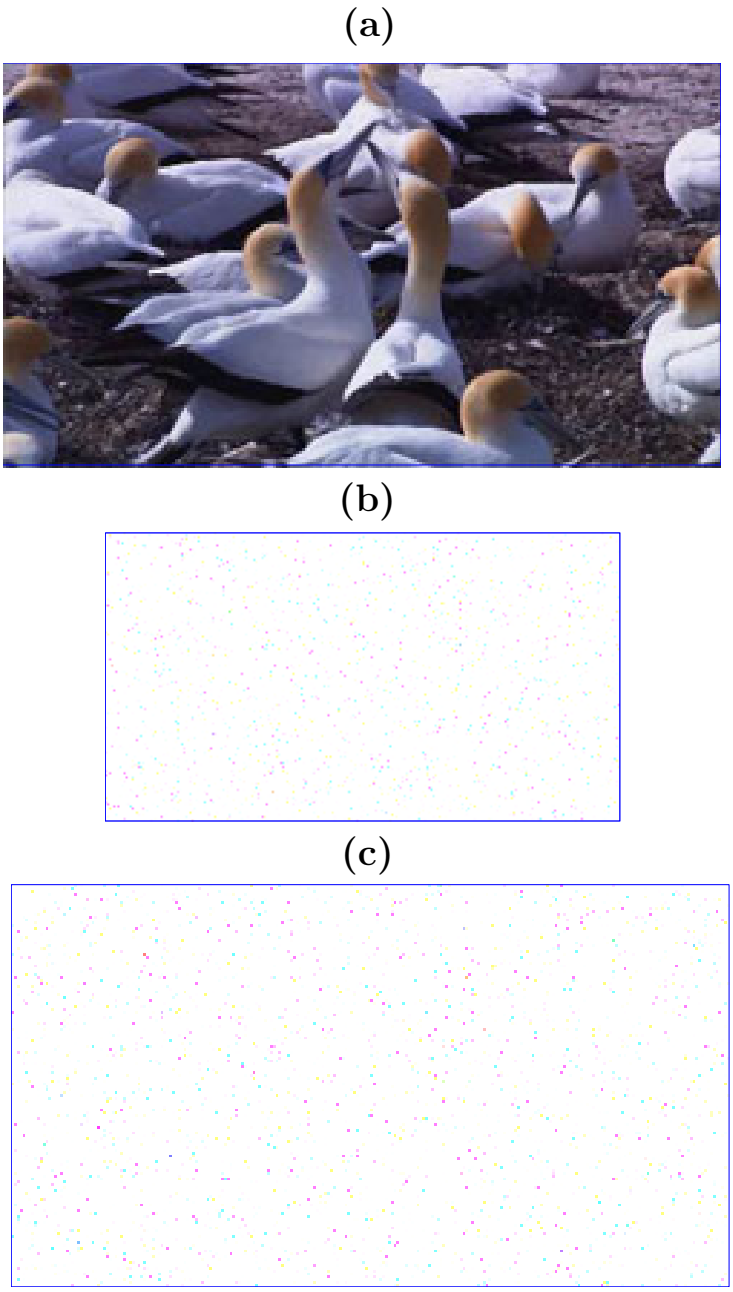

Fig. 1. (a) Original image (extracted from Windows7_OS video frequency: wild aninal.wmv). (b) a decrypted image via a key stream generated by RC4 PRNG with a different "random" initial condition randint(1,256,[0 255]), (c) a decrypted image via a key stream generated by Matlab PRNG with a different "random" stream randint (1, 840000,[0, 255]).

stream, and $\mathcal{C} = \{c_1, c_2, \cdots, c_n\}$ a ciphertext stream. Then, the stream encryption scheme with avalanche effect (SESAE) is described as follows.

(1) The ciphertext $\mathcal{C} = E(\mathcal{M}, \mathcal{P})$ is defined by

$$c_i = \begin{cases} p_i \ if \ m_i = 0, \\ \sim p_i \ if \ m_i = 1, \end{cases} \tag{4}$$

where $\sim p_i$ is defined to be the bit string obtained by replacing all 0s in p_i with 1s, and all 1s in p_i with 0s.

(2) The corresponding decrypted plaintext $\mathcal{M} = E^{-1}(\mathcal{C}, \mathcal{P})$ is determined by

$$m_i = \begin{cases} 0 \ if \ c_i = p_i, \\ 1 \ if \ c_i \neq p_i. \end{cases} \tag{5}$$

Figure 2(a) shows an RGB image birds extracted from Windows7_OS video frequency wild aninal.wmv, whose size is 250×140 pixels. Use it as a plaintext with a $250 \times 140 \times 3 \times 8 = 840000$ binary codes. Using the key streams generated by the two PRNGs encrypts the plaintext, we can obtain the decrypted texts without any errors. Using 100 key streams generated via the two PRNGs with randomly disturb initial conditions decrypt the encrypted image, respectively. Avalanche effects appear. The maximum number and minimum number of zero codes in the two 100 decrypted images are 1815 (the corresponding image is shown in Fig. 1(b)), 1623 and 1849 (the corresponding image is shown in Fig. 1(c)), 1632, respectively. Significant effects have appeared

5 Conclusions

The first new result of this paper is to propose the three randomness postulates on ideal binary d-bit Segment PRNGs, which is a generalization to Golomb's postulates on the randomness for binary pseudorandom sequences.

The second new result is to propose the test suite for binary d-bit segment PRNGs. When $d = 2$, this suite can be considered to be the FIPS140-2 test suite for binary PRNGs. Using the similar approaches proposed in Section 3, one can generalize the SP800-22 test suite for binary d-bit segment PRNGs. We will discuss this issue elsewhere. "The DIEHARD test suite is not very stringent and the user has little flexibility for changing that. The package also requires that the random numbers to be tested are in a binary file in the form of 32-bit (exactly) integers. This file is to be passed to the testing procedures. This setup is quite restrictive"[8].

The third new result is to use the test suite to test the randomness for the RC4 8-bit segment PRNG and the Matlab 8-bit segment PRNG. Further simulations show that the two PRNGs are able to generate the avalanche effect stated in ref. [10].

The results of this paper suggest that the further research along this line is promising.

Acknowledgments. The authors would like to thank the anonymous referees for their valuable comments. This project is supported by the National Natural Science Foundation of China (Grant Nos. 61074192, 61170037).

References

1. Binder, K., Heermann, D.W.: Monte Carlo Simulation in Statistical Physics, An Introduction, 4th edn. Springer (2002)
2. Ferguson, N., Schneier, B., Kohno, T.: Cryptography Engineering: Design Principles and Practical Applications. Wiley Publishing (2010)
3. Wegenkittl, S.: Gambling Tests for Pseudorandom Number Generator. Mathematics and Computers in Simulation 55, 281–288 (2001)
4. Knuth, D.E.: The Art of Computer Programming, Seminumerical Algorithms, 3rd edn., vol. 2. Addision-Wesley, Boston (1997)
5. Marsaglia, G.: Diehard test suite (1996), `http://www.stat.fsu.edu/pub/diehard/`
6. NIST: FIPS PUB 140-2, Security Requirements for Cryptographic Modules. NIST, Gaithersburg, MD (2001)
7. Rukhin, R., Soto, J., Nechvatal, J., et al.: A Statistical Test Suite for Random and Pseudorandom Number Generator for Cryptographic Applications. NIST Special Publication (2001)
8. Ecuyer, P.L., Simard, R.: TestU01: A C Library for Empirical Testing of Random Number Generators. ACM Transactions on Mathematical Software 33, 1–40 (2007)
9. Min, L., Chen, T., Zang, H.: Analysis of fips 140-2 test and chaos-based pseudorandom number generator. In: The Proc. of the 5th Chaotic Modeling and Simulation International Conference, Antens, Greece, June 12-15, pp. 345–352 (2012)
10. Min, L., Chen, G.: A novel stream encryption scheme with avalanche effect. European Physics J. B. (submitted, 2013), `http://www.paper.edu.cn/releasepaper/content/201301-1185`
11. Golomb, S.W.: Shift Register Sequences. Laguna Hills, Aegean (1982)

A Novel Adaptive Tropism Reward ADHDP Method with Robust Property

Jing Chen[1] and Zongshuai Li[2]

[1] School of Information Technology Engineering,
Tianjin University of Technology and Education, 300222 Tianjin, China
[2] Aeronautical Automation College, Civil Aviation University of China, 300300 Tianjin, China
jingchen0828@139.com, lizongshuai8@163.com

Abstract. According to the autonomous learning problem for the two-wheeled self-balancing robot, a novel adaptive tropism reward ADHDP with robust property was proposed, which can get the online adaptive tropism reward information. The whole learning system used a form of three networks, including action neural networks (ANN), adaptive tropism reward neural networks (ATRNN) and critic neural networks (CNN). The design of adaptive tropism reward neural networks took example from the learning mechanism of actor-critic structure. And through the primary binary reward signal, the continuous secondary reward signal can be got adaptively and become the basis of critic neural networks learning. Through the simulation in two-wheeled self-balancing robot, we can conclude that the proposed learning mechanism is effective and has a better progressive learning property. The optimal learning performance is got finally. Through the comparison of statistical experiment, it can be found that the proposed method has a certain anti-noise ability and the robust learning performance is better.

Keywords: Action-dependent heuristic dynamic programming (ADHDP), Two-wheeled self-balancing robot, Autonomous learning, fixed-point balance, robust learning.

1 Introduction

Action-dependent heuristic dynamic programming (ADHDP) method is a kind of adaptive dynamic programming (ADP) method, and it don't need to know the model information during learning, so it is a kind of model-free autonomous learning method. Although the design of the reward function is always 0-1 function or some designed function [1].

In the 1990s, researchers in hierarchy reinforcement learning proposed that during reinforcement the single reward prediction can be replaced by the combination of various reward prediction. Kimura and Kobayashi proposed the idea of hierarchy reinforcement learning, and applying the Q-learning to implement the high-level reinforcement learning and with the local linear Actor-Critic controller to implement the low-level learning, and using this method in the problem of cart-pole control, but

D. Liu et al. (Eds.): BICS 2013, LNAI 7888, pp. 288–295, 2013.

that the learning speed of the proposed method is not better than the common non-hierarchy RL[2,3]. In 2002, Li etc. apply the hierarchy reinforcement learning method in the multi-agent scheduling system [4]. And in 2011, He Haibo etc. [5] proposed a three-network architecture for on-line learning and optimization based on adaptive dynamic programming combining the original reward signal and internal reward signal, and made some simulation in the cart-pole system and three-level inverted pendulum system, but the detail theory validation was not enough. In 2012, S. Li etc. proposed the similar three-network architecture adaptive dynamic programming method with the multiple target and multiple scale representation and made some proof [6]. Botvinick and Barto have studied the neurophysiological principle of hierarchy organization [7], and two kinds of TD prediction error were defined. They proposed that the prefrontal cortex play an important part in the hierarchy reinforcement learning.

Inspired by the hierarchy of reinforcement learning and the neurophysiological principle, we proposed a kind of on-line adaptive tropism reward production mechanism on the basis of ADHDP method. For an agent, the proposed autonomous learning system made the tropism reward come into being adaptively. The whole system included three networks, separately named as action neural networks (ANN), adaptive tropism reward neural network (ATRNN) and the critic neural networks (CNN), and that the proposed learning system can get the internal secondary reward reinforcement signal through the primary reinforcement signal, and then get the aims of on-line learning, optimization and control.

2 Architecture Design of the Adaptive Tropism Reward System

The basis thought of the proposed adaptive tropism reward system is to built two prediction networks for the agent, one is for prediction of the primary reward signal, and another is for the continue tropism reward signal. The whole learning architecture appears as a hierarchical style, which is shown in Figure 1.

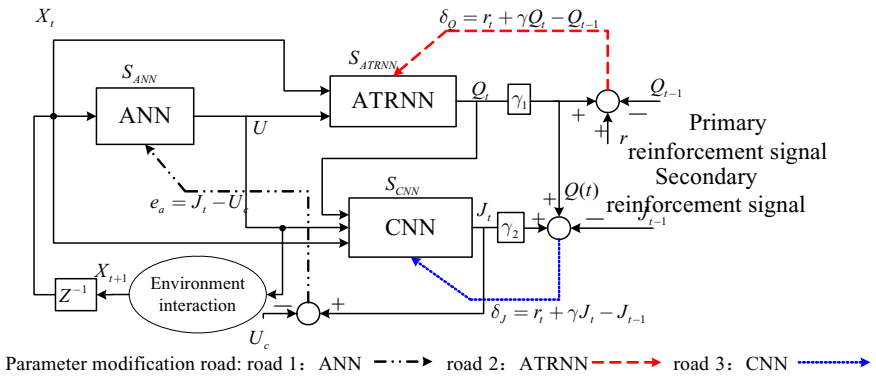

Fig. 1. Schematic of on-line adaptive tropism reward learning mechanism

In Figure 1, $X^c = [X^{a\mathrm{T}}, U^{\mathrm{T}}, Q^{\mathrm{T}}]^{\mathrm{T}}$ and the tropism reward function $Q(t)$ is the estimation of future reward discount sum, and the output of the CNN $J(t)$ is the estimation of future tropism reward discount sum, such as formula (1) and (2).

$$Q(t) = E\left\{r(t+1) + \gamma_1 r(t+2) + \gamma_1^2 r(t+3) + \cdots\right\} \tag{1}$$

$$J(t) = E\left\{Q(t+1) + \gamma_2 Q(t+2) + \gamma_2^2 Q(t+3) + \cdots\right\} \tag{2}$$

3 On-Line Adaptive Learning and Modification of Tropism Reward Neural Networks

The whole learning system contains the modification of three networks, as shown in Figure 1, and the modification error for ANN, ATRNN and CNN are shown in formula (3-5).

$$e_{ANN}(t) = J(t) - U_c(t) \quad E_{ANN}(t) = \frac{1}{2} e_{ANN}{}^2(t) \tag{3}$$

$$e_{QNN}(t) = r(t) + \gamma_1 Q(t) - Q(t-1) \quad E_{QNN}(t) = \frac{1}{2} e_{QNN}{}^2(t) \tag{4}$$

$$e_{CNN}(t) = Q(t) + \gamma_1 J(t) - J(t-1) \quad E_{CNN}(t) = \frac{1}{2} e_{CNN}{}^2(t) \tag{5}$$

During the learning process, the primary reward signal $r(t)$ can be seen as the high-level cognition, and the "good and bad" or "success and failure" could be denoted by the simple binary signal 0 and -1. The secondary reinforcement signal $Q(t)$ is a continuous value containing more information, and is used to improve the learning and generalization performance. The modification rule for ANN, ATRNN and CNN (denoted by $S_{ANN}, S_{ATRNN}, S_{CNN}$) can be denoted as formula (6)~(8).

$$\Delta S_{ANN}(t) = -\alpha_a \frac{\partial E_{ANN}(t)}{\partial S_{ANN}(t)} = -\alpha_a \frac{\partial E_{ANN}(t)}{\partial J(t)} \frac{\partial J(t)}{\partial U(t)} \frac{\partial U(t)}{\partial S_{ANN}(t)} \tag{6}$$

$$\Delta S_{ATRNN}(t) = -\alpha_q \frac{\partial E_{ATRNN}(t)}{\partial S_{ATRNN}(t)} = -\alpha_q \frac{\partial E_{ATRNN}(t)}{\partial Q(t)} \frac{\partial Q(t)}{\partial S_{ATRNN}(t)} \tag{7}$$

$$\Delta S_{CNN}(t) = -\alpha_c \frac{\partial E_{CNN}(t)}{\partial S_{CNN}(t)} = -\alpha_c \frac{\partial E_{CNN}(t)}{\partial J(t)} \frac{\partial J(t)}{\partial S_{CNN}(t)} \tag{8}$$

4 Neural Networks Implementation and Algorithm Step

The proposed three-network adaptive action critic learning mechanism is different with the traditional way, and the critic networks and the adaptive tropism reward networks are shown in Figure 2. and the algorithm can be implemented by the following steps.

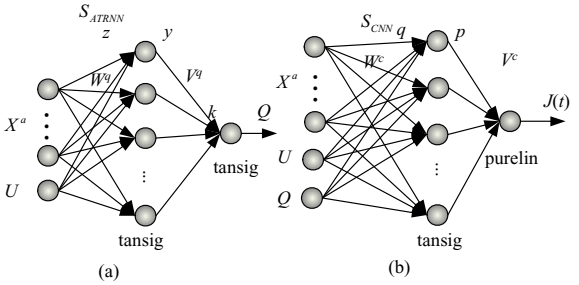

Fig. 2. Realization of adaptive tropism reward NN and CNN

Step 1: Initialization of the ANN, ATRNN and CNN weights, set the maximum of the trial and run step $trial_{\max}$, $step_{\max}$, Initialization of the state variables and normalization;

Step 2: If $trial < trial_{\max}$, $Q(0) = 0, J(0) = 0$, and $step = 1$, the system state back to the initial state.

Step 3: If $step < step_{\max}$, loop

(1) Based on the feedback states, get the primary reward signal r, decrease the learning step factor, and calculate U through ANN, and calculate the tropism reward Q and the output of CNN J;

(2) Modify the weights of ATRNN based on formula (7);

(3) Modify the weights of CNN based on formula (8);

(4) Modify the weights of ANN based on formula(6). Output the optimal action U, and act on the agent, transform to the next state;

(5) If the feedback system state is not beyond range, then $step \leftarrow step + 1$, if $step = step_{\max}$, then get out from the loop, and stop learning. Otherwise, $trial \leftarrow trial + 1$, go back to **Step 2**; if $trial = trial_{\max}$, the learning process stop with failure, and the process is over.

Step 4: Stop

In order to make the weights in the proper range, usually the weights should be normalized in the modification process, such as:

$$W(t+1) = \frac{W(t) + \Delta W(t)}{\left\| W(t) + \Delta W(t) \right\|_1}, V(t+1) = \frac{V(t) + \Delta V(t)}{\left\| V(t) + \Delta V(t) \right\|_1} \tag{9}$$

Where, $\left\| \mathrm{A} \right\|_1 = \max(\mathrm{sum}(\mathrm{abs}(\mathrm{A})))$.

5 Experiment Study in the Rigid TWSBR

5.1 Two-Wheeled Self-balancing Robot

We did the experiment in the rigid two-wheeled self-balancing robot for the study, and the robot system diagram is shown in Figure 3.

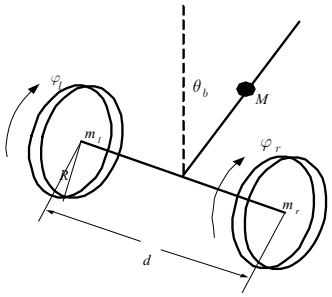

Fig. 3. Robot system diagram

Where, $q = (\theta_b, \varphi_l, \varphi_r, \dot{\theta}_b, \dot{\varphi}_l, \dot{\varphi}_r)^{\mathrm{T}}$ is the system state variables, respectively denoting as inclination, left and right wheel angular displacement, inclination angular velocity, left and right wheel; M is the robot body mass; m_l and m_r are the mass of the left and right wheels; R denotes the wheel's radius; d denotes the distance of the two wheels.

5.2 Fixed-Point Balance Learning Experiments

Using the proposed learning mechanism, we did the fixed-point balance learning experiment on the rigid TWSBR system.

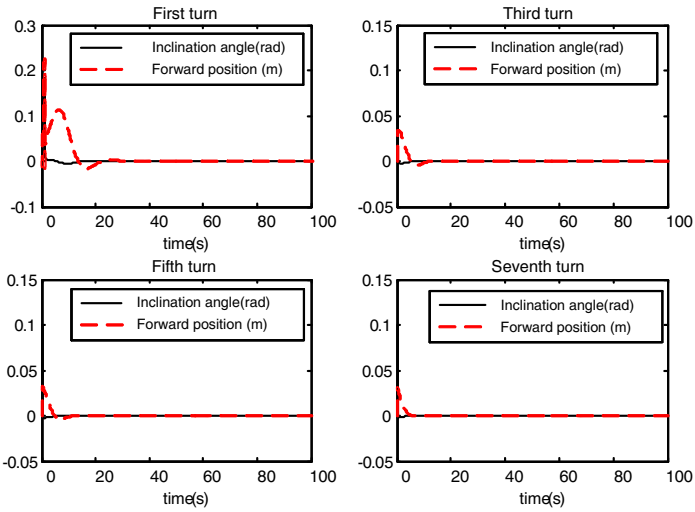

Fig. 4. Gradual optimization and balance performance

During the learning process, we choose the following parameters: $n = 4$, ANN, ATRNN and CNN are respectively 4-20-1, 5-20-1 and 6-20-1 MLP network,

$step_{\max} = 10000$, $trial_{\max} = 500$, $\gamma_1 = \gamma_2 = 0.95$, The feedback state is $X^a = X_1 = [\theta_b, \dot{\theta}_b, R(\varphi_l + \varphi_r)/2, R(\dot{\varphi}_l + \dot{\varphi}_r)/2]^{\mathrm{T}}$, the initial inclination angle is $0.1rad$, and the sampling time is $0.01s$. $\tau_l = u_1 + u_2; \tau_r = u_1 - u_2$, where, u_1 is the forward control, and u_2 is the rotated control.

u_1 is the output of the ANN neural network, u_2=0 . After at least 3 times' trials the robot can acquire the balance skill. In the initial experiments, the robot can maintain balance and return to the initial position after about 30s. Get the fixed-point balance skills, to continue the learning process a number of times, in the end, with the same initial state, the robot will be balanced and the robot go back to the initial position after about 5s. Fixed-point balance learning simulation results of turn 1,3,5,7 are drawn, and the gradual optimization performance is shown in Figure 4.

5.3 Robustness Testing Experiment

In the real world, because the detector itself performance or unpredictable changes in the environment may cause disruption to the robot, in order to enable the robot to complete motion balancing control tasks, the robot must have a certain degree of robustness. In order to simulate real-world environments, we add different Gaussian noise amplitude signal to the control input to verify robust learning performance to the measurement noise of the proposed learning model.

Suppose that there is Gaussian white noise during the detecting of the inclination angle, i.e. $\theta_b^{\ c} = \theta_b^{\ s} + \sigma \cdot N(0,1)$. $\theta_b^{\ s}$ denotes the actual angle value, while $\theta_b^{\ c}$ denoted the measured values.

In order to test the control performance in the existing of measurement noise, we made some comparison with the traditional the ADHDP method. The comparisons are shown in Figure 5 a) b).

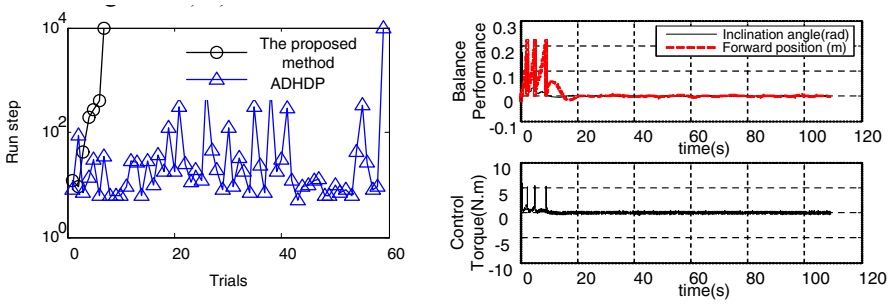

a) learning performance comparison b) Performance of the proposed method

Fig. 5. Performance comparison with the existing of measure noise

Results can be seen from Figure 5, in the presence of measuring noise cases, Adaptive increase in rewards network makes the whole learning system with fast learning speed, its gradual learning performance is better than traditional learning methods.

In order to have a quantitative description of the learning ability in noisy, we do a statistical experiment. Initial angle is the random value between [-0.1,0.1]rad. In the same learning parameter situation, respectively in no noise, and Gaussian noise ($\sigma = 0.001$), and Gaussian noise ($\sigma = 0.005$), Gaussian noise ($\sigma = 0.01$), using the traditional method and the proposed method respectively for 20 times independent experiment, we calculate out the average test number and make some comparison both in measurement noise exists situation. Statistics results are shown in Table 1.

Table 1. Statistical data of Number of Trial in different measure noise

Method / Noise	The proposed method		The traditional ADHDP method	
	Success rate	Average trials	Success rate	Average trials
No nosise	100%	7.3	100%	6.1
$\sigma = 0.001$	100%	7.25	100%	41.4
$\sigma = 0.005$	100%	7.5	100%	94.5
$\sigma = 0.010$	100%	7.75	95%	159.8

Through Table 1 we can conclude that, the noise amplitude's increase make the trials increase, but the learning speeds of the proposed method is not sensitive to measurement noise. And when measuring noise increases, the increase of the trial number has been slow. Under the Gaussian noise $\sigma = 0.01$ conditions, learning success 100% has been ensured, and only needs average 7.75 trials. While with the conventional methods we made 20 times test and in the learning process, under Gaussian noise conditions, 1 experiment has been tested no acquisition balance for 500 times, failed to learn, learning success rate of 95%, after up to 159.8 test in order to learn successfully.

6 Conclusion

A novel on-line adaptive tropism reward ADHDP method is presented, which is an adaptive critic method, through the introduction of adaptive tropism reward network the online adaptive learning mechanism can make the learning system get the orientation information adaptively, thus the learning effect is improved. Through the simulation in rigid two-wheeled self-balancing robot, we can conclude that the proposed learning mechanism is effective and has a better progressive learning property. This method does not require mathematical models of systems, and can achieve a fixed-point balance control. The optimal learning performance is got finally. The proposed method is a kind of model-free method, which is the advantage, and we don't need to know the model of the robot system. Through the comparison of statistical experiment, it can be found that the proposed bionic autonomous learning method has a better robust learning performance.

References

1. Wang, Z.-Y., Dai, Y.-P., Li, Y.-W., et al.: A kind of utility function in adaptive dynamic programming for inverted pendulum control. In: 2010 International Conference on Machine Learning and Cybernetics (ICMLC), pp. 1538–1543 (2010)
2. Doya, K.: Efficient nonlinear control with actor–tutor architecture. In: Mozer, M.C., Jordan, M.I., Petsche, T. (eds.) Advances in Neural Information Processing Systems, vol. 9, pp. 1012–1018. MIT Press, Cambridge (1997)
3. Doya, K.: Reinforcement Learning in Continuous Time and Space. Neural Computation 12(1), 219–245 (2000)
4. Li, X., Yang, Y., Xu, X.: Multiagent AGV dispatching system based on hierarchical reinforcement learning. Control and Decision 17(3), 292–296 (2002)
5. He, H., Ni, Z., Fu, J.: A three-network architecture for on-line learning and optimization based on adaptive dynamic programming. Neurocomputing 78(1), 3–13 (2012)
6. Liu, B., Li, S., Lou, Y., et al.: A hierarchical learning architecture with multiple-goal representations and multiple timescale based on approximate dynamic programming. Neural Computing & Applications, 1–17 (2012)
7. Botvinick, M.M., Niv, Y., Barto, A.C.: Hierarchically organized behavior and its neural foundations: A reinforcement learning perspective. Cognition 113(3), 262–280 (2009)

A Novel Clinical Expert System for Chest Pain Risk Assessment

Kamran Farooq[1], Amir Hussain[1], Hicham Atassi[1,2], Stephen Leslie[3], Chris Eckl[4], Calum MacRae[5], and Warner Slack[6]

[1] Department of Computing Science and Mathematics, University of Stirling, FK9 4LA, UK
[2] Brno University of Technology, Department of Telecommunications, Czech Republic
[3] Cardiac Unit, Raigmore Hospital, Inverness, IV2 3UJ, UK
[4] Sitekit Labs, Isle of Skye, Inverness, IV51 9HL, UK
[5] Brigham and Women's Hospital, Cardiovascular Division, Boston MA 02115, US
[6] Beth Israel Deaconess Medical Center, Harvard Medical School, Boston MA 02446, US
kfa@cs.stir.ac.uk, ahu@cs.stir.ac.uk, atassi@feec.vutbr.cz, stephen.leslie@nhs.net, chris.eckl@sitekit.net, cmacrae@partners.org, wslack@bidmc.harvard.edu

Abstract. Rapid access chest pain clinics (RACPC) enable clinical risk assessment, investigation and arrangement of a treatment plan for chest pain patients without a long waiting list. RACPC Clinicians often experience difficulties in the diagnosis of chest pain due to the inherent complexity of the clinical process and lack of comprehensive automated diagnostic tools. To date, various risk assessment models have been proposed, inspired by the National Institute of Clinical Excellence (NICE) guidelines to provide clinical decision support mechanism in chest pain diagnosis. The aim of this study is to help improve the performance of RACPC, specifically from the clinical decision support perspective. The study cohort comprises of 632 patients suspected of cardiac chest pain. A retrospective data analysis of the clinical studies evaluating 14 risk factors for chest pain patients was performed for the development of RACPC specific risk assessment models to distinguish between cardiac and non cardiac chest pain. In the first phase, a novel binary classification model was developed using a Decision Tree algorithm in conjunction with forward and backward selection wrapping techniques. Secondly, a logistic regression model was trained using all of the given variables combined with forward and backward feature selection techniques to identify the most significant features. The new models have resulted in very good predictive power, demonstrating general performance improvement compared to a state-of-the-art prediction model.

Keywords: RACPC risk assessment, Chest pain decision support system, Clinical decision support system for chest pain based on NICE Guidelines.

1 Introduction

Coronary heart disease (CHD) is the most common reason of death in the United Kingdom, and the fatality rate in the UK is still higher than many European countries

D. Liu et al. (Eds.): BICS 2013, LNAI 7888, pp. 296–307, 2013.

[1]. This condition is associated with an annual mortality between 2.8% to 6.6% per annum [2]. Patients who present with chest pain continue to present a major diagnostic challenge for both primary and secondary care physicians. This is due, in part, to the low specificity of chest pain as a symptom of significant coronary artery disease and the danger of misdiagnosis in patients who are at risk of major cardiac events. Furthermore, chest pain is a very common symptom, between 20% and 40% of the general population will experience chest pain in their lives [3] with up to 1% of visits to a general practitioner due to chest pain [4]. Chest pain is also common presenting complaint in patients attending A and E accounting for approximately 5% of visits to the emergency department. Furthermore, up to 40% of emergency hospital admissions are due to chest pain [5]. Even when patients are reviewed in the hospital setting with relatively easy access to diagnostic tests, it is estimated that between 2-5% of acute myocardial infarction patients is discharged inappropriately in the United Kingdom [6]. These individuals often have a very poor outcome, and are a leading cause of malpractice lawsuits each year [7].

The rest of the paper is organized as follows:

Section 2 reviews the state of the art in the clinical risk assessment and decision support mechanism for the chest pain patients, focusing specifically on the RACPC clinical study for Raigmore Hospital. Section 3 explains our methodology for the development of a machine learning based, novel expert system for the risk assessment of RACPC patients. Section 4 presents preliminary results which include validation and testing results using real chest pain patients' data acquired from the specialized chest pain clinic (RACPC) based at the Raigmore Hospital. Some concluding remarks and a brief discussion on future work is presented in section 5.

2 Background

Rapid Access Chest Pain Clinics

In 2001, the National Service Framework for Coronary Heart Disease made a commitment to have 50 rapid access chest pain clinics (RACPC) in England by April 2001 [8]. These clinics were designed to allow direct access to cardiology expertise without the need for accident and emergency assessment or admission to a medical ward. Rapid access chest pain clinics (RACPCs) would appear to be reliable and efficient to carry out the assessment of patients with suspected of angina and serious chest pain conditions [9].

Clinical Guidelines

Several clinical guidelines exist for the administration of patients with chest pain symptoms. [SIGN, ACC] and more recently, NICE made available standardized guidelines to ensure clinical governance for the management of recent onset chest pain. [10] However, producing clinical guidelines is not sufficient and implementation of guidelines presents a significant challenge. Several barriers to implementation of guidelines exist throughout the patient pathway, from problems with delayed referral, limited access to specialists and to specialist tests and rationing of some treatments. It remains difficult to ensure that all health care professionals are

aware of new guidelines and implement them. This results from ever increasing demands on health care professional's time and increasingly complex treatment regimes for patients. This is a particular problem for general and primary care physicians who are required to maintain a breadth of skills and knowledge base in a number of areas of medicine. Enforced embedding of clinical guidelines or clinical care pathways into paper or electronic referral systems is one approach to overcoming these barriers.

Clinical Features

There are several stages in the management of patients with suspected cardiac chest pain. The initial assessment should determine if it's likely that this patient is describing chest pain of a cardiac origin. This requires knowledge of the clinical history and risk factor profile of the individual patients. There are several algorithms that can be used to assess the most significant risk factor responsible for the disease outbreak. The algorithm used in the recent NICE guideline is based on the age, gender, risk factors and the typicality of the chest pain [11].

Diagnostic Tests

A resting ECG should be performed promptly in all patients complaining of chest pain. In order to further assess the patient further there are a range of available diagnostic tests including non-invasive functional testing (such as exercise ECG, stress echocardiography, myocardial perfusion scanning, and stress MRI [12]) or anatomical testing such as CT coronary angiography [13] or conventional diagnostic coronary angiography. Which test used will depend on each individual patient but also in part the relative availability at a local level.

Treatment

Treatment usually always involves medication but may also involve more invasive strategies such as coronary artery stenting and coronary artery bypass surgery. The timing of treatments and the need for invasive treatments such as stenting or coronary artery bypass grafting requires to be assessed on a case by case basis and decision making can be complex.

2.1 Conventional Retrospective and Prospective Risk Assessment Models Based on NICE Guidelines for RACPC Patients

The National Institute for Health and Clinical Excellence (NICE) recently released guidelines for the investigation of chest pain of recent onset. In one of the recent clinical case studies, the effect of these guidelines has been investigated in [14]. Their study suggested that patients attending RACPC will have a greater likelihood of CAD than predicted by NICE. They also made the recommendation that individual hospitals should investigate their RACPC cohorts prior to implementing the NICE guidelines.

In [15], the authors have carried out the investigation of chest pain of recent onset and recommended that the clinical risk assessment and risk stratification within a diagnostic/risk assessment model. Their study suggested that one in ten patients routinely excluded from cardiac investigation by the NICE algorithm have CAD and just over one in a hundred of them have a (major adverse cardiac event) MACE episode. Although these patients are considered low risk, they account for one third of adverse cardiac events in patients attending RACPC.

In a study conducted in [15], researchers undertook retrospective data analysis of 435 chest pain patients to investigate whether NICE guidelines had improved hospital's service provision by decreasing the number of further investigations required to make a diagnosis, and to see if the hospital's costs had increased now that the less expensive exercise tolerance tests were not recommended. Their study concluded that implementing NICE guidance reduced the number of investigations needed per patient, and did not increase the healthcare cost of the cardiology department in the short term [16].

2.2 RACPC Patient Data

Rapid access chest pain clinics have improved diagnosis of incident angina those with high risk of cardiovascular disease, but misdiagnosis rates are high and a recent study showed that a third of all cardiac events in subsequent follow-up occurred in those diagnosed with non-cardiac chest pain. We carried out a clinical case study comprises of 632 patients (male: 348 55 % of male, female: 45%; median age 61 years) attending rapid chest pain clinics (RACPC) at Raigmore Hospital between July 2009 and September 2011. Data were collated from clinical systems and patients' notes were considered where data were missing.

3 Methodology

3.1 RRAM (RACPC Risk Assessment Model)

We have exploited machine learning techniques to develop novel risk assessment models for RACPC by following iterative development Lifecycle. The block diagram explains the different stages involved in the development of risk assessment machine learning models for the chest pain clinic.

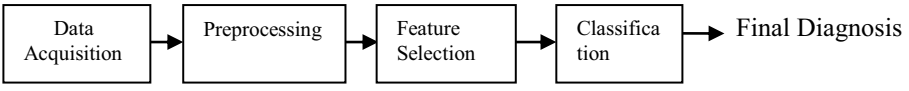

3.2 Data Acquisition

In data acquisition stage, we extracted data from various database servers; excel spreadsheets and where required doctor notes were taken into consideration to complete the retrospective case study/analysis of each patient. The acquired data were then normalized and held in a dedicated Ms Access database for further data analysis. The number of features was preselected through prior and ongoing consultations with the consultant cardiologist from Raigmore Hospital. We mutually identified 12 risk factors/variables out of the given 40 variables/risk factors. We also retrospectively completed episodic data analysis of 632 patients which are used for this case study.

Table 1. Risk Factors and Final Diagnoses

Features/Risk Factors		**Targets/Final Diagnosis**	
	Acronym		**Number of Patients**
Smoker	SMR	Acute Coronary Syndrome	9
Number of Cigarettes	NOC	Angina	274
Number of Years Smoked	YOS	Arrhythmia	11
Age	AGE	Declined Investigation	4
Pathway	PWY	GI Pain	39
Sex	SEX	Heart Failure	2
Diabetes Type	DAB	Syndrome X	5
Hypertension	HPT	Valve disease	3
Raised Cholesterol	CHL	Myocarditis	1
Initial Assessment	INA	Non Cardiac Symptoms	284
ETT Result	ETT		
CT Result	CTT	**Total patients**	**632**
MPS Result	MPS		
Anigo Result	ANG		

3.3 Preprocessing

In preprocessing stage, we transformed free text and categorical data values into numeric values for further processing. We carefully selected “Non cardiac symptom” as one of the major classes also set as the target result. As it can see in table 1, there are a number of target values/classes with minimal amount of patients associated with them such as Myocarditis, Syndrome X, Heart Failure etc. which is why we decided to work with only two major targets, namely “Non Cardiac Symptoms (with 284 patients, also the control group)) and “Angina” (comprises of 274 patients). We considered this as a binary classification problem focusing on “ Non Cardiac Symptoms” (“0”) and “Cardiac related symptoms” by merging all of the cardiac related classes into “1” class.

3.4 Feature Selection

The feature selection is a crucial issue for any pattern recognition task. The aim of this is to identify those features which are most relevant to the classification task. In the clinical domain, the *t*-test is frequently used to assess the feature quality using the *p*-value. This method belongs to two filtering methods which don't take into account the classification algorithm used and instead, evaluate the feature quality according to some statistical measurements. On the other hand, the feature selection methods known as wrappers usually show a high performance in terms of feature selection as the process of feature selection is controlled in each iteration by the classification accuracy of classifier used. There exist several types of such method, including forward selection, backward selection, and sequential floating forward selection. Among these options, we employed Forward selection (FS) and Backward selection (BS) for our experiments. Both algorithms choose the best features in an iterative manner. The difference between two wrapping techniques is that in the case of Forward Selection- one feature that yields best classification accuracy is added in each iteration whereas in the Backward Selection scenario- it starts off with the entire set of features, discarding one feature at a time to identify the best classification accuracy [17].

3.5 Classification

For classification purposes, we employed two widely used classifiers in the field of expert systems. The first one is based on decision trees (DT). Decision analysis is inspired by a theory of decision-making known as "subjected expected utility theory ". Decision trees are based on a normative model of decision making, meaning it describes the actions a decision-maker should take if they use the available information logically and rationally. In clinical decision analysis, decision problems are normally constructed as a decision tree [18]. By organizing the clinical domain in this manner, the problem can be analysed and the optimum choice determined. The branches/nodes of the decision trees represent both the probability (likelihood) of a particular outcome occurring and the value (utility) a decision maker attaches to that outcome. Decision Trees provide excellent clinical analysis capabilities for clinicians. It allows problematic decisions to be examined in detail, the use of research evidence to inform the decision, and recommends optimum solutions in complex situations where no right answer readily presents itself. They also promote holistic care as patients and their careers have the opportunity of expressing how they would feel about receiving different treatment options. By explicitly structuring the decision to be made in the form of a tree, it is possible to identify exactly how and why a particular decision was taken This could provide a valuable basis for reflection on and discussions of clinical decisions in nursing practice [19].

The second classifier is logistic regression (LR), which is a classification method based on linear modelling. Statistical disease prediction models for the clinical risk assessment are being used extensively to estimate and predict the likelihood of a medical prognosis. Regression models have long been fundamental to healthcare

authorities and research institutions, and more recently as clinical decision aids. In particular, logistic regression has been widely deployed for the risk estimation and prediction of clinical outcomes [20]. Logistic regression is a widely used machine learning algorithm among clinicians because of its transparency. It is a multivariable method which means that it tries to establish a functional relationship between two or more independent predictor/ variables and one outcome (dependent) variable; generally speaking, the outcome variable of a logistic regression is categorical (i.e. it can assume only a finite number of states) [16].

4 Experimental Setup and Results

We tested all possible combinations of classifiers and feature selection methods to identify the best approach among them. The validation was performed by applying leave-one-out validation technique.

The results for all possible combinations are reported in Table X. As it can be seen, several evaluation criteria are taken into account in order to make a fair comparison of methods under examination. These measurements are the most standard for assessing pattern recognition and expert systems. It is worth mentioning here that the advantage of the Mathew's correlation is that it takes into consideration all elements of the confusion matrix (true and false positive and negatives).

The results in Table 2 suggest that the decision tree based classifier combined with forward selection (DT-FS) gives the best performance in terms of Mathew's correlation, recall, weighted accuracy and unweighted accuracy. The ROC curves for all suggested setups are illustrated in figure 1. As the best performance was achieved by DT-FS setup, the pseudo code of feature selection and classification for this setup is reported.

4.1 Final Diagnosis

Figure 3 illustrates the weighted classification accuracies in each iteration for different experimental setups. These results are also reported in tabular format in table 3. The highlighted cells in the mentioned table represent the most significant features. For example, the highest classification accuracy for BS-LR was achieved by using features from iteration 4 to 13 (starting with NOC and ending with ANG). As it can be seen in the case of FS-DT, in spite of the fact the highest classification accuracy was achieved using 6 features, only 4 of them were considered because the difference in terms of classification accuracy was not statistically significant. It can also be seen through statistics given in table 3 that there are two (ANG and INA) common features among all experimental setups. It is also evident that the "CT Scan Result" appears to be relevant for FS-DT, BS-DT and BS-LR methods.

Table 2. Classification results in terms of several evaluations

Method	Unweighted accuracy	Weighted accuracy	Precision	Recall	F-measure	Matthew's Correlation
DT-FS	77.8481	78.4604	72.4138	85.1351	78.2609	0.5674
DT-BS	77.6899	77.3454	80.7471	79.1549	79.9431	0.5483
LR-FS	74.6835	74.4212	77.0115	77.0115	77.0115	0.4884
LR-FS	74.6835	74.4536	76.7241	77.1676	76.9452	0.4888

SET $Z_0 = \emptyset$ *// output feature group*
SET $i = 1$ *// iteration index*
SET $j = 1$ *// feature index*
SET $k = 1$ *// validation index*
SET $N_{\mathrm{f}} = 14$ *// number of features*
SET $N_{\mathrm{it}} = 14$ *// number of iterations*
SET $N_{\mathrm{pt}} = 632$ *// number of patterns (patients)*

// U is the entire set of patterns (subjects). $U = \{S_j\}$ for *j*=1,2,…, N_{pt}

FOR *i*=1 **TO** N_{it} *// main cycle*

FOR *j*=1 **TO** N_{f} *// features cycle*

FOR *k*=1 **TO** N_{pt} *// leave one out validation cycle*

$Z_{\mathrm{tr}} = \{U\}/\{S_k\}$ *// training set*
$Z_{\mathrm{te}} = \{S_k\}$ *// testing set*

// Train a classifier c by using training set Z_{tr} *and training function T, add feature j*

$$c = T(Z_{\mathrm{tr}}((Z_i \cup F(j)))$$

// Classifiy testing set Z_{te} *by classifier c and classifying function C, add feature j*

$$ca_k = C(\boldsymbol{c}, Z_{\mathrm{te}} \cup F(j))$$

ENDFOR *// end of validation cycle*

$CA_j = \frac{1}{N_{\mathrm{pt}}} \sum_{k=1}^{N_{\mathrm{pt}}} ca_k$ *// get the classification accuracy*

ENDFOR *// end of features cycle*

$f^+ = \mathrm{argmax}\ CA_j$ *// find feature with maximum classification accuracy*
$Z_{i+1} = Z \cup f^+$ *// add the selected feature to group Z*

ENDFOR *// end of main cycle*

Fig. 1. Pseudo code of feature selection and classification

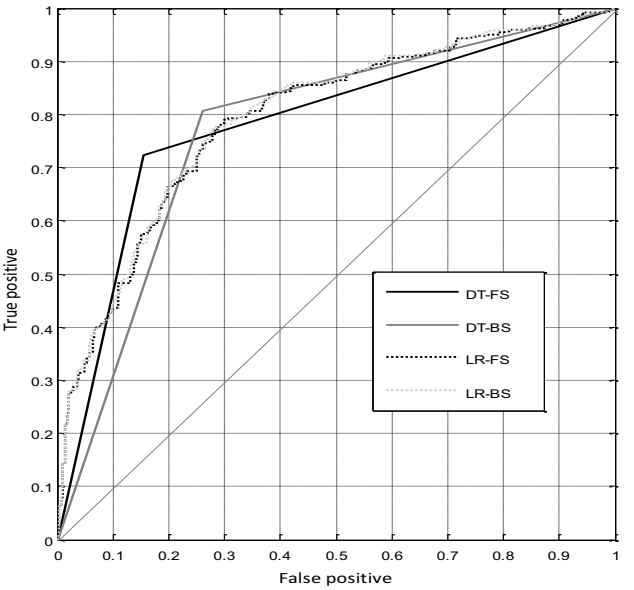

Fig. 2. ROC curves for different experimental setups

Table 3. Weighted classification accuracies in each iteration

Iteration	FS-DT		BS-DT		FS-LR		BS-LR	
1	**ANG**	64.7867	MPS	76.0240	**INA**	66.0596	ETT	74.3423
2	**INA**	71.7298	NOC	76.5198	AGE	67.8100	CHL	74.2776
3	CT	77.3454	CHL	76.8395	**ANG**	71.9423	DAB	74.4212
4	ETT	78.4341	SMR	77.1127	SEX	72.6789	NOC	74.4536
5	DAB	78.4341	ETT	77.1592	MPS	73.3831	MPS	73.8931
6	SEX	78.4604	DAB	76.8719	YOS	74.0550	SMR	73.3042
7	HPT	77.5943	YOS	73.6421	NOC	73.9113	HPT	73.8141
8	CHL	76.9650	AGE	75.0000	HPT	73.9902	YOS	73.6705
9	MPS	74.2492	PWY	77.3069	PWY	74.3099	CT	72.7113
10	NOC	73.9619	SEX	76.6270	ETT	74.3099	PWY	72.6789
11	PWY	76.3761	HPT	77.3454	CT	74.3099	SEX	71.9423
12	SMR	75.3379	CT	71.7298	SMR	74.4212	**INA**	68.1743
13	AGE	75.1153	**INA**	64.7867	DAB	74.1339	**ANG**	62.0690
14	YOS	75.1153	**ANG**		CHL	74.1663		

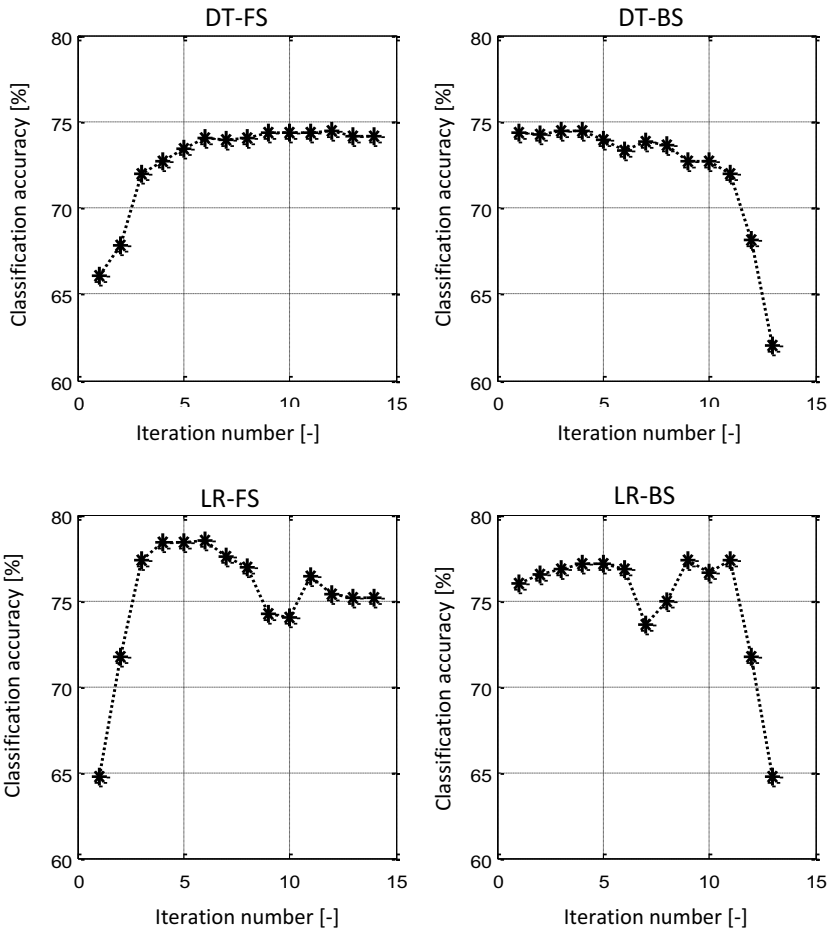

Fig. 3. Graphical output of weighted classification accuracies using different setups

5 Conclusions

In this paper, we presented a pilot case study of RACPC patients. We proposed an alternative risk assessment mechanism for RACPC based on novel real patient data (comprises of 632 patients along with 14 risk factors, carefully selected by the Consultant Cardiologist) acquired from Raigmore Hospital in the UK. We exploited two different techniques for both feature selection and classification, namely forward and backward wrapping techniques for feature selection and logistic regression and a decision tree for classification. The experimental results suggested the use of forward selection combined with decision tree classifier shows the best performance in terms of distinguishing among cardiac and non cardiac patients. The weighted accuracy of the proposed model was 78.46% , whereas the Mathews's correlation was 0.5674.

In light of the experimental results obtained through aforementioned classification techniques, we observed that “Angio Result”, “Initial Assessment” and “CT Result” are the key indicators for the clinicians to diagnose cardiac chest pain in early stages. The most significant risk factors (after dropping test results) among all methods were "AGE, SEX, Years of Smoking, Smoking, Hypertension and Number of Cigarettes patient Smoke". These, of course, will need to be clinically validated in future larger scale clinical trials in order for them to be considered for the possible inclusion in the relevant clinical guidelines.

The future work will aim to investigate more sophisticated techniques for feature selection and classification. We are going to expand on a number of other classes /diagnoses after acquiring additional data to satisfy their selection criteria.

References

[1] Unal, B., et al.: Explaining the decline in coronary heart disease mortality in England and Wales between 1981 and 2000. Circulation 109, 1101 (2004)
[2] Jones, M., et al.: Systematic review: prognosis of angina in primary care. Family Practice 23, 520 (2006)
[3] Stern, S., et al.: Presenting symptoms, admission electrocardiogram, management, and prognosis in acute coronary syndromes: differences by age. The American Journal of Geriatric Cardiology 13, 188–196 (2004)
[4] Ruigómez, A., et al.: Chest pain in general practice: incidence, comorbidity and mortality. Family Practice 23, 167 (2006)
[5] Nandalur, K.R., et al.: Diagnostic Performance of Stress Cardiac Magnetic Resonance Imaging in the Detection of Coronary Artery Disease: A Meta-Analysis. Journal of the American College of Cardiology 50, 1343–1353 (2007)
[6] Garg, P., et al.: Impact on service provision for non-invasive cardiac imaging following NICE recommendations: an observational study. Postgraduate Medical Journal 87, 445 (2011)
[7] Feuchtner, G.M., et al.: 64-MDCT for diagnosis of aortic regurgitation in patients referred to CT coronary angiography. American Journal of Roentgenology 191, W1 (2008)
[8] McArthur Rouse, F.: Critical care outreach services and early warning scoring systems: a review of the literature. Journal of Advanced Nursing 36, 696–704 (2001)
[9] Tenkorang, J.N., et al.: A rapid access cardiology service for chest pain, heart failure and arrhythmias accurately diagnoses cardiac disease and identifies patients at high risk: a prospective cohort study. Heart 92, 1084 (2006)
[10] Williams, M., et al.: Cardiac and coronary CT comprehensive imaging approach in the assessment of coronary heart disease. Heart 97, 1198 (2011)
[11] Dewey, M., Hamm, B.: Cost effectiveness of coronary angiography and calcium scoring using CT and stress MRI for diagnosis of coronary artery disease. European Radiology 17, 1301–1309 (2007)
[12] Abdulla, J., et al.: 64-multislice detector computed tomography coronary angiography as potential alternative to conventional coronary angiography: a systematic review and meta-analysis. European Heart Journal 28, 3042 (2007)
[13] Diamond, G.A., Forrester, J.S.: Analysis of probability as an aid in the clinical diagnosis of coronary-artery disease. New England Journal of Medicine 300, 1350–1358 (1979)

[14] Patterson, C., et al.: The effect of applying NICE guidelines for the investigation of stable chest pain on out-patient cardiac services in the UK. QJM 104, 581–588 (2011)
[15] Ashrafi, R., et al.: NICE recommendations for the assessment of stable chest pain: assessing the early economic and service impact in the rapid-access chest pain service. Postgraduate Medical Journal (2013)
[16] Farooq, K., Hussain, A., Leslie, S., Eckl, C., MacRae, C., Slack, W.: An ontology driven and bayesian network based cardiovascular decision support framework. In: Zhang, H., Hussain, A., Liu, D., Wang, Z. (eds.) BICS 2012. LNCS, vol. 7366, pp. 31–41. Springer, Heidelberg (2012)
[17] Kamran Farooq, A.H., Leslie, S., Eckl, C., Slack, W.: Ontology Driven Cardiovascular Decision Support System, May 23-26 (2011)
[18] Dowding, D.: Examining the effects that manipulating information given in the change of shift report has on nurses' care planning ability. Journal of Advanced Nursing 33, 836–846 (2008)
[19] Dowding, D., et al.: Conceptualising decision making in nursing education. Journal of Research in Nursing 17, 348–360 (2012)
[20] Pawlak, Z.: Rough set approach to knowledge-based decision support. European Journal of Operational Research 99, 48–57 (1997)

The Research of Thermal Power Unit Based on Improved Neural Network Generalized Predictive Control*

Licong Yuan[1], Hujun Ling[2], and Tao Sun[1]

[1] Inner Mongolia University of Technology,
College of Electric Power, 010080 Huhhot, China
wylc102@163.com
[2] Inner Mongolia University of Technology, 010080 Huhhot, China
260797817@qq.com

Abstract. With the development of electric power, Large-scale Generating Unit in heat power plant is a system which is complex, nonlinear and difficulty to establish accurate model, and etc. So it is hard to make system gain optimum running effect with conventional control strategy. Aiming at characteristic of generating unit, GA-LM algorithm optimization BP neural network is used to identify the coordinated control system for establishing a predictive model in Generalized predictive control strategy, achieves predictive control with online rolling optimization and real time feedback revision. Simulation results show its effectiveness.

Keywords: Levenberg-Marquardt, GA, BP Neural Network, Generalized predictive control, Generating unit.

1 Introduction

Power Generating is a complex production process. It has a strong coupling, time-varying, large lag and other features. The object parameter uncertainty when various perturbation effects, establishing an accurate model is difficult, the large-scale production process are complicated and difficult to control.

In recent years, with wider application of artificial neural network in solving nonlinear control problems, it can make the approximation of complex nonlinear relationship, to be able to learn and adapt to the dynamic characteristics of the uncertain system robustness and generalization ability. The BP network is widely used for system model identification and control. But its slow rate of convergence, it is difficult to meet the requirements of real-time control with adaptive features [1].

LM algorithm as the improved gauss-newton method, with the ordinary BP algorithm has good convergence and convergence speed advantages. Genetic algorithm with strong macro-search capability, and can find the global optimal solution with high probability, so use it to complete the pre-search can better

* This work is supported by National Nature Science Foundation under Grant 69964001; Inner Mongolia Autonomous Region Nature Science Foundation under Grant 200408020802.

D. Liu et al. (Eds.): BICS 2013, LNAI 7888, pp. 308–316, 2013.

overcome the shortcomings of the BP algorithm. Therefore using GA and LM algorithm to optimize the BP neural network (hereinafter referred to as GA - LM network) to establish a mathematic model of the system.

Generalized Predictive Control is Clarke and some other scientific family in retained the DMC, MAC of the multi-step prediction optimization strategy on the basis of introducing adaptive Control strategy and put forward, through the Generalized feedback correction eliminate Control the system steady deviation, and rolling optimization to replace the traditional optimal Control, and improve the system of real-time and anti-interference ability [2]. Limitations of traditional optimal control methods in the industrial process, GPC as its new modified optimal control method greatly enhances the applicability and robustness of the algorithm.

This paper based on the GA - LM algorithm of BP network to nonlinear, large time delay and time-varying large unit plant coordinated control system to establish forecast model, and by use of the generalized predictive control method for control for large unit plant coordinated control problem solving provides a very good way.

2 Theoretical Study

2.1 Based on the Optimized BP Network Forecast Model

The thermal power unit plant coordinated control system is a multi-variable nonlinear complex control object. Has proven mathematically for a forward three-layer neural network can achieve any nonlinear mapping, can approximate any complex function. First establish a three-layer BP neural network to approximate the controlled object[3].

2.2 Levenberg-Marquardt Algorithm

LM algorithm is a standard numerical optimization techniques fast algorithm can also be referred to as an improved Gauss-Newton algorithm than the steepest descent method convergence and fast convergence [4].

Let y_0 represents r is the output of the first training samples i section j, $y_{ij}^{'}$ is network predicted output, w is a right value and input x_i, the formula is:

$$\min E(w) = \sum_{i=1}^{p}\sum_{j=1}^{Q}\left(y_{ij} - y_{ij}^{'}(w, x_i)\right)^2 \equiv \sum_{k=1}^{m} r_k^2 \tag{1}$$

Formula: $m = i + p(j-1)$, r_k is i training layer first j output residuals.

If the calculation of target function E the connection weights of the first order derivative, $Jacobian$ array:

$$J = [\nabla r_1 \cdots \nabla r_m]^T \tag{2}$$

The formula: ∇r_1 is the n -dimensional vector of $r_1^{'}$, $\nabla r = \left[\frac{\partial r_i}{\partial w_1} \cdots \frac{\partial r_i}{\partial w_n}\right]$.

E of second order partial derivative matrix is called $Hessian$ array. For most seeking E extremum problems, if we take the appropriate residuals, can use this approximation. It is also the basic principle of the Gauss-Newton algorithm, that minimize the sum of the second power:

$$J^{'}Jp = -J^{'}r \tag{3}$$

$$w^{(k+1)} = w^k + \alpha p \tag{4}$$

Formula: J and r said in $w^{(k)}$ of estimate, p is forward (search) direction, is usually $w^{(k)}$ a decrease (feasible) direction; α is adaptive adjustment step length, usually take for optimal step length, in order to make function value decline as far as possible.

In practice, in order to alleviate the most advantage of the singular problem, it can make the objective function in close to the most advantages, in extreme value point nearby characteristic approximate quadratic sex, so as to speed up the convergence process optimization. Usually by the Hessian matrix E in the main diagonal matrix of each element is added a small positive, this is the basic idea of LM algorithm.

$$\left(J^{'}J + \mu I\right)p = -J^{'}r\,. \tag{5}$$

$$w^{(k+1)} = w^k + \alpha p\,. \tag{6}$$

2.3 Genetic Algorithm

The genetic algorithm is a draw on the biological natural selection and genetic mechanisms of random search optimization method. It does not depend on gradient information. Its essence is a kind of parallel, randomized, global search method, therefore, easy to get the global optimal solution.

Genetic algorithm is by selection, crossover and mutation suddenly three basic operator composition.

1) Choice is to select quality individuals from the old population, eliminated some individuals generate new populations of the process, to improve the average fitness of the population. Choice method has roulette method, the expectation value method, competition method, and keeps the optimal individual method, etc.

2) Cross is will choose the population after the individual in the mating pool randomly pairing, called father generation. According to the selected cross way and certain crossover probability, the pair of an individual's genes in part exchange, form a pair of progeny. Cross method a little cross, multipoint crossover and uniform cross, etc.

3) Suddenly variation is set according to the variation rate of the population of some individual gene seat, with opposite genes replacement, get a new individual.

Using genetic algorithm, LM algorithm combined with BP neural network can overcome the blind option value BP neural network training, slow convergence and easy to fall into local minimum.

Specific thoughts as: first use BP neural training, and produce a group of training weights, will then genetic algorithm of the initial population set to BP neural network training form right value, according to the BP neural network of global error setting the fitness function of the genetic algorithm, the fitness value calculation. And retain the best individual, residual individual genetic algorithm operating generate new individual and and retaining the best individual together constitute a new population, when they reach a certain evolution algebra, produce the optimized BP neural network weights. Continue to train the network, the LM algorithm to calculate the BP network training process with the right amount of value adjustments until you meet the initial set accuracy.

Optimizing neural network identification of the structure shown in Fig.1:

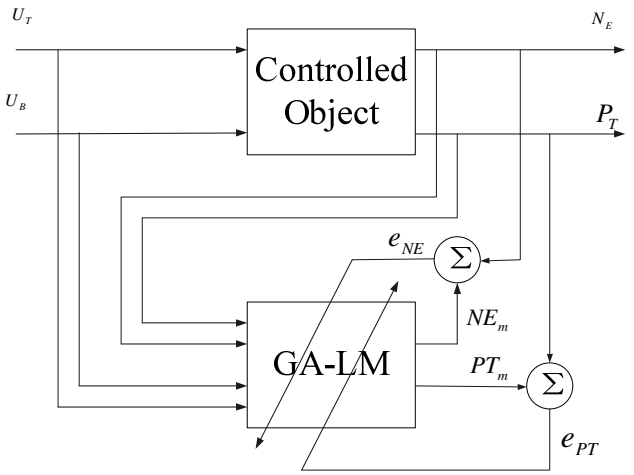

Fig. 1. GA-LM neural network system identification structure

2.4 Rolling Optimization

Performance index function:

$$J=\sum_{i=d}^{N1}[y_r(t+i)-y_p(t+i)]^2+\sum_{j=1}^{Nu}\lambda_i[\Delta u(t+j-1)]^2 \tag{7}$$

Formula (7), N_1 is Maximum prediction horizon, N_u is control horizon, λ_i is weighting constant, Δu is control increment, $y_r(t)$ is reference trajectory, $y_p(t+i)$ is the model prediction output of neural network.

Thus to the performance index function at each sampling instant use gradient descent method draw E control law, according to the generalized predictive control rolling optimization, and ultimately control quantity desirable for formula(8)[5]:

$$u(t+1)=u(t)+[1,0,\cdots,0](I+\mu\lambda)^{-1}\mu\delta y_u e\,. \tag{8}$$

Formula (8), μ is optimization step of gradient descent, is worked out by the trained neural network weights and the derivative of sigmoid function, e is prediction output error, it is worked out by prediction output and reference trajectory.

Therefore, using this method to calculate the control law and the solving diophantine compared to reduce the computation accelerate the calculation speed.

2.5 Feedback Correction

Prediction model output can not be fully consistent with the actual object. So it requires feedback to correct predictive model. In the algorithm of GA-LM neural network generalized predictive control, it detects the actual output at each step, and compares with model output to receive error message. It corrects GA-LM neural network model with error message. This process can be online, also be offline. To satisfy real-time requirements, it commonly learns and corrects online. The error between actual output and model output is showed as formula (9):

$$e_m(k)=y(k)-y_m(k)\,. \tag{9}$$

The prediction model output after feedback correction is showed as formula (10):

$$y_p(k+d)=y_m(k+d)+he_m(k)\,. \tag{10}$$

Formula (10) h is error correction coefficient.

2.6 The Control System Configuration

As mentioned above, the GA-LM neural network-based generalized predictive control, GA-LM neural network prediction model to optimize the controller and feedback correction of three parts, its structure is shown in Fig.2.

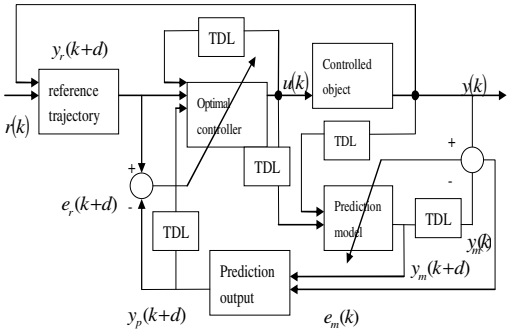

Fig. 2. GA-LMGPC System Structure

3 Research of the Delayed Model Simulation

Power plant boiler, boiler-turbine coordinate control system can be seen as a binary inputs and binary outputs system after reasonable simplified. The two input of it: turbine regulating valve opening instruction Ut, boiler burning rate instruction Ub. The two output of it: main steam pressure Pt, practical power of the unit Ne.

The transfer function of the delayed 300MW unit plant in 100% and 70% load operating conditions are expressed respectively as follows:

$$\begin{bmatrix} N_E \\ P_T \end{bmatrix} = \begin{bmatrix} \dfrac{4.665s(99s+1)e^{-15s}}{(582s^2+50s+1)(4.1s+1)} & \dfrac{2.069(311s+1)e^{-10s}}{(149s+1)^2(22.4s+1)} \\ -0.142(0.04+\dfrac{0.96}{70s+1}) & \dfrac{0.1265(205s+1)e^{-3s}}{(128s+1)^2(11.7s+1)} \end{bmatrix} \begin{bmatrix} \mu_T \\ \mu_B \end{bmatrix} . \tag{11}$$

$$\begin{bmatrix} N_E \\ P_T \end{bmatrix} = \begin{bmatrix} \dfrac{1.483s(150s+1)e^{-10s}}{(632s^2+40s+1)(2.7s+1)} & \dfrac{2.116(457s+1)e^{-8s}}{(221s+1)^2(21.8s+1)} \\ -0.828(0.01+\dfrac{0.99}{97s+1} & \dfrac{0.1649(275s+1)e^{-3s}}{(168s+1)^2(11.5s+1)} \end{bmatrix} \begin{bmatrix} \mu_T \\ \mu_B \end{bmatrix} . \tag{12}$$

Simulating it with the control strategy based on GA-LM neural network generalized predictive on the computer.

First, model training it using BP network optimized with GA-LM algorithm and ordinary BP algorithm at the same time, then compare the error curve which is shown in Fig.3.

The ordinary BP algorithm(200Epochs, Goal is 0.1) and GA-LM algorithm(13Epochs, Goal is 0.0001) is shown in Fig.3.

Seen from figure, model training with GA-LM algorithm is much faster than ordinary BP algorithm does.

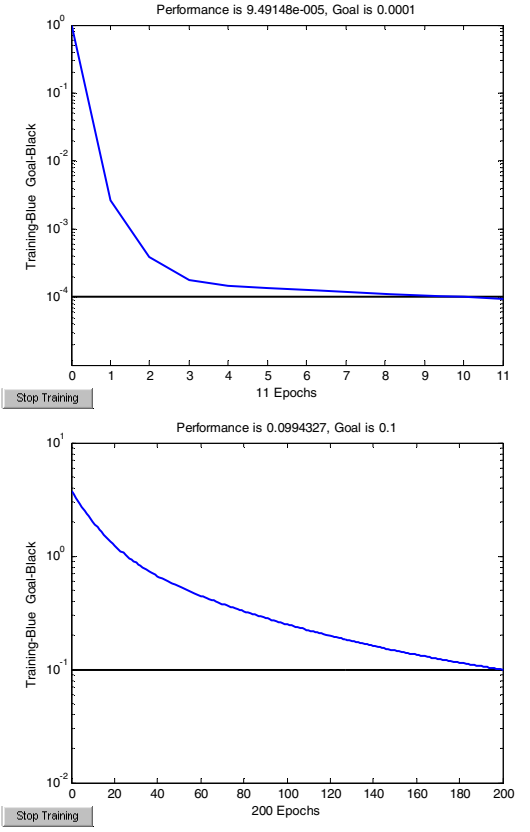

Fig. 3. The changing curve of training error based on network model

Second, the delayed unit plant with the optimized neural network generalized predictive control strategy is simulated.

Select the sampling period T=10s(the selected experience is: $T_{95}/T=(5\sim15)s$, T_{95} is the rise time of the transition process rising to 95%, sampling period can be obtained through the analysis of the step response of power and system pressure.) model length N=1000, predictive step length P=10, control step length M＝3, control weighting matrices R＝[0.8 0.2], the constrained values of 0<Pt< 20 MPa, 0<Ne< 300MW, power set value is Ne=300MW, pressure set value is Pt=18Mpa ; The controller parameters are unchanged at 70% load to observe the robustness of NNGPC, the set value and constrained value of Pt remained unchanged. the set value of Ne is 210MW. The simulation result of the control system is shown in Fig.4.

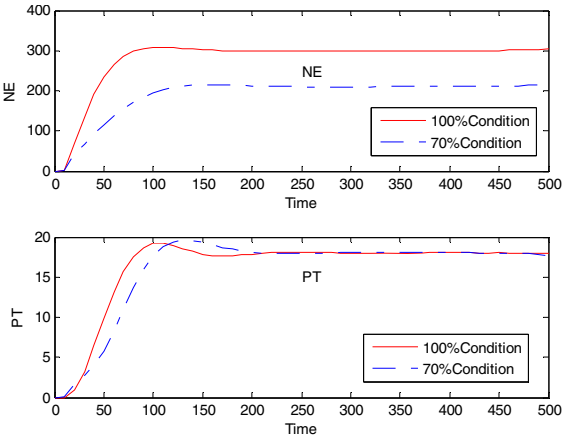

Fig. 4. Variable Load Response Curve of GA-LM GPC

In Fi.4, the solid line is the output curve to adjust the controller parameters in 100% load model, the dotted line is the output curve to switch to 70% load model and maintain the controller parameters constant. The simulation results show that the GA-LM neural network generalized predictive control applied to the unit coordinated control system can guarantee the system track the power and the main steam pressure setting fastly and smoothly and show a good adaptability in larger delay coordinated control system. In both load condition, the control system can guarantee a good dynamic and static characteristics, small overshoot, short adjusting time, stable output variables.

For purposes of comparison, the most widely used Smith Estimating PID control in the modern large-scale thermal power unit coordinated control are selected to overcome the pure delay on the performance of the control system. In 100% working condition, the PID controller parameters of μ_T and μ_B were set as follows:

kp1=0.001, ki1=0.000025, kd1=0.0152 ;

kp2=0.2, ki2=0.23, kd2=1.14

The output curve of Ne and Pt are shown by solid lines in Fig.5: In the 70% condition, the PID controller parameters are remained unchanged in order to observe the robustness of the PID control and the model adaptation, the Ne and Pt output curve are shown in the dashed line in Fig.5.

As can be seen from Figure 5 Simulation results, Ne and Pt step response curve swings, power settings can not be quickly tracked, Ne shows equal amplitude oscillation in 70% load. It can be seen that the control effects of the PID controller Smith predictor compensation package on delay, multi-variable object is not ideal, otherwise, the strategy based on GA-LM GPC has more robust, and can adapt to the requirements of model uncertainty of the large unit power plant.

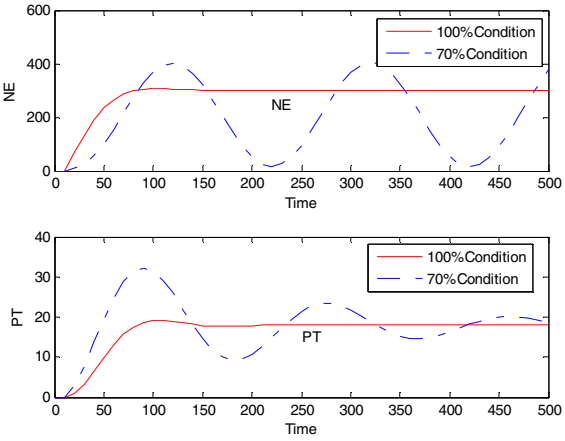

Fig. 5. Variable Load Response Curve of PID Control

4 Conclusion

In this paper, training the neural network model with GA-LM algorithm and identificating the mathematical model of multi-variable nonlinear system rapidly using BP network against the characteristic of the charged object of the large unit plant and combined with the widespread problem in coordinated control. At the same time, the trained neural network parameters are used to obtain the generalized predictive control rate. That avoids solving Diophantine equations to reduce the amount of calculation.

The simulation results show that the method ensures the power and the main steam pressure track their settings in the system operation smoothly and has a better robustness; the strategy is more effective than the conventional coordinated control strategy in unit plant control.

References

1. Lin, W., Hu, Y.: The automatic control technology of unit plant. China Electric Power Press, Beijing (2008)
2. Zhng, L., Liu, T., Sun, Y., Li, Q.: Research of genetic algorithm optimization neural network weights blind equalization algorithm based on real number coding. J.Computer Engineering and Applications 45, 162–164 (2009)
3. Hecht-Nielsen, R.: Theory of the back-propagation neural networks proceedings. In: Int. Conf. on Neural Networks (I), pp. 569–600. IEEE Press, New York (1989)
4. Peng, Y., Xue, Z.: Fuzzy Optimization Neural Network Model Based on Levenberg-Marquardt Algorithm. J. Water Resources and Power (2011)
5. Zhu, J.: The smart predictive control and its application, pp. 16–17. Zhejiang University Press, Hangzhou (2000)

A Review of Artificial Intelligence and Biologically Inspired Computational Approaches to Solving Issues in Narrative Financial Disclosure

Saliha Minhas[1], Soujanya Poria[2], Amir Hussain[1], and Khalid Hussainey[1]

[1] Dept. of Computing Science, Univerity of Stirling, FK9 4LA, Scotland
[2] Dept. of Computing Science, Jadavpur University, West Bengal, India
szm@stir.ac.uk, ahu@cs.stir.ac.uk,
soujanya.poria@ieee.org, khaled.hussainey@stir.ac.uk

Abstract. Indisputably, financial reporting has a key role to play in the efficient workings of capitalist economies. Problems related to agency and asymmetric information (Jensen and Meckling, 1976) would abound and cripple financial markets, as it has done when left unchecked (Enron, WorldCom and Tyco). However for too long, quantitative data has monopolised the assessment and prediction role within this arena and this has contributed to the failures, borne out by research (Kumar & Ravi, 2007). As qualitative data proliferates, containing value relevant information it needs to be factored into the analysis. This paper reviews work on financial narrative disclosures and looks at conventional artificial intelligence and more recent biologically inspired computational approaches to catapult the domain to more progressive methods of using linguistic data in evaluations.

Keywords: Narrative Financial Disclosure, Biologically Inspired, SenticNet.

1 Introduction

"Efficient allocation of resources in an economy, capital market development, liquidity in the market, decreased cost of capital, lower return volatility, and high analyst forecast accuracy" (Kothari, Li and Short , 2009)

To reach this aim, narrative disclosures can play a significant role, especially given the deluge of unstructured content that abounds and could contain value relevant information. However, despite this potential by far analysis and prediction has been predominantly performed using quantitative data. There is a reason why the saying 'number's don't lie' prevails and not 'the text doesn't lie'. Numerical data is just easier to deal with, whereas text is riddled with ambiguities and difficult to decipher for humans, let alone computers. However, given the deluge, taming text must be done. Within the Financial Reporting domain it would significantly enhance decision making powers of stakeholders. The next section reviews research work in narrative financial reporting to appreciate the task at hand. Thereafter, significant artificial intelligence/biologically inspired approaches are examined to assess their capabilities to decipher content. In particular, the potential of Sentic Computing (Cambria and Hussain, 2012) cyrstalized into SenticNet, an opinion mining engine will be

D. Liu et al. (Eds.): BICS 2013, LNAI 7888, pp. 317–327, 2013.

examined. This is built on ontological affective common sense representation and seeks to mimic cognitive processes in handling linguistic data. Preliminary results from this engine run on extracts of company annual reports will be given.

2 Literature Review - Narrative Disclosures

Despite being overshadowed by the reams of work in numerical analysis, deciphering narrative disclosure in accounting documents has had its proponents. A catalogue of significant research in this field is given in appendix one. This research can be examined from two angles, delineated below:

2.1 A Review of Methodology Applied to Understand the Narrative Content

Merkl-Davies et al (2013) developed a taxonomy to give structure to the relationship between research paradigms and text analysis approaches. They correctly point out that content analysis is the main textual analysis approach used within accounting narrative domain. It involves "*draw*[*ing*] *inferences from data by systematically identifying characteristics within the data"* (Clatworthy et al, 2001). Within content analysis, two approaches are typically taken: "form orientated" analysis, which involves routine counting of words or concrete references, and "meaning orientated" analysis, which focuses on analysis of the underlying themes in the texts under investigation (Smith and Taffler, 2000). Form orientated can be quantitative, use of proxies is common to enable statistical analysis or it can be qualitative, searching for occurrence of predefined content categories within texts. As Davies et al (2013) argue what methodology is chosen depends on the aims of the research.

Other studies (Li, 2008; Jones and Shoemaker, 1994) have looked at readability of narratives to typically check if the management obfuscation hypothesis is being played out. This is assessed by a readability formula that counts language variables in a text in order to provide a measure of reading difficulty for readers. Still others (Demers and Vega, 2008; Brennan et al, 2008) have looked at rhetorical manipulation, use of certain linguistic choices to influence meaning. This would again be relevant in the area of impression management and fraudulent activity.

Another nuance within content analysis work is that it can be performed either with a dictionary or a statistical based approach. In the former, dictionaries are employed to pick up the meaning and polarity of the text. For example (Kothari, Li and Short, 2009) put words into categories through use of a word list and then ascertained polarity (positive/negative) using the General Inquirer dictionary. Whereas, (Feldman et al., 2010) used Loughran and Macdonald's (2011) financial word list with polarity for detecting (positive/negative) tone. This has been touted as being more relevant for the financial domain. Typically once polarity of text has been determined, the results are quantified and used within regression analysis. There is a number of significant studies performed in this manner (Tetlock, 2007, Kothari, Li and Short, 2009, Huang, 2011). The use of dictionaries can be cumbersome as they need to be updated and require expert manual effort. Statistical approaches use a variety of

generative, probabilistic models based on bag of words approach and maximizing the likelihood of the observed word being in a class to gauge meaning (Manning and Shutze, 1999). The main criticism is the lack of lexical analysis done, therefore poor capture of semantics.

Smith and Taffler (2000) used OCP and SPSS to perform content analysis. They attempted to capture both themes and words. They looked for certain keywords that denote profitability, dividends, resignations etc. They also captured themes by examining combinations of words that would fit into designated thematic components. Keywords and captured themes are given numerical scores to correlate with bankruptcy (tested using failed firms). The scores are fed into linear discriminant models which show that chairman's statement in annual reports highly correlative with bankruptcy.

Beattie et al (2004) use content analysis software to code each sentence into one of ten categories and into four dimensions. Coders go through the software to aid in this process. Although methodology is comprehensive in the review of annual report narratives, it was labour intensive. Hussainey (2003) attempted to move away from manual analysis, with a view to capturing forward looking statements in narratives by drawing up keyword list that were indicative of this class. There are a number of other similar manual/semi-automated content analysis performed (Botosan, 1997; Ahmed et al.,1999; Kothari, Li and Short, 2009; Li, 2011). The main problem with these approaches is that it requires human interaction and judgement and is thus subject to reliability issues (such as inter coder agreement on terms), it is error prone and expensive. Therefore samples sizes tend to be small. There has been some recent work in the accounting narrative domain using a more complete computerised content analysis and is now delineated.

Li (2010) categorised 30,000 sentences containing Forward Looking Statement (FLS) into two dimension (positive/negative) and content (profitability, operations, liquidity). This training data is fed into a Naïve Bayes algorithm which is used to categorize the tone and content of about 13 million FLS. The problem with this approach is that no lexical analysis is done, each word is deemed independent of any other word and categorisation is often done using frequencies computed as prior/conditional probabilities. This is simplistic/naïve from a linguistic point of view.

Demers and Vega (2008) use dictionaries to measure linguistic tone to determine optimism and certainty in narratives. This is then build into a Bayesian learning model which predicts that sentiments expressed as linked to stock returns. Similarly, Tetlock (2007) and Feldman (2008) detect the relationship between sentiment expressed in narratives and stock market reactions. The former looks at frequencies of negative words, whereas the latter uses dictionaries to determine polarity.

Brown and Tucker (2010) used the vector space model of information retrieval to determine similarities in accounting statements. The similarity of any two documents is measured by the angle between the two vectors representing the documents, a smaller angle indicates more similar documents. TF-IDF weighting function was used within the vectors, this picks up words that are more salient in document as compared to the corpus. This vector space comparison can also be done at sentence level.

Qiu et al (2004) build a Support Vector Machine (SVM) based predictive model based on textual content and experimented with different feature selection methods. Balakrishnan et al (2010) again use a bag of word approach with TF/IDF scores to develop a predictive model where linguistic data predicts performance. Detection of financial misreporting has attracted research work, given the rise in fraudulent activity. Hobson et al (2012) build on cognitive dissonance theory (Festinger, 1957) - psychological discomfort when one's actions and beliefs are discrepant. They look for emotions such as fear, uncertainty, guilt, shame which give a high cognitive dissonance marker score that are indicative of deception. They apply this approach to non-verbal cues to CEO speech samples. Goel (2008) build an SVM classifier used to detect fraud. Linguistic features such as active/passive voice (look at personal pronouns used), uncertainty markers, readability index, tone, usage of proper nouns, type-token ratio etc were used. This helped to distinguish fraudulent annual reports from non-fraudulent reports. Generally researchers perform linguistic analysis identifying a set of "lying words" that pertain to deceptive language (Larcker and Zakolyukina , 2011; Newman et al., 2003; Loughran and McDonald, 2009).

The above research has still failed to capture the true potential of natural language processing capabilities. In particular, to guage tone, sentiment in narratives, to distinguish it from factual statement falls short of opinion mining and sentiment analysis potential. Some of these technologies will be examined in the Section 3. In general, there is still a paucity of research that uses Biologically Inspired/Artificial Intelligence approaches that can utilise the knowledge gained from the research into accounting narratives (see appendix one) and that can extract meaning from text.

2.2 A Review of the Findings of Methodology Applied

Appendix one, gives an overview of salient research in the accounting narrative research. As said by Qui et al (2004)"…these studies emanate from the intuitive recognition of a link between the textual report content and corporate performance". This indeed is characteristic of the findings outlined in appendix one, the narratives are correlated with variables, some of which are proxied eg Kothari et al (2009) used the cost of capital, stock return volatility and analyst forecast dispersion to proxy for firm risk. In the majority of cases it is found that the narratives have information content of a predictive nature (see appendix one) or that it sheds light on management actions or explains industry specific disclosure practices. In all the text analysis of narratives conducted the researchers were keen to pick up forward looking information and tone as it relays messages that can be significant for stock markets and industry analysts. This was primarily done using keyword searches, which can be improved upon by concept based opinion mining tools (Cambria and Hussain, 2012).

Recently the literature has been dominated by looking for linguistic cues that are indicative of impression management or fraud. Of primary importance in any textual analysis is the picking out of the most representative features. This has been more of a challenge given the ambiguous nature of these phenomena. Merkl-Davies and Brennan (2007) identified six strategies used for concealment. Two of these obfuscate bad news by manipulating verbal information and four strategies emphasize good

news by manipulating verbal and/or numerical information. The challenge is to develop features that would pick up such semantics. For example Goal (2008), used word frequencies, syntactic and surface level features for fraud detection.

The research delineated in appendix one also indicates that agency and information asymmetry, proprietary cost, self-attribution bias are all found to be empirically linked to disclosure. One of the main ways that researchers have used (Feldman, 2010; Tetlock, 2007; Li, 2010) to capture firm intention is tone. Therefore any analysis and prediction that is done using narrative content needs to take into account the industry background, management motivations and biases. For example we know that in highly competitive industries or firms operating in a highly litigious environment, poor performance are all likely to lead to less disclosure or attempts to blame external circumstances for unfavourable results. Any approach that can represent such knowledge and correctly capture tone would improve predictive modelling that seeks to guage future company performance.

In sum, it can be said that voluntary disclosure literature appears to offer an opportunity to increase understanding of the role of accounting information in firm valuation and corporate finance. This knowledge could be represented within biologically inspired systems through the use of an ontology or expert system, which with the semantics extracted from the actual linguistic data could lead to improve predictive capabilities of financial models.

3 Artificial Intelligence (AI) - Biologically Inspired Approaches

Ekbia (2010) outlined some of the main approaches in AI and their basic understanding of intelligence. They are outlined below with brief reviews on their applicability to the financial domain:-

Knowledge-Intensive AI is motivated by the idea that a vast amount of knowledge is the key to intelligence, in particular machines need to be given common sense knowledge for it to understand the meaning of concepts. SenticNet would fall under this umbrella, as would expert systems. These are programs that use information in a knowledge base, using a set of inference procedures, to solve problems that require significant human expertise for their solution. Expert systems (ES) lend themselves to dealing with qualitative data, as the knowledge base can be updated and inference mechanism adjusted. The information is used to mimic the decision making of experts. Expert Sytems have been used in forecasting for example FINEVA (FINancian AVAaluation) is a multicriteria knowledge-based ES to assess firm performance and viability. The output of this system demonstrates the ranking of analyzed firms based on class of risk. Within narratives the determinant of disclosure could be added to the knowledge base eg poor readability could be resultant from poor performance, fraud or that prevalence of good news and self references are indicative of good firm prospects or higher number of forward looking statements given to counteract stock prices which poorly reflect future earnings. In financial prediction and planning domain, several ES have been compared to statistical

methods. Results given by Bahrammirzaee (2010) indicate that Experts systems outperform. However ES provide a prescription and not a prediction. That means that if a goal is given then, a knowledge based ES suggests a course of action, while a simulation model predicts the consequences of a selected course of action under some experimental conditions (Bahrammirzaee, 2010).

Case-Based AI. The premise of this approach is that people reason and learn from experience and that the knowledge acquired from experience, captured in *cases*, is central to their understanding of the world. This would translate into AI as indexing cases as they occur so that, much later, they can be remembered and efficiently retrieved in "similar" situations. The algorithm would use such "experience" to reason about the task at hand. Sheng-Li et al (2009) argue that Case Based Reasoning (CBR) has good predictive capabilities, it is non parametric method which does not require any data distribution assumptions, an incremental learning technique that can retain new cases without reprocessing. However the determination of similar cases can be problematic. The authors propose a hybrid model for the financial prediction task: CBR augmented with Genetic Algorithm (GA) and the fuzzy K nearest neighbour (KNN) method. GAs are used to compute the optimal weight vectors of financial variables and KNN are used to compute distances between cases. The authors in their conclusion contend that financial ratios extracted for the knowledge elicitation task can be extended to pick up more features of interest with which to compare cases. This is again where the technique could be augmented with narrative content that would aid the prediction task. Both CBR and Artificial Neural Networks (ANN) have been intensively used in the finance domain. The evidence indicates that CBR can be better in some areas for example (Behbood, 2011) conclude that it gives better results when markets deviate from a stable equilibrium. Other researchers have also found it to have superior performance that ANN (Slonim, 2001; Shen 2012). This approach utilises one of the fundamentals of brain like activity, learning. It learns from experience and uses that knowledge to make new deductions

Biologically Inspired or Artificial Intelligence. These are models and techniques inspired by natural mechanisms, such as those studied in Biology. Examples would include Artificial Neural Networks (ANN), Machine Learning (ML), and Genetic Algorithms (GA). In Finance, they have been used in areas such as, business failure prediction, debt risk assessment, security market applications, financial forecasting, portfolio management, fraud detection and insurance. For example ANNs have been designed using financial data of banking customers as the input vector and the actual decisions of the credit analyst as the desired output vector. The objective of the system would be to imitate the human expert in granting credit and setting credit limits. Bahrammirzaee (2010) in his comprehensive review of ANN, finds that they outperform traditional statistical approaches but questions their accuracy. This he concludes is due to the difficulty of determining the proper size and structure of a neural net for a given problem, poor pattern matching capabilities and prediction based on past events which may not be repeated, especially within a financial setting. Within forecasting, typically financial ratios are used to feed into these models,

accuracy could be significantly enhanced by using data captured from narratives. For example sentiment polarity extracted by SenticNet or building up features from grammar rules, context analysis at the sentence level to capture company strategic intentions or likelihood of bankruptcy. This could be quantified and fed to the ANN.

Furthermore, within the realm of machine learning Chi et al (2011) use both financial and non-financial features with SVM model for financial distress prediction and get improved results as compared with approaches that use only financial features. SVM overcome the weakness ANN which tend to converge on local optimum with respect to the training data and generalise better with respect to the test data. SVM are known as maximal margin classifier in which the classification problem can be represented as an optimization process.

Genetic Algorithms have been used to find parameters for an SVM for diagnosing business crises (Chih-Hung W and Gwo-Hshiung Tzeng, 2007). Genetic algorithms find the optimal set of features which are then added to the feature set, boosting performance of the SVM classifiers.

Outwith these 3 main approaches, hybrid systems are worth mentioning because ''hybridization'' (e.g., mixing different functions in order to perform a complex task) would also fall into the realm of Artificial Intelligence (AI). For example, Kuo et al (1996) designed a system for stock market forecasting that concerned qualitative and quantitative factors simultaneously. This system was composed of integrating NN (Neural Net) for quantitative factors and fuzzy Delphi model for qualitative factors and got acceptable results. Hybrid systems typically combine the power of statistical models with neural nets and get superior result (Bahrammirzaee, 2010). Neural Nets are merged with Fuzzy Logic mechanisms or probabilistic methods. These tools can also be used on their own and fall under the soft computing category. They are widely used in financial applications as are tolerant to imprecision and uncertainty, which a human expert would deal with regularly. For example, Tan et al (2005) propose Genetic complementary learning system (a combination of the Genetic Algorithm and Neural Nets). It is based on hippocampus-inspired learning that is believed to be a mechanism underlying pattern recognition in human. This coupled with GA the authors contend offer good solutions to stock price and bank failure prediction task. The authors themselves in the conclusion advocate that its predictive capabilities would be enhanced with more narrative content inclusion.

To date the success of any prediction and modelling techniques employed using narratives have rested on the correct identification of features that capture semantics of the data in question. Within financial narratives for example a number or researchers have tried to pick up tone/sentiments expressed to link it to performance, strategic intentions, potential bankruptcy [see Appendix One]. However keyword searches are limited to syntactic analysis and fail to capture meaning which can be dispersed within natural language.

4 Preliminary Results – SenticNet

To correct this deficiency, Cambria et al (2012) propose a concept based technology (SenticNet) using an ontology ConceptNet (a common sense knowledge base) tuned

to picking up emotive content, using biologically-inspired affective categorisation model that can potentially describe the full range of emotional experiences. Dimensionality reduction techniques are employed to cluster similar concepts together. This when deployed within a financial narrative setting could pick up tone with polarity rating, more accurately. Loughran and Macdonald, 2012 (will be referred to as L&M)) build up a dictionary of words that denote sentiment in Finance, these could be used to build up the concepts within ConceptNet. For example L&M argue that words such as (*tax, costs, loss, capital, cost, expense,* and *expenses*) denoted as "negative" words generally. Within a financial setting, firm *costs*, sources of *capital,* or the amount of *tax* paid are neutral in nature; managers using this language are merely describing their operations. Once such relationships are captured within ConceptNet, SenticNet with its polarity detection and clustering techniques can classify sentences by tone. Thereafter once a sentence has been correctly tagged for its polarity, it can be used as training data to aid classification (this was done by Cambria et al, 2013 using Artificial Neural Network, which was fed affectively annotated text using SenticNet [43][44]). The above approach was followed (L&M's financial wordlist was incorporated into SenticNet) and the algorithms were run over extracts (the management discussion and analysis section) from ten company annual reports within the UK Food and Beverage sector. Some of the sentences passed to SenticNet with results are shown in appendix two. SenticNet was able to pick up the correct tone in all sentences that were put through it. This would be highly beneficial as tone within a financial context is taken as indictor of company performance, likely stock markets returns, used in fraud detection, early warning of company distress and impression management. Plethora of researchers have used tone to guage firm behaviour [see Appendix One]. Diction (the words that the author uses) are one of the main ways to determine tone (Nordquist, 2012) and this is what SenticNet is performing, examining words and the concepts that are enveloped within these words, demystified using an affective ConceptNet ontology.

5 Discussion and Conclusion

It is generally accepted that outbreak of corporate financial crises have been preceded by symptoms and alarms. Predictive modelling within finance has missed out on forecasting some big blunders. A significant contributing factor is that it has failed to take into account the abounding narrative content which many have touted to be key to knowledge discovery. The focus solely on non-text derived quantitative data is limiting as it is mostly backward-looking, point-in-time measures and therefore leads to inaccurate prediction. Research done on narrative disclosure strongly indicate that value relevant information is contained in documents such as annual reports, business news, analyst reviews. The question boils down to how to extract the relevant semantic information contained in textual format for use in analysis and prediction tasks? SenticNet for opinion mining was mentioned as a way forward to capture semantics in a robust and complete manner. SenticNet correctly picked up tone from extracts of company annual reports. This would greatly aid predictive capabilities of

financial models as tone from extensive research in narratives has been shown to be an accurate indicator of firm intention and prospects. To build Biologically Inspired or Cognitive Systems a vital component is learning and using it to improve its performance. This is where SenticNet can be developed further to completely build computational model that mimic the human brain. Within finance analysis and prediction could be done using the captured semantics through cognitive systems like SenticNet and then results fed into Machine Learning algorithms, as shown by Cambria et al (2013). Similarly, semantics of non-opinionated data could be captured through ontologies, probabilities, lexical analysis as part of the building blocks for cognitive systems. What techniques are chosen depends on the task at hand. The question that needs to be asked is "What data structures are useful for representing knowledge and what algorithms operate on those knowledge structures to produce intelligent behaviour?" (Lee and Ho, 2009). Bahrammirzaee, (2010) concludes after reviewing previous research that the accuracy of these artificial intelligent methods is superior to that of statistical methods in dealing with financial problems, especially with regard to nonlinear patterns.

References

1. Ahmed, K., Courtis, J.K.: Associations between corporate characteristics and disclosure levels in annual reports: a meta-analysis. British Accounting Review 31(1), 35–61 (1999)
2. Bahrammirzaee, A.: A comparative survey of artificial intelligence applications in finance: artificial neural networks, expert system and hybrid intelligent systems. Neural Computing and Applications 19(8) (2010)
3. Balakrishnan, R., Qiu, X.Y., Srinivasan, P.: On the predictive ability of narrative disclosures in annual reports. European Journal of Operational Research 202, 789–801 (2010)
4. Beattie, V., McInnes, W., Fearnley, S.: A methodology for analysing and evaluating narratives in annual reports: a comprehensive descriptive profile and metrics for disclosure quality attributes. Accounting Forum 28(3), 205–236 (2004)
5. Behbood, V.: Intelligent financial warning model using Fuzzy Neural Network and case-based reasoning. In: 2011 IEEE Symposium on Computational Intelligence for Financial Engineering and Economics, CIFEr (2011)
6. Botosan, C.A.: Disclosure level and the cost of equity capital. The Accounting Review 72(3), 323–349 (1997)
7. Brennan, et al.: Impression management: developing and illustrating a scheme of analysis for narrative disclosures – a methodological note. Accounting, Auditing and Accountability Journal 22(5), 789–832 (2007)
8. Brown, Tucker: Large-Sample Evidence on Firms Year-over-Year MD&A Modifications. Journal of Accounting Research 49(2) (2010)
9. Cambria, E., Hussain, A.: Sentic Computing: Techniques, Tools, and Applications. Springer, Dordrecht (2012) ISBN: 978-94-007-5069-2
10. Cambria, E., Mazzocco, T., Hussain, A.: Application of multi-dimensional scaling and artificial neural networks for biologically inspired opinion mining. Biologically Inspired Cognitive Architectures (2013), doi:10.1016/j.bica.2013.02.003
11. Chi, X., et al.: Financial distress prediction based on SVM and MDA methods: the case of Chinese listed companies. Quality and Quantity 45(3), 671–686 (2011)

12. Wu, C.-H., Tzeng, G.-H.: A real-valued genetic algorithm to optimize the parameters of support vector machine for predicting bankruptcy. Expert Systems with Applications 32, 397–408 (2007)
13. Clatworthy, M., Jones, M.J.: The effect of thematic structure on the variability of annual report readability. Accounting, Auditing and Accountability Journal 14(3), 311–326 (2001)
14. Demers, Vega: Linguistic Tone in Earnings Announcements: News or Noise?Linguistic Tone in Earnings Announcements: News or Noise? In: FRB International Finance Discussion Paper (2008)
15. Ekbia, H.: Fifty years of research in artificial intelligence. Annual Review of Information Science and Technology 44(1) (2010)
16. Feng, L.: The Information Content of Forward-Looking Statements in Corporate Filings—A Naïve Bayesian Machine Learning Approach. Journal of Accounting Research 48(5) (2010)
17. Feldman, R., Govindaraj, S., Livnat, J., Segal, B.: Management tone change, post earnings announcement drift and accruals. Review of Accounting Studies 5(4), 915–953 (2010)
18. Festinger, L.: A theory of cognitive dissonance. Stanford University Press, Stanford (1985) (first published 1957)
19. Goel, S., Gangolly, J.: Can Linguistic Predictors Detect Fraudulent Financial Filings? Journal of Emerging Technologies in Accounting 7(1), 25–46 (2010)
20. Hobson, J.L., et al.: Analysing Speech to Detect Financial Misreporting. Journal of Accounting Research 50 (2012)
21. Hussainey, K., Schleicher, T., Walker, M.: Undertaking Large-scale Disclosure Studies when AIMR-FAF Ratings are not available: the Case of Prices Leading Earnings. Accounting and Business Research 33(4), 275–294 (2003)
22. Huang, X., et al.: Tone Management. Social Science Research Network (2011)
23. Jensen, M., Meckling, W.: Theory of the Firm: Managerial Behavior, Agency Costs and Ownership Structure. Foundations of Organizational Strategy (1976)
24. Jones, M.J., Shoemaker, P.A.: Accounting Narratives: A Review of Empirical Studies of Content and Readability. Journal of Accounting Literature 13, 142–184 (1994)
25. Kothari, S., Li, X., Short, J.: The Effect of Disclosures by Management, Analysts, and Business Press on Cost of Capital, Return Volatility, and Analyst Forecasts: A Study using Content Analysis. The Accounting Review (September 2009)
26. Kumar, R., Ravi, V.: Bankruptcy prediction in banks and firms via statistical and intelligent techniques. A Review, European Journal of Operational Research (2007)
27. Kuo, R.J.: Integration of artificial neural networks and fuzzy Delphi for stock market forecasting. In: IEEE International Conference on Systems, Man, and Cybernetics (1996)
28. Larcker, D., Zakolyukina, A.: Detecting Deceptive Discussions in Conference Calls. Journal of Accounting Research 50(2) (2011)
29. Li, F.: Annual report readability, current earnings, and earnings persistence. Journal of Accounting and Economics 45, 221–247 (2008)
30. Li, F.: The Information Content of Forward-Looking Statements in Corporate Filings—A Naïve Bayesian Machine Learning Approach. Journal of Accounting Research 48(5) (December 2010)
31. Loughran, T., McDonald, B.: Barron's Red Flangs: Do They Actually Work? Working Paper,University of Notre Dame (2009)
32. Merkl-Davies, D.M., Brennan, N.M., Vourvachis, P.: A taxonomy of text analysis approaches in corporate narrative reporting research, working paper, Centre for Impression Management in Accounting Communication, Bangor Business School, UK (2013)

33. Merkl-Davies, D., Brennan, N.: Discretionary Disclosure Strategies in Corporate Narratives: Incremental Information or Impression Management? Journal of Accounting Literature 26, 116–196 (2007)
34. Manning, Shutze: Foundations of Statistical Natural Language Processing (Book) (1999)
35. Newman, M.J., Pennebaker, D., Berry, S.: Lying words: Predicting deception from linguistic styles. Personality and Social Psychology Bulletin 29(5), 665–675 (2003)
36. Nordquist, R.: Grammar & Composition Guide Book (2012)
37. Shen, Q., et al.: CBR case retrieval model research in business financial distress warning based on gray relation. In: Proceedings - IEEE Symposium on Robotics and Applications, ISRA 2012 (2012)
38. Li, S.-T., Ho, H.-F.: Predicting financial activity with evolutionary fuzzy case-based reasoning. Expert Systems with Applications, 411–422 (January 2009)
39. Slonim, T.: Design issues in fuzzy case-based reasoning. Fuzzy Sets and Systems 117(2) (2001)
40. Smith, M., Taffler, R.J.: The chairman"s statement: a content analysis of discretionary narrative disclosures. Accounting, Auditing and Accountability Journal 13(5), 624–646 (2000)
41. Tetlock, P.: Giving Content to Investor Sentiment: The Role of Media in the Stock Market. The Journal of Finance 62(3), 1139–1168 (2007)
42. Tan, T., et al.: Brain-inspired Genetic Complementary Learning for Stock Market Prediction. In: The 2005 IEEE Congress on Evolutionary Computation (2005)

Subject-Orientation as a Method to Specify the Cooperation of Active Entities in the uCepCortex Project

Albert Fleischmann[1], Egon Börger[2], and Harald Lerchner[3]

[1] Metasonic AG, Pfaffenhofen/Hettenshausen, Germany
albert.fleischmann@metasonic.de
[2] Universita di Pisa, Dipartimento di Informatica, Italy
boerger@di.unipi.it
[3] Johannes Kepler University Linz, Department of Business Information Systems, Austria
harald.lerchner@jku.at

Abstract. The aim of the uCepCortex project is to develop an exocortex based on Ubiquitous Complex Event Processing as an Artificial Cognitive System and to investigate how to enhance human cognitive abilities, manage assistive robots, and their cooperation with humans via an exocortex system. In order to develop applications based on these artefacts the requirements of these applications have to be defined in a technology independent manner. This means an abstract model of the planned application has to be described. In this article we describe a notion of model which supports the specification of autonomous agents and their interaction by events. This notion has a precise semantics which is defined by Abstract State Machines (ASM). Such models can be transformed into executable programs.

Keywords: Process, Abstract State Machine, Agent, Subject oriented process notation.

1 Introduction

In the uCepCortex project humans, robots, software applications work together to reach a common goal. These entities are more or less autonomous meaning that when they receive requests from other agents to perform an action they decide themselves whether to perform it or not. “An agent is an entity, such as a person or software component, that is capable of action”[4]. In the uCepCortex project robots and all other cognitive entities are also seen as agents. Agents are producer and consumer of events. An event is anything that happens [4][2]. In uCepCortex agents of different technologies cooperate by producing and consuming events to get the required result. This means systems developed with uCepCortex entities can be seen as processes. A process “is a collection of related, structured activities or tasks that produce a specific service or product (serve a particular goal) for a particular customer or customers”[3]. In order to specify the requirements of a system to be created “It is essential to have intuitively understandable models” (see page 15 in [1]).

D. Liu et al. (Eds.): BICS 2013, LNAI 7888, pp. 328–337, 2013.

Up to now notations which allow specifying requirements on an agent-and-event based philosophy have some major draw backs, in particular for business processes. It is difficult "to attain a coherent view of the entire business process, since its state is now distributed" and "there is a greater chance that the business process will fail to meet any overarching constraints placed upon its operation. This is because the process is constructed through dynamic, on the fly agreements, rather than through preset rules" [3]. Traditional process notations describe processes from a centralized perspective. This results in problems if non deterministic behaviors have to be described, as they appear normally in the intended applications of the uCepCortex results [7].

In the following section we want to describe a notation which allows one to describe agent oriented systems in a simple way including nondeterministic behaviors. This notation has been successfully applied in many academic and industrial business process management projects e.g. FI-TS [17], NEC [18] Swisscom[19], and has a precise formal semantic which is outlined thereafter.

In the uCepCortex project it is intended to investigate whether this notation is appropriate for building models for uCepCortex applications.

2 Subject Oriented Notation

2.1 Fundamentals of the Subject Oriented Approach

In our notation subjects represent the behavior of an active entity. A specification of a subject does not say anything about the technology used to execute the described behavior. This differs from agent-oriented concepts. Subjects communicate with each other by exchanging messages. Messages have a name and a payload. The name should express the theme of a message informally and the data are the payload transported. Internally subjects execute local activities such as calculating a price, storing an address etc. A subject sends messages to other subjects, expects messages from other subjects and executes internal actions. All these activities are done in sequences which are defined in a subject's behavior specification. Subject-oriented process specifications are embedded in a context. A context is defined by the organization and the technology in which a process is executed. Subject-oriented system development has been inspired by various process algebras (see e.g. [10], [11], [12]), by the basic structure of nearly all natural languages (Subject, Predicate, Object) and the systemic sociology developed by Niklas Luhmann (an introduction can be found in [13]). In the active voice of many natural languages a complete sentence consists of the basic components Subject, Predicate and Object(s). The subject represents the active element, the predicate the action and the object is the entity on which the action is executed. In the organizational theory developed by Luhmann the smallest organization consists of communication executed between at least two information processing entities [13]. (This is a definition from a sociologist not from a computer scientist.) Figure 1 summarizes the different inspirations of S-BPM.

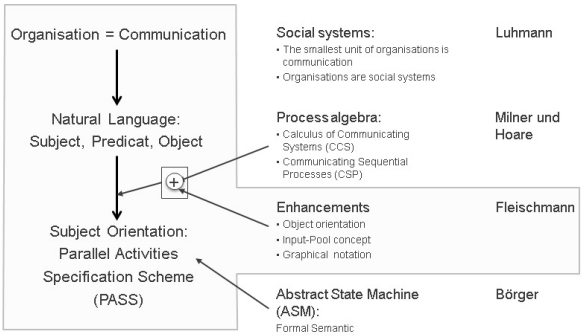

Fig. 1. Concepts of Subject Oriented Process models

2.2 Subjects: Interactions and Behavior

The basic concepts of process modeling in S-BPM are introduced by a simple process. We want to describe how the flight of a remote controlled artificial bird is controlled by a human and the flight is influenced by the wind. Fig. 2 shows an illustration of the problem and the communication structure of the problem.

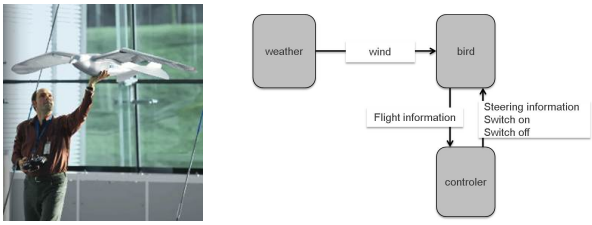

Fig. 2. Remote control of an artificial gull

In a first step we want to build an abstract model of the problem. Each entity is considered as subject and these subjects communicate with each other by exchanging messages. For exchanging messages each subject has an input pool which is similar to a mail box. A sender deposits its message in the input pool of the receiver. This input pool can be structured. The modeler can define how many messages of which type and/or from which sender can be deposited and what the reaction is if these restrictions are violated. This means the type of synchronization during message exchange can be individually specified.

Our model contains besides the messages for flying the gull also messages for switching on and off the subject “Bird”. The subject “Weather” influences the flight of the bird. This influence is modeled by the message “wind”. The subject “Controller” can send the message steering information to the bird. The bird sends back the message “flight information”. In reality the message “flight information” can be implemented by the Controller watching the bird by his eyes.

The communication structure gives only an overview of our system. Now we want to go into details. The behavior of each subject is described. Subjects send messages to other subjects, receive messages from other subjects and execute internal actions. First we consider the behavior of the subject “Weather”. This subject sends permanently the message wind to the subject “Bird”. Fig. 3 shows the behavior of subject “Weather”.

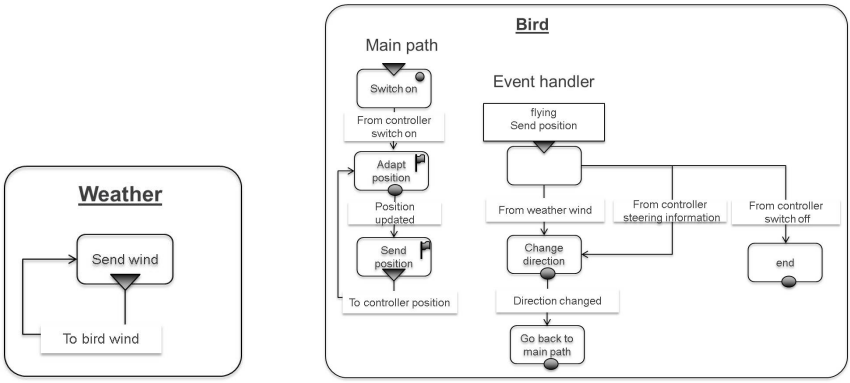

Fig. 3. Behavior of Subject "Weather" and Subject “Bird”

In Fig. 3 on the right side the behavior of subject “Bird” is shown. It consists of two parts, the main path and the event handler. The main path describes the normal flight behavior of the bird.

In the initial state the bird receives the message “switch on” from the subject “Controller”. The subject executes the internal function “adapt position” which means it flies. The result of that function is an updated position which is sent to the subject “Controller”. The states “Adapt Position” and “Send Position” are marked with a flag. This means that in these states the main path can be interrupted by message “wind” from the subject “Weather”, or by the message “steering information” or “switch off” from the subject “Controller”. If a message “wind” is in the input pool of subject “Bird” the behavior of the subject “Bird” is continued in state “Change Direction” of the event handler. In that state the direction is changed corresponding to the wind speed and direction. The same happens if the message “steering information” arrives from the subject “Controller”. After executing function “change direction” the behavior of the subject “Bird” is continued in the state of the main path where it was interrupted.

If the message “switch off” from the subject “Controller” is received, the bird runs into an end state. Fig. 4 shows the behavior of subject “Controller”.

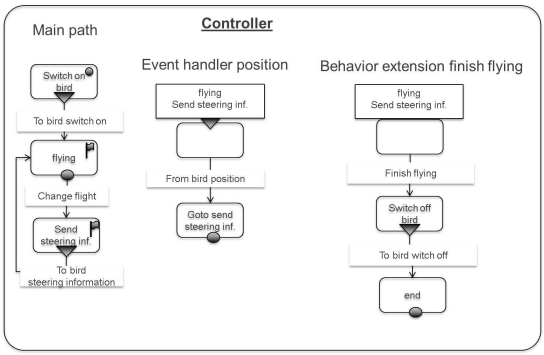

Fig. 4. Behavior of Subject "Controller"

The behavior of the subject “Controller” consists of three parts. The main path starts by switching on the subject “Bird”. After that the subject “Controller” executes the internal function “flying”. This function is finished with the result “Change Flight” which means the controller wants to change the flight of the bird. In the succeeding state the message “steering information” is sent to the subject “Bird”. With that message the bird gets some new flight information (direction, speed etc.). The main path can be interrupted if a message “bird position” comes from the bird. Then the main path is left and the subject “Controller” jumps into the event handler. The event handler forces the subject “Controller” to calculate new steering information and then to jump to the state “Steering Information” to send corresponding flight information to the subject “Bird”.

In its internal function state “flying” the subject “Controller” may have the “idea” to finish the flight session. This means the internal function “flying” may end with the result “Finish flying”. In this case the subject “Controller” left the main path and is continued in the behavior extension. In the behavior extension the subject “Controller” just sends the message “Switch off” to the subject “Bird” and the succeeding state is an end state whereby the flight session is finished.

With this simplified example we want to show the major concepts to build models for heterogeneous systems which consist of several autonomous entities and where communication is not deterministic.

2.3 Subjects and Objects

Up to now we did not mention data or the objects with their predicates in order to get complete sentences. Fig. 5 shows how subjects and objects are connected. The internal function ” Adapt position” uses internal data to prepare the data for the “Send position” message. These position and direction data is sent as payload of the message ”Send Position”. The internal functions in a subject can be realized as methods of an object or functions implemented in a service if service oriented architecture is used.

These objects have an additional method for each message. If a message is sent, the method allows one to get the values of the data sent with it and if a message is received the corresponding method is used to store the received data in the object.

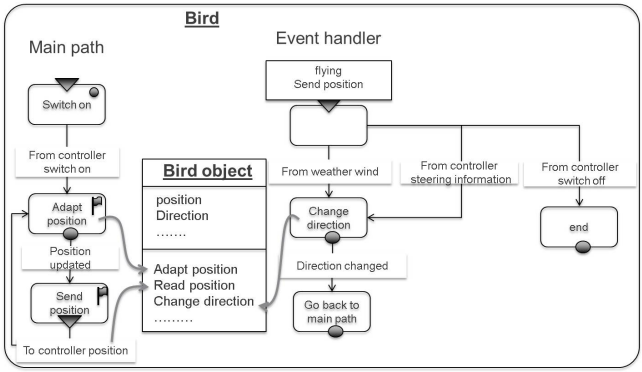

Fig. 5. Subjects and Objects

2.4 Subjects and Agents

In S-BPM subjects come with a behavior definition. In the implementation phase entities which are capable to execute actions are assigned to subjects. These agents can be humans, machines, a piece of software or a combination of all. The mapping of subjects to agents is called context of a process model. Agents execute the activities as specified in the subject definition. Process models can be executed at several locations or environments, e.g., the same process model may be used in any context. The model is always the same only the agents are different. The abstract resource subject allows one to describe process models independently of the specific environment in which a model is executed. A subject model is also independent of the type of agents (human, software etc.) executing a subject behavior. Furthermore an agent can be responsible for executing different subjects in various processes. Every employee typically is involved in more than one process. For example, employees may be involved not only in their usual work processes (controlling flying bird robots) but also in other processes such as application for vacation. Fig. 6 shows iconic representations of agents assigned to the subjects.

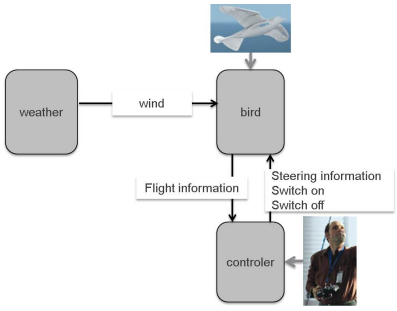

Fig. 6. Context of the "Remote Control" Process

2.5 Formal Interpreter of Subject Based Specifications

The concept of an Abstract State Machine has been developed by Yuri Gurevich [16]. To support hierarchical modular system development Egon Börger added the ASM refinements (for provably correct stepwise transformations of abstract models into executable code) [15]. These three concepts constitute the basis for a scientifically well-founded practical system engineering method known as ASM Method [8]. It has been used successfully for the design and the analysis (experimental validation and mathematical verification) of numerous software and embedded hard-software systems (see [8]).

Conceptual Foundations. ASMs provide a universal mathematical framework for semantic modelling of dynamic systems, given that they describe the evolution of mathematical algebras (or structures in the sense of mathematical logic), i.e. arbitrary sets with a collection of arbitrary operations defined on them. Such algebras allow one to represent arbitrary data structures and form the states of ASMs, generalizing the state notion of Finite State Machines (FSM). The evolution of states of an ASM is described by its program, a finite set of transition rules of the following form (cf. [8]):

If *Condition* then *Updates*

Condition (also called *guard*) is a Boolean-valued expression. *Updates* is a finite set of assignments. (Appropriate definitions support standard algorithmic notations, like LET, IF-THEN-ELSE, etc.) A single ASM computation step in a given state consists in executing simultaneously all updates of all transition rules whose guard is true in the state, if these updates are consistent, in which case the result of their execution yields the next state [8, p. 30]. This is the mathematical core of the semantics of (single-agent sequential as well as multi-agent distributed) ASMs.

An Abstract Interpreter Model for S-BPM. The ability to simulate arbitrary computational systems on their given level of abstraction, without implementing them in terms of software, qualifies ASMs for high-level system design and analysis [9]. The ASM method has constituents which are similar to those of S-BPM, thus permitting intertwining them from a structural and methodological perspective [9].

The behaviour of a subject in a process can be described using the three fundamental types of activities: send, receive, and function. Each subject is detailed through a so-called Subject Behaviour Diagram (SBD) which can be interpreted as directed graph. A graph consists of nodes connected by edges. Each node represents a state in terms of ASMs. At each state the underlying subject performance of one of the three activities is assigned to the state. One can understand an edge as transition from one state to the next. A transition can only occur once the activity assigned to a node has been completed. In order to manage alternative transitions each edge corresponds to a termination condition of the executed activity.

The following example of the ASM rule BEHAVIOR shows how to process a graph. The rule BEHAVIOR is invoked with the underlying subject and a state. It uses the rules PROCEED, START und PERFORM.

```
BEHAVIOR (subj , state) =
    if SID_state(subj ) = state then
        if Completed(subj , service(state), state) then
            let edge =
                select_Edge ({e ∈ OutEdge(state) | ExitCond(e)(subj , state)})
                    PROCEED (subj , service(target(edge)), target(edge))
        else PERFORM (subj , service(state), state)
where
    PROCEED (subj , X , node) =
        SID_state(subj ) := node
        START (subj , X , node)
```

Fig. 7. Rule BEHAVIOR, taken from [8] p. 320

This ASM can be read in the following way: Each subject is in a given state at each time (called as SID_State). A transition from the current state to the next state within the subject behaviour diagram can only occur if the service (equal to the assigned activity) is completed. Therefore the rule PERFORM will be executed until the predicate *Completed* confirms that the service has been completed. The edge to be taken to the successor state is selected by the function $\text{select}_{\text{Edge}}$.

Through the transition to the successor state the rule PROCEED sets the new current state of the subject (SID_State) and starts with the rule START the service (= activity) which is assigned to the successor state. The rules PERFORM and START remain abstract and are to be refined in successive steps.

Fig. 8 shows the complete structure of the interpreter. The function BEHAVIOR shown in Fig. 7 uses the function PERFORM. This function uses TryAlternative and so on. The size of the complete interpreter is only nine A4 pages.

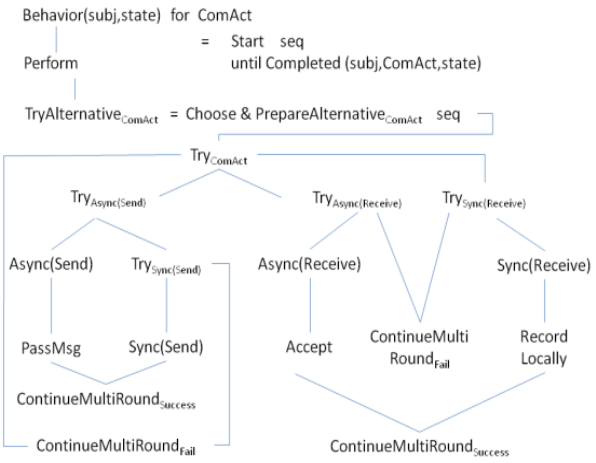

Fig. 8. Structure of the abstract Interpreter, taken from [8] p. 337

3 Conclusion and Future Work

The described concepts will be challenged in a complex use case whose structure is shown in Fig. 9. In this use case a mass event will be managed in order to avoid panic. Monitors are used to watch the people and in the case of signs of a beginning panic robots are used to structure the flow of people.

In order to use the subject oriented notation domain specific messages can be predefined including the data which are transported with messages.

Additionally it has to be investigated whether subjects can be also used as specifications for complex event processing agents [6].

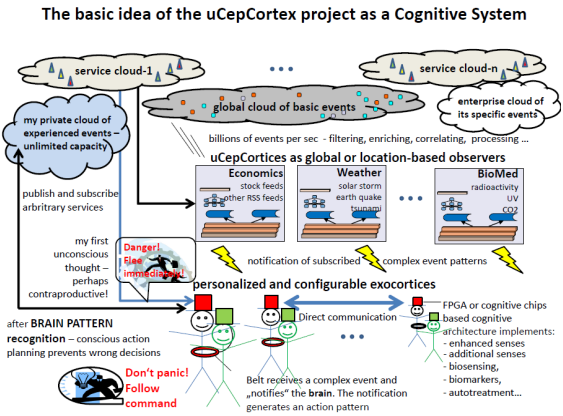

Fig. 9. Use case of the uCepCortex project [20]

References

1. Sterling, L.S., Taveter, K.: The Art of Agent-Oriented Modeling. MIT Press, Cambridge (2009)
2. Luckham, D.: Event Processing for Business. John Wiley & Sons, Hoboken (2012)
3. Jennings, N.R., et al.: Autonomous Agents for Business Process Management. Applied Artificial Intelligence 14, 145–189 (2000)
4. Chandy, K.M., Schulte, R.W.: Event Processing. Mac Graw-Hill, New York (2010)
5. Wooldridge, M.: An Introduction to Multi Agent Systems. John Wiley & Sons, Chichester (2002)
6. Fleischmann, A., Schmidt, W., Stary, C., Strecker, F.: Nondeterministic events in business processes. In: La Rosa, M., Soffer, P. (eds.) BPM 2012 Workshops. LNBIP, vol. 132, pp. 364–377. Springer, Heidelberg (2013)
7. Fleischmann, A., Schmidt, W., Stary, C., Obermeier, S., Börger, E.: Subject Oriented Business Process Management. Springer, Heidelberg (2012)
8. Börger, E., Stärk, R.: Abstract State Machines: A Method for High-Level System Design and Analysis. Springer, Berlin (2003)

9. Börger, E.: The subject-oriented approach to software design and the abstract state machines method. In: Stary, C. (ed.) S-BPM ONE 2012. LNBIP, vol. 104, pp. 1–21. Springer, Heidelberg (2012)
10. Hoare, A.: Communicating Sequential Processes. Prentice-Hall (1985)
11. Milner, R.: Communicating and Mobile Systems: The Pi-Calculus. Cambridge University Press (1999)
12. Milner, R.: Communication and Concurrency, Prentice Hall (1989)
13. Berghaus, M.: Luhmann leicht gemacht. Böhlau Verlag (2011)
14. Börger, E.: Construction and Analysis of Ground Models and their Refinements as a Foundation for Validating Computer Based Systems. Formal Aspects of Computing J. 19, 225–241 (2007)
15. Börger, E.: The ASM Refinement Method Formal Aspects of Computing 15, 237–257 (2003)
16. Gurevich, Y.: Evolving algebras 1993: Lipari Guide. In: Börger, E. (ed.) Specification and Validation Methods, pp. 9–36. Oxford University Press (1995)
17. Konjack, G.: Case study: AST order control processing. In: Buchwald, H., Fleischmann, A., Seese, D., Stary, C. (eds.) S-BPM ONE 2009. CCIS, vol. 85, pp. 115–120. Springer, Heidelberg (2010)
18. Nakamura, S., Tan, T., Hirayama, T., Kawai, H., Komiyama, S., Hosaka, S., Nakamura, M., Yuki, K.: CGAA/EES at NEC corporation, powered by S-BPM: The subject-oriented BPM development technique using top-down approach. In: Schmidt, W. (ed.) S-BPM ONE 2011. CCIS, vol. 213, pp. 215–231. Springer, Heidelberg (2011)
19. Walke, T., Witschi, M., Reiner, M.: Case study @ swisscom (Schweiz) AG: iPhone 5 self-service order app and process-workflows. In: Fischer, H., Schneeberger, J. (eds.) S-BPM ONE 2013. CCIS, vol. 360, pp. 264–273. Springer, Heidelberg (2013)
20. http://www.citt-online.com/downloads/uCepCortex-proposal-2G-Athens.ppt

A Review of DC Micro-grid Protection

Yuhong Xie[1], Jia Ning[1], Yanquan Huang[1], Junbo Jia[2], and Zhihui Jian[1]

[1] School of Electrical Engineering, Southwest Jiaotong University,
Chengdu, Sichuan, China, 610031
[2] School of Engineering, Temasek Polytechnic, Singapore 529757

Abstract. In this paper, an overview of DC micro-grid is described, which includes the status of DC micro-grid protection and its future development. The paper presents the key techniques of DC micro-grid protection. So far, standards, guidelines and techniques for DC micro-grid protection are well behind AC system. This paper summarizes the protective devices and protective methods of different DC micro-grid structures. The protective devices include fuses, circuit breakers and power-electronic switches. According to a series of research achievements, the paper points out the technological gaps and proposes some ideas for DC micro-grid protection in the future.

Keywords: DC Micro-grid, Protection, Protective Devices, Structures, Technological Gaps.

1 Introduction

Under the pressures of energy growth demand and environmental protection, distributed generation based on renewable energy resources has been receiving spotlights. The concept of micro-grid appeared to optimize the distributed generation to make up a smart system. DC micro-grid as an adaptive control system brings a convenience and high efficiency for integrating the distributed resources. DC micro-grid system can support plug and play functionality. Meanwhile, DC micro-grid system can reduce the losses in power transmission and improve power quality. Therefore, DC micro-grid has become an efficient means to integrate distributed resources. However, the research of DC micro-grid system is lag from the research level in AC micro-grid system. The reason why DC micro-grid system can not be widely used is lack of realizable protection means, standards and guidelines.

In 1990s, Sweden, Japan, France and The U.S. start to research [1], [2] DC power supply in data center. With the development of technology in DC micro-grid, DC system was applied in practice gradually use for shipboard [3], [4], spaceflight and automatic system, especially in electric traction DC power supply.

Nowadays, Japan, EU and the U.S. have set up professional research institution and demonstration project in residence DC power supply [5], [6].In China, research in dc micro-grid is still at an embryonic stage [34]. The government has established some organizations to start research in this field. As we know, the structures of DC micro-grid are varied and the control strategy may be different. So that different protective methods were emerged in research and engineering field.

D. Liu et al. (Eds.): BICS 2013, LNAI 7888, pp. 338–347, 2013.

This paper presents an overview of research of DC micro-grid to date. The significance of this work is to identify that DC system has higher efficiency than AC micro-grid system and it is feasible in application.

2 DC Micro-grid

A DC micro-grid is a network consists of generators, wind power system, photo-voltaic system, fuel cell system, energy storages such as super-capacitors and batteries, loads and so on. Resources and loads are integrated to DC bus through power electronic converters and protective devices (PD), connected to the utility grid at the point of common coupling (PCC) [3], [8]. Generally, the loads are supplied from the local resources and, if necessary, from the utility grid. The power also can export to the utility grid when the power produced by local resources exceeds the loads' power.

In DC micro-grid system, all kinds of resources can be in parallel to a DC bus or more. Using voltage droop of control, the system become more stable and efficient. There are some types of DC micro-grid system structure [7], [8], [9]. Example of Multi-terminal DC micro-grid System structure is shown in Fig. 1. Multi-terminal DC micro-grid system was first presented in the early 1990s. Consequently, the system becomes more robust and reliable.

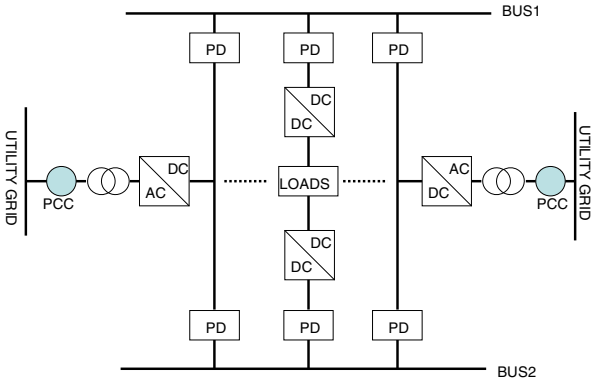

Fig. 1. Multi-terminal DC micro-grid system structure

3 DC Micro-grid Protection

A DC micro-grid system in application must be reliable and stable to operate as a UPS. Therefore, a good functionality protective system with high reliability is needed. The protective system consists of protective devices, protective relays and grounding. Due to the particularity of DC micro-grid, with bidirectional power flow, the AC power protective system can not be applied to DC micro-grid system directly. For a long time, most of the researches of power protective system are in AC field. As a start point,

experiences in power system, especially in power supplying for DC traction system and DC transmission [10], [11], can guide us to design a protective system to apply to DC micro-grid system. Short-circuit current calculation and fault detection have been discussed in [12], [13].

The challenges facing to DC protective system are arc extinguishing rapid and security. According to [14], protective system designed for micro-grid should obey the following criteria: reliable, speedy, well-performance, economical and simple.

3.1 Protective Devices

The power electronic converters containing protective functions can be used. Besides, other protective devices available commercially for DC micro-grid system are fuses and circuit breakers (CB) including molded-case circuit breakers (MCCB) and isolated-case circuit breakers [15], [16].Because of DC micro-grid system doesn't have natural zero current condition, devices designed for DC micro-grid system must be able to extinguish the arc rapidly and safely.

3.1.1 Fuses

Fuses are common used in a low-impedance system, mostly applying to DC traction, battery protection. Selection of fuse depends on the current-time and voltage ratings of system. In DC micro-grid system, the key point is to calculate the system time constant [15]. The rise time, determined by the system time constant, directly affects the operation of fuse to cut off the current. In a DC micro-grid system with a small time constant (<2.5ms), the fuse link will melt rapidly and extinguish the arc. If the time constant is up to 6 ms, with longer rise time, the temperature of fuse link increase slowly so that the heat-absorbing material cannot cool the arc, leading to the arc cannot be extinguished quickly [17]. In addition, fuses applied to DC micro-grid system should prevent fuse malfunction from transient over current. Fuses are a kind of economical protective devices. However, considering the performance of reliability and simplicity, fuses are not qualified to DC micro-grid protection because of it is inconvenient to be installed and difficult to difference transient effects and faults. In general, the best scheme is that fuses operate as secondary protection.

3.1.2 Circuit Breakers

In DC micro-grid system, resources interface to the DC bus through power electronic converters. Some of them, for example, generator and wind power system, will produce variable frequency transient interference. So that, DC micro-grid system needs large capacity of the capacitors to filter ripple wave and decoupling.

While a DC bus short circuit is happening, the capacitors rapidly discharge into fault point resulting in a surge current, the value depending on the filter design. The CBs maybe trip due to the transient current [18]. The impact of capacitors discharge in DC protective system has been identified specifically [19]. For example, the upstream and downstream CBs operate at the same time, or worse, the upstream CB trips but the closest CB doesn't. Furthermore, the loads capacitors discharge also contributes to the surge current probably result in more unwanted CBs tripping.

Besides, if the fault cannot be isolated rapidly, the CBs may be destroyed. For example, when the CBs instantaneous trip is exceeded, but the peak current doesn't sustained at a high enough value for long enough, the CB contacts cannot open completely so that the arc sustained burning even lead to the contacts to weld together during the fault[20].

Therefore, it is important to guarantee the CBs trip accurately and completely. The traditional CBs limiting the speed of fault isolation and recovery are not suit for DC micro-grid system, the voltage above 325V. Vacuum circuit breakers and hybrid solid state/vacuum interrupters are born to solve the limitation [21], [22].

These high-speed CBs are designed to apply to high voltage DC system. Even in a system with large time constant, the high-speed CBs still have a perfect performance, isolating the fault within 0.01 s. The application of high-speed CBs in DC system improves the reliability of DC protective system but at greater cost. However, this solution is a palliative. A suggestion was proposed by [23], [24]. According to the papers, to decrease the capacity of DC bus capacitors maintaining the performance criteria of the system, by means of using small capacity of film capacitors and active compensation device to replace the traditional large capacity of electrolytic capacitors, is an efficient approach.

3.1.3 No-Load Switches and Solid State Switches

Fast no-load switches are electro-mechanical devices, applying to isolate portions or zones to separate the health part from fault section of the system. Solid State Switches are semiconductor devices. They are able to interrupt current in μsec level [25], [26]. The schematic of current interrupter is shown in Fig. 2. For example [27], [28], gate turnoff thyristor (GTO), insulated-gate bipolar transistor (IGBT) and integrated gate-commutated thyristor (IGCT), are often used to DC protective system in especial in military without considering the cost. Solid State Switches have a well-function of current limitation [29], [30], as shown in Fig. 3. They can also apply to a high voltage level system [26], [31].

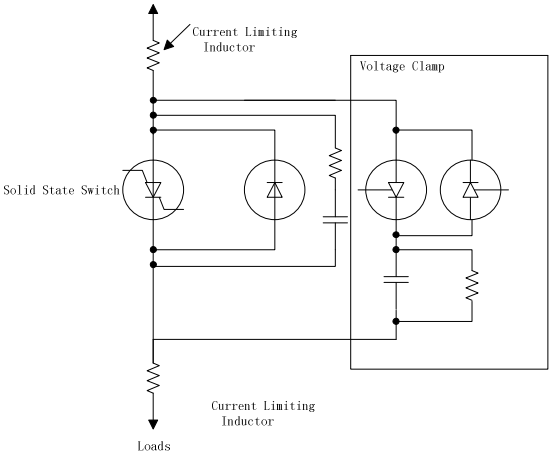

Fig. 2. Solid state current interrupter

Besides, according to the characteristic of DC single wizard transmission, by means of adding a series diode at branch of load-side can prevent the backflow of converter capacitive current while a DC bus short circuit is happening [32]. That helps to reduce the damage of DC bus short circuit, meanwhile, eliminating the potential of fire disaster.

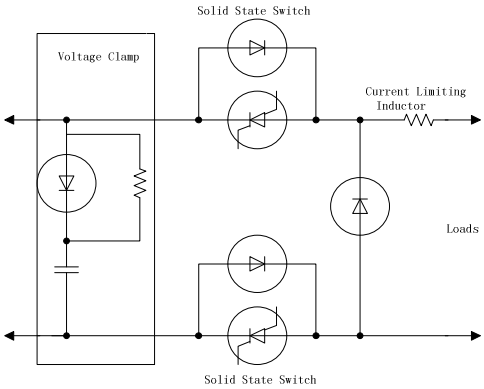

Fig. 3. Load protective current limiter

3.1.4 Multi-functional Patch Panel and Plug

Because of there is no natural zero current condition in DC system, the patch panel and plug needs to be redesigned. A feasible scheme was proposed by [33]. The structure is shown in Fig. 4 [34]. At power on stage, the main circuit will be closed in uncharged condition, and then, driving circuit closed to increase the main circuit current. So that the impact of surge current can be controlled. On the contrary, at power off stage, the driving circuit will be opened to force the current flow past the free-wheeling diode, and then separating the patch panel and the plug, there will be no arc.

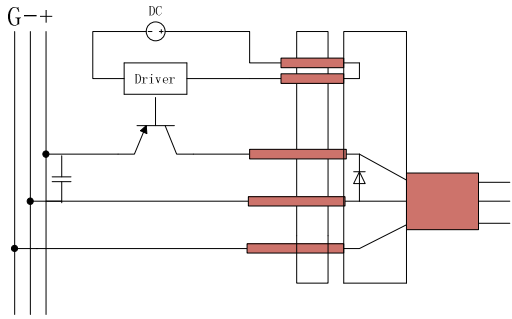

Fig. 4. Multi-functional patch panel and plug

3.2 Protective Relays

Generally, high-speed DC CBs can be set to trip if the current exceeds 1-4 p.u.. However, in some condition, for example, a fault with high impedance has occurred, protective relays are needed to calculate time derivatives and step changes of currents to determine whether the breakers trip or not.

3.3 Grounding

Grounding is a very important approach for fault detection and safety [35]. There are many different modes in power system discussed in [36], [37]. A DC micro-grid can be ungrounded, high impedance grounded, or low impedance grounded. Two types of grounding, TN-S system and IT system, are discussed in this paper.

In TN-S DC micro-grid system, the middle point of converter and battery connected to ground (T), and the metal skins of equipment connected to the neutral and protective earth (N). The neutral wire and protective wire are separated wires, connected at the side of grounding (S). While a ground fault is occurring, a large ground current and a large DC-link voltage transient are easily detected and the fault can be quickly cleared. So TN-S system can be applied to DC micro-grid especially power supplying for houses, commercial centers and factories.

In IT DC micro-grid system, neutral of converter and battery ungrounded or high impedance grounded (I), and the metal skins of equipment connected to ground independent of the neutral (T). As a result, there is a small ground fault current and voltage transient. On one hand, a small fault current causes a difficulty for fault detection. On the other hand, a small fault current and voltage transient will not do serious damage to the system. If only a single ground fault is occurring, the system can still operate stably for a reasonable period of time. To increase the impedance of each load can limit the voltage transient but results in higher losses.

An example of DC micro-grid protection presented by Salomonsson [38] was shown in Fig. 5. The calculation of fault current was treated in [39], [40], [41]. It is a TN-S ground system. So that the faults illustrated are easily to be detected. Fault F1 and F2, with large fault current, are potential threatening to damage the power electronic converters in parallel to the DC bus. To protect the converters, high-speed DC CBs are used in this system. When fault F1 or fault F2 is occurring, large fault currents (i_{ac} and i_{batt}) are detected causing PD1 and PD3 opened. The DC bus voltage drops to zero. If fault F3 is occurring, PD5 and PD6 will sense a large current meanwhile causing a bus voltage drop, and then PD5 and PD6 both trip. So that the faulted feeder is isolated. Fault F4 is similar to fault F3, in this system, with low-impedance. While fault F4 is occurring, PD7 will trip. Above are protective measures of each unit. To improve the reliability of protective system, this requires that the PDs coorperate with each other. PD1-PD4 are backup protection for the feeder protection. Otherwise, PD5-PD8 are backup protection if PD1-PD4 do not clear the bus faults. In addition, PD5-PD8 must be faster than PD1-PD4 to prevent a malfunction of PD1-PD4 while a feeder fault is occurring. Besides, fuses can be connected on the AC side of the converters to act as backup protection for the converters [35].

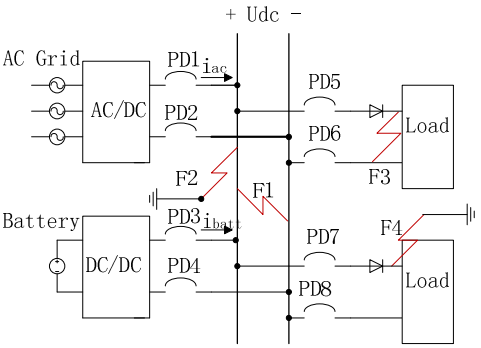

Fig. 5. Detailed scheme of protective system

Another example of Protective topology multi-terminal DC micro-grid system shown in Fig. 6 was presented by Tang and Ooi [42]. The three buses are supplied by three voltage source converters (VCS). This paper proposes the handshaking method to protect DC system. In this system, for example, a fault occurs on Bus1. Each VSC will select a fast DC switch to trip owing to the abnormal current. The rule of selection is: the switch selected is the one carrying the largest positive fault current. In this case, VSC1 selects SW11, and VSC2 selects SW12. However, for VSC3, which switch will be selected depends the distance fromVSC3 to the faulted pole. As a matter of fact, it doesn't matter whether SW33 or SW23 will be selected. The paper assumes that SW33 is selected. According to the handshaking method, from the result of the selection, VSC1 distinguishes Bus1, VSC2 distinguished Bus1 and VSC3 distinguishes bus3 as potential faulted line. By analyzing the handshaking method, we find out that the non-faulted bus will always connected to a VSC at one end through a closed switch. The final result is determined by voting. So Bus1 is selected and isolated. After isolating the fault, the system needs to be re-configured. Then the three VSCs recover the output to supply the buses. The opened switch will be re-closed if the switch senses the voltage on both sides exceeding the pre-set value. So that SW33 is re-closed, then the system restore to a regular condition.

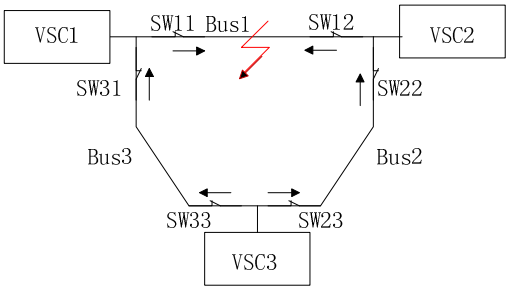

Fig. 6. Protective topology of multi-terminal DC system

Besides, a DC zonal electric system was presented in [3]. The system is a revised version considered by the U.S. navy for shipboard electrical system [43], [44]. With redundant design, it makes the system more stable and robust. The protective method is similar to the multi-terminal DC system.

4 Conclusion

This paper represents the structures of DC system and the DC protective system. To utilize the DC protective devices available commercially, a reliable protective system could be designed, so that the application of DC micro-grid system is feasible. It is an ideal solution to integrate the distributed resources since DC micro-grid system has a higher efficiency and easier to be controlled than AC micro-grid system. In order to promote the scale of DC micro-grid system in practice, unified standards and guidelines need to be formulated as quickly as possible.

So far, the DC protective technology is not developed enough. Maybe the power-electronic devices can be extensive used in DC system. And the protective function of VSC can be exploited further aiming to make the protective system to be as simpler as possible.

References

1. Zhu, X.: New high voltage direct current power supply system for data communication Equipment abroad. Designing Techniques of Postes and Telecommunication (2009)
2. My Ton, Brian Fortenbery.: DC Power for Improved Data Center Efficiency [R/OL] (2008)
3. Ciezki, J.G., Ashton, R.W.: Selection and stability issues associated with a navy shipboard DC zonal electric distribution system. IEEE Transactions on Power Delivery (2000)
4. Su, C.L., Yeh, C.T.: Probabilistic security analysis of shipboard DC zonal electrical distribution systems. In: IEEE Power and Energy Society General Meeting (2008)
5. Kakigano, H., Miura, Y., Ise, T.: Fundamental characteristics of DC micro-grid for residential houses with cogeneration system in each house. In: 2008 IEEE Power and Energy Society General Meeting, Pittsburgh, PA, USA (2008)
6. REbusTM DC Microgrid: Technical Overview (2010)
7. Marnay, C., Rubio, F., Siddiqui, A.: Shape of the microgrid. In: IEEE Power Engineering Society Winter Meeting, pp. 150–153 (2001)
8. Lu, W., Ooi, B.T.: Multiterminal LVDC system for optimal acquisition of power in wind-farm using induction generators. IEEE Trans. Power Electron 17(4), 558–563 (2002)
9. Lu, W., Ooi, B.T.: Optimal acquisition and aggregation of offshore wind power by multiterminal voltage-source hvdc. IEEE Trans. 18(1), 201–206 (2003)
10. Wang, H., He, B.: Transmission Line Aggrate Protection and Its Implementation. Power System Technology (2005)
11. Paul, D.: DC traction power system grounding. IEEE Transactions on Industry Applications 38(3), 818–824 (2002)
12. Sutherland, P.: DC short-circuit analysis for systems with static sources. IEEE Trans. Ind. Appl. 35(1), 144–151 (1999)

13. Feng, X., Ye, Z., Liu, C., Zhang, R., Lee, F., Boroyevich, D.: Fault detection in dc distributed power systems based on impedance characteristics of modules. In: Proc. Conf. Rec. IEEE Ind. Appl. Soc. Annu. Meeting, Rome, Italy, October 8-12, vol. 4, pp. 2455–3462 (2000)
14. Cuzner, R.M., Venkataramanan, G.: The status of DC micro-grid protection. In: IEEE Industry Applications Society Annual Meeting, Edmonton, Alberta, Canada (2008)
15. Brozek, J.P.: DC Overcurrent Protection—Where We Stand. IEEE Transactions on Industry Applications 29(5), 1029–1032 (1993)
16. Gregory, G.D.: Applying Low Voltage Circuit Breakers in Direct-Current Systems. IEEE Transactions on Industry Applications, 650–657 (1995)
17. IEEE Guide for the Protection of Stationary Battery Systems. IEEE Std.1375-1998 (1998)
18. Baran, M., Mahajan, N.R.: PEBB based DC system protection: opportunities and challenges. In: Proceedings of the IEEE Power Engineering Society Transmission and Distribution Conference, PES TD 2005/2006, Dallas, TX, USA (2006)
19. Siu, A.: Discrimination of miniature circuit breakers in a telecommunication DC power system. In: Telecommunications Energy Conference, pp. 448–453 (1997)
20. Yao, G., Wang, Z.: A Circuit Structure of High Voltage Direct Current Circuit Breaker and Its Test Methods. In: CESSE (2011)
21. Genji, T., Nakamura, O., Isozaki, M., Yamada, M., Morita, T., Kaneda, M.: 400 V class high-speed current limiting circuit breaker for electric power system. IEEE Transactions on Power Delivery 9(3), 1428–1435 (1994)
22. Krstic, S., Wellner, E., Bendre, A., Semenov, B.: Circuit Breaker Technologies for Advanced Ship Power Systems. In: IEEE Electric Ship Technology Symposium (2007)
23. ABB circuit breakers for direct current applications (2009)
24. Shimizu, T., Jin, Y., Kimura, G.: DC ripple current reduction on a single-phase PWM voltage-source rectifier. IEEE Transactions on Industry Applications (2000)
25. Krstic, S., Wellner, E., Bendre, A., Semenov, B.: Circuit Breaker Technologies for Advanced Ship Power Systems. In: IEEE Electric Ship Technology Symposium (2007)
26. Commerton, J., Zahzah, M., Khersonsky, Y.: Solid state transfer switches and current interruptors for mission-critical shipboard power systems. In: IEEE Electric Ship Technologies Symposium (2005)
27. Tennakoon, S., McEwan, P.: Short-circuit interruption performance of thyristor circuit breakers. In: Proc. IEEE APEC, Orlando, FL, vol. 2, pp. 832–838 (1994)
28. Meyer, J.M., Rufer, A.: A dc hybrid circuit breaker with ultra-fast contact opening and integrated gate-commutated thyristors (igcts). IEEE Trans. Power Del. 21(2), 646–651 (2006)
29. Brice, C.W., Dougal, R.A., Hudgins, J.L.: Review of Technologies for Current-Limiting Low-Voltage Circuit Breakers. IEEE Transactions on Industry Applications (1996)
30. Chunlian, J., Dougal, R.: Current Limiting Technique Based Protection Strategy for an Industrial DC Distribution System. In: IEEE International Symposium on Industrial Electronics, vol. 2, pp. 820–825 (2006)
31. Crowley, T., O'Brien, H., Shaheen, W.: Evaluation of 10 kV, 80 kA Si SGTO Switching Components for Army Pulsed Power Applications. In: Power Modulator Symposium Conference Record, May 14-18, pp. 240–243 (2006)
32. Cairoli, P., Kondratiev, I., Dougal, R.: Ground Fault Protection for DC Bus Using Controlled Power Sequencing. In: IEEE SoutheastCon 2010 Conference: Energizing Our Future, Charlotte-Concord, NC, USA (2010)
33. Lee, F.C.: Sustainable Buildings and Nanogrids (2010)

34. Weimin, W., Yuanbin, H., Pan, G.: Key Technologies for DC Micro-Grids. Transactions of China Electrotechnical Society 1(1), 98–106 (2012)
35. IEEE Recommended Practice for the Design of DC Auxiliary Power Systems for Generating Stations. IEEE Std. 946-2004 (2004)
36. Low-Voltage Electrical Installations, IEC 60 364-1 (2005)
37. Paul, D.: DC Traction Power System Grounding. IEEE Trans. Ind. Appl. 38(3), 818–824 (2002)
38. Salomonsson, D., Söder, L., Sannino, A.: An Adaptive Control System for a DC Microgrid for Data Centers. IEEE Transactions on Power Delivery 24(3), 1405–1414 (2009)
39. IEEE Guide for the Protection of Stationary Battery Systems, IEEE Std. 1375-1998 (1998)
40. ABB Power Breaker Catalogue (2009)
41. Evox Rifa Electrolytic Capacitors, EVOX RIFA (2007)
42. Tang, L., Ooi, B.-T.: Locating and Isolating DC Faults in Multi- Terminal DC Systems. IEEE Transactions on Power Delivery 22(3), 1877–1884 (2007)
43. Baran, M., Mahajan, N.R.: DC Distribution for Industrial Systems: Opportunities and Challenges. IEEE Trans. Ind. Appl. 39(6), 1596–1601 (2003)
44. Baran, M., Mahajan, N.: Overcurrent Protectiong on Voltage-Source-Converter-Based Multiterminal DC Distribution Systems. IEEE Transactions on Power Delivery 22(1), 406–412 (2007)

Multicast Routing Algorithm Based on Network Coding

Dongming Tang[1,2], Xianliang Lu[1], and Juguang Li[2]

[1] School of Computer Science and Engineering,
University of Electronic Science and Technology of China, Chengdu, China
[2] School of Information Engineering,
Southwest University of Science and Technology, Mianyang, China
dmtang@hotmail.com, xlu@uestc.edu.cn, ljg_express@263.net

Abstract. Network coding has been proved can approach the max-flow min-cut limit of the network graph and can improve the performance of multicast communication. Considering the advantages of Dijkstra shortest path algorithm and network coding respectively, an improved multicast routing algorithm based on network coding is proposed in this paper. The details of algorithm are given to construct a proper multicast topology for data transmission. The simulation results show proposed algorithm has an apparent advantage of throughput and load balance compared with shortest path distribution tree algorithm, and has better advantage than previously proposed multicast routing algorithm based on network coding in terms of the metrics of load balance.

Keywords: Network coding, multicast communication, multicast routing.

1 Introduction

The network coding, proposed by Ahlswede et al. [1], generalizes traditional routing by allowing intermediate network nodes to generate new packets by coding operations on incoming data packets. By this way, the network throughput can approach the max-flow min-cut limit of the network graph. Subsequently, it has been further shown that linear network coding is sufficient to achieve the multicast capacity [2]. Linear network coding regards the messages as vectors of elements in a finite field, and the encoding function is a simple linear combination over the finite field. The framework of random linear network coding was proposed in [3], which shifts network coding research from theory to practical applications. An algebraic framework was introduced in [4] for investigating capacity issues in networks using linear codes, and the technique made a connection between certain systems of polynomial equations and the solutions to network problems. For single source linear multicast at the maximal data rate, the polynomial-time algorithm was presented in [5] and [6], in which the linear algebra, network flows and randomization/derandomization were combined together.

However, all above papers assume the availability of dedicated network resources, and scant attention is paid to the problem of determining the allocation of network resources to dedicate to a particular connection or set of connections. So,

D. Liu et al. (Eds.): BICS 2013, LNAI 7888, pp. 348–357, 2013.

Lun et al. [7] took the cost consideration from routed packet networks and applied it to coded packet networks. They found the minimum-cost sub-graphs that allow given multicast connections to be established (with appropriate coding) over coded packet networks, and then gave a distributed minimum-cost routing algorithm. Chi et al. [8] proposed the routing algorithms of network coding based multicast for low-rate multicast and high-rate multicast respectively, and the routing performance simulation results verified the effectiveness of the algorithms. Wang et al. [9] presented a new multicast routing algorithm to search the routing groups from source node to each receiver node by using reduction network, and they showed the performances of the routing algorithm are improved at a great extent in resource consumption and load balance.

Only considering the multicast based on network coding, in this paper, we propose a detailed algorithm to find proper transmission paths from source to multi-receivers in multicast network. The algorithm optimizes the sharing of links in paths, increase the multicast routing performance. We evaluate our algorithm by using a series of simulation experiments, and the proposed algorithm can bring tangible benefits compared with the other multicast routing algorithms (traditional multicast algorithm based on shortest path distribution tree and the previously proposed multicast routing based on network coding), when considering throughput and load balance.

The remainder of the paper is organized as follows. Section 2 discusses the principle of network coding and the context of multicast routing. Section 3 proposes the multicast routing algorithm based on network coding. We take performance simulations for algorithm in section 4. Finally, we conclude this paper in Section 5.

2 Network Coding and Multicast Routing

2.1 Network Coding

we explain coding operations of network coding in directed acyclic networks and use random linear network coding on finite field $GF(q)$, where q denotes the size of finite field. A node encodes a new packet p_i by linearly combining n original packets x_j as $p_i = \sum_{j=1}^{n} f_{ij} x_j$, where f_{ij} are the random elements belonged to a finite field $GF(q)$ having q elements.

The benefit of random linear network coding can be exemplified through the classic example depicted in Fig.1. Each link in the topology has unit capacity as shown in Fig.1(a), and the source S want to transmit packets a and b, containing binary information symbols, to receivers X and Y. It's easy to check the value of max-flow from source node to every receiver node is 2. The goal is to maximize the receiving rate at the two receiver nodes X and Y in a multicast session. Fig.1 (b) shows that the intermediate node T has to carry out two individual transmissions of a and b by the traditional multicast routing. However, as illustrated in Fig.1(c), with network coding, node T can code a new packet $a+b$, with the "+" operation

defined in a finite field, and forwards the new packet to X and Y. The receiver X can recover b as $b = a + (a + b)$, and similarly Y can recover a. So, we can see the network coding realizes the multicast max-flow.

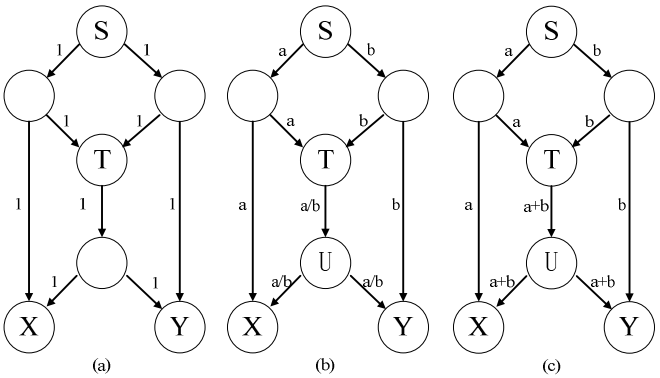

Fig. 1. Examples of network coding

Other than achieving the max-flow and improving the throughput of multicast, network coding also offers other benefits, such as load balance and lower bandwidth consumption.

2.2 Multicast Routing

Multicast, which means transmitting information from the source to a set of receiver nodes, is a mode of connection used widely in network communications. The key problem of multicast communication is a proper multicast routing selection. In traditional multicast communications, to seek a minimum-cost multicast tree is a Steiner tree problem, which is well known to be NP-complete problem. In fact, the fundamental topological structure of multicast, whether it is IP-layer or application-layer, is a tree. Hence, every multicast group member in the tree has only one path from the source root, and its throughput is limited by this path [10]. It's not easy to add other paths from the source to each receiver node to increase throughput.

However, finding minimum-cost sub-graphs in coded packet networks is much easier, and one can find optimal sub-graphs in polynomial time in many cases [7]. Just as the examples illustrated by Fig.1, by appropriate use of network coding, the communication network will achieve the maximum throughput without increasing commensurate cost or complexity.

3 Multicast Routing Algorithm

3.1 Preliminary

We consider a network graph with a source node s and a set of multicast group members as receiver nodes. We first introduced the notion of *k*-redundant multicast graph and disjoint paths defined in [10].

Definition 1 (*k-redundant multicast graph*). A *k*- redundant multicast graph for single-source multicast is a directed acyclic graph (DAG) which has the following two properties:

1) The set of all nodes *A* is the union of three disjoint subsets $\{s\} \cup A_I \cup A_T$:

$\{s\}$, the source, indegree(*s*) = 0 and outdegree(s) > 0;

A_I , the intermediate nodes (who are not members of the multicast group), denoted by u_i , $1 \le i \le n_I$, $1 \le$ indegree(u_i) $\le k$ and outdegree(u_i) > 0;

A_T , the receiver nodes (i.e., multicast group members), denoted by t_i , $1 \le i \le n_t$, indegree(t_i) = k and outdegree(t_i) = 0;

2) If each edge in the graph has unit-bandwidth, then for any node whose indegree is k , its individual max-flow is k .

Definition 2 (*disjoint paths*). The disjoint paths are two paths from s to t , which do not share any common edges.

Then, given a node t with indegree k in a *k*-redundant multicast graph with source s and unit-bandwidth edges, t has k disjoint paths from s if and only if t has individual max-flow of k .

At last, we give the definition of path stamp, which gives the effective hints to search the proper disjoint path from source node s to each receiver node. By using path stamp, we can build the disjoint paths from source node to a receiver node, and we are able to guarantee the paths from source node to different receiver nodes have more shared links.

Definition 3 (*path stamp*). For a path from s to t_i , $1 \le i \le n_t$, we denote $ps(i)$ the path stamp of every intermediate node to indicate the fact that a path has went through this node. When $ps(i) = 1$, we say the intermediate node is on the path from s to t_i , while $ps(i) = 0$ indicates the node is not on the path from s to t_i .

3.2 Algorithm

For the convenience of discussion, we consider the case of 2-redundant multicast graphs to explain our proposed routing algorithm. So, for receiver nodes t_i with indegree 2 in a 2-redundant multicast graph with source s and unit-bandwidth edges, if we can search two disjoint paths between source s and every receiver node t_i , we can realize the multicast max-flow.

Combining with the demand of network coding and definition of path stamp, we modify the judgment rules of conventional Dijkstra shortest path algorithm to search the proper path between source and receiver node. When checking cumulative cost of each neighbor node of the last determined node, we consider not only the smallest distance of them, but also the path stamp of the neighbor nodes. Without loss of generality, we assume all the links in the multicast graph have the same capacity, and the distance of every two neighbor nodes in the multicast graph is 1.

The multicast routing algorithm based on network coding is shown as follows.

Step 1. Initialize the network.

Consider the directed acyclic graph $G(V,E)$, set the source node s, t_i receiver nodes, and the distance of any two neighbor nodes $d_{mn}=1$ for $(m,n)\in E$.

Step 2. Build the first path.

Build the first path p_{i1} from source node s to current t_i by modified Dijkstra shortest path algorithm. For all the intermediate nodes on the path, we set $ps(i,1)=1$. Set $i=i+1$ and repeat step 2 until we have searched the proper path for each t_i. In this step, when two paths have the same shortest distance, we give priority to the unused links (not been set path stamp in the head of the link, i.e., $ps(j,1)=0$, $j\neq i$) to build the path for receiver nodes. By this way, more links can be selected to balance the traffic load in the network.

Step 3. Build the second path

Build the second disjoint path p_{i2} from source node s to current t_i by modified Dijkstra shortest path algorithm. In this step, we only give priority to the unused links (not been set path stamp in the head of link, i.e., $ps(i,1)=0$) to build the path for receiver nodes. By this way, more links can be selected to share the traffic load in the network.

For example, when we build the path p_{22} from source s to receiver node t_2, to meet the disjoint rule, we do not concern the link which has been set path stamp $ps(2,1)=1$, which means the link has been used by p_{21} in step 2. And we do select the links used by other receiver nodes to increase the possibility of sharing of the link and decrease the probability for coding.

Set $i=i+1$ and repeat step 3 until the second disjoint path has been searched for each t_i.

Step 4. When two proper disjoint paths have been found for all receiver nodes, the algorithm stopped. From the results of the multicast routing algorithm, we can get a paths-cluster with two disjoint paths for each receiver node. The intermediate nodes, which have more than one incoming links, are network coding nodes.

When generalizing to *k*-redundant multicast graph, we only need to execute step 2 once and repeat step 3 $k-1$ times.

3.3 Example

We give an example of 2-redundant multicast graph, depicted in Fig.2, to explain our proposed algorithm.

In Fig.2 (a), in which t_i, $1\le i\le 4$, are the four receivers in the multicast group and s is the source node. Each link has the same bandwidth of 1. The first paths p_{i1} from source node s to corresponding t_i are shown in Fig.2 (b). In Fig.2 (c), the second disjoint paths p_{i2} are shown, in which the path p_{22} is the links set of $\{s\to c\to f\to i\to t_2\}$, p_{32} is the links set of $\{s\to d\to g\to j\to t_3\}$ and p_{42} is the links set of $\{s\to c\to g\to j\to t_4\}$.

Fig.2 (d) shows the determined disjoint paths in the final result, and the detailed of disjoint paths information from source node to each receiver node are list in Table 1.

Table 1. The disjoint paths of each receiver node

	p_1	p_2
t_1	$\{s \to a \to t_1\}$	$\{s \to b \to e \to h \to t_1\}$
t_2	$\{s \to b \to e \to h \to t_2\}$	$\{s \to c \to f \to i \to t_2\}$
t_3	$\{s \to c \to f \to i \to t_3\}$	$\{s \to d \to g \to j \to t_3\}$
t_4	$\{s \to d \to t_4\}$	$\{s \to c \to g \to j \to t_4\}$

It's obviously that almost all links take part in to balance the traffic load, and most links are shared in different paths from source node to different receiver nodes. So, the proposed multicast routing algorithm based on network coding is a scheme of link-optimization, decreasing the redundant links ($a \to e$ and $b \to f$) and keeping only the necessary the intermediate nodes to implement network coding. From Fig.2 (d), we can see that intermediate node g is the network coding node for there are two incoming links on it.

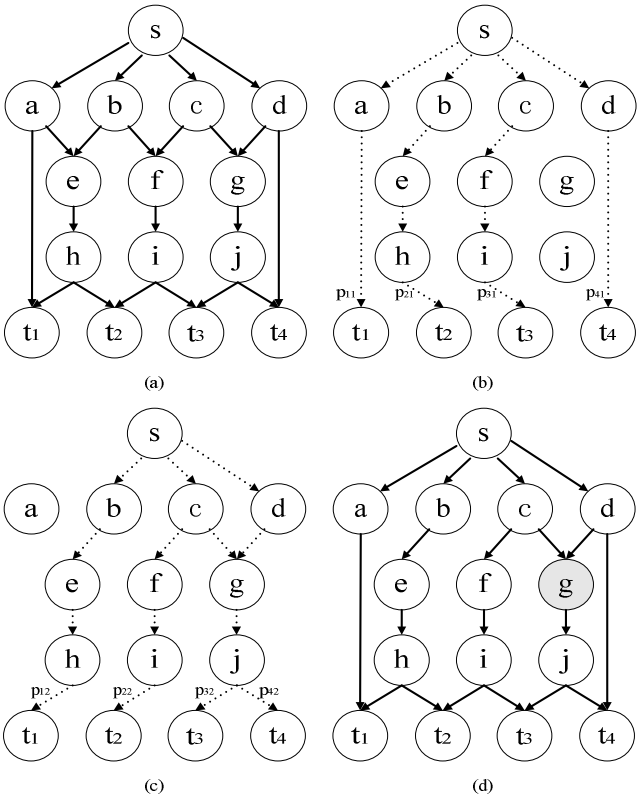

Fig. 2. Examples of 2-redundant multicast routing

4 Performance Simulations

We process the simulation experiments in this section to investigate our algorithm. We want to compare the performance of our proposed algorithm with traditional multicast algorithm based on shortest path distribution tree (Algorithm 1 in short) and previously proposed multicast routing algorithm based on network coding (Algorithm 2 in short)[9]. We generate a 2-redundant multicast graph illustrated in Fig.2 (a) and the random network as the experiment networks in our simulation, respectively. After running 100 times we get the average value as the final result. We consider the performance in terms of throughput and the load balance.

4.1 2-redundant Multicast Network

Fig.3 shows the average throughput of each receiver node in 2-redundant network, and the proportion of background traffic varies from 0% to 50%. The source node sends data by constant bit rate so that the data rate at each link on the path to a receiver node is 10 bit/unit time. The throughput is defined as the average received data per unit time, which can be recovered to original data, by each receiver node. So, we can observe that throughput of multicast routing algorithm based on network coding can achieve higher throughput than Algorithm 1. But the performance of two algorithms falls with the increase of background traffic, and the proposed algorithm falls quicker than Algorithm 1. For the encoding operation in intermediate nodes, the multicast routing based on network coding is sensitive to the correctness of data. With the increase of background traffic, the probability of data loss or receiving the incorrect data is increased, and one bit loss or incorrect will result in failing to decode the received data and decreasing the throughput of network.

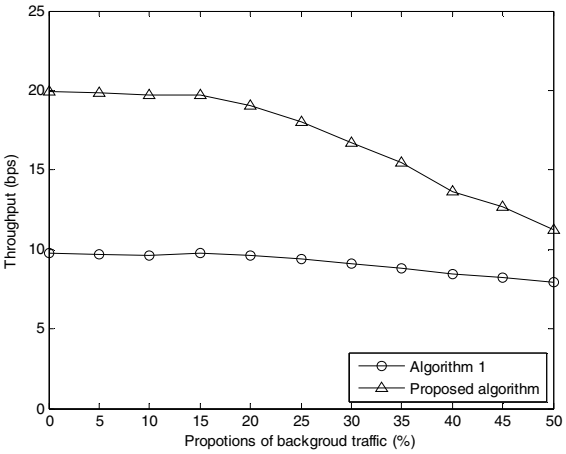

Fig. 3. Throughput in 2-redundant network

We check the performance of load balance, which means how much traffic load is distributed to an entire network, in the experiment network. From Fig.2 (d), we can see, in multicast routing based on network coding, there are 19 links take part in the multicast communication. While the example of the shortest path distribution tree is similar to Fig.2 (b), and there are only 12 links compose the shortest path distribution tree. The performance of load balance of the proposed algorithm based on network coding is much better than that of Algorithm 1, for more links are used to share the traffic load to build the disjoint paths for each receiver node.

4.2 Random Network

The 2-redundant multicast network is an idealized network model and has some remarkable difference with real network topology. We generate the 30-nodes random network topology by Waxman model in this section to be the experiment network. The selected receiver nodes in random network have different indegree, and then there are different numbers of disjoint paths from source node to different receiver nodes. To make the algorithm feasible, we define the numbers of disjoint paths as the minimum indegree of all receiver nodes. We randomly select 5 nodes to be the receiver nodes, and the minimum indegree of the 5 nodes is 4. The source node sends data by constant bit rate so that the data rate at each link on the path to a receiver node is 30 bit/unit time.

Fig.4 shows the average throughput of each receiver node in 30-nodes random network, and the proportion of background traffic varies from 0% to 50%. It's obviously that the network coding has the same ability to increase throughput in random network, and has the same downward trend with the increase of background traffic. But the performance of throughput falls dramatically comparing with that of 2-redundant network, and has fallen by more than half when the background traffic reaches 50%.

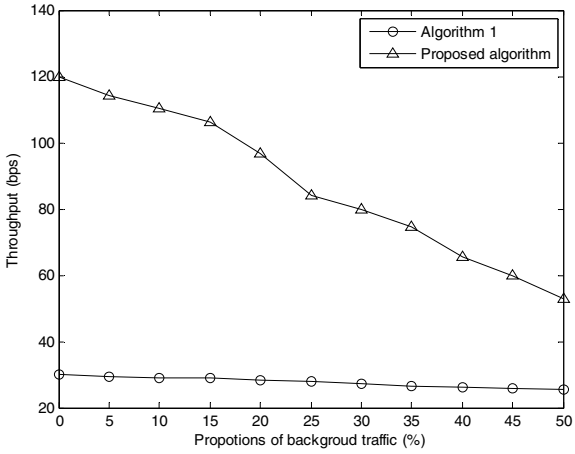

Fig. 4. Throughput in 30-nodes random network

To check the performance of load balance in random network, we generate 4 random networks with different nodes, and define the 25% of nodes in networks as the receiver nodes. Table 2 shows the number of links that take part in multicast communication of three routing algorithms.

Table 2. The load balance of random network

Nodes/links	20/42	25/55	30/93	35/130
Algorithm 1	15	20	35	44
Algorithm 2	25	34	49	60
Proposed algorithm	26	39	51	68

For all of the three algorithms in Table 2, we note that the number of links, which take part in multicast communication, increases with the rising number of nodes in random network. But the proposed algorithm can utilize almost half of links in network to take part in multicast communication at the same random network, which then make traffic load to be distributed more widely than other algorithms.

5 Conclusion

In this paper, we propose a multicast routing algorithm based on network coding, which is a scheme of link-optimization, to balance and share the traffic load and to improve the multicast communication performance in network. We run simulation experiments, and the simulation results show that, the multicast routing algorithm based on network coding has an apparent advantage of throughput and load balance, compared with shortest path distribution tree algorithm. Furthermore, in terms of the metrics of load balance, the proposed algorithm shows the better advantage than previously proposed multicast routing algorithm based on network coding.

References

1. Ahlswede, R., Cai, N., Li, S.-Y.R., Yeung, R.W.: Network information flow. IEEE Transactions on Information Theory 46, 1204–1216 (2000)
2. Li, S.Y.R., Yeung, R.W., Cai, N.: Linear network coding. IEEE Transactions on Information Theory 49(2), 371–381 (2003)
3. Ho, T., Koetter, R., Medard, M., Karger, D., Effros, M.: The Benefits of Coding over Routing in a Randomized Setting. In: Proceedings of the International Symposium on Information Theory, pp. 442–447 (2003)
4. Koetter, R., Medard, M.: An algebraic approach to network coding. IEEE/ACM Transactions on Networking 11(5), 782–795 (2003)

5. Sanders, P., Egner, S., Tolhuizen, L.: Polynomial time algorithms for network information flow. In: 15th ACM Symposium on Parallel Algorithms and Architectures, San Diego, CA, pp. 286–294 (2003)
6. Jaggi, S., Chou, P.A., Jain, K.: Low complexity algebraic multicast network codes. In: Proc. ISIT, Yakohama, Japan, p. 368 (2003)
7. Lun, D.S., Ratnakar, N., Medard, M., Koetter, R., Karger, D.R., Ho, T., Ahmed, E., Zhao, F.: Minimum-cost multicast over coded packet networks. IEEE Trans. Inf. Theory 52(6), 2608–2623 (2006)
8. Chi, K., Yang, C., Wang, X.: Performance of network coding based multicast. IEE Proc.-Commun. 153(3), 399–404 (2006)
9. Wang, J., Liu, J., Wang, X.: Performance Analysis of Multicast Routing Algorithm Based on Network Coding. Journal of Electronics & Information Technology 30(11), 2605–2608 (2008)
10. Zhu, Y., Li, B., Guo, J.: Multicast with Network Coding in Application-Layer Overlay Networks. IEEE Journal on Selected Areas in Communications 22(1), 1–13 (2004)

An Intelligent Tutoring System Based on Speech Assessment for Spoken English Learning in China*

Yingli Liang and Jun Xu

School of Education Technology, South China Normal University,
510631, Guangzhou, China
Yingliliang208@163.com, xuj@scnu.edu.cn

Abstract. With the development of mobile Internet, speech technology has matured. In education, automatic speech assessment technology has been gradually applied in language learning. Since intelligent tutoring system is distinguished by its one-on-one individualized teaching effects, this paper has proposed an intelligent tutoring system based on speech assessment for spoken English learning in China. The system provides context of situation for English learning as well as automatic assessment services. The results show that the assessment is of high validity and reliability and the system is greatly helpful for Chinese middle school students to learn spoken English.

Keywords: intelligent tutoring system, speech assessment, English learning.

1 Introduction

Human language is the most important, effective, common and convenient means for social communication. English has become an international language, spoken English learning is one of the most important research in the area of Applied Linguistics. With the implementation of the new curriculum reform in China, there is increasing emphasis on the cultivation of interpersonal skills such as listening and speaking. In Guangdong, Jiangsu and Shandong provinces in China, the Test of Spoken English has become an important part of the college entrance examination. Specially, the total score of listening and speaking exam for English in Guangdong college entrance examination is 15 points, accounting for 10% of the total score. However, as a non-native speakers of a second language, the large number of primary and secondary school students, and even college graduates, after ten years of learning English could only read or write and hardly listen and speak. "deaf English" and "dumb English" has been plagued Chinese students in learning English. In the face of such unspeakable pain, as one of the educational researcher, we should seriously consider the serious problems that exist in the current spoken English teaching and learning.

* This work was supported in part by Guangdong Provincial Department of Science and Technology under Grant 2012A080104021.

D. Liu et al. (Eds.): BICS 2013, LNAI 7888, pp. 358–365, 2013.

1.1 Spoken English Learning in China

Language environment, or more precisely, the context of situation is the key issue in the linguistics study[1]. Context is extremely important from the point of view of applied linguistics analysis, and is prerequisite to effectively improve speaking skills. English linguist Firth[2] and Halliday[3]have done in-depth analysis and discussion in English context, and consider that the context of spoken English has a great effect on spoken English learning. However, for Chinese English teaching, English spoken environment is basically concentrated in the classroom and there is few other speaking practice environment. Especially in the vast rural areas, the students' oral English learning environment is of extreme scarcity and they hardlyl have any opportunities to practice. It can be said that the lack of spoken English learning environment is the primary cause of "dumb English".

Reading, retelling is an important way to improve English listening and speaking ability. However, speaking practise alone is just not enough, oral communication needs to Initiate and conduct dialogues by two or more partners to interact efficiently[4]. Then during the interactive process, detecting their own spoken conversation, pronunciation, grammar errors and make targeted rectify to improve the speaking skills is important. In the same time, the reliability and validity of the evaluation are also significant factors for the oral test. Therefore, spoken English assessment and feedback is extremely important. Nevertheless, the limited number of spoken English faculty is obviously difficult to meet this demand, and in some backward areas, the capacity of the teaching staff is difficult to guarantee the quality of spoken English teaching. In such cases, assessemnt is difficult to carry out, which becomes one of the bottlenecks in restricting students' spoken English learning.

In summary, the lack of spoken English learning environment rusults that it is ifficult to provide students with effective practice situations. The difficulty in assessing spoken English leads to insufficient interaction. They are the two prominent problems in the current Chinese Spoken English Teaching. In response to these problems, to build a one-on-one personalized learning environment by technical means, and to automate the spoken English assessment, that is speech assessment, and provide immediate feedback for students should be one of the effective solutions for spoken English learning.

1.2 Speech Assessment

With the emergence of cloud computing, wide application of 3G communication, and the promotion of the wave of mobile Internet, speech technology develops rapidly. Human-machine speech interaction is achieved with the help of speech technology, and then human-machine communication becomes as simple as interpersonal communication. Speech technology involves multidisciplinary research areas, including the study of acoustics, signal processing, information theory, linguistics and computer science and many other fields. Speech technology mainly includes three important research area, including speech synthesis, speech recognition and speech assessment technology. Speech synthesis technology transforms any text information

into a natural and smooth speech, which is called Text-to-Speech, also known as text-to-speech conversion technology, to make the machine speak. Corresponding to speech synthesis technology, speech recognition makes that the machine converts speech signal into a corresponding text or commands through the process of identifying and understanding.

In recent years, the rapid development of Education, Culture and Communication, speech assessment technology has made great progress and has been widely used. Speech assessment technology belongs to the field of Computer Assisted Language Learning. It is able to automaticlly detect students' pronunciation error, give correction guidance or suggested score. The computer assisted Mandarin or English pronunciation assessment can be achieved. The efficiency and effectiveness of spoken English learning can be greatly improved. Speech assessment includs the establishment of the standard pronunciation model, the analysis of the rhythmic quality of speech segment and machine scoring mapping with human scoring. Speech assessment framework shows as in Fig. 1.

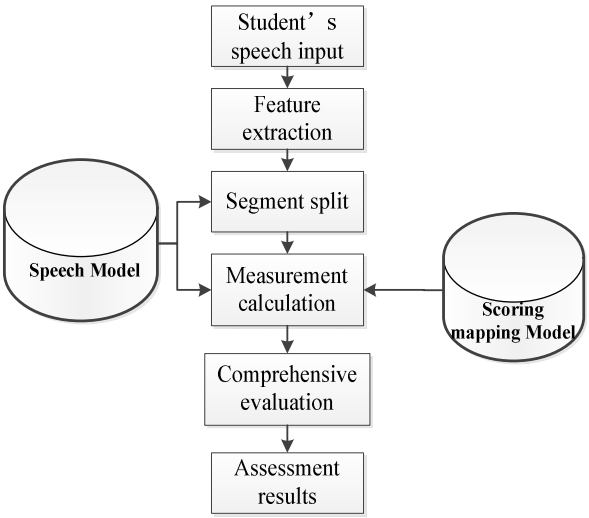

Fig. 1. Speech assessment framework

It needs to build speech model and ratings mapping model beforehand in speech assessment. Firstly, speech model is usually built based on large-scale standard pronunciation corpus, from which to get the data of the standard pronunciation. After feature extraction, it builds a speech model that enables a computer to automatically analyze the pronunciation of what is the standard pronunciation. Secondly, non-standard speech corpus is collected and. After a series of processing including its feature extraction and segments cutting, based on the standard acoustic models, computers can automatically analyze its acoustic gap to the standard speech pronunciation. At the same time, experts complete error detection as well as human scoring manually to annotate the non-standard speech corpus. Afterwards data mining technology is used to achieve the mapping from computer automatic scoring to human

scoring, in which process that it can make the computer automatically learn how the experts scores as well as their scoring rules. That is, the computer has the rating capacity of the experts'.

The whole speech assessment process is as following[3]: first, executing speech feature extraction from student's speech; second, splitting the speech segments based on the well trained speech model(usually using the Viterbi algorithm), and calculating the pronunciation quality measurements; last, converting the measurements into intuitive scores using the well trained score mapping model.

As speech technology continues to mature and widely used in the process of language learning, using computer-assisted spoken English learning to promote English teaching is increasingly becoming a hotspot in current research[5-7].

2 System Design

Intelligent tutoring system (ITS) plays an important role and effects significantly in one-on-one personalized teaching[8]. It consists of three components: student model, domain model and tutoring model. Student model is the core of ITS, the student's ability level is the most important characteristic of the student model. It can objectively reflect the student's knowledge and skill level. And assessment is the most direct approach to get these information which represent the student's ablility. Therefore, this study proposes that to build student model based on the assessment technology. Domain model and student model is the basis of tutoring model, and further more, tutoring model is the bridge between domain model and student model. From pedagogy perspective, the essence of tutoring model is to make adaptive decision-making and to provide personalized recommendation services. Fig. 2 shows their mutual contact.

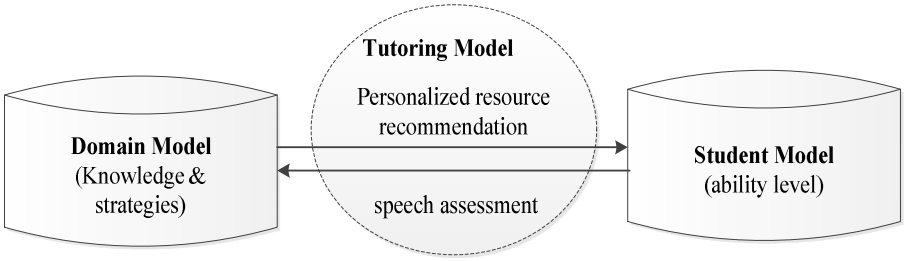

Fig. 2. Relationships among domain model, tutoring model and student model in an ITS

Linguistic research shows that reading and retelling are effective ways to improve their English speaking skills. Therefore, in this study proposes the following exercises types, including imitation read aloud, retelling, situational dialogues nd other spoken English practice activities. As the speech assessment engine, the accuracy of pronunciation, fluency, integrity and rhythmicity will be its main assessment parameters.

This study proposes an intelligent tutoring system for spoken English learning based on speech assessment. The proposed system flow is shown in Fig. 3.

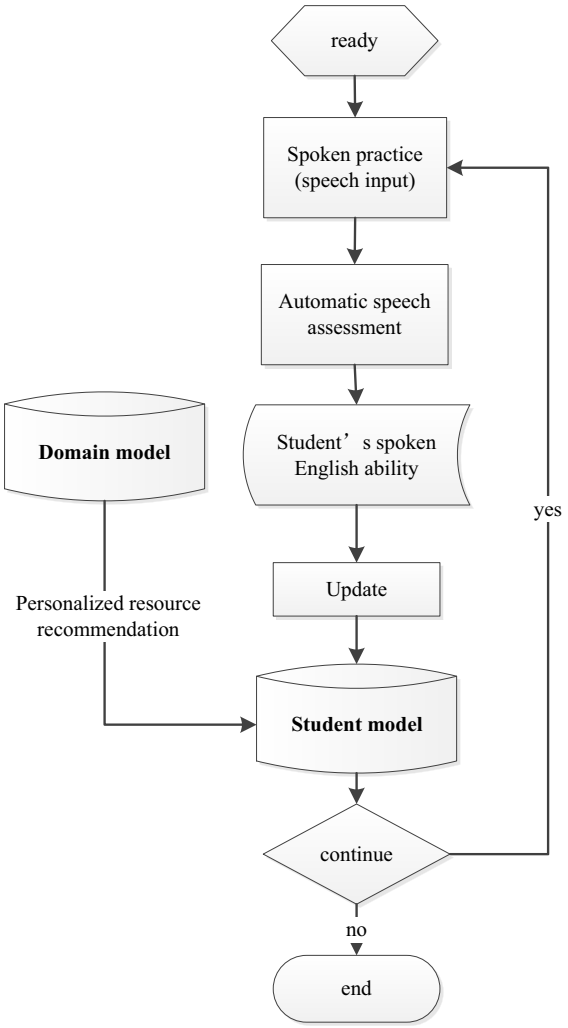

Fig. 3. System flow chart

First, as for the domain knowledge of spoken English, we build the speech corpus-based domain model, which is one component of the speech assessment engine and the basis of the evaluation criteria. On the one hand, we need to determine the important speech features that are able to identify the quality of the speech. In the present study, these features include pronunciation accuracy, fluency, integrity and rhythmicity. On the other hand, we need to build the acoustic model, language model and scoring model. The acoustic model is a software component that enables the engine to identify the word. Language model is a software component which allows the engine to distinguish words with similar pronunciations(e.g. it is able to identify that the student speaks "the red cup" rather than "the read cup"). Scoring model is about the

computer's imitation human score, which is similar to the evaluation criteria. The three models provide services for speech assessment engine.

Secondly, we build student model based on the speech assessment data. The student takes part in reading aloud, retelling, situational dialogues and ther spoken English practice activities. The speech assessment engine takes the student speech signal as the input data, on the basis of knowledge in the field of English spoken, extract the characteristics of the input speech, implements automatic speech assessment, proposes scores according his performance in accuracy, fluency, integrity and rhythmicity. The score reflects student's speaking ability which will be the update basis of student model. With the growth of the time, the system uses the collected data to automatically improve the spoken English speech domain knowledge model, which will make the assessment engine be more and more accurate to represent students' speaking ability.

Finally, tutoring model continuously updates students' speaking ability, provides instant feedback on learning suggestions and recommends personalized resources to students in line with his current spoken English level. Then the student get into the next round of learning.

This study proposes an intelligent tutoring system for spoken English learning based on speech assessment methods and technique. Its prototype and main functions are designed. In the system, the student can take part in the situational dialogue practice. The context of situation is created with the help of multimedia by computer. By means of automatic speech assessment, the student interacts smoothly and naturally with the computer, feeling like that a pair of partners are continuously taking. As for the feedback interface of the speech assessment system, after the student compelets his speech execises, the system automaticlly assesses his speech input according to his pronunciation accuracy, fluency integrity and rhythmicity. Then a suggested score is given. For commen practice, detailed and immediate feedback will be put forward to the students. Since the system function is still being complete, the feedback will be improved in the next stage. The score reflects the student's current spoken English level. According to the student's speaking ability, adaptive learning resources will be recommended to students. The whole process simulates human for one-on-one personalized teaching.

3 Experiments

The prototype system has been applied in spoken English learning for middle school students. In language testing, correlation analysis of the scores provided by human assessment and automated scoring system is generally considered as an argument of the validity of automated speech assessment method. This experiment around the criterion-related validity. This experiment carries out the criterion-related validity studies. First, we validates the accuracy and effectiveness of the automatic speech assessment. Since the system has been applied in English oral test of senior high school entrance examination Zhanjiang, Guangdong province,we randomly select 100 examinees and their scores from this examination. In the exmination, there are 5 question types, including sentence reading, paragraph reading, retelling, situational dialogues and oral composition. In order to get human scores and machine scores, we

collect all the speech audio and then carry on human scoring by human teachers and automated speech scoring by our system.

Then we import the human scores and machine scores(automated speech assessment) into the software SPSS 17.0 for windows. The sample size is 100. In order for Pearson correlation analysis, we then check the distribution of HumanScoring and MachineScoring. The effect is positive. The preanalysis show that the two variables is a linear relationship(see Fig. 4).

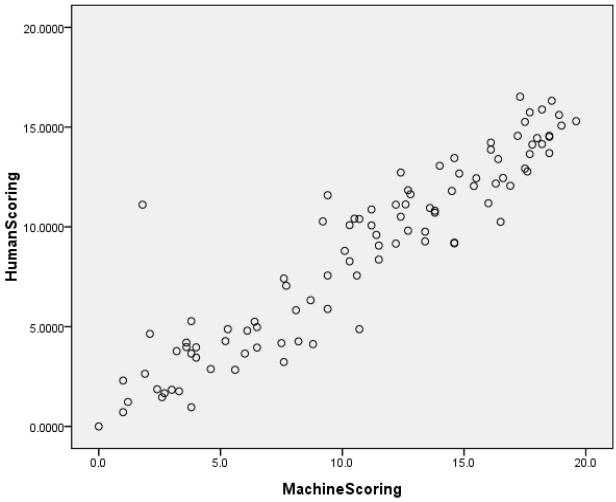

Fig. 4. Linear relationship between human scores(HumanScoring) and machine scores(MachineScoring)

Second, we have conducted a sample survey and the results show that 96% students support that the system effectively promote spoken English learning, as shown in Fig. 5.

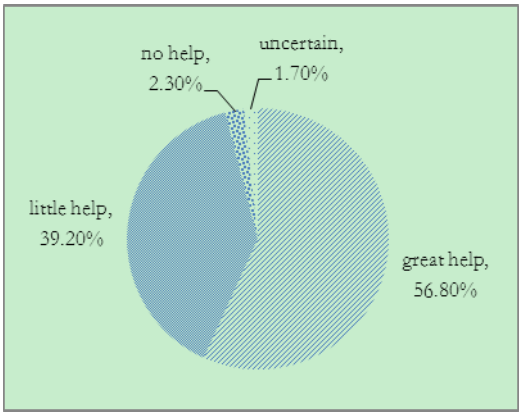

Fig. 5. Survey results

4 Conclusion

With the mobile Internet wave rising, speech technology has made crucial breakthrough in its development and large-scale applications. Spoken language learning has a more urgent demand for speech assessment in education. For millions of Chinese studetns, context of situation shortage and spoken English assessment difficulty have been critical issues in a long time that need to be solved. This paper design an intelligent tutoring system for spoken English learning based on speech assessment. The results show that the system can effectively assist students' spoken English learning. However, the system functions need to be further improved, especially in human-computer interaction between the students and the system as well as the feedback design. How to design effective type of exercises according to the applied linguistics research and build a more meaningful speaking practice situation will be our focus in next step for improvement.

Acknowledgments. We thank Guangdong Provincial Department of Science and Technology. We also thank Dr. Dongqing Wang for helpful conversations, Hou Han for analyses with the samples, and Wei Yan for excellent technical assistance.

References

1. Firth, J.R.: Personality and language in society. The Sociological Review 42, 37–52 (2011)
2. Firth, A., Wagner, J.: On discourse, communication, and (some) fundamental concepts in SLA research. The Modern Language Journal 81, 285–300 (1997)
3. Halliday, M.A., Hasan, R.: Language, context, and text: Aspects of language in a social-semiotic perspective (1989)
4. Arias, J.P., et al.: Automatic intonation assessment for computer aided language learning. Speech Communication 52, 254–267 (2010)
5. Xi, X., et al.: Automated scoring of spontaneous speech using SpeechRaterSM v1. 0, Educational Testing Services Research Report (2008)
6. Wei, C.: Detecting Off-Task Speech (2012)
7. Chen, L., et al.: Systems and Methods for Assessment of Non-Native Spontaneous Speech. Google Patents (2009)
8. Nkambou, R., et al.: Advances in Intelligent Tutoring Systems, vol. 308. Springer (2010)

Fault Detection Filter Design for Certain Networked Control System

Yuqiang Chen, Wei Lu, and Zhiyan Xu

The 3rd Department, Aimin West Street No. 136,
LangFang HeBei, China 065000
chenyuq2002@163.com

Abstract. This paper is concerned with fault detection filter design of certain discrete-time networked systems with delays. Based on the traditional fault detection filter, a novelty fault detection observer was designed to compensate the delay by iteration. The fault reference model was introduced, and an augumented residual system was derived. With the H_∞ theory, a fault detection schem was proposed based on the H_∞ filter. With the *LMI*, the observer gain and the post filter matrix could be got. Simulation results gave an illustration of the proposed design.

Keywords: Fault Detection, NCS, LMI.

1 Introduction

Networked control systems (NCSs) have received increasing attentions in recent years. One of the particular problems on analyzing and designing NCSs is the network-induced delays, which has become a crucial factor for the stability of the NCS. Furthermore, the continuous plant coupled with the digital controller can be named hybrid system, especially, when there is time delay happening, the system also should be modeled as a discrete time delay system. Recently, the network-induced delays have been modeled in various probabilistic ways [1,2,3]. In these networked control system applications, the delay can be modeled as a random process described by a Markov chain with a finite number of states. Each state in this Markov chain reflects the loading of the network or a processor at a given time [4]. It is worth mentioning that the binary random delay has gained much research interest because of its simplicity in describing network-induced delays [5], and the references therein.

The fault detection and isolation (FDI) problem has attracted persistent attention because of the increasing complexity and safety demand of real time systems [6]. There is an urgent need to consider the FDI problem for networked systems. Recently, there have been some research interests on network based FDI problems, see the survey paper [7-11,14] and the references therein.

In this paper, we aim to solve the fault detection problem for a class of Networked Control Systems with random sensor delays and disturbances. Assume that the Maximum allowable delay [12] – τ_{MAD} is gotten prior. With the delay, the system can

D. Liu et al. (Eds.): BICS 2013, LNAI 7888, pp. 366–376, 2013.

still maintain stability. State 1 denotes delay happening, state 0 denotes no delay. The system is stochastic switching between the two states. A sufficient condition for the existence of the desired fault detection filter is established in terms of certain linear matrix inequality (LMI). When this LMI is feasible, the explicit expression of the desired fault detection filter can be determined. A numerical example is provided to demonstrate the usefulness of the present methods.

2 Problem Formulation and Preliminaries

Generally, an observer can be designed to achieve fault detection for the system as following,

$$\begin{cases} \hat{x}(i+1) = F\hat{x}(i) + Bu(i) + D(y(i-hT) - \hat{y}(i-hT)) \\ \hat{y}(i) = H\hat{x}(i) \end{cases} \tag{1}$$

where $\hat{x} \in R^n$ denotes the state estimated vector, $u \in R^p$ denotes the control input vector, $\hat{y} \in R^m$ denotes the measurable estimated output vector , the matrix D is to be calculated. It's obvious that the network delay was not considered in the design of the observer. Thus the performance of the residual generator will be influenced by network delay. In order to compensate the network transmission delay, an iterator is used to predict the measurement output and redesign the state observer.

Based on the output data up to *i-hT,* the state predictions from *i-hT+1* to *i* are constructed as

$$x_{i-hT+1|i-hT} = Ax_{i-hT|i-hT-1} + Bu_{i-hT} + Mf_{i-hT}$$

Where $x_{i-hT+1|i-hT} \in R^n$ is the one-step ahead state prediction at time *i-hT*.

$$\begin{aligned} x_{i-hT+2|i-hT} &= Ax_{i-hT+1|i-hT} + Bu_{i-hT+1} + Mf_{i-hT+1} \\ &\vdots \\ x_{i|i-hT} &= Ax_{i-1|i-hT} + Bu_{i-1} + Mf_{i-1} \end{aligned}$$

Which results in

$$x_{i|i-hT} = A^{hT}x_{i-hT} + B\sum_{j=1}^{h} A^{j-1}u_{i-j} + M\sum_{j=1}^{h} A^{j-1}f_{i-j}$$

With the known delay, we can design the state observer, which can compensate the network delay as following

$$\begin{cases} \hat{x}(i+1) = F\hat{x}(i) + Bu(i) + D(Cx_{i|i-hT} - \hat{y}_i) \\ \hat{y}(i) = H\hat{x}(i) \end{cases} \tag{2}$$

In the NCS, to make the system stable, we have to consider the delays of feedback and forward as the Fig1.

But with the strong computing ability of the smart nodes, we can avoid considering the delay of forward for locating the controller and fault detection module together. In this paper, we make some assumption for convenience. It is assumed that the control and supervision stations for process (1) are located together;

- We assume that the delays are random but bounded;
- The Maximum Allowable Delay (τ_{MAD}) is gotten;

Remark : If the parameters of fault detection algorithm are re-computed according to the delay gotten on-line, it is difficult for the smart nodes to achieve it for the complexity of the algorithm every time. Thus the bounded delay -τ_{MAD} is used to simplify the design. Though some conservatism is brought, it will be a feasible practical application scheme for Networked Control Systems.

- Sensor delay doesn't affect the disturbance.

Under these assumptions, the process (1) will be changed to the following equation:

$$\begin{cases} x(k+1) = Ax(k) + Bu(k) + Ed(k) + Ff(k) \\ y(k) = Cx(k) \end{cases} \tag{3}$$

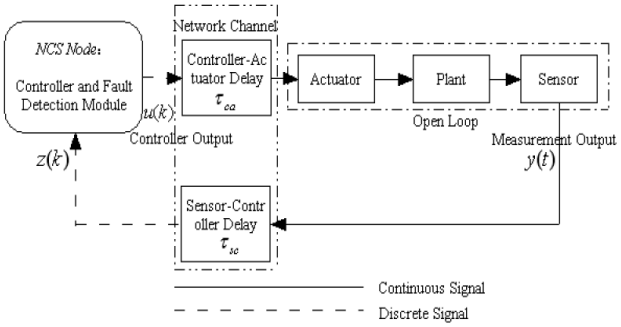

Fig. 1. [7] Fault Detection for NCSs

3 Robust Fault Detection Observer Design

3.1 The Modeling of Time Delay in the Feedback Channel

Because the time delay happens randomly, one of the difficulties of fault detection for NCS is to model the time delay. According to the assumption above, the fault detection observer is designed at the controller site, which is based on two different modes. One is '0' denotes there is no delay; the other is '1' denotes there happens delay, and the delay is Maximum Allowable Delay (τ_{MAD}). From the figure 2,

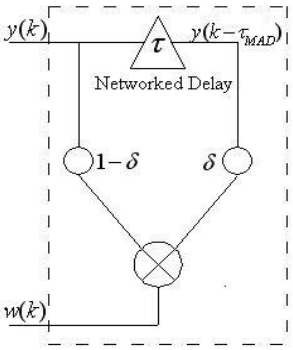

Fig. 2. The Measurement Delay Model

we can get the time delay model. No matter how many delay is, we take the $y(k-\tau_{MAD})$ as the delayed measurement. The random of the system represents stochastic switching between the two modes. With the bounded delay - τ_{MAD}, the NCS can be kept stability. At the controller site, we have measurement signal:

$$w_k = (1-\delta)y_k + \delta y_{k-\tau_{MAD}} \tag{4}$$

where δ is modeled as a discrete-time Markov chain with two state space $\varphi = \{0,1\}$

3.2 Design of Robust Fault Detection Observer

Based on the output (3) of the plant, we constructed the following equation as the injection output of the observer.

$$v_k = (1-\delta)\hat{y}_k + \delta \hat{y}_{k-\tau_{MAD}} \tag{5}$$

Thus the observer is designed as following,

$$\begin{aligned} &\hat{x}(k+1) = A\hat{x}(k) + Bu(k) + H(w_k - v_k) \\ &= A\hat{x}(k) + Bu(k) + H[(1-\delta)(y(k) - \hat{y}(k)) \\ &+ \delta(y(k-\tau_{MAD}) - \hat{y}(k-\tau_{MAD}))] \end{aligned} \tag{6}$$

Let $m_k = \delta$, we can let $m_k = 1$ denotes that the delay occurs at the kth time step, and $m_k = 0$ denotes no delay happens. Where m_k is modeled as a Markov chain with two states taking values as $\varphi = \{0,1\}$, and the transition probability matrix at time k is given by:

$$\Pi_k := \begin{bmatrix} p_{11}(k) & p_{12}(k) \\ p_{21}(k) & p_{22}(k) \end{bmatrix} (k = 0,1,2,\cdots) \tag{7}$$

$$P\{m_k = j \mid m_{k-1} = i\} = p_{ij}$$

Where $p_{ij}(k)(i, j = 1,2; k = 0,1,2,\cdots)$ is the conditional probability. Hence the $p_{ij}(k)$ satisfies the relation:

$$0 \le p_{ij}(k) \le 1, p_{1j}(k) + p_{2j}(k) = 1, i, j = 1,2; k = 0,1,2,\cdots \quad (8)$$

From the plant (3) and model (6), we can get the state error equation:

$$e(k+1) = (A - HC(1-m_k))e(k) - HCm_k e(k-\tau_{MAD}) + Ed(k) + Ff(k) \quad (9)$$

and the residual is

$$r(k) = W(w_k - \upsilon_k) = WC((1-m_k)e(k) + m_k e(k-\tau_{MAD})) \quad (10)$$

where W is the weighting gain. The coefficient matrices are functions of the random parameter- m_k .

The error equation (10) can be reduced to a discrete-time Markov jump system with time delay. From the equation, we can see that if the equation is robust stability without the fault term, the observer can be used to detect fault during the system running and the residual can be signal of the occurrence of the fault. Without fault term, the equation (10) is changed as equation (11):

$$e(k+1) = (A - HC(1-m_k))e(k) - HCm_k e(k-\tau_{MAD}) + Ed(k) \quad (11)$$

The equation is consistent with the discrete time jump linear state-delay systems of Cao [11]. When the system operates on the *ith* mode ($d_k = i$), the matrices can be denoted as following:

$$A_{1i} = A - HC(1-m_k) \ , \ A_{2i} = -HCm_k \quad (12)$$

We can use a stochastic Lyapunov function $V(\cdot)$ (Kushner),

$$V_k(x_k, m_k) \overset{\Delta}{=} x_k^T P(m_k) x_k + \sum_{l=k-d}^{k-1} x_l^T Q x_l . \quad (13)$$

With the proof in Cao [11], we can get the

Theorem 1. [13]. The free-jump system is stochastically stable if there exist $Q > 0$ and $P_i > 0, i = 1,\cdots s$, satisfying the coupled *LMIs*

$$M_i = \begin{bmatrix} A_{1i}^T \tilde{P}_i A_{1i} - P_i + Q & A_{1i}^T \tilde{P}_i A_{2i} \\ A_{2i}^T \tilde{P}_i A_{1i} & -Q + A_{2i}^T \tilde{P}_i A_{2i} \end{bmatrix} < 0 \ i = 1,\cdots s \quad (14)$$

Where

$$\tilde{P}_i = \sum_{j=1}^{s} p_{ij} P_j, i = 1, \cdots s \tag{15}$$

To get the robust H_∞ disturbance attenuation for the discrete-time residual above, we can get the following theorem.

Theorem 2. The residual system possesses the γ -disturbance attenuation property, that is

$$\|r\|_2 < \gamma \|d\|_2, \tag{16}$$

for all $d \in l_2[0, N-1]$, $d \neq 0$,if there exist $Q > 0$ and $P_i > 0, i = 1, \cdots s.$ satisfying the following coupled *LMIs*,

$$\Theta_i \overset{\Delta}{=} \begin{bmatrix} \psi_i & A_{1i}^T \tilde{P}_i A_{2i} + C_{1i}^T C_{2i} & A_{1i}^T \tilde{P}_i E \\ * & -Q + A_{2i}^T \tilde{P}_i A_{2i} + C_{2i}^T C_{2i} & A_{2i}^T \tilde{P}_i E \\ * & * & -\gamma^2 I + E^T \tilde{P}_i E \end{bmatrix} \tag{17}$$

where * represents blocks that are readily inferred by symmetry and

$$\psi_i \overset{\Delta}{=} A_{1i}^T \tilde{P}_i A_{1i} - P_i + Q + C_{1i}^T C_{1i} \tag{18}$$

Proof: As to the residual system (10) and (11), in the following, we assume zero initial condition that is

$$e_k = 0, k \in \{-\tau_{MAD}, \cdots, 0\},$$

And define

$$J_N \overset{\Delta}{=} \|r\|_2^2 - \gamma^2 \|d\|_2^2 = E\{\sum_{j=0}^{N-1} (r_j^T r_j - \gamma^2 d_j^T d_j)\}$$

From the Theroem 1, we can see that

$E\{V_N(e_N, m_k)\} = E\{\sum_{k=0}^{N-1} [V_{k+1}(e_{k+1}, m_{k+1}) - V_k(e_k, m_k)]\}$ Hence, for any nonzero $w \in l_2[0, N-1]$,

$J_N = E\{\sum_{k=0}^{N-1} (r_j^T r_j + V_{k+1}(e_{k+1}, m_{k+1}) - V_k(e_k, m_k) - \gamma^2 d_j^T d_j)\} - E\{V_N(e_N, m_N)\}$ So

$J_N \leq E\{\sum_{k=0}^{N-1} (r_j^T r_j + V_{k+1}(e_{k+1}, m_{k+1}) - V_k(e_k, m_k) - \gamma^2 d_j^T d_j)\} = \sum_{k=0}^{N-1} (\sigma_k^T \Theta_i \sigma_k) < 0$

where $\sigma_k \overset{\Delta}{=} [e_k^T, e_{k-\tau_{MAD}}^T, d_k^T]^T$. Therefore, the dissipativity inequality (16) holds for $N > 0$. In other words, we have $r \in l_2[0, N-1]$ for any nonzero $d \in l_2[0, N-1]$, and $\|r\|_2 < \gamma \|d\|_2$

To design the foregoing observer, we will make some transition for the equation (17) to be easy to calculate the observer gain H. Define $X_i = P_i^{-1}$. Pre and post-multiplying (17) by $diag(X_i, I)$, it is easy to find that matrix inequalities are feasible if and only if

$$\begin{bmatrix} -X_i + X_i Q X_i & 0 & 0 & U_{1i}^T & (C_{1i}X_i)^T \\ 0 & -Q & 0 & U_{2i}^T & C_{2i}^T \\ 0 & 0 & -\gamma^2 I & U_{3i}^T & 0 \\ U_{1i} & U_{2i} & U_{3i} & -Z & 0 \\ C_{1i}X_i & C_{2i} & 0 & 0 & -I \end{bmatrix} < 0 \tag{19}$$

Where

$$U_{1i}^T \overset{\Delta}{=} [\sqrt{p_{i1}}(A_{1i}X_i)^T \cdots \sqrt{p_{is}}(A_{1i}X_i)^T] \tag{20}$$

$$U_{2i}^T \overset{\Delta}{=} [\sqrt{p_{i1}}A_{2i}^T \cdots \sqrt{p_{is}}A_{2i}^T] \tag{21}$$

$$U_{3i}^T \overset{\Delta}{=} [\sqrt{p_{i1}}E^T \cdots \sqrt{p_{is}}E^T]$$

$$Z \overset{\Delta}{=} diag(X_i \cdots X_s) \tag{22}$$

Let $R = Q^{-1}$ and continue to simplify the matrix inequalities (19) as following inequality equation (23) with Schur Lemma.

We can see that (23) is not a typical *LMIs* which is nonlinear because there is an inverse matrix Q^{-1}. However it can be solved using a cone complementarity linearization algorithm (*Ghaoui, L. EI* 1997 [12]) as following:

$$\min_{X_1, X_2, H, Q, R} tr(QR) \tag{23}$$

And let $R = Q^{-1}$, subject to

$$\begin{bmatrix} -X_i & 0 & 0 & U_{1i}^T & (C_{1i}X_i)^T & X_i \\ 0 & -Q & 0 & U_{2i}^T & C_{2i}^T & 0 \\ 0 & 0 & -\gamma^2 I & U_{3i}^T & 0 & 0 \\ U_{1i} & U_{2i} & U_{3i} & -Z & 0 & 0 \\ C_{1i}X_i & C_{2i} & 0 & 0 & -I & 0 \\ X_i & 0 & 0 & 0 & 0 & -R \end{bmatrix} < 0 \quad i = 1, \cdots, s \tag{24}$$

$$\begin{bmatrix} Q & I \\ I & R \end{bmatrix} \geq 0 \tag{25}$$

The feasible solution of above minimization problem can be found by the following iterative algorithm.

Algorithm 1:

(1). Find a feasible solution $[X_{10}, X_{20}, H_0, Q_0, R_0]$ satisfying (23) and (24).

(2). Solve the following *LMI* problem for $[X_1, X_2, H, Q, R]$, $\min_{X_1, X_2, H, Q, R} tr(QR)$ subject to (23) and (24).

(3). Set $Q_{i+1} = Q$ and $R_{i+1} = R$

(4) If the condition (23) is satisfied, there exits the observer gain H, which is gotten by the equation (12). If the condition (23) is not satisfied, set $i = i + 1$ and go to step (2). If *i* is bigger than the specified maximum of iterations, then the program exits. Where matrix *H*is the required observer gain. The algorithm can be readily implemented with the aid of *Matlab LMI* control toolbox.

4 Numerical Example

To illustrate the proposed fault detection scheme, a numerical example is considered in this section. The parameters of the discrete-time linear system with two modes are given as the follows:

$$A = \begin{bmatrix} 0.006738 & 0.506 \\ 0 & 0.9983 \end{bmatrix}, B = \begin{bmatrix} 0.002261 \\ 0.005507 \end{bmatrix},$$
$$C = \begin{bmatrix} 2.21 & 0 \end{bmatrix}.$$

Assume that the transition probability matrix is given by

$$p = \begin{bmatrix} 0.7 & 0.3 \\ 0.4 & 0.6 \end{bmatrix}, \tag{26}$$

The Maximum Allowable Delay -τ_{MAD} = 10 steps.

$$w_k = (1 - m_k) y_k + m_k y_{k-\tau_{MAD}} \tag{27}$$

Where $m_k \in \{0,1\}$, we can get the state error equation. With it we can get the observer gain H under fault-free condition.

$$e_{k+1} = [A - HC(1 - m_k)]e_k - HCm_k e_{k-\tau_{MAD}} + Ed(k) \tag{28}$$

Thus, as to the discrete-time Markov jump system with time delay,

For mode $m_k = 0$, the system matrices are given by

$$A_{11} = A, A_{21} = HC \tag{29}$$

For mode $m_k = 1$, the system matrices are given by $A_{12} = A + HC, A_{22} = 0$, and

$$\begin{aligned} \tilde{P}_1 &= p_{11}P_1 + p_{12}P_2 \\ \tilde{P}_2 &= p_{21}P_1 + p_{22}P_2 \end{aligned}, \tag{30}$$

Using the *LMI* tool we can achieve the observer gain from the matrix equality (19) as following:

$H_1 = [0.4282;0.4260]$, for the mode $m_k = 0$;

$H_2 = [0.0038;0.0016]$, for the mode $m_k = 1$.

Update to now, the designed fault detection module can be used to monitor the distributed system by running on the smart node.

In addition, the unknown disturbance *d(k)* is supposed to be random noise which is uniform distribution over [-0.3,0.3], and the sample period is 5*ms*, and the fault signal *f(k)* is given as the Fig3:

$$f(k) = \begin{cases} 1, for \quad k = \quad 400, \quad 401, \quad \cdots, \quad 1000 \\ 0, others \end{cases}$$

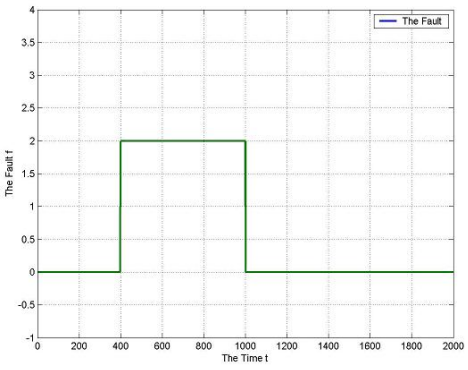

Fig. 3. Fault f(k)

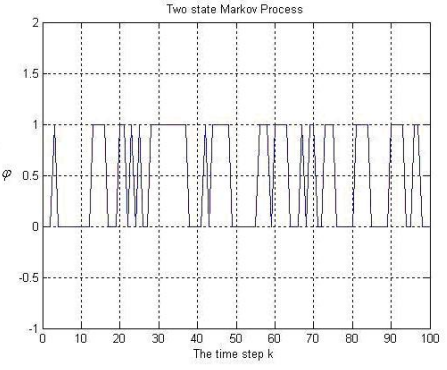

Fig. 4. Measurement mode over network

A two states stochastic variable φ is used to describe the measurement mode with random delays, as is shown in Fig4. Fig5 shows the generated residual signal r_k. We

selected a threshold as $J_{th} = E\{\sum_{k=0}^{2000} r^T(k)r(k)\}^{1/2}$. After the simulations, we get an average value $J_{th} = 8.4800$. Through comparison, we can see that 9.411 = r(405) > Jth, thus the fault can be detected in the Maximum Allowable Delay $-\tau_{MAD}$ after its occurrence.

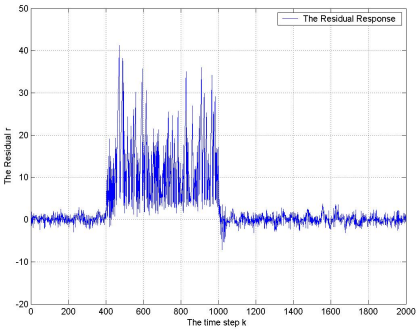

Fig. 5. Residual signal *r*

5 Conclusion

In this paper, we have studied the fault detection problem for certain *NCS* with stochastic time delays, which is modeled as a Markov jump process. The Maximum Allowable Delay is introduced to simplify the practical application on the smart node. We then formulate the fault detection observer design with *LMI*, and the stability of the error system is tested. Assumptions have brought conservatism which can reduce the performance of the fault detection system. One of our future research topics would be how to reduce the conservatism.

References

1. Nilsson, J.: Real-time Control Systems with Delays, Ph.D. dissertation. Department of Automatic Control Lund Institute of Technology, Lund, Sweden (1998)
2. Krtolica, R.: Stability of linear feedback systems with random communication. International Journal of Control 29(4), 925–953 (1994)
3. Nilsson, J., Bernhardsson, B., Wittenmark, B.: Stochastic analysis and control of real-time systems with random time delays. Automatica 34(1), 57–64 (1998)
4. Chen, Y.-Q., Xu, Z.-Y.: Real-time Fault Detection Based on Simulink. Journal of System Simulation 19(1), 226–229 (2007)
5. Yang, F., Wang, Z., Hung, Y.S., Gani, M.: H∞ Control for Networked Systems With Random Communication Delays. IEEE Trans. Automat. Control 51(3), 511–518 (2006)
6. Patton, R.J., Frank, P.M., Clark, R.N.: Issues of Fault Diagnosis for Dynamic Systems. Springer (2000)

7. Chen, Y., Xiao, B., Xu, Z.: Fault Detection Filter Design For Networked Control System With Communication Delays. In: The Sixth International Conference on Intelligent Systems Design and Applications (ISDA 2006), pp. 867–872 (2006)
8. Winstead, V.: Observers for Fault Detection In Networked Systmes with Random Delays. In: Proceedings of the 2004 American Control Conference, Boston, pp. 2457–2462 (June 2004)
9. Zhang, P.: Fault Detection of networked control systems with missing measurements. In: 5th Asian Control Conference, July 20-23, vol. 2, pp. 1258–1263 (2004)
10. Kim, D.-S., Lee, Y.S., Kwon, W.H., Park, H.S.: Maximum allowable delay bounds of networked control systems. Control Engineering Practice 11, 1301–1313 (2003)
11. Cao, Y.-Y.: Stochastic Stabilizability and H∞ Control for Discrete-time jump linear systems with time delay. Journal of the Franklin Institute 336, 1263–1281 (1999)
12. Ghaoui, L.E., Oustry, F., Aitrami, M.: A cone complementarity linearization algorithm for static output feedback and related problems. IEEE Transactions on Automatic Control 42, 1171–1176 (1997)
13. Chen, Y., Xiao, B., Xu, Z.: Fault Detection Filter Design For Networked Control System With Communication Delays. In: The Sixth International Conference on Intelligent Systems Design and Applications (ISDA 2006), pp. 867–872 (2006)
14. Chen, Y.-Q., Duan, Z.-G., Liu, Y.-B., Wang, R.-P.: Fault Detection for Networked Control System with Random Delays. In: 2008 IEEE International Conference on Robotics, Automation and Mechatronics (RAM 2008), pp. 95–100 (2008)

Trace Representation of Quasi-negacyclic Codes

Xiuli Li* and Chenghua Fu

School of Mathematics and Physics,
Qingdao University of Science and Technology,
Qingdao 266000, China
lixiuli2004@tom.com

Abstract. The alphabet decomposition of quasi-negacyclic codes is developed. By the use of the Chinese Remainder Theorem (CRT), or of the Discrete Fourier Transform (DFT), the ring $F_q[X]/\langle x^m + 1\rangle$ can be decomposed into a direct product of fields. The trace representation for quasi-negacyclic codes generalizes nicely the trace representation of cyclic and quasi-cyclic codes. Furthermore quasi-negacyclic codes are constructed by Vandermonde matrices.

Keywords: quasi-negacyclic codes, trace, Discrete Fourier Transform.

1 Introduction

Constacyclic codes constitute a remarkable generalization of cyclic codes, hence form an important class of linear codes in the coding theory (see [1],[3]-[5],[8]-[10]). And, constacyclic codes also have practical applications as they can be encoded with shift registers.

Definition 1. Let F_q be the Galois field with q elements and $\lambda \in F_q^*$. A subset C of F_q^n is called a λ-constacyclic code of length n if

(1) C is a subspace of F_q^n;
(2) if $c = (c_0, \cdots, c_{n-1})$ is a codeword of C, then $T_\lambda(c) = (\lambda c_{n-1}, c_0, \cdots, c_{n-2})$ is also a codeword in C.

1-constacyclic codes are cyclic codes. -1-constacyclic codes are called negacyclic codes.

Any negacyclic code C of length n over a finite field F_q is identified with an ideal of the quotient algebra $F_q[X]/\langle x^n + 1\rangle$ where $\langle x^n + 1\rangle$ denotes the ideal generated by $x^n - \lambda$ of the polynomial algebra $F_q[X]$. For more details, see [2,5].

As another generalization of cyclic codes, quasi-cyclic codes have been around for more than 35 years. They constitute a remarkable generalization of cyclic codes (see [1],[3]-[4],[6]-[10]). Many good quasi-cyclic codes were discovered in [11].

* This research is supported by natural scientific foundation of China (10971252), science and technology program of Qingdao(10-3-4-4-2-jch), technology development project of colleges and universities of ShanDong(J10LA57) and reward fund for outstanding young and middle-aged scientists of ShanDong(BS2011DX011).

D. Liu et al. (Eds.): BICS 2013, LNAI 7888, pp. 377–386, 2013.

Most of the works has been concentrated on the algebraic-combinatorial computers search. In [8], San Ling and Patrick Solé introduced a new algebraic approach to quasi-cyclic codes over finite fields and gave a trace representation that generalizes that of cyclic codes.

In this work, we propose to view quasi-negacyclic codes of length lm and index l over a field F_q as codes over the polynomial ring

$$R_m = F_q[X]/\langle x^m + 1\rangle.$$

We generalize the method in [8] to quasi-negacyclic codes over finite fields . When m is coprime with the characteristic of F_q, the ring $F_q[X]/\langle x^m + 1\rangle$ can be decomposed into a direct sum of fields. This decomposition can be achieved by either the Chinese Remainder Theorem (CRT) or the Discrete Fourier Transform (DFT).

The paper is organized in the following way. Section II contains some basic notations and definitions, and develops the alphabet decomposition of quasi-negacyclic codes using the CRT. Section III tackles the same problem with the DFT which results in a trace representation of quasi-negacyclic codes that generalizes nicely the trace representation of cyclic and quasi-cyclic codes. Section IV develops applications of the above theory for Vandermonde construction of quasi-negacyclic codes.

2 Quasi-negacyclic Codes

Let F_q be the Galois field with $q = p^r$ elements. Let $F_q[x]$ denote the polynomials in the indeterminate x with coefficients in F_q and $R_m = F_q[x]/\langle x^m + 1\rangle$ such that $gcd(m, p) = 1$, $m \geq 2$.

Definition 2. A subset C of F_q^{lm} is called a quasi-negacyclic code of length lm and index l if

(1) C is a subspace of F_q^{lm};

(2) if $c = (c_{0,0}, \cdots, c_{0,l-1}, c_{1,0}, \cdots, c_{1,l-1}, \cdots, c_{m-1,0}, \cdots, c_{m-1,l-1})$ is a codeword of C, then $T_{-1,l}(c) = (-c_{m-1,0}, \cdots, -c_{m-1,l-1}, c_{0,0}, \cdots, c_{0,l-1}, \cdots, c_{m-2,0}, \cdots, c_{m-2,l-1})$ is also a codeword in C.

When $p = 2$, the quasi-negacyclic codes are just quasi-cyclic codes. In the following of this paper, we always suppose that p is odd.

Define a map $\phi : F_q^{lm} \to R_m^l$ by

$$\phi(c) = (c_0(x), c_1(x), \cdots, c_{l-1}(x)),$$

where $c_j(x) = \sum_{i=0}^{m-1} c_{i,j}x^i \in R_m$, $0 \leq j \leq l-1$.

Let $\phi(C)$ denote the image of C under ϕ. Since ϕ is a bijection, we may denote $c \in C$ by $\phi(c)$. The map ϕ induces a one-to-one correspondence between quasi-negacyclic codes over F_q of length lm and index l and linear codes over R_m of length l.

The dual $C^\perp$ of a code C is understood with respect to the standard inner product. A code C is self-dual if $C = C^\perp$. We now proceed to the study of duality for linear codes over R_m, in relation with the duality of codes over F_q. We define a "conjugation" map on R_m as one that acts as the identity on the elements of F_q and sends x to $x^{-1} = -x^{m-1}$, and is extended F_q-linearly.

On F_q^{lm}, we define the usual *Euclidean inner product*: for

$$a = (a_{0,0}, \cdots, a_{0,l-1}, \cdots, a_{m-1,0}, \cdots, a_{m-1,l-1})$$

and

$$b = (b_{0,0}, \cdots, b_{0,l-1}, \cdots, b_{m-1,0}, \cdots, b_{m-1,l-1}),$$

define

$$a \cdot b = \sum_{i=0}^{m-1} \sum_{j=0}^{l-1} a_{ij} b_{ij}.$$

On R_m^l, we define the *Hermitian inner product*: for $a(x) = (a_0(x), \cdots, a_{l-1}(x))$ and $b(x) = (b_0(x), \cdots, b_{l-1}(x))$, define

$$a(x) * b(x) = \sum_{j=0}^{l-1} a_j(x)\overline{b_j(x)}.$$

Theorem 1. Let $a, b \in F_q^{lm}$. Then $(T_{-1,l}^k(a)) \cdot b = 0$ for all $0 \le k \le m-1$ if and only if $\phi(a) * \phi(b) = 0$.

Proof: The condition $\phi(a) * \phi(b) = 0$ is equivalent to

$$0 = \sum_{j=0}^{l-1} a_j(x)\overline{b_j(x)} = \sum_{j=0}^{l-1} \left(\sum_{i=0}^{m-1} a_{ij} x^i \right) \left(\sum_{t=0}^{m-1} b_{tj} x^{-t} \right). \tag{1}$$

Comparing the coefficients of x^k on both sides, (1) is equivalent to

$$\sum_{j=0}^{l-1} \left(\sum_{i=0}^{k-1} a_{ij} b_{m-k+i,j} - \sum_{i=k}^{m-1} a_{ij} b_{i-k,j} \right) = 0 \tag{2}$$

for all $0 \le k \le m-1$. (2) means precisely that $(T_{-1,l}^{m-k}(a)) \cdot b = 0$. For $0 \le k \le m-1$, $1 \le m-k \le m$. Since $T_{-1,l}^m(a) = -a$, then (2) is equivalent to $(T_{-1,l}^k(a)) \cdot b = 0$ for all $0 \le k \le m-1$.

By applying Theorem 1 with b belonging to a quasi-negacyclic code C of length lm and index l over F_q, we obtain the following.

Theorem 2. Let C be a quasi-negacyclic code of length lm and index l over F_q and $\phi(C)$ be its image in R_m^l under ϕ. Then $\phi(C)^\perp = \phi(C^\perp)$, where the dual in F_q^{lm} is taken with respect to the Euclidean inner product, while the dual in R_m^l is taken with respect to the Hermitian inner product.

Theorem 3. The dual of a quasi-negacyclic code of length lm and index l over F_q is a quasi negacyclic code of length lm and index l over F_q.

Proof: Suppose that C is a quasi-negacyclic code of length lm and index l over F_q. Then

$$C^{\perp} = \{b \in F_q^{lm} : \ a \cdot b = 0 \ for \ any \ a \ \in C\}.$$

For any $a \in C, T_{-1,l}^k(a) \in C$ $(0 \leq k \leq m-1)$. Then $T_{-1,l}^k(a) \cdot b = 0, 0 \leq k \leq m-1$. Since $T_{-1,l}^k(a) \cdot b = 0$ is equivalence to $a \cdot T_{-1,l}^{m-k}(b) = 0$, $0 \leq k \leq m-1$. Then $T_{-1,l}^k(b) \in C^{\perp}$, $0 \leq k \leq m-1$. Thus $C^{\perp}$ is a quasi-negacyclic code of length lm and index l over F_q.

For any monic polynomial $f(x) = \sum_{i=0}^{r} a_i x^i$ of degree r $(a_r = 1)$ over F_q, let $\overleftarrow{f(x)}$ denote a polynomial given by

$$\overleftarrow{f(x)} = x^r f\left(\frac{1}{x}\right) = \sum_{i=0}^{r} a_{r-i} x^i.$$

Furthermore, if $a_0 \neq 0$, then let $f^*(x) = \frac{1}{a_0}\overleftarrow{f(x)}$, $f^*(x)$ is called the *reciprocal polynomial* of $f(x)$. It is clear that $(f(x)g(x))^* = f^*(x)g^*(x)$ and $(f^*(x))^* = f(x)$ for any monic polynomials $f(x), g(x) \in F_q[x]$ such that the constant terms of $f(x)$ and $g(x)$ are non zero elements. In particular, if a polynomial is equal to its reciprocal polynomial over F_q, then it is called *self-reciprocal* over F_q.

Remark 1. Let $f(x)$ be a monic irreducible polynomial with non zero constant terms in $F_q[x]$. If $deg(f(x)) = 1$, $f(x)$ is self-reciprocal implies that $f(x) = x+1$ or $f(x) = x-1$. If $deg(f(x)) \neq 1$, $f(x)$ is self-reciprocal implies that the degree of $f(x)$ is even.

If $x^m + 1 = g(x)h(x)$, where $g(x), h(x) \in F_q[x]$ are monic polynomials, then $x^m + 1 = (x^m + 1)^* = g^*(x)h^*(x)$. Thus for any monic irreducible polynomial dividing $x^m + 1$ over F_q, its reciprocal polynomial also divides $x^m + 1$ over F_q and is also irreducible over F_q. Since $gcd(m, p) = 1$, the polynomial $x^m + 1$ can be factorized into distinct irreducible polynomials as follows

$$x^m + 1 = f_1(x) \cdots f_s(x) h_1(x) h_1^*(x) \cdots h_t(x) h_t^*(x), \tag{3}$$

where $f_i(x)$ $(1 \leq i \leq s)$ are monic irreducible self-reciprocal polynomials over F_q while $h_j(x)$ and its reciprocal polynomial $h_j^*(x)$ $(1 \leq j \leq t)$ are both monic irreducible polynomials over F_q. We say that $h_j(x)$ and $h_j^*(x)$ form a reciprocal polynomial pair. Note that s and t both depend on n and q. Therefore, we regard them as two functions of the pair (n, q).

Consequently, from CRT it follows that

$$R_m = \frac{F_q[x]}{\langle x^m + 1 \rangle} = \left(\bigoplus_{i=1}^{s} \frac{F_q[x]}{\langle f_i(x) \rangle} \right) \oplus \left(\bigoplus_{j=1}^{t} \left(\frac{F_q[x]}{\langle h_i(x) \rangle} \oplus \frac{F_q[x]}{\langle h_i^*(x) \rangle} \right) \right). \tag{4}$$

The direct sum on the right-hand side is endowed with the coordinate-wise addition and multiplication.

For convenience, we denote $\frac{F_q[x]}{\langle f_i(x)\rangle}$ by G_i, $\frac{F_q[x]}{\langle h_j(x)\rangle}$ by H_j, $\frac{F_q[x]}{\langle h_j^*(x)\rangle}$ by K_j. Then

$$R_m^l = \left(\bigoplus_{i=1}^{s} G_i^l\right) \oplus \left(\bigoplus_{j=1}^{t} \left(H_j^l \oplus K_j^l\right)\right).$$

In particular, every R_m-linear code C of length l can be decomposed as

$$C = \left(\bigoplus_{i=1}^{s} C_i\right) \oplus \left(\bigoplus_{j=1}^{t} \left(C_j' \oplus C_j''\right)\right),$$

where C_i is a linear code over G_i of length l, C_j' is a linear code over H_j of length l and C_j'' is a linear code over K_j of length l, $1 \le i \le s$, $1 \le j \le t$.

Every element of R_m may be written as $\mathbf{r}(x)$ which is in $F_q(x)$. $\mathbf{r}(x)$ may also be written as an $(s+2t)$-tuple:

$$(r_1(x), \cdots r_s(x), r_1'(x), r_1''(x), \cdots, r_t'(x), r_t''(x)),$$

where $r_i(x) \in G_i$ $(1 \le i \le s)$, $r_j'(x) \in H_j$ and $r_j''(x) \in K_j$ $(1 \le j \le t)$. The $r_i(x)$, $r_j'(x)$ and $r_j''(x)$ may be also considered as polynomials in $F_q[x]$.

For a monic irreducible polynomial $f(x) \in F_q[x]$ that divides $x^m + 1$, the quotients $F_q[x]/\langle f(x)\rangle$ and $F_q[x]/\langle f^*(x)\rangle$ are isomorphism as rings. The isomorphism is given by

$$F_q[x]/\langle f(x)\rangle \to F_q[x]/\langle f^*(x)\rangle$$
$$r(x) + \langle f(x)\rangle \to r(x^{-1}) + \langle f^*(x)\rangle.$$

Here x^{-1} can be replaced by $-x^{m-1}$. For $r(x) \in F_q[x]/\langle f(x)\rangle$, we denote $r(x)$'s image by $\overline{r(x)}$. Therefore, the element of $\overline{\mathbf{r}(x)}$ can be expressed as

$$\left(\overline{r_1(x)}, \cdots \overline{r_s(x)}, \overline{r_1''(x)}, \overline{r_1'(x)}, \cdots, \overline{r_t''(x)}, \overline{r_t'(x)}\right).$$

For vectors $\mathbf{c} = (c_1, \cdots, c_l), \mathbf{d} = (d_1, \cdots, d_l) \in (F_q[x]/\langle f(x)\rangle)^l$, the Hermitian inner product of $\mathbf{c}$ and $\mathbf{b}$ on $(F_q[x]/\langle f(x)\rangle)^l$ is

$$c * d = \sum_{i=1}^{l} c_i \overline{d_i}. \tag{5}$$

In the case where $f(x)$ is self-reciprocal and $deg(f(x)) = 1$, since the map $r(x) \to \overline{r(x)}$ is the identity, the Hermitian inner product (5) is the usual Euclidean inner product on F_q.

In the case where $f(x)$ is self-reciprocal and $deg(f(x)) = 2d$ with d a positive integer, $F_q[x]/\langle f(x)\rangle$ is isomorphic to $F_{q^{2d}}$ and the map $x \to x^{-1}$ is just the map $x \to x^{q^d}$. Hence the map $r(x) \to \overline{r(x)}$ is the map $r(x) \to r(x)^{q^d}$. In this case, the Hermitian inner product (5) coincides with the usual the Hermitian inner product defined on $F_{q^{2d}}$.

Let $\mathbf{a}, \mathbf{b} \in R_m^l$, $\mathbf{a} = (\mathbf{a}_0(x), \cdots, \mathbf{a}_{l-1}(x))$ and $\mathbf{b} = (\mathbf{b}_0(x), \cdots, \mathbf{b}_{l-1}(x))$. We may write

$$\mathbf{a}_i(x) = (a_{i1}(x), \cdots, a_{is}(x), a'_{i1}(x), a''_{i1}(x), \cdots, a'_{it}(x), a''_{it}(x))$$

and

$$\mathbf{b}_i(x) = (b_{i1}(x), \cdots, b_{is}(x), b'_{i1}(x), b''_{i1}(x), \cdots, b'_{it}(x), b''_{it}(x)),$$

where $a_{ij}(x), b_{ij}(x) \in G_j$, $a'_{ik}(x), b'_{ik}(x) \in H_k$ and $a''_{ik}(x), b''_{ik}(x) \in K_k$, $1 \le j \le s$, $1 \le k \le t$. Then

$$\mathbf{a} * \mathbf{b} = \sum_{i=0}^{l-1} \mathbf{a}_i(x)\overline{\mathbf{b}_i(x)}$$

$$= \left(\sum_{i=0}^{l-1} a_{i1}\overline{b'_{i1}}, \cdots, \sum_{i=0}^{l-1} a_{is}\overline{b_{is}}, \sum_{i=0}^{l-1} a'_{i1}\overline{b''_{i1}}, \sum_{i=0}^{l-1} a''_{i1}b_{i1}, \cdots, \sum_{i=0}^{l-1} a'_{it}\overline{b''_{it}}, \sum_{i=0}^{l-1} a''_{it}\overline{b'_{it}} \right).$$

In particular, $\mathbf{a} * \mathbf{b} = 0$ if and only if $\sum_{i=0}^{l-1} a_{ij}(x)\overline{b_{ij}(x)} = 0$ $(1 \le j \le s)$ and $\sum_{i=0}^{l-1} a'_{ik}(x)\overline{b''_{ik}(x)} = \sum_{i=0}^{l-1} a''_{ik}(x)\overline{b'_{ik}(x)} = 0$ $(1 \le k \le t)$.

Theorem 4. A linear code C over R_m of length l is self-dual with respect to the Hermitian inner product, or equivalently, a quasi-negacyclic code of length lm and index l over F_q is self-dual with respect to the Euclidean inner product, if and only if

$$C = \left(\bigoplus_{i=1}^{s} C_i \right) \oplus \left(\bigoplus_{j=1}^{t} (C'_j \oplus (C'_j)^{\perp}) \right).$$

For $1 \le i \le s$, C_i is a self-dual code over G_i of length l with respect to the Hermitian inner product and, for $1 \le j \le t$, C'_j is a linear code of length l over H_j and $(C'_j)^{\perp}$ is its dual with respect to the Hermitian inner product.

3 Trace Formula

Let F_q be the Galois field with $q = p^r$ elements, p is an odd prime number. If L is an extension of degree s of F_q, then the trace of $x \in L$ down to F_q is

$$Tr_{L/F_q}(x) = x + x^q + x^{q^2} + \cdots + x^{q^{s-1}}.$$

Let m be a positive integer with $gcd(m, q) = 1$. $R_m = F_q[x]/\langle x^m + 1 \rangle$. The roots of $x^m + 1$ are δ^{2i+1}, $0 \le i \le m-1$, where δ is a primitive $2m$-th root of unity in some extension field F of F_q. Let $\xi = \delta^2$, which is a primitive m-th root of unity in F. Let O_{2m} be the set of odd integers from 1 to $2m-1$.

In (4), the direct factors on the right-hand side correspond to the irreducible factors of x^m+1. There is a one-to-one correspondence between these factors and the q-cyclotomic cosets modulo $2m$. Denote by U_i $(1 \le i \le s)$ the q-cyclotomic coset corresponding to $f_i(x)$, V_j and W_j $(1 \le j \le t)$ the q-cyclotomic cosets corresponding to $h_j(x)$ and $h_j^*(x)$, respectively.

For $\mathbf{a} \in F_q^m$. Define the Discrete Fourier Transform (DFT) of $\mathbf{a}$ to be the vector $(A_0, \cdots, A_{m-1}) \in F^m$, where

$$A_i = \sum_{j=0}^{m-1} a_j \delta^{(2i+1)j}, \quad 0 \le i \le m-1.$$

A_i is called the i-th Fourier coefficient of $\mathbf{a}$. We define the DFT of an element $a(x) \in R_m$ to be the DFT of the corresponding vector $\mathbf{a}$ (so that $A_i = a(\delta^{2i+1})$). We make F_q^m into a ring by usual addition and componentwise multiplication ($\mathbf{a} \star \mathbf{b} = (a_0 b_0, \cdots, a_{m-1} b_{m-1})$). Finally, we define a generalization of the Mattson-Solomon polynomial of $\mathbf{a}$ (and $a(x)$) as

$$A(Z) = \sum_{i=0}^{m-1} A_i Z^i.$$

We state the following facts about this transform.

Lemma 1. ([2]) Let θ: $R_m \to F^m$ be the negacyclic DFT map defined by $\theta(a(x)) = (A_0, \cdots, A_{m-1})$. Suppose that $a(x), b(x) \in R_m$. Then

(1) θ is a ring homorphism.
(2) $A_i^q = A_{(iq + \frac{q-1}{2})}$.
(3) If $0 \le t \le m-1$, then

$$a_t = \frac{1}{m} \sum_{i=0}^{m-1} A_i \delta^{-(2i+1)t} = \frac{1}{m} \delta^{-t} A(\delta^{-2t}).$$

(4) $\sum_{t=0}^{m-1} a_t b_t = \frac{1}{m} \sum_{i=0}^{m-1} A_i B_{-i-1}$.

(All subscripts are calculated module m.)

Let $\overline{A}_k = A_{\frac{k-1}{2}}$ for $k \in O_{2m}$. Then

$$\overline{A}_k^q = A_{\frac{k-1}{2}}^q = A_{\frac{k-1}{2} q + \frac{q-1}{2}} = A_{\frac{kq-1}{2}} = \overline{A}_{kq};$$

$$a_t = \frac{1}{m} \sum_{i=0}^{m-1} \overline{A}_{2i+1} \delta^{-(2i+1)t};$$

$$\sum_{t=0}^{m-1} a_t b_t = \frac{1}{m} \sum_{i=0}^{m-1} \overline{A}_{2i+1} \overline{B}_{-(2i+1)}.$$

(All subscripts are calculated module $2m$.)

Let G_i, H_j and K_j denote the Galois extensions of F_q corresponding to the polynomials $f_i(x)$, $h_j(x)$ and $h_j^*(x)$, with corresponding cyclotomial cosets U_i, V_j and W_j. For $h \in U_i$, $\overline{A}_h \in G_i$, and for $h \in V_j$ (resp. W_j), $\overline{A}_h \in H_j$ (resp. K_j). For each i, choose and fix some $u_i \in U_i$. For each j, choose and fix some $v_j \in V_j$

and $w_j \in W_j$. Then $\overline{A}_{u_i} \in G_i$, $\overline{A}_{v_j} \in H_j$, and $\overline{A}_{w_j} \in K_j$. To the $(s+2t)$-tuple $(\overline{A}_{u_1}, \cdots, \overline{A}_{u_s}, \overline{A}_{v_1}, \cdots, \overline{A}_{v_t}, \overline{A}_{w_1}, \cdots, \overline{A}_{w_t})$, we associate the element

$$\sum_{t=0}^{m-1} a_t x^t \in \frac{F_q[x]}{\langle x^m + 1 \rangle}$$

where

$$ma_t = \sum_{i=1}^{s} Tr_{G_i/F_q}(\overline{A}_{u_i} \delta^{-u_i t}) + \sum_{j=1}^{t} Tr_{H_j/F_q}(\overline{A}_{v_j} \delta^{-v_j t})$$

$$+ \sum_{j=1}^{t} Tr_{K_j/F_q}(\overline{A}_{w_j} \delta^{-w_j t}),$$

where, for any extension L of F_q, $Tr_{L/F}$ denotes the trace from L to F_q. For a vector $\mathbf{a}$, by its Fourier transform, we simply mean the vector whose i-th entry is the Fourier transform of the i-th entry of $\mathbf{a}$. By the trace of $\mathbf{a}$ we mean the vector whose coordinates are the traces of the coordinates of $\mathbf{a}$.

This description gives the following trace parametrization for quasi-negacyclic codes over finite fields, analogous to the trace description of quasi-cyclic codes codes in [8].

Theorem 5. Let F_q be the Galois field with $q = p^r$ elements, p is a prime number. Let m be a positive integer with $gcd(m, q) = 1$. Let δ be a primitive $2m$-th root of unity in some extension field F of F_q. Then, for any l, the quasi-cyclic codes over F_q of length lm and index l are precisely given by the following construction: write $x^m + 1 = f_1 \cdots f_s h_1 h_1^* \cdots h_t h_t^*$, where f_i are monic irreducible factors that are self-reciprocal, and h_j are monic irreducible factors whose reciprocals are h_j^*. Write $F_q[x]/\langle f_i \rangle = G_i$, $F_q[x]/\langle h_j \rangle = H_j$, and $F_q[x]/\langle h_j^* \rangle = K_j$. Let U_i (resp., V_j and W_j) denote the cyclotomic coset of Z/mZ corresponding to G_i(resp., H_j and K_j) and fix $u_i \in U_i$, , $v_j \in V_j$ and $w_j \in W_j$. For each i, let C_i be a code of length l over G_i, and for each j, let C'_j be a code of length l over H_j and let C''_j be a code of length l over K_j. For $\mathbf{x}_i \in C_i$, $\mathbf{y}_j \in C'_j$, and $\mathbf{z}_j \in C''_j$, and for each $0 \leq k \leq m-1$, let

$$c_k((\mathbf{x}_i), (\mathbf{y}_j), (\mathbf{z}_j)) = \sum_{i=1}^{s} Tr_{G_i/F_q}(\mathbf{x}_i \delta^{-u_i k}) + \sum_{j=1}^{t} Tr_{H_j/F_q}(\mathbf{y}_j \delta^{-v_j k})$$

$$+ \sum_{j=1}^{t} Tr_{K_j/F_q}(\mathbf{z}_j \delta^{-w_j k}).$$

Then the code

$$C = \{c_0((\mathbf{x}_i), (\mathbf{y}_j), (\mathbf{z}_j)), \cdots, c_{m-1}((\mathbf{x}_i), (\mathbf{y}_j), (\mathbf{z}_j)) :$$

$$\forall \mathbf{x}_i \in C_i, \forall \mathbf{y}_j \in C'_j, \forall \mathbf{z}_j \in C''_j\}$$

is a quasi-negacyclic code over F_q of length lm and index l. Conversely, every quasi-negacyclic code over F_q of length lm and index l is obtained through this construction. Moreover, C is self-dual with respect to the Euclidean inner product if and only if the C_i are self-dual with respect to the Hermitian inner product and $C_j'' = (C_j')^{\perp}$ for each j with respect to the Hermitian inner product.

4 The Vandermonde Construction

Let m be a positive integer with $gcd(m, q) = 1$. Let $R_m = F_q[x]/\langle x^m + 1\rangle$. The roots of $x^m + 1$ are δ^{2i+1}, $0 \le i \le m-1$, where δ is a primitive $2m$-th root of unity in some extension field F of F_q. Suppose that $F = F_q$. The polynomial $x^m + 1$ splits completely as follows

$$x^m + 1 = (x - \delta)(x - \delta^3) \cdots (x - \delta^{2m-1}).$$

From the Fourier transform in Section III, for $\mathbf{a} = (a_0, a_1, \cdots, a_{m-1}) \in F_q^m$, we have

$$(A_0, A_1, \cdots, A_{m-1}) = (a_0, a_1, \cdots, a_{m-1})V,$$

where

$$V = \begin{pmatrix} 1 & 1 & \cdots & 1 \\ \delta & \delta^3 & \cdots & \delta^{2m-1} \\ \vdots & \vdots & \cdots & \vdots \\ \delta^{m-1} & \delta^{3(m-1)} & \cdots & \delta^{(2m-1)(m-1)} \end{pmatrix}$$

is the $m \times m$ Vandermonde matrix.

For a given positive integer l, let $\mathbf{c}_0, \cdots, \mathbf{c}_{m-1} \in F_q^l$ be m vectors. The construction

$$(\mathbf{c}_0, \cdots, \mathbf{c}_{m-1})V^{-1}$$

gives an element of R_m^l. If C_i $(0 \le i \le m-1)$ are linear codes over F_q of length l, and $c_i \in C_i$ for $0 \le i \le m-1$, then we obtain a linear code over R_m of length l, which then corresponds to a quasi-negacyclic code over F_q of length lm and of index l.

Theorem 6. Let F_q be a finite field and m an integer coprime with the characteristic of F_q, q is odd. Assume that F_q^* contains an element δ of order $2m$. Let $C_0, C_1, \cdots, C_{m-1}$ be linear codes of length l over F_q. Then the Vandermonde product of $C_0, C_1, \cdots, C_{m-1}$ is a quasi-negacyclic code over F_q of length lm and index l. Moreover, when F_q and m are as above, every quasi-negacyclic code of length lm and index l over F_q is obtained via the Vandermonde construction.

References

1. Barbier, M., Chabot, C., Quintin, G.: On quasi-cyclic codes as a generalization of cyclic codes. Finite Fields and Their Applications 18, 904–919 (2012)
2. Blackford, T.: Negacyclic duadic codes. Finite Fields and Their Applications 14, 930–943 (2008)

3. Cao, Y.: Structural properties and enumeration of 1-generator generalized quasi-cyclic codes. Designs, Codes and Cryptography 60, 67–79 (2011)
4. Cao, Y., Gao, J.: Constructing quasi-cyclic codes from linear algebra theory. Designs, Codes and Cryptography 67(1), 59–75 (2013)
5. Dinh, H.Q.: On the linear ordering of some classes of negacyclic and cyclic codes and their distance distributions. Finite Fields and Their Applications 14, 22–40 (2008)
6. Han, S., Kim, J.-L., Lee, H., Lee, Y.: Construction of quasi-cyclic self-dual codes. Finite Fields and Their Applications 18, 613–633 (2012)
7. Kamiya, N.: Quasi-Cyclic Codes from a Finite Affine Plane. Designs, Codes and Cryptography 38, 311–329 (2006)
8. Ling, S., Solé, P.: On the Algebraic Structure of Quasi-Cyclic Codes I: Finite Fields. IEEE Transactions on Information Theory 47(7), 2751–2760 (2001)
9. Solé, P., Yemen, O.: Binary quasi-cyclic codes of index 2 and skew polynomial rings. Finite Fields and Their Applications 18, 685–699 (2012)
10. Venkaiah, V.C., Aaron Gulliver, T.: Quasi-cyclic codes over F_{13} and enumeration of defining polynomials. Journal of Discrete Algorithms 16, 249–257 (2012)
11. Chen Z.: (2011), `http://www.tec.hkr.se/~chen/research/codes/` (accessed Septemper 2011)

On a New-Member-Joining-Protocol Design Using Bivariate Polynomials Based DKG Algorithms

Qian Wu[1] and Yanyan Yang[2]

[1] School of Information Engineering, Minzu Univ. of China
27 Zhongguancun South St., Beijing, China, P.R.
wuqian@muc.edu.cn
[2] Technology School of Engineering, Portsmouth University
Portsmouth PO1 2UPWinston Churchill Ave, Beijing, UK
linda.yang@port.ac.uk

Abstract. In many wireless mobile applications, new member joining problem often occurs when a new player hopes to get a share of private key in order to join a multi-player group, which has jointly generated a pair of private and public keys based on some distributed key generation (DKG) protocols. We propose a New-Member-Joining (NMJ) protocol built upon bivariate polynomials based DKG scheme to completely solve the problem. A proof of security of the protocol in terms of correctness and secrecy is present.

Keywords: New-Member-Joining protocol, bivariate polynomials Threshold cryptography, Distributed Key Generation.

1 Introduction

It is in general impractical to orchestrate a trusted third party to generate and distribute key shares to users in many wireless mobile computing environments. Typically a set of n players in group could make use of a distributed key generation scheme to jointly generate a pair of public and private keys according to the distribution defined by a underlying threshold cryptosystem [1][2] without assuming the existence of any trusted party. In such a scenario, with the public key disclosed in the clear, the private key is shared by n players, each of which has its own unique secret share, such that any sufficiently large subset of the n players can reveal or use the key. The security parameter of such a system is called the threshold, t, which is the number of players that can be corrupted without the key being compromised. In contrary to widely adopted distributed key generation schemes for discrete-log cryptosystems [3][4] based on univariate polynomials, a distributed key generation scheme for discrete-log cryptosystems using bivariate symmetric polynomials is nevertheless proposed as BDKG [5], which works in a two-phased manner: firstly, the group of non-disqualified players, Q, is selected, and players in Q jointly generate a random secret key such that all players in Q have a share of the secret key; secondly, the public value associated to the shared secret is made. It is proved the BDKG is

D. Liu et al. (Eds.): BICS 2013, LNAI 7888, pp. 387–394, 2013.

efficient in computation, simple and flexible in applications, and is proven secure against static adversaries.

We present in this paper a solution for the new member joining problem based on the BDKG. Assuming that players P_1, …, P_n, whose identities will be assigned with their own indices, constituting a group G, have jointly generated a pair of private and public keys $<x,y> \in Z_q \times Z_p$ by the BDKG scheme, where p is a large prime and q a large prime dividing $p-1$, each player P_i ($i \in \{1,2,\ldots,n\}$) holds a share s_i of the secret key x, and any $t+1$ players among P_1, …, P_n can jointly recover x. When a new good player P_m ($m \neq 1,2,\ldots,n$) hopes to hold a share of x and to become a member of G, players in G can independently provide P_m with information on the above secret value and need not exchange information with other players in G. The security of such new member joining protocol can be proved in terms of correctness and secrecy.

The paper will proceed as follows. In Section 2 we outline a brief summary of BDKG algorithms. Section 3 describes the details of the NMJ protocol, with security proof followed in Section 4. Section 5 concludes the paper finally.

2 BKDG Algorithms Outline

BDKG, is based on so-called bivariate symmetrical polynomials and can work with less than $(n-2)/3$ corrupted players. The description of BDKG is based on some group G[6] which is a cyclic additive group of prime order q. BDKG can be described over multiplicative cyclic group with an element of prime order q, e.g, Z^*_p where p is a large prime and q divides $(p-1)$.

Assume a system involves a group of n players, which are modeled by probabilistic polynomial-time Turing machines. The players are connected by a complete network of private point-to-point channels. In addition, each player has access to a dedicated broadcast channel to broadcast message, which either reaches all recipients in random order, or none. The messages, sent on either a point-to-point or the broadcast channel, are received by their recipients within some fixed time bound. It is supposed that an adversary, A, can corrupt up to t of the n players in the network, where $t < (n-2)/3$; and the computational power of adversary is adequately modeled by a probabilistic polynomial time Turing machine. Finally we define the adversary as static in that before the protocol executes, the adversary has already decided which player to corrupt during the execution of the protocol.

With assumptions that the identity of each player is assigned with his own index, the BKDG algorithms can be summarized as follows.

1. Start with a dealing phase so that all players know q, G, P, where q is a large prime, G is an addition cyclic group of prime order q, P is the generator of G.
2. Generating secret value x (the process called *Joint-VSS*(t)):
   a) Each player P_i randomly chooses a bivariate symmetrical polynomial $f_i(x,z)$ over Z_q of degree t :

$f_i(x,z)=\sum_{k=0}^{t}\sum_{j=0}^{t} a_{kj}^{(i)}x^k z^j$ where $a_{00}^{(i)}=z_i$, $a_{kj}^{(i)} \in Z_q$,

the degree of both x and z equals to t, and $a_{kj}^{(i)}=a_{jk}^{(i)}$. And then, P_i computes $h_m^i(x)=f_i(x,m)$ as follows:

$h_m^i(x)=f_i(x,m)=\sum_{k=0}^{t}\sum_{j=0}^{t} a_{kj}^{(i)}x^k m^j$,

and securely send $h_m^i(x)$ to P_m, here m=1,2,…,n.

b) After receiving $h_m^i(x)$, P_m computes $h_{mk}^i=h_m^i(k)$ and securely sends it to P_k, here k=1,2,…,n.

c) For each m=1,2,…,n, player P_k checks if

$$h_{mk}^i=h_k^i(m) \quad (1)$$

If there are at least t+1 formulas that are not via checking, P_k broadcasts a complaint against P_i

d) Each player P_i who receives at most t complaints broadcasts $h_k^i(x)$ that satisfies Eq.1. Each of other $n-2$ players, P_j, checks if $h_k^i(j)=h_j^i(k)$. If $h_k^i(j)=h_j^i(k)$, P_j broadcasts "YES", otherwise "NO " .

e) Any player P_i marks as disqualified if:

P_i received at least t+1 complaints in Step (c), or there are at least t+1 players that broadcast "NO "in Step (d).

f) Each player then builds the set of non-disqualified players Q.

g) The distributed secret value s is not explicitly computed by any player, but it equals

$s=\sum_{i\in Q} Z_i \mod q$. Each player P_i computes:

$h_i(x)=\sum_{j\in Q} h_i^j(x)=\sum_{j\in Q} f_j(x,i)$ and sets his share of the secret as:

$S_i=\sum_{j\in Q} h_i^j(0) \bmod q$

3. Revealing: $y=sP$.

a) Each player P_i, $i\in Q$, broadcasts $A_{0k}^{(i)}=a_{0k}^{(i)}P$ for k=0,1,2,…,t

b) Each player P_j, $j\in Q$ verifies the values broadcast by the other players in Q, namely, for each $i\in Q$, P_j checks if

$$h_j^i(0)P = \sum_{k=0}^{t} j^k A_{0k}^{(i)} \quad (2)$$

If the check fails for an index i, P_j complains against P_i by broadcasting the value $h_j^i(0)$ that satisfies Eq.1 but does not satisfies Eq.2. For players P_i who receive at least one valid complaint, i.e. value which satisfies Eq.1 not Eq.2., the other players can jointly compute $z_i = f_i(0,0)$, $f_i(0,z)$, and $A_{0k}^{(i)}$ for $k=0,1,\ldots,t$, with Lagrange interpolation. For all players in Q, set $y_i = A_{00}^{(i)} = z_i P$. Compute: $y = \sum_{i \in Q} y_i$

c) $y_i = A_{00}^{(i)} = z_i P$. Compute $y = \sum_{i \in Q} y_i$

3 New-Member-Joining Protocol

3.1 The Problem Definition

We consider the following case: To perform some specific task, such as distributed signature, the private key generator (PKG) of ID-based cryptography, a group G initially formed by n players $P_1, P_2, \ldots, P_n$ that jointly generate a pair of public and private keys $<s,y>$ of G, and among whom $t+1$ players can reconstruct the private key s, where $s \in Z_q^*$, $y=sP$, P is a generator of G, which is a cyclic additive group of prime order q. To be better competent for its works in mobile ad hoc networks, G is often required to be highly dynamic and decentralized, that is, new players may join the group G at any time, and when they do, they must be provided with shares of private key s, by other players in G, since it may be unreasonable to assume that a trusted entity is able to provide a new player with such share. The above case that we describe often occurs in lots of applications [5,6,7].

We assume above private key s is generated by n players $P_1, P_2, \ldots, P_n$ using BDKG in section 2. We also assume that these n players jointly generate a bivariate symmetrical polynomial as follows,

$$f(x,z) = \sum_{i=0,j=0}^{t} a_{ij} x^i z^j, \text{ and } , f(0,0) = s$$

and each player P_i, $i \in \{1,2,3,\ldots,n\}$, gets a share $h_i(x)$ of $f(x,z)$, and a share S_i of s.

3.2 The Protocols

When a good player wants to join G, under the assumption that this new player has a secure channel with each player of G, we propose two protocols according to the two kinds of cases, Protocol-1 and Protocol-2. We further define the honesty as follows: one player in group G is honest if he sends correct message to new member in accordance with the provision of new-member-joining protocol, or else dishonest.

Protocol-1 is based on the assumption that each player of G is honest. When a new player P_{new} joins G, he requests and receives corresponding information from at least t+1 players from G. More specifically the protocol must be realized as follows:

1. P_{new} chooses a set G_0 of at least t+1 players from G. Without loss of generality, we assume this set of players is G_0={ P_1, P_2, …, P_{t+1}}.
2. P_{new} requests to be accepted as a member of G.
3. Each P_i of G_0 sends to P_{new} the piece of information $h_i(new)$.
4. Then, P_{new} computes his share polynomial h_{new} of $f(x,z)$ with $h_{new}(i)=h_i(new)$ and Lagrange interpolation:

$$h_{new}(x)=\sum_{i=1}^{t+1}\prod_{i\neq j}\frac{x-j}{i-j}h_{new}(i)=\sum_{i=1}^{t+1}\prod_{i\neq j}\frac{x-j}{i-j}h_i(new)$$

However, the assumption of each player of G is honest is impractical or impossible in many contexts. We must consider the case that some players of G are dishonest. Suppose that there are at most k ($k\leq t$) dishonest players in G, hence modify the above protocol-1 as follows to have protocol-2:

1. P_{new} chooses a set G_0 of at least n players from G. Without loss of generality, we assume this set of players is G_0={ P_1, P_2, …, P_n}.
2. P_{new} requests to be accepted as a member of G.
3. Each P_i of G_0 sends to P_{new} the piece of information $h_i(new)$, $y_i(=s_iP)$.
4. Then, P_{new} computes as follows:

$(S_1,s_{new},h_{new}(x))=EC\text{-}Interpolate(h1(new), h2(new),..., hn(new))$

$(S_2,v_{new},g_{new}(x)) = EC-Interpolate(y_1,y_2,\ldots,y_n)$

*5. Compute $y_{new}=s_{new}P$, choose t players P_{i1}, …, P_{it} from $S_1\cap S_1$, get function $g_1(x)P$ by polynomial interpolation for $y_{new},y_{i1},\ldots,y_{it}$, where $g_1(x)$ is a polynomial with degree of t.

*6. P_{new} accepts s_{new} and $h_{new}(x)$ and regards s_{new} as a share of private key s if $g_1(0)P=v_{new}=sP$.

In Protocol2, we use notation $(S,v,f(x))=EC\text{-}Interpolate(v_1, v_2, \ldots, v_n)$ for public reconstruction of a value through polynomial interpolation with the use of error-correcting codes. If $\{v_1,v_2,\ldots,v_n\}$ is a set of values such that at least $n-k$ of them lie on $f(x)$, where $f(x)$ is either polynomial or a function with form of $f_1(x)P$ ($f_1(x)$ is polynomial) , and $n>2k+t$, then $v=EC\text{-}Interpolate(v_1, v_2, \ldots, v_n)=f(0)$, S is a set which consists of the index of v_i which lie on $f(x)$. The polynomial can be computed using the method of [9] or any other standard error-correction mechanism, such as the Berlekamp-Welch decoder [10].

In Protocol2, Step 5 and Step 6 mainly make the new member P_{new} believe that s_{new} held by him is a share of private key s. However, making use of the shuffling technique presented in [11], we can ensure that private key s is secure, but, we would be able to convince P_{new} that s_{new} held by him is a share of private key s.

4 Security Analysis

The security of the new-member-joining protocol is defined in terms of correctness and secrecy. Correctness property requires that, even though there are at most dishonest k($k\le t$) players, new member correctly gets a share of private key s. By secrecy, we mean New member does not get any information on private key s; AND, any $d(d\le t)$ players in G do not get any information on a share of private key s which is obtained and is held by new member.

We have to further ensure the correctness and the secrecy of the new-member-joining protocol. Only the security of Protocol-2 shall be considered since Protocol-1 is a special case of Procotol-2. Assume that the number of dishonest players is at most k($k\le t$) , thus $n>2k+t$, then the correctness of Procotol-2 is a direct result of [9]. Hence we only prove the secrecy of the NMJ protocol.

Lemma 1. *By Protocol2, new member does not get any information on s.*

Proof. Assume players $P_1, \ldots, P_n$ jointly generate bivariate symmetric polynomial over Z_q, i.e.

$$f(x,z)=\sum_{i=0,j=0}^{t} a_{ij}\ x^i z^j, and, f(0,0)=s$$

and $a_{ij}=a_{ji}$, by BDKG. Thus, $f(x,z)$ is denoted as $f(x,z)=X^TAY$, where

$$X=(1,x,\ldots,x^t)^T$$
$$Y=(1,y,\ldots,y^t)^T$$

A is a symmetric matrix, X^T denotes the transpose of X. New member P_{new} gets a share s_{new} of private key s and a polynomial $h_{new}(x)=\sum_{i=0}^{t} a_i x^i = X^T Z$ over Z_q by BDKG, where $Z=(a_0,a_1,\ldots,a_t)^T$.

In order to prove that P_{new} does not get any information on private key s, we will show that, given any $a \in Z_q$, there exists a symmetric matric A_a and a bivariate symmetric polynomial $f_a(x,y)=X^T A_a Y$ over Z_q so that it satisfies $f_a(0,0)=a$ and $f_a(new,x) \equiv h_{new}(x) \ (mod\ q)$.

In the rest of proof, we denote *new* as m and assume $1 \le m < q$. Then $X^T Z \equiv X^T A_a M \ (mod\ q)$, where $M=(1,m,\ldots,m^t)^T$ i.e, for any $X \in \{1\} \times (Z_q)^t$, $X^T(A_a M - Z) \equiv 0 \ (mod\ q)$.

Thus, we get $A_a M \equiv Z \ (mod\ q)$ which is an equation set regarding entries of $A_a=(a_{ij})_{1 \le i \le t+1, 1 \le j \le t+1}$ as variables. Because we require that A_a is a symmetric matrix and $a_{11}=a$, the above equations set has $\frac{(t+1)^2-(t+1)}{2}-1$ free variables. Then there are $q^{\frac{(t+1)^2-(t+1)}{2}-1}$ symmetric matrices satisfying the above equations set.

Lemma 2. *Any $d(d \le t)$ players in G does not get any information on a share*

Proof. It is sufficient to prove the lemma in the case where $d=t$. If t players in G does not get any information on a share s_m of s which is gotten and is held by new member P_m with Protocol2, then neither does fewer than t players. Here, without loss of generality, let these t players $P_1, \ldots, P_t$. Then each P_i, $1 \le i \le t$, gets $h_m(i)(=h_i(m))$. Because, for any $a \in Z_q$ we can construct a polynomial $h^0(x)$ which satisfies $h^0(0)=a$, $h^0(1)=h_m(1)$, …, $h^0(t)=h_m(t)$. Thus these t players don't get any information on s_m.

Therefore *Protocl-2 has the secrecy property.*

5 Conclusions

In this paper, we present a new member joining (NMJ) protocol using bivariate symmetric polynomials based distributed key generation scheme. The protocol completely solves the new member joining problem in a group communication

environment without resorting to any trusted third party, and requiring no exchange of random information among players. The proof of security of the new-member-joining protocol is provided in terms of correctness and secrecy.

References

1. Canetti, R., Gennaro, R., Jarecki, S., Krawczyk, H., Rabin, T.: Adaptive security for threshold cryptosystems. In: Wiener, M. (ed.) CRYPTO 1999. LNCS, vol. 1666, pp. 98–115. Springer, Heidelberg (1999)
2. Desmedt, Y.G., Frankel, Y.: Threshold cryptosystems. In: Brassard, G. (ed.) CRYPTO 1989. LNCS, vol. 435, pp. 307–315. Springer, Heidelberg (1990)
3. Pedersen, T.P.: A threshold cryptosystem without a trusted party. In: Davies, D.W. (ed.) EUROCRYPT 1991. LNCS, vol. 547, pp. 522–526. Springer, Heidelberg (1991)
4. Gennaro, R., Jarecki, S., Krawczyk, H., Rabin, T.: Secure distributed key generation for discrete-log based cryptosystems. In: Stern, J. (ed.) EUROCRYPT 1999. LNCS, vol. 1592, pp. 295–310. Springer, Heidelberg (1999)
5. Wu, Q., et al.: On A Practical Distributed Key Generation Scheme Based on Bivariate Polynomials. In: WiCom 2011, pp. 338–342 (2011)
6. Narasimha, M., et al.: On the Utility of Distributed Cryptography in P2P and MANETs: The Case of Membership Control. In: IEEE International Conference on Network Protocols, pp. 336–345 (2003)
7. Saxena, N., et al.: Efficient Node Admission for Short lived Mobile Ad Hoc Networks. In: IEEE International Conference on Network Protocols (2005)
8. Deng, H., et al.: Threshold and identity-based key management and authentication for wireless Ad Hoc networks. In: International Conference on Information Technology: Coding and Computing (ITCC 804), vol. 1, pp. 107–115 (2004)
9. Stinson., D.R., et al.: An application of covering designs: determining the maximum consistent set of shares in a threshold scheme. Ars Comb 53 (1999)
10. Berlekamp, et al.: Error correction of algebraic block codes. US Patent 4,633,470 (2006)
11. Kong, J., et al.: Providing robust and ubiquitous security support for MANET. In: IEEE ICNP (2001)

Dynamic Model and Sliding Adaptive Control of a Chinese Medicine Sugar Precipitation Process

Qingwei Li[1] and Hongjun Duan[2]

[1] School of Resources and Materials, Northeastern University at Qinhuangdao, Qinhuangdao, China
lqwday@126.com
[2] School of Control and Engineering, Northeastern University at Qinhuangdao, Qinhuangdao, China
dhj@mail.neuq.edu.cn

Abstract. A model dedicated to Chinese medicine sugar precipitation was designed, without consideration of crystal size distribution. Sliding mode adaptive control algorithm was proposed for the uncertain nonlinear systems based on Lyapunov's stability theory. The system was divided into nominal model and lumped disturbance term which embodies model mismatch, parameter uncertainties, and disturbances. Adaptive control was adopted to approach the uncertain input coefficients of system, robust control was introduced to reduce the lumped disturbance to a small bound in finite time, and sliding mode control was adopted to eliminate the tracking errors of the uncertain nonlinear system ultimately. The scheme is robust for the uncertainties and overcomes the chattering in the input of sliding mode control. It was applied to the precipitation control of sucrose-glucose mixed solution, and the validity of the proposed algorithm was supported by simulation results.

Keywords: batch processes, precipitation of mixed solution, nonlinearity, sliding mode adaptive, Chinese medicine.

1 Introduction

Precipitation is a unit operation for achieving the extraction of a solute from a saturated solution, which is widely developed in pharmaceutical, chemical and food industries. Due to the strong nonlinearity of this process, its monitoring and control remain an interesting challenge in terms of quality and global efficiency improvement. Commonly, growth and nucleation kinetics are represented in terms of the supersaturation, i.e. the difference between the solution and the saturation concentrations. The state of supersaturation can be reached by mean of cooling, evaporation or use of a solvent.Due to widespread applications of precipitation process, optimal operation and efficient on-line control strategy of the precipitation process are necessary in order to enhance their performance in terms of product quality and energy usage [1]. On-line control during batch precipitation offers the possibilities for improved crystal product quality, shorter process times, and reduction

D. Liu et al. (Eds.): BICS 2013, LNAI 7888, pp. 395–405, 2013.

or elimination of compromised batches [2]. Precipitation of mixed solution is a batch process. Batch process is usually related with the formulation of a control problem in terms of economic or performance objective at the end of the process [3]. Despite the long history and widespread application of batch process, there remains a number of problems associated with its control, mainly related the complex nonlinear dynamics with nonideal mixing, and various disturbances characteristic to these systems [4]. In recent years, there has been a growing interest in the optimization control of batch processes, which are suitable for responsive manufacturing of low volume and high value-added products [5-6]. However, it is usually very difficult to obtain the accurate models due to the complexity of the processes, and it is also difficult to implement them for on-line optimization since optimization based on mechanistic models is usually very time-consuming [7]. The repetitive nature of batch process operations allows that the information of previous batch runs can be used to improve the operation of the next batch. The current PID control strategy has proved to be inadequate regarding the strong nonlinearities of the crystallization process. This statement of fact leads to the proposition of alternative controlled variable and a more suitable control algorithm to improve the process control and the global process efficiency. Of late, the relative algorithms are mainly iterative learning control (ILC) [8-10] and nonlinear model-based predictive control (NMPC) [11-12]. However, the batch numbers of some industry processes are restricted, in other words, the cycle of each batch process is very long, and so the above-mentioned algorithms are inapplicable. For example, it claims almost seven days for one batch Chinese medicine produce. The content of effective components is discrepant for the medicinal materials from different producing areas. These come into being tremendous challenge for the steady productions of different batch processes.

Due to robustness properties against uncertainty, sliding mode control (SMC) has become very popular and enjoys a wide variety of application areas [13-14]. A new output feedback, variable structure-like tracking controller for a general class of nonlinear, MIMO (multi-input multi-output), mechanical systems whose uncertain dynamics are first-order differentiable [15-16]. However, there generally exists model mismatch between batch processes, and serious model mismatch decreases the control precision inevitably. In this paper, the designed method of sliding mode adaptive controller was studied for a class of nonlinear systems. The uncertain parameters are approached in real time by adaptive control, the disturbance and unmodeled dynamics are reduced by robust control to a tiny bound in finite time, and the tracking error of the uncertain nonlinear system is ultimately eliminated by sliding mode control. The chattering in the control process is overcome. The sliding mode adaptive controller is simulated for the precipitation control of sucrose-glucose mixed solution. The sugars are precipitated according to their respective crystal rates, and sucrose and glucose track their respective concentration setpoints in real time.

2 Process Modeling

A model dedicated to precipitation monitoring and control of Chinese medicine is developed. The most widely approaches investigated to describe sugars extraction

take into account four physical--chemical phenomena: nucleation, agglomeration, growth and dissolution. These investigations lead to the development of models of high purity liquors [19]. Little information is available about the stage where multiple sugars could be co-precipitated. There, low grade Chinese medicine crude solutions (impure solutions) contain a high proportion of impurities, which considerably changes their properties. It makes it difficult to adapt the models in all the process. To overcome this difficulty, the most usual approach consists of considering nucleation, agglomeration and dissolution negligible during the growth phase, in supersaturated conditions [20]. In other words, crystal growth phenomena are assumed to be preponderant. The precipitation step of Chinese medicine sugar is performed through a crystallizer, operating by a continuously agitator, as illustrated in Fig.1. The portal (a) provides access to the crystallizer internals. The crystallizer widens at the lower section (b) to accommodate the crystallizer jacket, to which coolant (e) and heating fluid (h) lines are connected. Mixing is achieved using an impeller driven from below (c). The process feed enters from above (f) and exits below (d). The temperature sensor is inserted from above (g).

Fig. 1. Crystallizer of Chinese medicine

The dynamic model proposed in this paper represents the mass balance for dissolved sucrose and glucose (m_s and m_g), crystals (m_{sc} and m_{gc}), sodium hydroxide solution (m_{sh}) and impurities (m_i). The phase changing from dissolved to crystallized sugar is expressed by a simple and nonreversible conversion. Thus, the evolution of mass of crystals is governed by the following expression:

$$\begin{cases} \dot{m}_{sc} = \alpha m_s \\ \dot{m}_{gc} = \beta m_g \end{cases} \tag{1}$$

where α and β are adjusted crystal parameters of sucrose and glucose respectively.

The evolution of dissolved sucrose and glucose results from the sucrose and glucose contained in the liquor supply, which depends on the mass fraction of dry

substance and on the purity of the solution, and from the disappearance of sucrose and glucose converted into crystals, according to Eq. (1):

$$\begin{cases} \dot{m}_{\mathrm{s}} = \rho_{\mathrm{f}} F_{\mathrm{f}} Bx_{\mathrm{fs}} Pte_{\mathrm{fs}} - \dot{m}_{\mathrm{sc}} \\ \dot{m}_{\mathrm{g}} = \rho_{\mathrm{f}} F_{\mathrm{f}} Bx_{\mathrm{fg}} Pte_{\mathrm{fg}} - \dot{m}_{\mathrm{gc}} \end{cases} \tag{2}$$

where ρ_{f} and F_{f} are the density[kg/m^3] and flow rate[m^3/s] of the feed syrup respectively, Bx_{fs} and Pte_{fs} are the mass fractions of sucrose and its dry substance respectively, Bx_{fg} and Pte_{fg} are the mass fractions of glucose and its dry substance respectively.The mass balance applied to the sodium hydroxide solution in the crystallizer leads to the following equation:

$$\dot{m}_{\mathrm{sh}} = \rho_{\mathrm{f}} F_{\mathrm{f}} \left(1 - Bx_{\mathrm{fs}} - Bx_{\mathrm{fg}}\right) + \rho_{\mathrm{sh}} F_{\mathrm{sh}} - \dot{m}_{\mathrm{vap}} \tag{3}$$

where ρ_{sh} and F_{sh} are the density[kg/m^3] and flow rate[m^3/s] of the sodium hydroxide solution respectively, m_{vap} is the emitted vapor mass[kg].The mass of impurities contained in solution is obtained using the following expression:

$$\begin{cases} \dot{m}_{\mathrm{i}} = \rho_{\mathrm{f}} F_{\mathrm{f}} \left(Bx_{\mathrm{fs}} + Bx_{\mathrm{fg}}\right)\left(1 - Pte_{\mathrm{fs}} - Pte_{\mathrm{fg}}\right) \\ m_{\mathrm{i}}(t) = m_{\mathrm{i}}(0) + \rho_{\mathrm{f}} F_{\mathrm{f}} \left(Bx_{\mathrm{fs}} + Bx_{\mathrm{fg}}\right)\left(1 - Pte_{\mathrm{fs}} - Pte_{\mathrm{fg}}\right) t \end{cases} \tag{4}$$

The initial value $m_{\mathrm{i}}(0)$ is obtained using the initial conditions. An energy balance applied to the magma in the crystallizer allows to express the mass of emitted vapor:

$$\dot{H}_{\mathrm{mg}} = \dot{Q} + \rho_{\mathrm{f}} F_{\mathrm{f}} h_{\mathrm{f}} + \rho_{\mathrm{sh}} F_{\mathrm{sh}} h_{\mathrm{sh}} + \lambda_{\mathrm{sc}} \dot{m}_{\mathrm{sc}} + \lambda_{\mathrm{gc}} \dot{m}_{\mathrm{gc}} - h_{\mathrm{vap}} \dot{m}_{\mathrm{vap}} \tag{5}$$

where H_{mg} is the enthalpy of the magma[J], $\dot{Q}$ is the heating power[W], h_{f} , h_{sh} ,and h_{vap} are the specific enthalpy of feed syrup, sodium hydroxide solution, and emitted vapor respectively[J/kg], λ_{sc} and λ_{gc} are the specific latent heat of sucrose and glucose respectively[J/kg].

The enthalpy variation of the magma can be written as follows:

$$\begin{cases} H_{\mathrm{mg}} = Cp_{\mathrm{mg}} m_{\mathrm{mg}} T_{\mathrm{mg}} \\ m_{\mathrm{mg}} = m_{\mathrm{s}} + m_{\mathrm{g}} + m_{\mathrm{sc}} + m_{\mathrm{gc}} + m_{\mathrm{sh}} + m_{\mathrm{i}} \end{cases} \tag{6}$$

$$\dot{H}_{\mathrm{mg}} = Cp_{\mathrm{mg}} m_{\mathrm{mg}} \dot{T}_{\mathrm{mg}} + Cp_{\mathrm{mg}} T_{\mathrm{mg}} \dot{m}_{\mathrm{mg}} \tag{7}$$

where, Cp_{mg} , m_{mg} , T_{mg} are the specific heat capacity[J/(K·kg)], mass[kg], and temperature[℃] of the magma respectively. During the crystallization process, the

temperature of the magma is available. It has been observed that its variation negligible compared to the mass variation. Consequently, it can be written:

$$\dot{H}_{\mathrm{mg}} \approx Cp_{\mathrm{mg}} T_{\mathrm{mg}} \dot{m}_{\mathrm{mg}} \tag{8}$$

From Eq.(5), the mass of vapor can be expressed as follows:

$$h_{\mathrm{vap}} \dot{m}_{\mathrm{vap}} = \dot{Q} + \rho_{\mathrm{f}} F_{\mathrm{f}} h_{\mathrm{f}} + \rho_{\mathrm{sh}} F_{\mathrm{sh}} h_{\mathrm{sh}} + \lambda_{\mathrm{sc}} \dot{m}_{\mathrm{sc}} + \lambda_{\mathrm{gc}} \dot{m}_{\mathrm{gc}} - Cp_{\mathrm{mg}} T_{\mathrm{mg}} \dot{m}_{\mathrm{mg}} \tag{9}$$

Substitute the expressions (1-4) into Eq.(9), it comes:

$$\begin{aligned} \left(h_{\mathrm{vap}} - Cp_{\mathrm{mg}} T_{\mathrm{mg}}\right) \dot{m}_{\mathrm{vap}} &= \dot{Q} + \rho_{\mathrm{f}} F_{\mathrm{f}} \left(h_{\mathrm{f}} - Cp_{\mathrm{mg}} T_{\mathrm{mg}}\right) \\ &+ \rho_{\mathrm{sh}} F_{\mathrm{sh}} \left(h_{\mathrm{sh}} - Cp_{\mathrm{mg}} T_{\mathrm{mg}}\right) + \alpha \lambda_{\mathrm{sc}} m_{\mathrm{s}} + \beta \lambda_{\mathrm{gc}} m_{\mathrm{g}} \end{aligned} \tag{10}$$

Let us denote:

$\boldsymbol{u} = \begin{bmatrix} u_1 & u_2 & u_3 \end{bmatrix}^{\mathrm{T}} = \begin{bmatrix} F_{\mathrm{f}} & F_{\mathrm{sh}} & \dot{Q} \end{bmatrix}^{\mathrm{T}}$ the input vector, $\boldsymbol{x} = \begin{bmatrix} x_1 & x_2 & x_3 \end{bmatrix}^{\mathrm{T}} = \begin{bmatrix} m_{\mathrm{s}} & m_{\mathrm{g}} & m_{\mathrm{sh}} \end{bmatrix}^{\mathrm{T}}$ the state vector. Considering model mismatch and unknown disturbance, from Eq.(1-3) and (10), the state space representation of the system is nonlinear and can be written as follows:

$$\begin{cases} \dot{\boldsymbol{x}} = \boldsymbol{f}\left(\boldsymbol{x}\right) + \boldsymbol{b}\left(\boldsymbol{x}\right)\boldsymbol{u} + \boldsymbol{d} \\ \boldsymbol{y} = \boldsymbol{x} \end{cases} \tag{11}$$

where

$$\boldsymbol{f}\left(\boldsymbol{x}\right) = \begin{bmatrix} -\alpha m_{\mathrm{s}} \\ -\beta m_{\mathrm{g}} \\ \dfrac{\alpha \lambda_{\mathrm{sc}} m_{\mathrm{s}} + \beta \lambda_{\mathrm{gc}} m_{\mathrm{g}}}{\vartheta} \end{bmatrix}; \quad \boldsymbol{b}\left(\boldsymbol{x}\right) = \begin{bmatrix} \rho_{\mathrm{f}} Bx_{\mathrm{fs}} Pte_{\mathrm{fs}} & 0 & 0 \\ \rho_{\mathrm{f}} Bx_{\mathrm{fg}} Pte_{\mathrm{fg}} & 0 & 0 \\ \rho_{\mathrm{f}} \left(\dfrac{h_1}{\vartheta} - Bx_{\mathrm{fs}} - Bx_{\mathrm{fg}}\right) & \rho_{\mathrm{sh}} \dfrac{h_2}{\vartheta} & -\dfrac{1}{\vartheta} \end{bmatrix};$$

$\vartheta = h_{\mathrm{vap}} - Cp_{\mathrm{mg}} T_{\mathrm{mg}}$, $h_1 = h_{\mathrm{vap}} - h_{\mathrm{f}}$, $h_2 = h_{\mathrm{vap}} - h_{\mathrm{sh}}$; $\boldsymbol{d}$ is the uncertain vector under model mismatch or disturbance vector.

3 Design of Sliding Mode Adaptive Controller

Extending system (11) into *n*th-order nonlinear systems as follows:

$$\begin{cases} \boldsymbol{x}^{(n)} = \boldsymbol{f}\left(\boldsymbol{x}, \dot{\boldsymbol{x}}, \cdots, \boldsymbol{x}^{(n-1)}\right) + \boldsymbol{b}\left(\boldsymbol{x}\right)\boldsymbol{u} + \boldsymbol{g} \\ \boldsymbol{y} = \boldsymbol{x} \end{cases} \tag{12}$$

The objective is to enable the output $\boldsymbol{y}$ to follow a desired trajectory $\boldsymbol{y}_{\mathrm{d}}$.

There exists a known positive constant η, such that $\left\|\boldsymbol{g}(\boldsymbol{x}, \dot{\boldsymbol{x}}, \cdots, \boldsymbol{x}^{(n-1)})\right\| \leq \eta$, $\forall \boldsymbol{x} \in R^{\mathrm{m}}$. $\|\cdot\|$ denotes the standard Euclidean norm.

Define the error vectors $\boldsymbol{e} \in R^{mn}$ and a sliding vector $\boldsymbol{s} \in R^{m}$ as follows:

$$\boldsymbol{e} := \left[\boldsymbol{x} - \boldsymbol{x}_{\mathrm{d}}, \dot{\boldsymbol{x}} - \dot{\boldsymbol{x}}_{\mathrm{d}}, \cdots, \boldsymbol{x}^{(n-1)} - \boldsymbol{x}_{\mathrm{d}}^{(n-1)}\right]^{\mathrm{T}} = \left[\boldsymbol{e}_1, \boldsymbol{e}_2, \cdots, \boldsymbol{e}_n\right]^{\mathrm{T}} \tag{13}$$

$$\boldsymbol{s} := \boldsymbol{e}_n + \lambda_{n-1}\boldsymbol{e}_{n-1} + \cdots + \lambda_1 \boldsymbol{e}_1 + \lambda_0 \int_0^t \boldsymbol{e}_1 \mathrm{d}\tau = \boldsymbol{e}_n + \sum_{i=1}^{n-1} \lambda_i \boldsymbol{e}_i + \lambda_0 \int_0^t \boldsymbol{e}_1 \mathrm{d}\tau \tag{14}$$

where, $\boldsymbol{x}_{\mathrm{d}}$ is the desired trajectory of $\boldsymbol{x}$; $\boldsymbol{e}_1 = \left[x_1 - x_{1\mathrm{d}}, x_2 - x_{2\mathrm{d}}, \cdots, x_m - x_{m\mathrm{d}}\right]^{\mathrm{T}}$ $= \left[e_1, e_2, \cdots, e_m\right]^{\mathrm{T}}$, $\boldsymbol{e}_2 = \left[\dot{e}_1, \dot{e}_2, \cdots, \dot{e}_m\right]^{\mathrm{T}}$, $\cdots$, $\boldsymbol{e}_n = \left[e_1^{(n-1)}, e_2^{(n-1)}, \cdots, e_m^{(n-1)}\right]^{\mathrm{T}}$; $\lambda_i > 0$.

Again define quantity $\boldsymbol{\delta} \in R^{m}$ as follows:

$$\boldsymbol{\delta} = \boldsymbol{x}_{\mathrm{d}}^{(n)} - \left(\lambda_{n-1}\boldsymbol{e}_n + \lambda_{n-2}\boldsymbol{e}_{n-1} + \cdots + \lambda_1 \boldsymbol{e}_2 + \lambda_0 \boldsymbol{e}_1\right) = \boldsymbol{x}_{\mathrm{d}}^{(n)} - \sum_{i=0}^{n-1} \lambda_i \boldsymbol{e}_{i+1} \tag{15}$$

Substitute (15) and (12) into the derivative of $\boldsymbol{s}$ in (14), and we obtain

$$\dot{\boldsymbol{s}} = \dot{\boldsymbol{e}}_n + \lambda_{n-1}\boldsymbol{e}_n + \cdots + \lambda_1 \boldsymbol{e}_2 + \lambda_0 \boldsymbol{e}_1 = \boldsymbol{x}^{(n)} - \boldsymbol{\delta} = \boldsymbol{f} + \boldsymbol{g} + \boldsymbol{b}\boldsymbol{u} - \boldsymbol{\delta} \tag{16}$$

The following sliding qualification must be attained

$$\frac{1}{2}\frac{\mathrm{d}\left(\boldsymbol{s}^{\mathrm{T}}\boldsymbol{s}\right)}{\mathrm{d}t} = \boldsymbol{s}^{\mathrm{T}}\dot{\boldsymbol{s}} < 0 \tag{17a}$$

s.t.

$$\boldsymbol{s}^{\mathrm{T}}\left(\boldsymbol{f} + \boldsymbol{g} + \boldsymbol{b}\boldsymbol{u} - \boldsymbol{\delta}\right) < 0 \tag{17b}$$

The control law of (12) can be designed as

$$\boldsymbol{u} = \boldsymbol{b}^{-1}(-\boldsymbol{f} - \overline{\boldsymbol{g}} + \boldsymbol{\delta} - \boldsymbol{k}\boldsymbol{s}) \tag{18}$$

where

$$\overline{\boldsymbol{g}} = \begin{cases} \eta \boldsymbol{s} / \|\boldsymbol{s}\|, & \|\boldsymbol{s}\| > \varepsilon \\ \eta \boldsymbol{s} / \varepsilon, & \|\boldsymbol{s}\| \leq \varepsilon \end{cases} \tag{19}$$

$\boldsymbol{k} = \mathrm{diag}\{k_1, k_2, \cdots, k_m\}$, $k_1, k_2, \cdots, k_m, \varepsilon$ are all positive constants.Transfer (18) into the form as follows:

$$\boldsymbol{u} = \frac{\boldsymbol{s}^{\mathrm{T}}}{\boldsymbol{s}^{\mathrm{T}}\boldsymbol{b}\boldsymbol{s}}\left(-\boldsymbol{f} - \overline{\boldsymbol{g}} + \boldsymbol{\delta} - \boldsymbol{k}\boldsymbol{s}\right)\boldsymbol{s} = \frac{\boldsymbol{s}}{\boldsymbol{s}^{\mathrm{T}}\boldsymbol{b}\boldsymbol{s}}\left(-\boldsymbol{s}^{\mathrm{T}}\boldsymbol{f} - \boldsymbol{s}^{\mathrm{T}}\overline{\boldsymbol{g}} + \boldsymbol{s}^{\mathrm{T}}\boldsymbol{\delta} - \boldsymbol{s}^{\mathrm{T}}\boldsymbol{k}\boldsymbol{s}\right) \tag{20}$$

Defin $\underline{\boldsymbol{x}} = \left[\boldsymbol{x}, \boldsymbol{x}_{\mathrm{d}}\right]^{\mathrm{T}}$, $\boldsymbol{s}_e = \boldsymbol{s} / \|\boldsymbol{s}\|$, $\beta(\underline{\boldsymbol{x}}) = \boldsymbol{s}_e^{\mathrm{T}}\boldsymbol{b}\left(\boldsymbol{x}\right)\boldsymbol{s}_e$, then

$$\boldsymbol{s}^{\mathrm{T}}\left(\underline{\boldsymbol{x}}\right)\boldsymbol{b}\left(\boldsymbol{x}\right)\boldsymbol{s}\left(\underline{\boldsymbol{x}}\right) = \boldsymbol{s}_e^{\mathrm{T}}\left(\underline{\boldsymbol{x}}\right)\boldsymbol{b}\left(\boldsymbol{x}\right)\boldsymbol{s}_e\left(\underline{\boldsymbol{x}}\right)\left\|\boldsymbol{s}\left(\underline{\boldsymbol{x}}\right)\right\|^2 = \beta\left(\underline{\boldsymbol{x}}\right)\left\|\boldsymbol{s}\left(\underline{\boldsymbol{x}}\right)\right\|^2 \tag{21}$$

Substitute (21) into (20), we obtain

$$\boldsymbol{u} = \frac{\boldsymbol{s}_e}{\beta}\left(-\boldsymbol{s}_e^{\mathrm{T}}\boldsymbol{f} - \boldsymbol{s}_e^{\mathrm{T}}\overline{\boldsymbol{g}} + \boldsymbol{s}_e^{\mathrm{T}}\boldsymbol{\delta} - \boldsymbol{s}_e^{\mathrm{T}}\boldsymbol{k}\boldsymbol{s}\right) \tag{22}$$

Let $\overline{\beta}$ be the evaluation of β, and of which optimal approach β^* is

$$\beta^* = \arg\min_{\overline{\beta}}\left(\sup_{\underline{\boldsymbol{x}} \in X}\left|\beta(\underline{\boldsymbol{x}}) - \overline{\beta}\right|\right) \tag{23}$$

where, $X \subseteq R^m$ is a region in which the state $\boldsymbol{x}$ and $\boldsymbol{x}_{\mathrm{d}}$ are constrained to reside.

Define the adaptive parameter error of β

$$\phi_\beta = \beta^* - \beta \tag{24}$$

The adaptive law can be gotten

$$\dot{\phi}_\beta\left(t\right) = -\dot{\beta}\left(t\right) = -\frac{\mu}{\beta^*}\boldsymbol{s}^{\mathrm{T}}\left(\boldsymbol{f} - \boldsymbol{\delta} + \boldsymbol{s}_e\eta\right) \tag{25}$$

where, μ is a positive constant which is adjustable.

According to the above analysis, we proposed the control law of system (12) as follows:

$$\boldsymbol{u} = \frac{\boldsymbol{s}_e}{\beta^*}\left(-\boldsymbol{s}_e^{\mathrm{T}}\boldsymbol{f} - \boldsymbol{s}_e^{\mathrm{T}}\overline{\boldsymbol{g}} + \boldsymbol{s}_e^{\mathrm{T}}\boldsymbol{\delta} - \boldsymbol{s}_e^{\mathrm{T}}\boldsymbol{k}\boldsymbol{s}\right) \tag{26}$$

Theorem 1: Given the uncertain nonlinear MIMO system (12), if the following condition is satisfied

$$\boldsymbol{s}_e^{\mathrm{T}}\boldsymbol{k}\boldsymbol{s}_e > \left(1/\|\boldsymbol{s}\| - 1/\varepsilon\right)\eta \tag{27}$$

Then the system is asymptotically stable under the controller (26) with the adaptive laws (25). Moreover, $\boldsymbol{s}, \boldsymbol{e}_1, \boldsymbol{e}_2, \cdots, \boldsymbol{e}_n \to \boldsymbol{0}$, $\beta^* \to \beta$, $\bar{\eta} \to \eta$ as $t \to \infty$.

Proof: Define a positive Lyapunov function by

$$V(\boldsymbol{s}) = \frac{1}{2}\boldsymbol{s}^{\mathrm{T}}\boldsymbol{s} + \frac{1}{2\mu}\phi_\beta^2 \tag{28}$$

Substitute (16) into the derivative of (28), we obtain

$$\dot{V}(\boldsymbol{s}) = \boldsymbol{s}^{\mathrm{T}}\dot{\boldsymbol{s}} + \frac{1}{\mu}\phi_\beta\dot{\phi}_\beta = \left(\boldsymbol{s}^{\mathrm{T}}\boldsymbol{f} - \boldsymbol{s}^{\mathrm{T}}\boldsymbol{\delta} + \boldsymbol{s}^{\mathrm{T}}\boldsymbol{g}\right) + \boldsymbol{s}^{\mathrm{T}}\boldsymbol{b}\boldsymbol{u} + \frac{1}{\mu}\phi_\beta\dot{\phi}_\beta \tag{29}$$

After Substituting (26) and (21) into the second item on the right-hand side of (29), we have

$$\boldsymbol{s}^{\mathrm{T}}\boldsymbol{b}\boldsymbol{u} = \frac{\boldsymbol{s}^{\mathrm{T}}\boldsymbol{b}\boldsymbol{s}_e}{\beta^*}\left(-\boldsymbol{s}_e^{\mathrm{T}}\boldsymbol{f} - \boldsymbol{s}_e^{\mathrm{T}}\bar{\boldsymbol{g}} + \boldsymbol{s}_e^{\mathrm{T}}\boldsymbol{\delta} - \boldsymbol{s}_e^{\mathrm{T}}\boldsymbol{k}\boldsymbol{s}\right)$$

$$= \frac{\beta\|\boldsymbol{s}\|}{\beta^*}\left(-\boldsymbol{s}_e^{\mathrm{T}}\boldsymbol{f} - \boldsymbol{s}_e^{\mathrm{T}}\bar{\boldsymbol{g}} + \boldsymbol{s}_e^{\mathrm{T}}\boldsymbol{\delta} - \boldsymbol{s}_e^{\mathrm{T}}\boldsymbol{k}\boldsymbol{s}\right) = \frac{\beta}{\beta^*}\left(-\boldsymbol{s}^{\mathrm{T}}\boldsymbol{f} + \boldsymbol{s}^{\mathrm{T}}\boldsymbol{\delta} - \boldsymbol{s}^{\mathrm{T}}\bar{\boldsymbol{g}} - \boldsymbol{s}^{\mathrm{T}}\boldsymbol{k}\boldsymbol{s}\right) \tag{30}$$

Substitute (30), (25), and (24) into (29), we obtain

$$\begin{aligned}\dot{V}(\boldsymbol{s}) &= \frac{\phi_\beta}{\beta^*}\boldsymbol{s}^{\mathrm{T}}\boldsymbol{g} + \frac{\beta}{\beta^*}\boldsymbol{s}^{\mathrm{T}}\left(\boldsymbol{g} - \bar{\boldsymbol{g}}\right) - \frac{\beta}{\beta^*}\boldsymbol{s}^{\mathrm{T}}\boldsymbol{k}\boldsymbol{s} - \frac{1}{\beta^*}\phi_\beta\|\boldsymbol{s}\|\eta \\ &\le \frac{\phi_\beta}{\beta^*}\|\boldsymbol{s}\|\eta + \frac{\beta}{\beta^*}\left(\|\boldsymbol{s}\|\eta - \boldsymbol{s}^{\mathrm{T}}\bar{\boldsymbol{g}}\right) - \frac{\beta}{\beta^*}\boldsymbol{s}^{\mathrm{T}}\boldsymbol{k}\boldsymbol{s} - \frac{\phi_\beta}{\beta^*}\|\boldsymbol{s}\|\eta \\ &= \frac{\beta}{\beta^*}\left(\left(\|\boldsymbol{s}\|\eta - \boldsymbol{s}^{\mathrm{T}}\bar{\boldsymbol{g}}\right) - \boldsymbol{s}^{\mathrm{T}}\boldsymbol{k}\boldsymbol{s}\right)\end{aligned} \tag{31}$$

Substitute (19) into (31) with $\|\boldsymbol{s}\| > \varepsilon$, it comes:

$$\dot{V}(\boldsymbol{s}) \le \frac{\beta}{\beta^*}\left(\left(\|\boldsymbol{s}\|\eta - \boldsymbol{s}^{\mathrm{T}}\frac{\boldsymbol{s}}{\|\boldsymbol{s}\|}\eta\right) - \boldsymbol{s}^{\mathrm{T}}\boldsymbol{k}\boldsymbol{s}\right) = -\frac{\beta}{\beta^*}\boldsymbol{s}^{\mathrm{T}}\boldsymbol{k}\boldsymbol{s} < 0 \tag{32}$$

Substitute (19) and (27) into (31), then

$$\dot{V}(\boldsymbol{s}) \le \frac{\beta}{\beta^*}\left(\left(\|\boldsymbol{s}\|\eta - \boldsymbol{s}^{\mathrm{T}}\frac{\boldsymbol{s}}{\varepsilon}\eta\right) - \boldsymbol{s}^{\mathrm{T}}\boldsymbol{k}\boldsymbol{s}\right)$$

$$= \frac{\beta}{\beta^*}\|\boldsymbol{s}\|^2\left(\left(\frac{1}{\|\boldsymbol{s}\|}-\frac{1}{\varepsilon}\right)\eta - \boldsymbol{s}_e^{\mathrm{T}}\boldsymbol{k}\boldsymbol{s}_e\right) \leq 0 \tag{33}$$

The equal sign comes into existence only when $\|\boldsymbol{s}\| = 0$, it indicates that $\lim_{t\to\infty}\boldsymbol{s} \to \boldsymbol{0}, \lim_{t\to\infty}\boldsymbol{e}_i = \boldsymbol{0}$ ($i = 1, 2, \cdots, n$). So the system is asymptotically stable. From (28), we know that $\lim_{t\to\infty}\phi_\beta \to 0$, i.e. $\lim_{t\to\infty}\beta^* \to \beta$.

4 Precipitation Control Simulation of Mixed Solution

The precipitation performance of the process can be increased by improving the crystal rate. This growth rate can be apprehended by following the crystal mass. In mixed solution, we set sucrose crystal mass and glucose crystal mass in different time, respectively, and they are tracked by the proposed control algorithm. Beyond this setpoint tracking, a second control objective is required, and consists in maintaining the solution in an appropriate supersaturated state, that is a metastable zone, as illustrated in Fig.2 and Fig.3. Solubility curves are denoted by solidlines, and nucleation curves are denoted by dotted lines.

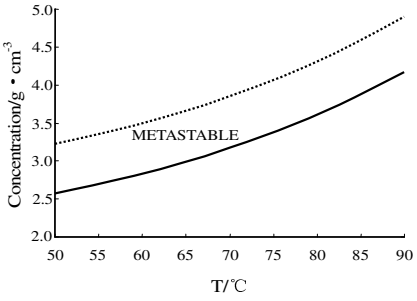

Fig. 2. Concentration trajectory of sucrose

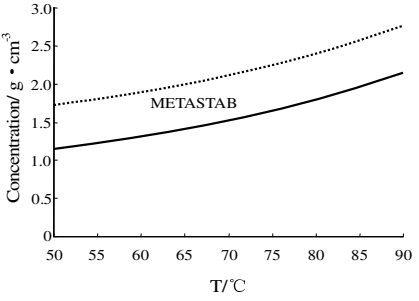

Fig. 3. Concentration trajectory of glucose

The controller parameters are as follows:

$\boldsymbol{k} = \mathrm{diag}\{0.6, 0.5, 0.4\}$, $\boldsymbol{g} = [5\cos t, 3\cos t, 2\cos t]^{\mathrm{T}}$, $\lambda = 2$, $\mu = 1$, $\eta = 8$, $\varepsilon = 2$, $\overline{\beta} = 1$ (the initial value of β).

The precipitation tracking curves of sucrose-glucose solution are illustrated in Fig.4, where M_{scd} , M_{sc} are the setpoints and tracking results of sucrose crystal masses; $M_{\mathrm{gcd}}, M_{\mathrm{gc}}$ are the setpoints and tracking results of glucose crystal masses. The concentration tracking curves of sucrose-glucose solution are illustrated in Fig.5, where C_{sd} , C_{s} are the setpoints and tracking results of sucrose concentration;

C_{gd} , C_g are the setpoints and tracking results of glucose concentration. From the simulation results in figure 4, we get to know that the crystal masses of sucrose-glucose track their respective setpoints commendably. From the simulation results in figure 5, we get to know that the concentrations of sucrose-glucose track their respective setpoints commendably.

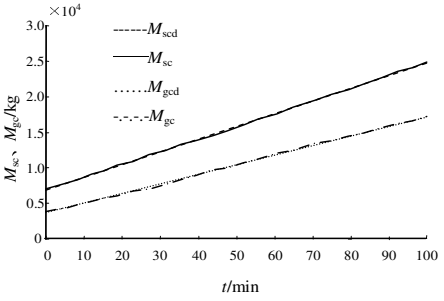

Fig. 4. Precipitation tracking curves

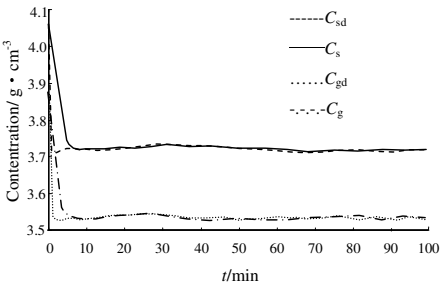

Fig. 5. Concentration tracking curves

5 Conclusion

In this paper, the objective was to develop a new control strategy of Chinese medicine sugar precipitation process, based, on the first hand, on a real-time control of the crystal mass evolution, and on the other hand, on a control of the solution concentration to maintain the magma in supersaturation conditions. A sliding mode adaptive robust was designed for a class of uncertain nonlinear systems with unknown disturbance. The uncertain parameters are approached in real time by adaptive control, the unknown disturbances were reduced by robust control to a tiny bound in finite time, and the tracking error was ultimately eliminated by sliding mode control.

The quivering in the control process was overcome. The validity was supported by the co-precipitation simulations of sucrose-glucose mixed solution. This method can be implemented on multi-solutions. The global performance of the closed-loop precipitation process has been studied with different crystallization setpoints, in terms of energy efficiency.

References

1. Paengiuntuek, W., Kittisupakon, P., Arpornwichanop, A.: Optimization and Nonlinear Control of a Batch Crystallization Process. Journal of the Chinese Institute of Chemical Engineers 39, 249–256 (2008)
2. Nagy, Z.K., Chew, J.W., Fujiwara, M.: Comparative Performance of Concentration and Temperature Controlled Batch Crystallizations. Journal of Process Control 18, 399–407 (2008)
3. Georgieva, P., Azevedo, S.F.D.: Neural Network-based Control Strategies Applied to a Fed-batch Crystallization Process. International Journal of Information and Mathematical Sciences 33, 224–233 (2007)

4. Nagy, Z.K.: Model Based Robust Control Approach for Batch Crystallization Product Design. Computers and Chemical Engineering 33, 1685–1691 (2009)
5. Bonvin, D.: Optimal Operation of Batch Reactors: A Personal View. Journal of Process Control 8, 355–368 (1998)
6. Chen, Z.G., Xu, C., Shao, H.H.: Batch Processes Optimization and Advanced Control—A Survey. Control and Instruments in Chemical Industry 30, 1–6 (2003)
7. Xiong, Z.H., Zhang, J.: Neural Network Model-based On-line Re-optimization Control of Fed-batch Processes Using a Modified Iterative Dynamic Programming Algorithm. Chemical Engineering and Processing 44, 477–484 (2005)
8. Xiong, Z.H., Zhang, J., Dong, J.: Optimal Iterative Learning Control for Batch Processes Based on Linear Time-varying Perturbation Model. Chinese Journal of Chemical Engineering 16, 235–240 (2008)
9. Zhang, J., Nguyen, J., Xiong, Z.H.: Iterative Learning Control of Batch Processes Based on Time Varying Perturbation Models. Journal of Tsinghua University (Sci. & Tech.) 48(S2), 1771–1774 (2008)
10. Jia, L., Shi, J.P., Qiu, M.S.: Nonrestraint-iterative Learning-based Optimal Control for Batch Processes. CIESC Journal 61, 1889–1893 (2010)
11. Damour, C., Benne, M., Boillereaux, L.: NMPC of an Industrial Crystallization Process Using Model-based Observers. Journal of Industrial and Engineering Chemistry 16, 708–716 (2010)
12. Fan, L., Wang, H.Q., Song, Z.H.: Iterative Optimal Control for Batch Process Based on Generalized Predictive Control. Control and Instruments in Chemical Industry 33, 25–28 (2006)
13. Liu, Z.L., Svoboda, J.: A New Control Scheme for Nonlinear Systems with Disturbances. IEEE Transactions on Control Systems Technology 14, 176–181 (2006)
14. Xu, H.J., Maj, M.: Robust Adaptive Sliding Control for a Class of MIMO Nonlinear Systems. In: AIAA Guidance, Navigation and Control Conference and Exhibit, Montreal, Canada, pp. 1–10 (2001)
15. Pai, M.C.: Design of Adaptive Sliding Mode Controller for Robust Tracking and Model Following. Journal of Franklin Institute 347, 1837–1849 (2010)
16. Ansarifar, G.R., Talebi, H.A., Davilu, H.: An Adaptive-dynamic Sliding Mode Controller for Non-minimum Phase Systems. Commun Nonlinear Sci. Numer Simulat. 17, 414–425 (2012)
17. Damour, C., Benne, M., Boillereaux, L.: Multivariable Linearizing Control of An Industrial Sugar Crystallization Process. Journal of Process Control 21, 46–54 (2011)
18. Wright, P.G., White, E.T.: A Mathematical Model of Vacuum Pan Crystallization. In: Proceedings of ISSCT 15th Congress, pp. 1546–1560 (1974)
19. Barth, S.: Utilization of FBRM in the Control of CSD in a Batch Cooled Crystallizer. Ph.D. Thesis, Georgia Institute of Technology (2006)
20. Damour, C., Benne, M., Boillereaux, L.: Multivariable Linearizing Control of an Industrial Sugar Crystallization Process. Journal of Process Control 21, 46–54 (2011)
21. Larsen, P.A., Patience, D.B., Rawlings, J.B.: Industrial Crystallization Process Control. IEEE Control System Magazine, 70–80 (2006)
22. Mesbah, A., Landlust, J., Huesman, A.E.M.: A Model-based Control Framework for Industrial Batch Crystallization Processes. Chemical Engineering Research and Design 88, 1223–1233 (2010)
23. Damour, C., Benne, M., Grondin-Perez, B.: Nonlinear Predictive Control Based on Artificial Neural Network Model for Industrial Crystallization. Journal of Food Engineering 99, 225–231 (2010)

Establishment of Tourism Geographic Information System to Promote Field Work in Tourism Management Major

Yan Liu

Lanzhou University of Finance and Economics
College of Business Administration
GanSu Province, China
liuyan4580@126.com

Abstract. As an applied discipline, tourism undergraduate education will be improved in practice teaching. With design for the tourism geographic information system, all students will participate in investigation, design, data collection, maintenance and management of the information system, which can undoubtedly improve employability of the students. In particular, in organization of data for the tourism information system, the participants will obtain comprehensive knowledge about tourism resources in the region to establish a complete database. As an applied discipline, tourism undergraduate education will be improved in practice teaching. With design for the tourism geographic information system, all students will participate in investigation, design, data collection, maintenance and management of the information system, which can undoubtedly improve employability of the students. In particular, in organization of data for the tourism information system, the participants will obtain comprehensive knowledge about tourism resources in the region to establish a complete database.

Keywords: Tourism GIS, software system, Expandability, tourism service.

1 Introduction

In recent years, increasing imbalance between supply and demand in the tourism talent market in China has been witness. On the one hand, tourism enterprising are imposing higher requirements on knowledge, ability and quality of such talents, while on the other hand, undergraduate in tourism have insufficient theoretical knowledge and ability of practice. Therefore, in the situation with a substantial shortage in high-level talents in the current tourism market, employment of tourism undergraduates is not optimistic. As an applied discipline, tourism undergraduate education must attach great importance to development of the students' comprehensive ability of practice while providing them with specialized theoretical proficiency. During development of the ability of practice, the experiment course will be a key part, which can develop the students in their tourism skills and ability in application of specialized theory. The experiment base will be required to provide an environment reaching or close to real

D. Liu et al. (Eds.): BICS 2013, LNAI 7888, pp. 406–415, 2013.

professional tourism activities, so construction of an experiment base can be improved with IT means including network, multimedia and rituality. Such technology will not be restricted by instruments and materials in the laboratory, and comprehensive, designing, innovative and barrier experiments can be established with low consumption. Currently, e-commerce of tourism is flourishing, and with improvement in technology of geographic information system (GIS), tourism GIS will be established as an important part in experiment course in the school in order to provide the students with knowledge about e-commerce and tourism geography, thus improving their ability of practice[1]. Meanwhile, the establishment of a tourism GIS in the experiment base on the campus can not only reduce the traveling of teachers and students between the school and enterprises, but also improve efficiency in field work. First of all, a tourism GIS will be designed according to demand set by tourists.

2 Design of Tourism GIS

2.1 Demand Analysis and Design Objectives of the System

Demand analysis refers to detailed analysis on the problem to be settled in order to make clear requirements on the problem, including data to be entered, result to be obtained and final output. Demand analysis is the most important step in the design and development of the GIS, and it will be decisive. Only with demand analysis can overall concept of the function and performance of the system be described into detailed system demand specification in order to lay foundation for the development. During the process, the system analyst and software engineer will determine the demand from customers. In practice, it is impossible for the final software to satisfy demand from customers or to be completed within the specified time.

What the tourists are the most concerned about is the selection of the hotel and transport, etc. when going to the attraction,.

After extensive investigation, the tourism GIS must be equipped with the following functions:

- Management on tourism spatial database (data backup, updating and upgrading);
- Operation of basic functions of the map (zooming in, zooming out, roaming, etc);
- Query about information on tourism space;
- Query about multi-source information on the attraction (picture, sound, video, etc);
- Query about traffic information;
- Analysis of tourism space (analysis of traveling route, query about adjacent facilities);
- GPS Tracking and tracing;
- Map output and printing functions.

According to results system demand analysis, procedure of the whole system is shown in figure 2.1:

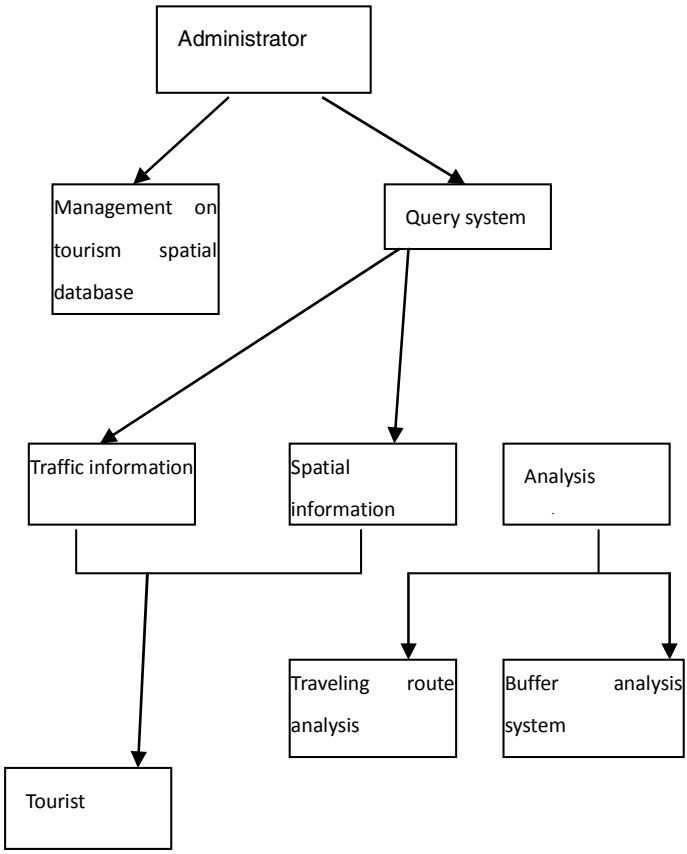

Fig. 1. System flowchart

In the system, the administrator will be responsible for maintenance of the system. Backup, updating and upgrading of the data in the system can be done in the tourism spatial database, and query about qualified tourism information can be made according to interests of the tourist in the query system so that the tourist can obtain knowledge about the interested attraction. Traffic information refers to the selection of traffic means including coaches, trains, planes according to actual needs of the tourist. Spatial information provides query about qualified information on tourism space according to interests of the tourist. With the analysis system, the tourist can make query with a combination of multiple restrictions by giving the target attraction. With analysis of the traveling route, comprehensive analysis of planning for the best route can be provided to the tourist by giving restrictions including the target attraction and cities to go by, etc. Tourists can make query about adjacent facilities by giving the target attraction with the buffer analysis system[3]. With GIS, tourists can finally obtain reference information for planning of the traveling route.

The design is for purpose of establishment of a tourism geographic information system, mainly providing tourists with attraction information for the destination, as well as supporting tourism information including traffic, shopping, hotel and

restaurant. Taking Gansu Province for instance, a multi-functional tourism GIS integrated with input, management and application will be achieved in order to provide uses with timely and accurate service to satisfy their demands and to provide basis for preparation of their traveling route and plan. With comprehensive consideration of required traveling information for tourists, the system is designed and developed to facilitate traveling of the tourists. Besides, it is also for training students majoring in tourism in their ability in background administration for the information system and collection of tourism information[2].

2.2 Principle for Design of the System

Design of the system is fundamentally decisive for the software system. A poor design of the system will produce a poor software system. Sticking to the idea of systematic engineering, the design will produce a scientific, rational and practical tourism GIS in Gansu Province. In the design and in future development, the following principles must be observed:

- Suitability

Suitability is the first indicator for assessment on the architecture, that is, whether the architecture is suitable for "functional demand" and "non-functional demand" of the software. Generally, software architecture will not be designated in the required document, and there is no one-to-one correspondence between the demand and the architecture, even no obvious correspondence. Therefore, the designer can give full play to the initiative, and according to characteristics of the demand, a suitable architecture will be designed with inference and induction. Designers lacking experience often focus on "functional demand" and neglect the "non-functional demand" which is exactly what reflects the design level.

- Structure stability

Architecture is the first element in design of the system, and work at the detailed design stage, including user interface design, database design, module design, data structure design, will all be carried out after determination of the architecture, and programming and test will come the last. Frequent change in the architecture will bring frequent change in the user interface, database, module and data structure built on the architecture, which will bring disorder in the project. Therefore, once design for the architecture is completed, it will maintain stable within a certain period for smooth implementation of subsequent work.

- Expandability

Expandability refers to the degree of ease for expansion of new functions of the software. With the developing commerce in society, there is a growing fast change in the demand, which will result in more and more important expandability. Change in demand will inevitably result in modification (or expansion) of functions of the software, and in case of software with poor expandability, costs for such modification (or expansion) will be very high. The software not expandable will lose possibility for development. Therefore, attention cannot be only paid to the stability, with the expandability neglected. A stable structure will be prerequisite for expandability of the

software system, or otherwise, it is impossible for development of the software as planned. Stability is the foundation for sustainable development of the system. To sum up, stability and expandability are both elements in the architecture design.

- Reusability Reusability refers to the reuse of something that already exists. It is the reflection of human wisdom, but not laziness, as the human beings make constant progress with utilization, improvement or innovation of results from their ancestors. Reusability will be obtained from design rather than chance encounter. To equip the architecture with good reusability, the designer design a universal architecture structure for reuse after analysis of common problems in the application domain.

2.3 System Architecture

With cores of basic space, attribute and multimedia tourism information and data including attractions, historical sites, natural sight, hotels, traffic route, etc, functional

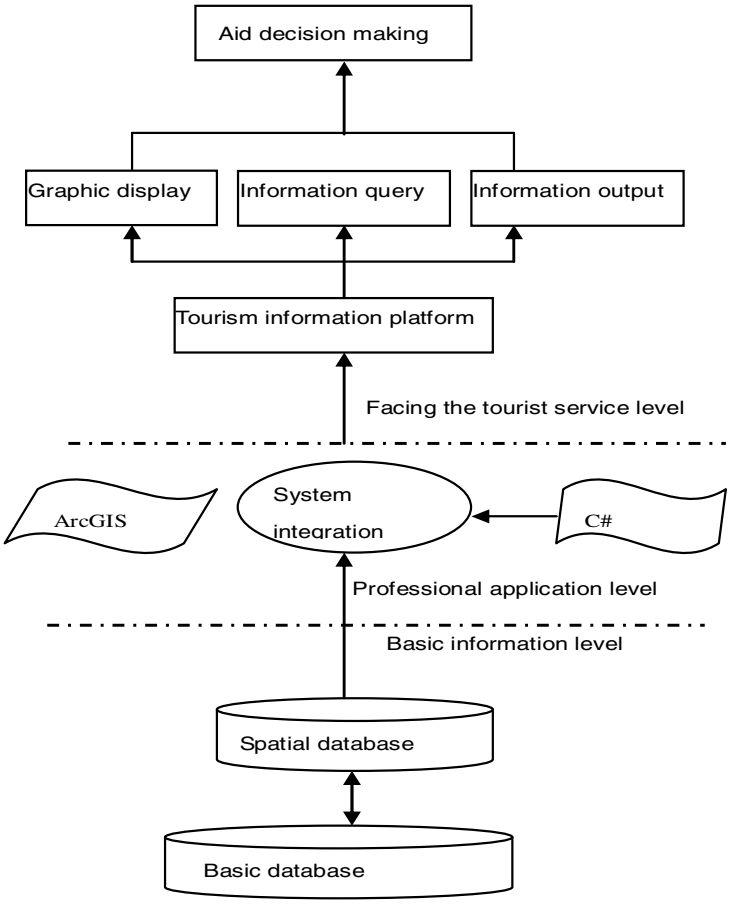

Fig. 2. Comprehensive information frame architecture

development of the system will be carried out according to matters related to satisfaction of tourists' demand, for purpose of providing tourists with reference proposal for traveling route and query about adjacent facilities so that the tourists can obtain more latest useful tourism information and more tourism service with high quality[4]. Figure 2 shows the system architecture:

2.4 System Function and Structure

Structure of functional modules in the system mainly includes management on tourism spatial database (data backup, updating and upgrading), operation of basic functions of the map (zooming in, zooming out, roaming, etc), query about information on tourism space, query about multi-source information on attractions (picture, sound, video, etc), query about traffic information, analysis of tourism space (analysis of traveling route, query about adjacent facilities), GPS tracking and tracing, map output and printing module group, etc. Figure 3. shows the functional structures in the system.

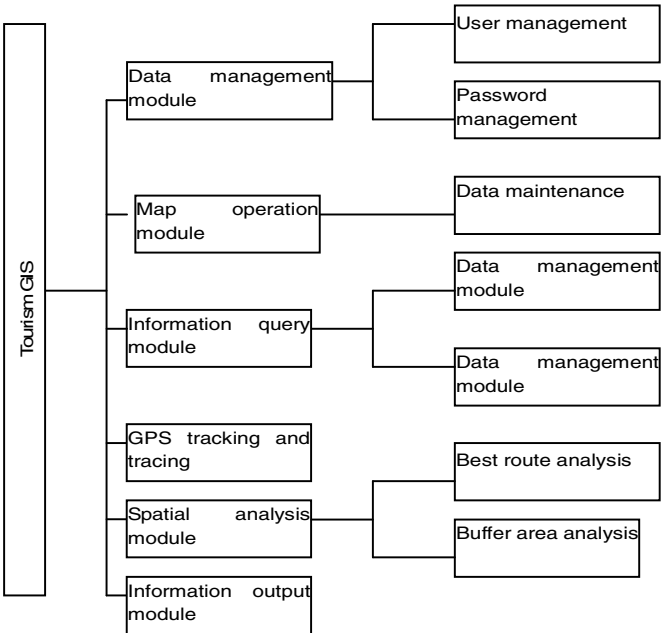

Fig. 3. System structure and function

2.5 Design for Functional Systems in the System

- Design of functions in the system must be targeted, that is, the design must be targeted towards the demand from users to satisfy users' demand to the greatest extent. According to the existing trend in development of software technology, a tourism GIS will be established by taking advantage of GIS technology, spatial database technology and data communication technology, etc in order to provide tourists with convenient service.

- Data management module,Data in data management module mainly include foregrounding maps, background attribute database and multimedia documents. Authorities for modification and updating of data will be provided to the system administrator, but not general users. With different authorities, users logging in to the system can carry out different operation on different modules, so individual users must be provided with certain authorities. Different users will see a different system after login, although it is in fact the same system, which further improves safety of the system by preventing users from modification of content beyond their authority.
- Map operation module,In the module, toolbars necessary for graphic browse and spatial attribute query and browse will be provided. The map operation module mainly includes map zooming, roaming, full-sized display, previous, next, click query about attribute, browse of spatial data, view refresh, distance measurement and navigation with eagle eye, etc.
- Information query module The information query module is mainly for query about information on spatial location with spatial attribute information, including query about information on attractions, hotel and cities, etc. All such information is involved with specific spatial location on the map, and with the query, specific location, relevant attribute information, pictures and video, etc can be displayed. Besides, query about coaches, trains and planes from Kunming to other major cities can also be made.
- Spatial analysis module, Spatial analysis module is a core in the system. Spatial analysis is a geographic data analysis technology for spatial arrangement based on geographic objects. It provide users with functions of multimedia query and analysis. Query about the best route can be achieved on the map, in which, with two attractions selected by the user, the system will carry out analysis and judgment of the shortest route according to road information on the map and a great amount of information saved in the database including length of roads so that it will help the user to select a desirable traveling route[5]. Besides, analysis of buffer area can be provided, such as attracts within 10km around the city, etc.

2.6 Design of System Database

Tourism data include spatial information and attribute information (information in text, photograph and video) on attractions, spatial information and attribute information on hotels and basic information related to tourism, such as spatial information with regard to roads, administrative regions, airports and railway station, etc. Tourism data in the system include the following two aspects: tourism map data of Gansu Province and basic attribute information related to tourism. On basis of determination of system objectives and thorough investigation into system functions, the data source will be determined. Such data mainly come from the traffic map of Gansu Province, tourism map of Gansu Province and information from tourism websites. Main data in the system will include spatial data (geographic data) and attribute data, which are shown in figure 4:

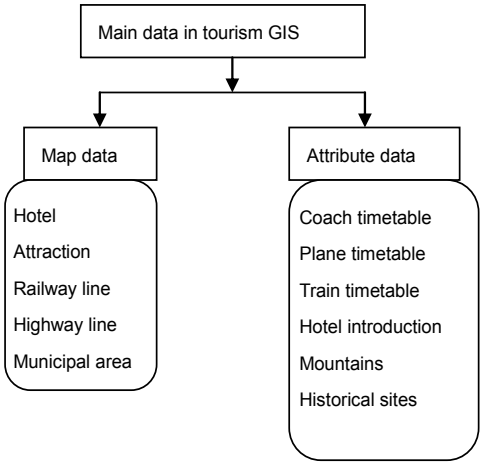

Fig. 4. Main data in tourism GIS

- Data organization, A characteristics to distinguish the tourism GIS from other GIS systems is its "multimedia attribute". The tourism information will be diversified due to its intrinsic nature, especially when combined with multimedia data. And with multimedia data, the tourism GIS will become more vivid, visual and interesting. Obviously, a successful tourism GIS must be capable of giving full play to the multimedia data, which is clearly reflected in the combination of multimedia data and geographic data in design and development. A mechanism with central processing is applied in the system, and the key is the processing efficiency. The multimedia data organized in the system with the principle of "taking the attraction and the city as the core as well as spatial data on the map" enables use to achieve considerable processing efficiency[6]. For example, during query about information on an attraction, the system can display photos and videos about the attraction in the photo area and video playing area, while providing the user with field information.

Introduction of database , The spatial database is the core and foundation of the GIS, and its quality will bring direct impact on the operation of the tourism information management system. Therefore, in design of the database, full consideration must be taken into existing data and various influencing factors, for purpose of rational design for the database in order to lay foundation for stable operation of the system. The system is composed of two parts: front-end collection system and management system. In the front-end collection system, ACCESS database is used, which is mainly for recording and entry of data. As a kind of relational database management system, ACCESS has the following main characteristics: single storage mode, which facilitates operation and management by the user; being object-oriented, which greatly simplify development by the user with achievement of database operation and management with approaches and attributes of the object; friendly interface, easier operation[7], etc. The above Geodatabase is the database used in the management system. Therefore, design for the database is composed of two parts: design for ACCESS database and design for Geodatabase database. For details, refer to figure 5 .

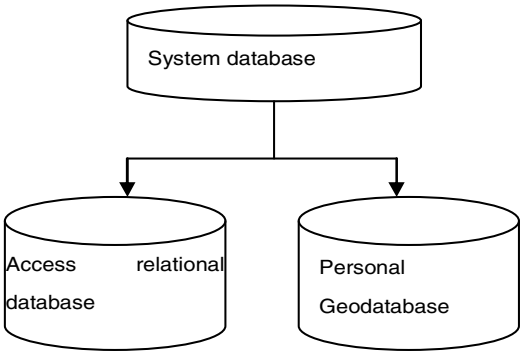

Fig. 5. System database

- ACCESS database Some attribute information is stored in ACCESS database, and according to actual tourism demands, many attributes are involved in the system, including respective attributes of spatial data, as well as other attribute information, such as basic information including train timetable (number, type, departure time, arrival time, run time and mileage, flight schedule and coach timetable. Except attribute information on some timetables, no respective attributes of spatial data is stored in the ACCESS database.
- Geodatabase database is a spatial database of geographic information for storage of geographic spatial information and attribute information of individual layers, including attractions, hotels, restaurants, traffic and administrative regions.

3 Conclusion

- By participating in the development and design of the tourism geographic information system, students majoring in tourism can carry out evaluation, planning, development and design for tourism resources, and obtain basic approaches for evaluation and development, utilization and protection of tourism resources. They can learn and master the application of e-commerce of tourism, and learn to carry out processing of tourism information and data, as well as statistical analysis of relevant data. With maps, models and audio and video data, they can obtain knowledge about distribution and characteristics of tourism resources in the experimental province. Through the above, students can really be improved in their ability in practice of tourism management through mutually beneficial learning and practice so that they can obtain proficiency required by tourism enterprises.

Acknowledgment. Foundation items:Lanzhou University of Finance and economics Subject of the project (2012) “The survey on the employment psychological of undergraduates from tourism management major”,Project Leader: Liu yan .

References

1. Chen, S., Peng, R.: Object-oriented Software Engineering, pp. 13–14. Publishing House of Electronics Industry (2003)
2. Craig, L., et al.: UML and Module Application: Object-oriented Analysis and Design Introduction, translated by Yao Shuzhen, et al, pp. 131–133. China Machine Press (2002)
3. Zhou, X., Yu, D., Zhang, J.: Research into Design Mode-based Software Architecture. Journal of Gansu University of Technology 19(6), 13–14 (2003)
4. Wei, Y., Tang, W., Guo, M.: Design for Database Access of DAO Mode-based JZEE Application
5. Xin, J.: Discussion on Construction of Experience-based Teaching Mode. Journal of Higher Education (3) (2005)

Author Index